Curso 2005/06
CIENCIAS Y TECNOLOGÍAS/13
I.S.B.N.: 84-7756-705-0

FERNANDO SALVADOR DELGADO TRUJILLO

Desarrollo de nuevos magnetos moleculares con ion malonato como ligando

Directores
CATALINA RUIZ PÉREZ
MIGUEL JULVE OLCINA

SERVICIO DE PUBLICACIONES
UNIVERSIDAD DE LA LAGUNA

SOPORTES AUDIOVISUALES E INFORMÁTICOS
Serie Tesis Doctorales

Agradecimientos

Me parece increíble poder estar escribiendo los agradecimientos que aunque será la primera hoja que aparecerá en el trabajo ha sido la última que se ha redactado. Mucha gente me viene a la mente en este momento y espero no olvidarme de nadie. Os agradezco a todos el gran apoyo que me habéis dado.

A mis compañeros de fatigas (Jorge, Óscar y Laura) precarios-becarios (como yo) con los que he compartido horas y horas no sólo en el laboratorio sino también fuera de él y que ¡han sido capaces de soportarme durante todo este tiempo!. Muchísimas gracias por hacerme pasar muy gratos momentos, hacerme reír cuando me encontraba más "pocho" y por todas esas buenas ideas que habéis aportado a este trabajo.

A Caty, Miguel (o Mikel) y Paco que han tenido tanta paciencia conmigo. Os agradezco un montón todo el apoyo que me habéis dado durante todo este tiempo. Sin vosotros este trabajo no hubiera sido posible. Sois los tres maravillosos. Miguel tienes que dejarme la receta de esas peras al vino que tan bien te quedan.

A las Marías. María Laz como verás casi ha desaparecido el color amarillo ... (estas cosas no se pueden escribir) que utilizaba para los átomos. Te agradezco muchísimo el apoyo que me has dado y los buenos ratos que me has hecho pasar cuando andaba un poco de capa caída (merci beaucoup). Eres estupenda. María Hernández, gracias también por tu apoyo.

También quisiera agradecer a Joaquín la ayuda que me ha dado. Muchísimas gracias.

No puedo olvidarme de Yolanda y José Ramón que aunque ahora ya no estén, son dos grandes amigos que tuve la suerte de conocer al comenzar el trabajo de tesis. A ver si nos vemos y podemos tomar una cerveza.

Qué no me olvide de toda la gente de Valencia: Eugenia, Alicia, Lumi, Emilio, Xelo, José, Joan, ... me habéis hecho sentir como en casa durante el tiempo que he pasado allí.

Muchísima gente me ha apoyado y me ha dado ánimos durante todo este tiempo: mis compañeros de facultad, mis amigos del GMT (Grupo Montañero de

Tenerife), los buenos amigos de l'Alliance Française (merci de l'encouragement que vous m'avez donné, je vous promets améliorer mon français et ne parler plus comme une vache espagnole).

Hay gente también muy especial a la que les agradezco su apoyo incondicional: a mis buenos amigos del Camino de Santiago: Estíbaliz (¡es qué es de Bilbao!); Dani de Jaén; Edu de Valencia; Antonio Carlos de Málaga (el quillo); Arturo de Vitoria,... Muchísimas gracias. Me alegro muchísimo de haber tenido la suerte de haberos conocido durante aquel mes caminando de Saint-Jean a Santiago. Un mes que no olvidaré jamás.

Lo más importante, gracias a mis padres, mis hermanos, mi abuela y a toda mi familia, por esos ánimos que me habéis dado en todo momento.

A mis padres,

"Il n'y a pas de recherche appliquée, il n'a que des applications de la recherche fondamentale".

Pascal

Índice

Tomo I

Tomo II

PARTE II: Trabajando con otros complejos de malonato

RESUMENES

Capítulo I

El Malonato protonado: la influencia de los enlaces de hidrógeno en el comportamiento magnético.

Objetivos de la Investigación

En los campos de la Química Supramolecular y el Magnetismo Molecular existe un gran interés en el estudio de las interacciones débiles (enlaces de hidrógeno, interacciones π···π, C-H···π, etc.), responsables del empaquetamiento molecular. Dentro de este contexto se está realizando un extenso estudio de las posibles interacciones que pueden existir entre los diferentes grupos funcionales de una molécula (a cada uno de los modos de interacción entre dos o más grupos funcionales se le denomina "*synthon*"), con el fin de ser capaces de comprender el empaquetamiento molecular y por consiguiente las propiedades macroscópicas que se derivan del mismo.

Con objeto de explorar este campo de la Química Supramolecular y de estudiar la influencia que pueden tener las interacciones débiles en las propiedades magnéticas de un material, se prepararon los compuestos que se presentan en este capítulo, usando como productos principales el ácido malónico (H_2mal), sus dos especies protonadas (Hmal$^-$ y mal^{2-}) y el ion paramagnético Cu^{2+}.

Planeamiento y Metodología utilizada

Inicialmente era necesaria la obtención de monocristales adecuados de los nuevos materiales con el fin de poder caracterizarlos estructuralmente mediante difracción de rayos X en monocristal. Con este fin se utilizó la técnica de crecimiento en solución. Para la preparación de los nuevos compuestos era necesario trabajar con diferentes pH, con el fin de controlar el nivel de protonación del grupo malonato.

Una vez obtenidos monocristales adecuados para su caracterización, estos fueron:

- Utilizados para su caracterización mediante análisis elemental.
- Montados en el difractómetro de rayos X de monocristal, obteniendo datos que permitieron la resolución estructural de los mismos.
- Molidos para obtener una muestra policristalina que permitiese caracterizar magnéticamente la muestra.

La síntesis química de los compuestos que se presentan en esta sección así como una descripción detallada de las medidas experimentales (difracción de rayos X, análisis elemental y medidas magnéticas) está recogida en la parte experimental de este capítulo.

Finalizada la caracterización estructural y magnética se procedió al estudio de los datos obtenidos.

Aportaciones originales y resultados

La preparación y caracterización de los materiales presentes en este capítulo nos ha permitido mostrar la influencia de los enlaces de hidrógeno en las propiedades magnéticas de un material (relación estructura-propiedad). Cabe destacar que se han obtenido nuevos motivos estructurales, no observados con anterioridad en compuestos de malonato de cobre(II).

El primer compuesto de fórmula $[Cu(Hmal)_2]$ (**1**) presenta una estructura que consiste en planos rectangulares de $Hmal^+$ y cobre (ver Figura 1), en el que el ácido malónico desprotonado actúa simultaneamente (ver Esquema 1.II) como ligando monodentado [ocupando una posición apical en el entorno del átomo metálico, siendo 2.5429(13) Å la distancia de enlace Cu-O] y bidentado (conformando el plano ecuatorial del metal). Cabe destacar que es la primera vez que se observa este tipo de coordinación en el ligando $Hmal^+$. Dentro del plano, los átomos de cobre están conectados mediante puente carboxilato ocupando éste, una posición ecuatorial en el entorno de uno de los átomos metálicos y una posición apical en el atómo metálico adyacente (las distancias entre átomos de cobre que definen el plano están recogidas en la Tabla 3). A este tipo de puente se le conoce como puente carboxilato ecuatorial-apical. Los planos rectangulares de cobre(II) se encuentran unidos entre sí mediante enlaces de hidrógeno dando lugar a una estructura tridimensional (ver Figura 2). Cabe destacar que mediante los enlaces por puente de hidrógeno las unidades mononucleares $[Cu(Hmal)_2]$, conforman una red bidimensional con una topología del tipo "*herringbone*" (espina de pez, ver Figura 4), no observada antes en compuestos de malonato.

Los enlaces de hidrógeno no son capaces de transmitir interacciones magnéticas intensas. Por este motivo y teniendo en cuenta que los átomos de cobre están unidos mediante puente carboxilato, dando lugar a planos rectangulares, los datos magnéticos se ajustaron utilizando la ecuación correspondiente a un plano de átomos de Cu(II) (ec. 1) siendo los resultados del ajuste: J = +0.104(4) cm^{-1}, g = 2.13(1) y $R = 2.46 \times 10^{-4}$ [J es el

paramétro de canje magnético, *g* la constante giromagnética y *R* el factor de acuerdo del ajuste definido como $\Sigma[(\chi_M)_{obs} - (\chi_M)_{calc}]^2/\Sigma[(\chi_M)_{obs}]^2$; $(\chi_M)_{obs}$ y $(\chi_M)_{obs}$ siendo las susceptibilidades magnéticas observadas y calculadas, respectivamente]. Los resultados obtenidos muestran la existencia de una débil interacción ferromagnética entre los iones de cobre a través del puente carboxilato, encontrándose dentro del rango observado para la interacción magnética a través del puente carboxilato que se presenta en este compuesto (ecuatorial-apical).

Los compuestos **2** y **3** son dos polimorfos de fórmula molecular $[Cu(H_2O)(H_2mal)(mal)]$ cuya estructura consiste en cadenas de malonato de cobre(II) unidas mediante el puente carboxilato del malonato ácido (siendo las distancias de enlace Cu-O largas, entre 2.368(2) y 2.616(2), ver Tablas 4 y 5), dando lugar a planos de cobre donde el anión malonato (mal^{2-}) y el ácido malónico (H_2mal) actúan de puente (ver Figura 5). Estos planos están unidos mediante enlaces de hidrógeno que contribuyen a la estabilización de la estructura global dando lugar a una red tridimensional (ver Figuras 7 y 8). El grupo malonato adopta simultáneamente (ver Esquema 1.I) la conformación de ligando bidentado y monodentado (conformando, junto con una molécula de agua), el plano ecuatorial de los átomos de cobre). Por su parte el ácido malónico exhibe una coordinación bis-monodentada (ver Esquema 1.III), observada por primera vez en estos compuestos. El grupo carboxilato del ligando malonato conecta posiciones ecuatoriales de dos átomos metálicos adyacentes exhibiendo el modo de coordinación *anti-syn*. Sin embargo, en el ácido malónico el grupo carboxilato que actúa de puente conecta posiciones apicales correspondientes a entornos de dos átomos de cobre próximos, mostrando una conformación *anti-anti*. Es importante tener en cuenta, que desde el punto de vista magnético, el puente carboxilato de tipo ecuatorial-ecuatorial, transmite con mayor intensidad la interacción magnética que el puente apical-apical. Por esta razón, las propiedades magnéticas de estos materiales se interpretaron suponiendo que estos compuestos estaban constituidos por cadenas regulares de cobre. Los datos magnéticos de **2** y **3**, fueron ajustados siguiendo la expresión para una cadena ferromagnética regular de iones cobre(II) (eqs. 3-5) siendo los resultados obtenidos: $J = +1.467(1)$ cm^{-1}, $g = 2.182(9)$ y $R = 5.4x10^{-4}$ para **2** y $J = 0.79(1)cm^{-1}$, $g = 2.179(2)$ y $R = 8.9x10^{-4}$ para **3**. Como se puede observar el valor de la interacción a través del puente carboxilato es del mismo orden en ambos compuestos (siendo diferentes los valores de interacción magnética debido a las pequeñas

diferencias estructurales que existen entre ambos materiales) y de naturaleza ferromagnética, al igual que en el conjunto de compuestos de malonato de cobre cuyas propiedades magnéticas han sido interpretadas.

Conclusiones

Tres nuevos compuestos de fórmulas $[Cu(Hmal)_2]$ (**1**) y $[Cu(H_2O)(H_2mal)(mal)]$ (**2** y **3**) en los cuales se encuentran presentes las tres posibles especies derivadas del ácido malónico (H_2mal, $Hmal^-$, mal^{2-}) han sido sintetizados y caracterizados magnética y estructuralmente. Los tres compuestos presentan estructuras en forma de capas de malonato de cobre que se encuentran unidas mediante enlances de hidrógeno dando lugar a redes tridimensionales. Las propiedades magnéticas de estos compuestos muestran que la efectividad del canje magnético está relacionado con el grado de desprotonación del malonato, siendo despreciable para H_2mal, muy débil para $Hmal^-$ y más efectivo para el grupo mal^{2-}. Desde el punto de vista estructural las distancias Cu-O parecen estar relacionadas también con el grado de desprotonación del ligando, siendo menores cuando el grado de desprotonación es mayor. Con la preparación y caracterización de estos nuevos materiales hemos mostrado que es posible obtener compuestos donde coexistan diferentes especies del mismo ligando y que la disposición de los mismos puede controlar las propiedades magnéticas de un material. Cabe destacar que desde el punto de vista estructural se han observado por primera vez redes de tipo "*herringbone*" en compuestos de malonato de cobre (ver Figura 4) y modos de coordinación nuevos para los grupos H_2mal y $Hmal^-$ (ver Esquema 1).

Capítulo II

Empaquetamiento cristalino y comportamiento magnético en compuestos alkalinos de malonato de cobre(II).

Objetivos de la Investigación

Los resultados obtenidos con la utilización del malonato protonado, expuestos en el capítulo anterior, pusieron de manifiesto que la introducción de un cation en los complejos de malonato de cobre(II) podría ser una buena estrategia para la obtención de materiales funcionales con interesantes propiedades magnéticas.

Con esta idea en mente, decidimos estudiar cómo afectaba la introducción de un ion alkalino M (M = Li, Na, K, Rb, Cs) al empaquetamiento del malonato de cobre(II) y consecuentemente, a sus propiedades magnéticas.

Como se indica en la introducción de este capítulo, otros compuestos de cobre(II) con puente carboxilato y metal alkalino habían sido caracterizados; no obstante, en la bibliografía consultada no se ha encontrado ningún estudio pormenorizado de la influencia del metal alkalino en la estructura y propiedades de dichos materiales.

Planeamiento y Metodología utilizada

Para poder llevar a cabo el estudio planteado, era necesario obtener buenos monocristales, que nos permitieran caracterizar estructuralmente las muestras. Como metales alkalinos se utilizaron los siguientes: Li, Na, K, Rb y Cs.

Los nuevos materiales fueron sintetizados utilizando la técnica de crecimiento en solución.

Una vez obtenidos monocristales adecuados para el estudio, estos fueron:

- Utilizados para su caracterización mediante análisis elemental.
- Montados en el difractómetro de rayos X de monocristal, obteniendo datos que permitieron la resolución estructural de los mismos.
- Molidos para obtener una muestra policristalina que permitiese caracterizar magnéticamente la muestra.

La síntesis química de los compuestos que se presentan en este capítulo así como una descripción detallada de las medidas experimentales (difracción de rayos X, análisis elemental y medidas magnéticas) está recogida en la parte experimental.

Una vez caracterizados estructural y magnéticamente los compuestos sintetizados, se procedió al estudio de las relaciones magneto-estructurales que se presentan en el siguiente apartado.

Aportaciones originales y resultados

El trabajo realizado supone una primera aproximación al estudio de la influencia de los metales alkalinos en el empaquetamiento, no sólo de los compuestos de malonato de malonato de cobre, sino también dentro del campo de los compuestos con puente carboxilato.

Se prepararon cinco nuevos compuestos de fórmula molecular $[Li(H_2O)]_2[Cu(mal)_2(H_2O)]$ (**1**); $[Na(H_2O)]_2[Cu(mal)_2]$ (**2**); $[K(H_2O)_{3/2}]_2[Cu(mal)_2]$ (**3**); $[Rb(H_2O)_{1/2}]_2[Cu(mal)_2]$ (**4**) and $[Cs(H_2O)]_2[Cu(mal)_2(H_2O)_2]$ (**5**).

La estructura del compuesto **1** consiste en unidades de $[Cu(mal)_2(H_2O)]^{2-}$ y $[Li(H_2O)_n]^+$ unidas mediante puente carboxilato y moléculas de agua -coordinadas a ambos metales- dando lugar a una estructura tridimensional, en la que los iones litio actúan como pilares entre las unidades de malonato de cobre(II) (ver Figura 1). Adicionalmente, enlaces de hidrógeno en los que intervienen oxígenos del ligando malonato y moléculas de agua, contribuyen a la estabilización de la estructura.

Una descripción detallada de los entornos de los metales (Cu, Li), así cómo de los modos de coordinación de ión malonato, se realiza en el texto de este capítulo. Cabe destacar que los iones de litio se encuentran conectados entre sí mediante puente carboxilato, dando lugar a cadenas de alkalinos (Figura 6). Veremos a lo largo de este resumen que existe una relación directa entre el tamaño del alkalino y la estructura resultante del compuesto del malonato de cobre.

Desde el punto de vista de las propiedades magnéticas, los iones alkalinos son iones diamagnéticos y por consiguiente no son capaces de transmitir la interacción magnética. Por esta razón, y teniendo en cuenta que en **1** cada unidad de $[Cu(mal)_2(H_2O)]^{2-}$ está conectada a cationes del tipo $[Li(H_2O)_n]^+$, la interpretación de las propiedades magnéticas de este complejo puede realizarse, considerando que está compuesto por unidades monoméricas aisladas (magnéticamente) de malonato de cobre(II). La interpretación de los datos magnéticos a través de una Ley de Curie-Weiss (ver Figura

34) corrobora la hipótesis adoptada, existiendo una muy débil interacción antiferromagnética debida a los enlaces de hidrógeno que conectan las diferentes unidades de cobre (ver Figura 5).

El compuesto **2** posee una estructura tridimensional compuesta por planos iónicos alternados de malonato de cobre(II) y $[Na(H_2O)]^+$, unidos mediante puente carboxilato y moléculas de agua coordinadas a ambos metales (Figura 7). Enlaces de hidrógeno en los que participan oxígenos de grupos malonato y moléculas de agua ayudan en el empaquetamiento cristalino, contribuyendo a la estabilización de la estructura.

En el texto se realiza una descripción muy detallada de la estructura de este compuesto. Destacamos aquí simplemente dos aspectos importantes del estudio realizado:

- Las unidades de malonato de cobre $[Cu(mal)_2]^{2-}$ se encuentran enlazadas entre sí a través de puente carboxilato Cu-O(ecuatorial)-C-O(apical)-Cu [siendo 1.954(2) y 2.601(2) Å las distancias de enlace Cu-O(ecuatorial) y Cu-O(apical), respectivamente] dando lugar a un plano rectangular de iones cobre (ver Figura 11).
- Los iones sodio se encuentran unidos en primera instancia a través de puente μ-oxo (en el que intervienen moléculas de agua coordinada y átomos de malonato) dando lugar a cadenas (ver Figura 12), las cuales, a su vez están conectadas entre sí, mediante puente carboxilato, conformando los planos de sodio que se muestran en la Figura 13.

La interpretación de los datos magnéticos de **2** (Figura 35) se hace suponiendo que la estructura consiste únicamente en planos rectangulares de cobre (recordar que los iones alkalinos son diamagnéticos y no son capaces de trasmitir la interacción magnética). Los datos experimentales se ajustan utilizando el modelo de la expresión de la ecuación 5 derivada de las series de expansión para planos cuadráticos de cobre. Los resultados del ajuste [J = +0.897(1) cm^{-1}, g = 2.175(1) and R = $3.8x10^{-5}$] indican la existencia de una interacción ferromagnética.

La estructura del compuesto **3** al igual que el compuesto **2,** consiste en planos alternados de malonato de Cu y de unidades de iones alkalinos (K en este caso). Ver la Figura 14. Aunque el empaquetamiento de la estructuras **2** y **3** presenta algunas diferencias notables (comparar la Figura 11 con la 18 y la 13 con la 20) en ambos casos el malonato de cobre se empaqueta dando lugar al mismo tipo de planos rectangulares,

donde los cobres están unidos mediante puente carboxilato del tipo Cu-O(ecuatorial)-C-O(apical)-Cu [siendo ahora 1.9417(15) y 2.689(2) Å los valores correspondientes a las distancias de enlace Cu-O(ecuatorial) y Cu-O(apical)].

La interpretación de los datos magnéticos del compuesto **3** (Figura 36), se realiza de forma similar al compuesto **2** siendo los resultados obtenidos, los siguientes: J = +0.774(2) cm^{-1}, g = 2.243(2) and R =6.9x10^{-5}. Como puede observarse la interacción sigue siendo ferromagnética pero es más débil en **3**. Esto es debido al aumento de la distancia Cu-O(apical) que hace que el solapamiento entre los orbitales magnéticos de los iones cobre (unidos mediante el puente carboxilato) sea menor, lo que se traduce en una reducción de la interacción magnética a través del puente.

Para el complejo de Rb (**4**), la estructura cambia ligeramente, aunque sigue manteniéndose la estructura tridimensional de capas de malonato de cobre y alkalino (ver Figura 21), ahora una de las distancias Cu-O(apical) = 3.138(7) Å (que en **2** y **3** daba lugar al plano rectangular de cobre) es tan alta (debido al aumento del tamaño del ion alkalino) que no puede considerarse una distancia de enlace. Esto lleva a que para el compuesto **4**, en lugar de formar planos rectangulares de cobre, las unidades de malonato se empaqueten dando lugar a cadenas (ver Figura 25 y 26), en las que los iones cobre están unidos a través de puentes del tipo Cu-O(ecuatorial)-C-O(apical)-Cu [1.941(6) y 2.589(7) Å para las distancias de enlace Cu-O(ecuatorial) y Cu-O(apical), respectivamente]. Cabe destacar que los iones de Rb se encuentran conectados (a través de puente μ-oxo y carboxilato) dando lugar a una estructura bidimensional que contrasta con las estructuras observadas anteriormente (ver Figura 27).

Los datos magnéticos (Figura 34) se han ajustado siguiendo la ley de una cadena regular de iones S = ½ [iones de cobre(II)] (ver eq. 1-3) siendo los resultados del ajuste: J = +0.82(3) cm^{-1}, g = 2.155(1) y R = 4.0x10^{-4}.

Finalmente la estructura del compuesto **5**, aunque consiste en una red tridimensional compuesta (al igual que los compuestos del **2-4**) en planos alternados de malonato de cobre y alkalino (Cs), ver la Figura 28. En este caso el tamaño del anión es tal que consigue alejar entre sí las unidades de malonato de cobre, las cuales se encuentran unidas ahora mediante enlaces de hidrógeno.

Las unidades de Cs, se encuentran unidas por enlaces de tipo μ-oxo dando lugar a una estructura bidimensional (ver Figura 33).

Desde el punto de vista magnético los datos experimentales se ajustaron siguiendo una ley de Curie-Weiss al igual que en **1**. Los resultados obtenidos del ajuste apuntan a la existencia de una muy débil interacción ferromagnética que tiene lugar a través de los enlaces de hidrógeno que unen las unidades de cobre entre sí.

Conclusiones

En este capítulo se hace una comparación detallada entre cada una de las estructuras obtenidas. Cabe destacar los siguientes resultados:

- El empaquetamiento de los iones alkalinos está directamente relacionado con su tamaño. Así observamos que estos iones se unen a través de puente μ-oxo dando lugar a dímeros (Li), cadenas (Na y K), cadenas dobles (Rb) y planos (Cs). Lógicamente este hecho tiene su influencia en el empaquetamiento de las unidades de malonato de cobre(II).
- Exceptuando el caso del Li, a medida que el tamaño del alkalino aumenta (Na, K, Rb y Cs), aumenta la distancia entre las unidades de cobre. Esto se traduce en una disminución de la interacción magnética. Variando el ion alkalino se observa una gran variedad de empaquetamientos cristalinos del malonato de cobre; dando lugar a unidades mononucleares unidas mediante enlaces de hidrógeno (Li, Cs), planos (Na y K) y cadenas (Rb).

Hemos demostrado que la utilización de los iones alkalinos puede ser útil cuando se desea controlar el empaquetamiento de las unidades de malonato de cobre. Estos resultados pueden ser extensibles a otros compuestos que contengan ligandos carboxilatos (oxalato, fumarato, acetato, etc,...)

Capítulo III

Empaquetamiento cristalino y comportamiento magnético en compuestos de amonio de malonato de cobre(II).

Objetivos de la Investigación

A la luz de los resultados obtenidos en el capítulo anterior donde pudimos comprobar la importancia del tamaño del ion alkalino en el empaquetamiento de las unidades de malonato y tras comprobar que la introducción de un ligando protonado puede ser una estrategia interesante en el diseño de nuevos materiales magnéticos (como pudimos observar en el capítulo I), decidimos abordar el estudio magneto-estructural en compuestos de malonato de cobre(II) donde se incluía como cation el grupo amonio (NH_4^+) y sus derivados {$[CH_3NH_3]^+$, $[H_3(CH_2)_2NH_3]^{2+}$, $[NH_3(CH_2)_3NH_3]^{2+}$, $[NH_3(CH_2)_4NH_3]^{2+}$}.

Siguiendo esta estrategia pensábamos aprovechar la amplia versatilidad que brindan las interacciones débiles (enlaces de hidrógeno fundamentalmente) en el diseño de estructuras moleculares (recordar el concepto de "*synthon*" que se utilizó en el capítulo I) y sacar provecho a la posibilidad de jugar con el tamaño del cation introducido (al igual que hicimos en el capítulo II y que nos dio tan buenos resultados) para poder controlar el empaquetamiento de las unidades de malonato de cobre.

Planeamiento y Metodología utilizada

Como comentamos en los objetivos, nuestro propósito inicial consistía en preparar compuestos de malonato de cobre utilizando como contraion el amonio y otros cuatro grupos derivados del mismo.

Los compuestos de fórmula molecular: $(NH_4)_2[Cu(mal)_2]$ (**1**), $(MeNH_3)$ $[Cu(mal)_2]$ (**2**), $(H_2en)[Cu(mal)_2(H_2O)]\cdot 2H_2O$ (**3**), (H_2pn) $[Cu(mal)_2]$ (**4**) y $(H_2bn)[Cu(mal)_2(H_2O)]\cdot H_2O$ (**5**) fueron preparados a partir de productos comerciales, tal y como se describe en la parte experimental de este capítulo.

Se utilizó como método de síntesis la evaporación lenta (para la obtención de los compuestos **1-3** y **5**) y el método de difusión lenta para el compuesto de **4**.

Monocristales apropiados para su caracterización estructural se obtuvieron para los compuestos aquí descritos **1-5**.

Para cada uno de los compuestos obtenidos se realizaron las siguientes medidas experimentales:

- Análisis elemental para determinar el contenido de C, H y N.
- Medidas de difracción de rayos X de monocristal cuyos datos permitieron la resolución estructural de cada uno de los compuestos preparados.
- Medidas de susceptibilidad magnética para poder caracterizar magnéticamente cada una de las muestras.

A continuación se exponen los resultados obtenidos.

Aportaciones originales y resultados

En la bibliografía no se recoge ningún trabajo que estudie cómo afecta el tamaño de un ion del tipo del amonio y sus derivados en el empaquetamiento cristalino y en las propiedades magnéticas de un complejo.

El trabajo aquí presentado supone una aportación nueva al campo de la Ingeniería Cristalina y del Magnetismo Molecular y pone de manifiesto la importancia de las interacciones débiles en la comprensión del empaquetamiento cristalino.

Al igual que en capítulos anteriores, en el texto de la tesis que acompaña a este resumen puede encontrarse una descripción detallada de cada una de las estructuras así como una pormenorizada comparación entre los resultados obtenidos para cada compuesto.

La estructura del compuesto **1**, consite en aniones de $[Cu(mal)_2]^{2-}$ que se encuentran unidos mediante puentes carboxilato de malonato dando lugar a una red aniónica tridimensional (Figura 5). El empaquetamiento de estas unidades es posible gracias a los grupos NH_4^+, los cuales mediante enlaces de hidrógeno contribuyen al acercamiento de las unidades de cobre y favorecen la aparición de la red tridimensional de malonato de cobre (Figura 1a). Teniendo en cuenta la estructura formada por cada una de las unidades constituyentes de este compuesto [el anión dimalonato de cobre(II) y el cation amonio] podemos considerar que la estructura del compuesto **1** consiste en dos redes iónicas interpenetradas, como se puede observar en la Figura 1b de este capítulo.

Desde el punto de vista magnético, como hemos comentado en los capítulos anteriores, los enlaces de hidrógeno no son capaces de transmitir de forma efectiva la interacción magnética. En este sentido, únicamente debemos considerar los puentes de tipo carboxilato para poder interpretar los datos magnéticos de este compuesto, por

consiguiente deberíamos ajustar los datos experimentales a una ley correspondiente a una red tridimensional de spin S = ½ [iones cobre(II)]. Desgraciadamente no existe ninguna ley teórica que permita realizar dicho ajuste. Ello es debido a la complejidad (alta dimensionalidad) de la red a tratar. No obstante, observando el comportamiento de la curva de $\chi_M T$ (χ_M siendo la susceptibilidad magnética) frente a T (ver Figura 29), podemos decir que la interacción es de naturaleza ferromagnética.

El compuesto **2** consiste en un empaquetamiento alterno de capas de aniones $[Cu(mal)_2]^{2-}$ y de cationes $(MeNH_3)^+$ unidos mediante puente carboxilato y enlaces de hidrógeno (ver Figura 8). Las capas aniónicas están compuestas por iones de cobre, unidos mediante puente malonato dando lugar a una plano rectangular de iones cobre (Figure 11) similar al observado en los compuesto de Na y K presentado en el capítulo II. Por su parte los cationes se encuentran unidos entre sí mediante enlaces de hidrógeno dando lugar a cadenas a lo largo del eje *c* cristalográfico. Estas cadenas catiónicas que se empaquetan a lo largo del eje *b* (dando lugar a planos iónicos), hacen de puente entre los planos aniónicos del malonato de cobre, contribuyendo a la estabilización de la estructura tridimensional del compuesto.

Desde el punto de vista magnético el compuesto consiste en planos rectangulares de iones Cu(II) (ver Figura 11) unidos mediante puente carboxilato del tipo Cu-O(ecuatorial)-C-O(apical)-Cu [1.9236(11) y 2.5620(15) Å para las distancias de enlace Cu-O(ecuatorial) y Cu-O(apical), respectivamente. Por consiguiente, la interpretación de los datos magnéticos experimentales se hizo mediante la serie de expansión recogida en la ecuación (1) que ha sido derivada del modelo bidimensional de Heisenberg para spines S = ½ ferromagnéticamente acoplados. Los resultados del ajuste (J = +0.755(1) cm^{-1}, g = 2.060(1) y R = $2.3x10^{-5}$) indican que existe una interacción débilmente ferromagnética que está de acuerdo con los resultados obtenidos en el capítulo II (ver Tabla 17 del presente capítulo).

Es posible, además de aumentar el tamaño del catión, variar el número de grupos dadores que éste posee. Estas variaciones en la naturaleza del grupo dador van a producir también un cambio en el empaquetamiento de las unidades de cobre(II) debido al diferente esquema de interacciones (enlaces de hidrógeno) que genera el nuevo catión. Así por ejemplo, en el complejo **3** descrito en el texto, se ha utilizado como catión, un derivado de amonio que posee dos grupos dadores: $(H_2en)^{2+}$. Mediante esta estrategia, conseguimos variar la estructura del compuesto, poniendo de manifiesto la

importancia de las interacciones débiles en el empaquetamiento cristalino. La estructura del compuesto **3** consiste en capas alternadas de aniones y cationes (Figura 14). Las capas aniónicas se encuentran formadas por unidades de $[Cu(mal)_2]^{2-}$ unidas mediante enlaces de hidrógeno (ver Figura 17). Estas capas de malonato de cobre se encuentran enlazadas mediante los grupos $(H_2en)^{2+}$ que conforman a su vez capas catiónicas, dando lugar a una estructura tridimensional neutra.

Como hemos comentado, las unidades de $[Cu(mal)_2]^{2-}$ se encuentran unidas mediante enlaces de hidrógeno, es por ello por lo que los datos magnéticos han sido ajustados siguiendo una ley de Curie-Weiss (Figura 29). Los resultados obtenidos indican la existencia de una muy débil interacción ferromagnética, como era de esperar debido a la naturaleza monodimensional de **3**.

Continuando con nuestra estrategia del estudio de las propiedades estructurales y magnéticas de compuestos derivados del amonio, seguimos preparando compuestos dónde aumentábamos el tamaño del catión $(H_2pn)^{2+}$ (**4**) y $(H_2bn)^{2+}$ (**5**), con el objeto de estudiar sus efectos.

El compuesto **4**, muestra una estructura en capas alternadas (ver Figura 19), similar a la observada en los compuestos anteriores. Ahora las unidades de malonato de cobre, se encuentran unidas mediante los grupos catiónicos, empaquetándose ambos en capas separadas a lo largo del plano *ac*. El aumento del tamaño del catión hace que las unidades de cobre se alejen entre sí de forma que estén prácticamente aisladas. Como se puede observar en la Figura 21 la distancia Cu-O(apical) (dibujada con una flecha de color amarillo), es tan larga [3.151(3) Å] que no puede considerarse como distancia de enlace. Cabe destacar aquí que la topología de los planos de malonato de cobre, es similar a la observada para el Na, el K (ver Figura 11 y 18 del capítulo II) y para el compuesto **2** del presente capítulo.

De forma similar a **2**, la interpretación de los datos magnéticos del compuesto **4** (ver Figura 31), se hizo en base a la eq. (1) que representa la susceptibilidad para una red bidimensional de spines S = ½ acoplados ferromagnéticamente. Los resultados obtenidos (J = +0.263(5) cm^{-1}, g = 2.066(4) and R = $1.2x10^{-4}$), indican la existencia de una interacción ferro que como vemos es de menor intensidad que la observada en el compuesto **2**, debido fundamentalmente al aumento de la distancia Cu-O(apical) (ver Tabla 17).

Finalmente, a pesar de que en el complejo **5**, la estructura también consiste en capas iónicas alternadas, la configuración de las mismas es muy diferente a la observada en los compuestos anteriores. En este caso, las unidades de malonato de cobre conforman un plano mediante enlaces de hidrógeno (presentando una topología diferente a la del compuesto **3** de este capítulo, comparar Figuras 17 y 26).

De forma similar al compuesto **3**, el complejo **5** presenta un comportamiento magnético que puede interpretarse mediante una ley de Curie-Weiss (Figura 29). El ajuste de la curva experimental confirma la existencia de una débil interacción magnética (prácticamente despreciable) a través de los enlaces de hidrógeno.

Conclusiones

En este capítulo hacemos un estudio detallado de cómo la naturaleza (tamaño y número de grupos dadores) del catión orgánico introducido produce cambios en el empaquetamiento del malonato de cobre.

A diferencia del capítulo II, dónde únicamente podíamos variar el tamaño del catión (catión inorgánico), en el presente capítulo jugamos también con el número de grupos dadores.

Hemos podido comprobar como, al igual que en el capítulo anterior el aumento del tamaño del grupo catiónico, produce, en general, un alejamiento de las unidades de $[Cu(mal)_2]^{2+}$ dando lugar a una disminución progresiva de la intensidad del canje magnético.

Cabe destacar también la gran importancia de los enlaces de hidrógeno, los cuales controlan, sin lugar a dudas, el empaquetamiento cristalino de cada uno de los compuestos descritos en este capítulo.

Capítulo IV

Redes supramoleculares en compuestos de malonato de cobre(II).

Objetivos de la Investigación

En el trabajo realizado anteriormente hemos podido comprobar que los enlaces de hidrógeno a pesar de ser considerados como interacciones débiles, son muy importantes y pueden llegar a controlar el empaquetamiento cristalino (recordar el malonato ácido del capítulo I y los grupos amonios del capítulo III).

En el presente capítulo, nuestro objetivo consistió en la modificación de la unidad de malonato de cobre [$Cu(mal)_2$] -utilizada hasta ahora- por otra del tipo [Cu(mal)L], siendo L un ligando de tipo azina que actuase como ligando terminal. Con esta estrategia pretendíamos estudiar como otro tipo de interacciones débiles, tales como las interacciones de tipo $\pi\cdots\pi$ (que se pueden dar entre los grupos aromáticos de los ligandos tipo azina), podían introducir cambios en el empaquetamiento cristalino.

Planeamiento y Metodología utilizada

Para poder llevar a cabo los objetivos previstos, elegimos inicialmente un grupo de ligandos tipo azina apropiados que pudiesen actuar como ligandos terminales: bis(2-piridil)keton (dpydiol); 2,2'-dipirildamina (dpa); 2-(2-piridil)imidazol (pyim); 2,3-bis(2-piridil)pirazina (dpp) y 1,10-fenantrolina (phen).

Utilizando el método de evaporación lenta y siguiendo el procedimiento descrito y en el apartado experimental, se realizó la síntesis de los seis compuestos que se describen en este capítulo: [Cu(dpydiol)(mal)(H_2O)]·$2H_2O$ (**1**); [Cu(dpa)(mal)(H_2O)]·H_2O (**2**); [Cu(pyim)(mal)(H_2O)]·H_2O (**3**); [Cu(dpp)(mal)(H_2O)]·$3/2H_2O$ (**4**); [Cu(phen)(mal)(H_2O)]·H_2O (**5**);[Cu_2(phen)$_2$(mal)(H_2O)$_3$](NO_3)$_2$·$2H_2O$ (**6**)

Una vez obtenidos cristales apropiados para cada uno de los compuestos, se caracterizaron mediante:

- Analísis elemental.
- Difracción de rayos X en monocristal.

- Medidas magnéticas en un magnetómetro Squid, únicamente para el compuesto **6** que como veremos es un complejo dinuclear de cobre. Las medidas magnéticas para los compuestos **1-5** no se realizaron debido a su naturaleza mononuclear.

A continuación se muestran los resultados obtenidos.

Aportaciones originales y resultados

El trabajo expuesto supone la descripción estructural de 6 nuevos compuestos de malonato de cobre y ha permitido poner de manifiesto que interacciones consideradas como débiles (enlaces de hidrógeno e interacciones de tipo π···π o C-H···π) son las que gobiernan el empaquetamiento cristalino y por consiguiente las propiedades de los materiales obtenidos. Este hecho es importante, dentro del campo de la Ingeniería Cristalina los resultados obtenidos pueden ser un buen punto de partida para el diseño de nuevos materiales basados en el anión malonato.

Una detallada descripción de cada una de las estructuras aquí presentadas, se puede encontrar en el texto. En este resumen discutiremos los puntos más destacados de cada una de ellas.

Como puede observarse en la Figura 1, el compuesto **1**, está formado por unidades de [Cu(dpydiol)(mal)(H_2O)] y moléculas de agua unidas entre sí mediante enlaces de hidrógeno (que aparecen dibujados como líneas discontinuas) e interacciones de tipo π···π entre los anillos aromáticos del grupo dpydiol (ver Tabla 2), dando lugar a una estructura tridimensional. Es importante destacar el papel que juegan las moléculas de disolvente (en este caso, moléculas de agua) en el empaquetamiento cristalino. Como puede verse en las Figuras 3 y 4, éstas son las responsables del empaquetamiento tridimensional de las unidades de malonato de Cu y dpydiol. Las moléculas de agua, junto con los átomos aceptores, dan lugar a patrones definidos, como por ejemplo los anillos de ocho y catorce miembros [$R_4^4(8)$ y $R_5^5(14)$, en la nomenclatura utilizada en la bibliografía] que pueden observarse en la Figura 3. Estos patrones facilitan la comprensión del empaquetamiento molecular. Finalmente la estructura del compuesto **1** se encuentra estabilizada mediante débiles interacciones de tipo π···π (Figura 1).

En el compuesto **2**, [Cu(dpa)(mal)(H_2O)]·H_2O, hay una molécula de disolvente menos que en el **1**. A pesar de ello, las unidades de [Cu(dpa)(mal)] se encuentran unidas mediante enlaces de hidrógeno (ver Tabla 5) de tipo O-H···O (Figura 7) y N-H···O

(Figura 8), dando lugar a una red tridimensional. Débiles interacciones de tipo π···π contribuyen a la estabilización de la estructura.

En lo que respecta a los patrones de agua observados, se pueden distinguir dos tipos diferentes (ver Figura 7): anillos de doce miembros $R_6^4(12)$ que dan lugar a cadenas dobles de malonato de cobre y anillos de dieciséis miembros $R_4^4(16)$ los cuales unen las cadenas dobles entre sí, dando lugar a capas que crecen en el plano perpendicular al eje *b* cristalográfico. Estos planos, se encuentran unidos entre sí mediante interacciones del tipo N-H···O donde intervienen las moléculas de agua no coordinadas y el grupo NH del ligando dpydiol (ver las líneas discontínuas en la Figura 5 y 8). Finalmente interacciones de tipo π···π refuerzan el contacto entre los diferentes planos de malonato de cobre (Figura 8).

Una estructura similar a la anterior se observa para el compuesto **3**. Planos de malonato de cobre donde las unidades de malonato están unidas mediante enlaces de hidrógeno (en los que intervienen moléculas de agua coordinadas y de cristalización ;ver Figura 11) están conectados entre sí mediante enlaces de tipo N-H···O (donde intervienen los grupos NH del ligando pyim y oxígenos del ligando malonato) e interacciones π···π (entre los anillos aromáticos del ligando pyim; ver Figura 12), como puede observarse en la Figura 9, dando lugar a una red neutra tridimensional.

En lo que respecta a los patrones de agua, en el complejo **3**, se pueden distinguir anillos de doce miembros [$R_4^4(12)$, ver Figura 11] formados por dos moléculas de agua de cristalización y dos grupos carboxilato del grupo malonato, relacionados mediante un centro de inversión.

Hasta el momento las interacciones que han controlado el empaquetamiento cristalino han sido: enlaces de hidrógeno del tipo O-H···O y N-H···O e interacciones débiles del tipo π···π. Con la utilización del ligando 2,3-bis-(2-piridil)-pirazina (dpp) en el complejo **4** conseguimos introducir una nueva interacción de tipo hidrofóbica (entre el anillo aromático del ligando dpp y la cadena alifática del grupo malonato; ver línea punteada de color negro en la Figura 13) que va a gobernar el empaquetamiento de las unidades de malonato de cobre. Este tipo de interacción sólo había sido caracterizada en un único compuesto de malonato de cobre [Borghi E., 1987, incluida en las referencias de este capítulo].

La estructura del compuesto **4**, puede ser vista como cadenas de [Cu(dpp)(mal)(H_2O)] unidas mediante enlaces de hidrógeno (ver Tabla 13 y Figuras 13 y 15) en los que intervienen moléculas de agua -coordinadas y de cristalización- y los oxígenos externos del grupo malonato. Enlaces de hidrógeno adicionales, en los que intervienen únicamente las aguas de cristalización [O(2w) y O(3w)] conectan las diferentes cadenas, dando lugar a una estructura tridimensional donde las cadenas de malonato de cobre crecen en dos direcciones diferentes: [½ ½ 0] y [½ -½ 0]. Este tipo de estructura en la que se entrelazan cadenas, no había sido observada nunca en compuestos de malonato. Creemos que su aparición se debe fundamentalmente a la combinación y competencia entre las interacciones hidrofóbicas (descritas en el párrafo anterior) y los enlaces de hidrógeno.

Utilizando el ligando 1,10-fenantrolina (phen) se prepararon los compuestos **5** y **6**. La estructura del compuesto **5** es similar a la de los compuestos **1**-**3**, planos de malonato de cobre (en los que las unidades de cobre se encuentran unidas mediante enlaces de hidrógeno; ver Tabla 16 y Figura 18) enlazados mediante interacciones de tipo π···π (entre los anillos aromáticos de la phen; ver Figuras 18 y 19). La principal diferencia entre los compuestos **1**-**3** y el **5** consiste en que en el presente compuesto el ligando azina no posee grupos NH que puedan actuar como dadores y unir los diferentes planos de malonato de cobre entre sí. De esta forma y teniendo en cuenta únicamente los enlaces de hidrógeno, el compuesto da lugar a redes bidimensionales (frente a las redes tridimensionales que presentaban los compuestos del **1** al **3**), consiguiéndose la tridimensionalidad de la estructura mediante interacciones débiles de tipo π···π. Este hecho pone de manifiesto la importancia de las interacciones π···π que hasta el momento parecía que contribuían de forma secundaria al empaquetamiento molecular.

En lo que respecta a los patrones de agua en este compuesto, pueden distinguirse, dentro del plano de malonato de cobre (Figura 18), anillos de ocho [$R_4^2(8)$] y doce miembros [$R_6^4(12)$], responsables del empaquetamiento a lo largo del plano *ac*.

Para terminar con la descripción de este compuesto se realiza una comparación del mismo con otro de fórmula similar [Cu(mal)(phen)(H_2O)]·3/2H_2O [Kwik W.-L. *et al.*, 1986; Borghi E., 1997, referencias recogidas en el presente capítulo]. Destacar únicamente que la preparación de ambos compuestos fue diferente, siendo en medio etanol para el compuesto **5** y en medio acuoso para [Cu(mal)(phen)(H_2O)]·3/2H_2O. Esto

hace que el número total de moléculas de aguas de cristalización sea diferente en ambos compuestos, lo que da lugar a un distinto empaquetamiento de las unidades de malonato de cobre en ambos complejos (comparar las Figuras 16 y 18, correspondientes a **5**, con las Figuras 20 y 21, correspondientes a [Cu(mal) (phen)(H_2O)]·3/2H_2O).

Mediante la introducción del contraion nitrato, se preparó el compuesto dinuclear **6** que consiste en unidades diméricas de cobre unidas a través de puente malonato (ver Figura 23). Estas unidades se encuentran a su vez ligadas mediante enlaces de hidrógeno e interacciones hidrofóbicas -entre los grupos aromáticos de la phen y la cadena alifática de los grupos malonato- y de tipo π···π -entre los grupos aromáticos de la phen- dando lugar a una red tridimensional (Figura 22).

Las propiedades magnéticas de los compuestos del **1**-**5** no fueron medidas debido a la naturaleza monomérica de los mismos. Las propiedades correspondientes al compuesto **6**, fueron analizadas mediante una ley de susceptibilidad magnética para un compuesto dinuclear de cobre. Los resultados obtenidos del ajuste: J = +6.22(3) cm^{-1}, θ = -0.042(2) K , g = 2.106(1) and R = 2.3x10^{-5} dan cuenta de la existencia de una interacción ferromagnética a través del puente Cu-O(ecuatorial)-C-O(ecuatorial)-Cu (puente carboxilato de malonato), de acuerdo con los resultados obtenidos para este tipo de puente en complejos de malonato de cobre(II).

Conclusiones

Tras la discusión de los resultados obtenidos, podemos concluir que interacciones generalmente consideradas como débiles (enlaces de hidrógeno O-H···O/ N-H···O e interacciones de tipo π···π y C-H···π) juegan un papel muy importante en la compresión del empaquetamiento cristalino y por consiguiente deben ser tenidas en cuenta en el diseño *a-priori* de nuevos materiales.

La combinación de un contraion y un ligando de tipo azina dio lugar a un compuesto dinuclear de cobre. Este método podría utilizarse para la preparación de nuevos complejos dinucleares.

Como reseña final, cabe destacar que se ha obtenido por primera vez en compuestos de malonato de cobre, un compuesto (**4**) en el que se entrelazan cadenas de malonato de cobre.

Capítulo V

De redes 1D a 3D: El uso de un ligando para controlar la estructura cristalina.

Objetivos de la Investigación

El estudio de la influencia de un protón (capítulo I), de una cation de tipo inorgánico (capítulo II) o de tipo orgánico (capítulo III) y/o la introducción de un ligando de tipo azina que pueda actuar como ligando terminal (capítulo IV), nos ha permitido comprobar la importancia que pueden tener dentro del campo de la Ingeniería Cristalina las interacciones débiles (enlaces de hidrógeno, π···π, C-H···π).

Existe un gran interés dentro de los campos de la Ingeniería Cristalina y del Magnetismo Molecular en comprender los mecanismos que controlan el empaquetamiento molecular.

Para el diseño de nuevos materiales funcionales, resulta conveniente ser capaces de predecir *a priori*, cómo los iones, o las unidades moleculares, van a ensamblarse para dar lugar a la estructura cristalina final. Concretamente en el campo del Magnetismo Molecular nos interesa conocer cómo los iones magnéticos van a unirse entre sí, ya que de este hecho depende el comportamiento magnético del compuesto sintetizado, y por tanto, sus posibles aplicaciones posteriores. Ligandos con N- y/o O-dadores se emplean frecuentemente en el diseño racional de nuevos materiales.

Conociendo la gran versatilidad del anión malonato, teniendo en cuenta la importancia de los enlaces de hidrógeno en el empaquetamiento molecular y haciendo uso de ligandos de tipo N- o/y O-dadores, decidimos afrontar el estudio del diseño racional de materiales moleculares con los complejos de malonato de cobre de dimensionalidad 1D, 2D y 3D.

Planeamiento y Metodología utilizada

Para la preparación de los nuevos compuestos pensamos conveniente utilizar los siguientes ligandos: N- y O-exo dentados (bpe y dpo) y los ligandos dpp y dien (dietilentriamina) que podían actuar como ligando puente entre los iones magnéticos.

Mediante los métodos de evaporación lenta y tubo en H; siguiendo los pasos indicados en el apartado de síntesis, se prepararon los siguientes compuestos con fórmula molecular: $\{(H_2bpe)[Cu(mal)_2]\}_n \cdot 4H_2O$ (**1**); $[Cu_2(dpp)(mal)_2(H_2O)_2]_n \cdot 7nH_2O$ (**2**); $\{[Cu(mal)_2(H_2O)_2][Cu(dien)]\}_n \cdot 4nH_2O$ (**3**); $[Cu(mal)(dpo)(H_2O)]_n$ (**4**); $[Cu(mal)(bpe)_{1/2}(H_2O)]_n \cdot nH_2O$ (**5**) and $[Cu_4(mal)_4(bpe)_3]_n \cdot 6H_2O$ (**6**).

Una vez obtenidos monocristales adecuados para la caracterización de cada unos de los productos descritos se realiza:

- Análisis elemental, para determinar la composición en % de C, H y N.
- Difracción de rayos X en monocristal, para determinar su estructura atómica.
- Medidas magnéticas de susceptibilidad con el fin de estudiar su comportamiento magnético.

Cabe comentar que en la resolución de la estructura del compuesto **2**, a temperatura ambiente, existía desorden térmico en alguna de las aguas de cristalización. Para intentar solventar este problema y tener la estructura de este compuesto bien resuelta, se realizaron medidas de difracción de rayos X en monocristal a 100 K. La resolución de la estructura mediante los datos de baja temperatura llevaron a unos resultados similares a los obtenidos a temperatura ambiente, pero en los que el desorden térmico de las moléculas de agua era mucho menor, permitiendo una mejor caracterización de la estructura.

Hecho esto procedimos al análisis de los resultados obtenidos para cada una de los compuestos sintetizados.

Aportaciones originales y resultados

En este capítulo se presentan seis nuevos complejos de malonato de cobre en los que se introduce un segundo ligando que puede actuar como puente entre los iones magnéticos. Asimismo, se discuten las propiedades magnéticas de cada uno de ellos en base a sus propiedades estructurales. Una descripción detalla de las propiedades tanto estructurales como magnéticas de cada uno de los compuestos presentados se puede encontrar en el texto de la tesis. En este resumen destacaremos los aspectos más relevantes.

El compuesto **1** consiste en unidades aniónicas de $[Cu(mal)_2]^{2-}$ unidas mediante puente carboxilato de malonato del tipo Cu-O(ecuatorial)-C-O(apical)-Cu [1.9341(11) y

2.6107(14) Å para las distancias de enlace Cu-O(ecuatorial) y Cu-O(apical), respectivamente], dando lugar a cadenas regulares de malonato de cobre (ver Figura 2). Estas cadenas están unidas entre sí mediante enlaces de hidrógeno en los que intervienen grupos $Hbpe^{+}$ y moléculas de agua, dando lugar a una red supramolecular tridimensional (Figura 4). Los datos magnéticos de este compuesto fueron interpretados mediante la ley de Baker para una cadena regular de spines S = ½ acoplados ferromagnéticamente. El ajuste de los datos experimentales (Figura 25) da cuenta de la existencia de una interacción de tipo ferromagnético [J = +0.049(1) cm^{-1}, g = 2.062(2)] a través del puente Cu-O(ecuatorial)-C-O(apical)-Cu (ver esquema 1). La interacción magnética es tan débil debido a la larga distancia de enlace Cu-O(apical) y a la ortogonalidad entre los planos ecuatoriales de los iones cobre que intervienen en el puente.

En el segundo complejo descrito en este capítulo, coexisten dos iones de cobre cristalográficamente diferentes [Cu(1) y Cu(2)]. No obstante, las diferencias geométricas entre ellos son mínimas (ver distancias y ángulos de enlace en la Tabla 4 y 5). El compuesto **2** está formado por cadenas de cobre, donde los iones magnéticos están conectados alternativamente por puente μ-oxo de tipo carboxilato [Cu-O(mal)-Cu; ocupando el oxígeno del puente una posición ecuatorial en unos de los cobres -1.929(2) Å para la distancia promedio Cu-O(ecuatorial)- y una otra apical en el cobre adyacente -2.775(3) Å para la distancia promedio Cu-O(apical)-] y puente dpp (ver Figura 5). Estas cadenas de cobre se encuentran unidas entre sí mediante enlaces de hidrógeno (ver Tabla 4 y 5) en los que intervienen moléculas de agua coordinadas y oxígenos del grupo malonato, dando lugar a planos que crecen perpendiculares al eje cristalográfico *b* (ver Figura 8a). Enlaces de hidrógeno adicionales, en los que intervienen las aguas de cristalización y alguno de los oxígenos del grupo malonato contribuyen al empaquetamiento cristalino, dando lugar a una red extendida tridimensional (ver Figura 8b).

Para la interpretación de los datos magnéticos del compuesto **2**, realizamos una búsqueda bibliográfica de compuestos de puente dpp [Sletten *et al.*, 1998; Grove H. *et al.*, 2000; Grove H. *et al.*, 2001, referencias recogidas en este capítulo] que nos permitió concluir que la interacción a través de este puente debe ser antiferromagnética y muy débil, siendo más importante el canje magnético a través del puente μ-oxo. Teniendo esto en cuenta, realizamos el ajuste de los datos experimentales (Figura 26) mediante

una ley de Blaeney-Bowers para un compuesto dinuclear de spines S = ½. Los resultados obtenidos [J = +2.866(4) cm^{-1}, g = 2.052(1), R = $1.1x10^{-5}$] indican la ocurrencia de una interacción ferromagnética a través del puente μ-oxo en el que interviene el grupo malonato.

El complejo **3** consiste en cadenas de tipo *"zigzag"* de cobre (ver Figura 9), donde los iones están conectados a través de puente carboxilato del tipo Cu-O(ecuatorial)-C-O(apical) [1.936(5) y 2.202(6) Å para las distancias de enlace Cu-O(ecuatorial) y Cu-O(apical), respectivamente], presentado una conformación *anti-syn*. Estas cadenas se encuentran unidas entre sí mediante enlaces de hidrógeno, en los que intervienen las moléculas de agua coordinada y oxígenos de malonato, dando lugar a capas que crecen a lo largo del plano *ab* (Figura 12). De forma similar al compuesto **2**, en **3**, estos planos de malonato de cobre se encuentran unidos mediante enlaces de hidrógeno en los que intervienen moléculas de agua de cristalización (Figura 9) dando lugar a una red tridimensional.

Los datos magnéticos del compuesto **3**, fueron analizados siguiendo la expresión derivada por Borrás-Almenar J.J. *et al.* para una cadena alternada ferro- y antiferromagnética de spines S = ½ (eq 3-5). La curva de χ_M vs. T (Figura 27), aumenta progresivamente hasta alcanzar un máximo entorno a 5 K, disminuyendo a partir de este punto. Este comportamiento es característico de la coexistencia de una interacción global ferromagnética (J_2) con una interacción mucho más débil de tipo antiferromagnética (J_1). Los resultados del ajuste fueron: J_1 = -1.48(1) cm^{-1}, J_2 = 10.4(1) cm^{-1}, g = 2.151(3), θ = 0.984(1) y R = $8.3x10^{-6}$. Es la primera vez que se observa una interacción antiferromagnética a través de puente carboxilato del malonato (Ver Tabla 17). Sin la introducción del parámetro θ que tuviese en cuenta la interacción entre cadenas, el acuerdo entre los datos experimentales y la curva teórica era menor (R = $2.3x10^{-4}$). Teniendo en cuenta el pequeño valor de la constante antiferromagnética J_1 y que el parámetro θ es de naturaleza ferromagnética, sería posible pensar que las dos interacciones a través de puente carboxilato en la cadena fuesen de naturaleza ferromagnética (J_1 siendo muy débilmente ferro) y la interacción entre cadenas, a través de enlaces de hidrógeno, fuese de carácter antiferromagnético. No obstante, la existencia de una gran distorsión en el entorno del Cu(2) podría explicar la aparición de una interacción antiferromagnética a través del puente carboxilato del malonato.

El ligando dpo ha sido utilizado normalmente para construir redes cuadradas. Con esta idea se fue utilizado inicialmente, pero el resultado obtenido desde el punto de vista estructural fue sorprendente. La estructura del compuesto **4** -con dpo- consiste en cadenas helicoidales dobles donde las unidades de malonato de cobre están unidas mediante puente dpo (ver Figura 13). Las cadenas helicoidales dobles de malonato de cobre están unidas mediante enlaces de hidrógeno (ver Tabla 10) del tipo C-H···O, donde los carbonos y oxígenos de la dpo y el anión malonato actúan como grupos dadores y aceptores, respectivamente (Figura 13). A su vez, estas cadenas dobles están conectadas entre sí mediante enlaces de hidrógeno donde intervienen las moléculas de agua coordinadas a los átomos de cobre -correspondientes a una cadena doble- y los átomos de oxígeno de malonato -pertenecientes a la cadena adyacente- (Figura 14), dando lugar a una estructura tridimensional.

Como podemos observar en la Figura 13, la separación entre unidades de $[Cu(mal)]^{2-}$ a través de puente dpo es tan larga [12.267(2) Å] que considerámos en un principio que no existiría interacción entre los iones magnéticos. No obstante las medidas experimentales (Figura 28) mostraban la existencia de una débil interacción antiferromagnética.

Una inspección detallada de la estructura nos llevó a pensar que esta interacción débilmente antiferro podía ser debida a la interacción magnética a través de:

- puente dpo (algo poco probable, debido a la larga distancia de separación entre los átomos de cobre)
- enlaces por puente de hidrógeno que unen las cadenas dobles entre sí [Cu-Ow-H···O-C-O-Cu; Figura 14b]
- y/o los enlaces del tipo C(dpo)-H···O(dpo) que mantienen unidas las cadenas helicoidales que dan lugar a las cadenas dobles [Cu-O(apical)···H-C-N-O(ecuatorial)-Cu; Figura 13b]

en los dos últimos casos la distancia donor···aceptor de los enlaces de hidrógeno son cortas (ver Tabla 10) con lo que no existe ninguna razón para poder despreciar, *a priori*, estos posibles caminos de canje. Desgraciadamente no existe ninguna expresión analítica que nos permitiera ajustar los datos magnéticos teniendo en cuenta los posibles caminos de canje. Para poder determinar el camino de canje predominante sería conveniente realizar algún cálculo teórico de tipo DFT.

Los dos últimos compuestos (**5** y **6**) fueron preparados con el ligando bpe, al igual que el complejo **1** presentado en este capítulo. El compuesto **5** consiste en cadenas "*zigzag*" de cobre donde los iones están unidos a través de puente *anti-syn* carboxilato del tipo Cu-O(ecuatorial)-C-O(ecuatorial)-Cu (ver Figura 17a). Las cadenas están unidas mediante el ligando bpe, dando lugar a planos ondulados, como puede observarse en la Figura 17b. Finalmente estos planos están conectados mediante enlaces de hidrógeno dando lugar a una red tridimensional.

Cabe destacar la formación de poros [9.2 x 11.3 Å] en este compuesto en los cuales se encuentran alojadas cadenas de agua (Figura 17b y 17c), ligadas a los poros mediante enlaces de hidrógeno.

Desde el punto de vista magnético la posible interacción a través de la bpe -debido a la larga separación [13.3768(9) Å] entre los Cu a través de la bpe-, puede despreciarse frente a la interacción existente a través del puente carboxilato. Por este motivo, los datos magnéticos de este compuesto (Figura 29) fueron tratados siguiendo la ley de Baker y Rushbrooke para una cadena regular de spines S = ½. Los resultados obtenidos del ajuste (J = +3.85(3) cm^{-1}, g = 2.155(3) y R = $1.4x10^{-5}$), indican la existencia de una interacción ferromagnética que se ajusta bien al tipo de puente observado.

Por su parte el compuesto **6** posee una estructura tridimensional compleja que se esquematiza en las Figuras 21 y 24. Básicamente, consiste en planos de malonato de cobre unidos entre sí mediante el ligando bpe. Los planos de cobre pueden considerarse formados por tetrámeros del metal unidos mediante puente carboxilato de tipo Cu-O(ecuatorial)-C-O(ecuatorial/apical)-Cu (esquematizados como líneas de color azul en la Figura 24) siendo la separación entre los iones cobre de 5.0082(10) y 4.9488(11) Å para las configuraciones ecuatorial-ecuatorial y ecuatorial-apical, respectivamente. Estas unidades tetranucleares se encuentran unidas, a su vez, mediante puentes μ-oxo (líneas rojas en la Figura 24) y puentes carboxilato del tipo Cu-O(ecuatorial)-C-O(apical)-Cu -líneas amarillas de la Figura 24- , siendo 3.4095(7) y 6.5268(13) Å la separación entre iones Cu a través del puente μ-oxo y carboxilato, respectivamente. Enlaces de hidrógeno entre las moléculas de agua y los oxígenos del malonato contribuyen a la estabilización de la estructura tridimensional.

Desde el punto magnético, existen siete caminos de canje posibles en **6** (ver esquema 2). Tal sistema resulta imposible de interpretar magnéticamente por lo que

tuvimos que realizar aproximaciones para poder obtener algún resultado cuantitativo. En primer lugar, consideramos que la interacción a través de la bpe era despreciable frente a la interacción a través de los puentes μ-oxo y carboxilato. En una segunda aproximación consideramos la interacción μ-oxo en la configuración que presenta en este complejo debía transmitir con menor intensidad la interacción magnética. Y finalmente, de los tres caminos de canje que quedaban, todos ellos a través de puente carboxilato, consideramos activos aquellos para los cuales la distancia entre los átomos de cobre que conectaran, fuera menor. Teniendo en cuenta estas aproximaciones, la interpretación de los datos magnéticos se reducía a considerar el complejo **6** compuesto por unidades tetranucleares de Cu. Utilizando la expresión recogida en las eq. 8-13 realizamos el ajuste de los datos experimentales introduciendo en esta ecuación un parámetro θ que tuviese en cuenta la interacción intermolecular entre las unidades tetraméricas. Los resultados del ajuste (ver Figura 30) aunque representan bien la curva experimental quedan ligeramente por encima de los valores obtenidos para el canje magnético a través de puente carboxilato. Esta sobreestimación de los valores de canje, debe ser explicada en función de las aproximaciones realizadas.

Conclusiones

Los resultados obtenidos en este capítulo muestran que resulta complicado predecir *a priori* las propiedades estructurales de un compuesto de malonato de cobre, debido a la probabilidad de existencia de una gran variedad de estructuras posibles (véase que se han obtenido tres compuestos diferentes con el ligando bpe, dos de ellos obtenidos en la misma síntesis: **5** y **6**). Así mismo, también resulta sorprendente la estructura del compuesto **4**, con dpo, donde las interacciones débiles controlan de forma dominante (frente al puente dpo) el empaquetamiento molecular.

Desde el punto de vista magnético los resultados obtenidos nos han permitido corroborar que el ligando malonato es un buen candidato para acoplar ferromagnéticamente dos iones con spin S = ½ (en todos los compuestos preparados en los que los iones de cobre(II) están unidos por puente carboxilato de malonato se observa la misma naturaleza en la interacción).

Capítulo VI

Nuevos compuestos homometálicos de malonato: Co(II), Ni(II) y Mn(II)

PARTE A: Co(II) y Ni(II)

Objetivos de la Investigación

En los resultados presentados hasta el momento, hemos tratado siempre con compuestos de malonato de cobre(II) en los que hemos ido introduciendo diferentes grupos (cationes inorgánicos y orgánicos, ligandos de tipo terminal y tipo puente). No obstante, no habíamos abordado el estudio de materiales homometálicos de malonato con otros iones de la primera serie de transición diferentes del Cu(II).

Los complejos de Zn(II) y Mn(II) habían sido caracterizados anteriormente, sin embargo, hasta el momento no había sido posible obtener cristales adecuados de los compuestos de malonato de Co(II) y Ni(II) que permitiesen su caracterización estructural mediante difracción de rayos X en monocristal. Únicamente, se había podido obtener muestra policristalina. Mediante difracción en polvo se habían determinado los parámetros de celdilla y se sabía que eran isoestructurales con el compuesto de malonato de Zn(II).

Nuestro objetivo al comenzar el trabajo descrito en este capítulo, consistía en la preparación y caracterización de los malonatos de Co(II) y Ni(II).

Planeamiento y Metodología utilizada

Para la obtención de cristales adecuados para su caracterización estructural, los malonatos de Co(II) (**1**) y Ni(II) (**2**) se prepararon siguiendo el método recogido en la sección de síntesis de este capítulo. Comentar que el gran avance frente a intentos anteriores fue la utilización de los acetatos de niquel y cobalto, los cuales permiten una síntesis mucho más limpia, donde no quedan residuos en la disolución. Ambos compuestos se prepararon por el método de evaporación lenta.

Una vez obtenidos y secados convenientemente los monocristales de ambos compuestos, estos se caracterizaron mediante:

- Análisis elemental para determinar el porcentaje cualitativo de C, N e H presentes en la muestra.
- Difracción de rayos X en monocristal para poder resolver la estructura cristalina.
- Medidas de susceptibilidad que permitieran una interpretación posterior de sus propiedades magnéticas.

A partir de los datos obtenidos, se realizó el estudio de relación estructura-propiedad cuyos resultados mostramos a continuación.

Aportaciones originales y resultados

Por primera vez, se obtuvieron monocristales de los malonatos de Co(II) y Ni(II). Esto supuso el poder caracterizar convenientemente las estructuras de ambos compuestos. Una descripción detalla, tanto de las estructuras como de las propiedades magnéticas, así como las relaciones magneto-estructurales de ambos compuestos, se puede encontrar en el texto. A continuación, resaltamos los aspectos fundamentales del estudio realizado.

Los dos compuestos son isoestructurales con el malonato de Zn(II) y consisten en planos corrugados formados por unidades de $[M(mal)_2(H_2O)_2]^{2-}$ y $[M(H_2O)_2]^{2+}$ [M = Co(II) (**1**) y Ni(II) (**2**)] unidas mediante puente carboxilato de tipo *anti-syn* (ver Figura 1a). Estos planos están conectados mediante enlaces de hidrógeno en los que intervienen moléculas de agua y oxígenos de malonato (ver Tabla 2 y Figura 1b). En la Tabla 3 pueden compararse las distancias y ángulos de enlace para ambos compuestos.

En lo que respecta a las propiedades magnéticas, el ion cobalto(II) presenta serias dificultades a la hora de abordar la interpretación de sus propiedades magnéticas debido a su naturaleza electrónica. El ión cobalto posee un estado fundamental $^4T_{1g}$ que posee un momento orbital no nulo y que debe ser tenido en cuenta en la interpretación de sus propiedades. Además, en función del entorno que posea el cobalto (la naturaleza de los ligandos que se coordinen a él y el tipo de geometría en que se disponen en torno al ión metálico), el estado fundamental puede romper su degeneración y desdoblarse, dando lugar a otros estados que pueden interaccionar entre sí. En resumen, para poder interpretar correctamente las propiedades magnéticas del cobalto es necesario utilizar el Hamiltoniano de la eq (1), donde el primer término corresponde con al acoplamiento spin-órbita (siendo κ el parámetro de reducción orbital). El segundo término del

Hamiltoniano tiene en cuenta el campo de los ligandos en un entorno en el que existe distorsión axial (provocando el desdoblamiento del estado fundamental) y el tercer corresponde a la interacción de Zeeman. Los resultados del ajuste de las propiedades magnéticas (ver Figura 4) de este compuesto -aplicando la ec(1) y utilizando diagonalización de matrices- están dentro de los valores esperados para iones cobalto(II). La desviación de los valores teóricos de $\chi_M T$ a baja temperatura para un ion cobalto aislado con respecto a los datos experimentales indican que debe existir una interacción de naturaleza antiferromagnética entre los iones cobalto(II) a través del puente carboxilato del malonato (ver Figura 4).

La curva de $\chi_M T$ vs T para el compuesto de Ni(II) (ver Figura 5) indica la existencia de una débil interacción ferromagnética, siendo la caída de la curva a bajas temperaturas debida al efecto de desdoblamiento a campo cero [típico en los iones de Ni(II)] o a una débil interacción antiferromagnética a través de los enlaces de hidrógeno. Mediante las series de expansión derivadas del modelo de Heisenberg para una red cuadrada de spines S = 1 (eq 2) se ajustan los datos experimentales correspondientes a T > 16 K. Los resultados obtenidos muestran la existencia de una débil interacción ferromagnética [J = +0.18(2) cm^{-1}] a través del puente carboxilato del malonato.

Conclusiones

Cabe destacar que la obtención de monocristales de las especies **1** y **2** ha permitido caracterizar estructuralmente estos compuestos. También ha sido posible medir sin problemas de impurezas las propiedades magnéticas de estos compuestos.

A pesar de que ambos son isoestructurales, la interacción a través del puente malonato en ambos iones da lugar a interacciones de naturaleza opuesta: antiferromagnética en **1** y ferromagnética en **2**. La explicación de este fenómeno debe buscarse en la diferente configuración electrónica de ambos metales.

Realizando un estudio de compuestos de malonato de Ni(II), Co(II) y Mn(II), llegamos a la conclusión que se resume en el esquema 1 de este capítulo: aunque el malonato homometálico de Mn(II) posee una estructura diferente de los malonatos de Co(II), Ni(II) y Zn(II) -los cuales son isoestructurales-, cuando se añade un ligando N-exo dentado de tipo piridil, las unidades de [M(mal)(H_2O)] se disponen siguiendo la misma topología independientemente del metal [M = Co(II), Ni(II), Zn(II), Mn(II)] utilizado.

PARTE B: Mn(II) [Estudio de difracción de neutrones]

Objetivos de la Investigación

El malonato de manganeso (Figura 6) había sido caracterizado previamente [Rodríguez-Martín et *al.*, 2003, recogida en las referencias de este capítulo], observando que presentaba un comportamiento magnético de *spin-canting* (Figura 7). Nuestro objetivo en esta parte del capítulo VI, consistió en obtener la estructura magnética (disposición de los momentos magnéticos) de este compuesto por debajo de la temperatura de orden [T = 2.7(1) K] mediante difracción de neutrones en polvo.

Planeamiento y Metodología utilizada

Siguiendo la síntesis descrita en la bibliografía para este compuesto [Rodríguez-Martín et *al.*, 2003, recogida en las referencias de este capítulo] se preparó muestra suficiente (10 gr) para poder realizar las medidas de difracción de neutrones en polvo.

Existía una serie de problemas experimentales:

- La estructura determinada por rayos X no permitía la caracterización de los átomos de hidrógeno (que tienen un bajo coeficiente de dispersión para rayos X, tener en cuenta que sólo posee un electrón), los cuales tienen una contribución importante en la difracción de neutrones. Para resolver este problema se realizaron medidas de difracción de neutrones en el equipo G4.2 del LLB (Laboratoire Léon Brilloin, Saclay) que permitió la determinación estructural completa.
- La presencia de los hidrógenos en la muestra crea un ruido de fondo que podía dar lugar a problemas en la interpretación de los datos magnéticos. Esto hizo necesario realizar una estadística conveniente de cada una de las medidas realizadas para disminuir este factor.
- El bajo número de iones magnéticos en la celdilla unidad (únicamente 4) implicaba la existencia de una débil señal para la muestra. Este problema se solucionaba, al igual que en el apartado anterior, mediante una buena estadística de los datos.

Las muestras cristalinas obtenidas de la síntesis se molieron para obtener un material policristalino apto para la difracción de neutrones en polvo. Esta muestra se midió:

- En el equipo G4.2 (equipo de difracción de neutrones no polarizados) a 280 y 5 K, para la obtención de la estructura cristalina completa (incluyendo átomos de H).
- En el equipo G4.1 a 5 K y a diferentes temperaturas por debajo de la temperatura de orden para observar el fenómeno de *spin-canting*.

Aportaciones originales y resultados

En la literatura existen pocos ejemplos de estructuras magnéticas de compuestos moleculares determinadas mediante difracción de rayos X. En este sentido los resultados obtenidos con el malonato de Mn(II) confirman la posibilidad de utilizar esta técnica en este tipo de compuestos para obtener información de la estructura magnética.

Una explicación detallada de cada uno de los pasos seguidos para la interpretación de los datos de neutrones se da en el capítulo de la tesis. En este resumen daremos una lista de los pasos seguidos en el tratamiento de los datos y comentaremos los resultados finales.

Los pasos seguidos fueron los siguientes:

- Determinación de la estructura mediante rayos X a temperatura ambiente y 100 K (ver Tablas 6 y 7)
- Búsqueda de los átomos de H, no encontrados mediante la técnica de rayos X, tratando los datos de difracción de neutrones del equipo G4.2 y utilizando un procedimiento de "*simulate annealing*" para modelizar los átomos de H de las moléculas de agua (ver el modelo utilizado en el esquema 1 y los resultados del ajuste del patrón experimental de neutrones en la Figura 12) no encontrados en el refinamiento de la estructura mediante difracción de rayos X.
- Refinamiento de la estructura completa del malonato de Mn, utilizando conjuntamente los datos de difracción de rayos X y de neutrones (G4.2) (ver resultados del ajuste del patrón de neutrones y de los datos de rayos X a 100 K en la Figura 13)
- Determinación de la estructura magnética mediante los datos de difracción de neutrones (G4.1).

Comparando los difractogramas del equipo G4.1 a 5 y 1.5 K (ver Figuras 16 y 17), pudimos comprobar cómo, por debajo de la temperatura de orden [T_c = 2.7(1) K] aparecen en el difractograma dos nuevos picos (marcados en la Figura 17),

correspondientes a la aparición de un cambio en la estructura magnética. El ajuste de los difractogramas por debajo de la temperatura de orden permitió obtener los valores de las componentes del momento magnético asociado a cada uno de los iones Mn(II) dentro de la celdilla unidad (ver Tabla 4). Este ajuste, nos permitió realizar un esquema de la estructura magnética (ver Figura 18) corroborando la existencia del comportamiento de *spin-canting*, debido a la aparición de un momento magnético espontáneo por debajo de la temperatura de orden (ver los valores de Mz en la Tabla 4).

Conclusiones

A pesar de los problemas experimentales que se planteaban al inicio del experimento (presencia de H en la muestra, número bajo de iones magnéticos en la celdilla unidad, estructura determinada parcialmente por difracción de rayos X), ha sido posible la determinación de la estructura magnética del malonato de Mn(II) por debajo de la temperatura de orden, utilizando la técnica de difracción en polvo de neutrones.

Los resultados obtenidos corroboran la existencia del fenómeno de *spin-canting*, permitiendo obtener los valores del momento magnético para cada uno de los iones Mn(II) que forma la celdilla unidad.

Capítulo VII

Una revisión estructural de los complejos heterometálicos de malonato

Objetivos de la Investigación

Estudios previos en complejos de malonato bimetálicos habían sido realizados previamente [Rodríguez-Martín Y. *et al.*, 2002a, referencia incluida en el capítulo VII] permitiendo la caracterización de complejos de malonato homometálicos MM' [M, M' = Mn(II), Co(II), Ni(II), Cu(II) y Zn(II)]. Únicamente en el caso de los complejos de NiMn y CoMn, no había sido posible la obtención de monocristales, imposibilitando la determinación de la estructura atómica de estos compuestos.

Los objetivos del trabajo expuesto en este capítulo consistían en la obtención de monocristales adecuados que permitieran una apropiada caracterización de los compuestos de malonato de NiMn y CoMn.

Planeamiento y Metodología utilizada

Múltiples intentos de síntesis fueron realizados. Los productos finales, se obtuvieron mediante el procedimiento descrito en la sección de síntesis utilizando los métodos de síntesis hidrotermal (**1**) y evaporación lenta (**2**).

La síntesis del compuesto **2** presenta una serie de problemas relacionados con la aparición de varias fases en el vaso de precipitados (malonato de Co, malonato de Mn, y disoluciones sólidas de ambas fases).

Para determinar si los cristales medidos poseían igual proporción de Co y Mn, a los cristales obtenidos se les realizó un análisis cuantitativo usando la microsonda de rayos X del microscopio electrónico (SEM) para determinar la cantidad de cada uno de los metales presentes. Los resultados determinaron que ambos se encontraban en igual proporción.

Determinada la proporción de ambos metales, se realizaron medidas de difracción de rayos X que permitieron la determinación estructural de ambos compuestos.

Aportaciones originales y resultados

En este capítulo, se caracterizan estructuralmente, por primera vez, mediante difracción de rayos X de monocristal los compuestos de NiMn (**1**) y CoMn (**2**).

El compuesto **1** es isoestructural con los complexos heterometálicos MM' de fórmula molecular $[M^{II}(H_2O)_6][Cu(mal)_2(H_2O)_2]$ (M = Cu y M' = Cu, Ni, Mn, Zn, Co) [Rodríguez-Martín Y. *et al.*, 2002b, referencia recogida en este capítulo]. Su estructura consiste en capas alternadas, aniónicas y catiónicas conectadas entre sí mediante enlaces de hidrógeno (Figura 2 y Tabla 2) dando lugar a redes extendidas tridimensionales. Las unidades aniónicas de $[Cu(mal)_2]^{2-}$ se encuentran conectadas entre sí mediante enlaces de hidrógeno en los que las moléculas de agua coordinadas al cobre actúan como dadores, dando lugar a capas que crecen en el plano *ab* (ver Figura 1a). Por su parte, las unidades catiónicas están unidas mediante enlaces de hidrógeno dando lugar a cadenas que se empaquetan a lo largo del eje *c* (Figura 1b). Finalmente, enlaces de hidrógeno en los que intervienen todas las moléculas de agua y los átomos de oxígeno del grupo malonato, conectan las diferentes capas entre sí, contribuyendo al empaquetamiento cristalino y dando lugar a una red supramolecular tridimensional.

El compuesto **2** posee una estructura similar a la de los malonatos homometálicos de Co(II) y Ni(II) discutidos en el capítulo VI. Al igual que estos compuestos la estructura de **2** consiste en capas corrugadas en las que las unidades de $[Co(mal)_2(H_2O)_2]^{2-}$ y $[Mn(H_2O)_2]^{2+}$ se encuentran enlazadas mediante puentes carboxylato en conformación *anti-syn*. A diferencia de los malonatos homometálicos, (donde únicamente hay un sólo tipo de puente carboxilato) en **2** existen dos tipos de puente en el plano, ambos de conformación *anti-syn* (ver Figuras 4a y 6 del presente capítulo y comparar con las Figuras 1a y 2 del capítulo VI). Estos planos están unidos mediante enlaces de hidrógeno en los que las moléculas de agua actúan como dadores (ver Figura 4b y Tabla 6), dando lugar a una estructura tridimensional.

Conclusiones

Por primera vez se ha podido caracterizar mediante difracción de rayos X de monocristal los compuestos de malonato de NiMn y CoMn. No obstante, es necesario resaltar que la obtención de este último producto resulta complicada, debido a la aparición de otras fases (malonato de manganeso, malonato de cobalto y disoluciones sólidas de ambas fases) en el vaso de precipitados.

Capítulo VIII

Desde redes de baja a alta dimensionalidad en compuestos de malonato de Co(II)

Objetivos de la Investigación

Al igual que en el capítulo IV y V, tras los primeros resultados obtenidos con los compuestos homometálicos de Co(II) y Ni(II) decidimos abordar el estudio de la preparación, caracterización estructural y magnética de complejos de Co(II) de dimensionalidad variable.

El estudio del ion Co(II) (cobalto de alto spin) como comentamos en el capítulo VI presenta cierta complejidad debido a que su estado fundamental $^4T_{1g}$ tiene un momento orbital no nulo. En este momento se están desarrollando nuevos métodos numéricos, que permiten resolver el Hamiltoniano para un ión cobalto de alto spin cuando se encuentra en un entorno octaédrico ligeramente distorsionado. Resultaba interesante preparar y caracterizar materiales de Co(II) en los que se variara la dimensionalidad de la red del ión de alto spin. De esta forma, se dispone de resultados experimentales que permiten poner a prueba los nuevos métodos de análisis.

Planeamiento y Metodología utilizada

Se prepararon siguiendo las síntesis descrita en el texto de la tesis seis compuestos de malonato de Co(II) de fórmula molecular: $\{[Co(mal)_2(H_2O)_2]Cd(H_2O)_2\}$ (**1**); $[Co_2(mal)_2(dpo)(H_2O)_6]\cdot 2H_2O$ (**2**); $[Co(mal)(phen)(H_2O)]\cdot 2H_2O$ (**3**); $[Co(mal)(3\text{-cnpy})(H_2O)]$ (**4**); $[Co_2(mal)_2(pym)(H_2O)]_n$ (**5**); $[Co_2(mal)_2(pyz)(H_2O)]_n$ (**6**).

Obtenidos monocristales apropiados para su caracterización se realizó:

- Análisis elemental para determinar la proporción de C, H y N presentes en la muestra.
- Difracción de rayos X en monocristal para caracterizar estructuralmente cada uno de los materiales.
- Medidas de susceptibilidad magnética con el fin de caracterizar cada unos de los compuestos obtenidos.

Finalmente se realizó el tratamiento de los datos experimentales cuya discusión se recoge en este capítulo.

Aportaciones originales y resultados

Cabe destacar entre los resultados de este capítulo, que se han preparado compuestos donde el ión cobalto, desde el punto de vista magnético se encuentra aislado (**1**), formando unidades dinucleares (**2**), cadenas (**3**), planos (**4**) y estructuras tridimensionales (**5**, y **6**). Los compuestos del **1**-**4** han servido para poner a prueba los nuevos métodos numéricos que permiten abordar el magnetismo de compuestos de cobalto de alto spin de baja y alta dimensionalidad. La interpretación de las propiedades magnéticas de los compuestos **5** y **6** no se han podido abordar de la misma forma, debido a la complejidad del sistema a tratar.

Desde el punto de vista estructural, como se puede observar en la introducción, no existe un gran número de compuestos de malonato de Co(II). Los nuevos compuestos preparados suponen un aporte de información estructural sobre el comportamiento y empaquetamiento del malonato de Co(II) y a permitido corroborar los indicios estructurales de los que se habló en el capítulo VI (ver esquema 1 del capítulo VI).

El compuesto $\{[Co(mal)_2(H_2O)_2]Cd(H_2O)_2\}$ (**1**), es isoestructural con el compuesto bimetálico de CoMn, descrito en el capítulo anterior. Su estructura consiste en planos rectangulares corrugados donde los aniones $[Co(mal)_2(H_2O)]^{2-}$ y cationes $[Cd(H_2O)]^{2+}$ se encuentran unidos mediante puente carboxilato que presenta configuración *anti-syn*. Estos planos son similares a los que presentan los complejos hometálicos de Co(II), Ni(II) y Zn(II), con la diferencia de que ahora se tienen dos caminos de canje diferentes: (comparar las Figuras 1a y 3 de este capítulo con las Figuras 1a y 2 del capítulo VI) Co(1)-O(1)-C(1)-O(3)-Cd(1e) y Co(1)-O(2)-C(3)-O(4)-Cd(1) [7.3950(12) y 5.6915(12) Å para la separación Co(1)··· Cd(1e) y Co(1)···Cd(1), repectivamente] (Figura 3 de este capítulo). Enlaces de hidrógeno en los que intervienen como dadores las moléculas agua coordinadas al Cd, contribuyen a estabilizar los planos bimetálicos. Finalmente estos planos -que crecen a lo largo plano cristalográfico *ab*- están conectados entre sí, mediante enlaces de hidrógeno en los que las moléculas de agua coordinadas al cobalto actúan como grupos dadores (ver Figura 1b y Tabla 4), dando lugar a una red tridimensional.

El ion cadmio, desde el punto de vista magnético es diamagnético. Por esta razón las propiedades magnéticas del compuesto **1**, pueden ser tratadas considerando que los iones cobalto(II) están aislados magnéticamente. Como comentamos anteriormente la naturaleza electrónica del cobalto(II) (cobalto de alto spin) complica su la interpretación de los datos magnéticos. Para un cobalto situado en un entorno octaédrico ligeramente distorsionado, debemos abordar el problema utilizando el Hamiltoniano de la eq (1); en el que el primer término ($-A\kappa\lambda\mathbf{LS}$) hace referencia al acoplamiento espin-órbita [A es 3/2 para la mayoría de los compuestos de cobalto, κ es el factor de reducción orbital que tiene en cuenta la covalencia de los enlaces entre el cobalto y los átomos coordinados a él y λ es el parámetro de acoplamiento espin-orbita (en torno a -170 cm^{-1})] el segundo término [$\Delta[\mathbf{L}_z^2-(1/3)L(L+1)]$] tiene en cuenta la distorsión axial (Δ) en el entorno del ión metálico -la cual es directamente proporcional a la distancia entre el estado fundamental y el primer estado excitado- y el tercer término ($\beta(-A\kappa\mathbf{L} + g_e\mathbf{S})H$) hace referencia a la interacción de Zeeman. A partir de este Hamiltoniano no es posible derivar ninguna expresión analítica para la susceptibilidad magnética en función de A, κ, λ y Δ. La única posibilidad de derivar dichos parámetros consiste en diagonalizar la matriz del Hamiltoniano correspondiente a la ec. (1) de forma numérica. Para evitar la problemas de sobreparametrización y teniendo en cuenta que en compuestos de Co(II) donde la influencia del campo cristalino es débil el valor de A = 3/2; se fija dicho valor en el ajuste. Los resultados obtenidos (A = 3/2, k = 0.81, λ = -159 cm^{-1}, Δ = 506 cm^{-1} y R = 1.93×10^{-4}) ajustan convenientemente la curva experimental (Figura 18) y se encuentran dentro del rango observado para complejos de Co(II) con entorno similar al complejo **1**.

El compuesto **2**, consiste en unidades dinucleares de cobalto(II) donde los iones cobalto se encuentran unidos mediante puente carboxilato (Figura 5) *anti-syn*. Curiosamente el dpo, que suele actuar como ligando puente, actúa en **2** como ligando terminal. Las unidades dinucleares se encuentran unidas entre sí mediante un complicado sistema de enlaces de hidrógeno (Figura 4 y Tabla 5) dando lugar a una capa hidrófila que crece en el plano *ac* cristalográfico. Estas capas se encuentras conectadas mediante enlaces de hidrógeno -en los que intervienen moléculas de agua dadoras y los átomos de oxígeno del dpo que quedan sin coordinar- junto con interacciones de tipo π···π entre los grupos aromáticos del dpo (Figura 4) dando lugar a

una red tridimensional. El ion malonato actúa como ligando puente uniendo dos iones cobaltos adyacentes, siendo 5.2566(13) Å la separación Co···Co a través del puente.

Las propiedades magnéticas de este compuesto se analizaron diagonalizando la matriz del Hamiltoniano de la ec. (1), mediante métodos numéricos, al que se le añadió un cuarto término que tuviese en cuenta la interacción entre los iones cobalto a través del puente carboxilato del malonato. Como puede observarse en la Figura 19, los datos experimentales ajustan bastante bien al modelo propuesto, siendo los resultados del ajuste: A = 3/2, k = 0.94 cm^{-1}, λ = -143 cm^{-1}, Δ = -433 cm^{-1}, $J \simeq 0$. El valor del canje magnético (J) es prácticamente cero, indicando que la interacción a través del puente malonato es muy débil.

El compuesto **3** consiste en cadenas "*zigzag*" de malonato de cobalto en las que los iones magnéticos están unidos mediante puente de tipo carboxilato (ver Figura 7a); la separación entre iones cobalto a través del puente es 5.3482(10) Å. Estas cadenas están unidas mediante enlaces de hidrógeno (ver Tabla 12) en los que intervienen aguas de cristalización y oxígenos de malonato dando lugar a planos hidrofílicos. Éstos, a su vez se encuentran conectados entre sí mediante interacciones débiles de tipo π···π y C-H···π dando lugar a una red tridimensional (Figura 7).

La interpretación de las propiedades magnéticas de este compuesto, mediante el modelo numérico descrito anteriormente, permitió el ajuste de los datos experimentales (Figura 20), obteniéndose como resultados del ajuste: A = 3/2, k = 0.97, λ = -167 cm^{-1} y Δ = 930 cm^{-1}, J = 0.06 cm^{-1}. Los valores obtenidos caen dentro del rango esperado, pero el valor de la interacción a través del puente es ahora de naturaleza ferromagnética, comportamiento que no se había observado antes en compuestos de malonato de cobalto.

El compuesto **4**, consiste en planos corrugados donde las unidades de $[Co(mal)(H_2O)_2]$ se encuentran unidas mediante dos puentes carboxilato diferentes (ver Figuras 11 y 13): Co(1)-O(1)-C(1)-O(3)-Co(1c) y Co(1)-O(2)-C(3)-O(4)-Co(1d) siendo 5.3876(6) y 5.3135(7) Å la separación entre Co(1)···Co(1c) y Co(1)···Co(1d), respectivamente. Estos planos se encuentran unidos mediante enlaces de tipo C-H···N y C-H···π, dando lugar a redes tridimensionales (Figura 11).

El ajuste de las propiedades magnéticas de este compuesto (Figura 21) conduce a los siguiente resultados: A = 3/2, κ = 0.89, λ = -175, Δ = -717 cm^{-1}, J = -0.13 cm^{-1}. Como puede observarse la interacción a través del puente carboxilato es

antiferromagnética (comportamiento encontrado en la mayoría de los complejos de malonato de cobalto).

Finalmente los compuestos **5** y **6** consisten en redes tridensionales de iones cobalto en los que las unidades de [Co(mal)(H_2O)] se encuentran unidas mediante dos tipos de puente carboxilato dando lugar a planos corrugados (ver Figuras 14 y 17). Estos planos se encuentran conectados mediante el ligando pirimidina (Figura 15a) y pirazina (Figura 15b).

Debido a la alta dimensionalidad de los complejos **5** y **6**, no es posible interpretar cuantitativamente el canje a través del puente carboxilato. Únicamente podemos concluir que la interacción magnética debe ser de naturaleza antiferromagnética (debido a que los valores de $\chi_M T$ a 2 K es menor que los esperados para un centro magnético aislado de cobalto). Ahora bien, esta interacción antiferromagnética puede ser debida al canje a través del puente malonato y/o pirazina/pirimidina.

Conclusiones

Desde el punto de vista estructural hemos podido comprobar con los compuestos **4-6** que se cumple el esquema 1 del capítulo VI en el que comentábamos que los compuestos homometálicos de malonato en los que se utiliza un ligando N-exo dentado de tipo piridil [M = Co(II), Ni(II), Zn(II) y Mn(II)] están constituidos por planos rectangulares y corrugados de iones metálicos que poseen la misma topología.

Desde el punto de vista magnético hemos conseguido una familia de compuestos de dimensionalidad variable, desde el punto de vista magnético (desde 0D hasta 3D) que nos ha permitido estudiar la interacción magnética a través del puente malonato.

Por primera vez en compuestos de malonato de cobalto se ha observado un comportamiento de naturaleza ferromagnética a través del puente carboxilato.

Capítulo IX

Nuevos complejos de malonatos de lantánidos: Ho(III), Sm(III) y Ce(III)

Objetivos de la Investigación

Hasta este momento hemos estudiado las características estructurales y magnéticas de compuestos de la primera serie de transición [M = Cu(II) (capítulos I-V) Co(II), Ni(II), Zn(II) y Mn(II) (capítulos VI-VIII)]. A lo largo del estudio realizado hemos podido comprobar la versatilidad del ligando malonato en la obtención de estructuras de muy diversa dimensionalidad en las que el ligando puede actuar como ligando puente o terminal. Hemos visto que el ligando malonato es un grupo apropiado para la construcción de todo tipo de redes (supramoleculares basadas en unidades mono- o dinucleares; cadenas, planos o redes tridimensionales).

Nuestro objetivo con el trabajo de este capítulo consiste en la extensión de nuestros estudios magneto-estructurales de complejos de malonato con elementos de la primera serie de transición, a los malonatos de lantánidos. Ello es debido al creciente interés que presentan estos materiales desde el punto de vista de sus aplicaciones (muestras fluorescentes, materiales magnéticos, precursores para óxidos, etc...).

Planeamiento y Metodología utilizada

A partir de los nitratos correspondientes y mediante la técnica de crecimiento en gel se prepararon los compuestos de fórmula molecular: $[Ho_2(mal)_3(H_2O)_5]\cdot 2H_2O$ (**1**); $[Sm_2(mal)_3(H_2O)_6]$ (**2**) y $[Ce_2(mal)_3(H_2O)_6]\cdot 2H_2O$ (**3**).

El problema que plantea el crecimiento en gel con los cristales de malonato de tierra raras es que resulta complicado limpiar bien la muestra y generalmente siempre quedan pequeñas impurezas.

Una vez obtenidos monocristales de los productos descritos se les realizó:

- Análisis elemental, para determinar la proporción de C, H y N que poseía cada uno de ellos.
- Medidas de difracción de rayos X en monocristal.
- Medidas de susceptibilidad magnética.

A continuación, se procedió al tratamiento de los datos obtenidos.

Aportaciones originales y resultados

Tres nuevos complejos de malonatos de tierras raras han sido caracterizados estructuralmente.

El compuesto **1** consiste en unidades de diaqua- y triaquaholmio(III) conectadas mediante puente carboxilato dando lugar a capas de Ho(III) corrugadas que crecen a lo largo del plano cristalográfico *ab* (ver Figura 1). Las separaciones más cortas entre átomos de holmio dentro del plano son (ver Figuras 1a y 5): 4.9314(5) [Ho(1)··· Ho(2)], 5.9648(6) [Ho(1)···Ho(2j)], 6.384(8) [Ho(2)···Ho(2j)], 7.0905(8) [Ho(1)···Ho(1k)] y 8.0555(9) Å [Ho(1)···Ho(1b)]. Enlaces de hidrógeno en los que intervienen moléculas de agua de cristalización y oxígenos de grupos malonato (ver Tabla 2) conectan las diferentes capas entre sí, dando lugar a una red tridimensional (Figura 2). Cabe destacar que dos átomos de holmio(III), cristalográficamente independientes, están presentes en **1**, estando hexa- y nonacoordinados (Figura 3), respectivamente. Ambos presentan entornos de coordinación distorsionados: prisma trigonal triapicado -Ho(1)- y antiprisma cuadrado -Ho(2)- (Figura 4). Geometrías similares se presentan en el complejo $[Eu_2(mal)_3(H_2O)_5]\cdot 3H_2O$ [Hansson E., 1973].

Los compuestos **2** y **3** presentan ciertas similitudes. Ambos presentan una estructura tridimensional, en la que los iones lantánidos se encuentran unidos mediante dos grupos malonato, cristalográficamente diferentes. La estructura de ambos compuestos se puede interpretar como el resultado del cruce entre cadenas dobles de lantánidos que crecen a lo largo de la dirección [101] (Figuras 7a y 8a) y cadenas simples que se crecen a lo largo del eje *b* cristalográfico. Enlaces de hidrógeno en los que intervienen moléculas de agua y átomos de oxígeno de los grupos malonato (ver Tablas 3 y 4) contribuyen a estabilizar la estructura tridimensional. Los átomos de samario y cerio están nonacoordinados (Figura 9) conformando un entorno de antiprisma cuadrado distorsionado (Figura 10). La principal diferencia entre ambas estructuras radica en las aguas de cristalización que presenta el compuesto **3**, las cuales hacen que la red de enlaces de hidrógeno sea diferente para ambas estructuras.

Desde el punto de vista magnético, la interpretación de las propiedades magnéticas de los complejos de tierras raras, presentados en este capítulo, resulta complicado, debido a que el estado fundamental $^{2S+1}\Gamma_J$ rompe su degeneración, dando lugar a un multiplete en el cual, la diferencia en energía entre los diferentes estados

depende del entorno del ion de tierra rara y de la naturaleza del campo de los ligandos. Este hecho hace que la aproximación de ión libre sea sólo válida a altas temperaturas (cuando todos los estados del multiplete ,generados por la rotura de la degeneración del estado fundamental, están térmicamente poblados) y no pueda ser aplicada en todo el rango de temperaturas. Por consiguiente, la disminución de los valores de $\chi_M T$ al bajar la temperatura (ver Figuras 13, 14 and 15) pueden ser debidos a:

- despoblación de los estados de mayor energía correspondientes al multiplete originado a partir del estado fundamental.
- existencia de una interacción antiferromagnética.

Sería necesario un estudio más detallado, incluyendo la influencia del campo de los ligandos en el Hamiltoniano, para la interpretación de los datos magnéticos de estos compuestos.

Conclusiones

Los resultados obtenidos indican que los iones lantánidos dan lugar a redes de alta dimensionalidad. Esto es debido a su alto número de coordinación. Interesantes perspectivas se abren en el campo de los malonatos de tierras raras con la introducción de nuevos ligandos y/o grupos aniónicos que pueden dar lugar a modificaciones en su estructura y por consiguiente en sus propiedades [tal y como vimos que ocurría en el caso de los iones de la primera serie de transición].

De acuerdo con la experiencia, las estructuras de los compuestos de lantánidos cambian frecuentemente a lo largo de la serie, debido a la contracción de los lantánidos, hecho que corroboran los resultados experimentales.

Capítulo X

Compuestos de malonato de manganeso(III): un intento para obtener precursores

Objetivos de la Investigación

Como hemos comprobado hasta el momento, los ácidos dicarboxílicos desprotonados -como el ión malonato- cuando actúan como puente entre iones paramagnéticos, dan lugar a compuestos polinucleares que son muy interesantes desde el punto de vista del campo del Magnetismo Molecular.

El ácido malónico, es apropiado en el diseño de materiales moleculares multifuncionales, debido a su gran versatilidad para actuar de puente entre iones paramagnéticos. No obstante, resulta complicado utilizarlo en el diseño *a priori* de materiales multifuncionales, ya que es complicado predecir cómo va actuar el ligando y por consiguiente cuáles van a ser las propiedades estructurales del nuevo compuesto.

Un diseño racional se ha hecho con otros ligandos dicarboxílicos (tales como el oxalato) en los que se conseguido sintetizar una unidad muy estable, denominada precursor, que puede utilizarse a modo de ladrillo en la "construcción" de nuevos materiales. Esta estrategia resulta muy interesante, ya que facilita enormemente el diseño de materiales que posean las propiedades que nosotros deseamos.

Con esta idea en mente, iniciamos un trabajo cuyo objetivo final era la consecución de un complejo estable de malonato que pudiera utilizarse como precursor.

Planeamiento y Metodología utilizada

Mediante el método de evaporación lenta se prepararon muestras policristalinas de los productos de fórmula molecular $PPh_4[Mn(mal)_2(H_2O)_2]$ (**1**) and $AsPh_4[Mn(mal)_2(H_2O)_2]$ (**2**). A partir de la recristalización de estas muestras se obtuvieron cristales correspondientes a **1** y **2**.

Obtenidos los cristales se realizo:

- Análisis elemental, difracción de rayos X y medidas de susceptibilidad magnética.

Los cristales obtenidos para el compuesto **1** difractaban débilmente y no pudieron ser utilizados para las medidas de difracción de rayos X en monocristal.

Los resultados estructurales obtenidos, se compararon con los del complejo $K_2[Mn(mal)_2(MeOH)_2][Mn(mal)_2]$ (**3**). Para estudiar el comportamiento de la unidad de $[Mn(mal)_2]^-$ en ambos compuestos.

Para sustentar los resultados magnéticos obtenidos se realizaron cálculos DFT modelizando el canje magnético a través de los puentes que unen a los átomos paramagnéticos en los compuestos **2** y **3**.

Aportaciones originales y resultados

El compuesto $AsPh_4[Mn(mal)_2(H_2O)_2]$ (**2**) se caracterizó estructural y magnéticamente.

La estructura del compuesto **2** consiste en aniones *trans*-diaquabis(malonato) manganeso(III) y cationes tetrafenilarsonio (Figura 1) unidos mediante enlaces de hidrógeno (Figuras 4a y b), fuerzas electrostáticas e interacciones de van der Waals. Dos iones manganeso(III) cristalográficamente independientes están presentes en **2**. Los aniones se encuentran unidos entre sí mediante enlaces de hidrógeno, en los que intervienen todas las moléculas de agua y átomos de oxígeno del malonato, dando lugar a una red bidimensional que crece en el plano cristalográfico *ab* (Figura 2). Las distancias Mn···Mn más cortas en el plano son 7.1557(7) [Mn(1)···Mn(2)], 7.1526(7) [Mn(1)···Mn(2e)], 9.8890(8) [Mn(1)···Mn(1f)] y 10.3410(13) Å [Mn(2)···Mn(2e)]. Los grupos $AsPh_4^+$ están conectados entre sí mediante interacciones de tipo π···π dando lugar a capas catiónicas. Finalmente, las capas aniónicas y catiónicas están unidas mediante interacciones de tipo C-H···O donde intervienen los átomos de carbono del grupo $AsPh_4^+$ y los átomos de oxígeno del anión malonato y de las moléculas de agua coordinadas al manganeso(III) (Tabla 4).

Comparando esta estructura con $K_2[Mn(mal)_2(MeOH)_2][Mn(mal)_2]$ (**3**), donde átomos de K^+ actúan como contraion (en lugar del $AsPh_4^+$), se observa que en **3**, las unidades de $[Mn(mal)_2]^-$ se encuentran unidas mediante puente carboxilato dando lugar a cadenas regulares donde se alternan los aniones $[Mn(mal)_2(MeOH)_2]^-$ y $[Mn(mal)_2]^-$ (Figura 5) [la separación Mn···Mn a lo largo de la cadena es 5.501 Å y el ángulo diédrico entre planos ecuatoriales de metales adyacentes es 49.4º].

Las cadenas de manganeso(III) están unidas a través de los iones de potasio dando lugar a una red tridimensional. Interacciones del tipo C-H···O entre los grupos metilo del etanol y los átomos de oxígeno, contribuyen a estabilizar la estructura.

La principal diferencia entre **2** y **3** es el tamaño del contraion. El gran tamaño del grupo $AsPh_4^+$ aumenta la separación entre las unidades de manganeso(III) mientras que el K de menor tamaño permite que estás puedan estar más próximas.

Las propiedades magnéticas **1-3** (ver gráficas 6-8) han sido interpretadas en base al Hamiltoniano de la ecuación 1 realizando las siguientes aproximaciones: la dependencia de la susceptibilidad con el parámetro de desdoblamiento rómbico (E) es despreciable y los parámetros D, $g_{||}$ y $g_{\perp}$ son los mismos para los dos manganesos cristalográficamente independientes. Bajo estas aproximaciones es posible llegar a una expresión analítica para la susceptibilidad magnética de un cadena y de un plano de Mn (eq 6 y 7, respectivamente). El ajuste de los datos experimentales magnéticos mediante estas expresiones, lleva a los siguientes resultados: D = -3.91 cm^{-1}, J = +0.081 cm^{-1} and g = 1.98 for **1**, D = -3.96 cm^{-1}, J = +0.072 cm^{-1} and g = 1.99 for **2** and D = -3.95 cm^{-1}, J = -0.19 cm^{-1} and g = 1.99 for **3**.

Un cálculo DFT (método B3LYP implementado en Gaussian03) utilizando los modelos que muestran la Figura 9 se realizó, para analizar las interacciones magnéticas entre iones manganeso(III). Los resultados del cálculo, mostrando el esquema de orbitales magnéticos obtenidos, se muestra en las Figuras 10 y 11.

Conclusiones

Dificultades en la caracterización y en la preparación de los materiales basados en $[Mn(mal)_2]^-$ hace que estos no sean muy apropiados para su utilización como precursores.

No obstante, el estudio realizado nos ha permitido establecer correlaciones magneto-estructurales interesantes. Comprobando, desde el punto de vista estructural, que el tamaño del contraion juega un papel muy importante en el empaquetamiento de las unidades de malonato de manganeso(III) [al igual que ocurría con el Cu(II), capítulos II y III]. Desde el punto de vista magnético han quedado caracterizados los compuestos **1-3**. Comprobando que para el caso particular de los compuestos **1** y **2**, los enlaces de hidrógeno son capaces de transmitir el canje magnético.

Capítulo XI

El complejo como precursor: Compuestos de Cromo(III)

Objetivos de la Investigación

Los intentos realizados, en el capítulo anterior, para la obtención de un adecuado precursor no permitieron obtener un resultado del todo satisfactorio.

Por ello, nos propusimos realizar pruebas utilizando el ion Cr(III) y obtener compuestos de este material con otros metales para comprobar su estabilidad como precursor.

Planeamiento y Metodología utilizada

Se sintetizó inicialmente el compuesto $K_4[Cr(OH)(mal)_2]_2 \cdot 6H_2O$ (**1**), para caracterizar estructuralmente la unidad $[Cr(OH)(mal)_2]_2^{4-}$ que queríamos utilizar como precursor.

Tras caracterizar el compuesto mediante análisis elemental y difracción de rayos X, preparamos dos compuestos básados en la unidad $[Cr(OH)(mal)_2]_2^{4-}$ con cobre(II) y niquel(II). Estos compuestos fueron de nuevo caracterizados mediante análisis elemental y difracción de rayos X.

Finalmente se realizó un estudio detallado de la estructura de cada uno de los compuestos sintetizados.

Aportaciones originales y resultados

Se han preparado y sintetizado tres nuevos complejos de malonato de Cr(III) de fórmula molecular: $K_4[Cr(OH)(mal)_2]_2 \cdot 6H_2O$ (**1**), $\{[Cu(tren)]_4[Cr_2(mal)_4(OH)_2]\}(ClO_4)_4 \cdot 8H_2O$ (**2**) y $[Ni(Htren)_2][Cr_2(mal)_4(OH)_2] \cdot 8H_2O$ (**3**).

El compuesto **1** consiste en unidades dinucleares de malonato de Cr(III), donde los iones metálicos se encuentran unidos mediante doble puente μ-oxo (Figura 2). Estas unidades están conectadas mediante iones potasio dando lugar a una red tridimensional en la que capas de Cr(III) y K se alternan (Figura 1). Una lista detallada de los entornos

(distancias y ángulos de enlace) de cada uno de los átomos se puede encontrar en la Tabla 2.

En **2** las unidades dinucleares de Cr(III) se encuentran unidas a cuatro grupos $[Cu(tren)]^{2+}$ mediante enlaces carboxylato de tipo *anti-syn*, dando lugar a una unidad hexanuclear (Figura 7). Estas unidades se encuentran unidas mediante enlaces de hidrógeno en los que intervienen moléculas de agua, oxígenos de malonato y grupos perclorato (ver Figura 6 y consultar Tabla 7), dando lugar a una red extendida tridimensional.

La estructura de **3**, consiste en aniones $[Cr(OH)(mal)_2]_2^{4-}$ y cationes $[Ni(tren)_2]^{2+}$ (Figuras 10 y 11) que se encuentran enlazados mediante enlaces de hidrógeno dando lugar a capas que crecen a lo largo del plano cristalográfico *ac*. Estos planos, a su vez, se encuentran conectados mediante enlaces de hidrógeno, donde moléculas de agua de cristalización actúan como átomos dadores (Figura 9), dando lugar a una estructura tridimensional.

Conclusiones

Como hemos podido ver en los tres casos descritos, la unidad $[Cr(OH)(mal)_2]_2^{4-}$ se ha mantenido estable, permitiendo la construcción de grupos de nuclearidad mayor (complejos hexanucleares en **2**). Si comprobamos la geometría del grupo $[Cr(OH)(mal)_2]_2^{4-}$ comparando los parámetros geométricos (distancias y ángulos de enlace de las Tablas 2, 5, 8) podemos comprobar que no hay grandes variaciones.

Aunque en el complejo **3**, los grupos $[Ni(tren)_2]^{2+}$ no se unan mediante puente carboxilato al complejo dinuclear de Cr(III), la unidad $[Cr(OH)(mal)_2]_2^{4-}$ es un buen candidato para actuar como un buen precursor en la preparación de nuevos materiales basados en malonato.

Un amplio campo se abre a la luz de los resultados obtenidos, con la preparación de nuevos complejos utilizando otros iones metálicos [Co(II), Mn(II), Zn(II)] y con lantánidos. Estas estrategias pueden combinarse con las utilizadas en los capítulos anteriores: utilización del malonato ácido (capítulo I), introducción de un cation inorgánico o orgánico (capítulos II y III), utilización de un segundo ligando para el estudio de las interacciones débiles y el aumento de la dimensionalidad de las redes obtenidas (capítulo IV y V).

Por tanto la obtención de un precursor estable, abre un nuevo campo de trabajo en el que el diseño de los nuevos materiales multifuncionales puede estar dirigido a la obtención de compuestos con las propiedades deseas.

CONCLUSIONES

Conclusiones

A lo largo del trabajo realizado en esta tesis, hemos podido comprobar, cómo diferentes estrategias pueden ser utilizadas para el estudio magneto-estructural de los compuestos de malonato.

En el capítulo I, se observó cómo la inclusión de las especies $Hmal^+$ y H_2mal afectaba al empaquetamiento de las unidades de malonato de cobre(II). En este capítulo, tres nuevos compuestos de fórmula molecular $[Cu(Hmal)_2]$ y $[Cu(H_2O)(H_2mal)(mal)]$ (presentando dos polimorfos) -en los cuales se encuentran presentes las tres posibles especies del ácido malónico (H_2mal, $Hmal^-$, mal^{2-})- fueron sintetizados y caracterizados magnética y estructuralmente. Los tres compuestos presentan estructuras laminares de malonato de cobre, que se encuentran unidas mediante enlances de hidrógeno, dando lugar a redes tridimensionales. Estructuralmente por primera se han observado vez redes de tipo "*herrigbone*" en compuestos de malonato de cobre y modos de coordinación nuevos para los grupos H_2mal y $Hmal^-$. Las propiedades magnéticas de estos compuestos, muestran que la efectividad del canje magnético está relacionado con el grado de desprotonación del malonato, siendo despreciable para H_2mal, muy débil para $Hmal^-$ y más efectivo para el grupo mal^{2-}. Desde el punto de vista estructural, las distancias Cu-O(mal) están relacionadas con el grado de desprotonación del ligando, siendo menores cuando el grado de desprotonación es mayor. Con la preparación y caracterización de estos nuevos materiales, hemos mostrado que es posible obtener compuestos donde coexistan diferentes especies del mismo ligando y que la disposición de los mismos, puede controlar las propiedades magnéticas de un material.

En el capítulo II, estudiamos la influencia del tamaño de un ión inorgánico en las propiedades magnéticas y estructurales de los malonatos de cobre. Cabe destacar los siguientes resultados:

- el empaquetamiento de los iones alkalinos está directamente relacionado con su tamaño. Así, observamos que estos iones se unen a través de puente μ-oxo dando lugar a dímeros (Li), cadenas (Na y K), cadenas dobles (Rb) y planos (Cs). Lógicamente, este hecho tiene su influencia en el empaquetamiento de las unidades de malonato de cobre(II).

- exceptuando el caso del Li, a medida que el tamaño del ion alkalino aumenta (Na, K, Rb y Cs), aumenta la distancia entre las unidades de cobre. Esto se traduce en una disminución general de la interacción magnética.
- variando el ion alkalino se observa una gran variedad de empaquetamientos cristalinos para el malonado de cobre: unidades mononucleares (Li, Cs), planos (Na y K) y cadenas (Cs).
- la utilización de los iones alkalinos puede ser útil cuando se desea controlar el empaquetamiento de las unidades de malonato de cobre. Estos resultados pueden ser extensibles a otros compuestos que contengan ligandos carboxilatos (oxalato, fumarato, acetato, etc,...)

En el capítulo III, realizamos un estudio detallado de cómo la naturaleza (tamaño y número de grupos dadores) de un catión orgánico, utilizado en la preparación de nuevos complejos malonatos de cobre(II), produce cambios en el empaquetamiento molecular. Hemos podido comprobar que el aumento del tamaño del grupo catiónico, produce en general, un alejamiento de las unidades de $[Cu(mal)_2]^{2+}$, dando lugar a una disminución progresiva de la intensidad del canje magnético. Cabe destacar la gran importancia de los enlaces de hidrógeno, los cuales controlan, el empaquetamiento cristalino de cada uno de los compuestos descritos en este capítulo.

En el capítulo IV, nuestro objetivo consistió en la modificación de la unidad de malonato de cobre $[Cu(mal)_2]$ por otra del tipo [Cu(mal)L], siendo L un ligando de tipo azina que actuase como ligando terminal. Con esta estrategia, pretendíamos estudiar como otro tipo de interacciones débiles, tales como las interacciones de tipo $\pi\cdots\pi$ (que se pueden dar entre los grupos aromáticos de los ligandos tipo azina), podían introducir cambios en el empaquetamiento cristalino. A la vista de los resultados obtenidos, podemos concluir que interacciones generalmente consideradas como débiles, (enlaces de hidrógeno O-H···O/ N-H···O e interacciones de tipo $\pi\cdots\pi$ y C-H···π) juegan un papel muy importante en el empaquetamiento cristalino, y por consiguiente, deben ser tenidas en cuenta en el diseño *a-priori* de nuevos materiales. La combinación de un contraion y un ligando de tipo azina, dio lugar a un compuesto dinuclear de cobre. Este método podría utilizarse para la preparación de nuevos complejos dinucleares.

Conociendo la gran versatilidad del malonato, la importancia de los enlaces de hidrógeno en el empaquetamiento molecular y el uso de ligandos de tipo N- o/y O-dadores para un diseño racional de nuevos materiales, en eñ capítulo V abordamos el diseño racional de materiales moleculares basados en el malonato de cobre, intentando obtener redes mono-, bi- y tridimensionales. El trabajo realizado nos permite concluir que:

- resulta complicado predecir *a priori* las propiedades estructurales de un compuesto de malonato de Cu. Prueba de ello, son los tres compuestos de diferente topología que se han obtenido con malonato de Cu y bpe. Asimismo, también resulta sorprendente la estructura del compuesto de fórmula molecular $[Cu(mal)(dpo)(H_2O)]_n$, donde las interacciones débiles, controlan (frente al puente dpo) el empaquetamiento molecular.
- los resultados obtenidos nos han permitido comprobar que el ligando malonato es un buen candidato para acoplar ferromagnéticamente dos iones con spin S = ½ (salvo en el complejo de fórmula $\{[Cu(mal)_2(H_2O)_2][Cu(dien)]\}_n \cdot 4nH_2O$, la interacción magnética entre los iones de cobre a través de puente carboxilato de malonato es de naturaleza ferromanética).

En el capítulo VIa abordamos el estudio estructural de los compuestos homometálicos de malonato de Ni(II) y de Co(II). Cabe destacar los siguientes aspectos:

- a pesar de que ambos compuestos son isoestructurales, la interacción a través del puente carboxilato del malonato da lugar a interacciones de naturaleza opuesta: antiferromagnética [Co(II)] y ferromagnética [Ni(II)]. La explicación a este fenómeno debe buscarse en la diferente configuración electrónica de ambos metales.

Realizando un estudio de compuestos de malonato de Ni(II), Co(II) y Mn(II), llegamos a la conclusión que se resume en el esquema 1 del capítulo VIa:

- aunque el malonato homometálico de Mn(II) posee una estructura diferente de los malonatos de Co(II), Ni(II) y Zn(II) -los cuales son isoestructurales-; cuando se añade un ligando N-exo dentado de tipo piridil, las unidades de $[M(mal)(H_2O)]$ se disponen siguiendo la misma topología, independientemente del metal M utilizado [M = Co(II), Ni(II), Zn(II), Mn(II)].

En el capítulo VIb, se caracterizó mediante difracción de neutrones en polvo la estructura magnética del malonato de Mn(II). A pesar de los problemas experimentales que se planteaban al principio del experimento (presencia de H en la muestra, número bajo de iones magnéticos en la celdilla unidad, estructura determinada parcialmente -sin hidrógenos- por difracción de rayos X), fue posible la determinación de la estructura magnética del malonato de Mn(II) por debajo de la temperatura de orden (T_c = 2.7 K). Los resultados obtenidos corroboran la existencia del fenómeno de spin-canting, permitiendo obtener los valores del momento magnético para cada uno de los iones Mn(II) que forma la celdilla unidad.

En el capítulo VII se pudo caracterizar, por primera vez, mediante difracción de rayos X de monocristal los compuestos de malonato de NiMn y CoMn. No obstante, es necesario resaltar que la obtención de este último complejo resulta muy complicada, debido a la aparición simultánea de otras fases (malonato de manganeso, malonato de cobalto y disoluciones sólidas de ambas fases) y es necesario seguir trabajando para mejorar la síntesis.

En el capítulo VIII, se abordó el estudio de complejos de malonato de Co(II) con ligandos que pudiesen actuar de puente, con la finalidad de obtener redes de dimensionalidad variable que nos permitieran estudiar el canje magnético a través del puente carboxilato. Tras los resultados presentados en este capítulo, cabe destacar que:

- hemos podido comprobar que los compuestos homometálicos de malonato en los que se utilizaba un ligando N-exo de tipo piridil estaban constituidos por planos rectangulares y corrugados de iones metálicos, tal y como habíamos establecido en el capítulo VIa.
- desde el punto de vista magnético hemos conseguido una familia de compuestos de dimensionalidad variable (desde 0D hasta 3D), que nos ha permitido estudiar la interacción magnética a través del puente malonato. Por primera vez en compuestos de malonato de cobalto se ha observado un comportamiento de naturaleza ferromagnética a través del puente carboxilato en el complejo de fórmula molecular $[Co(mal)(phen)(H_2O)]\cdot 2H_2O$.

En el capítulo IX, ampliamos el estudio de malonatos a los iones lantánidos. De los resultados obtenidos podemos concluir que:

- con iones lantánidos es posible obtener redes de alta dimensionalidad, debido a su alto número de coordinación,.
- interesantes perspectivas se abren en el campo de los malonatos de tierras raras con la introducción de nuevos ligandos y/o grupos aniónicos que pueden dar lugar a modificaciones en su estructura y por consiguiente en sus propiedades [tal y como vimos que ocurría en para el caso de los iones de la primera serie de transición].

Finalmente en los capítulos X y XI pretendíamos obtener un precursor de malonato que nos permitiera el diseño de forma racional de nuevos materiales multifuncionales. El uso del Cr(III) resulta muy prometedor, pudiendo utilizarse la unidad $[Cr(OH)(mal)_2]_2^{4-}$ como un buen precursor para la preparación de nuevos materiales basados en malonato.

Un amplio campo se abre a la luz de los resultados obtenidos:

- preparación de nuevos complejos utilizando otros iones metálicos [Co(II), Mn(II), Zn(II)], y/o lantánidos.
- la estrategia de síntesis con precursor pueden combinarse con las utilizadas en los capítulos anteriores: utilización del malonato ácido (capítulo I), introducción de un cation inorgánico o orgánico (capítulos II y III), utilización de un segundo ligando para el estudio de las interacciones débiles y el aumento de la dimensionalidad de las redes obtenidas (capítulo IV y V).

Por tanto la obtención del precursor $[Cr(OH)(mal)_2]_2^{4-}$ abre un nuevo campo de trabajo en el que el diseño de los nuevos materiales multifuncionales dirigido a la obtención de compuestos con las propiedades deseas.

Universidad de La Laguna

DEPARTAMENTO DE FÍSICA FUNDAMENTAL II

"DESARROLLO DE NUEVOS MAGNETOS MOLECULARES CON ION MALONATO COMO LIGANDO"

"DEVELOPMENT OF NEW MOLECULAR MAGNETS BASED ON THE MALONATE ION"

TOMO I

FERNANDO SALVADOR DELGADO TRUJILLO

MEMORIA PARA OPTAR AL GRADO DE DOCTOR EN FÍSICA

Index

Volume I

Volume II

PART II: Working with other Malonate Complexes

PART III: New perspectives of malonate complexes

Molecular magnets and clusters exhibit a number of unusual phenomena of scientific interest, some having potential for practical applications. Tunneling and quantum coherence are of interest in components for possible use in quantum computing, while local thermo-induced spin-crossover transitions may bring revolutionary progress in the design of large-size displays due to spin dependence of the color of some magnetic molecules [Gatteschi D., 1994]. Light-induced spin transitions can modify magneto-optical properties and may be used in photonic switches [Coronado E. *et al.*, 1996]. Manganese magnetic complexes undergoing similar transitions, trigger a photosynthesis reaction and act as a catalyst [Girerd J.-J., 1998]. Finally the use of magnetic molecules in biomedicine is growing rapidly. An example is the use of such molecules attached to pathogens in blood removed from the body, which can then be filtered magnetically before the blood is reintroduced. Another example is the use of such molecules to enhance the NMR relaxation rate in specific target areas where greater contrast is needed for magnetic resonance imaging [Coronado E. *et al.*, 1996].

The present thesis couples our research in the study of these new magnetic materials: synthesis of new hybrid or metallo-organic materials; growth and preparation of single crystal samples, detailed measurements of magnetic susceptibility; X-ray diffraction; and neutron (structure and magnetic) diffraction. In a parallel way, extensive crystal growth methods have to be performed to complement and guide the experimental program.

Supramolecular chemistry, or chemistry beyond the molecule, has allowed us to build new molecular materials in the solid state. The crystal engineering concepts also help us to establish connections between the crystal structure of molecular materials and their properties. Crystal engineering, or design, links the domains of intermolecular interactions, crystal structures and crystal properties. Without interactions there cannot be structures, and without worthwhile properties as a goal, there cannot be sufficient reason for designing structures.

A major conclusion that emerges from our work is the great utility of defining the crystal structure as a network. This will be true for all varieties of molecular crystals ranging from simple monomers to coordination polymers that incorporate both inorganic and organic components. The design of this kind of complexes does not only

include the coordination but also the supramolecular chemistry, the use of weak interactions (hydrogen bonding, C-H···N, C-H···π. π-π) to guide the formation of specific structures. Among these weak interactions, the hydrogen bonds play a very important role in molecular recognition and crystal packing. The employment of these interactions in a rational and cooperative way is more effective in the control of the crystal packing and the crystal structure and therefore in the properties that these materials are going to have.

The aim of this thesis is to investigate the factors that control the way in which the malonate-containing complexes self-assemble, highlighting the main structural characteristics of the extended molecular networks, discussing the magnetic properties which result as a consequence of the specific arrangement of the paramagnetic metal ions in space.

The main investigatory techniques used in this thesis are the CCD X-ray diffraction and the SQUID susceptibility magnetometry. The physics of CCD-diffractometer and SQUID susceptibility magnetometer are given succinctly in Appendix A and B, respectively.

Finally, in this work we present, the malonic acid as a fruitful tool for the construction of new molecular magnets. This study is organized attending the metal and the dimensionality of the structure, and then the magnetic properties are explained attending to the bridging mode of the malonate ligand and the nature of the magnetic orbitals of the paramagnetic centres. Thus, playing with the stoichiometry and with the nature of other complementary ligands, very interesting compounds with a controlled dimensionality and nice magnetic properties have been prepared.

References

Coronado E., P. Delhaes P., Gatteschi D. and Miller J.S. (Eds), *Molecular magnetism: From molecular assemblies to the devices*, NATO ASI Series E, vol. 321, Kluwer Academic Publishing, **1996**.

Gatteschi D., *Adv. Mater.* **1994**, *6*, 635.

Girerd, J.-J. in proceedings of ESF Workshop *Molecular clusters: Magnetism and quantum size effects*, Florence, Italy, November 28-December **1998**.

INTRODUCTION

Malonic acid: a fruitful tool for the construction of new molecular magnets

Dicarboxylic ligands are frequently used as bridging ligands in the design of polynuclear complexes which exhibit interesting magnetic properties. The ability of the carboxylato bridge to mediate significant ferro- or antiferromagnetic interactions between the magnetic centres accounts for their use. The most widely studied dicarboxylic ligand is the oxalate $(C_2O_4)^{2-}$ anion. It usually adopts the coordination the η^4-chelation, acting as a bis-bidentate ligand, bridging the metal centres in an *anti-anti* fashion (see Scheme a) [Hernández-Molina M. *et al.*, 2001a].

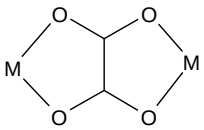

two η^4 chelates
anti-anti bridging mode

Scheme a

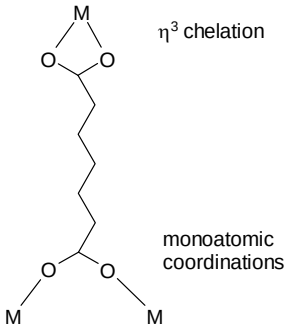

Scheme b

In addition, other coordination modes have also been observed, but they are not so adequate in the transmission of the magnetic coupling. The higher members of the dicarboxylic series exhibit the characteristic chelate coordination of the CO_2^- group, the η^3-chelation, which can be accompanied with one or two monoatomic coordinations, other chelate modes being forbidden by steric reasons [Hornick C. *et al* , 2000; Rabu P. *et al.*, 2001] (see Scheme b).

Malonic acid is widely used in many important fields as a result of its excellent coordination ability. The malonic acid complexes with lanthanides and transition metals have been used in the fluorescent probe technique, solid fluorescent materials, biological active materials and modifiers of polyethylene. Therefore, studies of the new complexes with malonic acid are quite valuable in theory and application.

The malonate anion is a dicarboxylic ligand with a singular behaviour different from the other dicarboxylic anions. In our previous investigations we have observed that with the 3*d* ions it can exhibit different coordination modes such as (a) bidentate [η^5-chelation] (b) bidentate [η^5-chelation] + unidentate and (c) bidentate [η^5-chelation] + bis(unidentate):

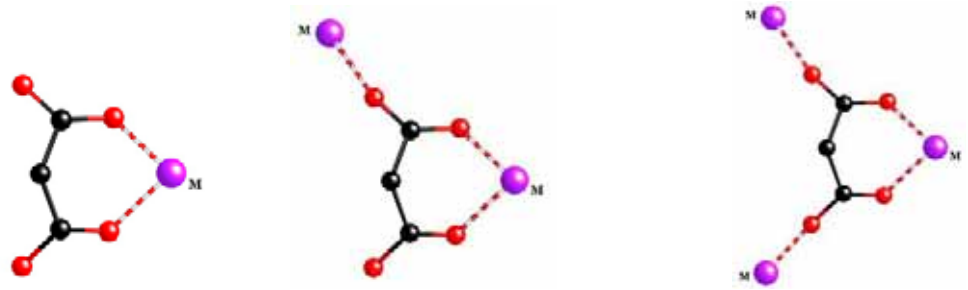

(a) **(b)** **(c)**

Other coordination modes, such as the η^3-chelation observed in the higher series have also been reported by other authors [Hornick C. *et al.*, 2000; Rabu P. *et al.*, 2001], but is less frequent with 3*d* metal ions. The bis-bidentate behaviour analogue to that exhibited by the oxalate is forbidden by steric reasons and this affects dramatically to the structure and properties of the malonate-containing complexes. The malonate ligand occupies one or two coordination positions and neutralizes two positive charges of the metallic ion, allowing the inclusion of other ligands in the coordination sphere of the metal. These complementary ligands can act as bridging or blocking ligands contributing to the interconnection or isolation of the spin carriers. Thus, combining the malonate with other bridging and/or blocking ligands we have been able to prepare monomers [Ruiz-Pérez C. *et al.*, 2000a; Hernández-Molina M. *et al.*, 2001b], dimmers [Ruiz-Pérez C. *et al.*, 2000a, Rodríguez-Martín Y. *et al.*, 2001a], trimers [Ruiz-Pérez C. *et al.*, 2000a], tetramers [Rodríguez-Martin Y. *et al.*, 2002a], infinite chains [Ruiz-Pérez C. *et al.*, 2000a, 2000b and 2000c; Sanchiz J. *et al.*, 2002], 2D [Rodríguez-Martín Y. *et al.*, 2001b] and 3D arrays [Rodríguez-Martín Y. *et al.*, 2002a and 2003].

Structural Chemistry of Malonate Compounds

1. Bridging modes of malonate

(a) bidentate (no-bridging)

In this coordination mode two of the malonate-oxygen atoms coordinate the metallic ion, the ligand behaving as η^5-bidentate, the rest of the oxygens may act as acceptors in hydrogen bonding. This mode is analogue to the η^4-bidentate chelate exhibited by the oxalate. The malonate acts as blocking ligand leading to isolated molecules that are interconnected through hydrogen bonding, exhibiting weak or no magnetic coupling among the metallic centres.

As examples we have the complexes of formula: $[M^{II}(H_2O)_6][Cu^{II}(mal)_2(H_2O)_2]$ (**1**) (M = Mn, Co, Ni, Cu and Zn) [Bimitrova G.I. *et al.*, 1974; Rodriguez-Martín Y. *et al.*, 2002b], $[Cu(mal)(bipym)(H_2O)]$ (**2**) (Figure 1a), and $[Cu_2(mal)_2(H_2O)_2(bipym)]$ (**3**) (Figure 1b) [Rodríguez-Martín Y. *et al.*, 2001a]. In **1**, four malonate oxygens fill the equatorial positions of the metallic ions, the rest of the coordination sites being occupied by water molecules. Other ligands may displace water molecules entering in the coordination sphere of the metallic ion, if they have a large size, they may keep the molecules isolated due to steric reasons, as in **2**. Some ligands can bridge the metallic ions, but if the malonate anion is kept as bidentate ligand the molecules remain isolated as in **3**, here the dimensionality and the magnetic coupling being governed by the complementary ligand.

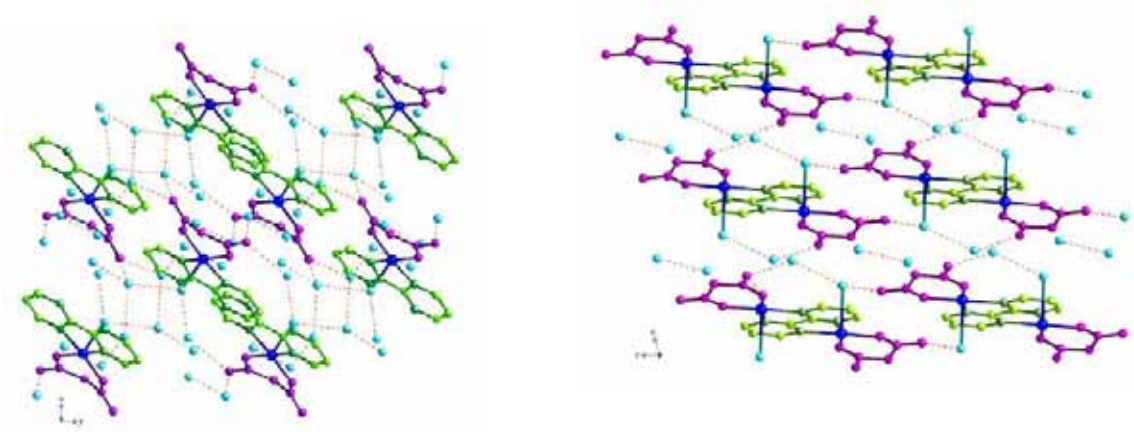

(a) **(b)**

Figure 1. Crystal packing of $[Cu(mal)(bipym)(H_2O)]$ (**2**) viewed down the crystallographic *c*-axis showing the extended 3D network **(a)** and crystal packing of $[Cu_2(mal)_2(H_2O)_2(bipym)]$ (**3**) viewed down the crystallographic *b*-axis, showing the extended 2D network, formed through water hydrogen bonding linkages (dashed lines). Hydrogen atoms have been omitted for clarity.

b) η^5-bidentate + unidentate

In this coordination mode, two of the malonate-oxygen atoms coordinate the same metal ion (bidentate) and another one is bound to an additional metal ion (monodentate), the ligand behaving overall as tridentate. The remaining oxygen acts as an acceptor in hydrogen bonding blocking the polymerisation in this direction.

The simplest compound exhibiting this coordination mode is that of formula $[(H_2O)_4Cu(\mu\text{-mal})Cu(mal)(H_2O)_2]$ (**4**) (Figure 2a) [Chattopadhyay D. *et al.*, 1993; Ruiz-Pérez C. *et al.*, 2000a]. This is a dinuclear compound where the Cu(1) and Cu(2) ions have octahedral and square pyramidal environments, respectively. The malonate oxygen atoms fill all the equatorial sites at Cu(1) and one apical position at Cu(2), the Cu(1)-O bond lengths being shorter than the Cu(2)-O ones.

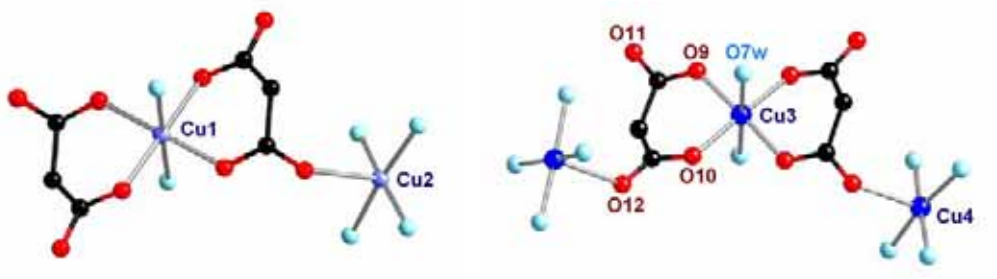

(a) **(b)**

Figure 2. (a) Perspective view of the $[(H_2O)_4Cu(\mu\text{-mal})Cu(mal)(H_2O)_2]$ dinuclear units in **4** and **(b)** view of the $[Cu_3(mal)_2(H_2O)_9]^{2+}$ trinuclear cation of the compound of formula $\{[Cu(H_2O)_4]_2[Cu(mal)_2(H_2O)]\}[Cu(mal)_2(H_2O)_2]\{[Cu(H_2O)_4][Cu(mal)_2(H_2O)_2]\}$ (**5**).

The $[Cu_3(mal)_2(H_2O)_9]^{2+}$ trinuclear cation (see Figure 2b) that occurs in the compound of formula $\{[Cu(H_2O)_4]_2[Cu(mal)_2(H_2O)]\}[Cu(mal)_2(H_2O)_2]\{[Cu(H_2O)_4][Cu(mal)_2(H_2O)_2]\}$ (**5**) [Ruiz-Pérez C. *et al.*, 2000a] is formed by a central aquabis(malonato)copper(II) entity which is linked to two peripheral tetraaquacopper(II) units through carboxylato bridges which exhibit the *anti-syn* configuration. The two crystallographically independent copper atoms [Cu(3) and Cu(4)] exhibit a distorted square pyramidal environments. Four coplanar carboxylate oxygen atoms from two malonato ligands with nearly identical bond lengths [1.938(4) and 1.941(2) Å for Cu(3)-O(9) and Cu(3)-O(10), respectively] build the basal plane around Cu(3), whereas a weakly coordinated water molecule [2.508(3) Å for Cu(3)-O(7w)] occupies the axial

position. The environment of the Cu(4) is built by four water molecules which occupy the equatorial positions and one malonate-oxygen atom which fills the apical site.

The compound $\{[Cu(H_2O)_3][Cu(mal)_2(H_2O)]\}_n$ (**6**) [Ruiz-Pérez C. *et al.*, 2000a]. (Figure 3) has a 1D polymeric structure. It consists of zigzag chains of copper(II) ions that exhibit a regular alternation of aquabis(malonato)copper(II) and triaqua-copper(II) units, the former being linked to the latter as bis-monodentate ligand through two *trans*-malonate-oxygen atoms. The chains run parallel to the *c*-axis, and they are interconnected through hydrogen bonding. The two crystallographically independent copper(II) ions [Cu(1) and Cu(2)] in **6**, have distorted square pyramidal surroundings. Four coplanar carboxylate-oxygen atoms [O(1), O(3), O(5), and O(6)], which are coordinated to Cu(1) define the basal plane around this metallic ion, whereas the apical position is occupied by a weakly coordinated water molecule O(1w). Three water molecules [O(2w), O(3w), and O(4w)] and one carboxylate oxygen O(7) build the basal plane around Cu(2), whereas another carboxylate-oxygen atom, O(2c) [(c) -*x*, 1/2-*y*, -1/2+*z*], occupies the axial position. Each malonate group adopts simultaneously the bidentate [at Cu(1)] and monodentate [at Cu(2)] coordination modes. Two slightly different carboxylate bridges, that exhibit the *anti-syn* conformation, alternate regularly within each copper(II) chain.

Figure 3. Perspective drawing of a fragment of the chain of compound $\{[Cu(H_2O)_3][Cu(mal)_2(H_2O)]\}_n$ (**6**)

Combining the malonate anion with blocking ligands, such as imidazole (Im) or methylimidazole (MeIm), 1-D polymeric structures can be obtained as those observed in compounds $[Cu(Im)_2(mal)]$ (**7**) and $[Cu(MeIm)_2(mal)]$ (**8**) (Figure 4) [Sanchiz J. *et al.*, 2002]. In these compounds, the copper ions have square pyramidal surroundings. Two malonato-oxygen atoms from a bidentate malonate anion and two imidazole/methylimidazole-nitrogens build the basal plane of the metal ions. The

bidenate malonate group acts simultaneously as monodentate ligand towards the neighbouring copper(II) atom filling an apical position (the Cu-O bond length being long) and leading to zigzag malonate-bridged copper chains.

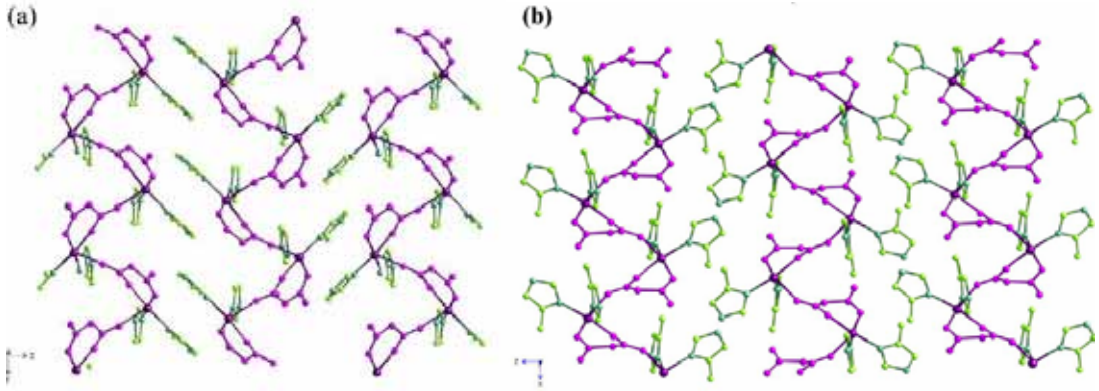

Figure 4. (a) Projection of compound $[Cu(Im)_2(mal)]$ (**7**) down the *a*-axis showing the parallel arrangement of the zigzag chains. **(b)** Projection of compound $[Cu(MeIm)_2(mal)]$ (**8**) down the *b*-axis showing the parallel arrangement of the zigzag chains and the columnar stacking of the MeIm ligands.

The crystal structure of $[Cu_4(mal)_4(H_2O)_4(2,4'\text{-bipy})_4]\cdot 2H_2O$ (**9**) [Rodriguez-Martín Y. *et al.*, 2002a] consists of $[Cu_4(mal)_4(H_2O)_4(2,4'\text{-bipy})_4]$ tetrameric neutral units, where copper(II) and malonate ions are located at the corners of a small planar square (Figure 5). The network is stabilized by the π-π stacking among the 2,4'-bipy ligands belonging to different tetrameric units, and hydrogen bonding between the coordinated water molecules and the free malonate-oxygen atoms. In the coordination sphere of the copper atoms, the malonate oxygens fill equatorial positions, the apical ones being occupied by water molecules. The 2,4'-bipy acts as a blocking ligand, since the location of the nitrogen in the 2 position doesn't allow further polymerisation.

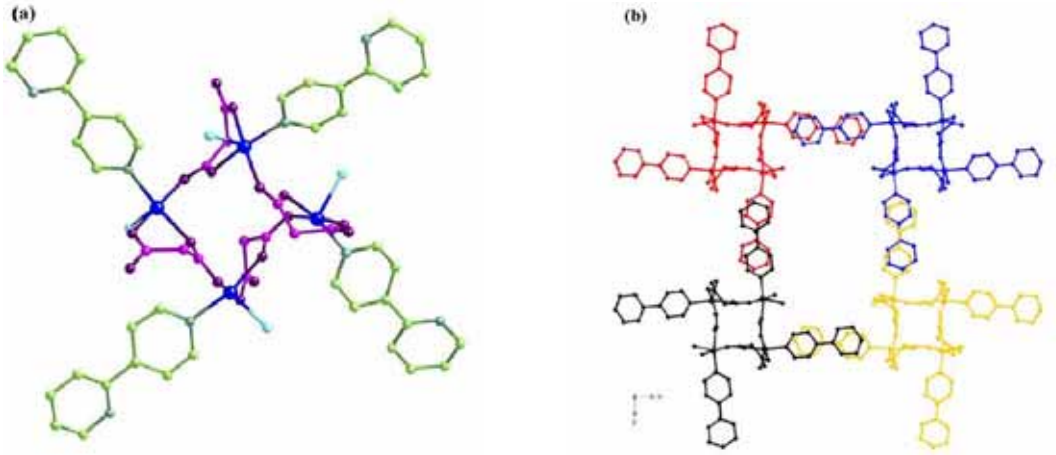

Figure 5. View of the tetrameric unit of the compound of formula $[Cu_4(mal)_4(H_2O)_4(2,4'\text{-bipy})_4]\cdot 2H_2O$ (**9**) **(a)** with a perspective view of the stacking of these units along the *c*-axis **(b)**.

$[Cu_4(mal)_4(H_2O)_4(4,4'\text{-bipy})]\cdot 2H_2O$ (**10**) [Rodríguez-Martín Y. *et al.*, 2001b] has a similar structure to that observed in **9**. The main difference is the ability of the 4,4'-bipy to act as a bidentate ligand, linking together the $Cu_4(mal)_4(H_2O)_4$ tetramers and leading to a 2D network (see Figure 6). This compound illustrates that it's possible to increase the dimensionality of a given compound by the introduction of the adequately bridging ligand.

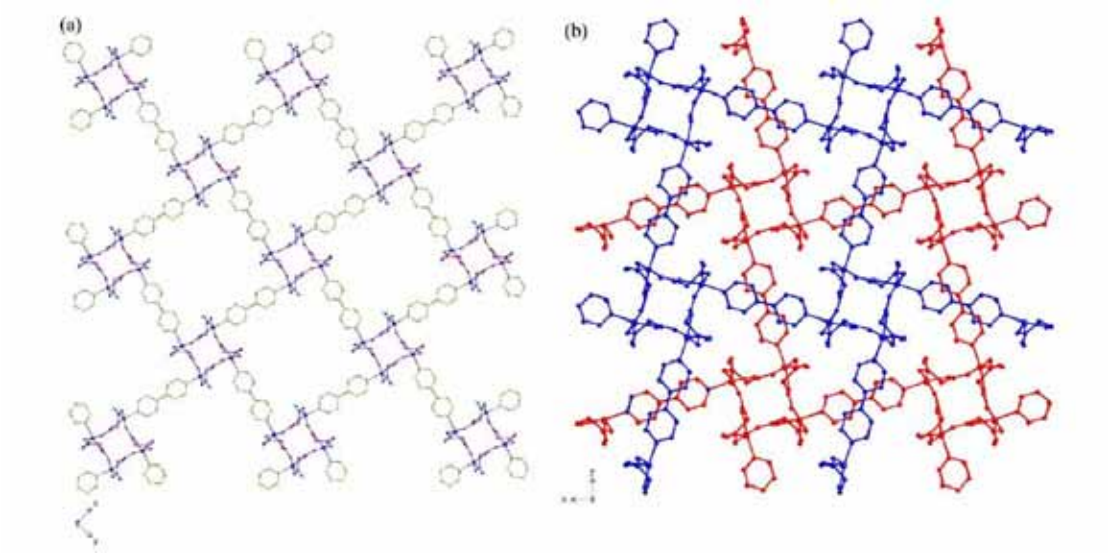

Figure 6. (a) Perspective view, along the *c*-axis, of the two types of square channels that occurs in $[Cu_4(mal)_4(H_2O)_4(4,4'\text{-bipy})]\cdot 2H_2O$ (**10**) when only the odd layers are drawn. **(b)** Perspective view of the layers stacked along the tetragonal *c*-axis.

The structure of $[Mn^{II}Cu^{II}(mal)_2(H_2O)_3]\cdot 2H_2O$ (**11**) [Ruiz-Pérez C. *et al.*, 2000c] is made up of neutral bimetallic chains (Figure 7) which are held together by means of long copper to malonate oxygen bonds [2.771(3) Å for Cu-O(apical) bond length], leading to a corrugated sheet-like structure. The crystal structure is stabilized by an extensive network of intra- and interlayer hydrogen bonds involving both coordinated and crystallization water molecules together with malonate-oxygen atoms. Each malonate group acts simultaneously as bidentate (towards the copper atom) and monodentate (towards manganese atom) ligand within the chain. The remaining carboxylate-oxygen atom interacts weakly with the copper atoms of the neighboring chains. Both carboxylato bridges adopt the *anti-syn* conformation.

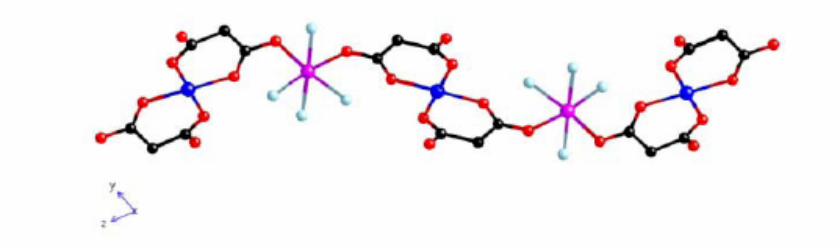

Figure 7. View of the $[Mn^{II}Cu^{II}(mal)_2(H_2O)_3]\cdot 2H_2O$ (**11**) chain down the *a*-axis. Crystallization water molecules and hydrogen bonding interactions are not drawn for the sake of clarity.

(c) Bidentate + bis(unidentate)

Two polymorphic malonate-bridged copper(II) complexes of formula $\{[Cu(bpy)(H_2O)][Cu(bpy)(mal)(H_2O)]\}(ClO_4)_2$ (**12**) (Figure 8) have been reported [Ruiz-Pérez C. *et al.*, 2000b]. Their structures consist of malonate-bridged cationic copper(II) *zigzag* chains which run parallel to the one crystallographic axis (*b*- or c-axis) and uncoordinated perchlorate anions. These chains are formed by $[Cu(bpy)(mal)(H_2O)]$ units which act as bis-unidentate ligands towards two adjacent $[Cu(bpy)(H_2O)]$ units through its OCCCO skeleton exhibiting an *anti-anti* conformation. Four crystallographically independent copper(II) atoms occur in both polymorphic compounds, all of them having distorted square pyramidal environments. The axial position is occupied by a water molecule, whereas the equatorial plane is formed by a chelating bpy and two carboxylate-oxygen atoms from a bidentate or two monodentate malonate ligands. Each malonate group exhibits simultaneously the bidentate and bis-monodentate coordination modes. The carboxylate bridges of the malonate ligands exhibit the *anti-syn* conformation.

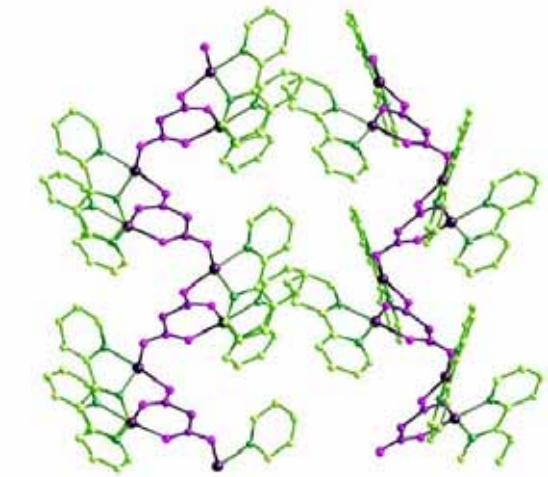

Figure 8. View of compound $\{[Cu(bpy)(H_2O)][Cu(bpy)(mal)(H_2O)]\}$ $(ClO_4)_2$ (**12**) showing the parallel arrangement of the chains along the *b*-axis. Hydrogen atoms and the perchlorate anions have been omitted for clarity.

The structure of the Mn(II) malonate compound (**13**) is made up by the polymerization of $[Mn(mal)(H_2O)_2]$ mononuclear units giving thus, a 2D array (Figure 9a) [Lis T. *et al.*, 1979; Rodríguez-Martín Y. *et al.*, 2003]. The manganese has an octahedral environment, four malonate-oxygen atoms building the basal plane around the metallic atom and two water molecules filling the apical positions. Each malonate anion chelates the metal, the remaining two oxygens bridging two adjacent metallic atoms. This structure is very original since the two malonate-carboxylate groups exhibit two different conformations, the *anti-anti* and the *anti-syn*, respectively. This asymmetry leads to a spin canting behaviour at low temperatures.

$[Mn(mal)(2,4'\text{-bipy})_{1/2}(H_2O)]$ (**14**) and $[Mn(mal)(4,4'\text{-bipy})_{1/2}(H_2O)]$ (**15**) [Rodríguez-Martín Y. *et al.*, 2003] (Figure 9) have similar structures in which layers of malonate-bridged manganese(II) ions are pillared by 2,4'-bipy or interconnected by 4,4'-bipy, affording a 2D (**14**) or 3D (**15**) structure, respectively. Each malonate anion chelates one metallic atom, the remaining two oxygen atoms bridge two neighbouring manganese(II) ions, forming thus malonate-bridged manganese layers. Therefore, three different malonate anions coordinate the metallic ion, the remaining two *trans* positions being filled by a terminal water molecule and a nitrogen from the aromatic molecule. All these compounds exhibit weak antiferromagnetic coupling.

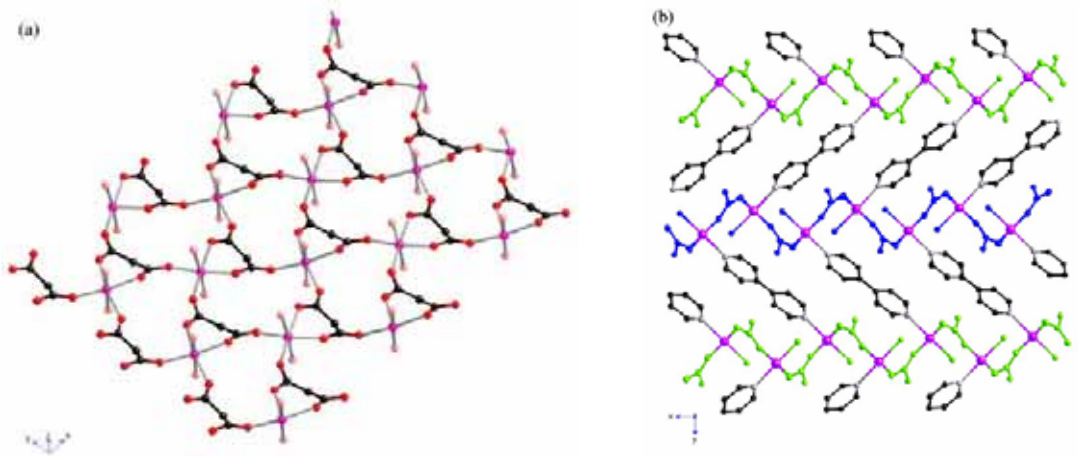

Figure 9. (a) Sheet structure of compound $[Mn(mal)(H_2O)_2]$ (**13**). **(b)** View of the crystal structure of $[Mn(mal)(4,4'\text{-bipy})_{1/2}(H_2O)]$ (**14**) along the *c*-axis. Hydrogen atoms have been omitted for clarity.

The structure of $[Cu_4(mal)_4(pyz)_2]\cdot 4H_2O$ (**16**) (Figure 10) is very similar to that of **10**, where two-dimensional layers were obtained by the assemblage of $Cu_4(mal)_4$ tetramers by means of bis-monodentate 4,4'-bipy ligands. In **16,** the tetramers are assembled by bis-monodentate pyrazine ligands. Each copper atom is in a quasi perfect

square pyramidal environment with three carboxylate-oxygen atoms from two malonate groups and one nitrogen atom from a pyrazine ligand building the equatorial plane. The main difference with the structure of **10** is the absence of a water molecule filling the apical position at the copper ion. This position is now occupied by a malonato oxygen atom from a tetramer unit belonging to a neighbouring layer. Consequently, the layers are interconnected each other leading to a three-dimensional structure. The four malonate-oxygen atoms are bonded to copper atoms: within each layer, the malonate adopts simultaneously the bidentate and monodentate coordination modes, the fourth carboxylate-oxygen acts also as monodentate being bound to a further copper atom from a neighboring layer.

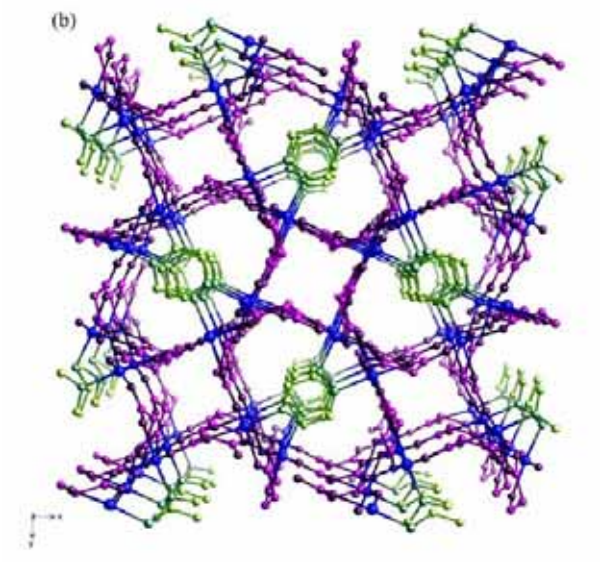

Figure 10. A view of the 3D structure of $[Cu_4(mal)_4(pyz)_2]\cdot 4H_2O$ (**16**) where the square grid layers are stacked along the *c*-axis showing the π-π overlap between pairs of pyrazine molecules. Hydrogen atoms have been omitted for clarity.

2. Geometrical aspects (bonds, angles,...)

In order to carry out a geometry study of the malonate ligand in homometallic malonate-containing metal complexes [M = Cu(II), Co(II), Ni(II), Mn(II) and Zn(II)], we have used the Cambridge Structural Database (CSD) [Allen F.H., 2002] search program ConQuest to retrieve the geometrical values of the malonate complexes from the CSD (version 5.26, August 2005). We searched for the geometrical parameters depicted in Figure 11. In the search, we included only those structures that have been solved at room temperature and with a R-factor < 10%. The ConQuest program cannot be used to depict the results obtained. Instead of ConQuest, we used the program Vista [version 2.3.8] included also in the CSD package to draw the histograms corresponding

to the distribution of the each geometrical value. The results obtained for each metal ion are shown in the following pages [Figure 12-14 and Tables 1 and 2]. It deserves to be note here that in the cases of nickel(II) and zinc(II) only three items have been found, for these metal ions we present the results in Tables instead of histograms. Few examples (only six) were found for cobalt(II).

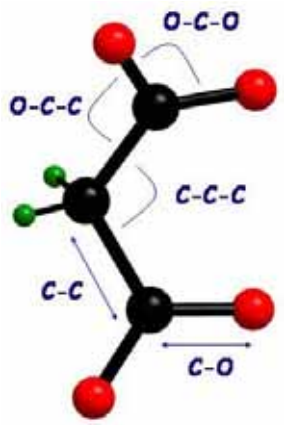

Figure 11. Schematic view of the malonate group, showing the geometric values included in the CSD search.

We can observe that there are no significant differences between the geometry values corresponding to the different metal ions. In all cases, each geometric parameter has a narrow range within it varies. Along this work, we are going to see that no long deviations from the values reported here, are going to been observed.

Finally, in order to study the coordination modes of the malonate ligand with the first transition metal ions, we carried out another search using the CSD search program ConQuest, to retrieve the cif files corresponding to the malonate-containing homometallic [Cu(II), Co(II), Ni(II), Mn(II) and Zn(II)] complexes. We restrain the search to those structures with a R-factor < 10% and obviously we skipped the structures that are going to be described in the present work. Once we got the cif files, we analyse one by one, the coordination of the malonate group/s that occur in each structure retrieved. To enhance this task we used the Mercury (version 1.3) program that allowed us to represent conveniently the coordination mode of the malonate groups for each compound. We have found 9 different coordination modes which are depicted in Schemes 1-9.

Homometallic Malonate-Containing Cu(II) Complexes (40 entries)

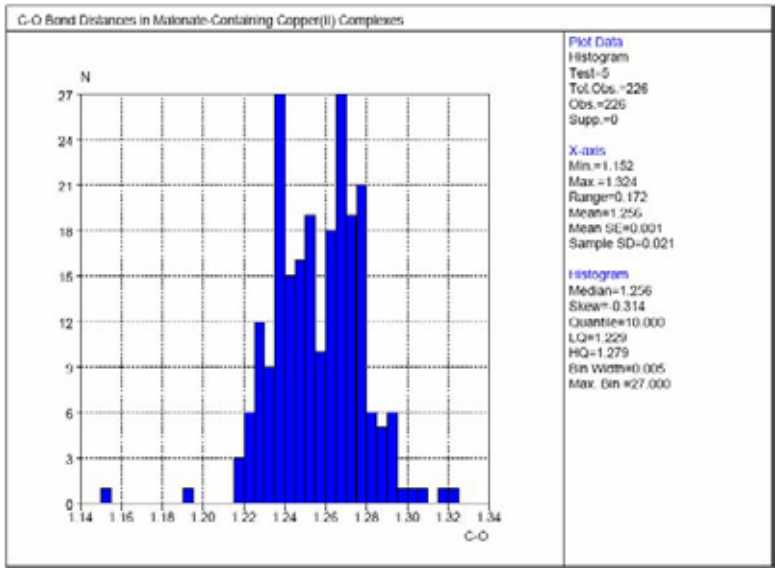

(a)

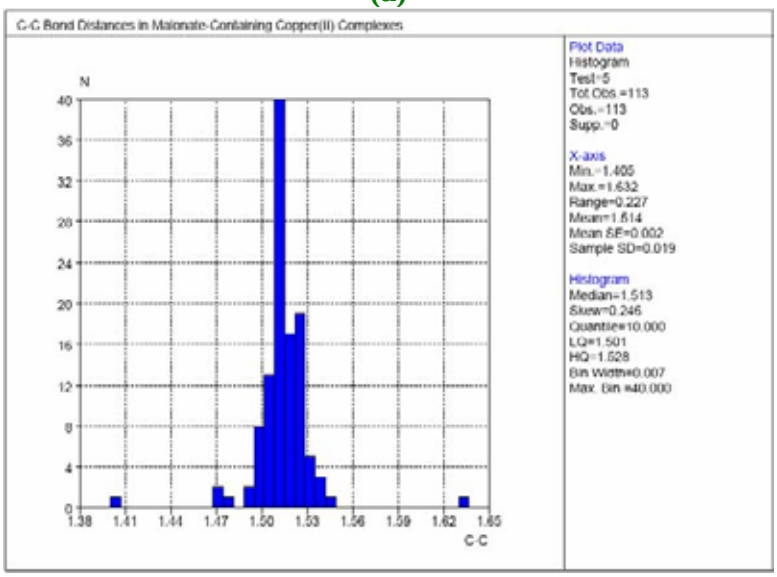

(b)

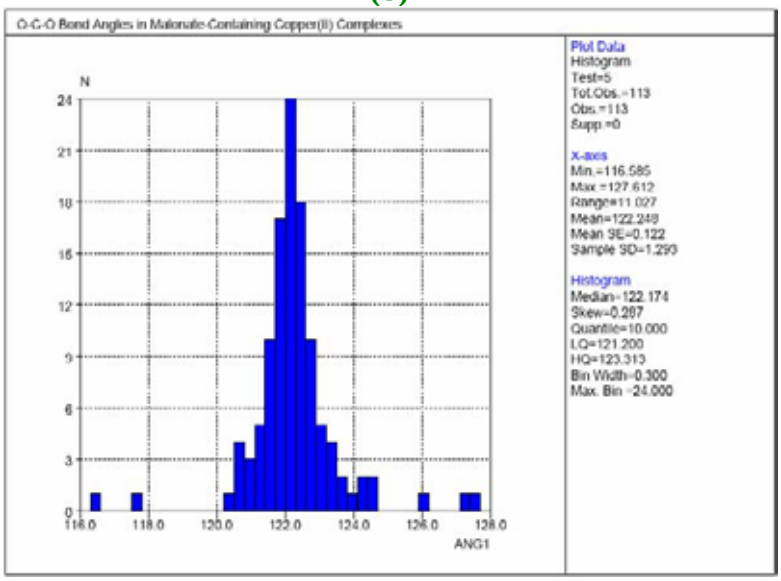

(c)

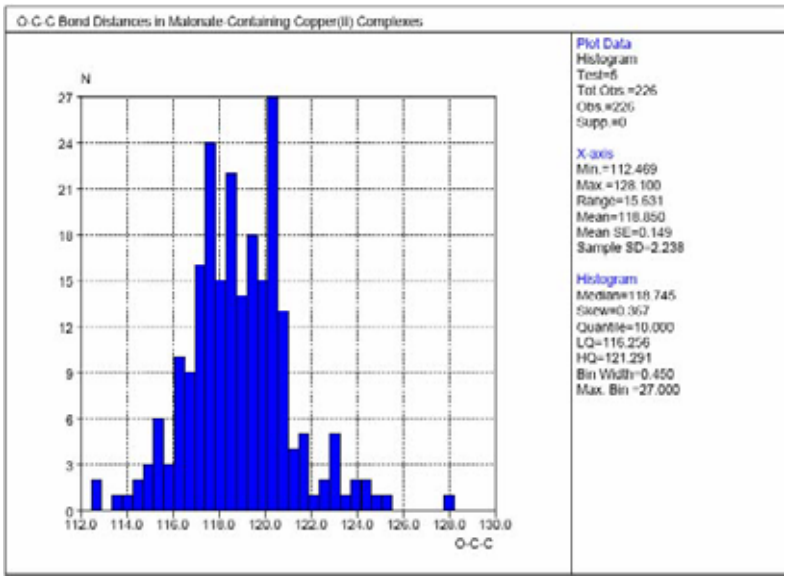

(d)

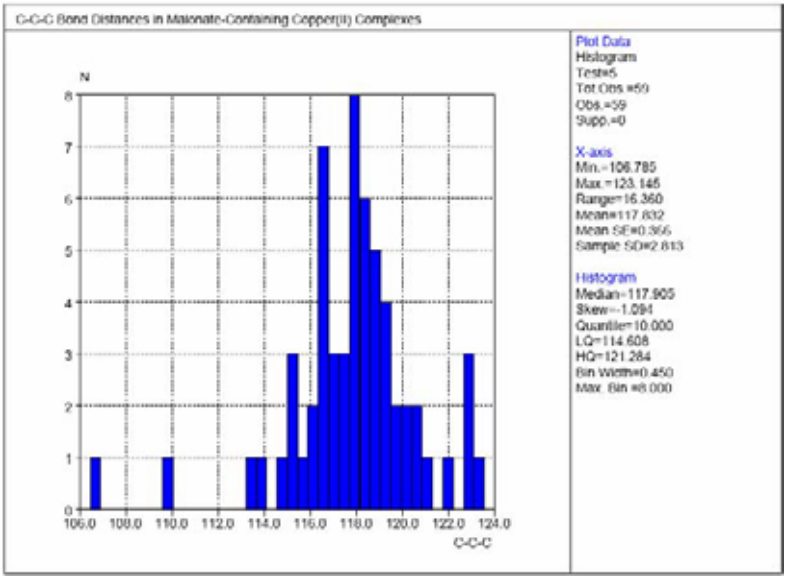

(e)

Figure 12. Histrograms corresponding to the distribution of C-O **(a)**, C-C **(b)** bond distances and O-C-O **(c)**, O-C-C **(d)** and C-C-C **(e)** bond angles for the malonate group in homometallic copper(II) complexes.

Homometallic Malonate-Containing Co(II) Complexes (6 entries)

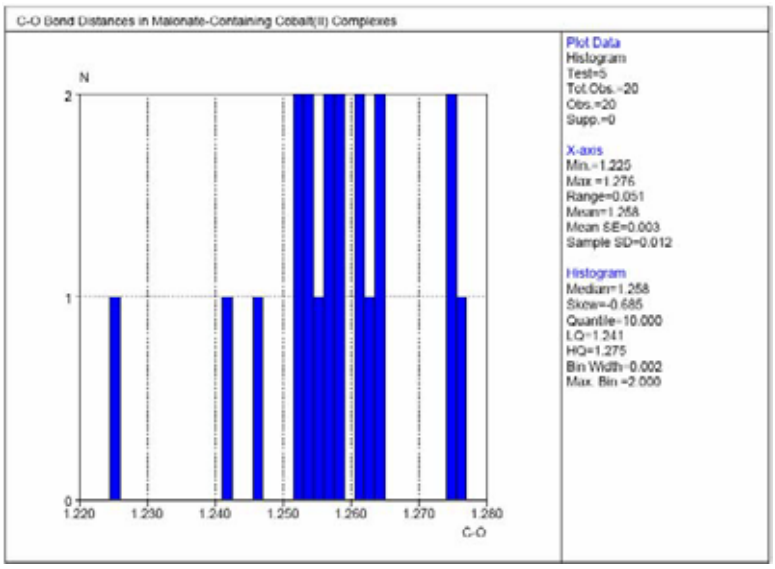

(a)

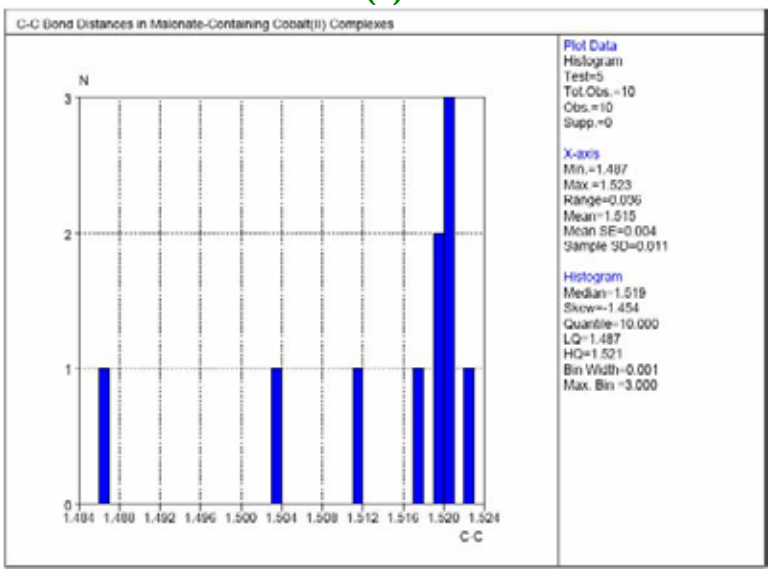

(b)

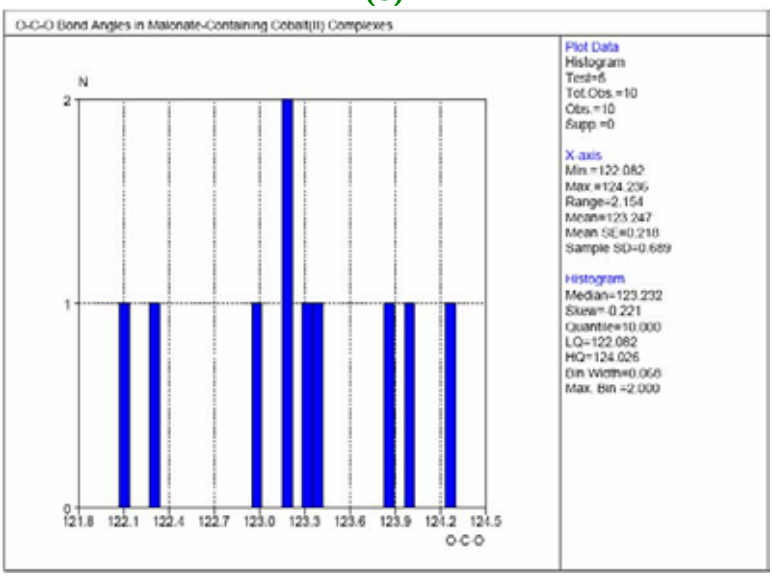

(c)

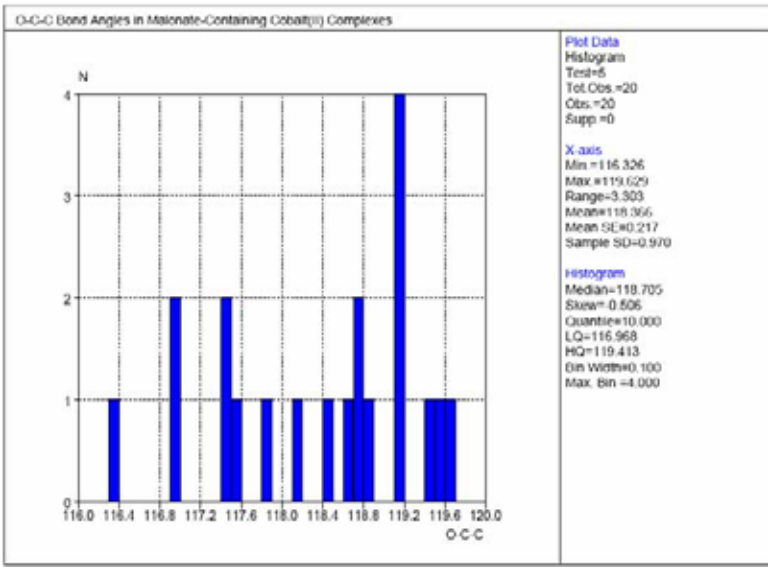

(d)

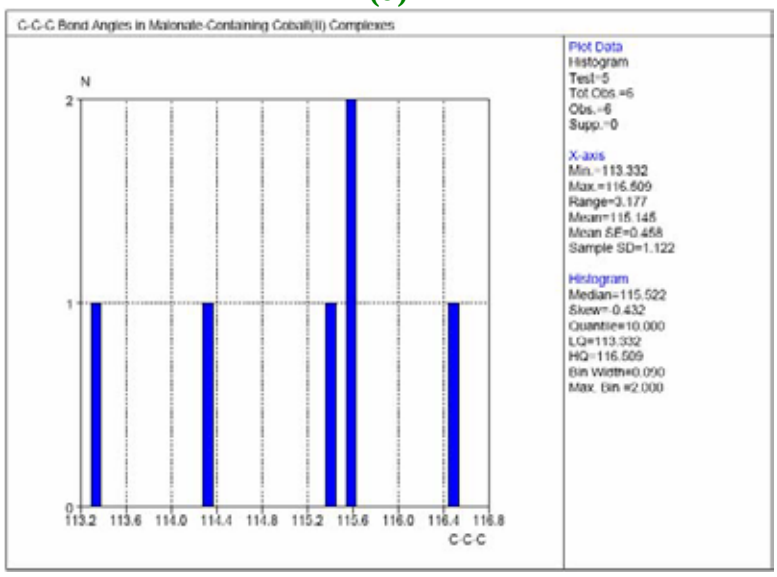

(e)

Figure 13. Histrograms corresponding to the distribution of C-O **(a)**, C-C **(b)** bond distances and O-C-O **(c)**, O-C-C **(d)** and C-C-C **(e)** bond angles for the malonate group in homometallic cobalt(II) complexes.

Homometallic Malonate-Containing Mn(II) Complexes (13 entries)

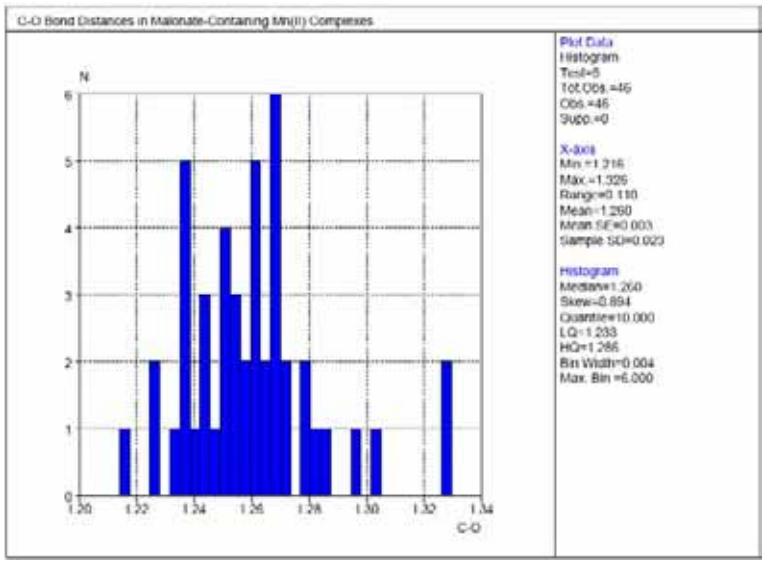

(a)

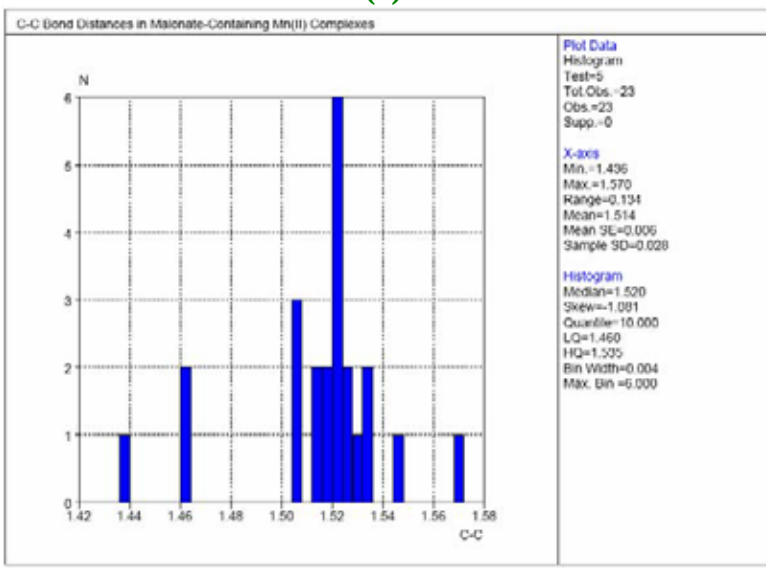

(b)

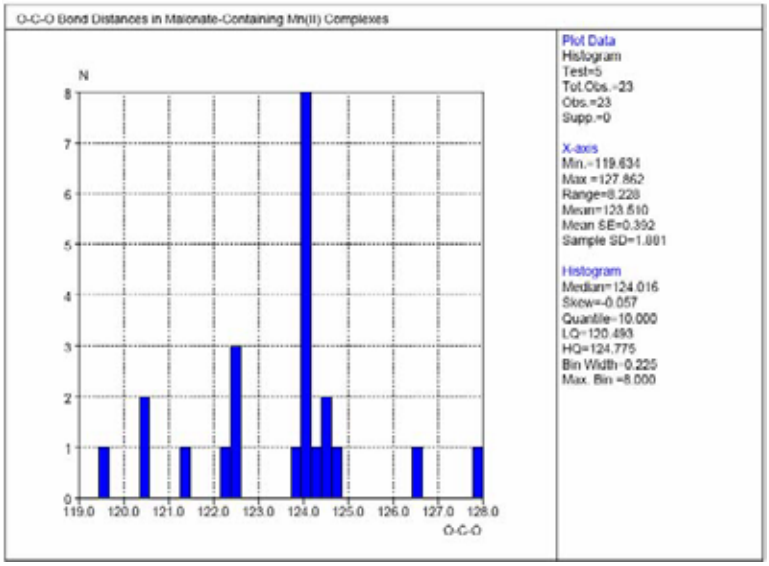

(c)

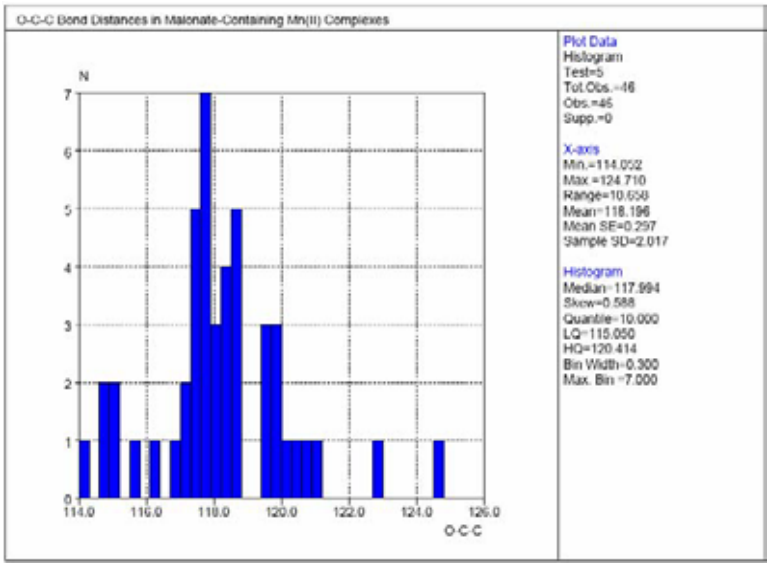

(d)

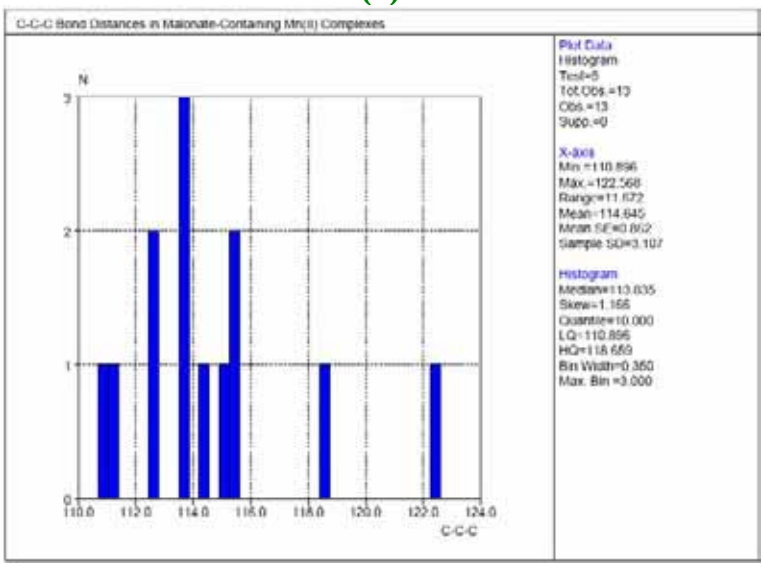

(e)

Figure 14. Histrograms corresponding to the distribution of C-O **(a)**, C-C **(b)** bond distances and O-C-O **(c)**, O-C-C **(d)** and C-C-C **(e)** bond angles for the malonate group in homometallic manganese(II) complexes.

Homometallic Malonate-Containing Zinc(II) Complexes (3 entries)

Table 1. Main bond distances (Å) and angles (º) for the malonate groups in homometallic Zinc(II) complexes.

Reference	C-C	C-O	O-C-O	O-C-C	C-C-C
Burrows A.D. *et al.*, 2000	1.516, 1.521	1.220-1.272	124.9, 124.8	115.8-119.4	108.4
Zhang X. *et al.*, 2003	1.510, 1.525	1.247-1.270	123.7, 124.1	116.0-119.9	115.1
Liu Q. *et al.*, 2004	1.517	1.258, 1.259	124.4	115.8, 119.8	115.4

Homometallic Malonate-Containing Nickel(II) Complexes (3 entries)

Table 2. Main bond distances (Å) and angles (º) for the malonate groups in homometallic Nickel(II) complexes.

Reference	C-C	C-O	O-C-O	O-C-C	C-C-C
Liu J.-G. *et al.*, 2004	1.520, 1.524	1.249-1.257	122.3, 122.7	115.2-122.3	123.8
Wang X.-D. *et al.*, 2004	1.520, 1.521	1.229-1.276	123.4, 123.8	116.7-119.5	118.0
Zheng Y.-Q. *et al.*, 2004	1.514	1.254, 1.267	122.8	117.5, 119.7	115.7

Schemes Showing the Coordination Modes of the Malonate Ligand

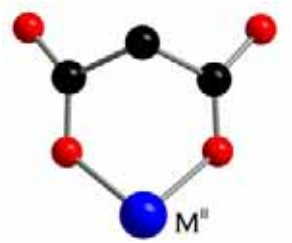

Scheme 1
M^{II} = Cu(II), Co(II), Mn(II), Ni(II), Zn(II)

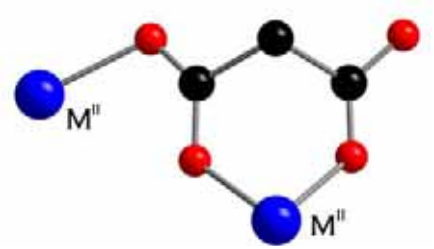

Scheme 2
M^{II} = Cu(II)

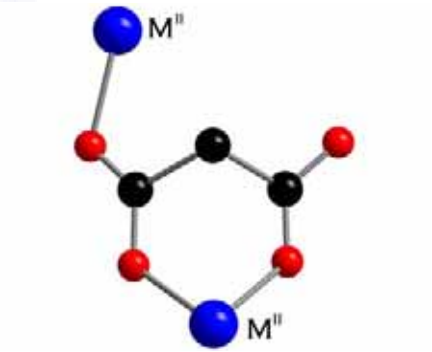

Scheme 3
M^{II} = Cu(II), Mn(II)

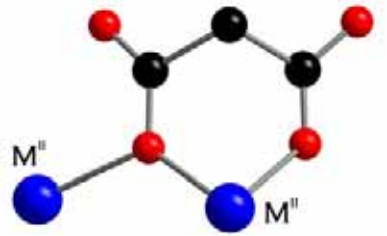

Scheme 4
M^{II} = Cu(II)

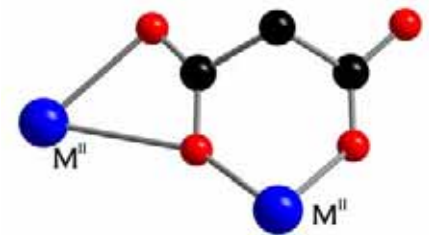

Scheme 5
M^{II} = Cu(II)

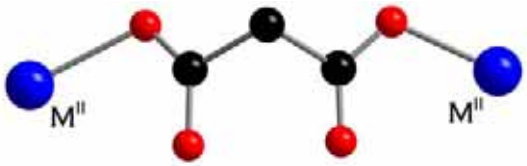

Scheme 6
M^{II} = Zn(II)

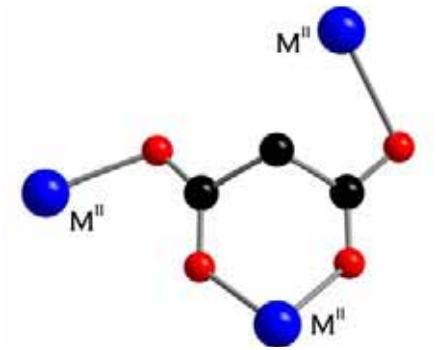

Scheme 7
M^{II} = Cu(II), Mn(II)

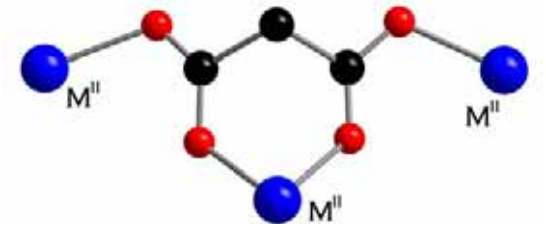

Scheme 8
M^{II} = Cu(II), Co(II), Mn(II), Ni(II), Zn(II)

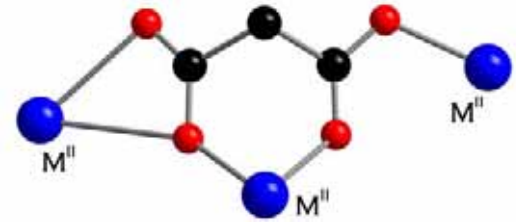

Scheme 9
M^{II} = Cu(II)

Magnetic Properties

The magnetic behaviour of a sample is usually detected by a substance's response, either attraction or repulsion, to a magnet. It arises from the way the electron spins interact with each other and with the external magnetic field. Every electron has a small magnetic moment associated with its quantum mechanical "spin". Since each orbital may have got as far as two electrons [one spin-up (↑) and one spin down (↓)] the spins cancel when both electrons are present. A molecule or ion which has two electrons in every orbital, it is a diamagnetic sample and it will be slightly repelled for an applied magnetic field. A molecule that has an odd number of electrons, it has got at least one unpaired electron, and consequently the molecule has a net spin. Such molecules or ions are usually sufficiently far apart to consider their spin-coupling energy is smaller compared to the thermal energy. In such a case the spins, that each individual molecule has got, do not couple and these molecules or ions form a very weak type of magnets called paramagnets. When spins are close enough, the spin-coupling energy increases and it may become large enough to enable an effective coupling between the neighbouring spins: called **ferromagnetic** (↑↑), when the coupling is paralell, or **antiferromagnetic** (↓↑), in the case of antiparalell coupling. Other behaviour is possible when in a sample one has two or more different spin carriers. **Ferrimagnets** occur when there are two or more different moments (essentially a different numbers of spins) on neighbouring sites which align antiferromagnetically. As they spins are different, they do not cancel, and lead to a net moment for the solid.

Magnetic behaviours different from the ferrimagnetism, ferromagnetism or antiferromagnetism may occur in the nature. The **metamagnetism,** for example occurs when a antiferromagnetic sample become a ferromagnetic one by the application of an external magnetic field. The **spin canting** behaviour is observed when two or more spins that couple antiferromagnetically are partially aligned, so they do not completely cancel, and they lead to a weak net magnetic moment for the solid.

Examples for all these situations have been found in malonato complexes, and they be showed below, but let's first explain how one can analyse the magnetic coupling between two paramagnetic centres by one of the models that more intuitively broaches this topic [Kahn, 1998].

The magnetic coupling among the magnetic centres is given by the value of *J*

(the intramolecular exchange interaction). The sign of *J* is indicative of the character of the interaction: antiferro- (negative) or ferromagnetic (positive) coupling. The magnitude of the interaction depends on the overlap between the orbitals where unpaired electrons are located (named as magnetic orbitals). Thus, for example for the carboxylato bridge, it will be affected by the possible bridging modes (*syn-syn, syn-anti* and *anti-anti*) that it can adopt. Therefore the nature (ferro- or antiferromagnetic) and the strengths of the coupling depend on the nature and the location of the magnetic orbitals of the spin carriers which are connected by a bridging ligand. We recall that an approximated value of *J* in copper(II) dinuclear complexes is given by eq (1), where S is the overlap integral between the two magnetic orbitals and β and j are their monoelectronic resonance and bielectronic exchange integrals, respectively.

$$J = 2j + 4\beta S^2 = J^F + J^{AF} \qquad (1)$$

Consequently, *J* can be seen as the sum of two terms; a ferromagnetic J^F and an antiferromagnetic J^{AF} one. Approximately J^{AF} is proportional to S^2, thus the stronger the overlap, the stronger the antiferromagnetic contribution. Usually the antiferromagnetic contributions are much larger than the ferromagnetic ones, but if the overlap integral is neglected either by accidental (due to the relative location between the magnetic orbitals) or by strict orthogonality (due to the nature and symmetry of the orbitals) between the magnetic orbitals of the spin carriers, the ferromagnetic contribution may dominate, leading to ferromagnetism. In most of our compounds the magnetic properties can be analyzed under these approximations having a satisfactory explanation of the magnetic properties.

Ferromagnetism

Most of the malonate-containing copper(II) complexes [see references of copper(II)-malonate complexes at the end of this Introduction] exhibit ferromagnetic interactions and both mechanisms (strict and accidental orthogonality) have been observed. The magnetic behaviour of these compounds can be explained on the basis of the bridging mode of the carboxylate group (*syn-syn, syn-anti* and *anti-anti*) and the relative orientation of the bridge within the coordination sphere of the copper ions it links (apical-apical, apical-equatorial or equatorial-equatorial). Let's see a few examples to illustrate both situations.

The magnetic behaviour of $[Cu_4(mal)_4(H_2O)_4(2,4'\text{-bipy})_4]\cdot 2H_2O$ (**9**) [Rodriguez-Martín *et al.*, 2002a] in the form of $\chi_M T$ *vs.* T plot [χ_M being the magnetic susceptibility per four copper(II) ions] is shown in Figure 15. The value of the $\chi_M T$ at room temperature is 1.65 $cm^3\ mol^{-1}\ K$, a value which is as expected for a four magnetically isolated copper(II) ions (g = 2.10, S = 1/2). Upon cooling, $\chi_M T$ increases reaching a plateau at 3 K ($\chi_M T$ = 3.24 $cm^3\ mol^{-1}\ K$), that corresponds to the value of a magnetically isolated square of four spin doublets, interacting ferromagnetically. The magnetic data for (**9**) can be analysed through the following theoretical Hamiltonian:

$$\hat{H} = -J(\hat{S}_1\cdot\hat{S}_2 + \hat{S}_2\cdot\hat{S}_3 + \hat{S}_3\cdot\hat{S}_4 + \hat{S}_4\cdot\hat{S}_1) \qquad (2)$$

The least-squares fit of the experimental data leads to a coupling constant of J = +12.3 cm^{-1}. This strong ferromagnetic coupling can be explained in the terms of the effective accidental orthogonality of the magnetic orbitals which results from the large dihedral angle (δ) subtended by the basal planes of adjacent copper(II) ions, linked by a carboxylate bridge, δ = 70º in **9** (δ = 0º maximum overlap, δ = 90º zero overlap).

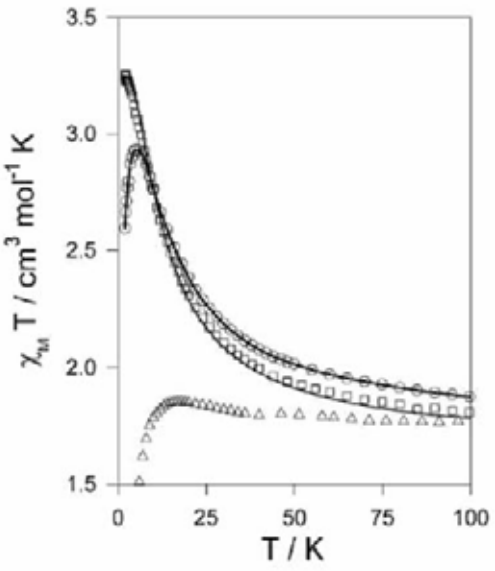

Figure 15. Thermal dependence of the $\chi_M T$ product for compounds **9** (□), **10**(O) and **16** (Δ) experimental curves; (-) best fit curves (see text).

Bulk ferromagnetic properties are only exhibited by high dimensional compounds, but the interpretation of the magnetic behaviour of these compounds remains difficult. So, we present here an example of one-dimensional copper(II) complex with easily comprehensive magnetic properties.

The magnetic properties of $\{[Cu(H_2O)_3][Cu(mal)_2(H_2O)]\}_n$ (**6**) under the form of $\chi_M T$ *vs.* T plot [χ_M being the magnetic susceptibility per two copper(II) ions] are shown in Figure 16. At high temperatures the value of $\chi_M T$ corresponds to two magnetically isolated copper(II) ions. On cooling, it remains practically constant up to 30 K and then it increases sharply.

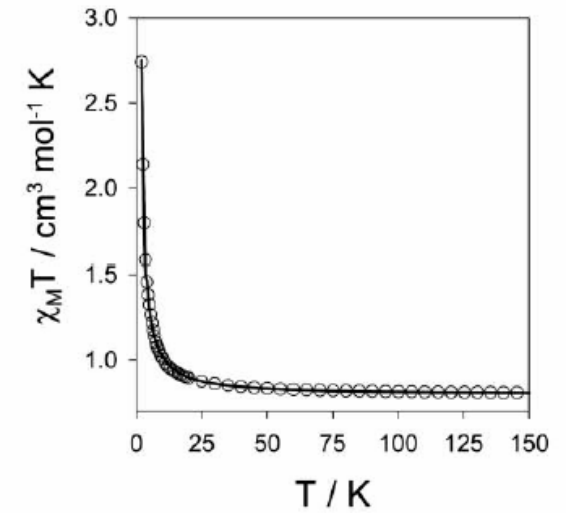

Figure 16. Thermal dependence of the $\chi_M T$ product in **6** $\{[Cu(H_2O)_3][Cu(mal)_2(H_2O)]\}_n$: (o) experimental data; (-) best fit curve (see text).

The structure of compound **6** consist of alternating chains of malonate-bridged copper(II) ions. The carboxylate groups exhibit the equatorial-equatorial (J_1) and the equatorial-apical (J_2) orientations. The spin Hamiltonian corresponding to such a system is:

$$\hat{H} = \sum_i -\left[J_1(\hat{S}_{2i} \cdot \hat{S}_{2i-1}) + J_2(\hat{S}_{2i} \cdot \hat{S}_{2i+1})\right] \qquad (3)$$

The best fit of the magnetic data leads to $J_1 = +3.0$ cm^{-1} and $J_2 = +1.9$cm^{-1}. The J_1 value can be explained on the basis of the angle between the basal planes of the copper(II) ions ($\delta = 85.9^{\circ}$), very close to the orthogonality, 90º. J_2 can be understood regarding the small overlap between the magnetic orbitals in the equatorial-apical orientation of the carboxylate bridge (strict orthogonality) see the following scheme.

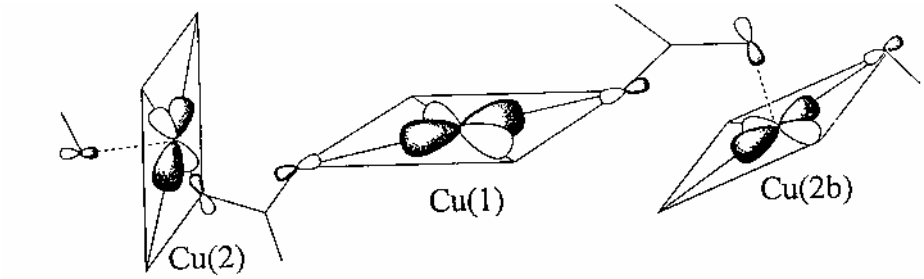

Antiferromagnetism.

The antiferromagnetic interaction is much more frequent than the ferromagnetic one, but in malonato-complexes this latter seems to be dominant, nevertheless some malonato-complexes exhibit antiferromagnetic coupling. One of those compounds is the dinuclear Ni(II) complex of formula $[(tren)Ni(\mu\text{-}mal)Ni(tren)(H_2O)](ClO_4)_2 \cdot 3H_2O$ (**17**) [Sanchiz J. *et al.*, 2005].

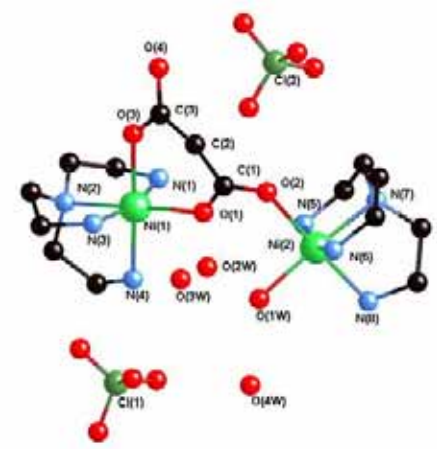

Figure 16. Molecular structure and atomic labels for $[(tren)Ni(\mu\text{-}mal)Ni(tren)(H_2O)](ClO_4)_2 \cdot 3H_2O$. Hydrogen atoms and the labels of the tren-carbons and perchlorate-oxygens have been omitted for clarity.

Its structure consist of $[(tren)Ni(\mu\text{-}mal)Ni(H_2O)(tren)]^{2+}$ cations, ClO_4^- anions and crystallization water molecules held together by means of hydrogen bonds. The *tren* groups act as blocking ligands whereas the malonate bridges two non-equivalent Ni(II) ions, acting simultaneously as bidentate [towards Ni(1)] and monodentate [towards to Ni(2)] ligand. The bridging carboxylate group exhibits the *anti-syn* coordination mode.

The thermal dependence of $\chi_M T$ [χ_M being the magnetic susceptibility *per* two nickel(II) ions] is shown in Figure 17. On cooling, $\chi_M T$ decreases smoothly up to 30 K and then, it rapidly falls to reach a value of 1.52 $cm^3\ mol^{-1}$ K at 1.8 K. This indicates the occurrence of a weak antiferromagnetic intramolecular interaction and/or a single-ion zero-field splitting of the Ni(II) ions (D). The result of the least-squares fit through the corresponding theoretical expression is $g = 2.175(3)$, $J = -0.20(2)\ cm^{-1}$, $D = 4.6(4)\ cm^{-1}$ and $R = 1.04 \times 10^{-4}$.

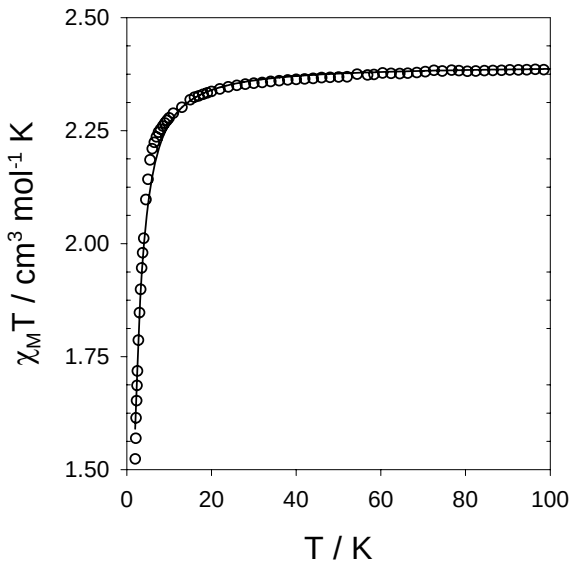

Figure 17. Thermal dependence of the $\chi_M T$ product of **17**: (o) experimetal data; (-) best fit curve (see text).

The value obtained for g and *D* lie within the range observed for the previously reported similar Ni(II) complexes [Ginsberg *et al.*, 1972; Duggan *et al.*, 1974; Vermaas *et al.*, 1977; De Munno *et al.*, 1993; Roman *et al.*, 1996; Calatayud *et al.*, 1996]. It is clear that the efficiency of the carboxylate group in the *anti-syn* bridging mode is drastically reduced compared to other related compounds in which the Ni(II) ions are bridged in the *anti-anti* mode (Scheme 1), such as in the bis-bidentate oxalate complexes.

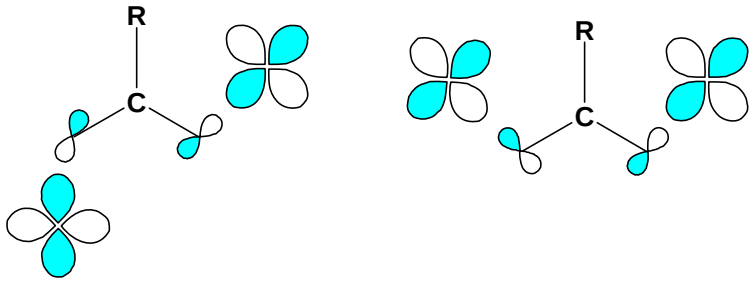

syn-anti *anti-anti*

The reduction of the intensity can be explained in terms of the contributions of the 2*p* oxygen orbitals belonging to the magnetic orbitals centered on the metal ions, which are much more favourably oriented to give an effective overlap in the *anti-anti* than in the *anti-syn* conformation.

Ferrimagnetism

Malonato-bridged bimetallic one-dimensional systems are good examples of ferrimagnetism. In the compound $[Mn^{II}Cu^{II}(mal)_2(H_2O)_3]\cdot 2H_2O$ [Ruiz-Pérez C. et al.,

2000c] an antiferromagnetic coupling takes place between the S = 5/2 Mn(II) and the S = 1/2 Cu(II) ions. Due to the different size of the respective spins, even exhibiting an antiferromagnetic coupling, the solid has got a net paramagnetic spin.

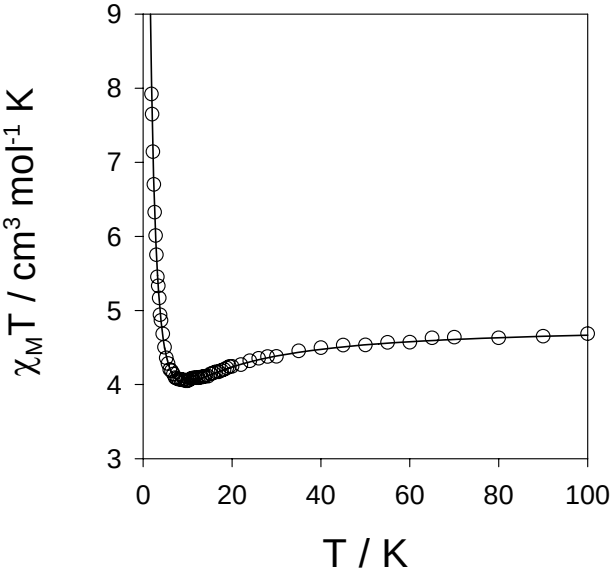

Figure 18. Thermal dependence of $\chi_M T$ product in **11** $[Mn^{II}Cu^{II}(mal)_2(H_2O)_3]\cdot 2H_2O$: (o) experimental data; (-) best fit curve.

The magnetic behavior in the form of the $\chi_M T$ versus T plot for **11** [χ_M being the magnetic susceptibility per copper(II) and mangense(II) ion] is shown in Figure 18. The minimum observed for the χT curve is typical in the ferrimagnetic compounds. The least-squares fitting of the data through the appropriate expression leads to J_{MnCu} = -4.5 cm^{-1}.

Spin canting

Spin canting, with T_c = 2.7 K, occurs in the sheet-like polymer $[Mn(mal)(H_2O)_2]_n$ (**13**). The structure of $[Mn(mal)(H_2O)_2]_n$ consist of high planarity layers of *trans*-diaquamanganese(II) units bridged by carboxylate-malonate groups in the *anti-anti* and *anti-syn* coordination modes (Figure 19).

Four carboxylate-oxygens from three malonate ligands fill the equatorial positions. The Mn···Mn interlayer distance is [5.421(2) Å] and the Mn···Mn separations through the *anti-anti* and *anti-syn* carboxylate bridges are 6.275(3) and 5.828(2) Å, respectively.

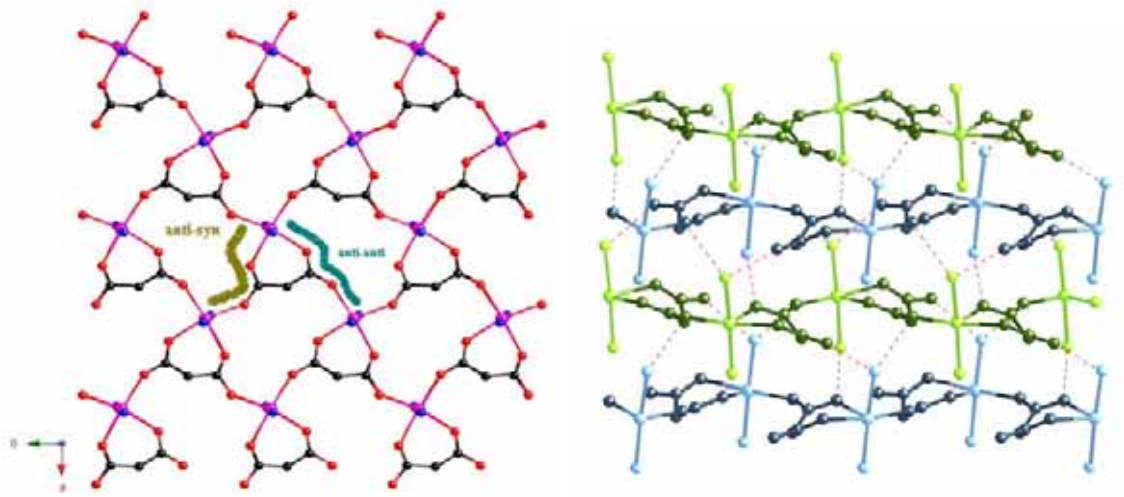

Figure 19. Perspective view, along the *c*-axis, of the layers of *trans*-diaquamanganese(II) units bridged by carboxylate-malonate groups in the *anti-anti* and *anti-syn* coordination modes **(a)** and view, along the *b*-axis, of a fragment of these layers held together by means of hydrogen bonds **(b)** in **13**.

The thermal dependence of the $\chi_M T$ product for $[Mn(mal)(H_2O)_2]_n$ [χ_M being the magnetic susceptibility per manganese(II) ion] is shown in Figure 20.

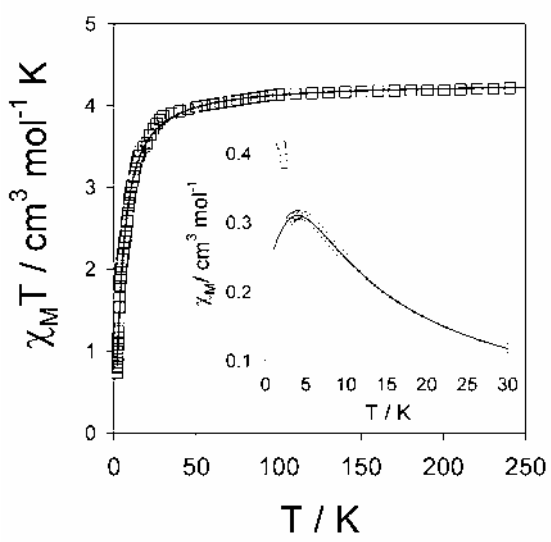

Figure 20. Thermal dependence of $\chi_M T$ product for $[Mn(mal)(H_2O)_2]_n$ (**13**): (□) experimental data; (-) best fit curve.

At room temperature, the value of the $\chi_M T$ product is equal to 4.30 cm^3 mol^{-1} K, a value which is as expected for a magnetically isolated manganese(II) ion (g = 2, S = 5/2). The $\chi_M T$ curve smoothly decreases on cooling, and below 100 K it decreases more rapidly. The susceptibility curve (see insert of Figure 20) shows a maximum at 4.3 K, and below 2.7 K it increases abruptly deviating from the theoretical curve. This behaviour is characteristic of a spontaneous moment due to the spin canting. Consequently, the compound exhibits a long range magnetic ordering below 2.7 K. The

spin canting takes place when the spins are not perfectly cancelled leading to a net magnetic moment. The spin canting can arise from (a) single-ion local anisotropy and/or (b) antisymmetric exchange [Dzyaloshinski J., 1958; Moriya T., 1960]

Given that six-coordinated Mn(II) has a the $^6A_{1g}$ ground state (state with a high isotropic character), the antisymmetric exchange must be responsible for the spin canting observed in $[Mn(mal)(H_2O)_2]_n$. The acentric character of the $Pca2_1$ space group of $[Mn(mal)(H_2O)_2]_n$ accounts for the occurrence of a spin canted structure for this compound. Although an antiferromagnetic interaction takes place among the Mn(II) ions, the absence of an inversion centre in the space group does not lead to a complete annulment of the spins and the solid has a non-cero magnetic moment.

References

Allen F.H. *Acta Cryst., Sect. B*, **2002**, 58, 380.

Bimitrova G.I., Ablov A.V., Kiosse G.A., Popovich G.A., Nmalinouskii T.I. and Bourshteyn I. F., *Dokl, Akad. Nauk SSSR*, **1974**, 216, 1055.

Calatayud M.L., Castro I., Sletten J., Cano J., Lloret F., Faus J., Julve M., Seitz G. and Mann K., *Inorg. Chem.*, **1996**, *35*, 2858.

Chattopadhyay D., Chattopadhyay S.K., Lowe P.R., Schwalde C.H., Mazumder S.K., Rana A. and Ghosh S., *J. Chem. Soc., Dalton Trans*., **1993**, 913.

De Munno G., Julve M., Lloret F., Derory A., *J. Chem. Soc., Dalton Trans*., **1993**, 1179.

Dzyaloshinski J., *J. Phys. Chem. Solids,* **1958**, 4, 241.

Duggan D.M., Barefield E.K. and Hendrickson D.N., *Inorg. Chem.* **1974**, 13, 2056.

Ginsberg A.P., Martín R.L., Brookes R.W. and Sherwood R.C., *Inorg. Chem.*, **1972**, 11, 2884.

Hernández-Molina M., Lorenzo-Luis P.A. and Ruiz-Pérez C., *CrystEngComm*, **2001a**, 3, 60.

Hernández-Molina M., Lorenzo-Luis P.A., Ruiz-Pérez C., Lloret F. and Julve M., *Inorg. Chim. Acta*, **2001b**, 313, 87.

Hornick C., Rabu P. and Drillon M., *Polyhedron*, **2000**, 19, 259.

Kahn O., *Comments Cond. Mat. Phys.*, **1994**, 17, 39-58.

Kahn O., *The Enciclopedia of Advanced Materials.*, Pergamon. **1994**. pp1665-1673.

Kwik W.-L., Ang K.-P. and Chan H.S.-O., *J. Chem. Soc., Dalton Trans*., **1986**, 2519.

Lightfoot P. and Snedden A., *J. Chem. Soc., Dalton Trans.*, **1999**, 3549.

Lis T. and Matuszewski J., *Acta Cryst*., **1979**, B35, 2212.

Mercury, version 1.3, Crystal Structure Visualization Program, Copyright CCDC 2001-2004.

Miller J.S. and Epstein. A. J., *Angew. Chem. Int. Ed. Engl.*, **1994**, 33, 385.

Moriya T., *Phys. Rev.,* **1960**, 120, 91.

Pei Y., Journaux Y. and Kahn. O., *Inorg. Chem.*, **1989**, 28, 100.

Rabu P., Rueff J.M., Huang Z.L., Angelov S., Souletie J. and Drillon M., *Polyhedron*, **2001**, 20, 1677.

Ray N.J. and Hathaway B.J., *Acta Cryst.*, **1982**, B38, 770.

Rodríguez-Martín Y., Sanchiz J., Ruiz-Pérez C., Lloret F. and Julve M., *Inorg. Chim. Acta*, **2001a**, 326, 20.

Rodríguez-Martín Y., Ruiz-Pérez C., Sanchiz J., Lloret F. and Julve M., *Inorg. Chim. Acta*, **2001b**, 318, 159.

Rodríguez-Martín Y., Hernández-Molina M., Delgado F.S., Pasán J., Ruiz-Pérez C., Sanchiz J., Lloret F. and Julve M., *CrystEngComm*, **2002a**, 4, 440.

Rodríguez-Martín Y., Sanchiz J., Ruiz-Pérez C., Lloret F. and Julve M., *CrystEngComm*, **2002b**, 4, 631.

Rodríguez-Martín Y., Hernández-Molina M., Sanchiz J., Ruiz-Pérez C., Lloret F. and Julve M., *Dalton Trans.*, **2003**, 2359.

Roman P., Guzmán-Miralles C., Luque A., Beitia J.I., Cano J., Lloret F., Julve M. and Alvarez S., *Inorg. Chem*. **1996**, *35*, 3741.

Ruiz-Pérez C., Sanchiz J., Hernández-Molina M., Lloret F. and M. Julve, *Inorg. Chem.*, **2000a**, 39, 1363.

Ruiz-Pérez C., Hernández-Molina M., Lorenzo-Luis P.A., Lloret F. and Julve M. *Inorg. Chem.*, **2000b**, 39, 3845.

Ruiz-Pérez C., Sanchiz J., Hernández-Molina M., Lloret F. and Julve M., *Inorg. Chim. Acta*, **2000c**, 298, 202.

Sanchiz J., Rodríguez-Martín Y., Ruiz-Pérez C., Mederos A., Lloret F. and Julve M., *New J. Chem.*, **2002**, 26, 1624.

Sanchiz J., Rodríguez-Martín Y., Hernández-Molina M., Ruiz-Pérez C., Lloret F. and Julve M., **2005***, article in preparation.*.

Veciana J., Rovira C. and Amabilino D.B., *Supramolecular Engineering of Synthetic Metallic Materials*. NATO ASI Series, **1998**, Vol. 518.

Vermaas A., Groeneveld W. L. and Reedijik J., *Naturforsch* **1977**, A32, 632.

Vista, version 2.3.8, Statistical Analysis and Display of Geometric Data, Copyright CCDC 1994-2002.

References for the Malonate-Containing Homometallic Complexes

Homometallic Malonate-Containing Copper(II) Complexes

Scheme 1

Chattopadhyay D., Chattopadhyay S.K., Lowe P.R., Schwalbe C.H., Mazumder S.K., Rana A. and Ghosh S., *J.Chem.Soc.,Dalton Trans.*, **1993**, 913.

Chawla S.K., Arora M., Nattinen K., Rissanen K. and Yakhmi J.V., *Polyhedron*, **2004**, 23, 3007.

Cui G.-H., Li J.-R., Hu T.-L. and Bu X.-H., *J. Mol. Struct.*, **2005**, 738, 183.

Filippova I.G., *Koord.Khim.(Russ.)(Coord.Chem.)*, **2000**, 26, 295.

Filippova I.G., Kravtsov V.Kh. and Gdanets M., *Koord. Khim. (Russ.)(Coord. Chem.)*, **2000**, 26, 860.

Gasque L., Moreno-Esparza R., Mollins E., Brianso-Penalva J.L., Ruiz-Ramirez L. and Medina-Dickinson G., *Acta Cryst.,Sect. C*, **1998**, 54, 1848.

Gasque L., Moreno-Esparza R., Mollins E., Brianso-Penalva J.L., Ruiz-Ramirez L. and Medina-Dickinson G., *Acta Cryst.,Sect. C*, **1999**, 55, 158.

Hay R.W., Danby A. and Lightfoot P., *Polyhedron*, **1997**, 16, 3261.

Kawata S., Kitagawa S., Machida H., Nakamoto T., Kondo M., Katada M., Kikuchi K. and Ikemoto I., *Inorg. Chim. Acta*, **1995**, 229, 211.

Kwik W.-L., Ang K.-P., Chan H.S.-O., Chebolu V. and Koch S.A., *J. Chem. Soc., Dalton Trans.*, **1986**, 2519.

Lin Z.-Z., Jiang F.-L., Chen L. and Hong M.-C., *Jiegou Huaxue (Chin.)(Chinese J. Struct. Chem.)*, **2004**, 23, 993.

Naumov P., Ristova M., Soptrajanov B., Drew M.G.B. and Ng S.W., *Croat. Chem. Acta*, **2002**, 75, 701.

Pajunen A. and Nasakkala E., *Finn. Chem. Lett.*, **1977**, 189.

Rodríguez-Martín Y., Sanchiz J., Ruiz-Pérez C., Lloret F. and Julve M., *Inorg. Chim. Acta*, **2001**, 326, 20.

Rodríguez-Martín Y., Sanchiz J., Ruiz-Pérez C., Lloret F. and Julve M., *CrystEngComm.*, **2002**, 4, 631.

Ruiz-Pérez C., Sanchiz J., Hernández-Molina M., Lloret F. and Julve M., *Inorg. Chem.* **2000**, 39, 1363.

Shen H.-Y., Bu W.-M., Liao D.-Z., Jiang Z.-H., Yan S.-P. and Wang G.-L., *Inorg. Chem. Comm.*, **2000**, 3, 497.

Sieron L., *Acta Cryst., Sect. E*, **2004**, 60, m297.

Suresh E. and Bhadbhade M.M., *Acta Cryst. ,Sect.C* ,**1997**, 53, 193.

Xiong Y., Tong M., An T. and Karlsson H.T., *Acta Cryst., Sect. C*, **2001**, 57, 1385.

Yilmaz V.T., Senel E. and Thone C., *Transition Met. Chem.*, **2004**, 29, 336.

Yilmaz V.T., Senel E. and Kazak C., *Solid State Sciences*, **2004**, 6, 859.

Zhao W., Fan J., Okamura T., Sun W.-Y. and Ueyama N., *New J. Chem.(Nouv. J. Chim.)*, **2004**, 28, 1142.

Scheme 2

Konar S., Mukherjee P.S., Drew M.G.B., Ribas J. and Chaudhuri N.R., *Inorg. Chem.*, **2003**, 42, 2545.

Ruiz-Pérez C., Sanchiz J., Hernández-Molina M., Lloret F. and Julve M., *Inorg. Chem.*, **2000**, 39, 1363.

Tosik A., Sieron L. and Bukowska-Strzyzewska M., *Acta Cryst., Sect. C*, **1995**, 51, 1987.

Yilmaz V.T., Senel E. and Thone C., *Transition Met. Chem.*, **2004**, 29, 336.

Scheme 3

Chattopadhyay D., Chattopadhyay S.K., Lowe P.R., Schwalbe C.H., Mazumder S.K., Rana A. and Ghosh S., *J. Chem. Soc., Dalton Trans.*, **1993**, 913.

Filippova I.G., Kravtsov V.Kh. and Gdanets M., *Koord. Khim. (Russ.)(Coord. Chem.)*, **2000**, 26, 860.

Naumov P., Ristova M., Soptrajanov B., Drew M.G.B. and Ng S.W., *Croat. Chem. Acta*, **2002**, 75, 701.

Ruiz-Pérez C., Sanchiz J., Hernández-Molina M., Lloret F. and Julve M., *Inorg. Chem.* **2000**, 39, 1363.

Sanchiz J., Rodríguez-Martín Y., Ruiz-Pérez C., Mederos A., Lloret F. and Julve M., *New J. Chem. (Nouv. J. Chim.)*, **2002**, 26, 1624.

Yilmaz V.T., Senel E. and Kazak C., *Solid State Sciences*, **2004**, 6, 859.

Scheme 4

Pajunen A. and Nasakkala E., *Finn. Chem. Lett.*, **1977**, 100.

Scheme 5

Rodríguez-Martín Y., Ruiz-Pérez C., Sanchiz J., Lloret F. and Julve M., *Inorg. Chim. Acta*, **2001**, 318, 159.

Scheme 7

Bie H.-Y., Yu J.-H., Zhao K., Lu J., Duan L.-M. and Xu J.-Q., *J. Mol. Struct.*, **2005**, 741, 77.

Liu T.-F., Sun H.-L., Gao S., Zhang S.-W. and Lau T.-C., *Inorg. Chem.*, **2003**, 42, 4792

Yilmaz V.T., Senel E. and Thone C., *Transition Met. Chem.*, **2004**, 29, 336.

Scheme 8

Liu T.-F., Sun H.-L., Gao S., Zhang S.-W. and Lau T.-C., *Inorg. Chem.*, **2003**, 42, 4792.

Liu Q., Li Y.-Z., Song Y., Liu and Xu Z., *J. Solid State Chem.*, **2004**, 177, 4701.

Sain S., Maji T.K., Mostafa G., Lu T.-H. and Chaudhuri N.R., *New J. Chem. (Nouv. J. Chim.)*, **2003**, 27, 185.

Zhang X., Lu C., Zhang Q., Lu S., Yang W., Liu J. and Zhang H., *Eur. J. Inorg. Chem.*, **2003**, 1181.

Zheng Y.-Q. and Ying E.-B., *J. Coord. Chem.*, **2005**, 58, 453.

Scheme 9

Ruiz-Pérez C., Hernández-Molina M., Lorenzo-Luis P., Lloret F., Cano J. and Julve M., *Inorg. Chem.*, **2000**, 39, 3845.

Homometallic Malonate-Containing Cobalt(II) Complexes

Scheme 1

Lin D.-D., Liu Y. and Xu D.-J., *Acta Cryst.,Sect. E*, **2003**, 59, m771.

Wang X.-D., Li L.-C., Liao D.-Z., Jiang Z.-H., Yan S.-P. and Cheng P., *J. Coord. Chem.*, **2004**, 57, 1577.

Scheme 8

Konar S., Mukherjee P.S., Drew M.G.B., Ribas J. and Chaudhuri N.R., *Inorg. Chem.*, **2003**, 42, 2545.

Lightfoot P. and Snedden A., *J. Chem. Soc., Dalton Trans.*, **1999**, 3549.

Xue Y.-H., Lin D.-D. and Xu D.-J., *Acta Cryst.,Sect. E*, **2003**, 59, m750.

Zheng Y.-Q. and Xie H.-Z., *J. Coord. Chem.*, **2004**, 57, 1537.

Homometallic Malonate-Containing Manganese(II) Complexes

Scheme 1

Sain S., Maji T.K., Mostafa G., Lu T.-H. and Chaudhuri N.R., *Inorg. Chim. Acta*, **2003**, 351, 12.

Shen L., *Acta Cryst.,Sect. C*, **2003**, 59, m128.

Wang Z.-X., Zhou X.-H., Yu W.-T. and Fu Y.-J., *Z. Kristallogr.-New Cryst. Struct.*, **2000**, 215, 423.

Zhang Q.-Z. and Lu C.-Z., *Acta Cryst., Sect. E*, **2004**, 60, m1778.

Scheme 3

Sain S., Maji T.K., Mostafa G., Lu T.-H. and Chaudhuri N.R., *Inorg. Chim. Acta*, **2003**, 351, 12.

Wei Y.-G., Zhang S.-W., Shao M.-C., Liu Q. and Tang Y.-Q., *Polyhedron*, **1996**, 15, 4303.

Scheme 7

Lis T. and Matuszewski J. Acta Cryst., Sect .B, **1979**, 35, 2212.

Scheme 8

Konar S., Manna S.C., Zangrando E., Mallah T., Ribas J. and Chaudhuri N.R., *Eur. J. Inorg. Chem.*, **2004**, 4202.

Liu Q., Li B., Xu Z., Sun X., Yu K.-B. and Li Y.-Z. *J. Coord. Chem.*, **2003**, 56, 771.

Maji T.K., Sain S., Mostafa G., Lu T.-H., Ribas J., Monfort M. and Chaudhuri N.R., *Inorg. Chem.*, **2003**, 42, 709.

Rodríguez-Martín Y., Hernández-Molina M., Sanchiz J., Ruiz-Pérez C., Lloret F. and Julve M., *Dalton Trans.*, **2003**, 2359.

Zheng Y.-Q. and Ying E.-B., *J. Coord. Chem.*, **2005**, 58, 453.

Homometallic Malonate-Containing Nickel(II) Complexes

Scheme 1

Liu J.-G. and Xu D.-J., *Acta Cryst., Sect. E*, **2004**, 60, m541.

Wang X.-D., Li L.-C., Liao D.-Z., Jiang Z.-H., Yan S.-P. and Cheng P., *J. Coord. Chem.*, **2004**, 57, 1577.

Scheme 8

Zheng Y.-Q. and Xie H.-Z., *J. Coord. Chem.*, **2004**, 57, 1537.

Homometallic Malonate-Containing Zinc(II) Complexes

Scheme 1

Zhao W., Fan J., Okamura T., Sun W.-Y. and Ueyama N., *J. Solid State Chem.*, **2004**, 177, 2358.

Scheme 6

Burrows A.D., Harrington R.W., Mahon M.F. and Price C.E., *J. Chem. Soc., Dalton Trans.*, **2000**, 3845.

Zhang Y., Li J., Chen J., Su Q., Deng W., Nishiura M., Imamoto T., Wu X. and Wang Q., *Inorg. Chem.*, **2000**, 39, 2330.

Scheme 8

Liu Q., Li Y.-Z., Song Y., Liu H. and Xu Z., *J. Solid State Chem.*, **2004**, 177, 4701.

Zhang X., Lu C., Zhang Q., Lu S., Yang W., Liu J. and Zhang H., *Eur. J. Inorg. Chem.*, **2003**, 1181.

PART I: COPPER(II) MALONATE COMPLEXES

CHAPTER I. The protonated malonate: the influence of hydrogen bonds on the magnetic behaviour.

CHAPTER II. Network formation and magnetic behaviour of Copper(II)malonate anions in alkali salts.

CHAPTER III. Network formation and magnetic behaviour of Copper(II)malonate anions in ammonium salts.

CHAPTER IV. Supramolecular networks in Copper(II) malonate complexes.

CHAPTER V. From 1D to 3D networks: the use of a ligand to control the crystal structure.

CONCLUSIONS

CHAPTER I.

The protonated malonate: the influence of hydrogen bonds on the magnetic behaviour.

Introduction

Recent years have witnessed an explosion of interest in both molecule-based magnetism and supramolecular chemistry. In the former field, the concept of the "magnetic brick" is widely applied to the description of the structures and magnetic characteristics of these materials. In the latter field, the idea of the "synthon" finds favour. A natural progression is to combine these two concepts and create supramolecular organised molecular magnets. In order to explore this idea we have chosen the flexible malonate ligand (dianion of 1,3-propanedioic acid, H_2mal) which provides several possibilities in creating supramolecular architectures, namely hydrogen bonding and bridging between "bricks" *via* carboxylate groups. In particular for some Cu(II)-containing coordination compounds it has been shown that the variation of possible supramolecular interactions can substantially influence the properties of the related coordination polymers [Kahn O. *et al.*, 1988; Larionova J. *et al.*, 1997; Plass W. *et al.*, 2001; Desplanches C. *et al.*, 2002a; Desplanches C. *et al.*, 2002b].

Over the past few years, our efforts have been focused on the use of malonate ligand in the control of molecular architectures with magnetic properties [Rodríguez-Martín Y. *et al.*, 2002; Ruiz-Pérez C. *et al.*, 2003; Pasán J. *et al.*, 2003a]. In this context, new perspectives are opened when malonate ligand is partially or totally protonated. Three new compounds containing different anionic malonate species (the neutral H_2mal, the monoanionic $Hmal^-$ and the dianionic mal^{2-}) were prepared and their crystal structures and magnetic properties were investigated. These compounds are interesting because they allow us to illustrate the influence of the hydrogen bonding interactions on the magnetic properties (even in mononuclear complexes).

In our current research work, we have obtained several structural motifs with copper(II) and malonate ions, but the highest dimensionality obtained was only one [Ruiz-Pérez C. *et al.*, 2000]. We were able to prepare two new high-dimensional copper(II)-malonate compounds containing protonated malonate ions: $[Cu(H_2O)(H_2mal)(mal)]$ (**2**) and (**3**). In this way, we increased the dimensionality without adding a new ligand. Also the magnetic properties of the three compounds are investigated and analysed.

Experimental

Materials and methods

Malonic acid, copper(II) chloride dihydrate, copper(II) nitrate trihydrate, sodium hydroxide, pyridine, THF (tetrahydrofurane) and absolute ethanol were purchased from commercial sources and used as received. Elemental analyses (C, H) were performed on a EA 1108 CHNS-O microanalytical analyzer. Magnetic susceptibility measurements on polycrystalline samples of compounds **1-3** were carried out with a Quantum Design SQUID magnetometer. Diamagnetic corrections for the constituent atoms were estimated from Pascal's constants [Earnshaw A., 1968] as -101×10^{-6} cm^3 mol^{-1} for **1** and -108×10^{-6} cm^3 mol^{-1} for compounds **2** and **3**. Experimental susceptibilities were also corrected for the temperature-independent paramagnetism [60 x 10^{-6} cm^3 mol^{-1} per Cu(II) ion] and the magnetization of the sample holder.

Synthesis

[Cu(Hmal)$_2$] (1). Malonic acid (2 mmol, 0.108 g) is added to an ethanolic solution (15 cm^3) of copper(II) chloride (2 mmol, 0.341 g) under continuous stirring. To this solution pyridine (1 mmol, 0.079 g) in THF solution (5 cm^3) is added. Single crystals of **1** were grown after 3 days as light blue prisms. Yield: 45%. Anal. Calcd. for $C_6O_8H_6Cu$: C, 26.71; H, 2.22. Found: C, 26.55; H, 2.31%.

[Cu(H$_2$O)(H$_2$mal)(mal)] (2). Malonic acid (2 mmol, 0.108 g) is added to an aqueous solution (40 cm^3) of copper(II) chloride (2 mmol, 0.341 g) under continuous stirring. To this solution an ethanolic solution (5 cm^3) of pyridine (1 mmol, 0.079 g) is added. Single crystals of **2,** as light blue prisms, were grown after a week. Yield: 40%. Anal. Calcd. for $C_6O_9H_8Cu$: C, 25.02; H, 2.78. Found: C, 25.15; H, 2.91%.

[Cu(H$_2$O)(H$_2$mal)(mal)] (3). Malonic acid (2 mmol, 0.108 g) is added to an aqueous solution (40 cm^3) of copper(II) nitrate (2 mmol, 0.483 g) under continuous stirring. To this solution an aqueous solution (10 cm^3) of sodium hydroxide (2 mmol, 0.080 g) is added under stirring. After two weeks, single crystals of **3** as light blue prisms were obtained together with a green powder material that was discarded. Yield: 5%. Anal. Calcd. for $C_6O_9H_8Cu$: C, 25.02; H, 2.78. Found: C, 25.12; H, 2.85%.

Crystal data collection and refinement

Single crystals of three compounds were mounted on a Bruker-Nonius KappaCCD diffractometer. Orientation matrix and lattice parameters were obtained by least-squares refinement of the reflections obtained by a θ-χ scan (Dirax/lsq method). Diffraction data for all compounds were collected at 293(2) K using graphite-monochromated Mo-K_α radiation (λ = 0.71073 Å). A summary of the crystallographic data and structure refinement is given in Table 1. The indexes of data collection were -7 ≤ h ≤ 9, -13 ≤ k ≤ 13, -16 ≤ l ≤ 17 for **1**; -6 ≤ h ≤ 9, -12 ≤ k ≤ 11, -19 ≤ l ≤ 21 for **2** and -12 ≤ h ≤ 8, -19 ≤ k ≤ 19, -14 ≤ l ≤ 21 for **3**. Of the 1127 (**1**), 2647 (**2**) and 2657 (**3**) measured independent reflections in the θ range 6.43 – 30º (**1**), 6.54 - 30º (**2**) and 6.42 – 30º (**3**), 879 (**1**), 2336 (**2**) and 1848 (**3**) have $I \geq 2\sigma(I)$. All the measured independent reflections were used in the analysis. All calculations for data reduction, structure solution, and refinement were done by standard procedures (WINGX) [Farrugia, L.J., 1999]. The structure was solved by direct methods and refined with full-matrix least-squares technique on F^2 using the SHELXS-97 and SHELXL-97 programs [Sheldrick, G.M. SHELX97, realease 97-2, 1998], respectively. The malonate and water molecules hydrogen atoms were located from difference Fourier maps and refined with isotropic temperature factors. The final Fourier-difference map showed maximum and minimum height peaks of 0.385 and -0.491 e $Å^{-3}$, 0.369 and -0.543 e $Å^{-3}$ and 0.459 and -0.504 e $Å^{-3}$, for **1**, **2** and **3**, respectively. The final geometrical calculations and the graphical manipulations were carried out with PARST97 [Nardelli M., 1995] and CRYSTAL MAKER [CRYSTAL MAKER 4.2.1, 2001] programs, respectively.

Crystal structures were deposited at the Cambridge Crystallographic Data Centre and the CCDC reference numbers are 237206 (**1**), 237207 (**2**), 237208 (**3**).

Table 1. Crystal data and details of structure determination for compounds **1-3**

Compound	**1**	**2**	**3**
Formula	$C_6H_6CuO_8$	$C_6H_8CuO_9$	$C_6H_8CuO_9$
M	269.64	287.66	287.66
Crystal system	orthorhombic	orthorhombic	orthorhombic
Space group	*P*bca	$P2_12_12_1$	*P*bca
a, Å	6.7424(5)	7.0880(10)	8.6409(11)
b, Å	9.3819(5)	8.767(2)	14.0972(10)
c, Å	12.4519(10)	15.147(3)	15.148(2)
V, Å^3	787.66(10)	941.2(3)	1845.2(3)
Z	4	4	8
T, K	293(2)	293(2)	293(2)
ρ_{calc} (Mg m^{-3})	2.274	2.030	2.071
F(000)	540	580	1160
λ (Mo-K$_\alpha$ Å)	0.71073	0.71073	0.071073
μ (Mo-K$_\alpha$, mm^{-1})	2.800	2.357	2.405
Extinction coefficient	0.153(5)	-	-
Number parameters/restraints	84 / 0	166 / 0	177 / 0
Goodness of fit (*S*)	1.074	1.077	1.035
R1, $I > 2\sigma(I)$ (all)	0.0278 (0.0419)	0.0330 (0.0416)	0.0411 (0.0753)
wR2, $I > 2s(I)$ (all)	0.0645 (0.0697)	0.0708 (0.0742)	0.0760 (0.0695)
Max/min electron density (e/Å^3)	0.385 / -0.491	0.369 / -0.543	0.459 / -0.504
Measured reflections (R_{int})	7201 (0.0377)	7373 (0.0673)	10712 (0.0587)
Independent reflections [$I > 2\sigma(I)$]	1127 (879)	2647 (2336)	2657 (1848)

Results and Discussion

Description of the structure of $[Cu(Hmal)_2]$ (1)

Complex **1** consists of layers containing $[Cu(Hmal)_2]$ neutral units that grow in the *ab*-plane (see Figure 1). They are linked through hydrogen bonds leading to a three-dimensional network (Figure 2).

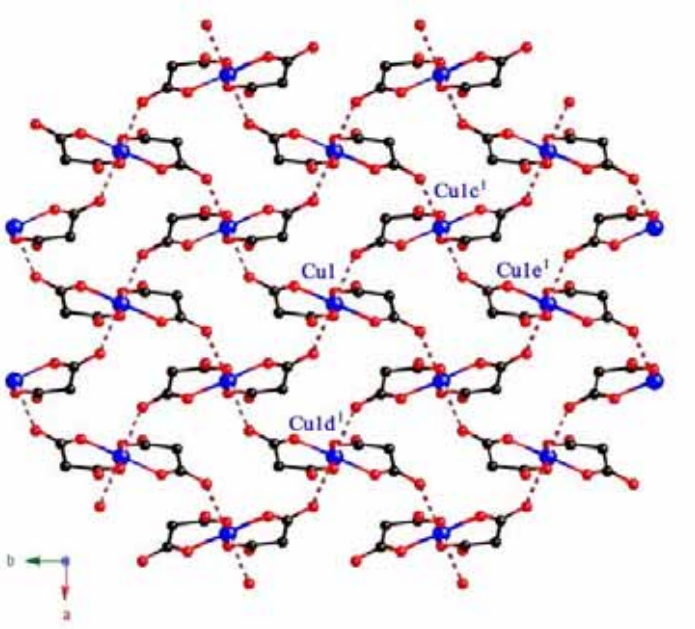

Figure 1. Perspective view, along the *c*-axis of a fragment of the hydrogen malonate-bridged layer of **1**. Apical bonds around copper(II) ions are drawn as broken lines.

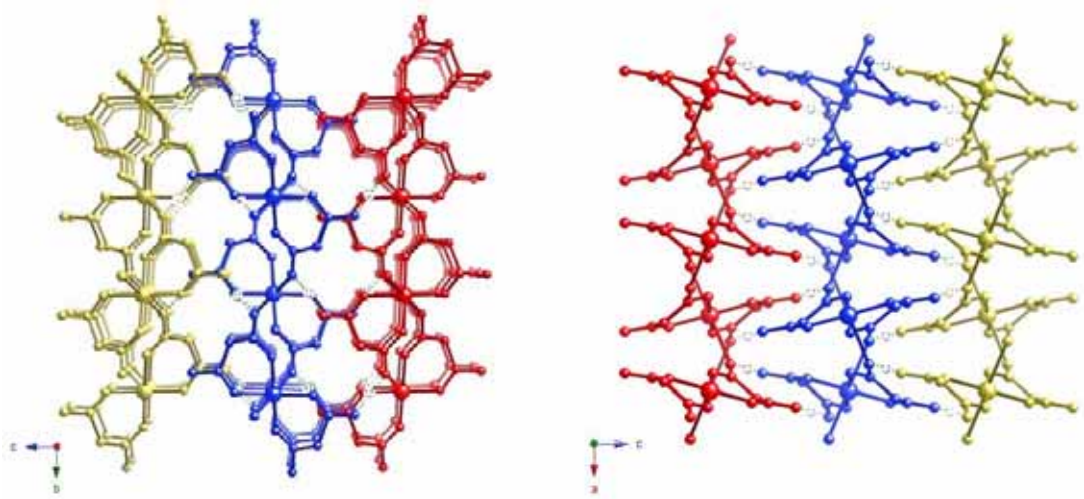

(a) **(b)**

Figure 2. (a) Perspective view of three adjacent layers of **1** down the *a*-axis. **(b)** Side view of three adjacent layers of **1** down the *b*-axis. Hydrogen bonds are drawn as broken lines.

Copper(II) ion lies on a $\bar{1}$ crystallographic site. Metal ion is six coordinated (see Figure 3) exhibiting a 4+2 elongated octahedral environment (ϕ = 54.1º and *s*/*h* = 1.474,

ϕ and *s/h* being the twist angle and compression ratio, respectively) [Stiefel E.I. *et al.*, 1972]. Four carboxylate-oxygen atoms from two different Hmal groups build the equatorial plane around Cu(1) [the mean bond distance being 1.9383(12) Å]. Whereas two carboxylate oxygen atoms from two Hmal units, occupy the apical positions of the metal ion [Cu(1)-O(apical) 2.5429(13) Å].

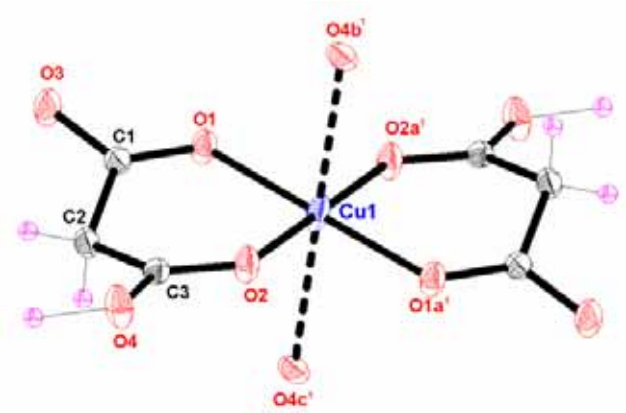

Figure 3. View of the metal environment in **1**. Thermal ellipsoids are drawn at the 50% probability level.

Table 2. Selected bond lengths (Å) and angles (º) for compound **1**[a]

Cu(1)-O(1)	1.9443(12)	Cu(1)-O(2)	1.9323(12)
Cu(1)-O(4b^1)	2.5429(13)	Cu(1)-O(4c^1)	2.5429(13)
O(1)-Cu(1)-O(2)	92.51(5)	O(1)-Cu(1)-O(2a^1)	87.49(5)
O(4b^1)-Cu(1)-O(1)	84.00(5)	O(4c^1)-Cu(1)-O(1)	96.00(5)
O(4b^1)-Cu(1)-O(2)	88.44(5)	O(4c^1)-Cu(1)-O(2)	91.56(5)
O(4b^1)-Cu(1)-O(1a^1)	96.00(5)	O(4c^1)-Cu(1)-O(1a^1)	84.00(5)
O(4b^1)-Cu(1)-O(2a^1)	91.56(5)	O(4c^1)-Cu(1)-O(2a^1)	88.44(5)

[a] The superscript indicates the compound which corresponds the symmetry code. Symmetry codes: (a^1) -*x*, -*y*+1, -*z*; (b^1) -*x*+1/2, *y*+1/2, *z*; (c^1) *x*-1/2, -*y*+1/2, -*z*.

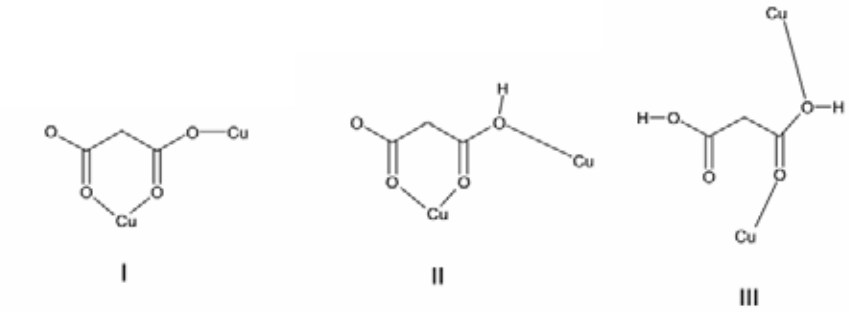

Scheme 1

Hmal$^-$ group (see Figure 3 and Scheme 1, II) acts simultaneously as bidentate [through O(1) and O(2) towards Cu(1)] and monodentate [through O(4) towards Cu(1)]. It has six membered-ring that exhibits a boat conformation with geometric values θ= 85.7(2)º, ϕ= 115.6(2)º [Cremer D. *et al.*, 1975]. The carboxylate-malonate groups

exhibit the *anti-syn* conformation and they connect an equatorial site of one copper atom with an apical position around an adjacent copper atom. The mean values of the C-C [1.499(2) Å] and C-O [1.256(2) Å] hydrogen malonate bond distances and O-C-O [121.73(15)º] bond angles agree well with those previously reported in other malonate-containing copper(II) complexes [see Introduction]. $Hmal^-$ group exhibits a coordination mode different from that observed in the reported copper(II) $Hmal^-$ compound [Lenstra A.T.H. *et al.*, 2001], where the ligand acts as bidentate towards the copper(II) ion.

Within the hydrogen malonate-bridged copper(II) layers one can distinguish tetranuclear units (see Figure 1). Each tetranuclear unit forms a 16-membered ring $[Cu-O-C-O-Cu]_4$ with the four copper(II) atoms located at the corners of a rhombus. Each copper(II) ion is linked to four other ones through *anti-syn* Hmal-carboxylate groups [the Cu···Cu distance being 5.7767(3) Å]. The shortest Cu···Cu separations within the layer are shown in Table 3.

Additional hydrogen bonds [O4···O($3f^{I}$) 2.447(2) Å; (f^{I}) *-x*, *y*-1/2, *-z*+1/2] lead to a three-dimensional network. Regarding the hydrogen bonds, the $[Cu(Hmal)_2]$ units build up a two-dimensional network that exhibits a (6,3) herringbone conformation (see Figure 4). The shortest copper···copper separations within the layer are shown in Table 3.

Table 3. Metal···Metal distances in **1**

Cu(1)···Cu($1c^{I}$)	5.7767(3)		
Cu(1)···Cu($1d^{I}$)	6.7424(5)	Cu(1)···Cu($1f^{I}$)	7.7953(4)
Cu(1)···Cu($1e^{I}$)	9.3819(5)	Cu(1)···Cu($1g^{I}$)	12.4519(10)

[a] Symmetry codes: (c^{I}) *x*-1/2, *-y*+1/2, *-z*; (d^{I}) *x*+1, *y*, *z*; (e^{I}) *x*, *y*-1, *z*; (f^{I}) *-x*, *y*-1/2, *-z*+1/2; (g^{I}) *x*, *y*, *z*-1

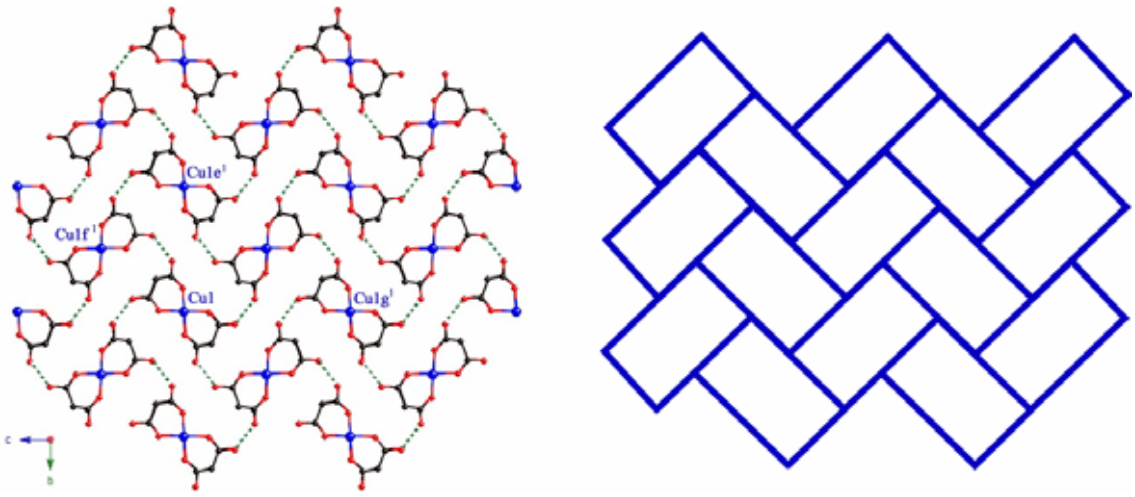

Figure 4. View, along the *a*-axis of a layer build-up from $[Cu(Hmal)_2]$ units through hydrogen bonds in compound **1**.

Description of the structure of [Cu(H$_2$O)(H$_2$mal)(mal)] (2 and 3)

Complexes **2** and **3** are polymorphous. Their structures consist of corrugated layers containing [Cu(H$_2$O)(H$_2$mal)(mal)] units linked by mal^{2-}-carboxylate groups in the *anti-syn* and H$_2$mal-carboxylate in the *anti-anti* bridging modes. These layers grow in the *ab*-plane (see Figure 5) and they exhibit intralayer and interlayer hydrogen bonds, the latter ones leading to a three-dimensional structure.

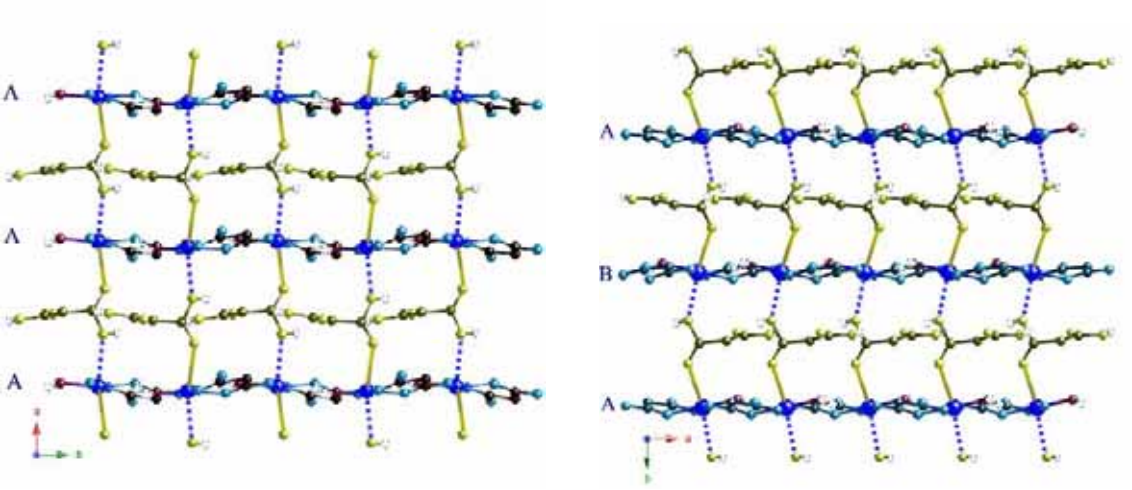

(a) **(b)**

Figure 5. View, along the *c*-axis, of a fragment of the malonate-bridged layer of **2** **(a)** and **3** **(b)**.

Main bond lengths and angles for compounds **2** and **3** are listed in Tables 4 and 5.

Table 4. Selected bond lengths (Å) and angles (º) for compound **2**

Cu(1)-O(1)	1.924(2)	Cu(1)-O(2)	1.933(2)
Cu(1)-O(4a^2)	1.956(2)	Cu(1)-O(1w)	1.943(2)
Cu(1)-O(11)	2.368(2)	Cu(1)-O(13b^2)	2.579(2)
O(1)-Cu(1)-O(2)	91.28(7)	O(4a^2)-Cu(1)-O(1w)	96.37(9)
O(1)-Cu(1)-O(4a^2)	175.14(8)	O(2)-Cu(1)-O(1w)	171.99(13)
O(1)-Cu(1)-O(1w)	87.11(8)	O(2)-Cu(1)-O(4a^2)	84.80(7)
O(11)-Cu(1)-O(1)	84.24(9)	O(13b^2)-Cu(1)-O(1)	82.96(8)
O(11)-Cu(1)-O(2)	86.57(9)	O(13b^2)-Cu(1)-O(2)	83.92(7)
O(11)-Cu(1)-O(4a^2)	98.36(9)	O(13b^2)-Cu(1)-O(4a^2)	93.75(8)
O(11)-Cu(1)-O(1w)	101.06(12)	O(13b^2)-Cu(1)-O(1w)	88.09(11)
O(11)-Cu(1)-O(13b^2)	163.85(7)		

[a] Symmetry codes: (a^2) -*x*, *y*-1/2, -*z*+1/2; (b^2) *x*-1, *y*, *z*

Table 5. Selected bond lengths (Å) and angles (º) for compound **3**

Cu(1)-O(1)	1.937(2)	Cu(1)-O(2)	1.906(2)
Cu(1)-O(3a^3)	1.953(2)	Cu(1)-O(1w)	1.958(2)
Cu(1)-O(11)	2.415(2)	Cu(1)-O(13b^3)	2.616(2)

O(1)-Cu(1)-O(2)	91.21(8)	O(3a^3)-Cu(1)-O(1w)	95.18(9)
O(1)-Cu(1)-O(3a^3)	85.16(7)	O(2)-Cu(1)-O(1w)	85.48(10)
O(1)-Cu(1)-O(1w)	176.15(10)	O(2)-Cu(1)-O(3a^3)	176.36(8)
O(11)-Cu(1)-O(1)	85.12(7)	O(13b^3)-Cu(1)-O(1)	91.45(8)
O(11)-Cu(1)-O(2)	84.34(7)	O(13b^3)-Cu(1)-O(2)	81.86(8)
O(11)-Cu(1)-O(3a^3)	95.18(7)	O(13b^3)-Cu(1)-O(3a^3)	98.37(7)
O(11)-Cu(1)-O(1w)	92.59(10)	O(13b^3)-Cu(1)-O(1w)	90.03(10)
O(11)-Cu(1)-O(13b^3)	165.70(7)		

[a] Symmetry codes: (a^3) *x*-1/2, *y*, -*z*+1/2; (b^3) -*x*+1/2, *y*+1/2, *z*

In both complexes the copper(II) ion [Cu(1)] is six-coordinated (see Figure 6) and it exhibits a 4+1+1 distorted octahedral conformation (ϕ = 52.9º and *s*/*h* = 1.414 for complex **2** and ϕ = 53.8º and *s*/*h* = 1.454 for complex **3**) [Stiefel E.I. *et al.*, 1972]. The equatorial sites around Cu(1) are occupied by three carboxylate-oxygen atoms from two different mal^{2-} ligands and one oxygen atom from a water molecule. Metal ion is shifted 0.0821(4) Å from the mean equatorial plane towards O(11), for compound **2** and 0.0159(3) Å towards O(13b^3) [(b^3) -*x*+1/2, *y*+1/2, *z*], for compound **3**. Two carboxylate-oxygen atoms from two different H_2mal groups fill the apical positions around copper(II). The Cu-O(equatorial) bond lengths [average values 1.939(2), 1.938(2) Å for **2** and **3**, respectively] are shorter than the Cu-O(apical) ones {2.368(2), 2.415(2) Å [Cu(1)-O(11)] and 2.579(2), 2.616(2) [Cu(1)-O(13b^3)] for **2** and **3**, respectively}.

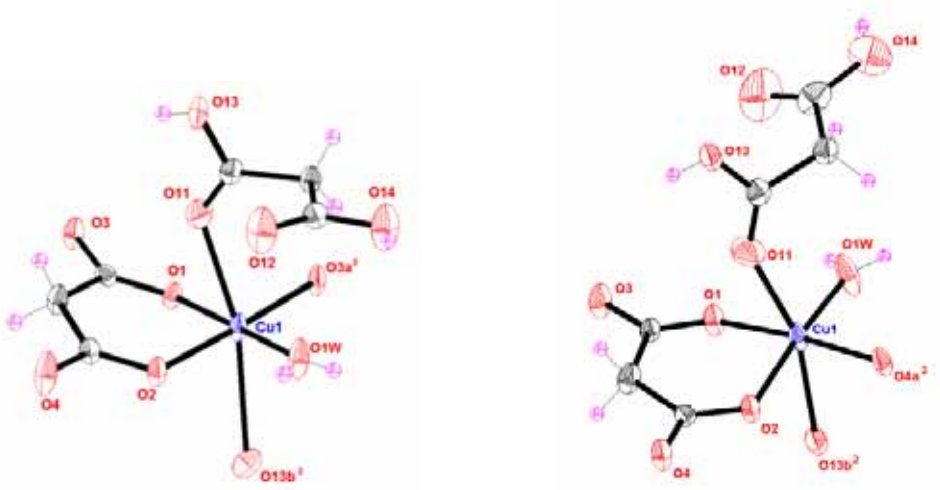

(a) **(b)**

Figure 6. View of the metal environment in **2** **(a)** and in **3** **(b)**. Thermal ellipsoids are drawn at the 50% probability level.

Two crystallographically independent malonate groups are present in both compounds: mal^{2-} (malonate anion) and H_2mal (malonic acid). The mal^{2-} group (see

Scheme 1, I) acts simultaneously as monodentate [through O(4) towards Cu(1c^2) for **2** and through O(3) towards Cu(1c^3) for **3**; (c^2) -*x*, *y*+1/2, -*z*+1/2, (c^3) -*x*+1/2, *y*, -*z*+1/2] and bidentate [through O(1) and O(2) towards Cu(1)]. Including the metal atom each malonate group forms a six-membered ring that exhibits an envelope conformation [θ= 56.0(6)º, ϕ= 124.3(6)º; θ= 59.7(4)º, ϕ= 127.7(4)º for **2** and **3**, respectively] [Cremer D. *et al.*, 1975]. The carboxylate-malonate groups exhibit the *anti-syn* conformation and they connect two equatorial positions of two structurally different Cu(1) metal ions.

Whereas the H_2mal ligand (see Scheme 1, III) acts as bis-monodentate [through O(11) towards Cu(1) for both compounds and through O(13) towards Cu(1d^2) for **2** and Cu(1d^3) for **3**; (d^2) *x*+1, *y*, *z*; (d^3) -*x*+1/2, *y*-1/2, *z*]. The coordination mode is different from the observed one in the reported copper(II) H_2mal containing compound, where the H_2mal group acts as bidentate ligand [Zhang Y. *et al.*, 1999]. The mean values of the C-C [1.502(4) Å and 1.503(4) Å for **2** and **3**, respectively] and C-O [1.255(3) Å (**2**) and 1.254(3) Å (**3**)] malonate bond distances and O-C-O [122.6(3) (**2**) and 122.5(3)º (**3**)] bond angles agree well with those previously reported in other malonate-containing copper(II) complexes [see Introduction].

Each Cu(1) ion is linked to two other ones along the *b*-axis (**2**) or *a*-axis (**3**) through *anti-syn* carboxylate groups involving the mal^{2-} ligand to afford zigzag chains (see Figure 5) [the shortest intrachain Cu···Cu distances being 5.0257(10) and 4.9323(6) Å for **2** and **3**, respectively], the values of the dihedral angles between the equatorial plane of the Cu(1) ion and the O(1)-C(1)-O(2) and O(2)-C(3)-O(4) mean planes are 17.1(2) and 15.8(2)º for **2** and 27.75(14) and 24.0(2)º for **3.** The equatorial planes of two consecutives Cu(1) ions along the chain-axis form dihedral angles of 1.76(8) (**2**) and 2.31(6)º (**3**). In addition, each Cu(1) ion is linked to two other ones, along the *a*-axis (**2**) or *b*-axis (**3**), through *anti-anti* carboxylate groups leading to a two-dimensional network (see Figure 5) [the shortest Cu···Cu distance being 7.0880(10) and 7.0536(6) Å for **2** and **3**, respectively]. Interestingly, the topology of the malonate-bridging copper(II) layers are quite different for both compounds. Regarding the relative position of the two apical sites around Cu(1) we have alternating (**2**) or regular (**3**) zigzag chains (see Figure 5). For compound **2**, the chains stack in a AAA sequence along the *a*-axis, whereas for **3** the chains stack along the *b*-axis in the ABAB sequence.

Additional hydrogen bonds involving water molecules and carboxylate-malonate (mal^{2-} and H_2mal) oxygen atoms contribute to stabilize the structure and lead to a three-dimensional structure. The extensive network of hydrogen bonds in **2** and **3** are

different. Although in both complexes appears similar intrachain hydrogen bonds involving the water molecule and the malonate-oxygen atoms [O(1w)···O($2a^2$) 2.652(3) Å (**2**); O(1w)···O($1a^3$) 2.707(3) Å (**3**); (a^2) -*x*, *y*-1/2, -*z*+1/2, (a^3) *x*-1/2, *y*, -*z*+1/2] the connections between chains through hydrogen bonds are quite different due to the relative position of the malonic acid within the chain. In **2**, we can distinguish an alternation in the position of the malonic acid along the *b*-axis. Each chain is connected to four adjacent ones leading to a three-dimensional network (see Figure 7). Whereas in **3** the position of the malonic acid within the chain, along the *a*-axis, is regular (see Figure 8). In **3**, each chain is connected through hydrogen bonds, involving malonic acid, to two other ones leading to a two-dimensional network. The relevant hydrogen bonds for all compounds are shown in Table 6.

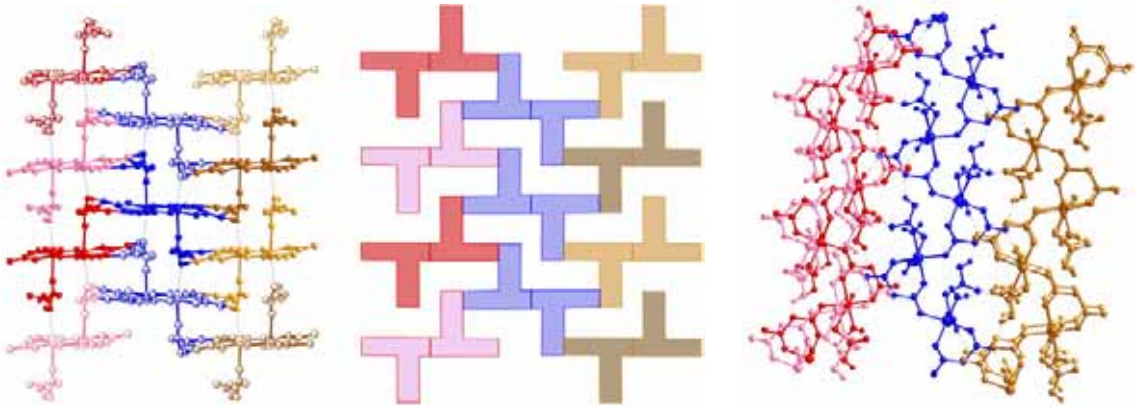

(a) **(b)**

Figure 7. (a) View of three adjacent layers of **2** along the *b*-axis **(b)** Perspective view, along the *a*-axis, of a chain connected to four adjacent ones through hydrogen bonds (broken lines).

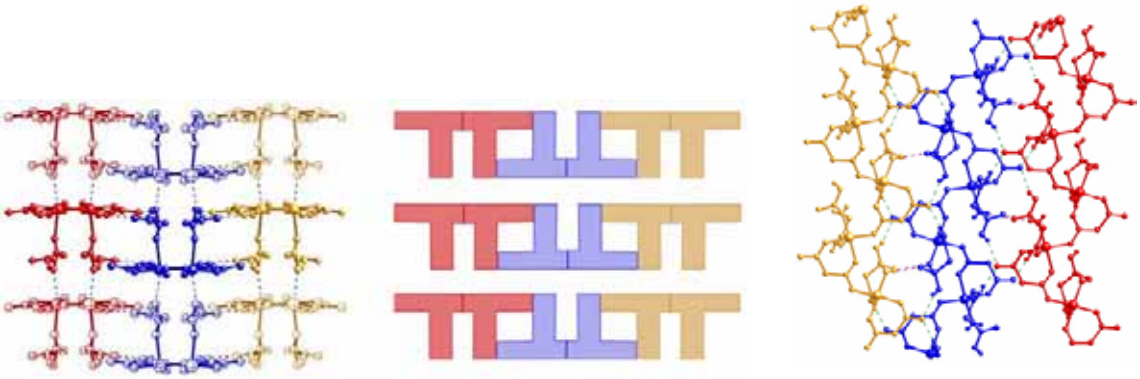

(a) **(b)**

Figure 8. (a) View of three adjacent layers of **3** along the *a*-axis. **(b)** Perspective view, along the *b*-axis, of a chain connected to two other ones through hydrogen bonds (broken lines).

Table 6. Relevant hydrogen bonds.

D-H···A	D···A / Å	D-H···A / º	D-H···A	D···A / Å	D-H···A / º
Compound 1					
O(4)···O(3f[1])	2.447(2)	170(4)			
Compound 2			**Compound 3**		
Intrachain			Intrachain		
O(1w)···O(2a[2])	2.652(3)	135(3)	O(1w)···O(1a[3])	2.707(3)	128(4)
O(1w)···O(4e[2])	3.221(3)	153(3)	O(1w)···O(3e[3])	3.088(3)	159(4)
Interlayer			Interlayer		
O(1w)···O(12f[2])	2.666(4)	173(5)	O(1w)···O(12f[3])	2.743(3)	178(4)
O(14)···O(3g[2])	2.766(3)	136(2)	O(14)···O(4f[3])	2.661(3)	156(5)
O(13)···O(3h[2])	2.543(3)	173(4)	O(13)···O(4g[3])	2.545(3)	171(5)

[a] Symmetry codes: (f[1]) –*x*, *y*-1/2, -*z*+1/2, (a[2]) –*x*, *y*-1/2, -*z*+1/2; (e[2]) *x*, *y*-*1*, *z*; (f[2]) *x*-1/2, -*y*-1/2, -*z*; (g[2]) *x*+1/2, -*y*-1/2, -*z*; (h[2]) *x*+1/2, -*y*+1/2, -*z*; (a[3]) *x*-1/2, *y*, -*z*+1/2; (e[3]) *x*-1, *y*, *z*; (f[3]) -*x*, -*y*, -*z*+1; (g[3]) -*x*+1, -*y*, -*z*+1.

Magnetic properties

The magnetic properties of compound **1** under the form of $\chi_M T$ vs. T plot are shown in the Figure 9. $\chi_M T$ at room temperature is 0.40 cm^3 mol^{-1} K, a value which is as expected for a magnetically isolated spin doublet. Upon cooling, $\chi_M T$ remains almost constant and at very low temperatures $\chi_M T$ deviates from the Curie law increasing smoothly to reach a value of 0.45 cm^3 mol^{-1} K at 2 K. The magnetization versus field curve (insert curve of Figure 9) runs slightly above the Brillouin function for a spin doublet, confirming an overall ferromagnetic coupling between the copper(II) ions in **1**. Although the coupling is extremely weak we can try to fit the data to the high-temperature expansion series derived from the 2D Heisenberg model for the S = 1/2 ferromagnetic quadratic lattice [Navarro R., 1990].

$$\chi = Ng^2\beta^2 S(S+1)/(3kT)\left[1+\sum_{n=1}^{8} a_n K^n\right] \qquad (1)$$

where K is $J/2kT$, J is the intrachain magnetic coupling parameter, N the Avogadro's number, g the Landé factor, β the Bohr magneton, k the Boltzman's constant and the a_n coefficients are taken for the square lattice. The spin Hamiltonian is defined as:

$$\hat{H} = \sum_i -J\hat{S}_i \cdot \hat{S}_{i+1} \qquad (2)$$

The best least-square fit parameters are J = 0.104(4) cm^{-1}, g = 2.13(1) and R = 2.4×10^{-4}. The calculated curve matches very well the experimental data in the whole temperature range.

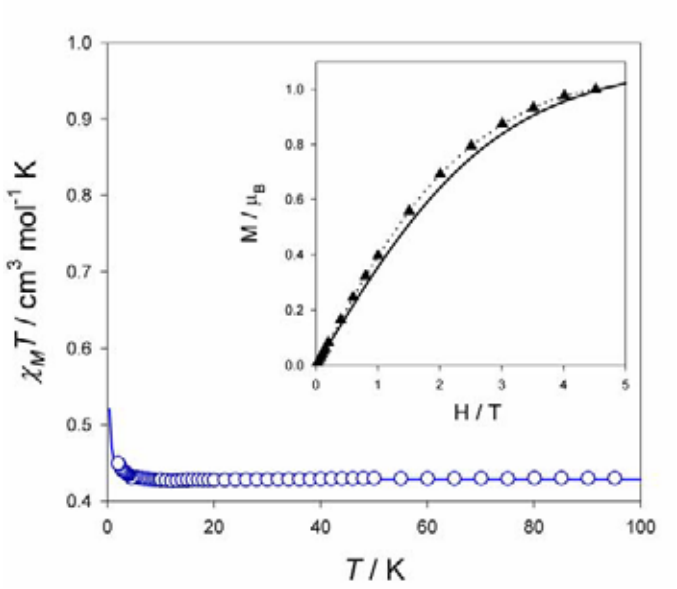

Figure 9. Thermal dependence of the $\chi_M T$ product for **1**: (**O**) experimental; (—) best-fit through equation (1). The inset shows the magnetisation versus H plot at 2.0 K for **1**: (▲) experimental; (—) Brillouin function for a spin doublet.

The ferromagnetic nature of the interaction can be explained since the Cu-O-C-O-Cu exchange pathway involves an equatorial position at one copper(II) ion and an axial position of the nearest neighbouring copper(II). This behaviour has been observed in other carboxylate bridged copper(II) complexes [Ruiz-Pérez C. *et al.*, 2000a; Gil de Muro I. *et al.*, 1998; Sanchiz J. *et al.*, 2002; Delgado, F.S. *et al.*, 2003; Pasán J. *et al.*, 2003b]. The magnetic orbital in the distorted octahedral surrounding exhibited by the copper(II) ions in **1** is defined by the four short equatorial Cu-O bonds, being thus mainly localized in the equatorial plane (essentially the $d_{x^2-y^2}$ orbital). A low spin density is expected in the axial position because some admixture of the d_{z^2} character due to the trigonal distortion of the metal environment. The small overlap between the magnetic orbitals of adjacent copper(II) ions through the out-of-plane exchange pathway reduces the antiferromagnetic contribution and the ferromagnetic one becomes dominant [Kahn O., 1993; Ruiz-Pérez C. *et al.*, 2000a; Pasán J. *et al.*, 2003a]. The extremely weak coupling can be attributed to the very long Cu-O(axial) distance [2.5429(13) Å] that decreases the intensity of the interaction.

The magnetic properties of compounds **2** and **3** under the form of $\chi_M T$ vs. T plot [χ_M being the molar susceptibility per copper(II) ion] are shown in the Figure 10. Compound **2** was measured in the 150-2 K temperature range, whereas **3,** due to the small amount of product obtained, was measured between 60 and 2 K. The insert curve shows the field dependence of the magnetization at 2 K for **2**. The magnetization curve of **3** is very similar to that of **2** and it's omitted for clarity. The solid line represents the Brillouin function for a spin doublet. The values of the $\chi_M T$ at the highest temperatures measured are 0.45 and 0.46 cm^3 mol^{-1} K, for **2** and **3** respectively, as expected for magnetically isolated spin doublets. Upon cooling, $\chi_M T$ continuously increase to reach a maximum value of 0.86 and 0.60 cm^3 mol^{-1} K, for **2** and **3** respectively. This behaviour is indicative of the occurrence of an overall ferromagnetic coupling between the copper(II) ions in both compounds, confirmed by the magnetization curves that run above the Brillouin curve for a spin doublet.

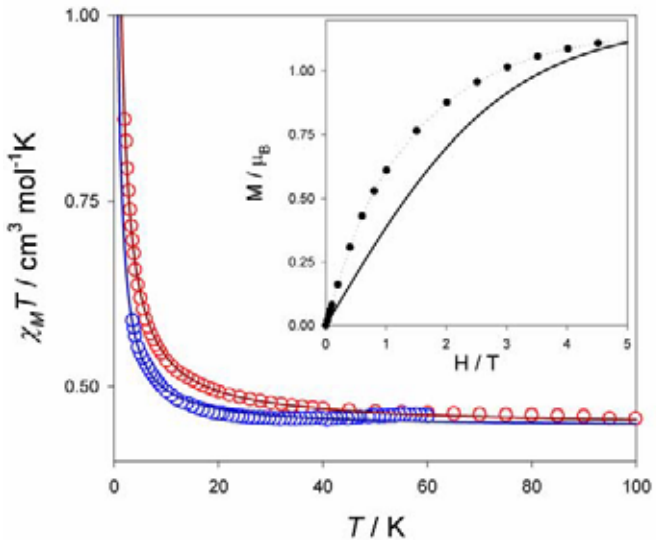

Figure 10. Thermal dependence of the $\chi_M T$ product for **2** (O) and **3** (O); the solid lines are the best-fit through equation (3). The inset shows the magnetisation versus H plot at 2.0 K for **2**: (●) experimental; (—) Brillouin function for a spin doublet.

The structure of **2** and **3** consist of $\{[Cu(H_2O)(H_2mal)(mal)]\}_n$ layers that are linked through hydrogen bonding to afford the 3D structure. However, the Cu-O($13b^3$) axial distance is so long [2.572(2) and 2.616(2) Å, for **2** and **3** respectively] that the magnetic data are better treated by means of the Baker and Rushbrooke model for a S = 1/2 ferromagnetic regular chain [Baker G.A. *et al.*, 1964]. [eqns. (3)-(5)]

$$\chi_M = \left(N\beta^2 g^2 / 4kT\right)\left(A/B\right)^{2/3} \qquad (3)$$

$$A = 1.0 + 5.7979916y + 16.902653y^2 + 29.376885y^3 + 29.832959y^4 + 14.036918y^5 \qquad (4)$$

$$B = 1.0 + 2.7979916y + 7.0086780y^2 + 8.6538644y^3 + 4.5743114y^4 \quad (5)$$

with $y = J/2kT$ and with the spin Hamiltonian defined as

$$\hat{H} = \sum_i -J\hat{S}_i \cdot \hat{S}_{i+1} \quad (6)$$

Best least-square fit parameters are J = 1.467(1) cm^{-1}, g = 2.182(9) and R = 5.4 × 10^{-4} for **2** and J = 0.79(1) cm^{-1}, g = 2.179(2) and R = 8.9 × 10^{-4} for **3.** The calculated curves match very well the experimental data in the whole temperature range for both compounds.

In order to elucidate if there is any magnetic exchange through the H_2mal, which may lead to a 2D magnetic system, the molecular field approximation has been applied to both set of data by means of equation (7).

$$\chi_{2D} = \frac{\chi_{1D}}{1 - \chi_{1D}(2Zj'/Ng^2\beta^2)} \quad (7)$$

where j is the interaction between the chains and Z is the number of nearest neighbour chains. Nevertheless, the results have not been improved, indicating that the 1D model is the best for the treatment of the magnetic data.

The intensity of the magnetic coupling in **2** and **3** is of the same order of magnitude, but slightly lower than the magnetic coupling observed in the compound $\{[Cu(H_2O)_3][Cu(mal)_2(H_2O)]\}_n$ [J = 3.0 cm^{-1}] [Ruiz-Pérez *et al.*, 2000]. The ferromagnetic nature of the coupling between the copper(II) ions through the *anti-syn* carboxylate-malonate bridge in **2** and **3** is in agreement with the data reported in the literature for other copper(II) malonate-complexes with this type of bridge [Baker G.A. *et al.*, 1964; Colacio E. *et al.*, 1999; Pasán J. *et al.*, 2003a]. Furthermore, the exchange coupling in carboxylate-bridged dinuclear compounds has been studied by DFT methods [Rodríguez-Fortea A. *et al.*, 2001]. In those studies was concluded that single carboxylate bridges exhibiting the *anti-syn* conformation can lead to moderate ferromagnetic coupling between copper(II) ions. The poor overlap between the orbitals of the carboxylate bridge in the *anti-syn* conformation and those of the metals bearing the unpaired electron [mainly the $d_{x^2-y^2}$ for a copper(II) in an elongated-octahedral environment] minimizes the antiferromagnetic contribution making the ferromagnetic one to become dominant. The difference in intensity of the coupling constant between **2** and **3** is 0.7 cm^{-1}. Although compounds **2** and **3** have the same chemical composition, they have many structural differences (bond distances and angles, dihedral angles,

distortions from ideal geometries of the metallic ions environments, crystalline structure) that in general can justify that small difference. On the other hand, it is not possible to attribute to one of them the responsibility for such a small difference.

References

Baker G.A., Rushbrooke G.S and Gilbert H.E., *Phys. Rev.*, **1964**, 135, A1272.

Colacio E., Domínguez-Vera J.M., Ghazi M., Krekäs R., Klinga M. and Moreno J.M., *Eur. J. Inorg. Chem.*, **1999**, 441.

Cremer D. and Pople J.A., *J. Am. Chem. Soc.*, **1975**, 97, 1354.

Crystal Maker 4.2.1. Crystalmaker Software., P.O. Box 183. Bicester, Oxfordshire, OX26 3TA. UK, **2001**.

Delgado F.S., Sanchiz J., Ruiz-Pérez C., Lloret F. and Julve M., *Inorg. Chem.*, **2003**, 42, 5938.

Desplanches C., Ruiz E., Rodríguez-Fortea A. and Alvarez S., *J. Am. Chem. Soc.,* **2002a**, 124, 5197.

Desplanches C., Ruiz E. and Alvarez S., *Chem. Comm.,* **2002b**, 2614.

Earnshaw A., *Introduction to Magnetochemistry*, Academic Press, London, **1968**.

Farrugia L.J., *J. Appl. Crystallogr.*, **1999**, 32, 837.

Gil de Muro I., Mautner F.A., Insausti M., Lezama L., Arriortua M.I., Rojo T., *Inorg. Chem.*, **1998**, 37, 3243.

Kahn O., Pei Y., Verdaguer M., Renard J.P. and Sletten J., *J. Am. Chem. Soc.,* **1988**, 110, 782.

Kahn O., *Molecular Magnetism*, VCH, New York, **1993**.

Larionova J., Chavan S.A., Yakhmi J.V., Gulbrandsen Froystein A., Sletten J., Sourisseau C. and Kahn O., *Inorg. Chem.,* **1997**, 36, 6374.

Lenstra A.T.H. and Kataeva O.N., *Acta Cryst. Sect. B*, **2001**, 57, 497.

Nardelli M., *J. Appl. Crystallogr.*, **1995**, 28, 659.

Navarro R., *Application of High- and Low-Temperature Series Expansions to Two-dimensional Magnetic Systems*, ed. L.J. de Jongh, Kluwer Academic Publishers, The Netherlands, **1990**.

Pasán J., Delgado F.S., Rodríguez-Martín Y., Hernández-Molina M., Ruiz-Pérez C., Sanchiz J., Lloret F. and Julve M., *Polyhedron,* **2003a**, 22, 2143.

Pasán J., Sanchiz J., Ruiz-Pérez C., Lloret F. and Julve M., *New J. Chem.*, **2003b**, 27, 1557.

Plass W., Pohlmann A. and Rautengarten J., *Angew. Chem. Int., Ed. Engl.,* **2001**, 40, 4207.

Roríguez-Fortea A., Alemany P., Álvarez S. and Ruiz E., *Chem. Eur. J.*, **2001**, 7, 627.

Rodríguez-Martín Y., Hernández-Molina M., Delgado F.S., Pasán J., Ruiz-Pérez C., Sanchiz J., Lloret F. and Julve M., *CrytsEngComm*, **2002**, 4, 522.

Ruiz-Pérez C., Sanchiz J., Hernández-Molina M., Lloret F. and Julve M., *Inorg. Chem.,* **2000,** 39, 1363.

Ruiz-Pérez C., Rodríguez-Martín Y., Hernández-Molina M., Delgado F.S., Pasán J., Sanchiz J., Lloret F. and Julve M., *Polyhedron,* **2003**, 22, 2111.

Sanchiz J., Rodríguez-Martín Y., Ruiz-Pérez C., Mederos A., Lloret F. and Julve M., *New J. Chem.*, **2002**, 26, 1624.

Sheldrick G.M., SHELXS-97 & SHELXL-97, Programs for Crystal Structure Analysis (Release 97-2). Institut für Anorganische Chemie der Universität, Tammanstrasse 4, D-3400 Göttingen , Germany, **1998**.

Stiefel E.I. and Brown G.F., *Inorg. Chem.*, **1972**, 2, 434.

Zhang X., Lu C., Zhang Q., Lu S., Yang W., Liu J. and Zhang H., *Eur. J. Inorg. Chem.*, **2003**, 1181.

CHAPTER II.

Network formation and magnetic behaviour of Copper(II)malonate anions in alkali salts.

Introduction

Research into the chemistry of coordination polymers has evolved rapidly in the last several years. In these polymeric materials a metal ion, a segment of an inorganic structural motif, or entire well-defined inorganic structures [Ciurtin D.M. *et al.*, 2003] are linked together by a rigid or flexible organic moiety to create an infinite organic-inorganic hybrid framework. Attributes of both the inorganic and organic moieties (*e.g.* available coordinations sites and coordination preferences, ligand flexibility and denticity) are transmited to the extended structure, hence the great potential for complexity and functionality of these materials [Hoskins R. *et al.*, 1990; Gardner G.B. *et al.*, 1995; Keller S.W., 1997; Abrahams B.F. *et al.*, 1994; Xu, Z. *et al.*, 2000]. A careful selection of ligands, metal centre and reaction conditions can confer control over the topology of the resulting frameworks. Copper(II)/carboxylates have been extensively employed in the construction of metal-organic networks, theirs properties and supramolecular behaviour have been studied extensively since the structure of $Cu_2(CH_3COO)_4{\cdot}2H_2O$ was first reported five decades ago [Van Niekerk J. N. *et al.*, 1953]. Although much of the attention has been focused on analogues of this complex, it became interesting to determine how other monovalent ions, especially the non-transition metals, can influence the self-assembly process. In this context, various Cu(II)-carboxylate derivatives that incorporate alkali metal ions, often sodium, have been reported in the last 20 years for ligands such as acetate [Hardt H.D. *et al.*, 1967; Seigrist T. *et al.*, 1996; Wu C. *et al.*, 2001; Warden A.C. *et al.*, 2003], croconate [Wang C.-C. *et al.*, 2002], picolinate [Chung Y.H. *et al.*, 1998], propionate [Goher M.A.S. *et al.*, 1994], azamacrocycle acetate derivatives [Weighardt K. *et al.*, 1982; Wong E.H. *et al.*, 2000], amino acids [Antolini L. *et al.*, 1988; Ng S.W. *et al.*, 1998], crown ether. [Gibney B.R. *et al.*, 1994] and alkoxo anions [Purdy P. *et al.*, 1995]. These studies have sparked interest in understanding the influence of alkali metal ions on the structure and the properties of transition metal complexes.

In the context of our magneto-structural research with malonate-bridged hetero (Cu-Mn and Ni-Na)-metallic complexes [Ruiz-Pérez C. *et al.*, 2000a and Ruiz-Pérez C. *et al.*, 2000b, respectively], we extended our work with the preparation, structural characterization and magnetic properties of the Cu(II)-malonate bricks ($[Cu(mal)_2]^{2-}$ and $[Cu(mal)_2(H_2O)]^{2-}$) with five monovalent ions from the alkaline group (Li, Na. K, Rb

and Cs). The results of this study are described below. In this way, we increased the dimensionality without adding a new ligand.

Experimental

Materials and methods

Malonic acid, copper(II) basic carbonate $Cu(CO_3)\cdot Cu(OH)_2$, Lithium hydroxide monohydrate $[Li(OH)\cdot H_2O]$, sodium hydroxide [Na(OH)], potassium hydrogencarbonate $[KHCO_3]$, rubidium carbonate $[Rb_2CO_3]$ and cesium carbonate $[Cs_2CO_3]$ were purchased from commercial sources and used as received. Elemental analyses (C, H) were performed on an EA 1108 CHNS-O microanalytical analyser. The magnetic susceptibility measurements were performed on a Quantum Design SQUID magnetometer operating at 250 G ($T < 20$ K) and 10000 G ($T \geq 20$ K) in the temperature range of 2-300 K for compounds **1**, **2**, **4** and **5** and operating at 500 G ($T < 10$ K) and 10000 G ($T \geq 10$ K) in the temperature range of 2-200 K for compound **3**. Diamagnetic corrections of all the constituent atoms were estimated from Pascal's constants [Earshaw, 1968] as -126×10^{-6}, -124×10^{-6}, -140×10^{-6}, -143×10^{-6} and -207×10^{-6} cm^3 mol^{-1} for compounds **1**-**5**, respectively. Magnetic data were also corrected for the temperature independent paramagnetism [60×10^{-6} cm^3 mol^{-1} per copper(II) ion] and the magnetization of the sample holder.

Synthesis

$[Li(H_2O)]_2[Cu(mal)_2(H_2O)]$ (1). Solid copper(II) basic carbonate (221 mg, 1 mmol) is added to an aqueous solution (5 cm^3) of malonic acid (416 mg, 4 mmol) under continuous stirring. The suspension is heated at 40-50 ºC, until a blue solution is obtained. This solution is filtered and mixed with an aqueous solution (5 cm^3) of lithium hydroxide (168 mg, 4 mmol). Single crystals of **1** as blue prisms were grown from the solution by slow evaporation at room temperature in a week. Yield 472 mg, 70 % (Found: C, 21.97; H, 3.10 %. Calc. for $C_6H_{10}O_{11}CuLi_2$: C, 21.45; H, 2.98 %).

$[Na(H_2O)]_2[Cu(mal)_2]$ (2). Compound **2** is obtained by the same procedure used for **1** but replacing the lithium hydroxide by sodium hydroxide (160 mg, 4 mmol). Single crystals of **2** suitable for X-ray diffraction were obtained by slow evaporation at room temperature within two weeks. Yield 525 mg, 75 % (Found: C, 21.00; H, 2.30 %. Calc. for $C_6H_8O_{10}CuNa_2$: C, 20.59; H, 2.28 %).

$[K(H_2O)_{3/2}]_2[Cu(mal)_2]$ (3). Compound **3** is obtained by the same procedure used for **1** but replacing the lithium hydroxide by potassium hydrogencarbonate (400 mg, 4 mmol). Single crystals of **3** as blue prisms were grown from the solution by slow evaporation at room temperature in a week. Yield 600 mg, 75 % (Found: C, 18.20; H, 2.55 %. Calc. for $C_6H_{10}O_{11}CuK_2$: C, 18.00; H, 2.50 %).

$[Rb(H_2O)_{1/2}]_2[Cu(mal)_2]$ (4). Compound **4** is obtained by the same procedure used for **1** but replacing the lithium hydroxide by rubidium carbonate (462 mg, 2 mmol). Single crystals of **4** as blue prisms were grown from the solution by slow evaporation at room temperature in two weeks. Yield 594 mg, 65 % (Found: C, 15.80; H, 1.45 %. Calc. for $C_6H_6O_9CuRb_2$: C, 15.76; H, 1.31 %).

$[Cs(H_2O)]_2[Cu(mal)_2(H_2O)_2]$ (5). Compound **5** is obtained by the same procedure used for **1** but replacing the lithium hydroxide by cesium carbonate (650 mg, 2 mmol). Single crystals of **5** as pale-blue prisms were grown from the solution by slow evaporation at room temperature in a few days. Yield 970 mg, 80% (Found: C, 11.95; H, 1.95 %. Calc. for $C_6H_{12}O_{12}CuCs_2$: C, 11.89; H, 1.98 %).

Crystal data collection and refinement of the structures

Single crystals of **1-5** were mounted on a Bruker-Nonius KappaCCD diffractometer. Orientation matrix and lattice parameters were obtained by least-squares refinement of the reflections obtained by a θ-χ scan (Dirax/lsq method). Diffraction data for all compounds were collected at 293(2) K using graphite-monochromated Mo-K_α radiation (λ = 0.71073 Å). Data collection and data reduction were done with the COLLECT [Hooft R.W.W., 1999] and EVALCCD [Duisenberg A.J.M. *et al.*, 2003] programs. Empirical absorption corrections were carried out using SADABS [SADABS, version 2.03, 2003] for all compounds. The indexes of data collection were $-8 \le h \le 8$, $-11 \le k \le 9$ and $-13 \le l \le 12$ for **1**, $-9 \le h \le 9$, $-13 \le k \le 11$ and $-23 \le l \le 12$ for **2**, $-8 \le h \le 10$, $-25 \le k \le 25$ and $-10 \le l \le 12$ for **3**, $-9 \le h \le 9$, $-12 \le k \le 12$ and $-22 \le l \le 15$ for **4** and $-9 \le h \le 8$, $-9 \le k \le 9$ and $-9 \le l \le 9$ for **5**. Of the 2591 (**1**), 1547 (**2**), 1683 (**3**), 2318 (**4**) and 1681 (**5**) measured independent reflections in the θ range 6.43 – 27.49 (**1**), 5.24 - 30 (**2**), 6.46 – 29.12 (**3**), 4.19 – 27.50 (**4**) and 6.46 – 27.49º (**5**), 2393 (**1**), 1071 (**2**), 1187 (**3**), 1671 (**4**) and 1523 (**5**) have $I \ge 2\sigma(I)$. All the measured independent reflections were used in the analysis. All calculations for data reduction, structure solution, and refinement were done by standard procedures (WINGX) [Farrugia L.J.,

1999]. The structure was solved by direct methods and refined with full-matrix least-squares technique on F^2 using the SHELXS-97 and SHELXL-97 programs [Sheldrick G.M., SHELX97, realease 97-2, 1998]. The hydrogen atoms of the malonate and water molecules were located from difference Fourier maps for compounds **1** and **2**. For compounds **3**-**5**, the hydrogen atoms of the water molecules were not found and those of the malonate were located from difference Fourier maps (**3**) or set in calculated positions (**4** and **5**). The hydrogen atoms for all compounds were refined with isotropic temperature factors. The final Fourier-difference map showed maximum and minimum height peaks of 0.313 and -0.289 e $Å^{-3}$ (**1**), 0.401 and -0.405 e $Å^{-3}$ (**2**), 0.484 and -0.304 e $Å^{-3}$ (**3**), 0.766 and -0.916 e $Å^{-3}$ (**4**) and 0.739 and -1.026 e $Å^{-3}$ (**5**). A summary of the crystallographic data and structure refinement is given in Table 1. The final geometrical calculations and the graphical manipulations were carried out with PARST97 [Nardelli M., 1995] and DIAMOND [DIAMOND 2.1d, 2000] programs, respectively.

Crystal structures were deposited at the Cambridge Crystallographic Data Centre and the CCDC reference numbers are 256111 (**1**), 256112 (**2**), 256113 (**3**), 256114 (**4**) and 256115 (**5**).

Table 1. Crystal data and details of the structure determination for compounds **1-5.**

Compound	**1**	**2**	**3**	**4**	**5**
Formula	$C_6H_{10}CuLi_2O_{11}$	$C_6H_8Cu_1Na_2O_{10}$	$C_6H_{10}Cu_1K_2O_{11}$	$C_6H_6CuRb_2O_9$	$C_6H_{12}Cs_2Cu_1O_{12}$
M	335.56	349.64	399.88	456.59	605.52
Crystal system	triclinic	orthorhombic	orthorhombic	orthorhombic	triclinic
Space group	*P*-1	*P*bca	*P*bcn	$P2_12_12_1$	*P*-1
a, Å	6.8515(3)	6.8270(10)	7.3985(7)	7.2224(6)	7.1166(6)
b, Å	8.8520(6)	9.517(2)	18.830(2)	9.4647(5)	7.1316(9)
c, Å	10.5293(7)	16.406(3)	9.3201(9)	17.017(2)	7.5211(6)
α, deg	80.655(6)	-	-	-	87.334(8)
β, deg	75.043(4)	-	-	-	79.428(7)
γ, deg	70.363(4)	-	-	-	86.698(8)
V, Å^3	579.07(6)	1065.9(3)	1298.4(2)	1163.25(18)	374.36(6)
Z	2	4	4	4	1
T, K	293(2)	293(2)	293(2)	293(2)	293(2)
ρ_{calc}, Mg m^{-3}	1.925	2.179	2.046	2.607	2.986
F(000)	338	700	804	868	316
λ (Mo-K$_\alpha$ Å)	0.71073	0.71073	0.71073	0.71073	0.71073
μ (Mo-K$_\alpha$, mm^{-1})	1.940	2.181	2.376	10.228	7.690
Extintion parameter	-	-	0.0116(12)	-	0.020(2)
Flack parameter	-	-	-	0.49(2)	-
Number parameters/restraints	221 / 0	104 / 0	102 / 0	163 / 0	97 / 0
Goodness of fit (*S*)	1.114	1.092	1.076	1.034	1.091
R1, $I > 2\sigma(I)$ (all)	0.020 (0.023)	0.037 (0.068)	0.034 (0.059)	0.050 (0.087)	0.027 (0.031)
wR2, $I > 2s(I)$ (all)	0.050 (0.052)	0.074 (0.085)	0.089 (0.098)	0.094 (0.104)	0.067 (0.069)
Max/min electron density (e/Å^3)	0.313 / -0.289	0.401 / -0.405	0.484 / -0.304	0.766 / -0.916	0.739 / -1.026
Measured reflections (R_{int})	5358 (0.014)	5136 (0.045)	8013 (0.023)	5038 (0.052)	3756 (0.040)
Independent reflections [$I > 2\sigma(I)$]	2591 (2393)	1547 (1071)	1683 (1187)	2318 (1671)	1681 (1523)

Results and discussion

Description of the structure of $\{[Li(H_2O)]_2[Cu(mal)_2(H_2O)]\}_n$ (1).

The structure of compound **1** consists of $[Cu(mal)_2(H_2O)]^{2-}$ anions and $[Li(H_2O)_n]^+$ (n = 1, 2) cations linked together by means of carboxylate bridges, water molecules and hydrogen bonds leading to a lithium pillared malonate copper(II) three-dimensional structure (see Figure 1).

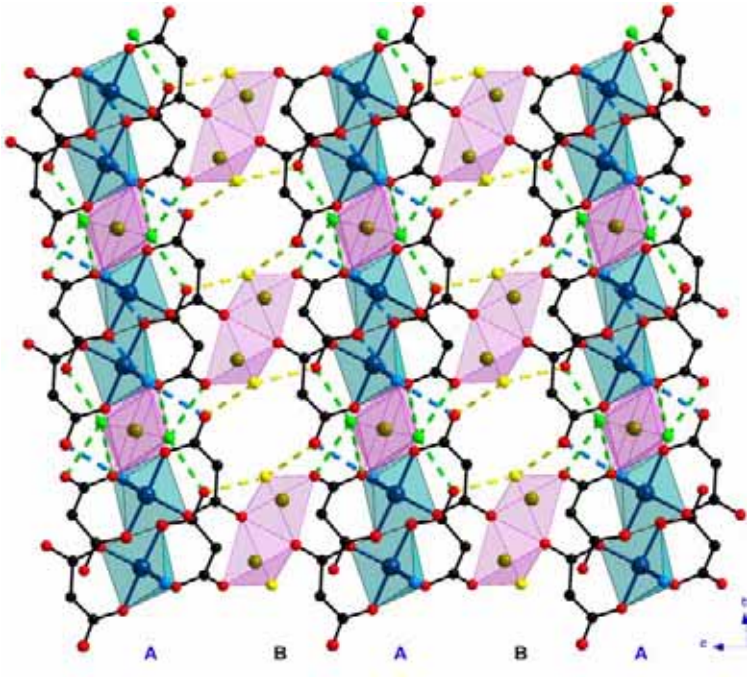

(a)

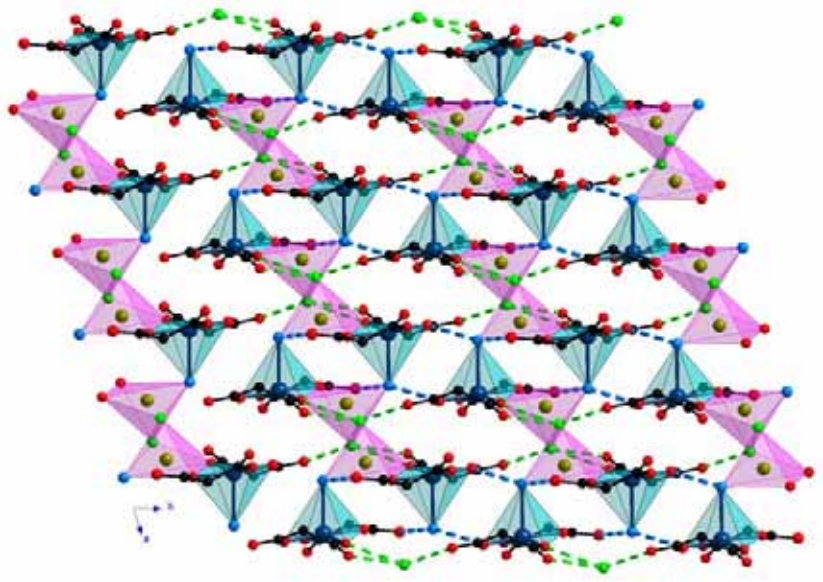

(b)

Figure 1. (a) Perspective view along the *a*-axis of the arrangement of the $[Cu(mal)_2(H_2O)]^{2-}$ and $[Li(H_2O)_n]^+$ units in **1**. **(b)** View of a fragment of the A-layer, along the *c*-axis in **1.** The hydrogen bonds are illustrated by broken lines (see text).

The copper(II) atoms are five-coordinated (Figure 2) with a distorted square pyramidal environment, the τ value being 0.264 (square-pyramidal and trigonal-pyramidal surroundings correspond to $\tau = 0$ and $\tau = 1$, respectively) [Addison A.W. *et al.*, 1984].

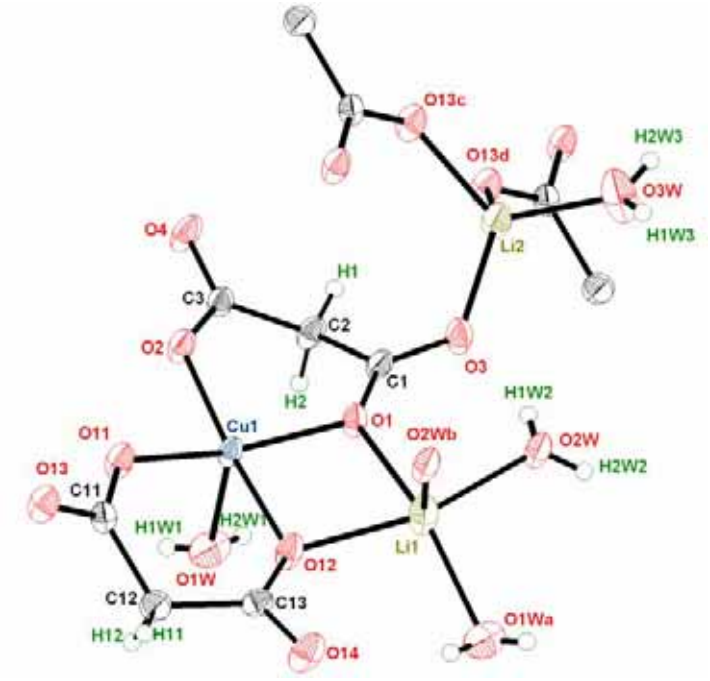

Figure 2. View of the metal environments in **1**. Thermal ellipsoids are drawn at the 50% probability level.

Selected bond lengths and angles for the metal environments in **1** are listed in Table 2. Four oxygen atoms from two crystallographically independent malonate groups build the equatorial plane around the metal atom [the Cu-O(equatorial) distances ranging from 1.9286(11)-1.9402(10) Å]. A water molecule occupies the apical position, the Cu(1)-O(1w) distance being 2.3705(14) Å. The metal atom is shifted by 0.2094(2) Å from the mean equatorial plane towards the apical water molecule. The bond distances and bond angles defined around the copper environment are in agreement with those observed in other malonate containing copper(II) complexes [see malonate-containing copper(II) complexes in the Introduction].

Table 2. Selected bond lengths (Å) and angles (°) for **1**[a]

Cu(1)-O(1)	1.9402(10)	Cu(1)-O(2)	1.9331(11)
Cu(1)-O(11)	1.9362(11)	Cu(1)-O(12)	1.9286(11)
Cu(1)-O(1w)	2.3705(14)		
O(1)-Cu(1)-O(2)	93.14(5)	O(11)-Cu(1)-O(12)	94.32(5)
O(1)-Cu(1)-O(11)	158.85(5)	O(2)-Cu(1)-O(12)	174.69(5)
O(1)-Cu(1)-O(12)	82.33(4)	O(2)-Cu(1)-O(11)	88.91(5)

O(1w)-Cu(1)-O(1)	95.16(6)	O(1w)-Cu(1)-O(2)	95.03(5)
O(1w)-Cu(1)-O(11)	105.63(6)	O(1w)-Cu(1)-O(12)	88.16(5)
Li(1)-O(1)	2.146(3)	Li(1)-O(12)	2.057(3)
Li(1)-O(1wa)	2.096(3)	Li(1)-O(2w)	1.969(3)
Li(1)-O(2wb)	2.055(3)		
O(1)-Li(1)-O(2w)	88.55(13)	O(12)-Li(1)-O(1wa)	99.87(14)
O(1)-Li(1)-O(1wa)	152.8(2)	O(12)-Li(1)-O(2w)	163.0(2)
O(1)-Li(1)-O(12)	74.54(10)	O(2w)-Li(1)-O(1wa)	95.78(14)
O(2wb)-Li(1)-O(1)	109.58(15)	O(2wb)-Li(1)-O(12)	94.72(13)
O(2wb)-Li(1)-O(1wa)	97.35(13)	O(2wb)-Li(1)-O(2w)	89.68(13)
Li(2)-O(3)	1.914(3)	Li(2)-O(3w)	1.873(3)
Li(2)-O(13c)	1.962(3)	Li(2)-O(13d)	1.999(3)
O(3)-Li(2)-O(3w)	112.28(15)	O(3)-Li(2)-O(13c)	112.84(14)
O(3w)-Li(2)-(13c)	115.8(2)	O(13d)-Li(2)-O(3)	121.9(2)
O(13d)-Li(2)-O(3w)	102.79(13)	O(13d)-Li(2)-O(13c)	89.43(12)

[a] Symmetry code: (a) -*x*, -*y*+1, -*z*+1; (b) -*x*+1, -*y*+1, -*z*+1; (c) -*x*+1, -*y*, -*z*+1; (d) *x*, *y*, *z*+1.

Two crystallographically independent lithium atoms [Li(1) and Li(2)] are present in **1** (see Figure 2). They are five [Li(1)] and four-coordinated [Li(2)]. Li(1) is bonded to three water molecules [O(1wa), O(2w), O(2wb)] and two carboxylate oxygen atoms [O(1) and O(12)] from two different malonate groups. They build a distorted square pyramid around the alkaline atom (see Figure 3a). Li(1) is shifted by 0.243(3) Å from the mean equatorial plane, which is defined by O(1), O(12), O(2w) and O(1wa). Li(2) is bound to a water molecule and three malonate oxygen atoms from three different malonate groups that form a distorted tetrahedron around it (see Figure 3b). The Li-O(malonate) and Li-O(w) bond distances are somewhat longer for Li(1) than for Li(2).

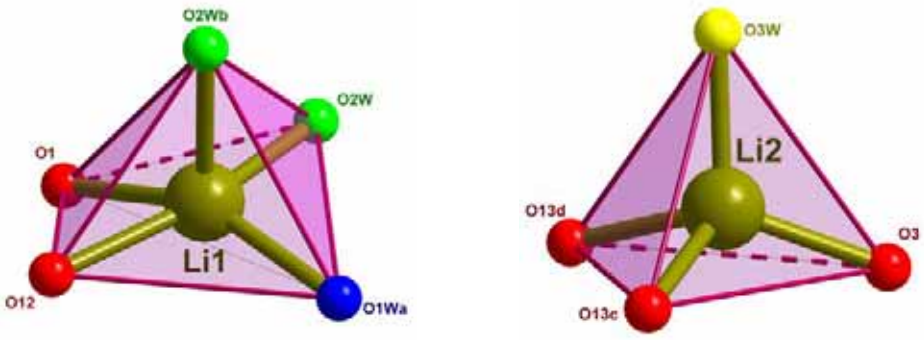

(a) **(b)**

Figure 3. Perspective drawing of the environment of the lithium atoms Li(1) **(a)** and Li(2) **(b)**. Symmetry codes: (a) -*x*, -*y*+1, -*z*+1; (b) -*x*+1, -*y*+1, -*z*+1; (c) -*x*+1, -*y*, -*z*+1; (d) *x*, *y*, *z*+1.

Two crystallographically independent malonate groups are present in **1**: L1 [C(1)-C(2)-C(3)] and L2 [C(11)-C(12)-C(13)] (see Figure 4).

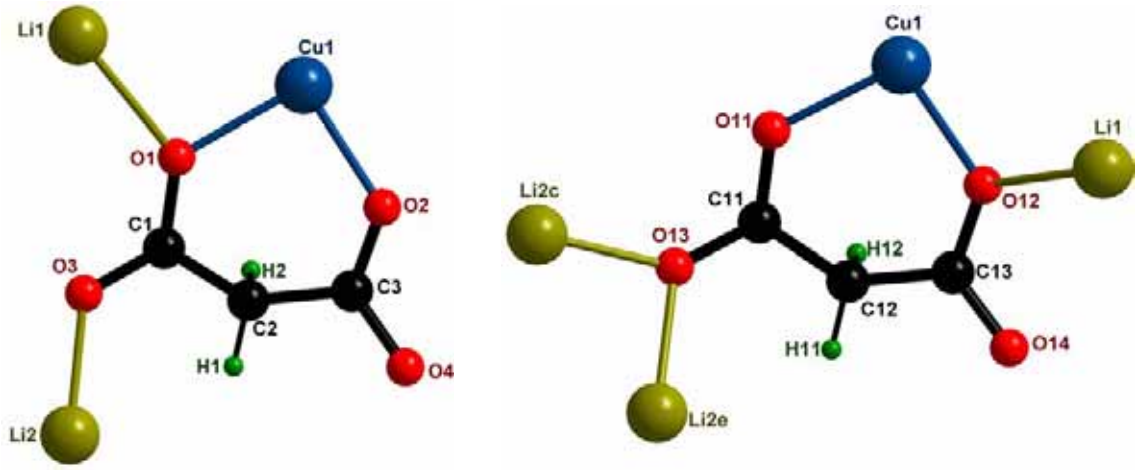

(a) **(b)**

Figure 4. View of the coordination mode of the malonato ligands in **1**: **(a)** L1 (*anti-syn* + η^5-chelation) and **(b)** L2 (outer bismonodentate + inner unidentate + η^5-chelation). Symmetry codes: (c) -*x*+1, -*y*, -*z*+1; (e) *x*, *y*, *z*-1.

L1 acts simultaneously as bridging ligand in the *anti-syn* conformation [through O(1) and O(3) towards Li(1) and Li(2), respectively] and bidentate [through O(1) and O(2) towards Cu(1)] ligand (see Figure 4a). It forms a six-membered ring [including the Cu(II) atom] that exhibits a boat conformation [Cremer D. *et al.*, 1975] [θ = 85.62(15)º and ϕ = 113.45(15)º]. On the other hand, L2 acts simultaneously as bis-monodentate bridging ligand [though O(13) towards Li(2c) and Li(2e); (e) *x*, *y*, *z*-1] and a monodentate ligand [through O(12) towards Li(1)] and as a bidentate ligand [through O(11) and O(14) towards Cu(1) (see Figure 4b). It forms a six-membered ring [including Cu(1)] that exhibits a distorted screw-boat conformation [Cremer D. *et al.*, 1975] [θ = 63.7(2)º and ϕ = 115.1(3)º]. The angles subtended by the malonate ligands at the copper atoms are 93.14(5) (L1) and 94.32(5)º (L2). Each copper atom is linked to two and three lithium ions through L1 and L2, respectively. The O(1)-C(1)-O(3) carboxylate-malonate group connects an equatorial position of Cu(1) with an apical site of Li(2), exhibiting the *anti-anti* conformation. Whereas, the O(11)-C(11)-O(13) group acts simultaneously as *anti-anti* [connecting Cu(1) and Li(2e)] and *anti-syn* [bridging Cu(1) and Li(2c)]. Furthermore, Cu(1) and Li(1) are linked through a double μ-oxo bridge involving two inner carboxylate-oxygen atoms from two different malonate groups (see Figure 2), which occupy equatorial positions at both metal environments [the Cu(1)-O(1)-Li(1) and Cu(1)-O(12)-Li(1) bond angles are 98.97(9) and 102.50(10)º, respectively]. The values of the malonate bond distances and angles of the malonate

ligands (see Table 3) agree with those observed in previous malonate-containing copper(II) complexes [see references of malonate complexes in the Thesis Introduction].

Table 3. Bond lengths (Å) and angles (º) for the malonate ligands in **1**

C(1)-C(2)	1.509(2)	C(2)-C(3)	1.515(2)
C(1)-O(1)	1.274(2)	C(3)-O(2)	1.271(2)
C(1)-O(3)	1.244(2)	C(3)-O(4)	1.238(2)
O(1)···O(2)	2.813(2)	O(3)···O(4)	4.391(2)
O(1)-C(1)-O(3)	122.24(13)	O(2)-C(3)-O(4)	122.55(14)
O(1)-C(1)-C(2)	118.55(13)	O(2)-C(3)-C(2)	120.38(13)
O(3)-C(1)-C(2)	119.18(13)	O(4)-C(3)-C(2)	117.06(13)
C(1)-C(2)-C(3)	116.06(13)		
C(1)-O(1)-Cu(1)	126.01(9)	C(3)-O(2)-Cu(1)	125.26(10)
O(1)C(1)O(3)-Cu(1)eq[a]	29.96(11)	O(2)C(3)O(4)-Cu(1)eq[a]	13.89(14)
C(11)-C(12)	1.514(2)	C(12)-C(13)	1.510(2)
C(11)-O(11)	1.270(2)	C(13)-O(12)	1.280(2)
C(11)-O(13)	1.246(2)	C(13)-O(14)	1.230(2)
O(11)···O(12)	2.834(2)	O(13)···O(14)	4.458(2)
O(11)-C(11)-O(13)	122.19(14)	O(12)-C(13)-O(14)	121.62(14)
O(11)-C(11)-C(12)	120.46(13)	O(12)-C(13)-C(12)	118.76(13)
O(13)-C(11)-C(12)	117.30(13)	O(14)-C(13)-C(12)	119.53(14)
C(11)-C(12)-C(13)	117.85(13)		
C(11)-O(11)-Cu(1)	126.12(10)	C(13)-O(12)-Cu(1)	128.55(10)
O(11)C(11)O(13)-Cu(1)eq[a]	28.44(14)	O(12)C(13)O(14)-Cu(1)eq[a]	12.14(11)

[a]dihedral angle (º) between the malonate carboxylate group and the mean equatorial plane of the metal.

The $[Cu(mal)_2(H_2O)]^{2-}$ units are held together by means of hydrogen bonds leading to a three-dimensional network (see hydrogen bonds in Table 4). First, each copper unit is linked to another symmetrically related [see Cu(1) and Cu(1f) units in Figure 5; (f) *-x*, *-y*, *-z*+1] through hydrogen bonds involving the O(1w) water molecule coordinated to the metal atom and the inner O(2) malonate oxygen atom. This structural feature leads to dinuclear anionic motifs [4.8446(4) Å for Cu(1)···Cu(1f)]. They are further linked to two other ones through hydrogen bonds (see Table 4) which involve the outer O(14) malonate oxygen atom and the O(1w) water molecule [5.4679(5) Å for the Cu(1)···Cu(1a) separation], giving thus a regular alternating copper(II) chain that

runs along the *b*-axis (Figure 5). Within the chain, additional hydrogen bonds (see green broken lines in Figure 5) that involve O(2w) [water molecule which is coordinated to Li(1)] connect adjacent links, stabilizing the anionic chain. Finally, these copper(II) chains are hydrogen bonded [O(4h)···H-O(3w)-H···O(14b); (h) -*x*+1, -*y*, -*z*+2] along the *a*-axis (see yellow broken lines in Figures 5 and 1a) though O(3w) [the water molecule coordinated to Li(2)] giving rise to a two-dimensional network.

Table 4. Relevant hydrogen bonds[a-c] for compound **1**

D-H···A	D···A/Å	H···A/Å	D-H···A/º
O(1w)-H(1w1)···O(2f)	3.037(2)	2.445(4)	148(3)
O(1w)-H(2w1)···O(14a)	2.905(2)	2.241(4)	147(3)
O(2w)-H(1w2)···O(3)	2.770(2)	2.071(3)	161(3)
O(2w)-H(2w2)···O(4g)	2.654(2)	1.88(3)	179(3)
O(3w)-H(1w3)···O(14b)	2.680(2)	1.97(3)	159(3)
O(3w)-H(2w3)···O(4h)	2.747(2)	1.98(3)	167(3)
C(2)-H(2)···O(14a)	3.301(2)	2.63(2)	131(2)
C(12)-H(12)···O(4f)	3.428(3)	2.59(3)	145(2)

[a] Symmetry transformations: (a) -*x*, -*y*+1, -*z*+1; (b) -*x*+1, -*y*+1, -*z*+1; (f) -*x*, -*y*, -*z*+1; (g) *x*, *y*+1, *z*; (h) -*x*+1, -*y*, -*z*+2; [b] A = acceptor; D = donor. [c] Symmetry transformations apply to acceptor atoms.

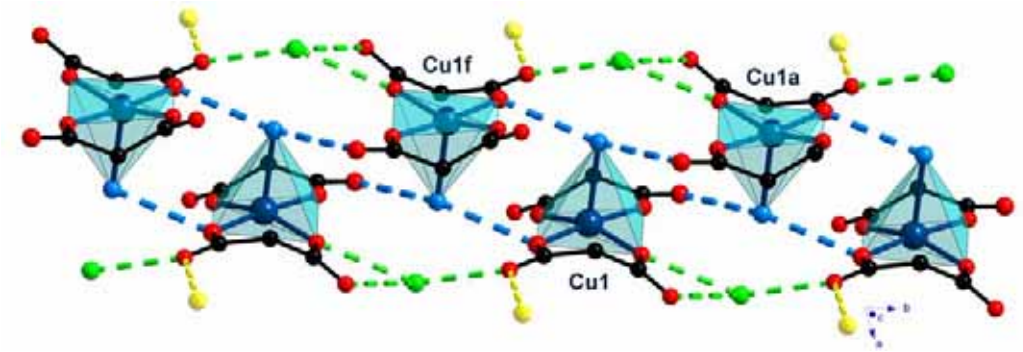

Figure 5. A perspective view of the malonato-copper(II) chains that grow along the *b*-axis. Hydrogen bonds are drawn as broken lines (see text).

Both Li(1) and Li(2) units are connected to the $\bar{1}$ symmetrically related ones through double μ-oxo like bridges (see Figure 6a). These bridges involve two water molecules at L(1) and two malonate-oxygen atoms at Li(2). The lithium···lithium separations through the double μ-oxo bridge are 2.854(5) and 2.814(4) Å for Li(1) and Li(2), respectively. Furthermore, these two crystallographically independent dimeric units are linked through the carboxylate bridge O(1)-C(1)-O(3), [the Li(1)···Li(2)

separation is 5.340(4) Å] affording an alternating chain along the [01-1] direction (see Figure 6b).

Finally, the copper(II) chains are pillared by $[Li(H_2O)_n]$ (n = 1, 2) units. The hydrogen bonded copper(II) chains are pillared along the *a*-axis by means of $[Li(1)(H_2O)_2]_2$ units affording an anionic layer which grows in the *ab*-plane (see Figure 1b). In addition, the chains are pillared along the *b*-axis by means of $[Li(2)(H_2O)]_2$ units, giving thus a neutral three-dimensional network: stacking of anionic and cationic sheets in a ABAB fashion (see Figure 1a).

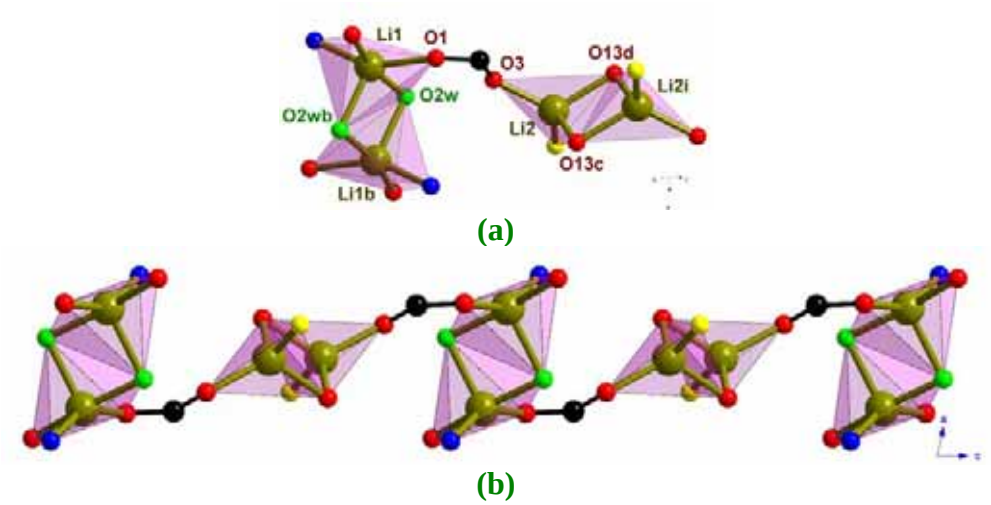

Figure 6. Perspective view of the arrangement of the lithium units: **(a)** $[Li(H_2O)_2]$ and $[Li(H_2O)]$ units linked through μ-oxo bridges; **(b)** A view, along the *b*-axis, of a part of the alkaline chains.

Description of the structure of $\{[Na(H_2O)]_2[Cu(mal)_2]\}_n$ (2).

The structure of this compound was previously reported after we obtained the single crystals [Barnes J.C. *et* al., 1997; Deng S.-L. *et al.*, 2002; Liu H.-L. *et al.*, 2004]. In spite of everything, we decided to include here its structure and magnetic properties in order to compare them with those of the other alkaline bismalonate copper(II) complexes with alkaline cations as counterions.

The structure of compound **2** consists of centrosymmetric $[Cu(mal)_2]^{2-}$ mononuclear anions and $[Na(H_2O)]^+$ cations that are held together by means of carboxylate bridges and water molecules, leading to a three-dimensional structure. An extensive network of hydrogen bonds contributes to stabilise the structure (see Figure 7).

Each copper atom lies on a $\bar{1}$ crystallographic site symmetry. The metal atom is six-coordinated (Figure 8) exhibiting a 4+2 elongated octahedral environment with

geometric values ϕ = 54.6º and *s/h* = 1.49 (ϕ and s/h being the twist angle and the compression ratio, respectively) [Stiefel E.I. *et al.*, 1972]. Four carboxylate-oxygen atoms from two crystallographically related malonate groups build the equatorial plane of the metal ion [the mean Cu(1)-O(equatorial) bond distance being 1.950(2) Å]. The apical positions are filled by two symmetrically related carboxylate oxygen atoms [the Cu(1)-O(apical) distance being 2.601(2) Å]. This long axial bond has been previously observed in other malonate copper(II) complexes [Delgado F.S. *et al.*, 2003 and 2004].

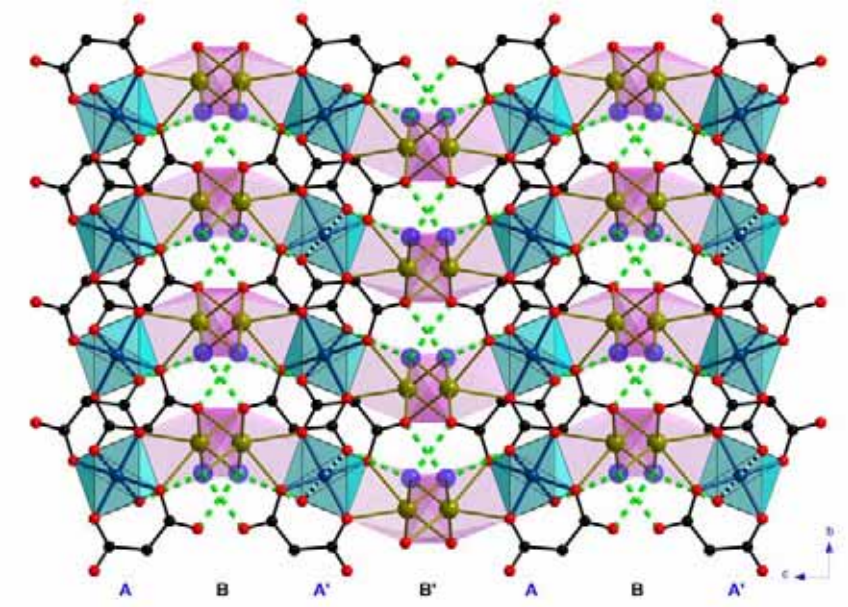

Figure 7. Perspective view along the *a*-axis of the three-dimensional network of compound **2** which built up by malonate-copper(II) and sodium units. The broken lines stand for the hydrogen bonds.

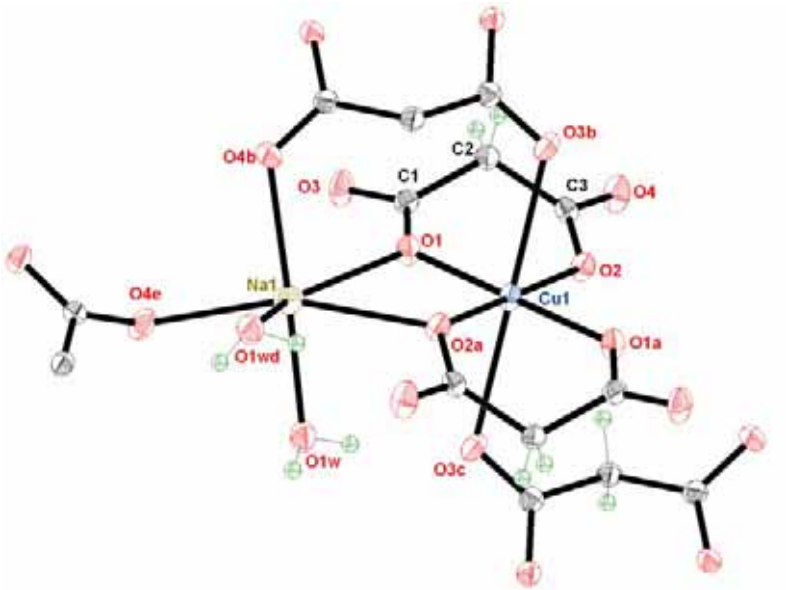

Figure 8. Perspective view of the metal environments in **2**. Thermal ellipsoids are drawn at the 50% probability level.

The main bond lengths and angles for the metal ions of **2** are listed in Table 5.

Table 5. Selected bond lengths (Å) and angles (º) for compound **2**[a]

Cu(1)-O(1)	1.954(2)	Cu(1)-O(2)	1.946(2)
Cu(1)-O(3b)	2.601(2)		
O(1)-Cu(1)-O(2)	93.72(7)	O(1)-Cu(1)-O(2a)	86.28(7)
O(3b)-Cu(1)-O(1)	88.66(7)	O(3b)-Cu(1)-O(1a)	91.34(7)
O(3b)-Cu(1)-O(2)	84.84(7)	O(3b)-Cu(1)-O(2a)	95.16(7)
Na(1)-O(1)	2.454(2)	Na(1)-O(2a)	2.578(2)
Na(1)-O(1wd)	2.385(2)	Na(1)-O(4e)	2.580(2)
Na(1)-O(1w)	2.364(2)	Na(1)-O(4b)	2.460(2)
O(1)-Na(1)-O(2a)	63.95(6)	O(2a)-Na(1)-O(1wd)	81.30(7)
O(1)-Na(1)-O(1wd)	141.81(9)	O(2a)-Na(1)-O(4e)	161.20(8)
O(1)-Na(1)-O(4e)	119.63(7)	O(2a)-Na(1)-O(1w)	84.23(7)
O(1)-Na(1)-O(1w)	90.42(8)	O(2a)-Na(1)-O(4b)	98.19(7)
O(1)-Na(1)-O(4b)	89.86(7)	O(1wd)-Na(1)-O(4e)	98.40(8)
O(4e)-Na(1)-O(1w)	77.42(8)	O(1wd)-Na(1)-O(1w)	101.87(8)
O(4e)-Na(1)-O(4b)	100.23(7)	O(1wd)-Na(1)-O(4b)	79.43(8)
O(1w)-Na(1)-O(4b)	177.43(9)		

[a] Symmetry codes: (a) *-x*, *-y*+1, *-z*; (b) *x*-1/2, *-y*+1/2, *-z*; (c) *-x*+1/2, *y*+1/2, *z*; (d) *x*-1/2, *y*, *-z*+1/2; (e) *x*, *-y*+1/2, *z*+1/2; (f) *x*+1/2, *-y*+1/2, *-z*

Alkaline ions are six-coordinated (see Figure 8). Four carboxylate-oxygen atoms from four monodentate malonate ligands and two *cis*-coordinated water molecules describe a distorted octahedral environment around the sodium atom (see Figure 9). The sodium-water oxygen bond lengths [2.364(2) and 2.385(2) Å] are somewhat shorter than the sodium-malonate oxygen ones [values ranging from 2.454(2) to 2.580(2) Å]. The Na-O bond lengths are in agreement with those observed in the bis(oxalate)cuprate(II) [Chananont P. *et al*., 1980; Gleizes A. *et al*., 1980] (2.385-2.587 Å) and bis(malonate)nickelate(II) [Ruiz-Pérez *et al.*, 2000b] (2.755-2.846 Å) sodium salts compounds. Large deviations from the ideal value of 90º are observed for some bond angles around the sodium atom [63.95(6), 77.42(8) and 79.43(8)º for O(1)-Na(1)-(2a), O(4e)-Na(1)-O(1w) and O(1wd)-Na(1)-O(4b), respectively].

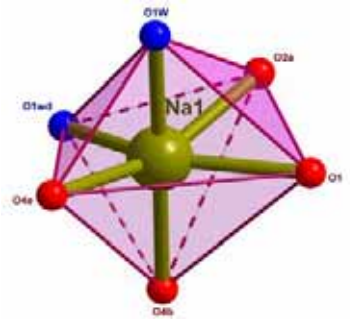

Figure 9. Perspective drawing of the sodium environment.

Each malonate group is coordinated to two copper and four sodium atoms (see Figure 10) adopting simultaneously monodentate [through O(1), O(2) and O(3) atoms towards Na(1), Na(1a) and Cu(1f) atoms respectively], bismonodentate [through the O(4) atom towards the Na(1g) and Na(1f) atoms; (g) *x*, -*y*+1/2, *z*-1/2] and bidentate [through O(1) and O(2) towards Cu(1)] coordination modes. It forms a six-membered ring [including the Cu(1) atom] that exhibits a slightly twist boat conformation [Cremer D. *et al.*, 1975] [θ = 83.2(3)º and ϕ = 110.8(3)]. The angle subtended by the malonate group at the Cu(1) atom is 93.72(7)º.

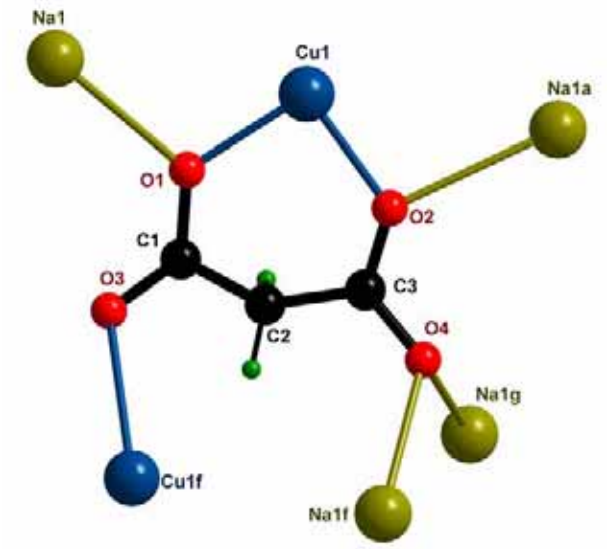

Figure 10. Coordination modes of the malonate ligand in **2.**

Each copper atom is linked to another copper through the O(1)-C(1)-O(3) carboxylate group exhibiting the *anti-anti* bridging mode. This bridge connects an equatorial position of Cu(1) with an apical one at Cu(1f). On the other hand, the other malonate-carboxylate group O(2)-C(3)-O(4) group exhibits simultaneously the *anti-anti* [Cu(1)-carboxylate-Na(1f)] and *anti-syn* [Cu(1)-carboxylate-Na(1g)] conformations. Furthermore, each copper atom is linked to two sodium atoms by means of μ-oxo bridges involving the inner oxygen atoms of the malonate groups [106.11(8) and 101.87(7)º for Cu(1)-O(1)-Na(1) and Cu(1)-O(2)-Na(1a), respectively] (see Figure 8). The values of the malonate bond distances and angles (see Table 6) are in agreement with those previously reported for malonate copper(II) complexes [see copper(II) malonate complexes in the Introduction].

Table 6. Bond lengths (Å) and angles (º) for malonate ligand in **2**[a]

C(1)-C(2)	1.520(3)	C(2)-C(3)	1.509(3)
C(1)-O(1)	1.285(3)	C(3)-O(2)	1.275(3)
C(1)-O(3)	1.232(3)	C(3)-O(4)	1.249(3)

O(1)···O(2)	2.846(2)	O(3)···O(4)	4.409(3)
O(1)-C(1)-O(3)	123.2(2)	O(2)-C(3)-O(4)	122.2(2)
O(1)-C(1)-C(2)	118.9(2)	O(2)-C(3)-C(2)	120.6(2)
O(3)-C(1)-C(2)	117.9(2)	O(4)-C(3)-C(2)	117.1(2)
C(1)-C(2)-C(3)	117.2(2)		
C(1)-O(1)-Cu(1)	125.59(15)	C(3)-O(2)-Cu(1)	125.9(2)
C(1)-O(3)-Cu(1f)	118.9(2)		
O(1)C(1)O(3)-Cu(1)eq[b]	26.1(3)	O(2)C(3)O(4)-Cu(1)eq[b]	20.9(2)

[a] Symmetry code: (f) *x*+1/2, -*y*+1/2, -*z*
[b] dihedral angle (º) between the malonate carboxylate group and the mean equatorial plane of the metal.

Each $[Cu(mal)_2]^{2-}$ unit is connected through the *anti-anti* carboxylate bridges to other four ones leading to malonate-bridged copper(II) anionic layers that grow in the *ab*-plane (Figure 11). The carboxylate-bridge connects an equatorial with an apical site from adjacent copper atoms. The dihedral angle between the mean equatorial planes of the adjacent copper atoms is 51.17(5)º. Within the layer, one can distinguish tetranuclear units that forms sixteen-membered rings $[Cu\text{-}O\text{-}C\text{-}O\text{-}Cu]_4$, the copper atoms being located at the corners of a rhombus [5.8562(9) Å for the Cu(1)···Cu(1b) separation]. The Cu(1)···Cu(1h) and Cu(1)···Cu(1i) separations within the layer (see Figure 11) are 6.8270(10) and 9.517(2) Å, respectively; (h) *x*+1, *y*, *z*; (i) *x*, *y*-1, *z*.

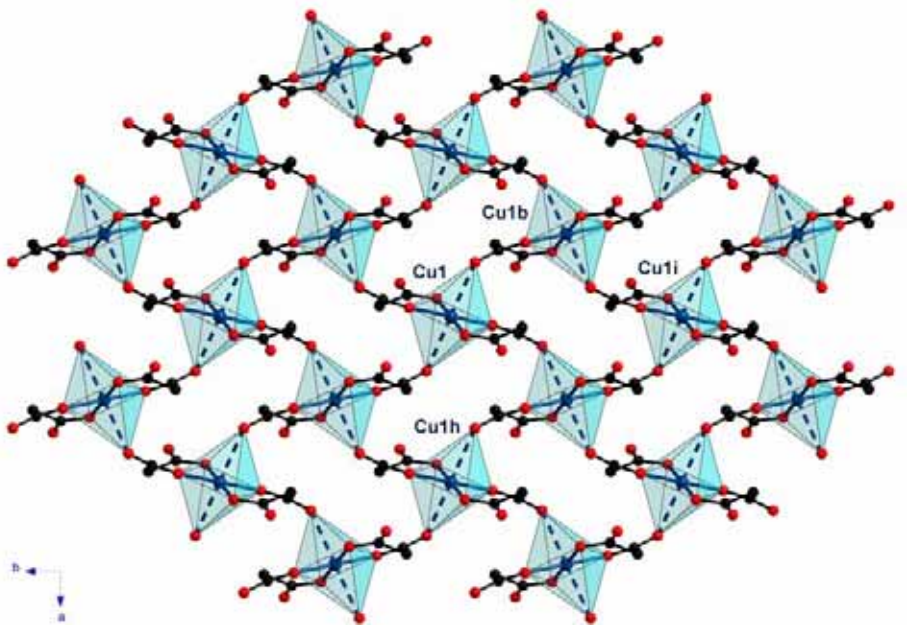

Figure 11. Perspective view along the *c*-axis, of a fragment of the malonate-bridged copper(II) layer in **2**. Apical bonds are drawn as broken lines.

Each $[Na(H_2O)]^+$ unit is connected to two other ones through a double μ-oxo bridge [involving a water molecule and a malonate-carboxylate oxygen atom, O(4)],

leading thus to a zigzag sodium chain (Figure 12). The shorthest Na···Na separation within the chain is 3.786(2) Å.

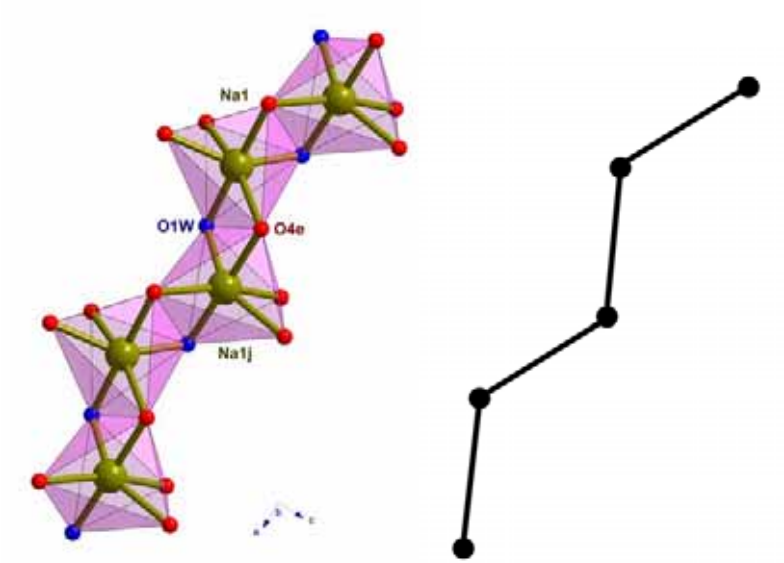

Figure 12. Perspective (left) and schematic (right) views of the $[Na(H_2O)]^+$ units linked through μ-oxo bridges [(j) x+1/2, y, -z+1/2].

Each chain is further linked to two adjacent ones, through *anti-syn* and *anti-anti* carboxylate bridges [O(2)-C(3)-O(4)], forming thus, a cationic layer that grows in the *ab*-plane (see Figure 13). Within these layers, alkaline chains are stacked in a c1 c2 c1 c2 manner (see scheme of Figure 13; c = chain).

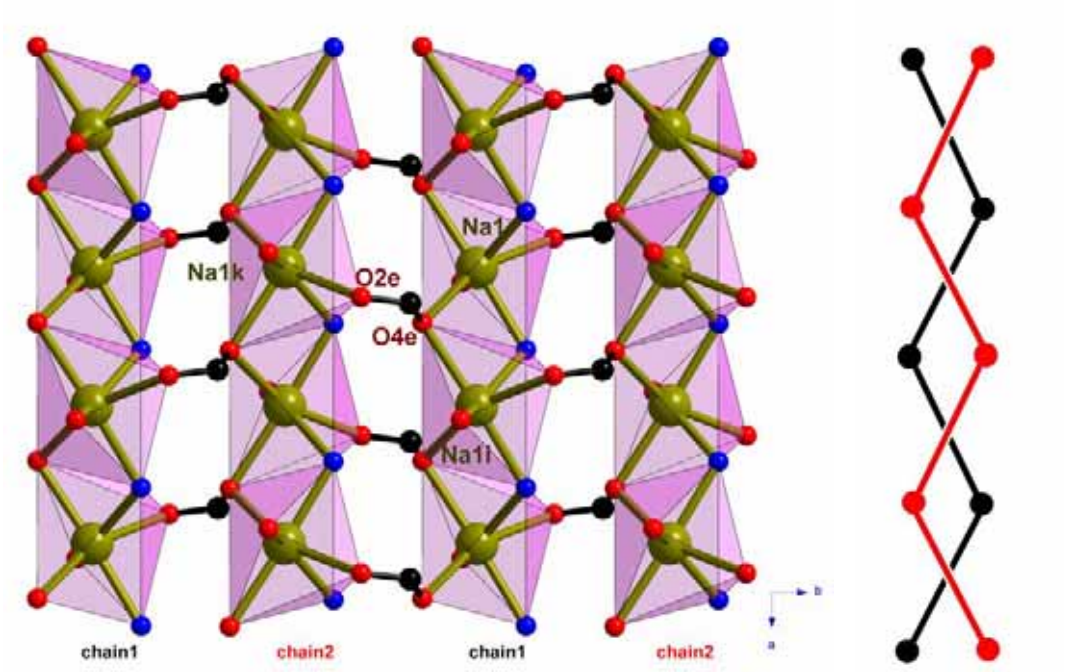

Figure 13. Perspective view along the *c*-axis of a carboxylate-bridged sodium layers (left) and schematic view along the *b*-axis of the stacking of the sodium chains within these layers (right); [(i) x, y-1, z; (k) -x, y-1/2, -z+1/2].

Anionic and cationic layers are held together by means of carboxylate-bridges and they are alternatively stacked in a ABA'B' fashion, leading to a three-dimensional network (see Figure 7). Additional hydrogen bonds (see Table 7) involving water molecules and carboxylate oxygen atoms stabilize the whole structure (see green broken lines in Figure 7).

Table 7. Relevant hydrogen bonds[a-c] for compound **2**

D-H···A	D···A/Å	H···A/Å	D-H···A/º
O(1w)-H(1w1)···O(4l)	2.723(2)	1.95(4)	169(4)
O(1w)-H(2w1)···O(3c)	2.754(3)	1.98(4)	171(4)
C(2)-H(1)···O(2m)	3.334(3)	2.50(3)	153(3)
C(2)-H(2)···O(1b)	3.503(4)	2.65(4)	161(3)

[a] Symmetry transformations: (b) *x*-1/2, -*y*+1/2, -*z*; (c) -*x*+1/2, *y*+1/2, *z*; (l) –*x*+1/2, -*y*+1, *z*+1/2; (m) -*x*+1/2, *y*-1/2, *z*. [b] A = acceptor; D = donor. [c] Symmetry transformations apply to acceptor atoms.

Description of the structure of $\{[K(H_2O)_{3/2}]_2[Cu(mal)_2]\}_n$ (3).

The structure of **3** is made up of $[Cu(mal)_2]^{2-}$ anions and $[K(H_2O)]^+$ cations which are linked together by means of carboxylate-malonate bridges and water molecules affording a three-dimensional structure (see Figure 14). An extensive network of hydrogen bonds (see green broken lines in Figure 14) involving water molecules and carboxylate-oxygen atoms contribute to the stabilisation of the whole structure.

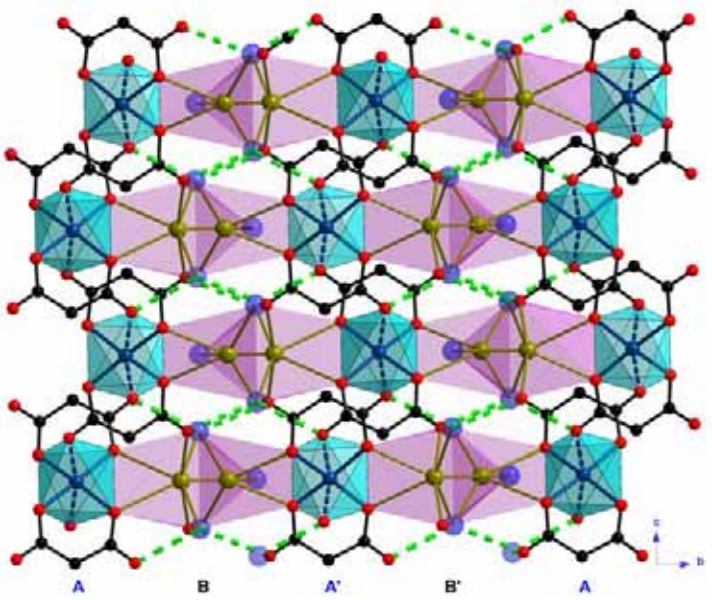

Figure 14. Perspective view along the *a*-axis of the three-dimensional structure of **3** which is made up of $[Cu(mal)_2]^{2-}$ and $[K(H_2O)]^+$ units. Hydrogen bonds are drawn as broken lines.

Each copper(II) atom lies on a two-fold axis. It is six-coordinated (see Figure 15) and exhibits a 4+2 elongated octahedron environment with geometric values ϕ = 53.9º and *s/h* = 1.55 [Stiefel E.I. *et al.*, 1972]. Selected bond lengths and angles for metal atoms in **3** are listed in Table 8.

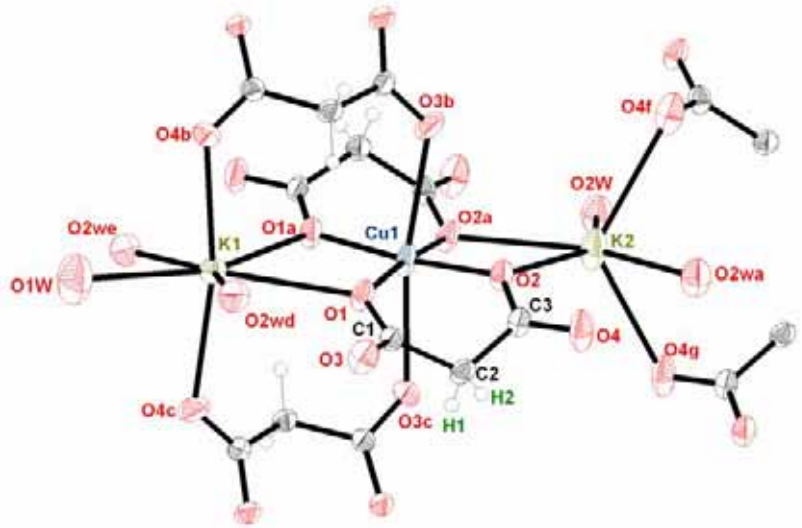

Figure 15. Perspective view of the metal environments in **3**. Thermal ellipsoids are drawn at the 50% probability level.

Four carboxylate-oxygen atoms from two bidentate malonate ligands define the equatorial plane around the copper atom [the values of the Cu(1)-O(equatorial) bonds are 1.9417(15) and 1.9400(12) Å]. Apical positions are occupied by two symmetry related carboxylate-oxygen atoms from other two monodentate malonate ligands. The Cu(1)-O(apical) bond is 2.6902(15) Å, a value which is quite long and that was never observed in the previously reported malonate-containing copper(II) complexes.

Table 8. Selected bond lengths (Å) and angles (º) for compound **3**[a]

Cu(1)-O(1)	1.9417(15)	Cu(1)-O(2)	1.9400(12)
Cu(1)-O(3b)	2.689(2)		
O(1)-Cu(1)-O(2)	92.38(6)	O(2)-Cu(1)-O(2a)	88.23(9)
O(1)-Cu(1)-O(1a)	87.88(9)	O(2)-Cu(1)-O(1a)	172.95(7)
O(1)-Cu(1)-O(2a)	172.95(7)	O(3b)-Cu(1)-O(1a)	89.70(6)
O(3b)-Cu(1)-O(1)	97.94(6)	O(3b)-Cu(1)-O(2a)	89.11(6)
O(3b)-Cu(1)-O(2)	83.29(6)	O(3b)-Cu(1)-O(3c)	169.42(6)
K(1)-O(1)	2.833(2)	K(1)-O(4b)	2.680(2)
K(1)-O(1w)	2.784(3)	K(1)-O(2wd)	2.777(2)
O(1)-K(1)-O(1a)	56.79(6)	O(4b)-K(1)-O(1)	100.41(5)
O(1)-K(1)-O(2wd)	76.78(5)	O(4b)-K(1)-O(1a)	89.56(5)
O(1)-K(1)-O(2we)	130.92(5)	O(4b)-K(1)-O(2wd)	83.57(6)
O(1)-K(1)-O(1w)	151.61(3)	O(4b)-K(1)-O(2we)	93.68(6)

O(1w)-K(1)-O(2wd)	75.98(4)	O(4b)-K(1)-O(1w)	84.36(4)
O(2wd)-K(1)-O(2we)	151.96(8)	O(4b)-K(1)-O(4c)	168.71(8)
K(2)-O(2w)	2.695(2)	K(2)-O(2)	2.754(2)
K(2)-O(4f)	2.908(2)		
O(2w)-K(2)-O(2wa)	133.71(8)	O(2)-K(2)-O(2a)	58.74(6)
O(2w)-K(2)-O(2)	142.49(5)	O(4f)-K(2)-O(2wa)	80.84(6)
O(2w)-K(2)-O(2a)	83.79(5)	O(4f)-K(2)-O(2)	118.35(5)
O(4f)-K(2)-O(2w)	76.24(6)	O(4f)-K(2)-O(2a)	113.90(5)
O(4f)-K(2)-O(4g)	119.35(8)		

[a] Symmetry codes: (a) *-x*, *y*, *-z*+1/2; (b) *-x*+1/2, *-y*-1/2, *z*-1/2; (c) *x*-1/2, *-y*-1/2, *-z*+1; (d) *x*+1/2, *y*+1/2, *-z*+1/2; (e) *-x*-1/2, *y*+1/2, *z*; (f) *x*, *-y*-1, *z*-1/2; (g) *-x*, *-y*-1, *-z*+1.

Two crystallographically independent potassium atoms, seven- [K(1)] and six-coordinated [K(2)] are present in **3** (see Figure 15). Both of them lie on a 2 crystallographically site symmetry. The K(1) atom exhibits a distorted pentagonal bipyramid environment (see Figure 16a): two symmetry related water molecules, two malonate-oxygen atoms and one water molecule (that lies on a two-fold axis) define the pentagonal plane around the K(1) atom [only a large deviation from the ideal value 72º is observed: O(1)-K(1)-O(1a) = 56.79(6)º]. The atoms deviate significantly from the planarity, the maximum deviation from the mean equatorial plane being 0.289(2) Å for O(1). The apical positions are filled by two carboxylate-oxygen atoms from two symmetry-related malonate groups. The environment of the K(2) atom is a distorted trigonal prism (see Figure 16b), the two trigonal bases of the polyhedron being defined by O(2), O(4g), O(1wa) and their symmetrically-related oxygen atoms. The potassium-water oxygen bond distance at K(2) [2.695(2) Å for K(2)-O(2w)] is somewhat shorter than the potassium-malonate oxygen ones [2.754(2) and 2.908(2) Å for K(2)-O(2) and K(2)-O(4f), respectively].

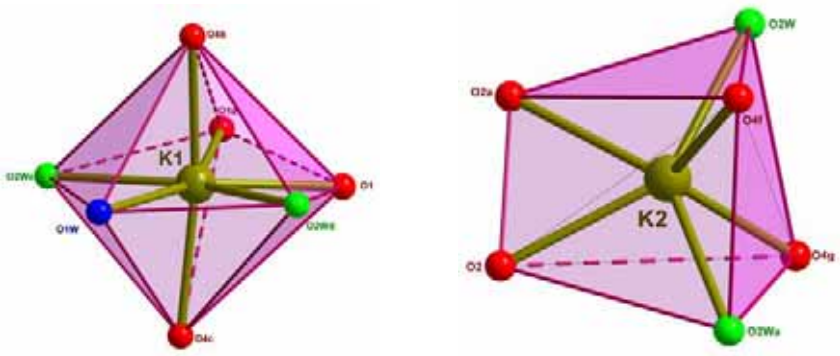

(a) **(b)**

Figure 16. Perspective drawings of the potassium environments in **3**.

The K-O bond distances observed in the oxalate-containing copper(II) potassium reported species: $K_2Cu(ox)_2 \cdot 2H_2O$ [Weichert, T. *et al.*, 1974] and $K_2Cu(ox)_2 \cdot 4H_2O$ [Fan *et al.*, 2001], range from 2.742(2) to 3.049(3) Å, in agreement with those observed in **3**.

Each malonate group in **3** is bonded to two copper and four potassium atoms (see Figure 17) adopting simultaneously the monodentate [through O(1), O(2) and O(3) atoms towards K(1), K(2) and Cu(1h) atoms respectively], bismonodentate [through O(4) towards K(1h) and K(2g); (h) $-x+1/2$, $-y-1/2$, $z+1/2$] and bidentate [through O(1) and O(2) towards Cu(1)] coordination modes. The angle subtended by the malonate ligand at Cu(1) is 92.39(5)º. The malonate group including the Cu(1) atom forms a six-membered ring that exhibits a boat conformation [Cremer D. *et al.*, 1975] [$\theta = 90.7(2)$º and $\phi = 117.7(2)$º].

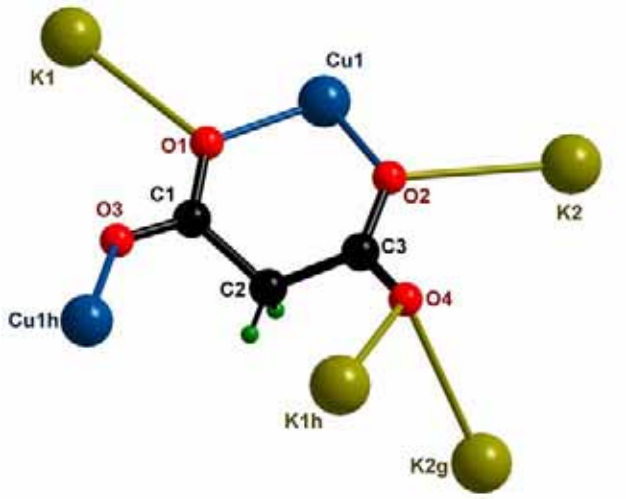

Figure 17. Coordination mode of the malonate ligand in **3**.

The carboxylate groups of the malonate ligand exhibit the *anti-anti* [Cu(1)-O(1)-C(1)-O(3)-Cu(1h)] and the *anti-syn* [Cu(1)-O(2)-C(3)-O(4)-K(1h); (h) $-x+1/2$, $-y-1/2$, $z+1/2$] conformations. The inner malonate-oxygen atoms connect each copper(II) atom with two alkaline ions by means of a μ-oxo bridge [the K(1)-O(1)-Cu(1) and K(2)-O(2)-Cu(1) bond angles being 107.66(6) and 106.52(6)º, respectively]. One of the outer carboxylate-oxygen atom [O(4)] acts as a μ-oxo bridge towards two potassium atoms [K(1h) and K(2g)]. The geometric values of the malonate group (see Table 9) are in agreement with those observed above.

Table 9. Bond lengths (Å) and angles (º) for the malonate ligand in **3**

C(1)-C(2)	1.512(3)	C(2)-C(3)	1.512(3)
C(1)-O(1)	1.275(2)	C(3)-O(2)	1.269(3)
C(1)-O(3)	1.236(2)	C(3)-O(4)	1.239(3)

O(1)···O(2)	2.801(2)	O(3)···O(4)	4.410(2)
O(1)-C(1)-O(3)	123.1(2)	O(2)-C(3)-O(4)	122.9(2)
O(1)-C(1)-C(2)	119.5(2)	O(2)-C(3)-C(2)	119.6(2)
O(3)-C(1)-C(2)	117.5(2)	O(4)-C(3)-C(2)	117.6(2)
C(1)-C(2)-C(3)	117.0(2)		
C(1)-O(1)-Cu(1)	125.20(13)	C(3)-O(2)-Cu(1)	125.48(14)
C(1)-O(3)-Cu(1h)	126.14(15)		
O(1)C(1)O(3)-Cu(1)eq[b]	24.4(2)	O(2)C(3)O(4)-Cu(1)eq[b]	30.6(2)

[a] Symmetry codes: (h) -*x*+1/2, -*y*-1/2, *z*+1/2

[b] dihedral angle (º) between the malonate carboxylate group and the mean equatorial plane of the metal.

Each $[Cu(mal)_2]^{2-}$ unit is linked to four other ones through *anti-anti* carboxylate-bridges (see Figure 18) leading thus, to an anionic malonate-bridged copper(II) layer that grows in the *ac*-plane. Each carboxylate-bridge connects an equatorial site and an apical site from two adjacent copper atoms. The dihedral angle between the mean equatorial planes of two consecutive copper atoms is 73.14(4)º. Within the layer, one can distinguish tetranuclear units that form sixteen-membered rings $[Cu\text{-}O\text{-}C\text{-}O\text{-}Cu]_4$ where the metal atoms occupy the corners of a rhombus. The shortest copper···copper separations within the layer are 6.2435(4), 7.3985(7) and 9.3201(9) Å for Cu(1)···Cu(1b), Cu(1)···Cu(1i) and Cu(1)···Cu(1j), respectively [(i) *x*+1, *y*, *z*; (j) *x*, *y*, *z*-1] (see Figure 18a). The malonate-bridged copper(II) layers stack in a AA'AA' sequence (see Figure 18b).

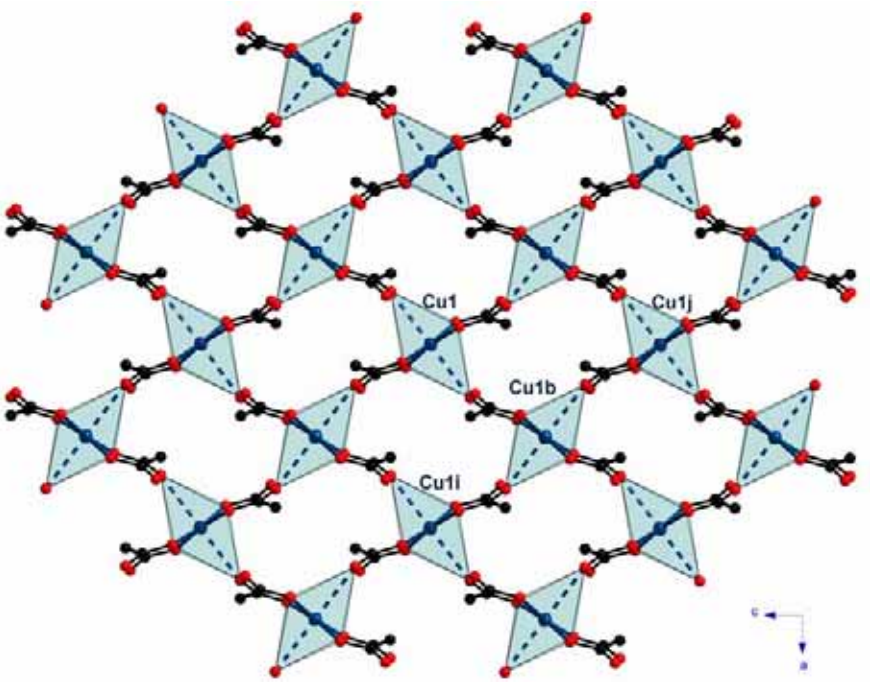

(a)

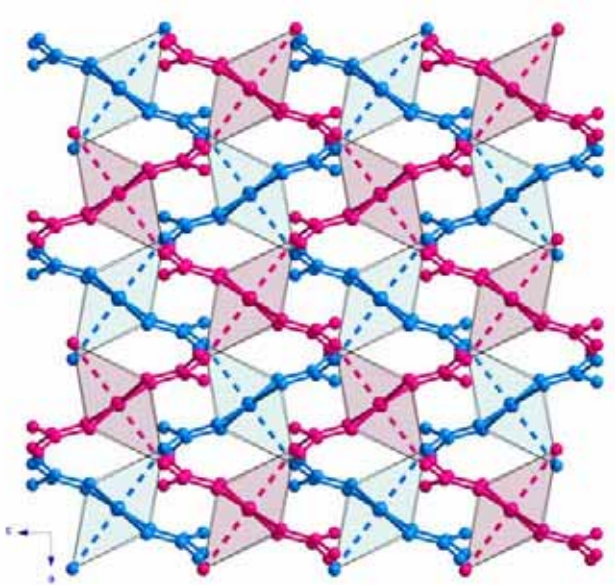

(b)

Figure 18. Perspective view, along the *b*-axis of **(a)** a fragment of the malonate-bridged copper(II) layer and **(b)** the stacking of two consecutives copper(II) layers in **3**. Broken lines represent the apical bonds around each copper atom.

The $[K(H_2O)]^+$ units are connected through double μ-oxo bridges of a water molecule [O(2w)] and a carboxylate-oxygen atom [O(4)], leading thus to a uniform zigzag alkaline chain that runs along the *a*-axis (see Figure 19). The shortest intrachain potassium···potassium distance is 4.0846(6) Å [K(1)···K(2d)].

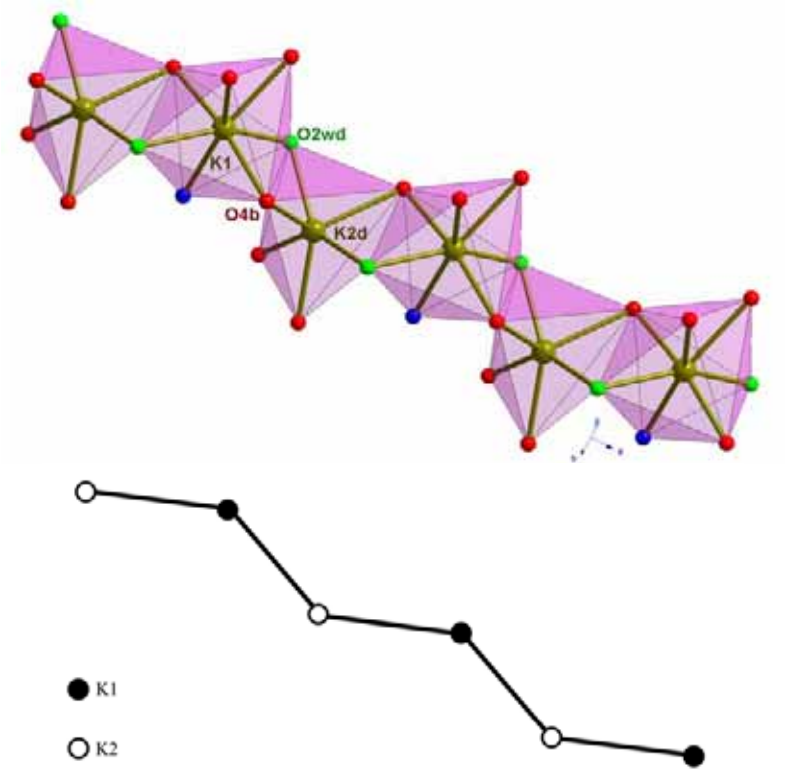

Figure 19. Perspective (top) and schematic (bottom) view of the $[K(H_2O)]^+$ units linked through μ-oxo bridges.

In addition, *anti-anti* [K(2)-bridge-K(1)] and *anti-syn* [K(2)-bridge-K(2)] malonate-carboxylate groups connect adjacent potassium chains, affording a cationic layer that grows in the *ac*-plane (Figure 20). Within the layer, the alkaline chains are stacked in a c1 c2 c1 c2 sequence (see Figure 20, c = chain). Comparing the structures of **2** and **3**, it deserves to be noted that although the alkaline layers stack in a similar sequence (BB'B'; see Figures 7 and 14), the topology of these layers are different, as we can see in the Schemes of Figures 13 and 20.

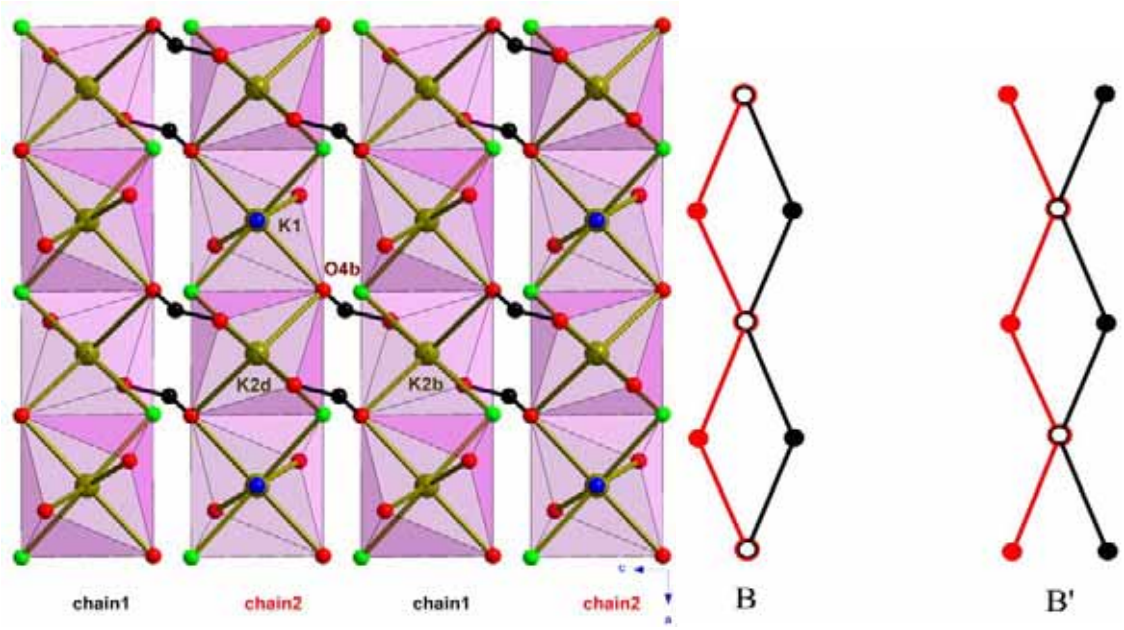

Figure 20. Perspective view along the *b*-axis of the carboxylate-bridged potassium layers (left) and schematic (right) view along the *c*-axis of the stacking of the alkaline chains within these layers.

Copper(II) and alkaline layers are linked through carboxylate-malonate bridges leading to a neutral three-dimensional structure (see Figure 14). They stack in a ABA'B'AB fashion similarly to compound **2**. Hydrogen bonds involving water molecules and malonate oxygen atoms (see Table 10) contribute to the stabilization of the three-dimensional network (see green broken lines in Figure 14).

Table 10. Relevant hydrogen bonds[a-c] for compound **3**

D-H···A	D···A/Å	H···A/Å	D-H···A/º
O(2w)-H···O(3k)	2.755(2)		
O(2w)-H···O(4a)	2.794(2)		
C(2)-H(1)···O(3c)	3.291(3)	2.55(3)	134(2)
C(2)-H(2)···O(1h)	3.569(3)	2.63(2)	163(2)

[a] Symmetry transformations: (a) -*x*, *y*, -*z*+1/2; (c) *x*-1/2, -*y*-1/2, -*z*+1; (h) -*x*+1/2, -*y*-1/2, *z*+1/2; (k) *x*-1/2, *y*-1/2, -*z*+1/2. [b] A = acceptor; D = donor. [c] Symmetry transformations apply to acceptor atoms.

Description of the structure of $\{[Rb_2(H_2O)]\ [Cu(mal)_2]\}_n$ (4)

The structure of compound **4** consists of $[Cu(mal)_2]^{2-}$ anions and $[Rb_2(H_2O)]^{2+}$ cations that are held together by means of carboxylate bridges and water molecules leading thus to a three-dimensional network (see Figure 21). Additionally hydrogen bonds contribute to stabilise the whole structure.

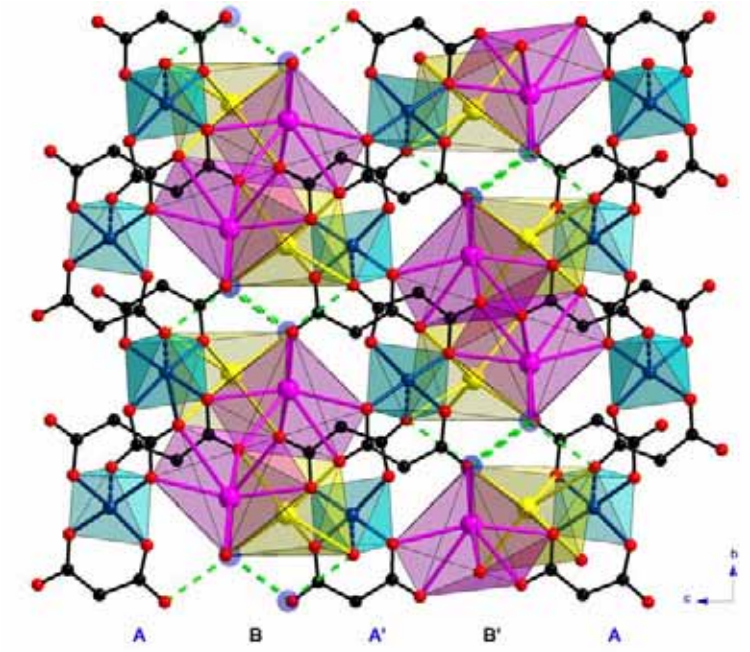

Figure 21. Perspective view, along the *a*-axis of the three-dimensional structure of **4**. Rb(1) and Rb(2) are drawn as yellow and pink solid spheres, respectively.

Each copper(II) atom is five-coordinated (Figure 22) and it exhibits a slightly distorted square pyramidal environment, the τ value being 0.137 [Addison A.W. *et al.*, 1984]. Selected bond lengths and angles for compound **4** are listed in Table 11.

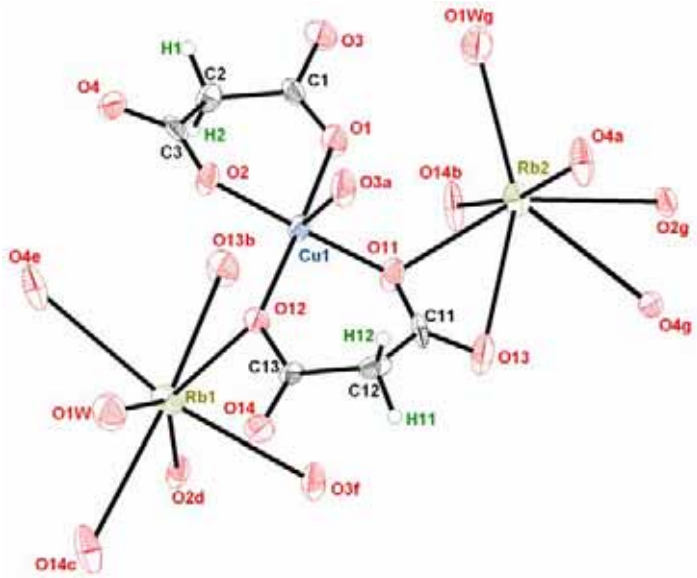

Figure 22. Perspective view of the metal environments in **4**. Thermal ellipsoids are drawn at the 50% probability level.

Table 11. Selected bond lengths (Å) and angles (º) for compound **4**[a]

Cu(1)-O(1)	1.941(6)	Cu(1)-O(2)	1.922(6)
Cu(1)-O(11)	1.916(6)	Cu(1)-O(12)	1.917(6)
Cu(1)-O(3a)	2.589(7)		
O(1)-Cu(1)-O(2)	92.4(3)	O(11)-Cu(1)-O(12)	91.4(3)
O(1)-Cu(1)-O(11)	88.1(3)	O(2)-Cu(1)-O(12)	89.0(3)
O(1)-Cu(1)-O(12)	167.8(3)	O(2)-Cu(1)-O(11)	176.0(3)
O(3a)-Cu(1)-O(1)	97.4(2)	O(3a)-Cu(1)-O(2)	84.5(2)
O(3a)-Cu(1)-O(11)	91.5(2)	O(3a)-Cu(1)-O(12)	94.9(2)
Rb(1)-O(12)	3.062(6)	Rb(1)-O(1w)	2.984(8)
Rb(1)-O(13b)	2.808(7)	Rb(1)-O(14c)	3.069(8)
Rb(1)-O(2d)	3.112(6)	Rb(1)-O(4e)	3.112(8)
Rb(1)-O(3f)	3.154(7)		
O(12)-Rb(1)-O(1w)	63.2(2)	O(1w)-Rb(1)-O(13b)	124.1(2)
O(12)-Rb(1)-O(13b)	73.0(2)	O(1w)-Rb(1)-O(14c)	66.8(2)
O(12)-Rb(1)-O(14c)	121.1(2)	O(1w)-Rb(1)-O(2d)	147.3(2)
O(12)-Rb(1)-O(2d)	144.0(2)	O(1w)-Rb(1)-O(4e)	75.4(2)
O(12)-Rb(1)-O(4e)	94.0(2)	O(1w)-Rb(1)-O(3f)	123.0(2)
O(12)-Rb(1)-O(3f)	89.9(2)	O(13b)-Rb(1)-O(14c)	165.9(2)
O(14c)-Rb(1)-O(2d)	80.6(2)	O(13b)-Rb(1)-O(2d)	87.7(2)
O(14c)-Rb(1)-O(4e)	101.9(2)	O(13b)-Rb(1)-O(4e)	74.8(2)
O(14c)-Rb(1)-O(3f)	92.3(2)	O(13b)-Rb(1)-O(3f)	88.2(2)
O(2d)-Rb(1)-O(4e)	110.2(2)	O(4e)-Rb(1)-O(3f)	160.5(2)
O(2d)-Rb(1)-O(3f)	58.7(2)		
Rb(2)-O(11)	2.876(7)	Rb(2)-O(13)	3.276(7)
Rb(2)-O(4a)	2.855(6)	Rb(2)-O(14b)	2.778(6)
Rb(2)-O(1wg)	2.833(7)	Rb(2)-O(2g)	2.968(7)
Rb(2)-O(4g)	3.061(6)		
O(11)-Rb(2)-O(13)	41.1(2)	O(13)-Rb(2)-O(4a)	80.9(2)
O(11)-Rb(2)-O(4a)	93.1(2)	O(13)-Rb(2)-O(14b)	109.3(2)
O(11)-Rb(2)-O(14b)	92.7(2)	O(13)-Rb(2)-O(1wg)	140.0(2)
O(11)-Rb(2)-O(1wg)	104.7(2)	O(13)-Rb(2)-O(2g)	111.5(2)
O(11)-Rb(2)-O(2g)	150.6(2)	O(13)-Rb(2)-O(4g)	69.3(2)
O(11)-Rb(2)-O(4g)	109.6(2)	O(4a)-Rb(2)-O(14b)	169.3(2)
O(14b)-Rb(2)-O(1wg)	87.9(2)	O(4a)-Rb(2)-O(1wg)	82.0(2)
O(14b)-Rb(2)-O(2g)	88.1(2)	O(4a)-Rb(2)-O(2g)	91.3(2)
O(14b)-Rb(2)-O(4g)	103.6(2)	O(4a)-Rb(2)-O(4g)	82.84(8)
O(1wg)-Rb(2)-O(2g)	104.7(2)	O(2g)-Rb(2)-O(4g)	42.3(2)
O(1wg)-Rb(2)-O(4g)	143.1(2)		

[a] Symmetry codes: (a) –*x*+1, *y*-1/2, -*z*-1/2; (b) -*x*, *y*+1/2, -*z*-1/2; (c) *x*-1/2, -*y*-1/2, -*z*; (d) *x*-1, *y*, *z*; (e) *x*-1/2, -*y*+1/2, -*z*; (f) -*x*, *y*-1/2, -*z*-1/2; (g) –*x*+1/2, -*y*, z-1/2.

Four carboxylate-oxygen atoms from two different malonate groups define the basal plane around the copper atom [the Cu(1)-O(equatorial) bond distances ranging

from 1.916(6) to 1.941(6) Å]. The apical position is occupied by a malonate-oxygen atom [2.589(7) Å for Cu(1)-O(apical)].

Two crystallographically independent seven-coordinated rubidium atoms [Rb(1) and Rb(2)] are present in **4** (see Figure 22). Rb(1) exhibits a highly distorted monocapped trigonal prism (see Figure 23a), the triangular bases being defined by O(1w), O(4e) and O(14c) and O(3f), O(12) and O(13b). Four carboxylate-oxygen atoms [O(13b), O(3f), O(14c), O(4e)] from four different malonate groups are quasi coplanar. The maximum deviation from the mean plane is 0.024(7) Å for O(13b). Rb(1) is shifted by 0.3343(9) Å from this mean plane towards O(1w) and O(12) atoms. The distances of the O(2d), O(1w) and O(12) atoms from the mean equatorial plane are 2.462(6), 2.583(7) and 3.112(6) Å, respectively. The O(2d)-Rb(1)-O(1w) and O(2d)-Rb(1)-O(12) bond angles that define the trigonal prism are 147.3(2) and 144.0(2)°, respectively. Six carboxylate-oxygen atoms from four malonate groups and one water molecule build a highly distorted pentagonal bipyramid around the Rb(2) atom (see Figure 23b). Two malonate-oxygen atoms [O(4a) and O(14b)] occupy the apical positions, whereas four oxygen atoms from two different carboxylate groups and a water molecule define a distorted equatorial plane around Rb(2) [the maximum shift from the mean equatorial plane being 0.335(6) Å for O(11)]. The metal atom is shifted by 0.1703(9) Å from the mean equatorial plane towards O(14b). The Rb-O bond distances are in agreement with those reported for the rubidium salt of the bisoxalate-cuprate(II) rubidium salt [2.902(2)-3.536(2) Å] [Kolitsh U., 2004].

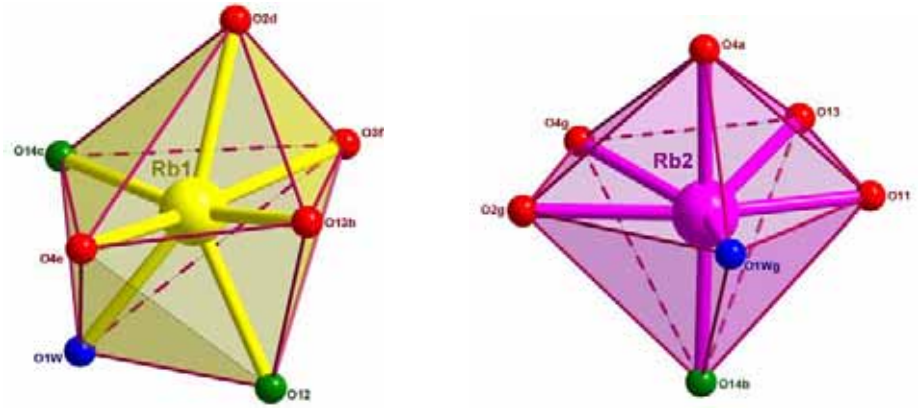

(a) **(b)**

Figure 23. Perspective drawings of the rubidium environments in **4**.

Two crystallographically independent malonate groups are present in **4**: L1 [C(1)-C(2)-C(3)] and L2 [C(11)-C(12)-C(13)] (see Figure 24). Both act as bridging ligands. L1 adopts simultaneously the monodentate [through O(2) towards Rb(1i)], the

bis-monodentate [through O(3) towards Rb(1b) and Cu(1h) and through O(4) towards Rb(1k) and Rb(2h)] and bidentate [through O(1) and O(2) towards Cu(1) and through O(2) and O(4) towards Rb(2j)] coordination modes. The angles subtended by the malonato group at the metal atoms are 92.4(3)º [O(1)-Cu(1)-O(2)] and 42.3(2)º [O(2)-Rb(2j)-O(4)] respectively. L2 acts as tris-monodentate [through O(11), O(12) and O(13) towards Rb(2), Rb(1) and Rb(1f), respectively], bis-monodentate [through O(14) towards Rb(2f) and Rb(1l); (l) *x*+1/2, -*y*-1/2, -*z*] and bidentate [through O(11) and O(12) towards Cu(1)].

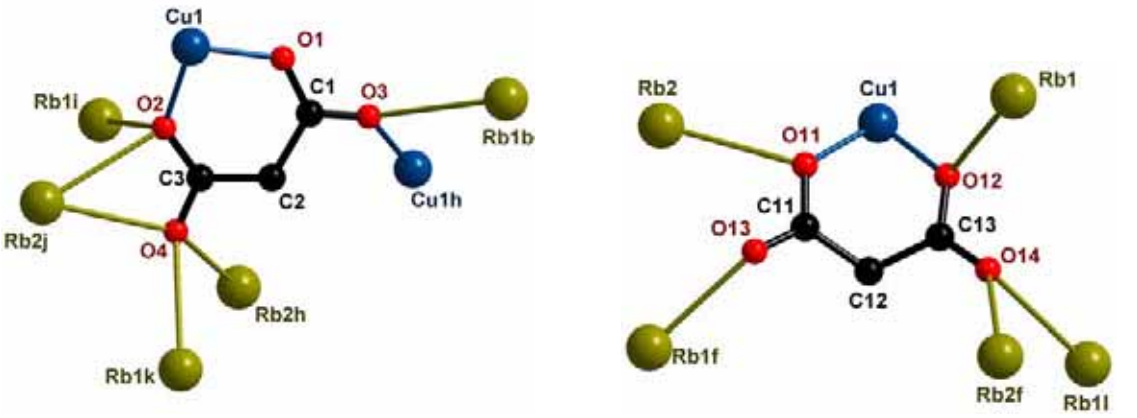

(a) **(b)**

Figure 24. Coordination modes of malonate ligands in **4**: L1 **(a)** and L2 **(b)**. Symmetry codes: (h) -*x*+1, *y*+1/2, -*z*-1/2; (i) *x*+1, *y*, *z*; (j) -*x*+1/2, -*y*, *z*+1/2; (k) *x*+1/2, -*y* + 1/2, -*z*; (l) *x*+1/2, -*y*-1/2, -*z*.

Both malonate groups form a six-membered ring [including the copper atom Cu(1)] that exhibits a boat conformation [Cremer D. *et al.*, 1975] [θ = 94.8(8)º and ϕ = 117.1(9)º for L1 and θ = 95.9(8)º and ϕ = 120.2(8)º for L2]. Each copper atom is linked to five rubidium atoms (through L1 and L2, respectively) and to one copper atom (through L1, involving an apical and an equatorial site). The carboxylate groups of the malonate ligands exhibits the *anti-anti* [Cu(1)-O(1)-C(1)-O(3)-Cu(1h), Cu(1)-O(2)-C(3)-O(4)-Rb(1k), Cu(1)-O(2)-C(3)-O(4)-Rb(2h) and Cu(1)-O(12)-C(13)-O(14)-Rb(2f)] and the *anti-syn* bridging conformations [Cu(1)-O(1)-C(1)-O(3)-Rb(1b), Cu(1)-O(11)-C(11)-O(13)-Rb(1f) and Cu(1)-O(12)-C(13)-O(14)-Rb(1l)]. The inner malonate-oxygen atoms connect the copper atoms with two alkaline ions by means of a μ-oxo bridge [118.3(3), 123.6(3), 123.5(3) and 113.3(3)º for Rb(1i)-O(2)-Cu(1), Rb(2j)-O(2)-Cu(1), Rb(2)-O(11)-Cu(1) and Rb(1)-O(12)-Cu(1), respectively]. The values of the bond length and angles for the malonate ligands (see Table 12) agree with those observed in previous copper(II) malonate complexes [see references of malonate complexes in the Introduction].

Table 12. Bond lengths (Å) and angles (º) for malonate ligands in **4**

C(1)-C(2)	1.516(13)	C(2)-C(3)	1.493(13)
C(1)-O(1)	1.258(10)	C(3)-O(2)	1.258(11)
C(1)-O(3)	1.260(11)	C(3)-O(4)	1.257(11)
O(1)···O(2)	2.787(9)	O(3)···O(4)	4.519(10)
O(1)-C(1)-O(3)	120.9(9)	O(2)-C(3)-O(4)	120.0(9)
O(1)-C(1)-C(2)	121.3(8)	O(2)-C(3)-C(2)	121.8(8)
O(3)-C(1)-C(2)	117.8(7)	O(4)-C(3)-C(2)	118.1(9)
C(1)-C(2)-C(3)	117.2(7)		
C(1)-O(1)-Cu(1)	124.7(6)	C(3)-O(2)-Cu(1)	125.1(6)
O(1)C(1)O(3)-Cu(1)eq[a]	27.0(6)	O(2)C(3)O(4)-Cu(1)eq[a]	31.9(6)
C(11)-C(12)	1.510(13)	C(12)-C(13)	1.524(13)
C(11)-O(11)	1.286(10)	C(13)-O(12)	1.279(10)
C(11)-O(13)	1.218(11)	C(13)-O(14)	1.226(11)
O(11)···O(12)	2.743(9)	O(13)···O(14)	4.507(11)
O(11)-C(11)-O(13)	121.9(9)	O(12)-C(13)-O(14)	123.1(9)
O(11)-C(11)-C(12)	119.3(8)	O(12)-C(13)-C(12)	118.6(8)
O(13)-C(11)-C(12)	118.7(8)	O(14)-C(13)-C(12)	118.2(8)
C(11)-C(12)-C(13)	118.0(7)		
C(11)-O(11)-Cu(1)	125.8(6)	C(13)-O(12)-Cu(1)	126.5(6)
O(11)C(11)O(13)-Cu(1)eq[a]	24.0(6)	O(12)C(13)O(14)-Cu(1)eq[a]	29.6(7)

[a]dihedral angle (º) between the malonate carboxylate group and the mean equatorial plane of the metal atom

The $[Cu(mal)_2]^{2-}$ units are linked to two other ones through *anti-anti* carboxylate bridges, leading to uniform malonate-bridged copper(II) chains which run parallel to the *b*-axis (see Figure 25). The shortest intrachain copper···copper separation is 6.1197(14) Å and the dihedral angle between the mean basal planes of adjacent copper atoms is 67.78(15)º. Each copper(II) chain is linked to four adjacent ones by hydrogen bonds (see green broken lines in Figure 25b) that involve water molecules and malonate-oxygen atoms leading to a three-dimensional network.

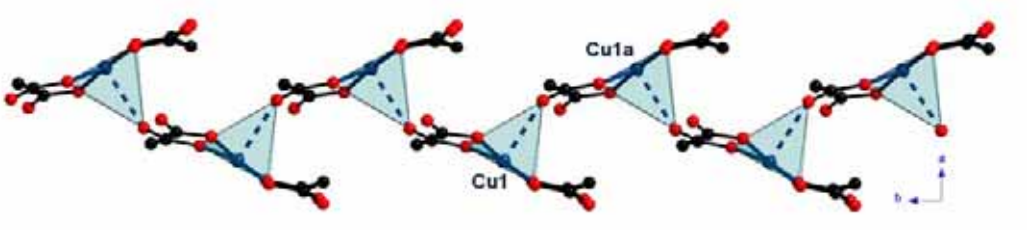

(a)

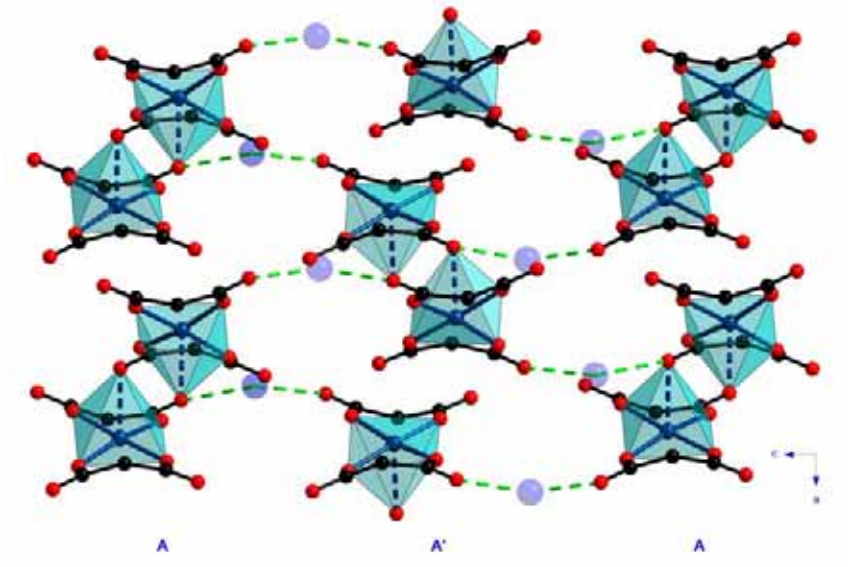

(b)

Figure 25. (a) Perspective view, along the *c*-axis of the malonate-bridged copper(II) chains in **4**. The apical bond of the metals atom is drawn as a blue broken line. **(b)** Perspective view, along the *b*-axis, of the arrangement of the copper(II) chains in **4**. Hydrogen bonds are illustrated as green broken lines.

It deserves to be noted that regarding the stacking of the copper(II) chains, in the *ab*-plane (Figure 26), one can distinguish a similar topology to that observed for the copper(II) layers in **2** and **3** (see Figures 11 and 18a).

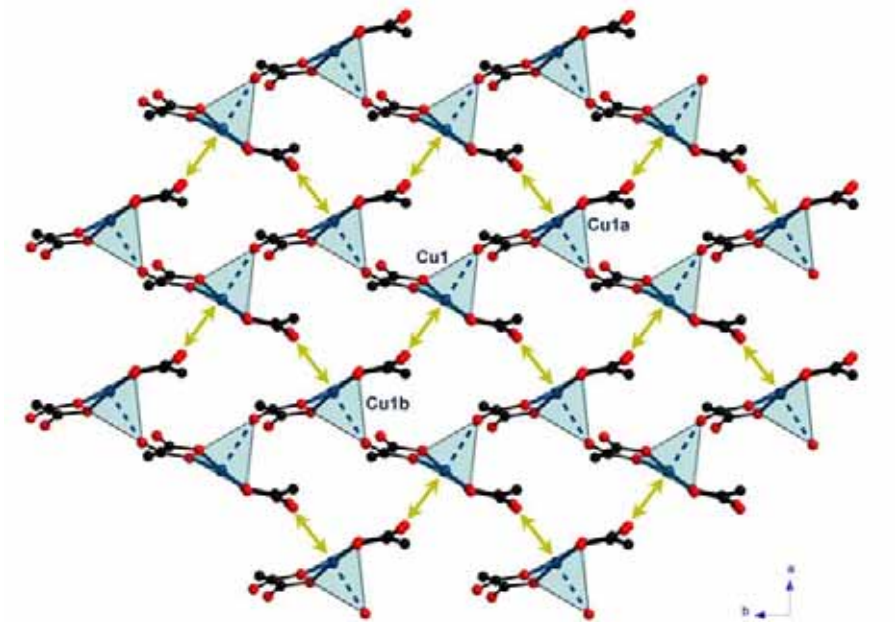

Figure 26. Perspective view of the malonate-bridged copper(II) chains which are stacked along the *a*-axis. The apical bond at the copper(II) is drawn as broken line. The yellow arrow represents the long Cu(1)···O(13b) distance (see text).

Unlike to the anionic layers in **2** and **3,** where each $[Cu(mal)_2]^{2-}$ unit is linked to four other ones equally distant [5.8562(9) (**2**) and 6.2435(4) Å (**3**) for Cu(1)···Cu(1b)],

there are two different separations between the $[Cu(mal)_2]^{2-}$ units in **4**, (see Figure 26): 6.1197(14) [Cu(1)···Cu(1a)] and 6.4355(15) Å [Cu(1)···Cu(1b)]. In the present complex, Cu(1) and Cu(1b) are not linked by a carboxylate-malonate bridge because the Cu(1)···O(13b) distance [3.138(7) Å] (highlighted as a yellow arrow in Figure 26) is too long to be consider as a bond. So, in **4** the greater size of the rubidium atom causes a larger separation of the copper(II) chains and breaks the uniform malonate-bridged copper(II) layer observed in **2** and **3**.

The rubidium cations units are linked together through μ-oxo bridges involving water molecules and some of the malonate oxygen atoms (Figure 27a).

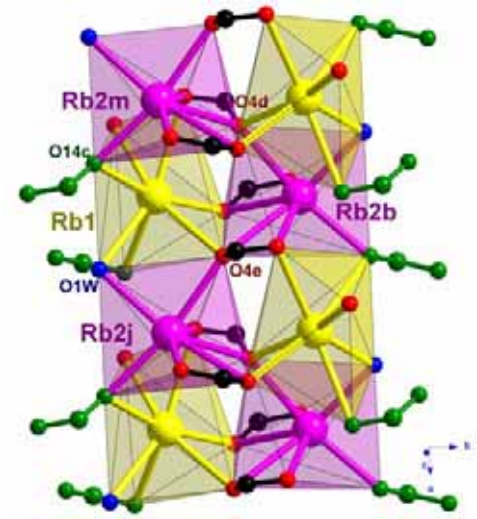

(a)

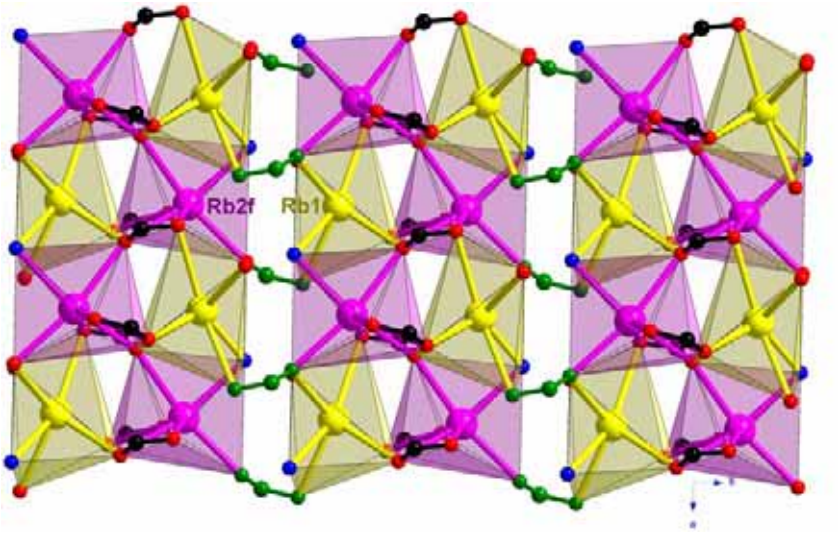

(b)

Figure 27. Arrangement of the rubidium cations in **4**. **(a)** Perspective view of the alkaline double helical chain and **(b)** the two-dimensional network built up by $[Rb_2(H_2O)]^{2+}$ linked through μ-oxo and carboxylate bridges; (m) $-x-1/2, -y, z+1/2$.

Each rubidium atom is connected to three other ones through double μ-oxo: Rb(1)-O(4e)/O(13b)-Rb(2b) [4.3628(12) Å for Rb(1)···Rb(2b)], Rb(1)-O(2d)/O(14c)-Rb(2m) [4.1218(14) Å for Rb(1)···Rb(2m)] and Rb(1)-O(4e)/O(1w)-Rb(2j) [4.1953(14) Å for Rb(1)···Rb(2j)]; and μ-oxo bridges: Rb(2b)-O(4d)-Rb(2m) and Rb(2b)-O(4e)-Rb(2j) [5.6406(13) Å for Rb(2)···Rb(2) separations], affording thus a double alkali helical chain which run along the *a*-axis. Furthermore, these cationic chains are connected through carboxylate-bridges [O(12)-C(13)-O(14)] leading to a two-dimensional network that grow in the *ab*-plane [see Figure 27b, the Rb(1)···Rb(2f) separation is 5.1034(12) Å].

Both copper(II) and alkaline layers are linked through carboxylate-malonate bridges and hydrogen bonds (see Table 13) leading to a neutral three dimensional structure (see Figure 21). The copper(II) and rubidium layers are stacked in a ABA'B'AB fashion.

Table 13. Relevant hydrogen bonds[a-c] for compound **4**

D-H···A	D···A/Å	H···A/Å	D-H···A/º
O(1w)-H···O(3j)	2.849(11)		
O(1w)-H···O(14)	2.743(11)		
C(2)-H(2)···O(13b)	3.322(11)	2.604(7)	131.0(5)
C(12)-H(11)···O(11f)	3.601(10)	2.646(6)	168(5)
C(12)-H(12)···O(1a)	3.658(11)	2.732(7)	160(5)

[a] Symmetry transformations: (a) -*x*+1, *y*-1/2, -*z*-1/2; (b) -*x*, *y*+1/2, -*z*-1/2; (j) -*x*+1/2, -*y*, *z*+1/2; (f) -*x*, *y*-1/2, -*z*-1/2. [b] A = acceptor; D = donor. [c] Symmetry transformations apply to acceptor atoms.

Description of the structure of $\{[Cs(H_2O)]_2[Cu(mal)_2(H_2O)_2]\}_n$ (5).

The structure of compound **5** is made up of $[Cu(mal)_2(H_2O)_2]^{2-}$ anions and $[Cs(H_2O)]^{+}$ cations that are held together by means of carboxylate bridges, water molecules and hydrogen bonds, leading thus to a three-dimensional network. (Figure 28).

The copper atom lies on a $\bar{1}$ crystallographic site symmetry. The metal ion is six-coordinated (see Figure 29) exhibiting a 4+2 elongated octahedral environment (ϕ = 54.6º and *s/h* = 1.40). Selected bond lengths and angles for compound **5** are listed in Table 14.

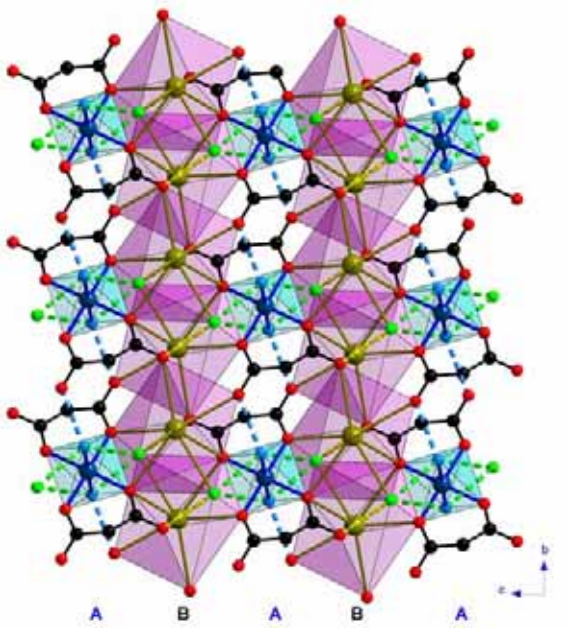

Figure 28. Perspective view of the three-dimensional network in **5**. The hydrogen bonds are represented by broken lines.

Four carboxylate-oxygen atoms from two different malonate groups build the equatorial plane of the metal ion [the values of the Cu(1)-O(equatorial) bond distances are 1.935(2) and 1.970(3) Å]. Apical positions are filled by two symmetrically-related water oxygen atoms [Cu(1)-O(apical) = 2.411(3) Å].

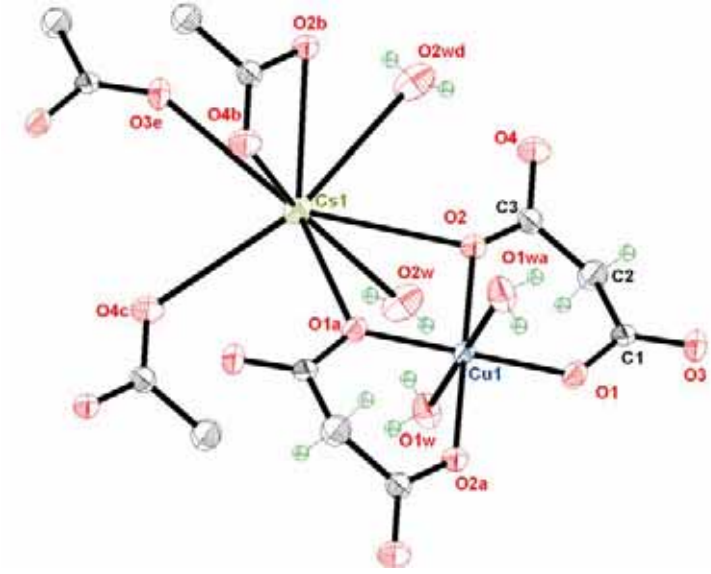

Figure 29. Perspective view of the metal environments in **5**. Thermal ellipsoids are drawn at the 50% probability level.

The cesium atom is eight-coordinated exhibiting a highly distorted square antiprism environment (see Figure 30). Two water molecules [O(2w) and O(2wd)] and two carboxylate-malonate oxygen atoms [O(3e) and O(4c)] conform one basal plane of the square antiprism [the maximum separations from the mean basal plane being

0.114(4) Å for O(2wd) and the Cs(1)-mean basal plane distance is 1.1449(2) Å]. The other basal plane of the antiprism anticube is slightly distorted [the maximum shift from the mean basal plane is 0.203(3) Å for O(4b)] and it is defined by four carboxylate-oxygen atoms from three different malonate groups [the Cs(1)-mean basal plane distance is 2.1613(2) Å]. The Cs-O bond distances for the cesium salt of the bis(oxalate) cupprate(II) $Cs_2Cu(ox)_2 \cdot 2H_2O$ [Pannhorst W. *et al.*, 1974] agree with those reported here.

Table 14. Selected bond lengths (Å) and angles (°) for compound **5**[a]

Cu(1)-O(1)	1.935(2)	Cu(1)-O(2)	1.970(3)
Cu(1)-O(1w)	2.414(3)		
O(1)-Cu(1)-O(2)	92.82(11)	O(1)-Cu(1)-O(2a)	87.18(11)
O(1w)-Cu(1)-O(1)	92.90(11)	O(1w)-Cu(1)-O(1a)	87.10(11)
O(1w)-Cu(1)-O(2)	94.50(11)	O(1w)-Cu(1)-O(2a)	85.50(11)
Cs(1)-O(1a)	3.040(3)	Cs(1)-O(2)	3.211(3)
Cs(1)-O(2w)	3.401(3)	Cs(1)-O(2b)	3.456(3)
Cs(1)-O(4b)	3.407(4)	Cs(1)-O(3e)	3.083(3)
Cs(1)-O(4c)	3.117(3)	Cs(1)-O(2wd)	3.311(4)
O(1a)-Cs(1)-O(2)	50.94(7)	O(2)-Cs(1)-O(2w)	68.82(8)
O(1a)-Cs(1)-O(2w)	88.96(8)	O(2)-Cs(1)-O(2b)	86.64(6)
O(1a)-Cs(1)-O(2b)	98.65(7)	O(2)-Cs(1)-O(4b)	91.77(7)
O(1a)-Cs(1)-O(4b)	73.33(7)	O(2)-Cs(1)-O(3e)	146.99(7)
O(1a)-Cs(1)-O(3e)	132.82(8)	O(2)-Cs(1)-O(4c)	134.55(7)
O(1a)-Cs(1)-O(4c)	88.97(8)	O(2)-Cs(1)-O(2wd)	73.05(8)
O(1a)-Cs(1)-O(2wd)	123.91(7)	O(2b)-Cs(1)-O(4b)	37.57(7)
O(2w)-Cs(1)-O(2b)	141.11(8)	O(2b)-Cs(1)-O(3e)	60.62(7)
O(2w)-Cs(1)-O(4b)	159.61(8)	O(2b)-Cs(1)-O(4c)	124.59(7)
O(2w)-Cs(1)-O(3e)	134.78(8)	O(2b)-Cs(1)-O(2wd)	72.72(7)
O(2w)-Cs(1)-O(4c)	93.43(9)	O(3e)-Cs(1)-O(4c)	74.25(8)
O(2w)-Cs(1)-O(2wd)	71.48(10)	O(3e)-Cs(1)-O(2wd)	91.86(8)
O(4b)-Cs(1)-O(3e)	65.40(8)	O(4b)-Cs(1)-O(2wd)	109.82(8)
O(4b)-Cs(1)-O(4c)	96.22(8)	O(4c)-Cs(1)-O(2wd)	142.24(9)

[a] Symmetry codes: (a) -*x*+1, -*y*, -*z*; (b) -*x*+1, -*y*, -*z*+1; (c) *x*, *y*-1, *z*; (d) -*x*, -*y*, -*z*+1; (e) *x*, *y*-1, *z*+1.

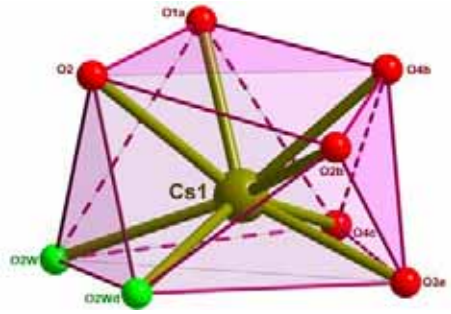

Figure 30. Perspective drawing of the cesium environment in **5**.

The malonate group (see Figure 31) adopts simultaneously the monodentate [through O(1), O(2), O(3) and O(4) towards Cs(1a), Cs(1), Cs(1g) and Cs(1f), respectively] and bidentate [through O(1) and O(2) towards Cu(1) and through O(2) and O(4) towards Cs(1b)] coordination modes. The angles subtended by the malonate group at the metal atoms are 92.89(9)º and 37.57(7)º for Cu(1) and Cs(1b), respectively.

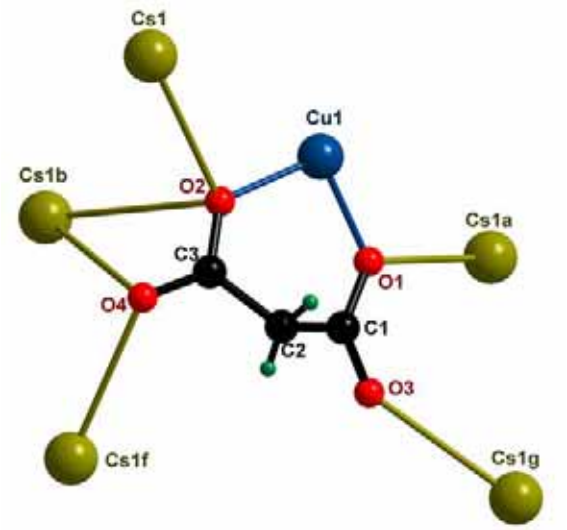

Figure 31. Coordination mode of the malonate ligand in **5** [(g) *x*, *y*+1, *z*-1].

The malonate ligand exhibit a six-membered ring [including the Cu(1) atom] that adopts a slightly distorted screw boat conformation [Cremer D. *et al.*, 1975] [θ = 79.7(3)º and ϕ = 114.4(4)º]. Each copper atom is linked to five cesiums atoms through the malonate ligand. The carboxylate groups exhibit the *anti-anti* [Cu(1)-O(2)-C(3)-O(4)-Cs(1f)] and the *anti-syn* [Cu(1)-O(1)-C(1)-O(3)-Cs(1g) and Cu(1)-O(2)-C(3)-O(4)-Cs(1b)] bridging conformations. The inner malonate oxygens connect the copper atoms with three cesium ions by means of a μ-oxo bridges [109.94(11), 102.83(9) and 122.12(12)º for Cs(1a)-O(1)-Cu(1), Cs(1)-O(2)-Cu(1) and Cs(1b)-O(2)-Cu(1) respectively]. The geometric parameters of the malonate group (see Table 15) agree with those observed in previously reported malonate-copper(II) complexes [see references concerning copper(II) malonate complexes in the Introduction].

Table 15. Bond lengths (Å) and angles (º) for malonate ligand in **5**

C(1)-C(2)	1.504(6)	C(2)-C(3)	1.514(5)
C(1)-O(1)	1.270(5)	C(3)-O(2)	1.264(5)
C(1)-O(3)	1.231(4)	C(3)-O(4)	1.254(5)
O(1)···O(2)	2.831(4)	O(3)···O(4)	4.421(4)
O(1)-C(1)-O(3)	122.0(4)	O(2)-C(3)-O(4)	122.7(4)
O(1)-C(1)-C(2)	118.9(3)	O(2)-C(3)-C(2)	119.9(3)

O(3)-C(1)-C(2)	119.1(3)	O(4)-C(3)-C(2)	117.4(4)
C(1)-C(2)-C(3)	117.3(3)		
C(1)-O(1)-Cu(1)	127.4(2)	C(3)-O(2)-Cu(1)	126.5(2)
O(1)C(1)O(3)-Cu(1)eq[a]	19.4(3)	O(2)C(3)O(4)-Cu(1)eq[a]	37.3(4)

[a]dihedral angle (º) between the malonate carboxylate group and the mean equatorial plane of the metal.

Hydrogen bonds (see Table 16) involving the O(1w) water molecule and the O(3) malonate oxygen atom connect the $[Cu(mal)_2]^{2-}$ units leading to regular malonate copper(II) chain which runs parallel to the *b*-axis [see Figure 32a, 7.1316(9) Å for Cu(1)···Cu(1c)]. These chains are stacked along the *a*-axis and they are held together by means of hydrogen bonds involving only water molecules (see green broken lines in Figure 32b). Finally, additional hydrogen bonds involving O(2w) water molecules and the O(4) outer malonate oxygen atoms connect each chain to four other ones (see yellow broken lines in Figure 32b) leading to a three-dimensional network.

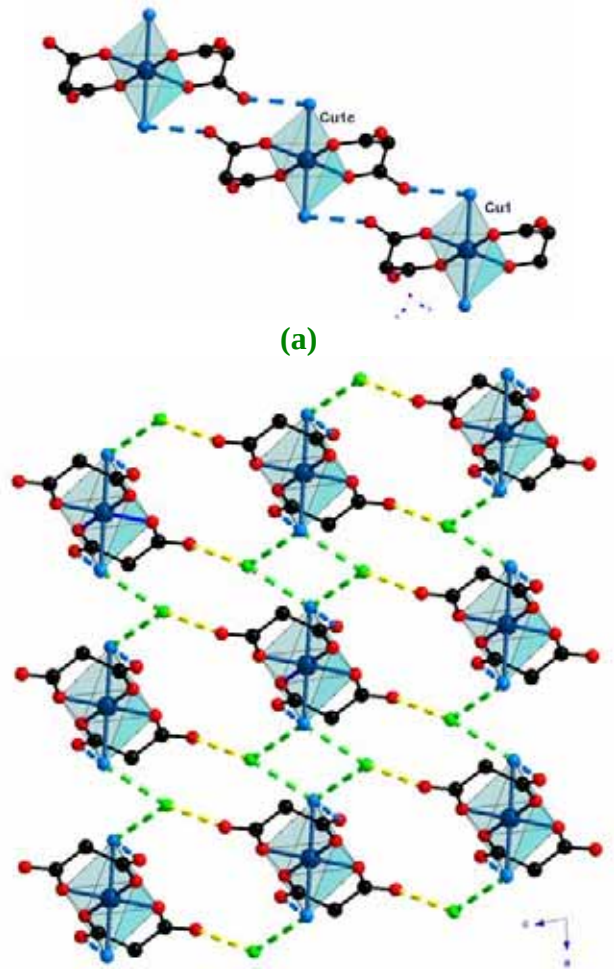

(a)

(b)

Figure 32. (a) Perspective view of the hydrogen bonded malonate copper(II) chain running parallel to the *b*-axis in **5**. **(b)** Projection down the *b*-axis of the malonate copper(II) chains, in **5**, which are held together by means of hydrogen bonds (broken lines).

Table 16. Relevant hydrogen bonds[a-c] for compound **5**

D-H···A	D···A/Å	H···A/Å	D-H···A/º
O(1w)-H(1w1)···O(3c)	2.708(4)	2.05(5)	165(5)
O(1w)-H(2w1)···O(2w)	2.771(5)	2.07(5)	155(6)
O(2w)-H(1w2)···O(1wh)	2.816(5)	2.19(6)	139(6)
O(2w)-H(2w2)···O(2wd)	2.748(5)	2.08(7)	160(8)
C(2)-H(1)···O(1wh)	3.570(5)	2.53(6)	161(4)

[a] Symmetry transformations: (c) *x*, *y*-1, *z*; (d) -*x*, -*y*, -*z*+1; (h) -*x*, -*y*, -*z*. [b] A = acceptor; D = donor.
[c] Symmetry transformations apply to acceptor atoms.

Each $[Cs(H_2O)_2]^+$ unit is linked to other three ones through three double μ-oxo bridges ($\bar{1}$ symmetrically related) affording thus to a two-dimensional network that grow in the *ab*-plane (Figure 33). The cesium···cesium separations and cesium-oxygen-cesium bond angles are 5.4486(6) Å and 108.76(11)º [Cs(1)-O(4b)-Cs(1k)], 4.3609(6) Å and 83,72(7)º [Cs(1)-O(2wd)-Cs(1d)] and 4.8529(6) Å and 93.38(6)º [Cs(1)-O(2b)-Cs(1b)]. Additional carboxylato bridges [O(1)-C(1)-O(3) and O(2)-C(3)-O(4)] help to stabilize the layer of rubidium(I) ions .

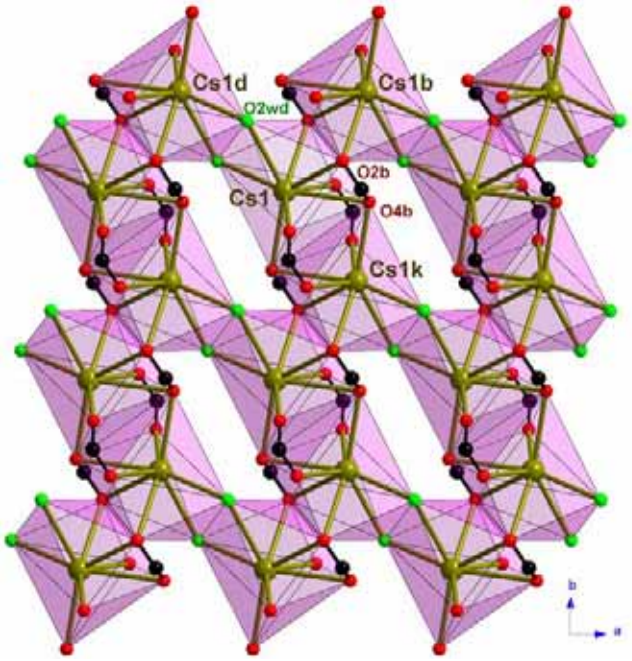

Figure 33. Perspective view along the *c*-axis, of an alkaline layer in **5** which is made up of $[Cs(H_2O)]^+$ units linked through μ-oxo and carboxylate bridges [Symmetry code: (k) -*x*+1, -*y*-1, -*z*+1].

Finally, the copper and cesium layers are linked through carboxylate-bridges and hydrogen bonds stacking in a ABAB sequence, leading thus to a neutral three-dimensional network (see Figure 28).

Magnetic properties

The magnetic properties of **1**, **4** and **5** under the form of $\chi_M T$ vs. T plot are shown in Figure 34, χ_M being the magnetic susceptibility per mol of Cu(II) ions. The values of $\chi_M T$ at room temperature are 0.41 (**1**), 0.43 (**4**) and 0.44 $cm^3mol^{-1}K$ (**5**). These values are as expected for a magnetically isolated spin doublet. Upon cooling, $\chi_M T$ remains almost constant following a Curie law and only at low temperatures the magnetic behaviour deviates from the Curie law. $\chi_M T$ slightly decrease in the case of **1** and increase for **4** and **5,** reaching a value of 0.69 $cm^3mol^{-1}K$ for **5**. These features indicate the occurrence of weak antiferro- (**1**) and ferromagnetic (**4** and **5**) interactions. The inset of the Figure 34 shows the magnetisation curve for **4** which runs above the Brillouin function for a spin doublet, confirming the occurrence an overall ferromagnetic interaction in this compound.

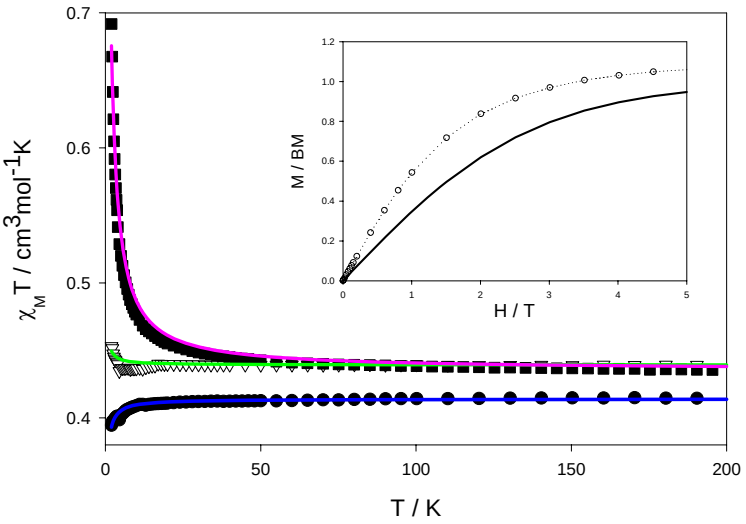

Figure 34. Thermal dependence of the $\chi_M T$ product of **1** (!)**, 4** (#)**,5** (∇); the solid lines are the best-fit curves (see text). The inset shows the magnetisation *versus H* plot at 2.0 K for 2: (C) Brillouin function for a spin doublet; (···) eye-guide line; (o) experimental data.

Compounds **1** and **5** have a mononuclear nature. The least-square fitting to the magnetic data of **1** and **5** through a Curie-Weiss law leads to $g = 2.101(2)$, $\theta = -0.106(4)$ cm^{-1} and $R = 2.1 \times 10^{-5}$ for **1** and $g = 2.164(1)$, $\theta = +0.046(8)$ cm^{-1} and $R = 7.2 \times 10^{-5}$ for **5** {where R is the agreement factor described as $\Sigma[(\chi_M)_{obs} - (\chi_M)_{calc}]^2/\Sigma[(\chi_M)_{obs}]^2$}. It deserves to be noted that the extensive hydrogen bonding interactions are not able to mediate any significant magnetic interaction in **1** and **5**.

From a magnetic point of view, the structure of compound **4** consists of uniform malonate bridged copper(II) chains. The magnetic data are treated by means of the

Baker and Rushbrooke model [Baker G. A., 1964] for a S = 1/2 regular ferromagnetic chain [eqns. (1)-(4)]

$$\chi_M = (N\beta^2 g^2 / 4kT)(A/B)^{2/3} \quad (1)$$

$$A = 1.0 + 5.7979916\,y + 16.902653\,y^2 + 29.376885\,y^3 + 29.832959\,y^4 + 14.036918\,y^5 \quad (2)$$

$$B = 1.0 + 2.7979916\,y + 7.0086780\,y^2 + 8.6538644\,y^3 + 4.57433114\,y^4 \quad (3)$$

with $y = J/kT$ and with the spin Hamiltonian defined as:

$$\hat{H} = \sum_i - J\hat{S}_i \cdot \hat{S}_{i+1} \quad (4)$$

The best least-square fit of the thermal dependence of $\chi_M T$ product leads to the following parameters J = +0.82(3) cm^{-1}, g = 2.155(1) and R =4.0x10^{-4}. The calculated curves match well the experimental data in the whole temperature range.

The thermal dependence of $\chi_M T$ product ($\chi_M T$ being the magnetic susceptibility per mol of copper(II) ions) for **2**-**3** is shown in Figure 35 and 36, respectively. The magnetic data measurements were done in the 2-300 (**2**) and 2-200 K (**3**) temperature range. $\chi_M T$ at the highest measured temperature is 0.44 (**2**) and 0.47 cm^{3}mol^{-1}K (**3**), values which are close to the value expected for a magnetically isolated spin doublet. Upon cooling, $\chi_M T$ remains almost constant up to 60 K, and then it smoothly increases, at lower temperatures, to reach at 2 K a value of 1.72 and 1.50 cm^{3}mol^{-1}K, for **2** and **3**, respectively.

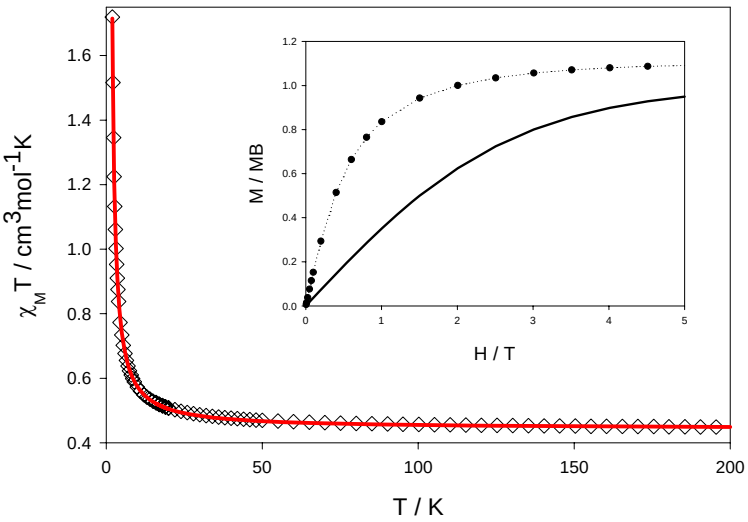

Figure 35. Thermal dependence of the $\chi_M T$ product of **2**: (◊) experimental data; (-) best fit curve (see text). The inset shows the magnetisation *versus* H plot at 2.0 K for 2: (C) Brillouin function for a spin doublet; (···) eye-guide line; (o) experimental data.

This behaviour is indicative of the occurrence of an overall ferromagnetic coupling between the copper(II) ions, confirmed by the magnetization curve that runs above the Brillouin curve for a spin doublet. The structure of both compounds consist of $[Cu(mal)_2]^{2-}$ layers that are held together by means of $[M(H_2O)]^{+}$ layers (M = Na, K) to afford a three-dimensional structure. We try to fit the magnetic data through the high-temperature expansion series derived from the 2D Heisenberg model for the S = ½ ferromagnetic quadratic lattice [Navarro R., 1990]:

$$\chi = Ng^2\beta^2 S(S+1)/(3kT)\left[1+\sum_{n=1}^{8} a_n K^n\right] \qquad (5)$$

where K is $J/2kT$, J is the intrachain magnetic coupling parameter, N the Avogadro's number, g the Landé factor, β the Bohr magneton, k the Boltzman constant. The a_n coefficients are taken for a square lattice. The spin Hamiltonian is defined as in eq (4). The best least-square fit parameters are J = +0.897(1) cm^{-1}, g = 2.175(1) and R = $3.8x10^{-5}$ (for **2**) and J = +0.774(2) cm^{-1}, g = 2.243(2) and R =$6.9x10^{-5}$ (for **3**). The calculated curve matched well the experimental data in the whole temperature range.

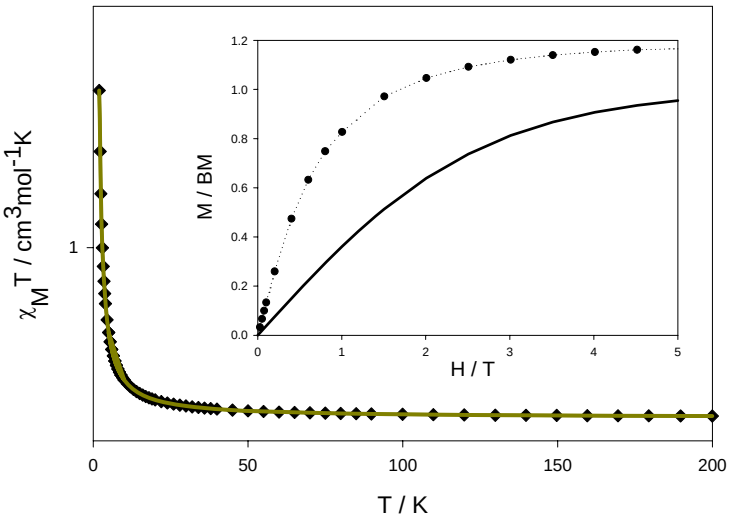

Figure 36. Temperature dependence of the $\chi_M T$ product of **3**: (♦) experimental data; (-) best fit curve (see text). The inset shows the magnetisation *versus* H plot at 2.0 K for 2: (C) Brillouin function for a spin doublet; (···) eye-guide line; (o) experimental data.

The magnetic behaviour of **4** is shown in the Figure 34 under the form of $\chi_M T$ vs. T (χ_M being the molar magnetic susceptibility per copper(II) ion). $\chi_M T$ at room temperature is 0.43 $cm^3mol^{-1}K$, a value which is as expected for a magnetically isolated spin doublet. Upon cooling $\chi_M T$ continuously increase to reach a maximum value of 0.69 cm^3mol^{-1} K at 2K. This behaviour is indicative of the occurrence of an overall

ferromagnetic coupling between the copper(II) ions, confirmed by the magnetization curve that runs above the Brillouin function for a spin doublet.

The weak ferromagnetic interaction observed in **2-4** can be explained considering the out-of-plane exchange pathway between adjacent copper(II) atoms. The unpaired electron of Cu(II) in this series is defined essentially by a $d_{x}2\text{-}_{y}2$ type magnetic orbital (the x and y axes being roughly defined by the copper to oxygen bonds) and it is mainly located in the equatorial plane defined by the malonate oxygen atoms due to the large apical-metal bond distances. A low spin density is expected in the axial positions because of some admixture of the d_{Z^2} character due to the trigonal distortion of the copper(II) environment. The shortest intermolecular magnetic exchange pathway in **2-4** [Cu-O-C-O···Cu] involve an equatorial position at one copper(II) atom and an apical position at the nearest neighbouring copper(II). Consequently, the overlap (S) between the magnetic orbitals of adjacent copper(II) ions is predicted to be very small reducing the antiferromagnetic contribution. The weak ferromagnetic coupling observed in these compounds is due to the accidental orthogonality between the magnetic orbitals through the out-of-plane exchange pathway. This behaviour have been previously observed in other malonate [Ruiz-Pérez C. *et al.*, 2000c; Sanchiz J. *et al.*, 2002; Delgado F.S. *et al.*, 2003 and 2004] and carboxylate bridged copper(II) complexes as oxalate [Gleizes A. *et al.*, 1980; Bloomquist D.R. *et al.*, 1981; Geiser U. *et al.*, 1987; Kou H.-Z. *et al.*, 1998; Grove H. *et al.*, 2002] and phenylmalonate [Pasán J. *et al.*, 2004], the effectiveness of the magnetic exchange depending on the structural features of each compound. The value of the ferromagnetic coupling are in good agreement with that observed in the above compounds. It deserved to be note that $[Cu(Hmal)_2]$ [J = 0.104(4) cm^{-1}] exhibit a malonate bridged copper(II) layer which topology is quite similar to the anionic two-dimensional copper(II) network one in **2** and **3**. The interaction is more effective for mal^{2-} compounds than in the $Hmal^{-}$ one due to the degree of the protonation of the malonate anion.

References

Abrahams B.F, Hoskins D.M. and Robson R., *Nature*, **1994**, 369, 727.

Addison A.W., Rao T.N., Reedijk J., Rijn J. and Verschoor G.C.J., *J. Chem. Soc., Dalton Trans.*, **1984**, 1349.

Antolini L., Menabue L., Saladini M. and Sola M., *Inorg. Chim. Acta*, **1988**, *152*, 17.

Baker G. A., Rushbrooke G.S. and Gilbert H.E., *Phys. Rev.*, **1964**, 135, A1272.

Barnes J.C. and Weakely T.J.R., Private deposition in the Cambridge Crystallographic Data Center, **1997**. CCDC reference code: RUWMUR.

Bloomquist D.R., Hansen J.J., Landee C.P., Willett R.D. and Buder R. *Inorg. Chem.*, **1981**, 20, 3308.

Chanannont P., Nixon P.E., Waters J.M. and Waters T.N., *Acta Crystallogr., Sect.B*, **1980**, 36, 2145.

Chung Y.H., Wei H.H., Liu Y.H., Lee G.H. and Wang Y., *Polyhedron*, **1998**, 174, 449.

Ciurtin D.M., Smith M.D. and zur Loye H.-C., *Dalton Trans.*, **2003**, 1245 *and references therein.*

Cremer D. and Pople J.A., *J. Am. Chem. Soc.*, **1975**, 97, 1354.

Delgado F.S., Sanchiz J., Ruiz-Pérez C., Lloret F. and Julve M., *Inorg. Chem.*, **2003**, 42, 5938.

Delgado F.S., Sanchiz J., Ruiz-Pérez C., Lloret F. and Julve M., *CrystEngComm.*, **2004**, 6, 443.

Deng S.-L., Long L.-S., Zheng L.-S. and Ng S.W., *Main Group Metal Chemistry*, **2002**, 25, 465.

DIAMOND 2.1d, Crystal Impact GbR, CRYSTAL IMPACT, K. Brandenburg & H. Putz GbR, Postfach 1251, D-53002 Bonn, Germany, 2000.

Duisenberg A.J.M., Kroon-Batenburg L.M.J. and Schreurs A.M.M., *J. Appl. Cryst.*, **2003,** 36, 220 (EVALCCD).

Earshaw A., *Introduction to Magnetochemistry*; Academic Press; London, **1968**.

Farrugia L.J., (*WINGX*), *J. Appl. Cryst*, **1999**, 32, 837.

Fan J., Sun W.-Y., Okamura T. and Yu K.-B., *Inorg. Chim. Acta*, **2001**, 319, 240.

Gardner G.B., Venkataraman D., Moore J.S. and Lees S., *Nature* **1995**, 374, 792.

Geiser U., Ramakrishna B.L., Willett R.D., Hulsbergen F.B. and Reedijk J., *Inorg. Chem.*, **1987**, 26, 3750.

Gleizes A., Maury F. and Galy J., *Inorg. Chem.*, **1980**, 19, 2074.

Gibney B.R., Kessissoglou D.P., Kampf J.W. and Pecoraro V.L., *Inorg. Chem.* **1994**, 33, 4840.

Goher M.A.S. and Mautner F.A., *Polyhedron*, **1994**, 13, 149.

Grove H., Sletten J., Julve M., Lloret F., Lezama L., Carranza J., Parsons S. and Rillema P., *J. Mol. Struct.*, **2002**, 606, 253.

Hardt H.D. and Street G., *Z. Anorg. Allg. Chem.*, **1967**, 350, 84.

Hooft, R.W.W., *COLLECT*. Nonius BV, Delft, The Netherlands, **1999**.

Hoskins R. and Robson R., *J. Am. Chem. Soc.* **1990**, 112, 1546.

Keller S. W., *Angew. Chem., Int. Ed. Engl.* **1997**, 36, 247.

Kolitsh U. *Acta Crystallogr., Sect. C*, **2004**, 60, m129.

Kou H.-Z., Liao D.-Z., Yang G.-M., Cheng P., Jiang Z.-H., Yan S.-P., Wang G.-L., Yao X.-K. and Wang H.-G., *Polyhedron*, **1998**, 17, 3193.

Liu H.-L., Mao H.-Y., Zang H.-Y., Xu C., Wu Q.-A., Li G., Yu Z. and Hou H.-Y., *Polyhedron*, **2004**, 23, 943.

Nardelli M., *J. Appl. Crystallogr.*, **1995**, 28, 659.

Navarro R., *Application of High- and Low-Temperature Series Expansions to Two-dimensional Magnetic Systems*, ed. L.J. de Jongh, Kluwer Academic Publishers, Dordrecht, **1990**.

Ng S.W,. Che X.M. and Yang G., *Acta Cryst. Sect. C,* **1998**, 54, 1389.

Pannhorst W. and Lohn J., *Z. Kristallogr.*, **1974**, 139, 236.

Pasán J., Sanchiz J., Ruiz-Pérez C., Lloret F. and Julve M., *Eur. J. Inorg. Chem.*, **2004**, 4081.

Purdy P., George C.F., *Polyhedron*, **1995**, 14, 761.

Ruiz-Pérez C., Sanchiz J., Hernández-Molina M., Lloret F. and Julve M., *Inorg. Chim. Acta*, **2000a**, 298, 202.

Ruiz-Pérez C., Hernández-Molina M., Sanchiz J., López T., Lloret F. and Julve M., *Inorg. Chim. Acta*, **2000b**, 298, 245.

Ruiz-Pérez C., Sanchiz J., Hernández-Molina M., Lloret F. and Julve M., *Inorg. Chem.*, **2000c**, 39, 1363.

SADABS, version 2.03. Bruker AXS Inc.: Madison, WI, **2000**.

Sanchiz J., Rodríguez-Martín Y., Ruiz-Pérez C., Mederos A., Lloret F. and Julve M., *New J. Chem.*, **2002**, 26, 1624.

Seigrist T., Chamberlain B.L., Ramirez A.P. and LoBrutto R., *J. Solid State Chem.* **1996**, 121, 61.

Sheldrick G.M., *SHELX97*, *Programs for Crystal Structure Anlysis (Release 97-2)*, Institüt für Anorganische Chemie der Universität, Tammanstrasse 4, D-3400 Göttingen, Germany, **1998**.

Stiefel E.I. and Brown G.F., *Inorg. Chem.*, **1972**, 11, 434.

Van Niekerk J.N. and Schoening F.K.L., *Acta Cryst. Sect. B*, **1953**, 31, 227.

Wang C.-C., Yang C.-H. and Lee G.-H., *Inorg. Chem.*, **2002**, 41, 1015.

Warden A.C., Hearn M.T.W. and Spiccia L., *Inorg. Chem.*, **2003**, 42, 7037.

Weichert T. and Lohn J., *Z. Kristallogr.*, **1974**, 139, 223.

Weighardt K., Bossek U., Chaudhuri P., Hermann W., Menke B.C., *Inorg. Chem.*, **1982**, 21, 1208.

Wong E.H., Weisman G.R., Hill D.C., Reed D.P., Rogers M.E., Condon J.S., Fagan M.A., Calabrese J.C., Lam K.-C., Guzei I.A. and Rheingold A.L., *J. Am. Chem. Soc.*, **2000**, 122, 10561.

Wu C., Lu C.-Z., Yang W.-B., Zhuang H.-H. and Huang J.S., *Inorg. Chem. Commun.*, **2001**, 4, 504.

Xu Z., White S., K. Thompson L., Miller D.O., Ohba M., Okawa H., Wilson C. and Howard J.A.H., *Dalton Trans.* **2000**, 1751.

CHAPTER III.

Network formation and magnetic behaviour of Copper(II)malonate anions in ammonium salts.

Introduction

The key factor in the design of metal complexes is mainly the use of polyfunctional ligands capable to bridge metal centers to form polymeric structures, whereas the tools used in organic crystal engineering are hydrogen bonds and other intermolecular contacts [Desiraju G.R., 1989]. Furthermore, coordination compounds with hydrogen bonding substituents present synthetic challenges in supramolecular chemistry, since metal ions may themselves coordinate to the electronegative atoms of ligands, which are sources of strong hydrogen bond donors or acceptors. Such hydrogen bonds are also used to connect monomeric metal complexes to obtain one-, two- or three-dimensional coordination frameworks [Beatty A.M., 2003]. Unfortunately, it is not yet possible to predict solid state structure merely from the chemical composition. This was the subject of John Maddox's, 1988 *Nature* editorial where he indicated that "One of the continuing scandals in the physical sciences is that it remains in general impossible to predict the structure of even the simplest crystalline solids from a knowledge of their chemical composition" [Maddox J., 1988]. While these statements may still be true in a strict sense even today, continuing efforts of various research groups around the globe to achieve the objective of crystal structure prediction have afforded significant progress toward this goal.

The term ‘crystal engineering’ was coined by G. M. J. Schmidt in the 1970s to address the problem of crystal structure prediction in the context of organic solid state photochemical reactions of cinnamic acids [Schmidt G.M.J., 1971]. The broad and more meaningful definition of crystal engineering was provided by G. R. Desiraju in 1989 as "the understanding of intermolecular interactions in the context of crystal packing and in the utilisation of such understanding in the design of new solids with desired physical and chemical properties" [Desiraju G.R., 1989]. Crystal engineering is now a rapidly developing interdisciplinary field with a wide scope for basic research and promising industrial applications which may also drive the basic research effort.

The most successful strategies of crystal engineering are based on a building block (or supramolecular synthon) approach, which simplifies the complex problem of structure prediction into a simple problem of network architecture (like making things out of LEGO blocks). For all practical purposes, the crystal structures are assumed to be networks, where molecules, metals, ions, etc., are considered as nodes and the

intermolecular interactions or coordination bonds represent node connections [Desiraju G.R., 1995]. The design of one, two, or three-dimensional crystalline network structures can thus be achieved by choosing the desired combination of nodes and connectors. For example, metal cations as the nodes, coordinated to simple linear bifunctional ligands as connectors will form a variety of 1D, 2D, and 3D architectures depending upon the metal coordination geometry and metal to ligand ratio as shown by Mike Zaworotko [Seddon K.R. *et al.*, 1998] Interestingly, many of these simple new frameworks have no precedence in naturally occurring solids and the bulk properties of these compounds remains largely unexplored.

Experimental

Materials and methods

Malonic acid, copper(II) basic carbonate [$Cu(CO_3)\cdot Cu(OH)_2$], ammonia, methylamine [$MeNH_2$], ethylenediamine [NH_2enNH_2], 1,3-propylenediamine [NH_2pnNH_2] and 1,4-butanediamine [NH_2bnNH_2] were purchased from commercial sources and used as received. Elemental analyses (C, H) were performed on an EA 1108 CHNS-O microanalytical analyser. The magnetic susceptibility measurements were performed on a Quantum Design SQUID magnetometer in the 2-100 K temperature range, operating at 250 G ($T \leq 10$ K) and 1000 G ($T > 10$ K) for **1**, at 1000 G for compounds **2**, **3** and **5**, and at 500 G ($T \leq 20$ K) and 1000 G ($T > 20$ K) for compound **4**. Diamagnetic corrections of all the constituent atoms were estimated from Pascal's constants [Earshaw, 1968] as 98 x 10^{-6}, 136 x 10^{-6}, 156 x 10^{-6}, 142 x 10^{-6}, 179 x 10^{-6} cm^3mol^{-1} for compounds **1-5**, respectively. Corrections for the tip of the Cu(II) ions (60 x 10^{-6} cm^3 mol^{-1}) were also done.

Synthesis

$(NH_4)_2$[Cu(mal)$_2$] (1). Solid copper(II) basic carbonate (110 mg, 0.5 mmol) is added to an aqueous solution (10 cm^3) of malonic acid (208 mg, 2 mmol) under continuous stirring. The suspension is heated at 40-50 ºC until a blue solution is obtained. This solution is filtered and diluted to 25 cm^3 by water addition. Finally, the pH was adjusted to 5 by adding an aqueous solution of ammonia (2M). Single crystals of **1** as sky blue prisms were grown from the solution by slow evaporation at room temperature in a

week. (Found: C, 23.96; H, 3.98; N, 9.19 %. Calc. for $C_6H_{12}N_2O_8Cu$: C, 23.71; H, 3.95; N, 9.22 %).

$(MeNH_3)_2[Cu(mal)_2]$ (2). Compound **2** is obtained by the same procedure used for **1** but replacing NH_3 by $MeNH_2$. Single crystals of **2** as blue plates were grown from the solution by slow evaporation at room temperature in a week. (Found: C, 28.89; H, 4,74; N, 8.68 %. Calc. for $C_8H_{16}N_2O_8Cu$: C, 28.93; H, 4.82; N, 8.44 %).

$(H_2en)[Cu(mal)_2(H_2O)]\cdot 2H_2O$ (3). Compound **3** is obtained by following the same procedure used for **1** but replacing NH_3 by en. Single crystals as blue prisms were obtained by slow evaporation at room temperature in a week. (Found: C, 25.45; H, 4,93; N 7.92 %. Calc. for $C_8H_{20}N_2O_{11}Cu$: C, 25.01; H, 5.21; N, 7.30 %).

$(H_2pn)[Cu(mal)_2]$ (4). Solid copper(II) basic carbonate (110 mg, 0.5 mmol) is added to an aqueous solution (10 cm^3) of malonic acid (208 mg, 2 mmol) under continuous stirring. The suspension is heated at 40-50 ºC, until a blue solution is obtained. This solution was filtered and diluted to 25 cm^3 by water addition. The beaker containing this solution was put into a closed vessel containing a methanolic solution (10 cm^3) of *pn* (1.5 mmol). Single crystals of **4** as deep blue rectangular plates were obtained by slow diffusion at room temperature within two weeks. (Found: C, 31.46; H, 4.63; N 8.30 %. Calc. for $C_9H_{16}N_2O_8Cu$: C, 31.42; H, 4.65; N, 8.14 %).

$(H_2bn)[Cu(mal)_2(H_2O)]\cdot H_2O$ (5). Compound **5** is obtained by the same procedure used for **1** but replacing NH_3 by bn. Single crystals of **5** as blue prisms were obtained by slow evaporation at room temperature in a week. (Found: C, 30.57; H, 5.61; N 7.13 %. Calc. for $C_{10}H_{22}N_2O_{10}Cu$: C, 30.47; H, 5.59; N, 7.11 %)

Crystal data collection and refinement of the structures

Single crystals of **1-5** were mounted on a Bruker-Nonius KappaCCD diffractometer. Orientation matrix and lattice parameters were obtained by least-squares refinement of the reflections obtained by a θ-χ scan (Dirax/lsq method). Diffraction data were collected at 293(2) K for **1-5** and also at 100(2) K for **1** (the diffraction data for **1** corresponding to the measurements at 293 and 100 K are denoted hereafter as **1a** and **1b**, respectively) using graphite-monochromated Mo-K_α radiation (λ = 0.71073 Å). Data collection and data reduction were done with the COLLECT [Hooft R.W.W., 1999] and EVALCCD [Duisenberg, A.J.M. et al., 2003] programs. Empirical absorption

corrections were carried out using SADABS [SADABS, version 2.03, 2003] for all compounds. The indexes of data collection were $-19 \leq h \leq 13$, $-23 \leq k \leq 22$, $-10 \leq l \leq 12$ for **1a**; $-17 \leq h \leq 16$, $-11 \leq k \leq 21$, $-11 \leq l \leq 10$ for **1b**;$-11 \leq h \leq 6$, $-10 \leq k \leq 11$, $-11 \leq l \leq 11$ for **2**; $-15 \leq h \leq 14$, $-10 \leq k \leq 10$, $-13 \leq l \leq 19$ for **3**; $-10 \leq h \leq 9$, $-9 \leq k \leq 12$, $-22 \leq l \leq 16$ for **4** and $-9 \leq h \leq 9$, $-15 \leq k \leq 17$, $-10 \leq l \leq 7$ for **5**. Of the 1264 (**1a**), 1076 (**1b**), 1449 (**2**), 3321 (**3**), 1425 (**4**) and 3146 (**5**) measured independent reflections in the θ range 6.76 – 29.98º (**1a**), 5.13 – 27.50º (**1b**), 6.42 – 27.50º (**2**), 6.47 – 27.50º (**3**), 5.10 – 27.50º (**4**) and 4.65 – 27.50º (**5**); 1171 (**1a**), 1009 (**1b**), 1255 (**2**), 2815 (**3**), 1144 (**4**) and 2680 (**5**) have $I \geq 2\sigma(I)$. All the measured independent reflections were used in the analysis. All calculations for data reduction, structure solution, and refinement were done by standard procedures (WINGX) [Farrugia, L.J., 1999]. The structure was solved by direct methods and refined with full-matrix least-squares technique on F^2 using the SHELXS-97[23] and SHELXL-97 [Sheldrick, G.M. SHELX97, realease 97-2, 1998] programs. The hydrogen atoms of the malonate and counterions in **1-4** were located from difference Fourier maps whereas they were set in calculated positions in the case of **5**. Water hydrogen bonds were not found for **3** and **5**. The hydrogen atoms for all compounds were refined with isotropic temperature factors. The final Fourier-difference map showed maximum and minimum height peaks of 0.254 and -0.257 e $Å^{-3}$ (**1a**), 0.303 and -0.336 e $Å^{-3}$ (**1b**), 0.244 and -0.438 e $Å^{-3}$ (**2**), 0.659 and -0.978 e $Å^{-3}$ (**3**), 0.297 and -0.580 e $Å^{-3}$ (**4**), 0.428 and -0.388 e $Å^{-3}$ (**5**). A summary of the crystallographic data and structure refinement is given in Table 1. The final geometrical calculations and the graphical manipulations were carried out with PARST97 [Nardelli, M., 1995] and DIAMOND [DIAMOND 2.1d, 2000] programs, respectively.

Crystal structures were deposited at the Cambridge Crystallographic Data Centre, the CCDC reference numbers being 253062 (**1a**), 253063 (**2**), 253064 (**3**), 253065 (**4**) and 253066 (**5**).

Table 1. Crystal data and details of structure determination for **1-5**

Compound	**1a**	**1b**	**2**	**3**	**4**	**5**
Formula	$C_6H_{12}Cu_1N_2O_8$	$C_6H_{12}Cu_1N_2O_8$	$C_8H_{16}CuN_2O_8$	$C_8H_{20}CuN_2O_{11}$	$C_9H_{16}CuN_2O_8$	$C_{10}H_{22}CuN_2O_{10}$
M	303.72	303.72	331.77	383.80	343.78	393.84
Crystal system	orthorhombic	orthorhombic	monoclinic	monoclinic	orthorhombic	monoclinic
Space group	*F*dd2	*F*dd2	$P2_1/c$	$P2_1/c$	*P*bcn	$P2_1$
a, Å	13.8481(3)	13.656(2)	8.6866(2)	11.670(2)	8.2680(4)	7.3346(3)
b, Å	16.4536(2)	16.4436(9)	9.0585(3)	8.408(2)	16.9351(9)	13.6142(3)
c, Å	9.1071(2)	9.0876(9)	8.9681(3)	15.323(3)	9.4736(5)	7.9365(3)
α, deg	-	-	-	-	-	-
β, deg	-	-	115.198(2)	93.38(3)	-	97.519(3)
γ, deg	-	-	-	-	-	-
V, Å^3	2075.06(7)	2040.6(4)	638.53(3)	1500.9(5)	1326.49(12)	785.68(5)
Z	8	8	2	4	4	2
T, K	293(2)	100(2)	293(2)	293(2)	293(2)	293(2)
ρ_{calc} (Mg m^{-3})	1.944	1.977	1.726	1.698	1.721	1.665
F(000)	1240	1240	342	796	708	410
λ (Mo-K$_\alpha$ Å)	0.71073	0.71073	0.71073	0.71073	0.71073	0.71073
μ (Mo-K$_\alpha$, mm^{-1})	2.142	2.178	1.748	1.514	1.686	1.444
Flack parameter	0.458(16)	0.97(2)	-	-	-	0.611(15)
Extinction coefficient	-	-	-	0.114(4)	-	-
Number parameters/restraints	103 / 1	103 / 1	120 / 0	256 / 0	124 / 0	209 / 1
Goodness of fit (S)	1.073	1.088	1.104	1.094	1.106	1.046
R1, $I > 2\sigma(I)$ (all)	0.020 (0.024)	0.023 (0.026)	0.023 (0.030)	0.039 (0.048)	0.043 (0.058)	0.037 (0.50)
wR2, $I > 2s(I)$ (all)	0.048 (0.049)	0.050 (0.051)	0.059 (0.062)	0.102 (0.108)	0.091 (0.096)	0.079 (0.083)
Max/min electron density (e/Å^3)	0.254 / -0.257	0.303 / -0.336	0.244 / -0.438	0.659 / -0.978	0.297 / -0.580	0.428 / -0.388
Measured reflections (R_{int})	3607 (0.023)	2259 (0.020)	3684 (0.015)	10895 (0.035)	5634 (0.022)	4412 (0.018)
Independent reflections [$I > 2\sigma(I)$]	1264 (1171)	1076 (1009)	1449 (1255)	3321 (2815)	1425 (1144)	3146 (2680)

Results and discussion

Description of the structure of $(NH_4)_2[Cu(mal)_2]$ (1)

Although this compound was previously synthesized [Charbonnier F. et *al.*, 1972] its structure and its magnetic properties were unknown. In the context of our magneto-structural studies with ammonium complexes we have synthesised and characterised it.

The structure of **1** is made up of $[Cu(mal)_2]^{2-}$ units that are held together by means of carboxylate-malonate groups affording an anionic three dimensional network (see yellow framework in Figure 1). The $[Cu(mal)_2]^{2-}$ units are further connected through hydrogen bonds involving NH_4^+ units leading to a neutral three-dimensional structure (see Figure 1).

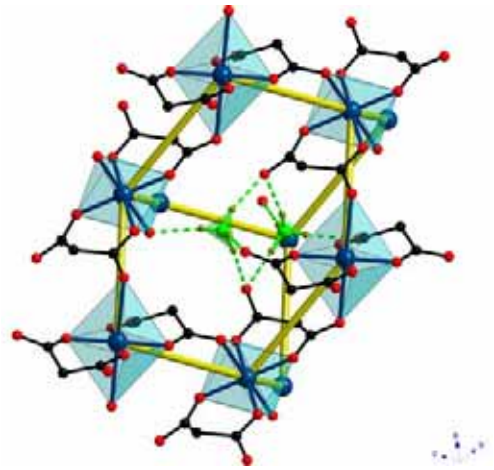

(a)

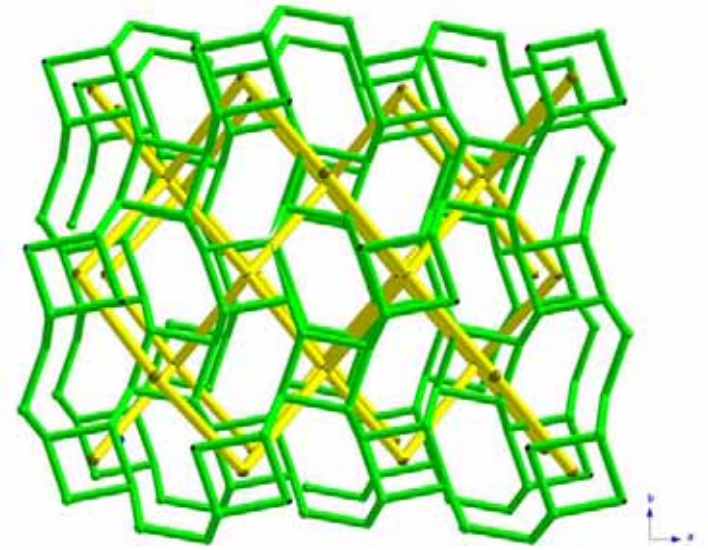

(b)

Figure 1. **(a)** View of a fragment of the 3D structure of **1** showing the $[Cu(mal)_2]^{2-}$ and NH_4^+ arrangement. **(b)** Schematic view, along the *c*-axis of the anionic malonate-bridged copper(II) (yellow) and cationic hydrogen bonded ammonium (green) networks in **1.**

Table 2. Selected bond lengths (Å) and angles (º) for **1**[a]

Cu(1)-O(1)	1.955(2)	Cu(1)-O(2)	1.9389(15)
Cu(1)-O(4b)	2.4813(14)		
O(1)-Cu(1)-O(2)	92.78(5)	O(1)-Cu(1)-O(1a)	87.68(9)
O(2)-Cu(1)-O(1a)	179.41(8)	O(2)-Cu(1)-O(2a)	86.77(9)
O(4b)-Cu(1)-O(1)	90.46(6)	O(4b)-Cu(1)-O(1a)	89.71(6)
O(4b)-Cu(1)-O(2)	89.92(6)	O(4b)-Cu(1)-O(2a)	89.91(6)
O(4b)-Cu(1)-O(4c)	179.77(4)		

[a] Symmetry codes: (a) -*x*, -*y*+1, *z*; (b) -*x*+1/4, *y*+1/4, *z*+1/4; (c) *x*-1/4, -*y* +3/4, *z*+1/4.

The copper atom lies on a binary axis. The metal atom is six-coordinated (see Figure 2 and Table 2) exhibiting a 4+2 elongated octahedron environment with geometric values ϕ = 59.0º and *s*/*h* = 1.44 (ϕ and *s*/*h* being the twist angle and the compresion ratio, respectively) [Stiefel E.I. et *al*., 1972]. Four inner oxygen atoms from two symmetrically related malonate groups build the equatorial plane [the maximum deviation from the mean equatorial plane being 0.07(2) Å for O(2)] around the metal atom [the mean Cu-O(eq) bond distance being 1.9471(16) Å]. Whereas two outer malonate oxygen atoms fill the apical positions [the Cu-O(ap) bond distance being 2.4813(14) Å].

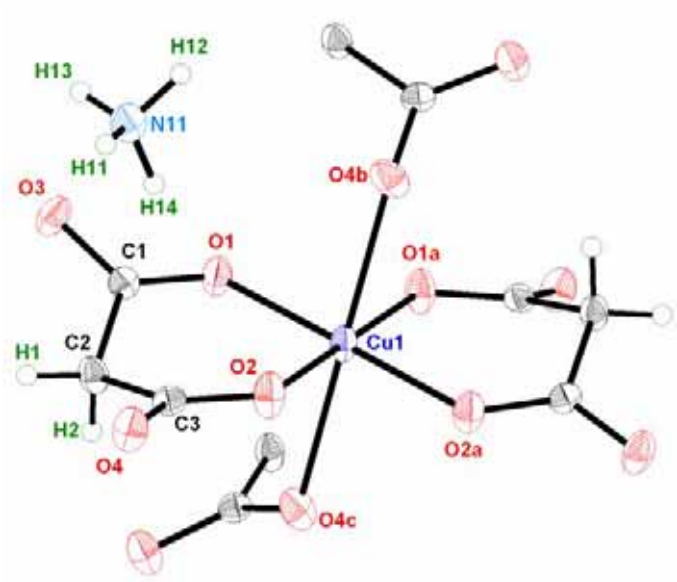

Figure 2. Perspective view of and the metal environment and the NH_4^+ cation in **1** with the numbering scheme. Thermal ellipsoids are drawn at the 50% probability level.

The malonate group acts simultaneously (see Figure 3) as bidentate [through O(1) and O(2) towards Cu(1)] and monodentate ligand [through O(4) towards Cu(1d); (d) -*x*+1/4, *y*-1/4, *z*-1/4]. The angle subtended by the malonate ligand at Cu(1) is

92.78(5)º. The malonate group with the copper atom form a six-membered ring that exhibits a distorted boat conformation [Cremer D. et *al.*, 1975] [θ = 77.2(2) and ϕ = 109.6(3)º]. The O(1)-C(1)-O(3) carboxylate-malonate group links equatorial and apical positions of two adjacent copper atoms exhibiting the bridging *anti-anti* conformation [the copper···copper separation is 5.8386(3) Å]. The malonate bond distances and angles (see Table 3) agree well with those previously reported [see references concerning the malonate-containing copper(II) complexes in the Introduction].

Table 3. Selected bond lengths (Å) and angles (º) for the malonate ligand in **1**[a]

C(1)-C(2)	1.511(3)	C(2)-C(3)	1.511(3)
C(1)-O(1)	1.263(2)	C(3)-O(2)	1.272(2)
C(1)-O(3)	1.251(3)	C(3)-O(4)	1.250(3)
O(1)···O(2)	2.820(2)	O(3)···O(4)	4.431(3)
O(1)-C(1)-O(3)	121.8(2)	O(2)-C(3)-O(4)	121.6(2)
O(1)-C(1)-C(2)	119.9(2)	O(2)-C(3)-C(2)	120.5(2)
O(3)-C(1)-C(2)	118.3(2)	O(4)-C(3)-C(2)	118.0(2)
C(1)-C(2)-C(3)	116.11(14)		
C(1)-O(1)-Cu(1)	126.45(14)	C(3)-O(2)-Cu(1)	127.72(14)
C(3)-O(4)-Cu(1d)	120.90(12)		
O(1)C(1)O(3)-Cu(1)eq[b]	23.9(2)	O(2)C(3)O(4)-Cu(1)eq[b]	18.5(2)

[a] Symmetry transformations: (d) -*x*+1/4, *y*-1/4, *z*-1/4.
[b] dihedral angle (º) between the malonate carboxylate group and the mean equatorial plane of the metal atom

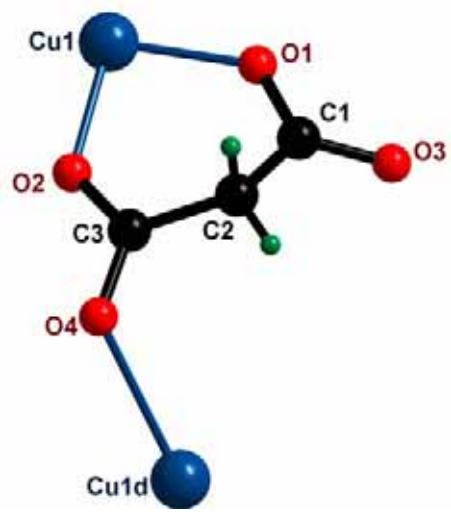

Figure 3. View of the coordination mode of the malonate ligand in **1.**

Each $[Cu(mal)_2]^{2-}$ unit is linked through carboxylate bridges in the *anti-anti* conformation to four other ones (see Figure 4), leading to a three-dimensional diamondoid framework (Figure 5). The dihedral angle between the mean equatorial

planes belonging to two consecutive metal atoms is 45.86º. The angles defined by nearest copper(II) atoms are (see Figure 4): 107.27º [C(1b)-Cu(1)-Cu(1d); (d) -*x*+1/4, *y*-1/4, *z*-1/4], 134.10º [Cu(1b)-Cu(1)-Cu(1e); (e) -*x*-1/4, *y*-1/4, *z*+1/4] and 90.42º [Cu(1b)-Cu(1)-Cu(1f); (f) -*x*-1/4, *y*+1/4, *z*-1/4]. These geometric values define the geometry of the six-membered ring (see scheme in Figure 4) which is the basic unit of the (6,4) copper(II) three dimensional structure.

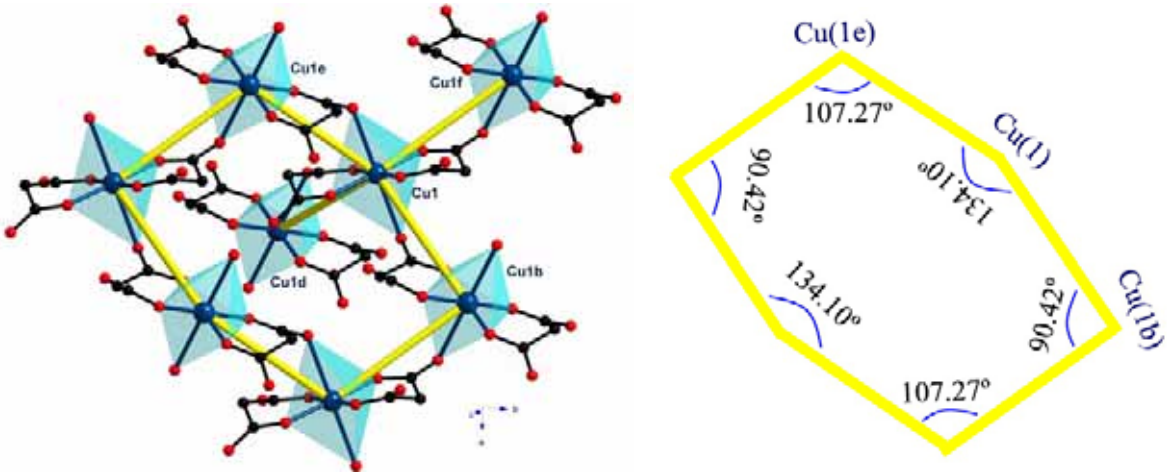

Figure 4. Perspective view of a fragment of the malonate-bridged copper(II) with a scheme showing some geometric values of the six-membered ring that conforms the anionic network.

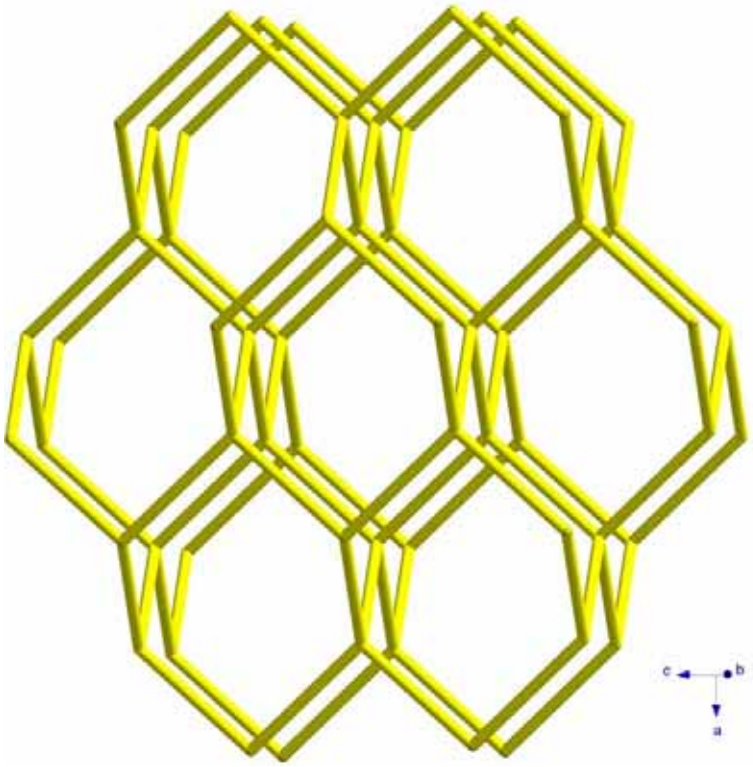

Figure 5. Schematic view of the diamondoid three-dimensional network.

The $[Cu(mal)_2]^{2-}$ units are further linked through hydrogen bonds involving malonate oxygen atoms and ammonium groups (see Figure 6a and Table 4).

Table 4. Hydrogen bonds[a-c] for compound **1**

D-H···A	D···A/Å	H···A/Å	D-H···A/º
N(11)-H(11)···O(3)	2.835(3)	2.02(4)	173(4)
N(11)-H(12)···O(3b)	2.843(2)	1.97(2)	161(2)
N(11)-H(13)···O(4g)	2.779(3)	1.97(5)	168(5)
N(11)-H(14)···O(3c)	2.931(2)	2.06(3)	163(2)
C(2)-H(1)···O(1d)	3.357(3)	2.64(2)	139(2)
C(2)-H(2)···O(2c)	3.428(3)	2.71(3)	145(2)

[a] Symmetry transformations: (b) -*x*+1/4, *y*+1/4, *z*+1/4; (c) *x*-1/4, -*y*+3/4, *z*+1/4; (d) -*x*+1/4, *y*-1/4, *z*-1/4; (g) *x*, *y*, *z*+1. [b] A = acceptor; D = donor. [c] Symmetry transformations apply to acceptor atoms.

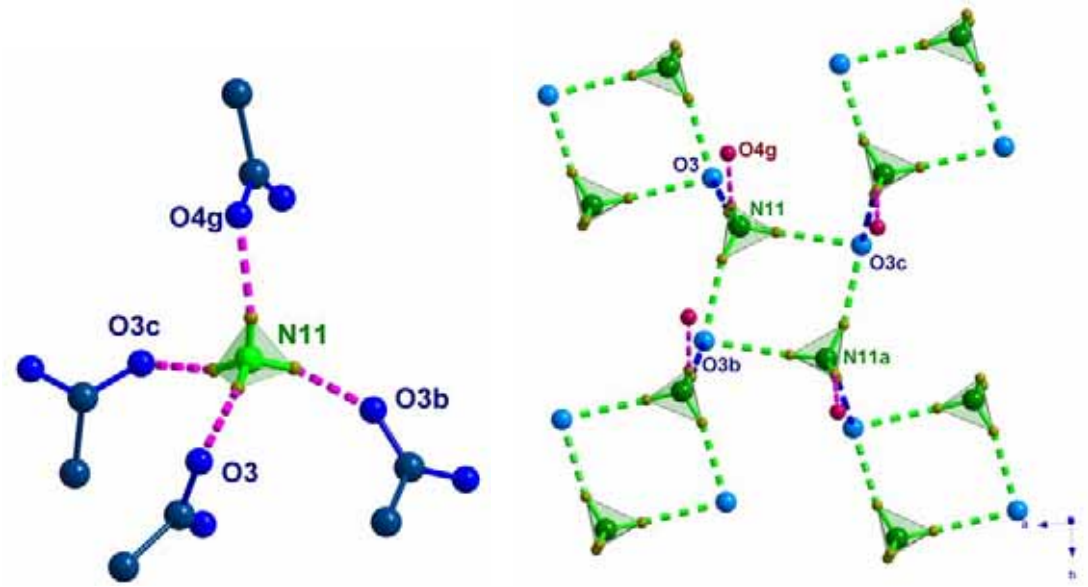

Figure 6. (a) A perspective view of one ammonium cation surrounded by four malonate carboxylate groups. **(b)** A view of a fragment of the cationic network where each ammonium pair unit is surrounded by four other ones.

Let us focus on the arrangement of the ammonium groups through hydrogen bonds. Each ammonium cation is linked to another symmetrically related one by means of a two-fold axis, through double N-H···O (green broken lines in Figure 6b) interactions leading to ammonium pairs. The N(11)···N(11a) separation is 3.769(2) Å. Furthermore, each pair is connected to other four ones by means of N-H···O (blue broken lines in Figure 6b) interactions, leading thus to a three-dimensional network (Figure 7a). Within this three dimensional network, one can distinguish hydrogen bonded chiral ammonium chains as shown in Figure 7b.

Additional N-H···O hydrogen bonds (purple broken lines in Figure 6a) help to stabilize the whole structure connecting the cationic and anionic networks.

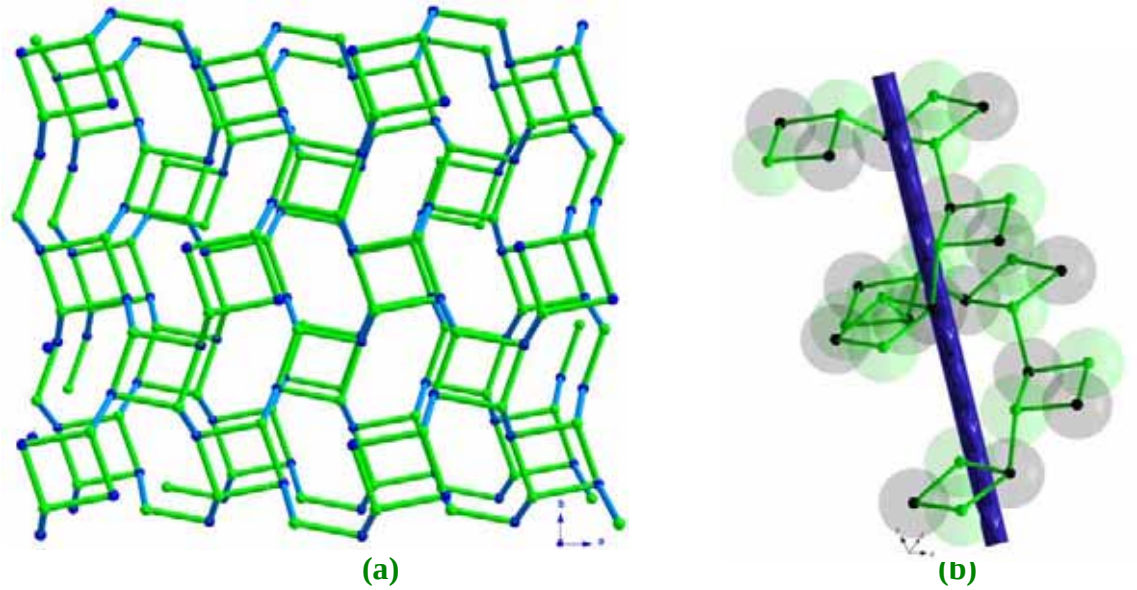

Figure 7. (a) Perspective view along the *c*-axis of the 3D hydrogen bonded ammonium network. **(b)** A side view of the chiral chain which forms this network.

Description of the structure of $(MeNH_3)_2[Cu(mal)_2]$ (2).

The structure of compound **2** consists of layers of anionic $[Cu(mal)_2]^{2-}$ units linked through carboxylate-malonate bridges. These layers are held together by means of hydrogen bonds involving the $CH_3NH_3^+$ groups, giving rise to a three-dimensional structure where anionic an cationic layers are stacked in a ABB'ABB' manner (see Figure 8).

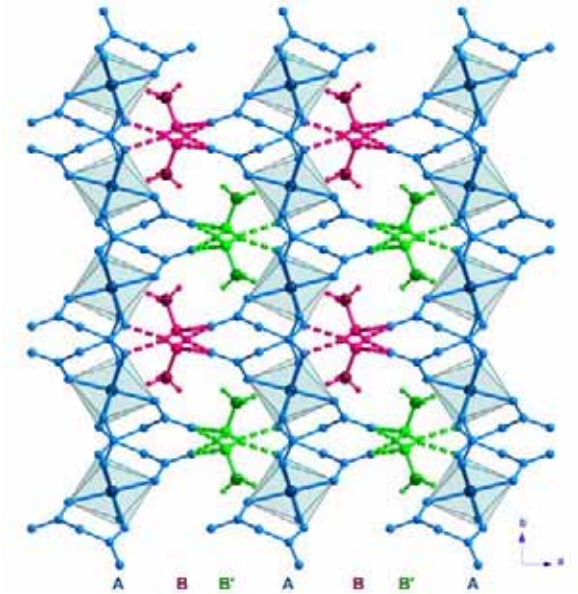

Figure 8. Perspective view along the *c*-axis of the arrangement of the $[Cu(mal)_2]^{2-}$ layers -blue coloured- and $CH_3NH_3^+$ units -green and purple coloured- in **2**. Hydrogen bonds are illustrated by broken lines.

Each copper atom lies on a $\bar{1}$ crystallographic site symmetry. The copper atom is six-coordinated and it exhibits an elongated 4+2 octahedron environment (Figure 9 and Table 5) with geometric values ϕ = 53.9º *s/h* = 1.50 [Stiefel E.I. et *al*., 1972]. Four carboxylate-oxygen atoms from two crystallographically related malonate groups define the equatorial plane of the metal atom [the mean Cu(1)-O(eq) bond distance is 1.9424(11)]. Apical positions are occupied by two symmetrically related carboxylate-oxygen atoms being 2.5620(15) Å the Cu(1)-O(ap) bond distance.

Table 5. Selected bond lengths (Å) and angles (º) for **2**

Cu(1)-O(1)	1.9236(11)	Cu(1)-O(2)	1.9613(10)
Cu(1)-O(3b)	2.5620(15)		
O(1)-Cu(1)-O(2)	91.81(5)	O(2)-Cu(1)-O(1a)	88.19(5)
O(3b)-Cu(1)-O(2)	94.96(5)	O(3b)-Cu(1)-O(1)	85.77(4)
O(3b)-Cu(1)-O(2a)	85.04(5)	O(3b)-Cu(1)-O(1a)	94.23(4)

[a] Symmetry codes: (a) -*x*, -*y*+1, -*z*; (b) *x*, -*y*+1/2, *z*+1/2; (c) –*x*, *y*+1/2, -*z*-1/2.

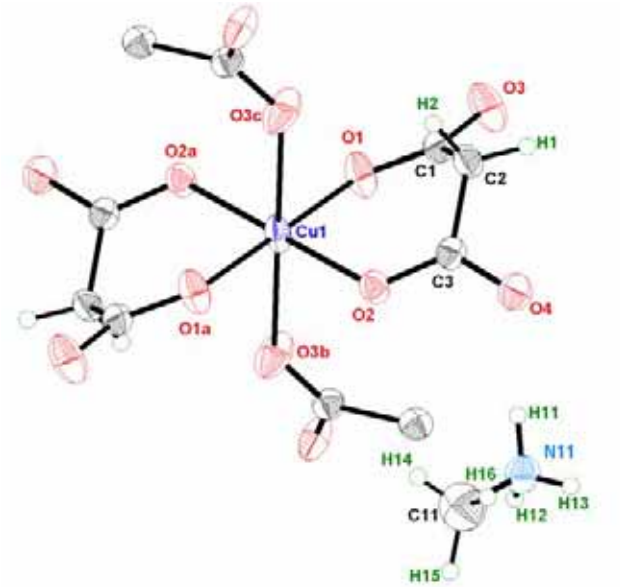

Figure 9. Perspective view of the metal environment and the $CH_3NH_3^+$ unit for **2** with the atom numbering. Thermal ellipsoids are drawn at the 50% probability level.

The malonate group acts simultaneously as bidentate [through O(1) and O(2) towards Cu(1)] and monodentate [through O(3) towards Cu(1d); (d) -*x*, *y*-1/2, -*z*-1/2] ligand (see Figure 10). The angle subtended by the malonate group at the Cu(1) atom is 91.81(5)º. The malonate group and the copper atom form a six-membered ring that exhibits a boat conformation [Cremer D. et *al*., 1975] [θ = 90.47(11) and ϕ = 122.91(12)º]. The O(1)-C(1)-O(3) carboxylate bridge exhibits the *anti-anti* conformation and it connects an equatorial and an apical position of two adjacent

copper atoms. The bond distances and angles of the malonate (see Table 6) agree well with those previously reported for other malonate-containing copper(II) complexes [see references in the Introduction].

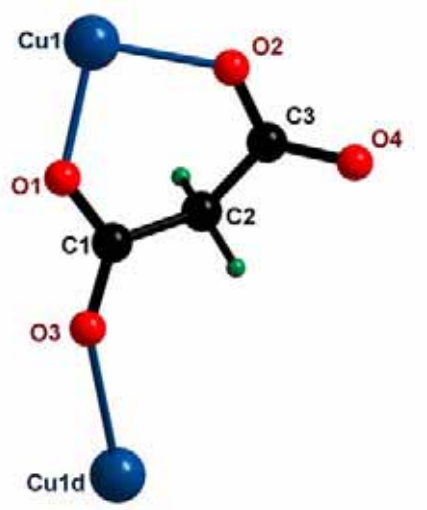

Figure 10. View of the coordination mode of the malonate ligand in **2**.

Table 6. Bond lengths (Å) and angles (º) for the malonate ligand in **2**

C(1)-C(2)	1.511(2)	C(2)-C(3)	1.513(2)
C(1)-O(1)	1.277(2)	C(3)-O(2)	1.263(2)
C(1)-O(3)	1.231(2)	C(3)-O(4)	1.248(2)
O(1)···O(2)	2.7897(13)	O(3)···O(4)	4.3432(15)
O(1)-C(1)-O(3)	122.25(15)	O(2)-C(3)-O(4)	122.64(13)
O(1)-C(1)-C(2)	117.96(13)	O(2)-C(3)-C(2)	119.69(13)
O(3)-C(1)-C(2)	119.74(14)	O(4)-C(3)-C(2)	117.67(14)
C(1)-C(2)-C(3)	114.99(12)		
C(1)-O(1)-Cu(1)	125.49(10)	C(3)-O(2)-Cu(1)	123.24(9)
C(1)-O(3)-Cu(1d)	136.45(11)		
O(1)C(1)O(3)-Cu(1)eq[b]	30.30(14)	O(2)C(3)O(4)-Cu(1)eq[b]	32.12(14)

[a] Symmetry transformations: (d) *-x*, *y*-1/2, -*z*-1/2.
[b] dihedral angle (º) between the malonate carboxylate group and the mean equatorial plane of the metal.

Each $[Cu(mal)_2]^{2-}$ unit is linked through carboxylate bridges in the *anti-anti* conformation to other four ones [the dihedral angle between the mean equatorial planes of adjacent copper atoms is 53.13(3)º] leading to a malonate-bridged copper anionic layer that grows in the *bc*-plane (Figure 11). Within each layer, one can distinguish tetranuclear units which form sixteen-membered rings $[Cu\text{-}O\text{-}C\text{-}O\text{-}Cu]_4$, the metal atoms being at the corners of a rhombus. The shortest Cu(1)···Cu(1) separations within

the layer are: 6.3734(1) Å [for Cu(1)···Cu(1c) and Cu(1)···Cu(1d)], 8.9681(3) [for Cu(1)···Cu(1e); (e) *x*, *y*, *z*-1] and 9.0585(3) Å [for Cu(1d)···Cu(1c)] (see Figure 11).

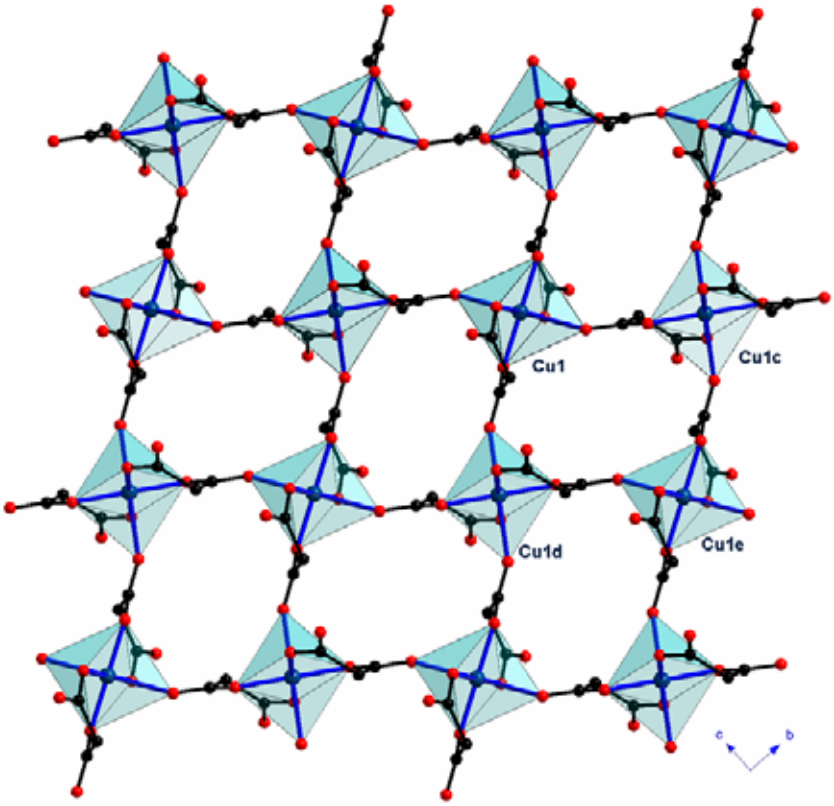

Figure 11. Perspective view of a fragment of the malonate-bridged copper(II) layer in **2**.

The $NH_3CH_3^+$ cations are held together by means of hydrogen bonds involving malonate-oxygen atoms (see Table 7 and Figure 12) affording zigzag chains that grow along the *c*-axis (see Figure 13). These chains are stacked in two different ways along the *b*-axis affording the B and B' cationic sheets that one can see in Figure 8.

Table 7. Relevant hydrogen bonds[a,b,c] for compound **2**

D-H···A	D···A/Å	H···A/Å	D-H···A/º
N(11)-H(11)···O(4)	2.760(2)	1.88(2)	175(2)
N(11)-H(12)···O(4b)	2.817(3)	1.96(3)	165(2)
N(11)-H(13)···O(1f)	2.818(2)	2.10(3)	155(3)
C(2)-H(1)···O(2g)	3.433(2)	2.58(2)	153(2)
C(2)-H(2)···O(3c)	3.123(2)	2.37(2)	137(2)
C(11)-H(15)···O(1h)	3.511(3)	2.63(3)	148(2)

[a] Symmetry transformations: (b) *x*, -*y*+1/2, *z*+1/2; (c) –*x*, *y*+1/2, -*z*-1/2; (f); *x*+1, -*y*+1/2, *z*+1/2; (g) *x*, -*y*+1/2, *z*-1/2; (h) *x*+1, *y*, *z*+1. [b] A = acceptor; D = donor. [c] Symmetry transformations apply to acceptor atoms.

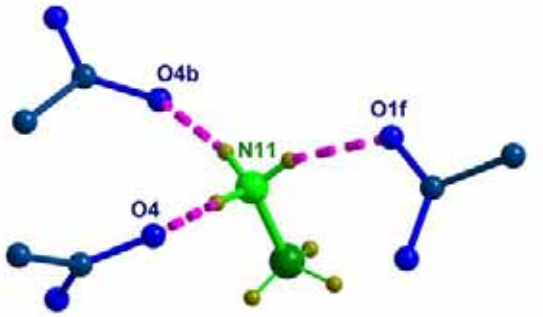

Figure 12. A view of the $CH_3NH_3^+$ cation surrounded by three malonate-carboxylate groups.

Finally, malonate-bridged copper(II) layers and cationic sheets, which are linked through hydrogen bonds, alternate following the ABB'ABB' sequence leading to a three-dimensional network (see Figure 8). Additional C-H···O interactions (Table 7) contribute to stabilize the whole structure.

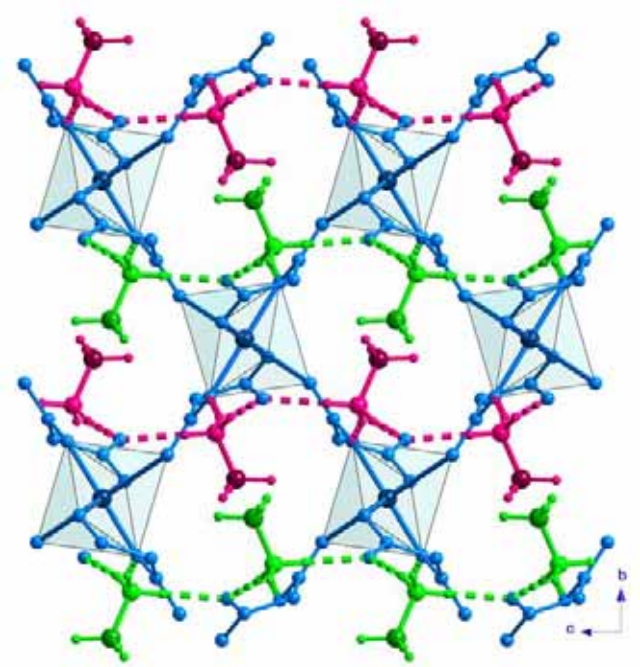

Figure 13. View along the *a*-axis of the arrangement of the $CH_3NH_3^+$ hydrogen-bonded chains (green and pink coloured) which link adjacent copper layers (blue coloured) in **2**.

Description of the structure of $(H_2en)[Cu(mal)_2(H_2O)]\cdot 2H_2O$ (3).

The structure of compound **3** consists of hydrogen bonded $[Cu(mal)_2(H_2O)]^{2-}$ anionic layers pillared through H_2en^{2+} cationic groups and crystallization water molecules (see Figure 14) leading to a three-dimensional network.

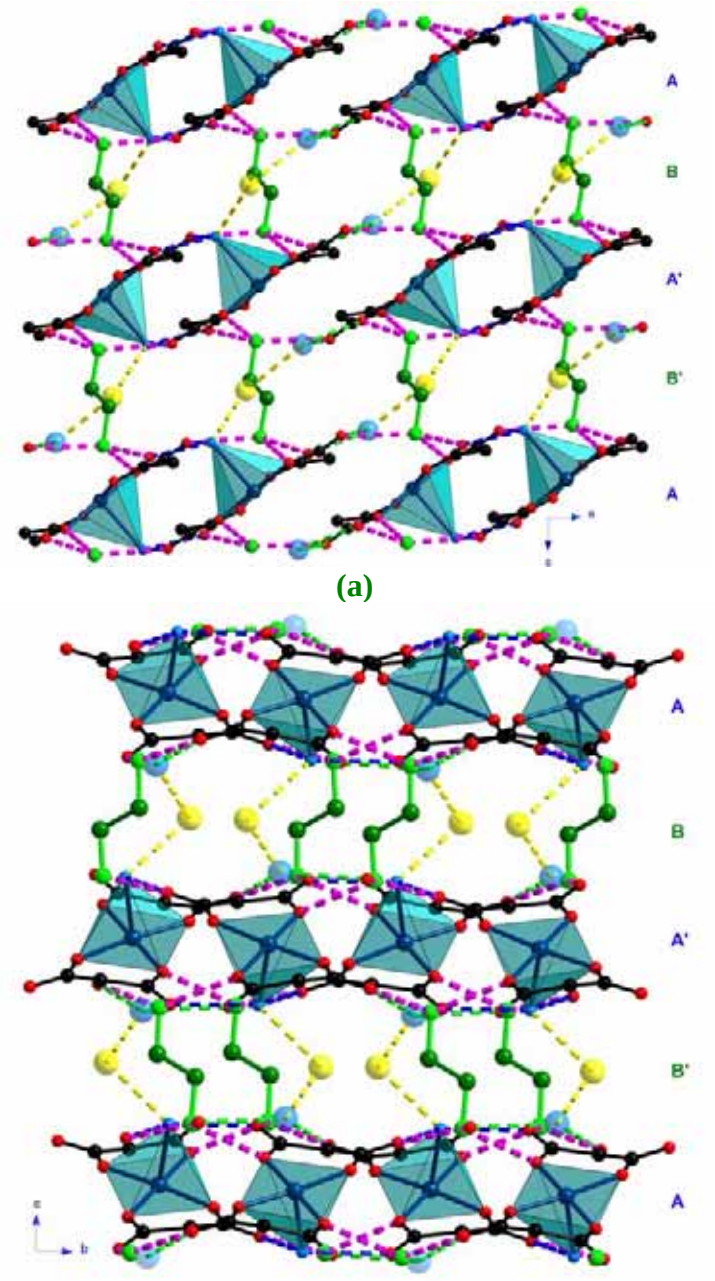

Figure 14. A perspective view of the pillared structure in **3** along the *b*- **(a)** and the *a*-axis **(b)**. Hydrogen bonds are drawn as broken lines. Hydrogen atoms are omitted for the sake of clarity. Crystallization water molecules are drawn as 30% transparency cyan (O2w) and yellow (O3w) balls.

Each atom is five-coordinated (see Table 8 and Figure 15) and it exhibits a slightly distorted square pyramidal environment (τ = 0.084) [Addison A.W. et *al.*, 1984]. Four carboxylate-oxygen atoms from two different malonate groups build the equatorial plane around the metal atom, the mean Cu-O(eq) bond distance being 1.931(2) Å. The apical position is occupied by a water molecule [Cu(1)-O(1w) = 2.442(2) Å]. The copper atom is shifted 0.0473(4) Å from the mean equatorial plane towards the apical position. Another water molecule [O(2w)] lies in the proximity of the

Cu(1) atom [O(2w)···Cu(1) = 2.758(3) Å] and it could be considered as weakly bonded to it.

Table 8. Selected bond lengths (Å) and angles (º) for **3**

Cu(1)-O(1)	1.925(2)	Cu(1)-O(2)	1.939(2)
Cu(1)-O(11)	1.936(2)	Cu(1)-O(12)	1.923(2)
Cu(1)-O(1w)	2.442(2)		
O(1)-Cu(1)-O(2)	92.78(7)	O(11)-Cu(1)-O(12)	93.11(7)
O(1)-Cu(1)-O(11)	86.79(7)	O(2)-Cu(1)-O(12)	87.30(7)
O(1)-Cu(1)-O(12)	174.52(7)	O(2)-Cu(1)-O(11)	179.55(6)
O(1w)-Cu(1)-O(1)	95.10(7)	O(1w)-Cu(1)-O(11)	91.74(7)
O(1w)-Cu(1)-O(2)	88.44(7)	O(1w)-Cu(1)-O(12)	90.37(7)

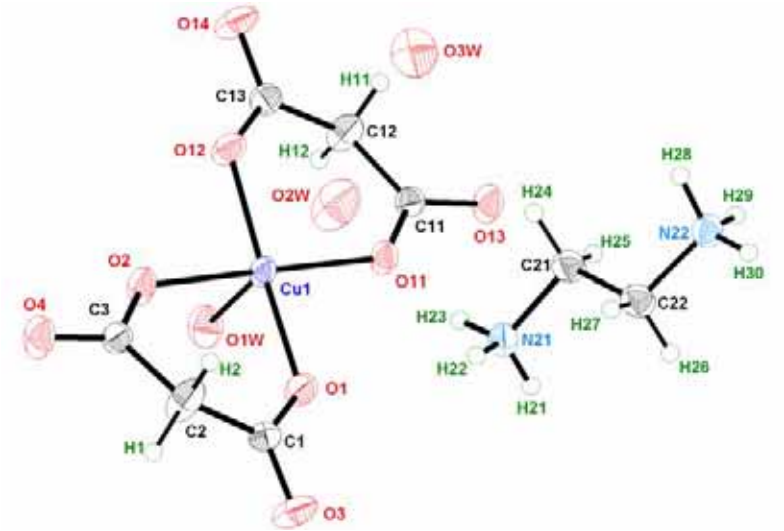

Figure 15. Perspective view of the asymmetric unit in **3** with the atom numbering. Thermal ellipsoids are drawn at the 50% probability level.

There are two symmetrically different malonate groups: L1 [C(1)-C(2)-C(3)] and L2 [C(11)-C(12)-C(13)]. Both of them act as bidentate ligands (see Figure 15) towards Cu(1). The values of the angle subtended by them at Cu(1) are 92.78(7) and 93.11(7)º for L1 and L2, respectively. Both chelating malonate groups form a six-membered ring (including the copper atom) that exhibits a boat conformation [Cremer D. et *al*., 1975] [θ = 115.6(3) and ϕ = 92.5(3) for L1 and θ = 122.5(3) and ϕ = 95.0(3) for L2]. The geometric values of L1 and L2 (see Table 9) agree well with those observed in other malonate-containing copper(II) complexes [see references in the Introduction].

Table 9. Bond lengths (Å) and angles (º) for the malonate ligands in **3**

C(1)-C(2)	1.514(3)	C(2)-C(3)	1.510(3)
C(1)-O(1)	1.259(3)	C(3)-O(2)	1.272(3)
C(1)-O(3)	1.236(3)	C(3)-O(4)	1.234(3)

O(1)···O(2)	2.797(2)	O(3)···O(4)	4.566(3)
O(1)-C(1)-O(3)	122.4(2)	O(2)-C(3)-O(4)	122.3(2)
O(1)-C(1)-C(2)	120.9(2)	O(2)-C(3)-C(2)	119.8(2)
O(3)-C(1)-C(2)	116.6(2)	O(4)-C(3)-C(2)	117.8(2)
C(1)-C(2)-C(3)	120.1(2)		
C(1)-O(1)-Cu(1)	127.25(15)	C(3)-O(2)-Cu(1)	127.46(15)
O(1)C(1)O(3)-Cu(1)eq[a]	20.0(2)	O(2)C(3)O(4)-Cu(1)eq[a]	23.2(2)
C(11)-C(12)	1.510(3)	C(12)-C(13)	1.514(3)
C(11)-O(11)	1.274(3)	C(13)-O(12)	1.259(3)
C(11)-O(13)	1.239(3)	C(13)-O(14)	1.239(3)
O(11)···O(12)	2.802(2)	O(13)···O(14)	4.593(3)
O(11)-C(11)-O(13)	122.1(2)	O(12)-C(13)-O(14)	121.5(2)
O(11)-C(11)-C(12)	120.0(2)	O(12)-C(13)-C(12)	122.0(2)
O(13)-C(11)-C(12)	117.9(2)	O(14)-C(13)-C(12)	116.5(2)
C(11)-C(12)-C(13)	120.3(2)		
C(11)-O(11)-Cu(1)	127.42(15)	C(13)-O(12)-Cu(1)	126.25(15)
O(1)C(1)O(3)-Cu(1)eq[a]	17.9(2)	O(2)C(3)O(4)-Cu(1)eq[a]	19.5(2)

[a]dihedral angle (º) between the malonate carboxylate group and the mean equatorial plane of the metal atom

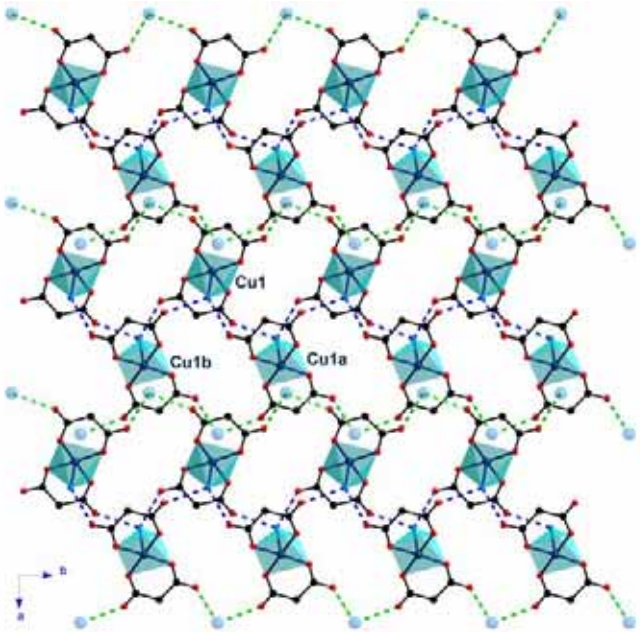

Figure 16. A perspective view along the *c*-axis of the packing of the $[Cu(mal)_2(H_2O)]^{2-}$ chains (one layer in Figure 14). Broken lines denote hydrogen bonds (see text). O(2w) crystallization water molecules are drawn as 60% transparency cyan balls.

Each $[Cu(mal)_2(H_2O)]^{2-}$ unit is linked to two other ones through hydrogen bonds (see blue broken lines in Figure 16) involving coordinated water molecules and the

outer malonate oxygen atoms (Table 10), affording thus, regular zigzag chains that run along the *b*-axis. Within each chain, additional hydrogen bonds involving the O(2w) water molecules and malonate oxygen atoms contribute to stabilize the chain connecting non-adjacent malonate copper(II) units (see green broken lines in Figure 16). The shortest copper···copper separations within the chain are: 7.1133(10) [Cu(1) ···Cu(1a); (a) -*x*+1, *y*+1/2, -*z*+3/2] and 8.408(2) Å [for Cu(1a)···Cu(1b); (b) -*x*+1, *y*-1/2, -*z*+3/2].

These hydrogen bonded chains are stacked along the *a*-axis, leading to malonate copper(II) sheets that grow in the *ab*-plane (Figure 16). Within the sheet, the copper chains are weakly linked together, because the long distance between O(2w) and Cu(1).

Table 10. Hydrogen bonds[a,b,c] for compound **3**

D-H···A	D···A/Å	H···A/Å	D-H···A/º
N(21)-H(21)···O(14d)	2.696(3)	1.88(3)	155(3)
N(21)-H(22)···O(4c)	2.792(3)	1.92(3)	165(3)
N(21)-H(23)···O(11)	2.773(3)	1.85(3)	168(3)
N(22)-H(28)···O(2e)	2.818(3)	1.84(4)	172(3)
N(22)-H(29)···O(13f)	2.783(3)	1.88(4)	166(4)
N(22)-H(30)···O(3g)	2.708(3)	1.86(3)	153(3)
C(2)-H(2)···O(3h)	3.368(4)	2.55(4)	131(3)
C(2)-H(2)···O(1h)	3.569(3)	2.63(2)	163(2)
D-H···A	D···A/Å	D-H···A	D···A/Å
O(1w)-H···O(13b)	2.891(3)	O(2w)-H···O(4c)	2.873(3)
O(1w)-H···O(14a)	2.696(3)	O(3w)-H···O(1we)	3.038(4)
O(2w)-H···O(3h)	2.744(3)	O(3w)-H···O(2w)	2.943(4)

[a] Symmetry transformations: (a) -*x*+1, *y*+1/2, -*z*+3/2; (b) -*x*+1, *y*-1/2, -*z*+3/2; (c) -*x*, *y*+1/2, -*z*+3/2; (d) *x*, *y*+1, *z*; (e) *x*, -*y*+1/2, *z*-1/2; (f) -*x*+1, -*y*+1, -*z*+1; (g) *x*, -*y*+3/2, *z*-1/2; (h) -*x*, *y*-1/2, -*z*+3/2. [b] A = acceptor; D = donor. [c] Symmetry operators apply to acceptor atoms.

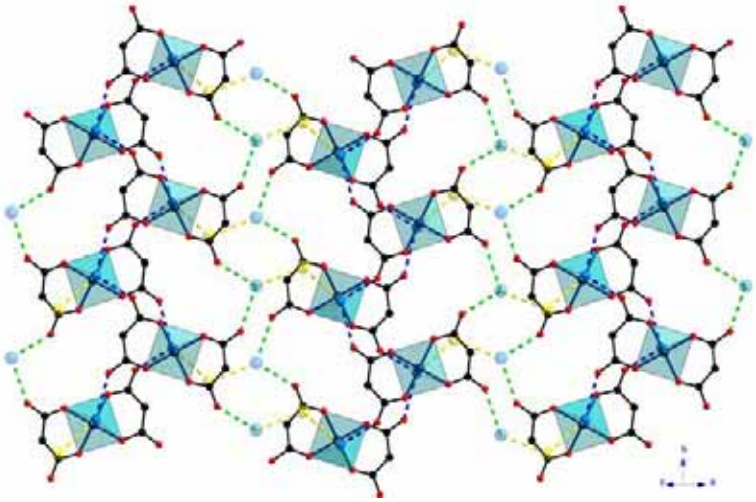

Figure 17. Perspective view along the [101] direction of the hydrogen bonded copper(II) layer. Hydrogen bonds are represented by broken lines. Crystallization water molecules are drawn as 50% transparency cyan (O2w) and yellow (O3w) balls.

Hydrogen bonds involving coordinated and non-coordinated water molecules (yellow broken lines in Figures 17 and 14) connect each malonate copper(II) chain to other two ones belonging to two adjacent copper(II) sheets chains, giving thus layers that grow along the [101] direction (see Figure 17).

The malonate-containing copper(II) chains are further pillared by H_2en^{2+} groups by means of hydrogen bonds (see Figure 18 and Table 10), along the *c*-axis, (see purple broken lines in Figure 14b) involving malonate-oxygen and H_2en^{2+}-nitrogen atoms, leading to a three-dimensional structure with alternating cationic and anionic sheets in the ABA'B' sequence (Figure 14b).

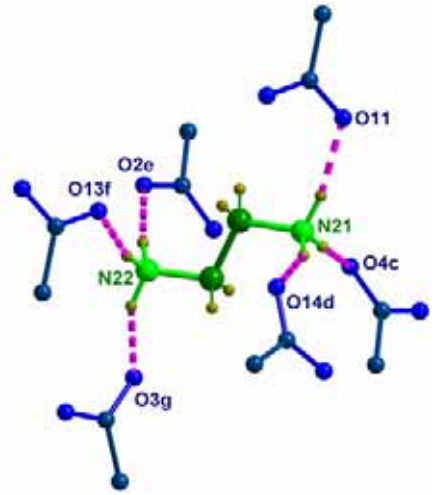

Figure 18. A view of one H_2en^{2+} cation surrounded by six malonate-carboxylate groups in **3**.

Description of the structure of $(H_2pn)[Cu(mal)_2]$ (4)

The structure of compound **4** consist of $[Cu(mal)_2]^{2-}$ anionic and H_2pn^{2+} cationic units held together by means of hydrogen bonds leading to a three-dimensional structure (see Figure 19) where anionic and cationic sheets are stacked following a ABA'B' sequence.

Each copper atom lies on a binary axis. It is four coordinated and it exhibits a distorted square planar environment (Figure 20). Selected bond lengths and angles for **4** are listed in Table 11. Four carboxylate-oxygen atoms from two symmetrically related malonate groups build up the equatorial plane around the metal atom. The O(1) and O(1a) atoms deviates 0.211(3) Å from the mean basal plane. The mean Cu-O bond distance is 1.915(2) Å. Although two symmetrically related malonate oxygens lie in the proximity of the copper environment [O(3b) and O(3c) atoms in Figure 21; (b) -*x*+1/2,

-*y*+1/2, *z*-1/2; (c) *x*-1/2, -*y*+1/2, -*z*+1], the value of the Cu···O separation [3.151(3) Å] is too large to be considered as bounded to the copper atom.

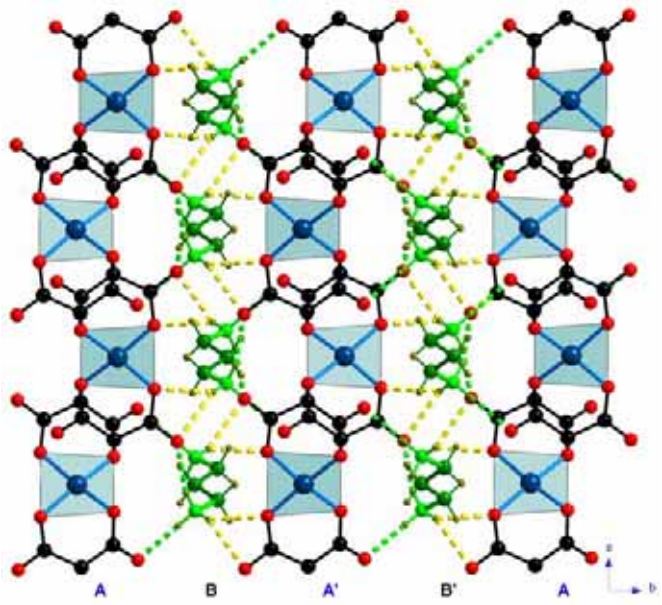

Figure 19. Perspective view of the stacking of the $[Cu(mal)]^{2-}$ and H_2pn^{2+} layers. Hydrogen bonds are drawn as broken lines.

Table 11. Selected bond lengths (Å) and angles (º) for **4**

Cu(1)-O(1)	1.919(2)	Cu(1)-O(2)	1.910(2)
O(1)-Cu(1)-O(2)	92.01(9)	O(1)-Cu(1)-O(1a)	88.32(15)
O(1)-Cu(1)-O(2a)	170.89(13)	O(2)-Cu(1)-O(2a)	89.09(12)

[a] Symmetry codes: (a) -*x*, *y*, -*z*+1/2.

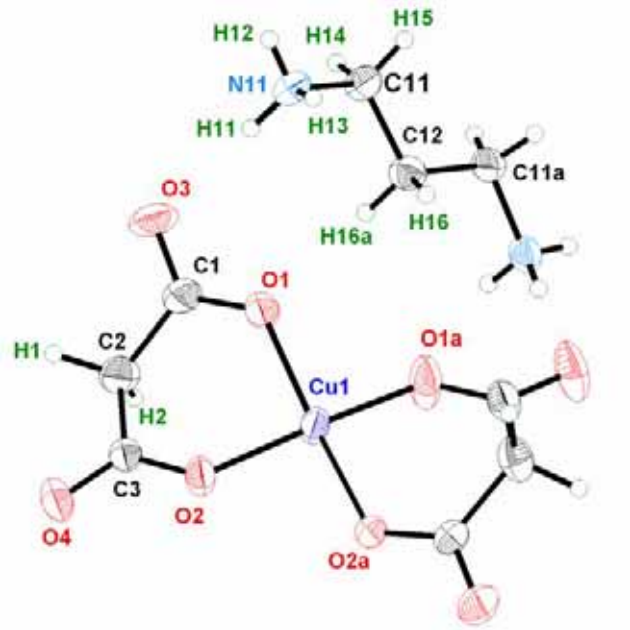

Figure 20. Perspective view of the metal environment and the H_2pn^{2+} cation in **4** with the numbering scheme. Thermal ellipsoids are drawn at the 50% probability level.

The malonate group acts as bidentate ligand towards Cu(1), the angle subtended by the ligand at the metal atom being 92.01(9)º. It forms (including the copper atom) a six-membered ring that exhibits a boat conformation [Cremer D. et *al.*, 1975] [θ= 113.9(4) and ϕ = 95.3(4)º]. The bond lengths and angles of the malonate ligand (see Table 12) agree well with those reported for other copper(II) malonate complexes [see references in the Introduction].

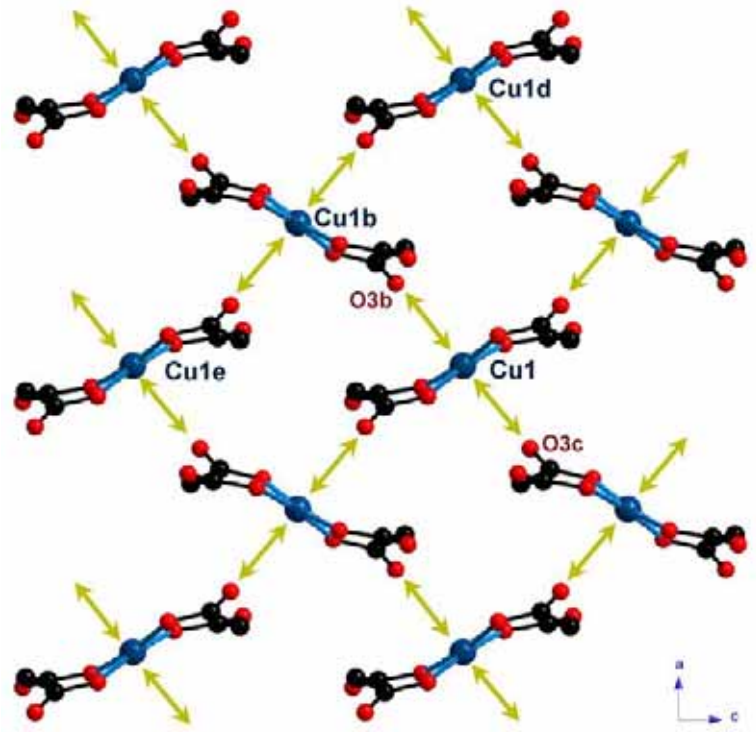

Figure 21. Partial view along the *b*-axis of the $[Cu(mal)]^{2-}$ stacking. The long Cu(1)···O(3) contacts are represented as yellow arrows.

Table 12. Bond lengths (Å) and angles (º) for malonate ligand in **4**

C(1)-C(2)	1.507(4)	C(2)-C(3)	1.521(4)
C(1)-O(1)	1.262(4)	C(3)-O(2)	1.268(3)
C(1)-O(3)	1.231(4)	C(3)-O(4)	1.238(3)
O(1)···O(2)	2.755(3)	O(3)···O(4)	4.537(3)
O(1)-C(1)-O(3)	122.2(3)	O(2)-C(3)-O(4)	121.1(3)
O(1)-C(1)-C(2)	119.8(3)	O(2)-C(3)-C(2)	120.3(3)
O(3)-C(1)-C(2)	118.0(3)	O(4)-C(3)-C(2)	118.5(3)
C(1)-C(2)-C(3)	117.8(3)		
C(1)-O(1)-Cu(1)	126.6(2)	C(3)-O(2)-Cu(1)	125.7(2)
O(1)C(1)O(3)-Cu(1)eq[a]	30.8(3)	O(2)C(3)O(4)-Cu(1)eq[a]	22.6(2)

[a]dihedral angle (º) between the malonate carboxylate group and the mean equatorial plane of the metal atom

The H_2pn^{2+} groups connect the $[Cu(mal)_2]^{2-}$ units through hydrogen bonds (see Figure 22 and Table 13; the central atom of the 1,3-propanediammonium group lies on a binary axis).

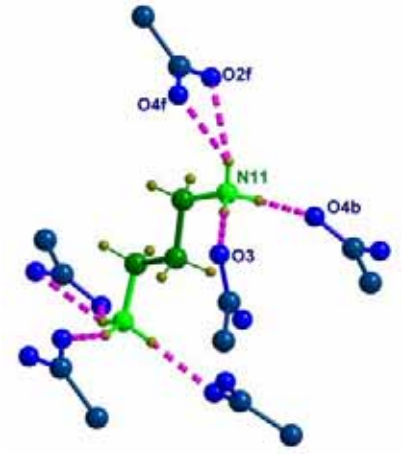

Figure 22. A view of a H_2pn^{2+} cation surrounded by six malonate-carboxylate groups in **4**.

Each $[Cu(mal)_2]^{2-}$ unit is hydrogen bonded to other four ones through N-H···O interactions (see green broken lines in Figure 23a) involving outer malonate oxygen atoms [O(3) and O(4)]. This arrangement gives rise to a neutral two-dimensional hydrogen bonded network which grows in the *ac*-plane (Figure 23a). These neutral layers are further linked through N-H···O bonds involving malonate-oxygen atoms from one carboxylate group [O(4)-C(3)-O(2), see Table 13] affording a three-dimensional network (see yellow broken lines in Figure 23b). This arrangement causes the stacking of the anionic bis(malonate)copper(II) and the cationic 1,3-propanediammonium sheets following the ABA'B'AB sequence along the *b*-axis, as seen in Figures 19 and 23b.

Table 13. Hydrogen bonds[a-c] for compound **4**

D-H···A	D···A/Å	H···A/Å	D-H···A/º
N(11)-H(11)···O(3)	2.867(4)	2.00(4)	177.(4)
N(11)-H(12)···O(2f)	2.972(3)	2.31(4)	141(4)
N(11)-H(12)···O(4f)	2.971(4)	2.31(4)	141(4)
N(11)-H(13)···O(4b)	2.788(4)	1.98(4)	159(4)
C(2)-H(1)···O(1g)	3.675(5)	2.66(5)	169(4)
C(11)-H(15)···O(3h)	3.604(4)	2.69(4)	170(3)

[a] Symmetry transformations: (b) -*x*+1/2, -*y*+1/2, *z*-1/2; (f) -*x*+1/2, *y*+1/2, *z*; (g) –*x*+1/2, -*y*+1/2, *z*+1/2; (h) *x*, -*y*+1, *z*-1/2. [b] A = acceptor; D = donor. [c] Symmetry transformations apply to acceptor atoms.

Looking at the arrangement of the $[Cu(mal)_2]^{2-}$ units in the *ac*-plane (see Figure 21), one can realize that the copper(II) units are distributed following a similar topology to that observed in other related complexes: $(MeNH_3)[Cu(mal)_2]$ (see Figure 11 in this chapter); $\{[Na_2(H_2O)_2][Cu(mal)_2]\}_n$, $\{[K(H_2O)]_2[Cu(mal)_2]\}_n$, $\{[Rb_2(H_2O)][Cu(mal)_2]\}_n$ (see Figures 11, 18a and 26 in the Chapter II) and $[Cu(Hmal)_2]$ (see Figure 1 in Chapter I). In this compound, one can also distinguish tetranuclear units that form sixteen-membered rings [Cu-O-C-O-Cu]$_4$ where the metal atoms occupy the corners of a rhombus. The shortest intralayer copper···copper separations are (see Figure 21): 6.4738(4) [Cu(1)···Cu(1b)], 8.2680(4) [Cu(1)···Cu(1d); (d) *x*+1, *y*, *z*], 9.4736(5) Å [Cu(1)···Cu(1e); (e) *x*, *y*, *z*-1]. The dihedral angle between the mean equatorial planes of two adjacent copper atoms is 63.28(7)º.

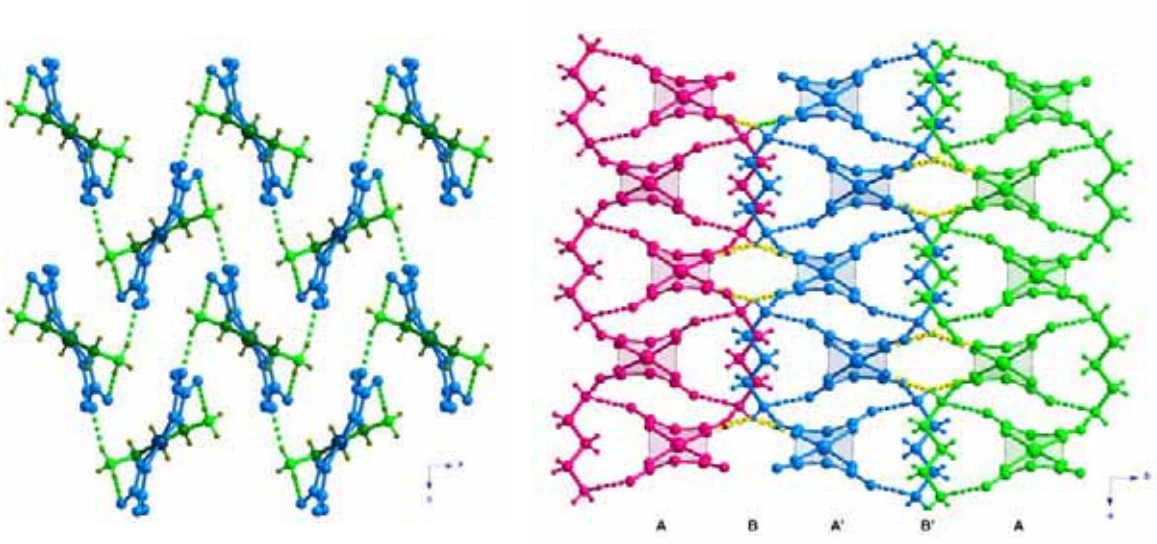

(a) **(b)**

Figure 23. Side view along the *b*-axis **(a)** and perspective view along the *c*-axis **(b)** of the stacking of the bis(malonate)copper(II) and 1,3- propanediammonium layers in **4**.

Description of the structure of $(H_2bn)[Cu(mal)_2(H_2O)]\cdot H_2O$ (5)

The structure of **5** is made up of $[Cu(mal)2(H_2O)]^{2-}$ anions, H_2bn^{2+} cations and crystallization water molecules that are held together by means of hydrogen bonds to afford a three-dimensional structure where anionic and cationic layers are stacked in a ABAB sequence (Figure 24).

Each copper atom is five-coordinated (see Figure 25 and Table 14) and it exhibits a slightly distorted square pyramidal environment ($\tau = 0.131$) [Addison A.W. et *al.*, 1984]. Four carboxylate-oxygen atoms from two crystallographically different malonate groups occupy the equatorial positions around the metal atom, the copper(II)

being shifted 0.1955(4) Å from the mean equatorial plane towards O(1w). One coordinated water molecule fills the apical position, the Cu(1)-O(1w) bond distance being 2.254(3) Å.

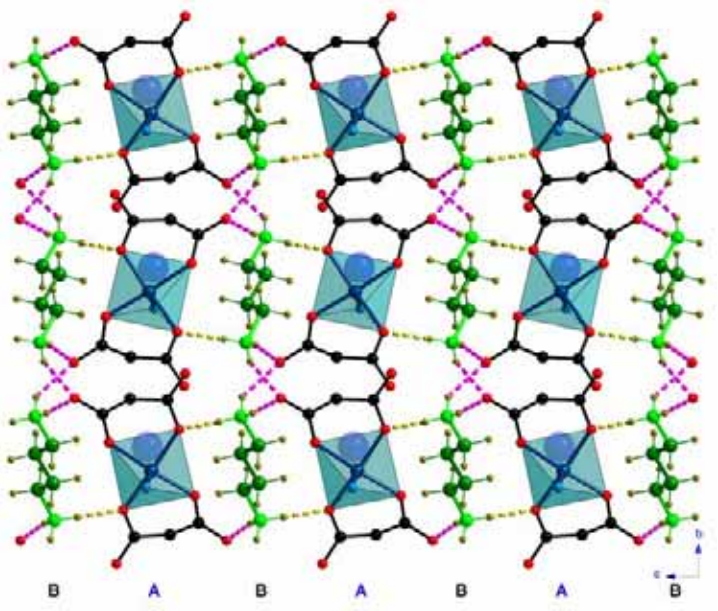

Figure 24. Perspective view along the *c*-axis showing the regular alternating of anionic and cationic layers in **5**. Hydrogen bonds are drawn as broken lines.

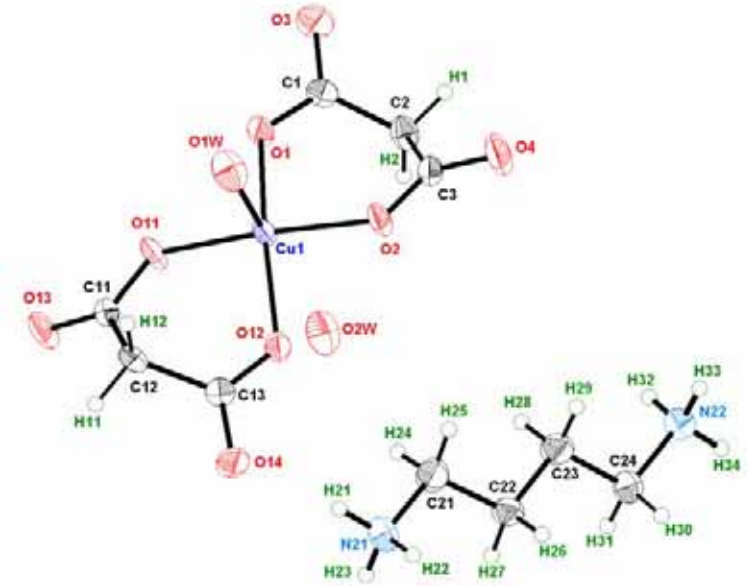

Figure 25. View of the asymmetric unit in **5** with the atom numbering. The thermal ellipsoids are drawn at the 50% probability level.

Table 14. Selected bond lengths (Å) and angles (º) for **5**

Cu(1)-O(1)	1.932(3)	Cu(1)-O(2)	1.931(3)
Cu(1)-O(11)	1.932(3)	Cu(1)-O(12)	1.960(3)
Cu(1)-O(1w)	2.254(3)		
O(1)-Cu(1)-O(2)	92.91(11)	O(11)-Cu(1)-O(12)	91.31(12)
O(1)-Cu(1)-O(11)	87.50(12)	O(2)-Cu(1)-O(12)	86.28(12)
O(1)-Cu(1)-O(12)	164.56(13)	O(2)-Cu(1)-O(11)	172.42(13)

O(1w)-Cu(1)-O(1)	93.41(12)	O(1w)-Cu(1)-O(11)	96.82(11)
O(1w)-Cu(1)-O(2)	90.71(11)	O(1w)-Cu(1)-O(12)	102.02(12)

Two malonate groups are present in **5**: L1 [C(1)-C(2)-C(3)] and L2 [C(11)-C(12)-C(13)]. Both act as bidentate ligands towards Cu(1) (see Figure 25), the values of th angle subtended by malonate groups at metal atom being 92.91(11) and 91.31(12)º for L1 and L2, respectively. They exhibit boat conformations [Cremer D. et *al.*, 1975] [θ = 81.0(3) and ϕ = 117.9(4) for L1 and θ = 89.6(3) and ϕ = 128.3(3)º for L2]. The bond lengths and angles of the malonate ligands (Table 15) are in good agreement with those observed in the previously malonate copper(II) complexes [see references in the Introduction].

Table 15. Bond lengths (Å) and angles (º) for the malonate ligands in **5**

C(1)-C(2)	1.491(5)	C(2)-C(3)	1.504(5)
C(1)-O(1)	1.263(5)	C(3)-O(2)	1.284(5)
C(1)-O(3)	1.258(5)	C(3)-O(4)	1.241(5)
O(1)···O(2)	2.800(4)	O(3)···O(4)	4.321(5)
O(1)-C(1)-O(3)	121.2(4)	O(2)-C(3)-O(4)	122.2(4)
O(1)-C(1)-C(2)	119.6(3)	O(2)-C(3)-C(2)	117.9(3)
O(3)-C(1)-C(2)	119.1(3)	O(4)-C(3)-C(2)	119.9(3)
C(1)-C(2)-C(3)	115.1(3)		
C(1)-O(1)-Cu(1)	125.9(3)	C(3)-O(2)-Cu(1)	126.2(2)
O(1)C(1)O(3)-Cu(1)eq[a]	27.9(2)	O(2)C(3)O(4)-Cu(1)eq[a]	32.6(3)
C(11)-C(12)	1.525(5)	C(12)-C(13)	1.514(5)
C(11)-O(11)	1.283(4)	C(13)-O(12)	1.271(5)
C(11)-O(13)	1.215(5)	C(13)-O(14)	1.225(4)
O(11)···O(12)	2.784(4)	O(13)···O(14)	4.353(4)
O(11)-C(11)-O(13)	122.1(4)	O(12)-C(13)-O(14)	122.3(4)
O(11)-C(11)-C(12)	117.3(3)	O(12)-C(13)-C(12)	118.9(3)
O(13)-C(11)-C(12)	120.6(3)	O(14)-C(13)-C(12)	118.8(3)
C(11)-C(12)-C(13)	115.4(3)		
C(11)-O(11)-Cu(1)	126.0(3)	C(13)-O(12)-Cu(1)	125.0(2)
O(1)C(1)O(3)-Cu(1)eq[a]	26.6(4)	O(2)C(3)O(4)-Cu(1)eq[a]	26.6(2)

[a]dihedral angle (º) between the malonate carboxylate group and the mean equatorial plane of the metal.

Each $[Cu(mal)_2(H_2O)]^{2-}$ unit is connected to two adjacent ones through O-H···O hydrogen bonds (blue broken lines in Figure 26; see Table 16) which involve the O(1w)

coordinated water molecule and malonate oxygen atoms, affording copper(II) chains that grow along the *b*-axis. The shortest intrachain copper···copper separation (see Figure 26) is 7.4880(7) Å [Cu(1)···Cu(1f); (f) -*x*, *y*-1/2, -*z*+1]. These chains are further linked through hydrogen bonds involving all water molecules and malonate oxygen atoms (see green broken lines in Figure 26), leading to a two-dimensional network that grows in the *ab*-plane. Finally, the layers are hydrogen bonded through N-H···O bonds (see Table 16) to afford a three-dimensional network (see Figure 24).

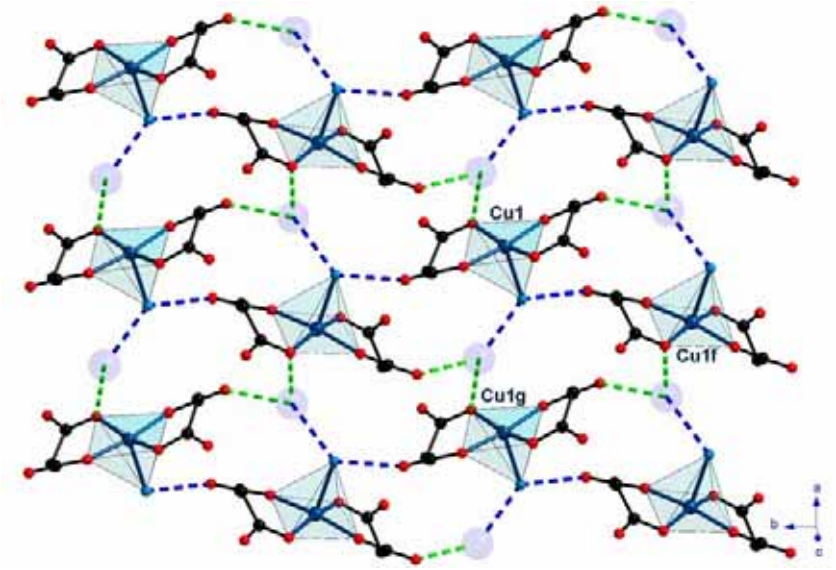

Figure 26. A Perspective view of a fragment of the hydrogen bonded $[Cu(mal)_2(H_2O)]^{2-}$ layer in **5**.

The H_2bn^{2+} groups are held together by means of hydrogen bonds involving malonate oxygen atoms (see Figure 27 and Table 16).

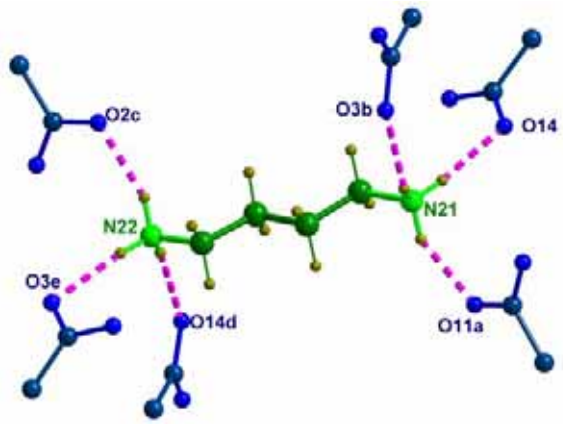

Figure 27. A view of the H_2bn^{2+} cation surrounded by six malonate-carboxylate groups in **5**.

They are also disposed in the *ab*-plane, linking the malonate copper(II) layers (see Figure 24). Looking at the arrangement of the H_2bn^{2+} groups, in the *ab*-plane, one realize they form a two-dimensional network through hydrogen bonds that exhibits a

herringbone type conformation (Figure 28) where some outer malonate-oxygen atoms are involved [O(3) and O(14); see purple broken lines in Figures 24 and 28]. Additional N-H···O hydrogen bonds involving some inner malonate oxygen atoms [O(2) and O(11)] contribute to stabilize the whole structure (see yellow lines in Figures 24 and 28).

Table 16. Hydrogen bonds[a-c] for compound **5**

D-H···A	D···A/Å	D-H···A	D···A/Å
O(1w)-H···O(13f)	2.723(4)	O(2w)-H···O(4b)	2.725(4)
O(1w)-H···O(2wg)	2.785(4)	O(2w)-H···O(12)	3.016(4)
D-H···A	**D···A/Å**	**H···A/Å**	**D-H···A/º**
N(21)-H(21)···O(14)	2.836(5)	1.956(3)	169.4(2)
N(21)-H(22)···O(11a)	2.780(4)	1.959(3)	152.6(2)
N(21)-H(23)···O(3b)	2.829(5)	2.101(3)	138.3(3)
N(22)-H(32)···O(2c)	2.863(4)	2.022(3)	157.2(2)
N(22)-H(33)···O(14d)	2.867(4)	2.041(3)	153.9(2)
N(22)-H(34)···O(3e)	2.843(5)	1.971(3)	166.1(2)
C(21)-H(24)···O(2w)	3.628(5)	2.717(3)	156.7(3)
C(23)-H(28)···O(1wc)	3.582(5)	2.654(3)	160.2(3)
C(22)-H(26)···O(2wa)	3.609(5)	2.709(3)	154.5(3)
C(24)-H(30)···O(1we)	3.735(5)	2.789(3)	165.1(3)
C(12)-H(11)···O(2wg)	3.731(5)	2.787(3)	164.4(2)

[a] Symmetry transformations: (a) *x*, *y*, *z*-1; (b) -*x*+1, *y*+1/2, -*z*+1; (c) *x*+1, *y*, *z*; (d) -*x*+1, *y*-1/2, -*z*; (e) *x*+1, *y*, *z*-1; (f) -*x*, *y*-1/2, -*z*+1; (g) *x*-1, *y*, *z*. [b] A = acceptor; D = donor. [c] Symmetry transformations apply to acceptor atoms.

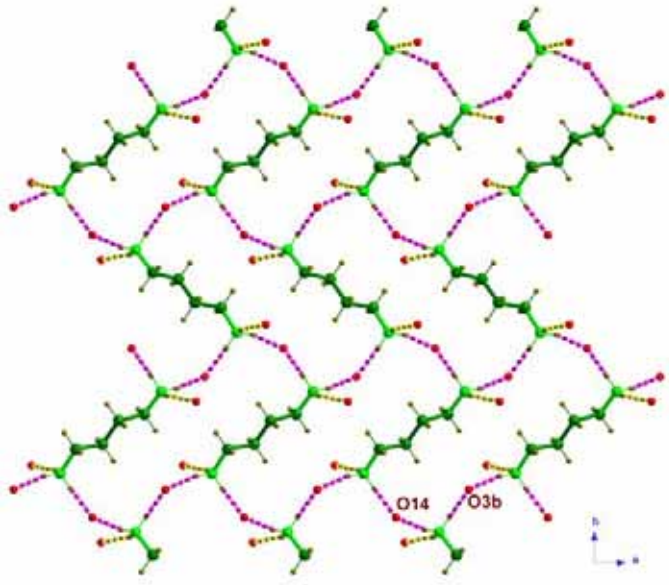

Figure 28. Perspective view of a fragment of the H_2bn^{2+} herringbone layer in **5**.

Magnetic Properties

The thermal dependence of $\chi_M T$ [χ_M is the magnetic susceptibility per mol of Cu(II) ions] in the temperature range 2-100 K for compounds **1**, **3** and **5** is shown in Figure 29.

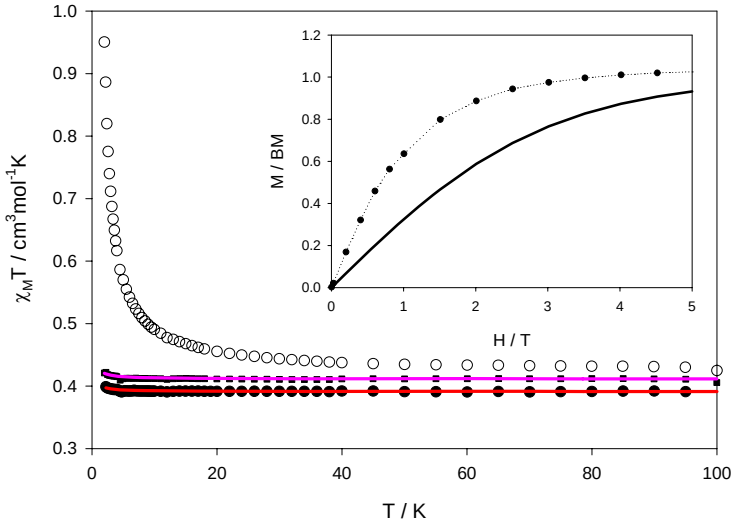

Figure 29. Thermal dependence of the $\chi_M T$ product of **1** (") **, 3** (!) **, 5** (#); the solid lines are the best-fit curves (see text). The inset shows the magnetisation *versus H* plot at 2.0 K for **1**: (C) Brillouin function for a spin doublet; (···) eye-guide line; (•) experimental data.

The values of $\chi_M T$ at the highest measured temperature are 0.39 (**3**) and 0.41 $cm^3mol^{-1}K$ (**5**). They are close to that expected for a magnetically isolated spin doublet. Upon cooling, a Curie law behaviour is observed down to 10 K. In the lower temperature range $\chi_M T$ smoothly increases to reach a value of 0.40 (**3**) and 0.42 $cm^3mol^{-1}K$ (**5**) at 2 K. This behaviour indicates the occurrence of a very weak (practically negligible) ferromagnetic coupling. This extremely weak ferromagnetic interaction in **3** and **5** is in agreement with their mononuclear nature. The least-square fitting of the magnetic data through a Curie-Weiss law leads (see Figure 29) to g = 2.042(1), θ = 0.034(3) cm^{-1} and $R = 1.0x10^{-5}$ (**3**) and g = 2.094(2), θ = 0.044(4) cm^{-1} and $R = 1.5x10^{-5}$ (**5**). R is the agreement factor defined as $\Sigma[(\chi_M)_{obs} - (\chi_M)_{calc}]^2/\Sigma[(\chi_M)_{obs}]^2$. As expected, the extensive hydrogen bonds present in both compounds are not able to mediate any significant coupling.

For compound **1**, the value of $\chi_M T$ at the highest measured temperature is 0.42 $cm^3\ mol^{-1}$ K, a value which is as expected for a magnetically isolated spin doublet. Upon cooling, $\chi_M T$ continuously increase to reach a value of 0.95 $cm^3\ mol^{-1}$ K at 2 K. This

behaviour indicates the occurrence of an overall ferromagnetic coupling. This is confirmed by the magnetization curve (see inset in Figure 29) which remains well above the Brillouin function for a spin doublet. The structure of **1** consists of a $[Cu(mal)_2]^{2-}$ units which are connected through out-of-plane carboxylate-malonate bridges leading to a three-dimensional malonate bridged copper(II) structure (see Figure 1b). There is no model to analyze such a system and we cannot introduce any approximation that allows us to simplify the system, consequently, the evaluation of the values of the magnetic coupling constant through the out-of plane carboxylate bridge is precluded in the present case. However, as the magnetic pathway involved in **1** is the same as that observed in **2**, **4** and in the alkaline-containing complexes presented in the previous chapter and given that in the case of an out-of-plane magnetic exchange pathway, the magnitude of the magnetic coupling depends mainly on the Cu-O(apical) bond distance (see Table 17), a value of the magnetic coupling in **1** somewhat above than that observed in compound **2** is predicted.

The magnetic properties of **2** and **4** under the form of $\chi_M T$ vs T plot [$\chi_M T$ being the magnetic susceptibility per mol of copper(II) ion] in the temperature range 2-100 K are shown in Figures 30 and 31, respectively. The values of $\chi_M T$ at 100 K are 0.42 and 0.40 $cm^3\ mol^{-1}\ K$ for **2** and **4**, respectively, values which are as expected for a magnetically isolated spin doublets. Upon cooling, $\chi_M T$ gradually increase, reaching a value of 1.22 (**2**) and 0.58 $cm^3\ mol^{-1}\ K$ (**4**) at 2 K. These features are indicative of the occurrence of an overall ferromagnetic coupling between the copper(II) ions.

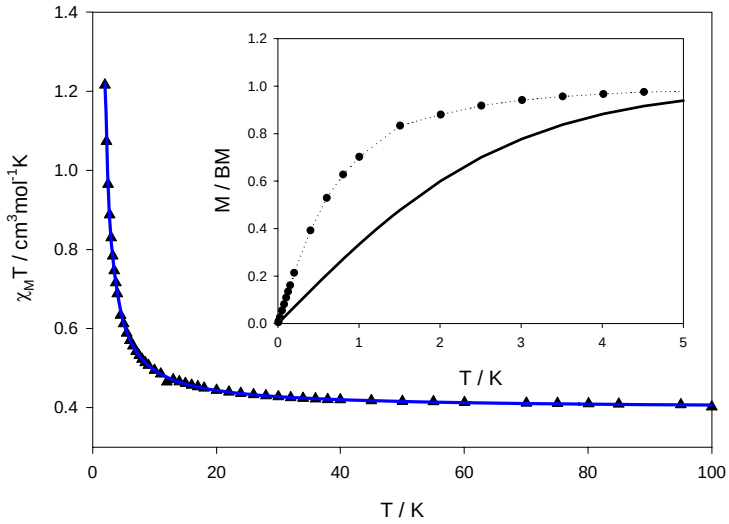

Figure 30. Temperature dependence of the $\chi_M T$ product of **2**: (▲) experimental data; (-) best fit curve (see text). The inset shows the magnetisation *versus* H plot at 2.0 K for **3**: (C) Brillouin function for a spin doublet; (···) eye-guide line; (•) experimental data.

The structure of **2** consists of $[Cu(mal)_2]^{2-}$ units which are held together by means of out-of-plane carboxylate bridges affording to a regular quasi-quadrate malonate-bridged copper(II) layer (see Figure 11). Although these layers are further linked through $MeNH_3^+$ groups, no significant coupling between magnetic centres of different layers is expected through this cation.

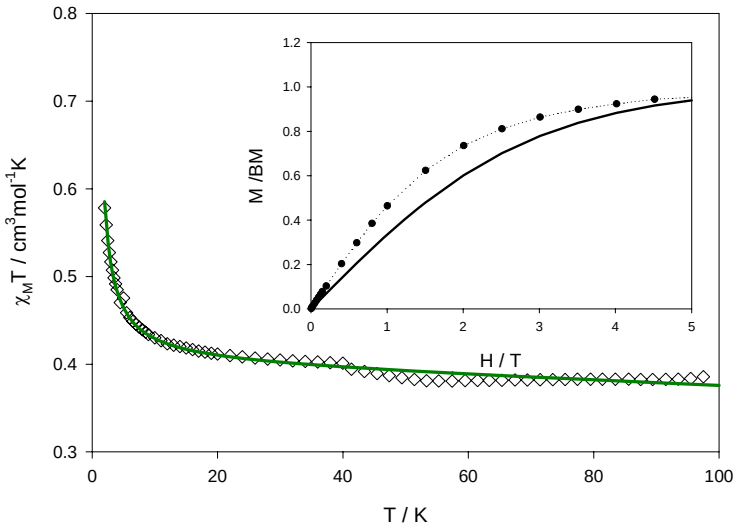

Figure 31. Thermal dependence of the $\chi_M T$ product of **4**: (◇) experimental data; (-) best fit curve (see text). The inset shows the magnetisation *versus H* plot at 2.0 K for **4**: (C) Brillouin function for a spin doublet; (···) eye-guide line; (•) experimental data.

Let us focus now in the structure of **4**. Although its structure consists of mononuclear $[Cu(mal)_2]^{2-}$ units which are connected through hydrogen bonds involving the H_2pn^{2+} groups, if one looks at the coordination sphere of the metal ion in **4**, one can see, that a [Cu-O(equatorial)-C-O(apical)···Cu] exchange pathway through the malonate ligand occurs, which connects equatorial and apical sites of adjacent copper(II) atoms [3.151(3) Å for the Cu···O(ap) separation; see Figure 21]. So, from a magnetic point of view, one can consider that each $[Cu(mal)_2]^{2-}$ unit in **4** is linked to other four ones through out-of-plane carboxylate bridges affording a regular quasi-quadratic malonate-bridged copper(II) layer, as observed for compound **2**.

We try to fit the magnetic data of **2** and **4** through the high-temperature expansion series derived from the 2D Heisenberg model for the S = ½ ferromagnetic quadratic lattice [Navarro R., 1990]

$$\chi = Ng^2\beta^2 S(S+1)/(3kT)\left[1+\sum_{n=1}^{8} a_n K^n\right] \qquad (1)$$

where $K = J/2kT$ and J is the intrachain magnetic coupling parameter. N, g, β and k have their usual meaning. The a_n coefficients are taken for a square lattice. The spin Hamiltonian is defined as:

$$\hat{H} = \sum_i -J\hat{S}_i \cdot \hat{S}_{i+1} \qquad (2)$$

The best least-squares fit parameters are: $J = +0.755(1)$ cm^{-1}, $g = 2.060(1)$ and $R = 2.3\text{x}10^{-5}$ (for **2**) and $J = +0.263(5)$ cm^{-1}, $g = 2.066(4)$ and $R = 1.2\text{x}10^{-4}$ for **4**. The calculated curve matched well the experimental data in the whole temperature range. The ferromagnetic coupling in **4** is smaller than that in **2**, due mainly to the longer axial Cu···O distance in the former compound. As seen in Table 17, the value of the magnetic interactions, in **2** and **4**, are in good agreement with other malonate complexes where the $[Cu(mal)_2]^{2+}$ units exhibit the same topology [two-dimensional malonate-bridged copper(II) networks where the metal atoms define a rhombohedral grid].

Table 17. Selected magneto-structural data for some related carboxylate(malonate)-bridged copper(II) complexes

Compound[a]	d_1[b]	d_2[c]	θ_1[d]	θ_2[e]	J[f]	Ref.
$[Na(H_2O)]_2[Cu(mal)_2]$	1.954(2)	2.601(2)	26.1(3)	51.17(5)	0.897(1)	Chap. II (**2**)
$[K(H_2O)_{3/2}]_2[Cu(mal)_2]$	1.9417(15)	2.689(2)	24.4(2)	73.14(4)	0.774(2)	Chap. II (**3**)
$(MeNH_3)_2[Cu(mal)_2]$	1.9236(11)	2.5620(15	30.1(1)	53.13(3)	0.755(1)	**2**
$(H_2pn)[Cu(mal)_2]$	1.919(2)	3.151(3)	30.8(3)	68.28(7)	0.263(5)	**4**
$[Cu(Hmal)_2]$	1.9323(12)	2.5429(13	19.5(2)	56.7(4)	0.104(4)	Chap. I (**1**)

[a] Abbreviations used: $MeNH_3^+ = CH_3NH_3^+$, $H_2pn^{2+} = [NH_3(CH_2)_3NH_3]^{2+}$. [b] Cu-O equatorial bond distance in Å. [c] Cu-O apical bond distance in Å. [d] Dihedral angle (º) between the malonate carboxylate group and the mean equatorial plane of the metal atom. [e] Dihedral angle (º) between the mean equatorial plane of adjacent copper atoms connected through out-of-plane carboxylate bridges. [f] Values of the magnetic coupling in cm^{-1}.

The weak ferromagnetic coupling observed in **1**, **2** and **4** can be explained keeping in mind the out-of-plane exchange pathway between adjacent metal ions. The unpaired electron of each copper(II) ion is defined by $d_{x^2-y^2}$ type magnetic orbital (the x and y axis being roughly defined by the short copper to oxygen bonds) and it is mainly located in the equatorial plane. The exchange pathway, in complexes **1**, **2** and **4**, involves an apical carboxylate-oxygen atom, so a small spin density is expected in the axial positions because of some admixture of d_{z^2} character. Therefore, the overlap (S)

between the magnetic orbitals belonging to adjacent copper atoms is expected to be very small and so, the antiferromagnetic contribution, which is proportional to the square of the overlap integral (S^2) in the Kahn's model [Kahn O., 1993] would be negligible. The weak ferromagnetic coupling observed in **1**, **2** and **4** is due to the accidental orthogonality between the magnetic orbitals described above. This behaviour has been observed in other malonate- and carboxylate-bridged complexes with long axial Cu···O separations as shown in the precedent chapter. The magnitude of the magnetic coupling, in this case, depends on structural parameters such as the value of the Cu-O(apical) distance and the dihedral angles between equatorial planes of adjacent copper(II) ions.

References

Addison A.W., Rao T.N., Reedijk J., Rijn J. and Verschoor G.C.J., *J. Chem. Soc., Dalton Trans.*, **1984**, 1349.

Beatty A.M., *Coord. Chem. Rev*., **2003**, 246, 131.

Charbonnier F. and Arnaud Y., *C.R.Acad.Science, Ser. C*, **1972**, 1515.

Cremer D. and Pople J.A., *J. Am. Chem. Soc.*, **1975**, 97, 1354.

Delgado F.S., Sanchiz J., Ruiz-Pérez C., Lloret F. and Julve M., *CrystEngComm.*, **2004**, 6, 443.

Desiraju G.R., Crystal Engineering: The Design of Organic Solids, Elsevier, Amsterdam, **1989**.

Desiraju G. R., *Angew. Chem. Int. Ed. Engl.*, **1995,** *34*, 2311.

DIAMOND 2.1d, Crystal Impact GbR, CRYSTAL IMPACT, K. Brandenburg & H. Putz GbR, Postfach 1251, D-53002 Bonn, Germany, 2000.

Duisenberg A.J.M., Kroon-Batenburg L.M.J. and Schreurs A.M.M., *J. Appl. Cryst.*, **2003,** 36, 220 (EVALCCD).

Earshaw A., *Introduction to Magnetochemistry*; Academic Press; London, **1968**.

Farrugia L.J. (*WINGX)*, *J. Appl. Cryst*, **1999**, *32*, 837.

Hooft, R.W.W. *COLLECT*. Nonius BV, Delft, The Netherlands, **1999**.

Kahn O., *Molecular Magnetism*, ed. John Wiley & Sons, **1993**.

Maddox J., *Nature* **1988**, *335*, 201.

Nardelli M., *J. Appl. Crystallogr.*, **1995**, *28*, 659.

Navarro R., *Application of High- and Low-Temperature Series Expansions to Two-dimensional Magnetic Systems*, ed. L.J. de Jongh, Kluwer Academic Publishers, Dordrecht, **1990**.

SADABS, version 2.03. Bruker AXS Inc.: Madison, WI, **2000**.

Schmidt G.M.J., *Pure Appl. Chem.* **1971**, 27, 647.

Seddon K.R., Zaworotko M.J. (eds.), *Crystal Engineering: The Design and Application of Functional Solids*, NATO, ASI series, **1998**.

Sheldrick, G.M. *SHELX97*, *Programs for Crystal Structure Anlysis (Release 97-2)*, Institüt für Anorganische Chemie der Universität, Tammanstrasse 4, D-3400 Göttingen, Germany, **1998**.

Stiefel E.I., Brown G. F. *Inorg. Chem.*, **1972**, 11, 434.

CHAPTER IV.

Supramolecular networks in Copper(II) malonate complexes.

Introduction

Crystal engineering with desired functions and fascinating topological architectures has become an area of increasing interest in recent years [Lehn J.-M., 1995: Desiraju G.R., 2001]. One of the most significant approaches in the field is to use robust modules or motifs to design supramolecular architectures [Desiraju G.R., 1995; Yaghi O.M. et *al.*, 1995]. In this context, discrete modules for inorganic-organic hybrid materials are linked to larger networks through coordinate bonds, covalent bonds, or other intermolecular secondary bonding interactions, such as hydrogen bonding, π-π stacking interactions, etc [Robson R., 2000]. Supramolecular chemistry has advanced to a stage at which one can design and construct molecular solids with specific network topologies. Especially hybrid polynuclear transition metal complexes have offered promising perspectives towards the developing of new functional materials [Coronado E. *et al.*, 2000]. A promising strategy for the construction of polynuclear systems is the hybrid inorganic/organic self-assembly approach in which the inorganic elements are linked by organic bridges, and many excellent examples have been reported.

It is well-known that the malonic acid can coordinate to metal ions. As a result, the mal^{2-} group can be used as both terminal and bridging ligand. The former affords monomeric crystal structures whereas the later allows extending arrays such as a dimer, one-dimensional (1D), or two-dimensional (2D) structure by using coordination bonding interactions.

However, the monomer compounds can also be built up to higher dimensional structures by secondary bonding interactions, such as hydrogen-bonding interactions, π-π stacking interactions, etc,...

Experimental

Materials and methods

Malonic acid, copper(II) basic carbonate $Cu(CO_3)\cdot Cu(OH)_2$, copper(II) acetate, copper(II) nitrate hemipentahydrate, bis(2-pyridyl)ketone, 2,2'-dipyridylamine, 2,3-bis(2-pyridyl)pyrazine, 1,10-phenantroline were purchased from commercial sources and used as received. 2-(2-pyridyl)imidazole was prepared by following a previously reported procedure [Reeder K.A. *et al.*, 1978]. Elemental analyses (C, H, N) were performed on an EA 1108 CHNS-O microanalytical analyser. The magnetic susceptibility measurements were performed on a Quantum Design SQUID

magnetometer in the 2-100 K temperature range, operating at 500 G ($T \leq 15$ K) and 1000 G ($T > 10$ K) for **6**. Diamagnetic corrections of all the constituent atoms were estimated from Pascal's constants [Earshaw, 1968] as 4.18×10^{-3} cm^3 $mol^{-1}$for compound **6**, respectively. Corrections for the tip of the Cu(II) ions (60×10^{-6} cm^3 mol^{-1}) were also done.

Synthesis

[Cu(dpydiol)(mal)(H_2O)]·2H_2O (1) [dpydiol = bis(2-pyridyl)methanediol]. Solid copper(II) basic carbonate (221 mg, 1 mmol) is added to an aqueous solution (15 cm^3) of malonic acid (104 mg, 2 mmol) under continuous stirring. The suspension is heated at 40-50 ºC, until a blue solution is obtained. This solution is filtered and mixed with solution of bis(2-pyridyl)ketone (368 mg, 2 mmol) in EtOH (5 cm^3). Single crystals of **1** as blue prisms were grown from the solution by slow evaporation at room temperature in a few days (Found: C, 40.24; H, 4.19; N, 6.87;calc. for $C_{14}H_{18}CuN_2O_9$: C, 39.82; H, 4.27; N, 6.64 %).

[Cu(dpa)(mal)(H_2O)]·H_2O (2) [dpa = 2,2'-dipyridylamine]. Compound **2** is obtained by the same procedure as **1** using 2,2'-dipyridilamine (160 mg, 2 mmol) instead of bis(2-pyridyl)ketone. Blue prisms of **2** suitable for X-ray diffraction were obtained by slow evaporation at room temperature within a week (Found: C, 41.85; H, 3.99;N, 11.00; calc. for $C_{13}H_{15}CuO_6N_3$: C, 41.85; H, 4.02; N, 11.27 %).

[Cu(pyim)(mal)(H_2O)]·H_2O (3) [pyim = 2-(2-pyridyl)imidazole]. Solid copper(II) basic carbonate (55 mg, 0.25 mmol) is added to an aqueous solution (15 cm^3) of malonic acid (52 mg, 0.5 mmol) under continuous stirring. The suspension is heated at 40-50 ºC, until a blue solution is obtained. This solution is filtered and mixed with an ethanolic solution (5 cm^3) of 2-(2-pyridyl)imidazole (38 mg, 0.25 mmol). Single crystals of **1** as pale blue plates were grown from the solution by slow evaporation at room temperature within a week (Found: C, 38.06; H, 3.64; N, 11.62;calc. for $C_{11}H_{13}CuN_3O_6$: C, 38.06; H, 3.75; N, 12.11%)**.**

[Cu(dpp)(mal)(H_2O)]·3/2H_2O (4) [dpp = 2,3-bis(2-pyridyl)pyrazine]. Solid copper(II) basic carbonate (55 mg, 0.25 mmol) is added to a 1:1 H_2O:acetonitrile solution (15 cm^3) of malonic acid (52 mg, 0.5 mmol) under continuous stirring. The suspension is heated at 40-50 ºC, during an hour. This solution is mixed with a solution of 2,3-bis(2-pyridyl)pyrazine (62 mg, 0.25 mmol) in acetonitrile (10 cm^3). The resulting dark green solution is filtered and allowed to evaporate at room temperature. Single

crystals of **1** as green plates were grown from this solution within a week (Found: C, 45.89; H, 3.36; N, 11.48; calc. for $C_{17}H_{17}CuN_4O_{6.5}$: C, 45.85; H, 3.82; N, 12.59%).

[Cu(phen)(mal)(H_2O)]·H_2O (5) [phen = 1,10-phenantroline]. Solid copper(II) acetate (22 mg, 0.1 mmol) is added to a solution of malonic acid (10 mg, 0.1 mmol) in EtOH (8 cm^3) under continuous stirring. The suspension is heated at 40-50 ºC. This solution is mixed with an ethanolic (5 cm^3) solution of 1,10-phenantroline (20 mg, 0.25 mmol). The dark blue solution which results of the mixture is filtered and allowed to evaporate at room temperature. Single crystals of **5** as blue plates were grown within a few days (Found: C, 47.16; H, 3.79;N, 7.29; calc. for $C_{15}H_{14}CuN_2O_6$: C, 47.14; H, 3.67; N, 7.33%).

[Cu_2(phen)$_2$(mal)(H_2O)$_3$](NO_3)$_2$·2H_2O (6) [phen = 1,10-phenantroline]. Solid copper(II) nitrate hemipentahydrate (466 mg, 2 mmol) is added to an aqueous solution (15 cm^3) of malonic acid (104 mg, 1 mmol) under continuous stirring. The suspension is heated at 40-50 ºC during 2 h. This solution is mixed with a solution of 1,10-phenantroline (160 mg, 2 mmol) in EtOH (5 cm^3). Finally, the blue solution which results of the mixture is filtered and allowed to evaporate at room temperature. Single crystals of **6** as dark blue prims were grown from the solution by slow evaporation at room temperature within a few days. (Found: C, 40.30; H, 3.40;N, 10.16; calc. for $C_{27}H_{28}Cu_2N_6O_{15}$: C, 40.32; H, 3.48; N, 10.45%).

Crystal data collection and refinement of the structures

Single crystals of five compounds were mounted on a Bruker-Nonius KappaCCD diffractometer. Orientation matrix and lattice parameters were obtained by least-squares refinement of the reflections obtained by a θ-χ scan (Dirax/lsq method). Diffraction data for all compounds were collected at 293(2) K using graphite-monochromated Mo-K_α radiation (λ = 0.71073 Å). Data collection and data reduction were done with the COLLECT [Hooft R.W.W., 1999] and EVALCCD [Duisenberg A.J.M. *et al.*, 2003] programs. Empirical absorption corrections were carried out using SADABS [SADABS, version 2.03, 2003] for all compounds. The indexes of data collection were $-7 \le h \le 10$, $-13 \le k \le 13$, $-12 \le l \le 13$ for **1**; $-10 \le h \le 10$, $-13 \le k \le 13$, $-15 \le l \le 16$ for **2**; $-9 \le h \le 9$, $-13 \le k \le 13$, $-11 \le l \le 13$ for **3**; $-21 \le h \le 21$, $-12 \le k \le 11$, $-29 \le l \le 23$ for **4** and $-8 \le h \le 10$, $-14 \le k \le 14$, $-22 \le l \le 22$ for **5** and $-11 \le h \le 11$, $-51 \le k \le 55$, $-14 \le l \le 12$ for **6**. Of the 3643 (**1**), 3978 (**2**), 2933 (**3**), 4198 (**4**), 6671 (**5**) and

8016 (**6**), measured independent reflections in the θ range 2.11 – 28.57º (**1**), 5.05 - 30º (**2**), 5.05 – 27.50º (**3**), 5.01 – 27.50º (**4**), 5.04 – 27.50º (**5**) and 4.03 – 30º (**6**), 3059 (**1**), 3203 (**2**), 1878 (**3**), 2644 (**4**) and 4869 (**5**)), 5224 (**6**), have $I \geq 2\sigma(I)$. All the measured independent reflections were used in the analysis. All calculations for data reduction, structure solution, and refinement were done by standard procedures (WINGX) [Farrugia L.J., 1999]. The structure was solved by direct methods and refined with full-matrix least-squares technique on F^2 using the SHELXS-97 and SHELXL-97 programs [Sheldrick G.M., SHELX97, realease 97-2, 1998]. All hydrogen atoms for compounds **1**, **2** and **5** were located from difference Fourier maps. For compounds **3, 4** and **6** the hydrogen atoms of the water molecules were not found and those of the pyridyl rings and malonate ligands were set in calculated positions. For all compounds, the hydrogen atoms were refined with isotropic temperature factors. The final Fourier-difference maps showed maximum and minimum height peaks of 0.876 and -0.467 e Å^{-3} (**1**), 0.433 and -0.321 e Å^{-3} (**2**), 0.708 and -0.521 e Å^{-3} (**3**), 0.809 and -0.312 e Å^{-3} (**4**), 0.370 and -0.306 e Å^{-3} (**5**) and 0.594/-0.436 e Å^{-3} (**6**), A summary of the crystallographic data and structure refinement is given in Table 1. The final geometrical calculations and the graphical manipulations were carried out with PARST97 [Nardelli M., 1995] and DIAMOND [DIAMOND 2.1d, 2000] programs, respectively.

Table 1. Crystal data and details of structure determination for compounds **1-6**.

Compound	**1**	**2**	**3**	**4**	**5**	**6**
Formula	$C_{14}H_{18}CuN_2O_9$	$C_{13}H_{15}CuO_6N_3$	$C_{11}H_{13}CuN_3O_6$	$C_{17}H_{17}CuN_4O_{6.5}$	$C_{15}H_{14}CuN_2O_6$	$C_{27}H_{28}Cu_2N_6O_{15}$
M	421.84	372.82	346.78	444.89	381.82	803.63
Crystal system	triclinic	triclinic	triclinic	monoclinic	triclinic	monoclinic
Space group	*P*-1	*P*-1	*P*-1	*C*2/c	*P*-1	$P2_1/c$
a, Å	7.9884(8)	7.2233(5)	7.0083(8)	16.9047(12)	8.0697(5)	7.9860(2)
b, Å	9.9682(10)	9.6170(5)	10.263(2)	9.6083(10)	11.0207(6)	39.540(2)
c, Å	10.9136(11)	11.4125(9)	10.3339(12)	23.0491(12)	17.6506(8)	10.2270(5)
α, deg	85.141(2)	87.670(6)	103.012(9)	-	88.248(4)	-
β, deg	76.697(2)	71.700(6)	103.305(9)	90.906(7)	79.767(4)	98.710(3)
γ, deg	75.294(2)	74.751(5)	106.116(10)	-	75.981(6)	-
V, Å^3	817.71(14)	725.43(8)	660.83(15)	3743.3(5)	1498.63(14)	3192.1(2)
Z	2	2	2	8	4	4
T, K	293(2)	293(2)	293(2)	293(2)	293(2)	293(2)
ρ_{calc} (Mg m^{-3})	1.713	1.707	1.743	1.579	1.692	1.672
F(000)	434	382	354	1824	780	1640
λ (Mo-K$_\alpha$, Å)	0.71073	0.71073	0.71073	0.71073	0.71073	0.71070
μ (MoK$_\alpha$, mm^{-1})	1.390	1.542	1.685	1.213	1.493	1.415
Number parameters/restraints	307 / 0	268 / 0	190 / 0	258 / 0	545 / 0	523 / 0
Goodness of fit (*S*)	0.979	0.987	1.096	1.124	1.010	1.088
R1, $I > 2\sigma(I)$ (all)	0.0368 (0.0434)	0.0366 (0.0570)	0.0675 (0.1234)	0.0734 (0.1264)	0.0349 (0.0640)	0.0559 (0.1004)
wR2, $I > 2s(I)$ (all)	0.0820 (0.0843)	0.0775 (0.0869)	0.1078 (0.1234)	0.1560 (0.1760)	0.0712 (0.0799)	0.1220 (0.1378)
Max/min electron density (e/Å^3)	0.876 / -0.467	0.433 / -0.321	0.708 / -0.521	0.809 / -0.312	0.370 / -0.306	0.594 / -0.436
Measured reflections (R_{int})	5444 (0.019)	7984 (0.020)	6133 (0.045)	11976 (0.036)	15613 (0.026)	20415 (0.0260)
Independent reflections [$I > 2\sigma(I)$]	3643 (3059)	3978 (3203)	2933 (1878)	4198 (2644)	6671 (4869)	8016 (5224)

Results and discussion

Description of the structure of [Cu(dpydiol)(mal)(H_2O)]·2H_2O (1)

The structure of **1** consists of [Cu(dpydiol)(mal)(H_2O)] mononuclear units and crystallization water molecules linked together by means of hydrogen bonds to afford a three-dimensional network (see Figure 1 and Table 2).

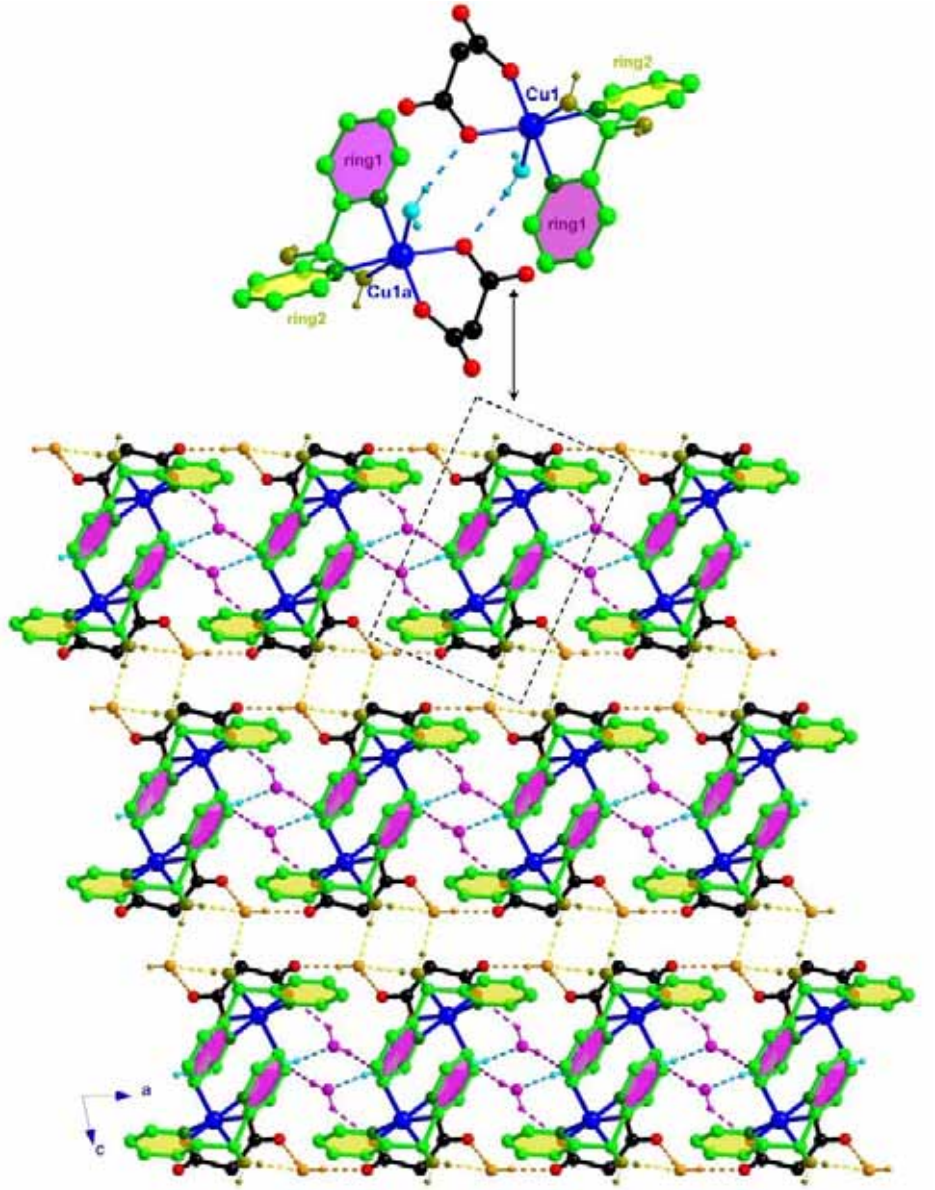

Figure 1. Projection down the *b*-axis showing the three-dimensional hydrogen bonded structure of **1**. Broken lines represent hydrogen bonds and the phenyl rings which participate in the same weak π-π stacking are drawn with the same colour.

Each copper atom is six coordinated CuN_2O_4 (Figure 2), forming a highly distorted 4+1+1 elongated octahedron environment with geometric values $\phi = 53.6^{\circ}$ and

s/h = 1.38 [Stiefel E.I. *et al*, 1972]. Selected bond lengths and angles for **1** are listed in Table 2.

Table 2. Selected bond lengths (Å) and angles (º), hydrogen bonds and weak interactions for **1**[a,b]

Copper environment			
Cu(1)-O(1)	1.955(2)	Cu(1)-N(11)	2.015(2)
Cu(1)-O(2)	1.946(2)	Cu(1)-N(12)	1.994(2)
Cu(1)-O(1w)	2.315(2)	Cu(1)-O(11)	2.593(2)
O(1)-Cu(1)-O(2)	90.20(7)	N(11)-Cu(1)-N(12)	89.63(8)
O(1)-Cu(1)-N(11)	89.92(8)	O(2)-Cu(1)-N(11)	179.06(8)
O(1)-Cu(1)-N(12)	167.15(8)	O(2)-Cu(1)-N(12)	90.46(8)
O(1)-Cu(1)-O(1w)	97.10(7)	N(11)-Cu(1)-O(1w)	90.09(8)
O(2)-Cu(1)-O(1w)	88.97(8)	N(12)-Cu(1)-O(1w)	95.74(8)
O(1)-Cu(1)-O(11)	94.38(7)	N(11)-Cu(1)-O(11)	69.39(7)
O(2)-Cu(1)-O(11)	111.53(6)	N(12)-Cu(1)-O(11)	73.47(7)
O(1w)-Cu(1)-O(11)	156.45(7)		
Hydrogen bonds			
D-H···A	D···A/Å	H···A/Å	D-H···A/º
O(1w)-H(1w1)···O(1a)	2.742(3)	2.00(3)	168(4)
O(1w)-H(2w1)···O(3w)	2.717(3)	2.05(3)	175(4)
O(2w)-H(1w2)···O(4)	2.639(3)	1.83(4)	177(4)
O(2w)-H(2w2)···O(3b)	2.688(3)	1.95(4)	174(4)
O(3w)-H(1w3)···O(2)	2.952(3)	2.30(4)	142(3)
O(3w)-H(2w3)···O(1wc)	2.829(4)	2.05(6)	166(5)
O(3w)-H(1w3)···O(3b)	3.110(3)	2.78(4)	107(3)
O(3w)-H(2w3)···O(3b)	3.110(3)	2.79(4)	107(4)
O(11)-H(21)···O(2wd)	2.628(3)	1.81(3)	177(3)
O(12)-H(22)···O(2we)	2.725(3)	2.08(3)	158(3)
Weak hydrogen bonds			
C(10)-H(10)···O(1a)	3.451(3)	2.58(3)	159(2)
C(10)-H(10)···O(1wa)	3.489(4)	2.85(3)	128(2)
C(12)-H(12)···O(3we)	3.281(3)	2.61(4)	130(2)
C(13)-H(13)···O(2we)	3.525(3)	2.85(2)	134(2)
C(13)-H(13)···O(3we)	3.394(3)	2.90(2)	117(2)
C(17)-H(17)···O(4f)	3.212(3)	2.48(3)	141(2)
C(18)-H(18)···O(2wf)	3.679(4)	2.88(3)	152(2)
C(19)-H(19)···O(1b)	3.521(3)	2.69(3)	145(2)
C(19)-H(19)···O(11b)	3.363(3)	2.61(3)	136(3)
C(20)-H(20)···O(3b)	3.368(3)	2.76(2)	129(2)

[a] Symmetry transformations: (a) –*x*, -*y*+1, -*z*+1; (b) *x*+1, *y*, *z*; (c) -*x*+1, -*y*+1, -*z*+1; (d) –*x*+1, -*y*+1, -*z*; (e) *x*-1, *y*+1, *z*; (f) *x*, *y*+1, *z*. [b] A = acceptor; D = donor.

Two malonate-oxygen and two dpydiol-nitrogen atoms build the equatorial plane around the metal atom [the maximum deviation from the mean equatorial plane

being 0.133(2) Å for N(11)]. The Cu-O bond distances [average value = 1.950 Å] are somewhat shorter that the Cu-N ones [average value = 2.005 Å]. The apical positions are occupied by a water molecule and an oxygen atom from one of the two hydroxil groups of the dpydiol ligand. [the Cu-Ow and Cu-O(hydroxil) bond distances being 2.315(2) and 2.593(2) Å, respectively]. The Cu-O(hydroxil) bond length [2.593(2) Å] is remarkably longer than those reported in the literature for other dpydiol-containing copper(II) compounds (values ranging from 2.323 to 2.477 Å) [Wang S.-L. *et al.*, 1986; Tangoulis V. *et al.*, 1997; Yang G. *et al.*, 1998; Serna, Z. *et al.*, 1999; Parker O.J. *et al.*, 2000; Breneman G.L. *et al.*, 2001; Reinoso S. *et al*, 2003; Steel P.J. *et al.*, 2003; Tong M.-L. *et al.*, 2004]. The metal atom is shifted by 0.1025(3) Å from the mean equatorial plane towards the coordinated water molecule. The values of the angles formed between the Cu-O(1w) and Cu-O(11) vectors with the normal line to the mean equatorial plane are 1.42(6) and 23.92(4)º, respectively (it deserves to be noted here that the ideal values for a regular octahedron are 0º for both angles, so the inclusion of the O(hydroxyl) atom in the metal environment causes a significant distortion of the copper's polyhedron.

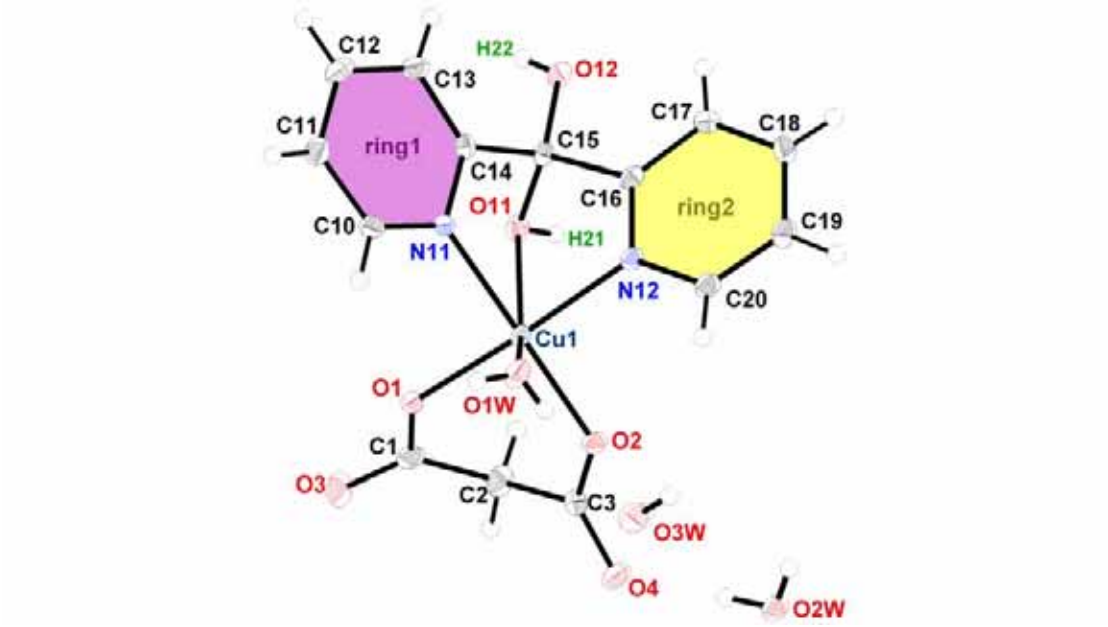

Figure 2. Perspective view of the asymmetric unit in **1** with the numbering scheme. Thermal ellipsoids are drawn at the 50% probability level.

Each malonate group (see Figure 2) act as a bidentate ligand [through O(1) and O(2) towards Cu(1)] and it has a six-membered ring (including the copper atom) that exhibits a boat conformation [Cremer D. *et al.*, 1975] with θ = 93.6(2)º and ϕ = 127.0(2)º. The bond distances and angles of the malonate ligand are listed in Table 3.

Table 3. Bond lengths (Å) and angles (º) for the malonate ligand in **1**

C(1)-C(2)	1.516(4)	C(2)-C(3)	1.519(4)
C(1)-O(1)	1.281(3)	C(3)-O(2)	1.279(3)
C(1)-O(3)	1.230(3)	C(3)-O(4)	1.229(3)
O(1)···O(2)	2.763(2)	O(3)···O(4)	4.317(3)
O(1)-C(1)-O(3)	121.9(2)	O(2)-C(3)-O(4)	123.5(2)
O(1)-C(1)-C(2)	118.1(2)	O(2)-C(3)-C(2)	117.9(2)
O(3)-C(1)-C(2)	120.0(2)	O(4)-C(3)-C(2)	118.5(2)
C(1)-C(2)-C(3)	114.0(2)		
C(1)-O(1)-Cu(1)	123.0(2)	C(3)-O(2)-Cu(1)	123.4(2)
O(1)C(1)O(3)-Cu(1)eq[a]	38.2(2)	O(2)C(3)O(4)-Cu(1)eq[a]	43.0(2)

[a]dihedral angle (º) between the malonate carboxylate group and the mean equatorial plane of the metal.

The bis(2-pyridyl)methanediol group coordinates the copper atom as a tridentate ligand (see Figure 2) as usually observed in the literature of the dpydiol-containing copper(II) complexes [see references cited above]. The angle subtended at the copper(II) atom by the dpydiol ligand is 89.63(8)º. Bond lengths and angles of the dpydiol ligand are listed in Table 4. The weak axial coordination of the O(11) atom to the copper accounts for the lengthening of the C(15)-O(11) bond when compared to the related C(15)-O(12) bond.

Table 4. Bond lengths (Å) and angles (º) for the dpydiol ligand in **1**

N(11)-C(10)	1.344(3)	N(12)-C(20)	1.343(3)
C(10)-C(11)	1.374(3)	C(20)-C(19)	1.365(4)
C(11)-C(12)	1.380(4)	C(19)-C(18)	1.378(4)
C(12)-C(13)	1.389(3)	C(18)-C(17)	1.380(4)
C(13)-C(14)	1.376(3)	C(17)-C(16)	1.380(3)
C(14)-N(11)	1.339(3)	C(16)-N(12)	1.341(3)
C(14)-C(15)	1.530(3)	C(16)-C(15)	1.527(3)
C(15)-O(11)	1.412(3)	C(15)-O(12)	1.384(3)
C(10)-N(11)-C(14)	118.7(2)	C(20)-N(12)-C(16)	118.5(2)
C(11)-C(10)-N(11)	122.3(2)	C(19)-C(20)-N(12)	122.4(2)
C(12)-C(11)-C(10)	118.9(2)	C(18)-C(19)-C(20)	119.1(3)
C(13)-C(12)-C(11)	119.0(2)	C(17)-C(18)-C(19)	119.3(3)
C(14)-C(13)-C(12)	118.9(2)	C(16)-C(17)-C(18)	118.5(2)
N(11)-C(14)-C(13)	122.2(2)	N(12)-C(16)-C(17)	122.2(2)
N(11)-C(14)-C(15)	114.0(2)	N(12)-C(16)-C(15)	114.6(2)
C(13)-C(14)-C(15)	123.6(2)	C(17)-C(16)-C(15)	123.2(2)
C(14)-C(15)-C(16)	111.1(2)	O(11)-C(15)-O(12)	113.3(2)
O(11)-C(15)-C(14)	103.3(2)	O(11)-C(15)-C(16)	109.7(2)
O(12)-C(15)-C(14)	113.1(2)	O(12)-C(15)-C(16)	106.4(2)

C(10)-N(11)-Cu(1)	122.9(2)	C(20)-N(12)-Cu(1)	123.1(2)
C(14)-N(11)-Cu(1)	118.4(2)	C(16)-N(12)-Cu(1)	118.3(2)

The six-membered ring Cu-N(11)-C(14)-C(15)-C(16)-N(12) (see Figure 2) adopts a boat conformation with geometric values ϕ = 121.28(14) and θ = 93.93(13)º [Cremer D. *et al.*, 1975]. The mean plane passing through N(11), C(14), C(16) and N(12) leaves the Cu(1) and C(15) atoms 0.8749(3) and 0.711(2) Å, respectively, above the plane. The geometry around the central C(15) atom is close to tetrahedral, the angles ranging from 103.3(2) [C(14)-C(15)-O(11)] to 113.1(2)º [C(14)-C(15)-O(12)] as previously reported. The pyridyl rings (denoted hereafter as ring1 and ring2, see Figure 2) are planar [the maxium deviations from the mean planes being 0.012(3) and 0.005(3) Å, for ring1 and ring2, respectively]. The dihedral angle between the two pyridyl rings is 53.43(8)º and those formed between the pyridyl rings and the *gem*-diol group [O(11)-C(15)-O(12)] are 66.4(2) (ring1) and 59.3(2)º (ring2). These values are far from that observed for the 2,2'-(dihydroxymethylene)dipyridinium dinitrate [Sommerer S.O. *et al.*, 1994] but agree well with those reported for other metal coordinated dpydiol-containing compounds.

Centrosymmetrically related [Cu(dpydiol)(mal)(H_2O)] units are pairwise connected through hydrogen bonds involving the coordinated water molecule and malonate oxygen atoms [see Figure 1 and 3, the Cu(1)···Cu(1a) separation being 5.3891(6) Å]. These copper(II) dimers are held together by means of hydrogen bonds involving water molecules [O(1w)···O(3w)···O(1w)] and malonate oxygen atoms [O(1w)···O(3w)···O(2) and O(4)···O(2w)···O(3)] leading to a ladder-like chain of copper ions that grows along the *a*-axis [see Figure 3, 7.3153(7) Å for Cu(1)···Cu(1c)].

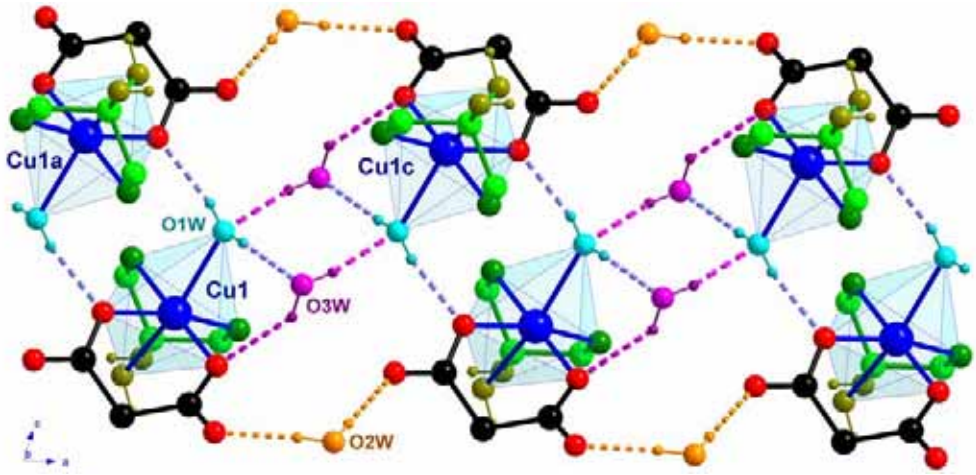

Figure 3. Partial view of the [Cu(dpydiol)(mal)(H_2O)] units connected through hydrogen bonds involving water molecules, giving thus a ladder-like chain that grows along the *a*-axis. The pyridyl rings of the dpydiol ligand were not drawn for clarity.

Looking at this 1D structure, one can distinguish two different H-bonding motifs: a $R_4^4(8)$ pattern involving only water molecules and a $R_5^5(14)$ motif involving carboxylate groups and water molecules. [$X_i^j(k)$: X = R indicates the motif is a ring; i and j is the number of donor and acceptor atoms, respectively, and k is the total number of atoms which forms the motif, including the hydrogen atoms] [Etter M.C., 1990]

These chains are connected each other through hydrogen bonds [see yellow broken lines in Figure 4] involving the *gem*-diol groups of the pyridyl ligands and one non-coordinated water molecule along the [0 1 1] and [0 1 -1] directions, affording a three-dimensional hydrogen bonded network.

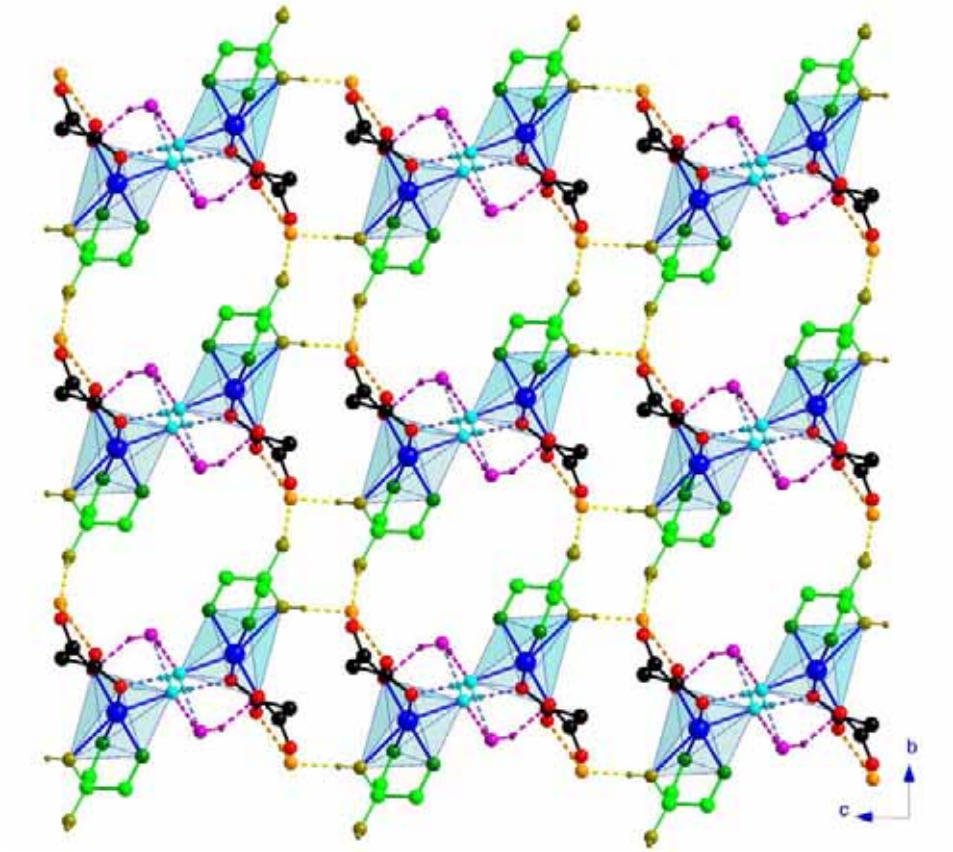

Figure 4. Perspective view, along the *a*-axis of the three-dimensional hydrogen bonded network in **1**. Hydrogen bonds are drawn as broken lines and pyridyl rings were skipped for the sake of clarity.

Looking at Figure 4, one can see that O(3w) (orange coloured in this figure) and the *gem*-diol groups (green and golden coloured atoms) form a $R_4^2(12)$ H-bonding pattern.

Weak intra- and interchain π-π interactions are present in **1**. Concerning the former ones (see ring1 in Figure 1), two pyridyl rings from adjacent dpydiol ligands are stacked in a face-to-face fashion (see yellow rings in Figure 1), the distance between the

mean planes of the pyridyl rings and the separation between the ring centroids being 3.504(2) Å and 3.789(3) Å, respectively. The other pyridyl rings (see purple rings in Figure 1) belonging to adjacent hydrogen bonded chains are stacked in an offset fashion, the distance between pyridyl rings and the separation between ring centroids being 2.753(2) and 5.606(3) Å, respectively.

Finally, weak C(aromatic)-H···O interactions contribute to stabilize the whole three-dimensional network (see Table 2).

Description of the structure of [Cu(dpa)(mal)(H_2O)]·H_2O (2)

The structure of **2** consists of [Cu(mal)(dpa)(H_2O)] mononuclear units and crystallization water molecules which are held together by means of hydrogen bonds and π-π interactions, leading to a three-dimensional structure (see Figure 5).

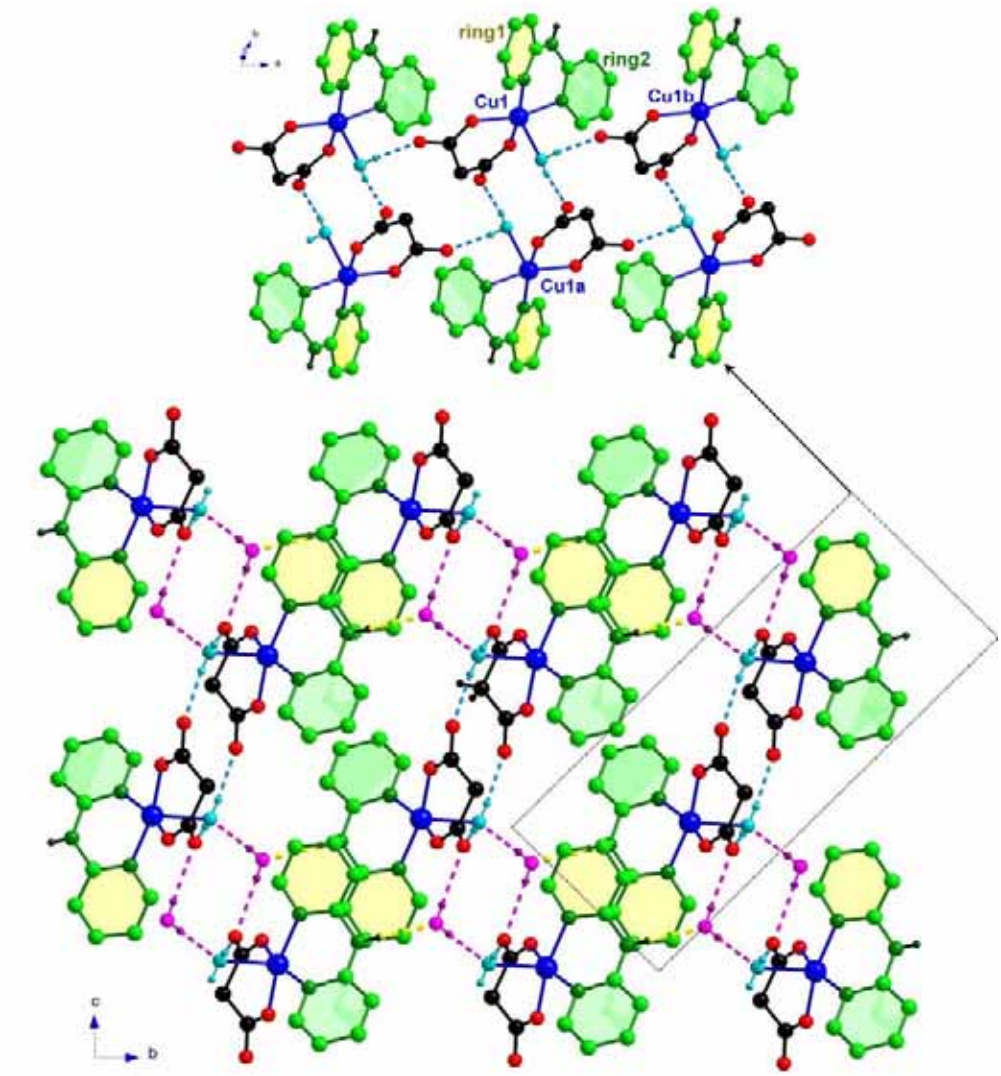

Figure 5. Perspective view along the *a*-axis of the crystal structure in **2**.

Selected bond lengths and angles of **2** with the relevant hydrogen bonds are listed in Table 5.

Each copper atom is five-coordinated and it exhibits a slightly distorted square pyramidal environment (see Figure 6), the geometric τ value being 0.04 [Addison A.W. *et al.*, 1984]. The equatorial plane around the copper atom is built by two malonate-oxygen and two dpa-nitrogen atoms, the maximum deviation from the mean equatorial plane, being 0.022(2) Å for N(11) [the average Cu-O and Cu-N bond lengths are 1.934(2) and 1.993(2) Å, respectively]. A water molecule occupies the apical position [the Cu-Ow bond length is 2.266(2) Å].

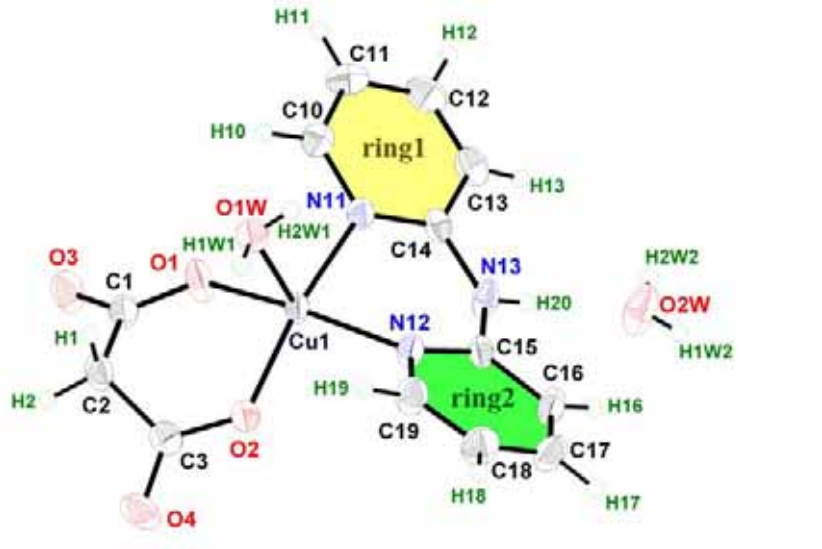

Figure 6. Perspective view of the asymmetric unit in **2** with the atom numbering. Thermal ellipsoids are drawn at the 50% probability level.

The copper atom is shifted by 0.2560(3) Å from the mean equatorial plane towards the apical water molecule. The bond distances and angles around the copper environment are into the range observed in other malonate- and dpa-containing copper(II) complexes [Youngme S. *et al.*, 2003; Du, M. *et al.*, 2003].

Table 5. Selected bond lengths (Å) and angles (º) and weak interactions for **2**[a,b]

Copper environment			
Cu(1)-O(1)	1.932(2)	Cu(1)-N(11)	1.988(2)
Cu(1)-O(2)	1.936(2)	Cu(1)-N(12)	1.998(2)
Cu(1)-O(1w)	2.266(2)		
O(1)-Cu(1)-O(2)	91.71(7)	N(11)-Cu(1)-N(12)	87.99(8)
O(1)-Cu(1)-N(11)	87.52(7)	O(2)-Cu(1)-N(11)	166.18(8)
O(1)-Cu(1)-N(12)	163.62(8)	O(2)-Cu(1)-N(12)	88.91(8)
O(1)-Cu(1)-O(1w)	97.53(8)	N(11)-Cu(1)-O(1w)	99.47(8)
O(2)-Cu(1)-O(1w)	94.31(8)	N(12)-Cu(1)-O(1w)	98.75(7)

Hydrogen bonds			
D-H···A	D···A/Å	H···A/Å	D-H···A/º
O(1w)-H(1w1)···O(4a)	2.705(3)	1.99(3)	170(4)
O(1w)-H(2w1)···O(3b)	2.702(3)	1.97(5)	173(5)
O(2w)-H(1w2)···O(1wc)	2.868(3)	2.14(4)	178(4)
O(2w)-H(2w2)···O(3d)	2.877(4)	2.21(5)	173(5)
N(13)-H(20)···O(2w)	2.835(3)	2.10(3)	178(3)
Weak hydrogen bonds			
C(2)-H(2)···O(4e)	3.589(4)	2.67(4)	175(3)
C(10)-H(10)···O(3f)	3.323(4)	2.58(3)	136(2)
C(13)-H(13)···O(1d)	3.202(3)	2.55(3)	134(3)
C(17)-H(17)···O(2g)	3.226(3)	2.55(4)	131(3)
C(19)-H(19)···O(4a)	3.561(4)	2.65(3)	173(3)

[a] Symmetry transformations: (a) –*x*+1, -*y*+1, -*z*; (b) *x*+1, *y*, *z*; (c) *x*, *y*+1, *z*; (d) –*x*, -*y*+2, -*z*+1; (e) –*x*, -*y*+1, -*z*; (f) –*x*, -*y*+1, -*z*+1; (g) –*x*+1, -*y*+2, -*z*. [b] A = acceptor; D = donor.

Each malonate group (see Figure 6) acts as a bidentate ligand [through O(1) and O(2) towards Cu(1)], the angle subtended at the copper atom being 91.71(7)º. It forms a six-membered ring, including the copper atom, that exhibits a boat conformation [Cremer D. *et al.*, 1975] with θ = 85.6(3) and ϕ = 119.0(3)º. Main malonate bond lengths and angles are listed in Table 6.

Table 6. Bond lengths (Å) and angles (º) for the malonate ligand in **2**

Malonate ligand			
C(1)-C(2)	1.519(3)	C(2)-C(3)	1.517(3)
C(1)-O(1)	1.266(3)	C(3)-O(2)	1.274(3)
C(1)-O(3)	1.242(3)	C(3)-O(4)	1.235(3)
O(1)···O(2)	2.775(2)	O(3)···O(4)	4.469(3)
O(1)-C(1)-O(3)	121.5(2)	O(2)-C(3)-O(4)	122.8(2)
O(1)-C(1)-C(2)	119.3(2)	O(2)-C(3)-C(2)	119.4(2)
O(3)-C(1)-C(2)	119.2(2)	O(4)-C(3)-C(2)	117.8(2)
C(1)-C(2)-C(3)	116.9(2)		
C(1)-O(1)-Cu(1)	128.4(2)	C(3)-O(2)-Cu(1)	127.9(2)
O(1)C(1)O(3)-Cu(1)eq[a]	19.1(2)	O(2)C(3)O(4)-Cu(1)eq[a]	18.9(2)

[a]dihedral angle (º) between the malonate carboxylate group and the mean equatorial plane of the metal atom

The dpa molecule acts as a bidentate ligand [through N(11) and N(12) towards Cu(1)] and it adopts the *trans-trans* conformation [Du M. *et al.*, 2003]. The angle subtended by the dpa at the copper atom is 87.99(8)º. This group has a six-membered

ring (including the copper atom) that exhibits a distorted screw-boat conformation with geometric values θ = 67.3(2) and ϕ = 124.4(3)º [Cremer D. *et al.*, 1975]. The amine-nitrogen atom of the dpa and the methylene-carbon atom of the malonate point to opposite directions. The pyridyl rings of the dpa are planar [maximum deviation from the mean planes being 0.014 and 0.037(3) Å for C(14) and C(15), respectively] as expected, whereas the dpa ligand as a whole deviates significantly from planarity. The dihedral angle between the pyridyl rings is 22.72(9)º, a value that remains into the range observed for other dpa-containing copper(II) complexes (values comprising in the range from 2.135 to 35.80º) [CCDC, The Cambridge Structural Database, ConQuest 5.25, Cambridge, November 2004 (Update February 2005); Allen F.H., 2002]. The bond lengths and angles of the dpa (see Table 7) agree with those reported for other copper(II) complexes with dpa and dicarboxylate as ligands [Karanovic L. *et al.*, 2002; Lu J.Y. *et al.*, 2002; Youngme S. *et al.*, 2003; Yang C.-H. *et al.*, 2003; Du M. *et al.*, 2003].

Table 7. Bond lengths (Å) and angles (º) for the dpa ligand in **2**

dpa ligand			
N(11)-C(10)	1.353(3)	N(12)-C(19)	1.354(3)
C(10)-C(11)	1.362(4)	C(19)-C(18)	1.364(4)
C(11)-C(12)	1.392(4)	C(18)-C(17)	1.392(4)
C(12)-C(13)	1.359(4)	C(17)-C(16)	1.360(4)
C(13)-C(14)	1.397(3)	C(16)-C(15)	1.406(3)
C(14)-N(11)	1.340(3)	C(15)-N(12)	1.342(3)
C(14)-N(13)	1.382(3)	C(15)-N(13)	1.373(3)
C(10)-N(11)-C(14)	118.2(2)	C(19)-N(12)-C(15)	118.3(2)
C(11)-C(10)-N(11)	123.1(3)	C(18)-C(19)-N(12)	123.0(3)
C(12)-C(11)-C(10)	118.4(3)	C(17)-C(18)-C(19)	118.4(3)
C(13)-C(12)-C(11)	119.4(3)	C(16)-C(17)-C(18)	119.6(2)
C(14)-C(13)-C(12)	119.5(3)	C(15)-C(16)-C(17)	119.2(2)
N(11)-C(14)-C(13)	121.4(2)	N(12)-C(15)-C(16)	121.1(2)
N(11)-C(14)-N(13)	120.2(2)	N(12)-C(15)-N(13)	120.0(2)
C(13)-C(14)-N(13)	118.4(2)	C(16)-C(15)-N(13)	118.9(2)
C(14)-N(13)-C(15)	128.8(2)		
C(10)-N(11)-Cu(1)	118.2(2)	C(19)-N(12)-Cu(1)	118.7(2)
C(14)-N(11)-Cu(1)	122.3(2)	C(15)-N(12)-Cu(1)	121.4(2)

The [Cu(dpa)(mal)(H_2O)] mononuclear units are connected each other by means of hydrogen bonds involving the coordinated water molecules and the outer malonate oxygen atoms [O(1w)···O(4a) and O(1w)···O(3b), see Table 5] leading to a ladder-like

copper(II) chain that runs parallel along the *a*-axis (see blue broken lines in Figure 5 and 7). The values of the intrachain distances are 6.8874(7) and 7.2233(7), respectively. These chains are further linked through hydrogen bonds involving the crystallization water molecules [O(2w)···O(1wc) and O(2w)···O(3d)] giving rise to a two-dimensional network that grows in the *ab*-plane (see Figure 7). Looking at this network, one can distinguish two cyclic motifs [Etter M.C., 1990]: a $R_6^4(12)$ (formed from two water molecules and one malonate-oxygen atom by an inversion centre) and a $R_4^4(16)$ (formed from two water molecules and two malonate groups centrosymmetrically related). The $R_6^4(12)$ ring exhibits a chair conformation (θ = 0º) [Cremer D. *et al.*, 1975].

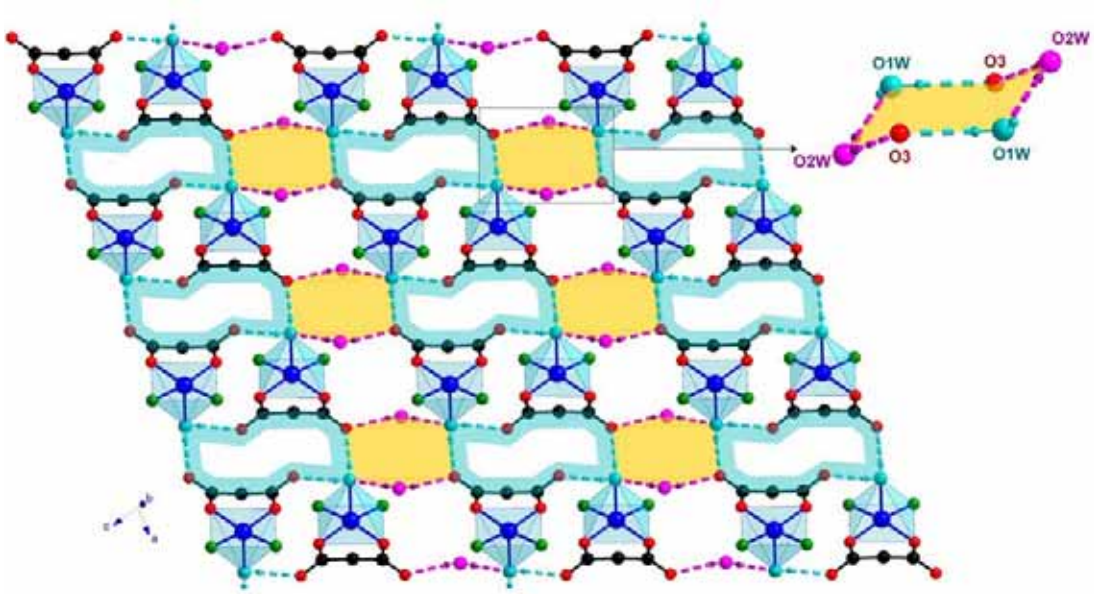

Figure 7. Perspective view of a fragment of the hydrogen bonded two-dimensional network, in **2**, that grows in the *ac*-plane. Hydrogen bonds are drawn as broken lines and the pyridyl rings of the dpa were omitted for clarity.

The hydrogen bonded layers are held together by means of N-H···O (yellow broken lines in Figure 8) and π-π interactions affording a three-dimesional structure. The pyridyl rings of the dpa ligands are stacked in an offset fashion, the separation between ring centroids and pyridyl rings being: 3.709(3) and 3.407(2) Å [between yellow rings] and 3.741(3) and 3.569(2) Å [between green rings] (see Figure 8). Additional weak hydrogen bonds (C-H···O) stabilize the whole three-dimensional structure (see Table 5).

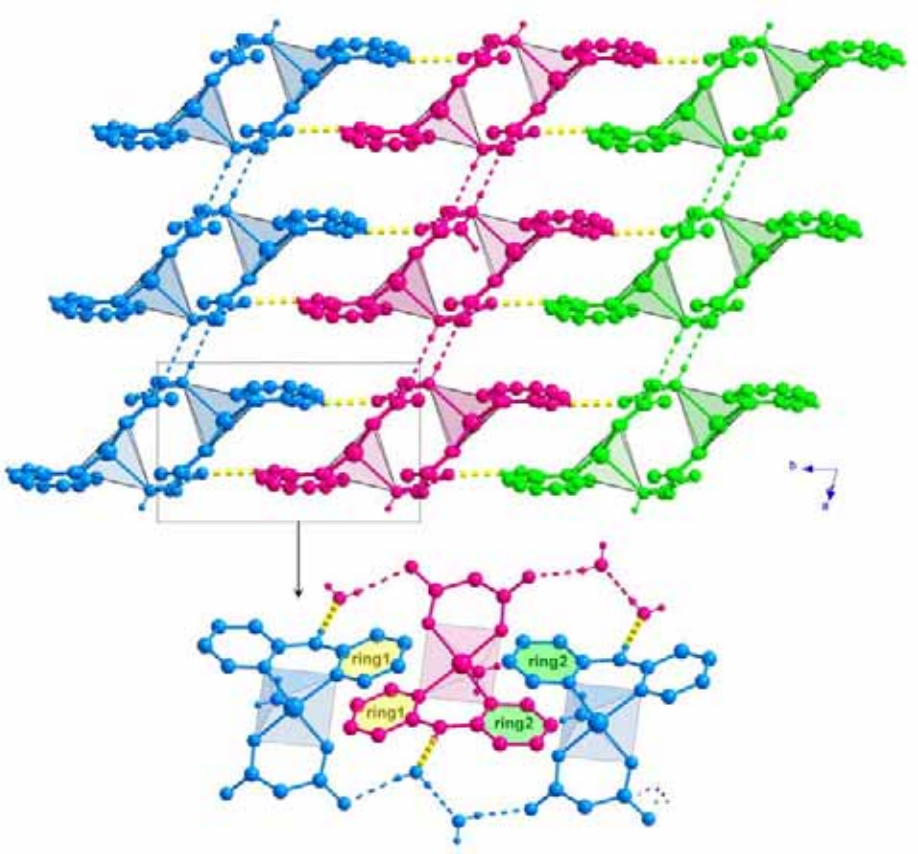

Figure 8. Perspective view along the [10-1] direction of the crystal packing of **2** with a fragment of the structure showing the π-π stacking. Each malonate copper(II) hydrogen bonded layer is coloured for clarity. The interlayer N-H···O hydrogen bonds are represented by yellow broken lines.

Description of the structure of $[Cu(pyim)(mal)(H_2O)]\cdot H_2O$ (3)

The structure of **3** consits of a three-dimensional network made up of $[Cu(pym)(mal)(H_2O)]$ mononuclear units and crystallization water molecules which are connected together by means of hydrogen bonds (Figure 9). Selected bond lengths and angles in **3** together with the relevant hydrogen bonds are listed in Table 8.

Each copper atom is five-coordinated and it exhibits a slightly distorted elongated square pyramidal environment (Figure 10), the geometric τ value being 0.06 [Addison A.W. *et al.*, 1984]. Two malonate oxygens and two pyim-nitrogen atoms, from bidentate malonate and pyim ligands, build the equatorial plane around the metal atom [the maximum deviation from the mean equatorial plane being 0.033(5) Å for N(11)]. The mean value of the equatorial Cu-O and Cu-N bond lengths are 1.928(3) and 1.997(4) Å, respectively. The apical position is filled by a water molecule, the axial Cu-O bond length [2.443(4) Å for Cu(1)-O(1w)] being significantly longer that the

equatorial ones. The copper atom is shifted by 0.1512(9) Å from the mean equatorial plane towards the apical water molecule.

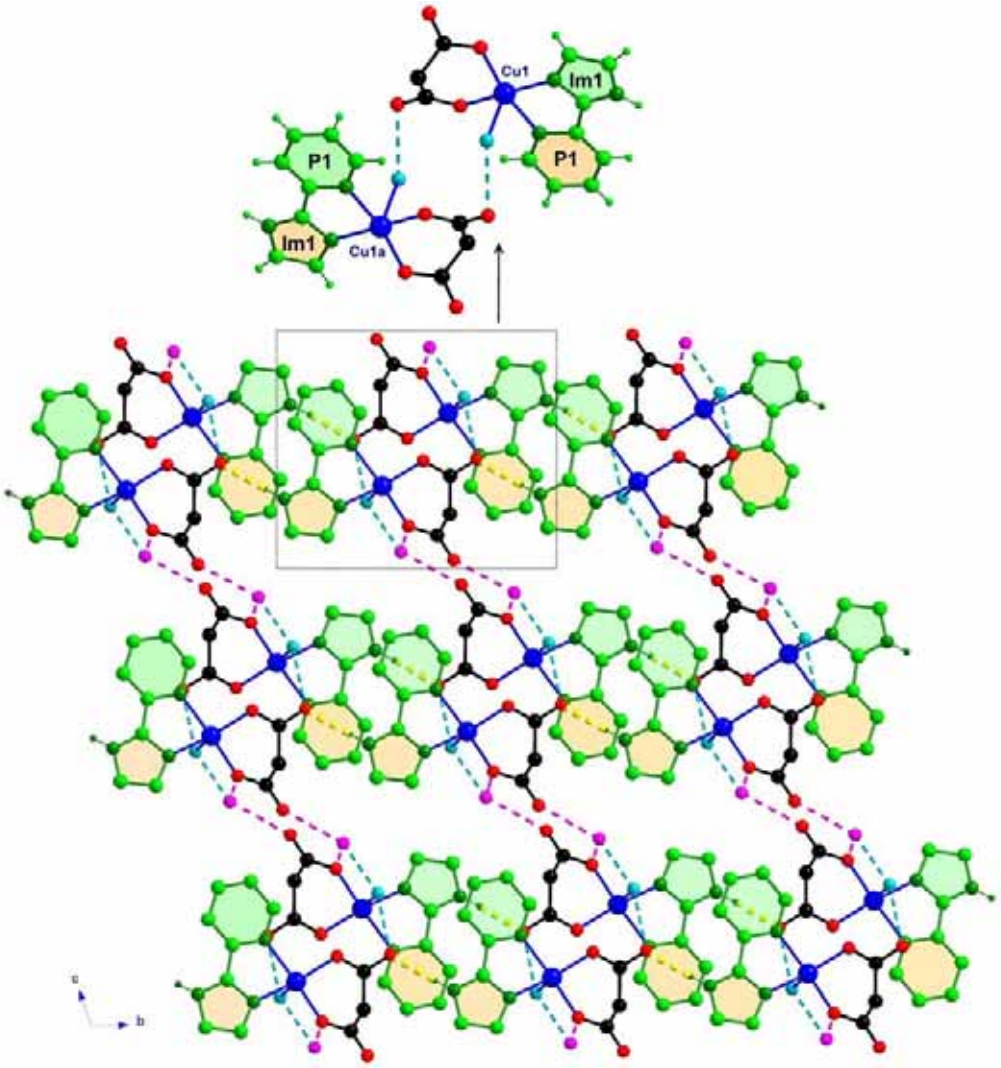

Figure 9. Perspective view along the *a*-axis of the crystal structure of **3**. The hydrogen bonds are represented by broken lines. The pyridyl rings participating in the same weak π-π interactions are drawn with the same colour.

Table 8. Selected bond lengths (Å) and angles (º) and hydrogen bonds for **3**[a,b]

Copper environment			
Cu(1)-O(1)	1.916(3)	Cu(1)-N(11)	1.972(4)
Cu(1)-O(2)	1.940(3)	Cu(1)-N(12)	2.021(4)
Cu(1)-O(1w)	2.443(4)		
O(1)-Cu(1)-O(2)	93.31(14)	N(11)-Cu(1)-N(12)	81.4 (2)
O(1)-Cu(1)-N(11)	90.7(2)	O(2)-Cu(1)-N(11)	171.3 (2)
O(1)-Cu(1)-N(12)	167.47(15)	O(2)-Cu(1)-N(12)	93.30(15)
O(1)-Cu(1)-O(1w)	100.6(2)	N(11)-Cu(1)-O(1w)	93.4(2)
O(2)-Cu(1)-O(1w)	93.5(2)	N(12)-Cu(1)-O(1w)	89.6(2)

Hydrogen bonds			
D-H···A	D···A/Å	D-H···A	D···A/Å
O(1w)-H···O(4a)	2.847(6)	O(2w)-H···O(1b)	2.845(7)
O(1w)-H···O(2w)	2.824(6)	O(2w)-H···O(3c)	2.769(7)
D-H···A	D···A/Å	H···A/Å	D-H···A/º
N(13)-H(13)···O(4d)	2.809(7)	1.951(4)	176.1(3)
C(2)-H(2)···O(2wd)	3.573(6)	2.631(3)	163.9(4)
C(14)-H(14)···O(4d)	3.456(7)	2.585(4)	155.9(4)
C(14)-H(14)···O(1we)	3.441(8)	2.705(4)	136.7(4)
C(16)-H(16)···O(3f)	3.329(8)	2.408(4)	170.1(4)

[a] Symmetry transformations: (a) –*x*+1, -*y*+1, -*z*+1; (b) *x*+1, *y*, *z*; (c) –*x*+1, -*y*+1, -*z*+2; (d) *x*, *y*+1, *z*; (e) –*x*+1, -*y*+2, -*z*+1; (f) *x*, *y*, *z*-1. [b] A = acceptor; D = donor.

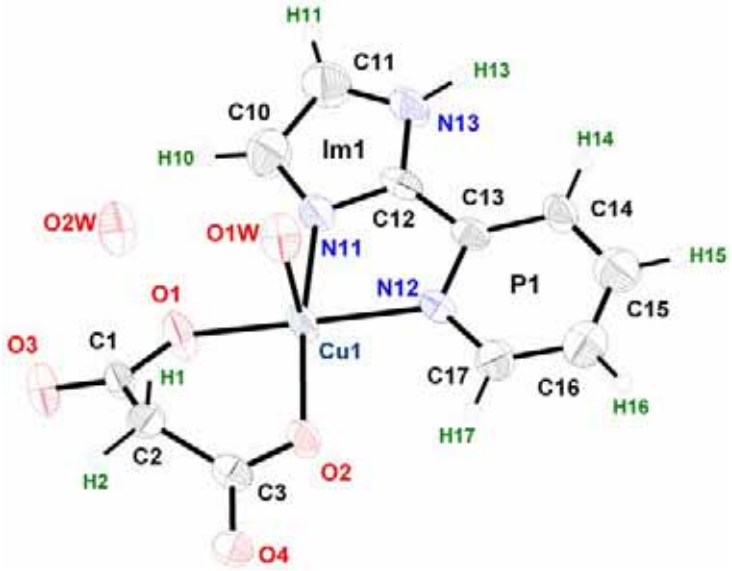

Figure 10. Perspective view of the asymmetric unit in **3** with the numbering scheme. Thermal ellipsoids are drawn at the 50% probability level.

Each malonate group (Figure 10) acts as a bidentate ligand [through O(1) and O(2) towards Cu(1)], the angle subtended at the metal atom being 93.31(14)º. It forms a six-membered ring (including the copper atom) that exhibits a boat conformation with geometric values θ = 91.4(5) and ϕ = 121.0(5)º [Cremer D. *et al.*, 1975]. The bond lengths and angles of the malonate ligand with other interesting geometric values are reported in Table 9.

Table 9. Bond lengths (Å) and angles (º) for the malonate ligand in **3**

Malonate ligand			
C(1)-C(2)	1.503(7)	C(2)-C(3)	1.490(7)
C(1)-O(1)	1.282(5)	C(3)-O(2)	1.274(5)

C(1)-O(3)	1.216(6)	C(3)-O(4)	1.252(5)
O(1)···O(2)	2.804(6)	O(3)···O(4)	4.349(6)
O(1)-C(1)-O(3)	122.4(5)	O(2)-C(3)-O(4)	121.5(5)
O(1)-C(1)-C(2)	117.2(5)	O(2)-C(3)-C(2)	119.3(4)
O(3)-C(1)-C(2)	120.4(4)	O(4)-C(3)-C(2)	119.1(4)
C(1)-C(2)-C(3)	117.2(4)		
C(1)-O(1)-Cu(1)	124.3(3)	C(3)-O(2)-Cu(1)	122.2(3)
O(1)C(1)O(3)-Cu(1)eq[a]	28.4(4)	O(2)C(3)O(4)-Cu(1)eq[a]	26.3(6)

[a]dihedral angle (º) between the malonate carboxylate group and the mean equatorial plane of the metal atom

The angle subtended at the copper atom by the bidentate pyim ligand is 81.4(2)º. The pyim ligand as a whole does not deviate significantly from the planarity, the dihedral angle between the imidazole and pyridyl rings being 1.0(3)º. The value of the inter-ring C(12)-C(13) bond length [1.444(7) Å] as well as the geometric parameters of the imidazole and pyridyl fragments of the pyim ligand (see Table 10) agree with those reported for this ligand in the complexes $[Cu(pyim)(C_2O_4)(H_2O)]\cdot 2H_2O$, $[Cu(pyim)(C_4O_4)(H_2O)_2]\cdot 2H_2O$, $[Cu(pyim)(H_2O)(dca)]_n$ (dca = dicyanamide anion) [Carranza J. *et al.*, 2003] and $[Cu(pyim)_2Br]ClO_4$ [Morsali A. *et al.*, 2003].

Table 10. Bond lengths (Å) and angles (º) for the pyim ligand in **3**

pyim ligand			
N(11)-C(10)	1.350(7)	N(12)-C(17)	1.339(7)
C(10)-C(11)	1.413(8)	C(17)-C(16)	1.354(8)
C(11)-N(13)	1.354(7)	C(16)-C(15)	1.351(8)
N(13)-C(12)	1.342(6)	C(15)-C(14)	1.384(8)
C(12)-N(11)	1.335(6)	C(14)-C(13)	1.362(7)
C(12)-C(13)	1.444(7)	C(13)-N(12)	1.343(6)
C(10)-N(11)-C(12)	105.5(4)	C(17)-N(12)-C(13)	118.0(4)
C(11)-C(10)-N(11)	109.6(6)	C(16)-C(17)-N(12)	124.0(5)
N(13)-C(11)-C(10)	105.0(5)	C(15)-C(16)-C(17)	117.1(6)
C(12)-N(13)-C(11)	108.1(4)	C(14)-C(15)-C(16)	121.1(6)
N(11)-C(12)-N(13)	111.8(5)	C(13)-C(14)-C(15)	118.3(5)
N(11)-C(12)-C(13)	119.1(4)	N(12)-C(13)-C(14)	121.5(5)
N(13)-C(12)-C(13)	129.1(5)	N(12)-C(13)-C(12)	112.3(4)
C(14)-C(13)-C(12)	126.2(5)		
C(10)-N(11)-Cu(1)	141.8(4)	C(17)-N(12)-Cu(1)	127.5(3)
C(12)-N(11)-Cu(1)	112.7(3)	C(13)-N(12)-Cu(1)	114.5(3)

Centrosymmetrically related [Cu(pyim)(mal)(H_2O)] units are pairwise connected through O(1w)-H···O(4) hydrogen bonds (see blue broken lines in Figure 9, and Table 8), the copper···copper separation being 6.3550(14) Å. These copper(II) dimers are further linked through O(1w)-H···O(2w) and O(2w)-H···O(malonate) hydrogen bonds leading to a two-dimensional network that grows in the *ac*-plane (Figure 11). Within the 2D-network, one can distinguish $R_4^4(12)$ hydrogen-bonding motifs [Etter M.C., 1990] formed from one water molecule and one malonate carboxylate group by an inversion centre.

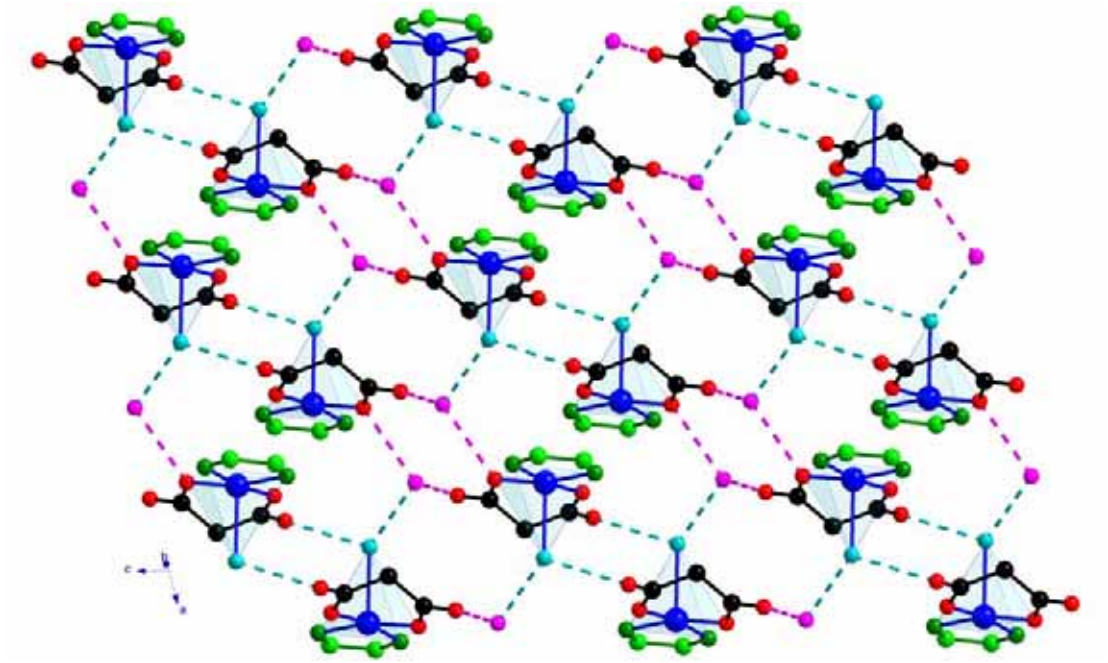

Figure 11. Perspective view of the [Cu(pyim)(mal)(H_2O)] units and crystallization water molecules, in **3,** which are connected through hydrogen bonds (broken lines) affording a 2D-network.

These layers are further connected through N(pyim)-H···O(mal) hydrogen bonds (see yellow broken lines in Figure 12) affording a three-dimensional structure. The imidazole and pyridyl rings from adjacent layers alternatively stack in an offset fashion (Figure 12). The separation between the ring centroids and the mean planes are 3.366(5) [C(P1)···Im1e], 3.113(5) [C(P1)···Im1g], 3.325(5) [C(Im1)···P1e] and 3.130(5) Å [C(Im1)···P1g] and the ring centroids distances are 4.190(7) [C(Im1e)···C(P1)], 4.628(7) [C(P1)···C(Im1g)], 4.190(7) [C(P1e)···C(Im1)] and 4.621(7) Å [Ce(Im1)···Ce(P1g)].

Additional weak C-H···O hydrogen bonds (see Table 8) contribute to stabilize the whole structure.

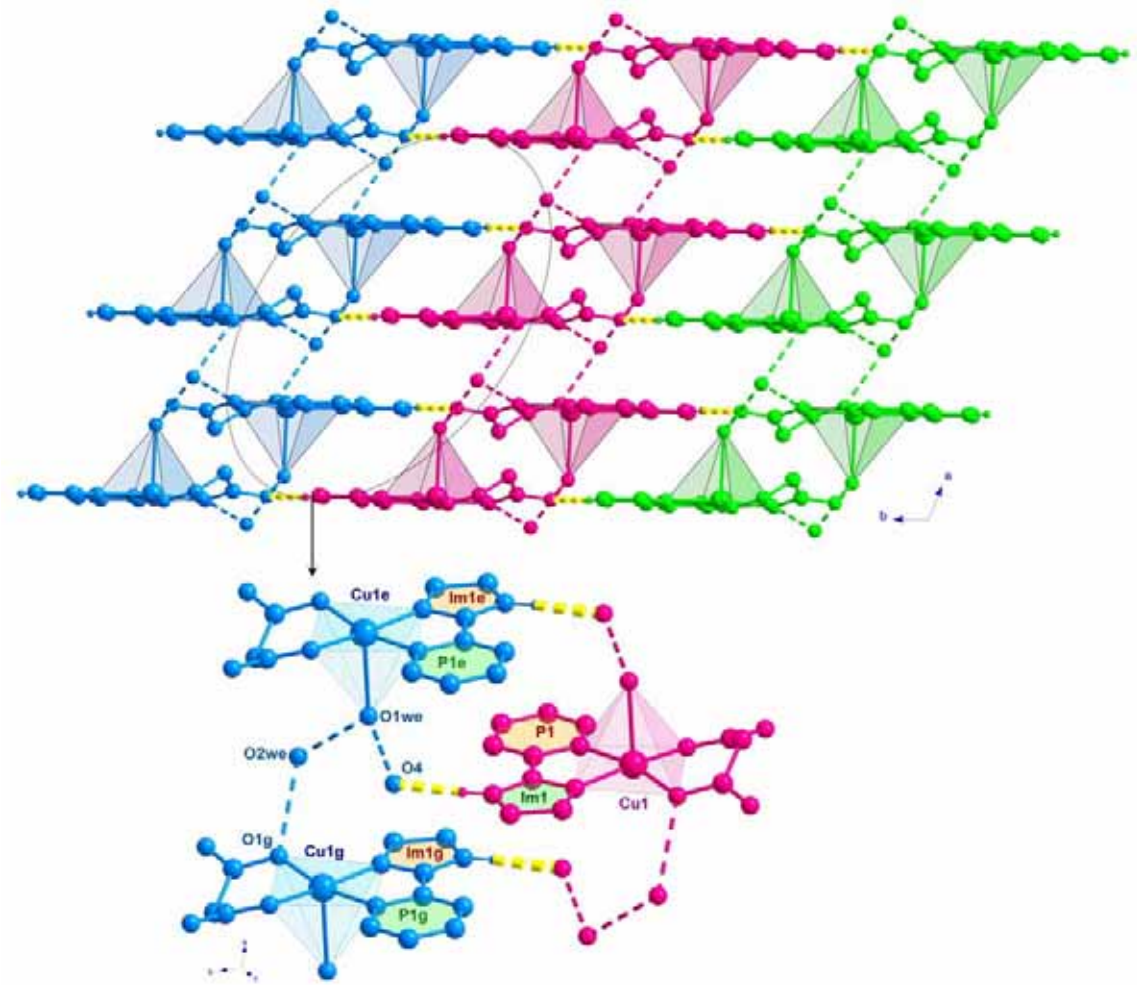

Figure 12. Perspective view along the *c*-axis of the crystal packing in **3** (top) with a fragment of the structure showing N-H···O (yellow broken lines) and weak π-π interactions (bottom).

Description of the structure of $[Cu(dpp)(mal)(H_2O)]\cdot 3/2H_2O$ (4)

The structure of **4** consists of $[Cu(dpp)(mal)(H_2O)]$ mononuclear units and crystallization water molecules held together by means of hydrogen bonds affording a three-dimensional structure. Additional hydrophobic interactions between the aromatic rings of the dpp molecule and the aliphatic chains of the malonate ligand contribute to the stabilization of the structure (Figure 13).

Selected bond lengths and angles with relevant hydrogen bonds in **4** are listed in Table 11.

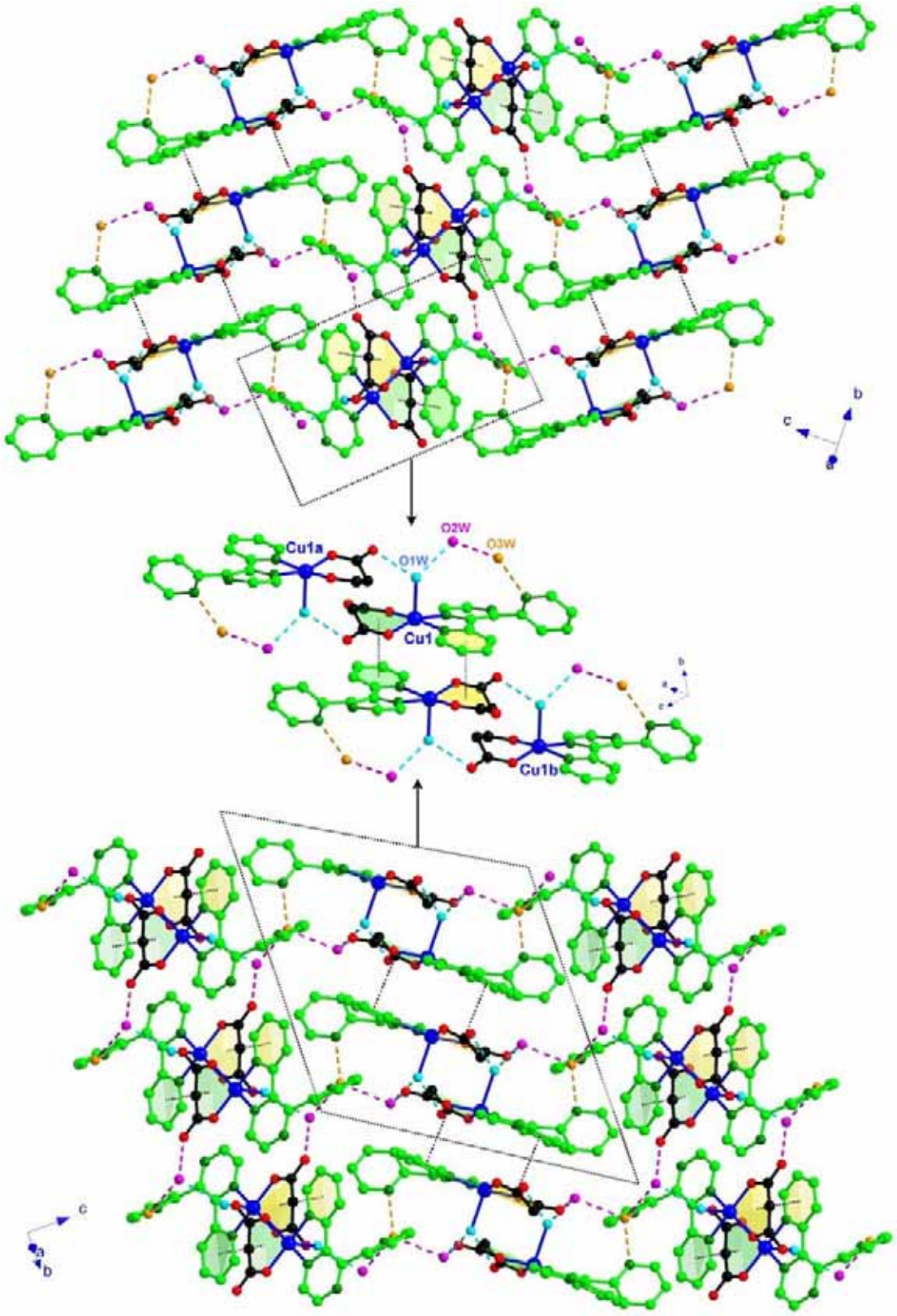

Figure 13. Perspective view along the [½ ½ 0] (top) and [½ -½ 0] (bottom) directions of the crystal packing in **4** with a view of a fragment of the structure (middle) showing some hydrogen bonds (drawn as broken lines) and the hydrophobic interactions (represented as dotted lines). Symmetry code: (a) -*x*+1/2, -*y*+1/2, -*z*+1; (b) -*x*, -*y*, -*z*+1.

Table 11. Bonds lengths (Å) and angles (º) and hydrogen bonds for **4**[a,b]

Copper environment			
Cu(1)-O(1)	1.910(4)	Cu(1)-N(11)	2.007(4)
Cu(1)-O(2)	1.925(4)	Cu(1)-N(12)	1.990(4)
Cu(1)-O(1w)	2.239(4)		
O(1)-Cu(1)-O(2)	93.1(2)	N(11)-Cu(1)-N(12)	79.7(2)
O(1)-Cu(1)-N(11)	92.5(2)	O(2)-Cu(1)-N(11)	160.0(2)
O(1)-Cu(1)-N(12)	168.1(2)	O(2)-Cu(1)-N(12)	91.4(2)
O(1)-Cu(1)-O(1w)	99.5(2)	N(11)-Cu(1)-O(1w)	99.2(2)
O(2)-Cu(1)-O(1w)	98.8(2)	N(12)-Cu(1)-O(1w)	90.7(2)
Hydrogen bonds			
D-H···A	D···A/Å	D-H···A	D···A/Å
O(1w)-H···O(4a)	2.742(6)	O(2w)-H···O(3w)	2.775(7)
O(1w)-H···O(2w)	2.665(7)	O(3w)-H···N(14)	2.850(7)
O(2w)-H···O(3c)	2.667(7)	O(3w)-H···N(14d)	2.850(7)
D-H···A	D···A/Å	H···A/Å	D-H···A/º
C(2)-H(1)···O(4a)	3.562(8)	2.611(4)	166.5(4)
C(11)-H(11)···O(4e)	3.338(8)	2.468(4)	155.8(4)

[a] Symmetry transformations: (a) -*x*+1/2, -*y*+1/2, -*z*+1; (c) -*x*, -*y*+1, -*z*+1; (d)-*x*, *y*, -*z*+1/2; (e) *x*-1/2, *y*+1/2, *z*. [b] A = acceptor; D = donor.

The copper(II) atom is five-coordinated and it exhibits a distorted square pyramidal environment (Figure 14) with a τ value of 0.135 [Addison A.W. *et al.*, 1984].

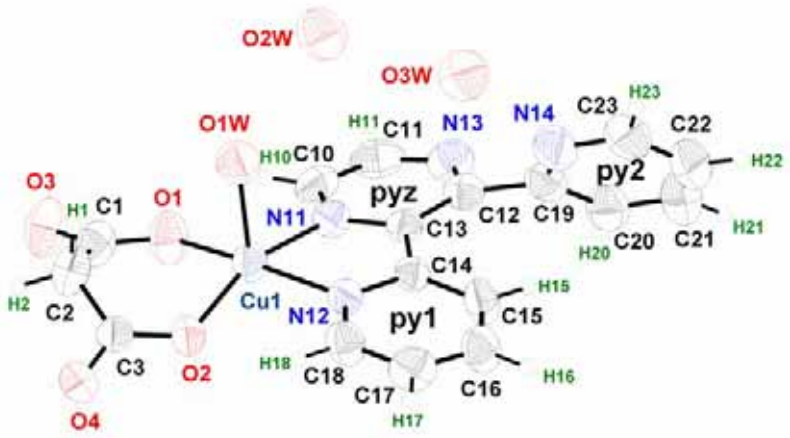

Figure 14. View of the asymmetric unit in **4** with the numbering scheme. Thermal ellipsoids are drawn at the 50% probability level.

Each copper atom is bonded to two dpp-nitrogen atoms [1.999(4) Å for the mean Cu-N bond length] and two malonate oxygen atoms [1.918(4) Å for the mean Cu-O bond length] in the basal plane and to a water molecule in the apical position [2.239(4) Å for Cu(1)-O(1w)]. The basal atoms do not deviate significantly from planarity, the maximum deviation from the mean basal plane being 0.081(4) Å for N(11). The

copper(II) atom is shifted by 0.2471(7) Å from the mean basal plane towards the apical water molecule.

The malonate group acts as bidentate ligand [through O(1) and O(2) towards Cu(1)] with a bite angle of 93.1(2)º (see Figure 14). It forms a six-membered ring (including the copper atom) that exhibits a boat conformation with geometric values θ = 93.0(6) and ϕ = 114(13)º [Cremer D. *et al.*, 1975]. The bond lengths and angles of the malonate ligand are reported in Table 12.

Table 12. Bond lengths (Å) and angles (º) for the malonate present in **4**

C(1)-C(2)	1.484(9)	C(2)-C(3)	1.489(8)
C(1)-O(1)	1.294(7)	C(3)-O(2)	1.271(6)
C(1)-O(3)	1.220(7)	C(3)-O(4)	1.232(6)
O(1)···O(2)	2.785(6)	O(3)···O(4)	4.420(7)
O(1)-C(1)-O(3)	122.4(6)	O(2)-C(3)-O(4)	122.1(5)
O(1)-C(1)-C(2)	119.6(5)	O(2)-C(3)-C(2)	119.3(5)
O(3)-C(1)-C(2)	118.0(6)	O(4)-C(3)-C(2)	118.5(5)
C(1)-C(2)-C(3)	119.1(5)		
C(1)-O(1)-Cu(1)	124.4(4)	C(3)-O(2)-Cu(1)	125.2(4)
O(1)C(1)O(3)-Cu(1)eq[a]	18.22(6)	O(2)C(3)O(4)-Cu(1)eq[a]	22.1(5)

[a]dihedral angle (º) between the malonate carboxylate group and the mean equatorial plane of the metal atom

The dpp ligand adopts a bidentate coordination mode (Figure 14) [through N(11) and N(12) towards Cu(1)], the angle subtended at the copper atom being 79.7(2)º. Hereafter we will refer to the pyrazine and the coordinated and uncoordinated pyridyl rings as pyz, py1 and py2, respectively (see Figure 14). The three aromatic rings of the dpp ligand are quite planar, the maximum deviation from the mean plane being 0.042(5) [C(12)], 0.015(6) [C(17)] and 0.037(8) Å [C(23)] in the pyz, py1 and py2 rings, respectively. The ligand as a whole strongly deviates from planarity. The dihedral angle between the mean planes of py1 and pyz rings is 12.61(14)º. The py2 ring is rotated by 54.9(2)º and 64.3º with respect to pyz and py1 rings, respectively. The bond lengths and angles of the dpp (see Table 13) are in agreement with those observed in the free dpp [Huang N.-T. *et al.*, 1991; Robertson K.N. *et al.*, 1998] and in the dpp-containing copper(II) complexes of formula: $[Cu(dpp)(H_2O)_2]_n(ClO_4)_{2n}\cdot 2nH_2O$ [Morgan L.W. *et al.*, 1992], $[Cu_2(dpp)(sq)_2(H_2O)_6]$ (sq = $C_4O_4^{2-}$ dianion of the squaric acid), $[Cu_2(dpp)(cr)_2(H_2O)_3]\cdot 2H_2O$ (cr = $C_5O_5^{2-}$ dianion of the croconic acid) [Sletten J. *et al.*, 1998], $[Cu(dpp)(H_2O)]n(NO_3)_{2n}\cdot 2n/3H_2O$, $[Cu(dpp)(H_2O)_2]_n(CF_3SO_3)_{2n}$, $[Cu(dpp)(H_2O)_2]_n$

$(A)_{2n}\cdot 2H_2O$ (A = BF_4^-, ClO_4^-) [Grove H. *et al.*, 2000], $[Cu(dpp)(N_3)_2]_n$, $[Cu(dpp)(NCO)_2]_n$, $[Cu(dpp)(NCS)_2]_2$, $[Cu(H_2O)(dpp)(NCS)_2]_2\cdot 2H_2O$ [Grove H. *et al.*, 2001a], $[Cu_2(dpp)(H_2O)(dmso)Cl_4]\cdot dmso$ (dmso = dimethyl sulfoxide), $[Cu_2(dpp)Cl_4]_n$ [Grove H. *et al.*, 2001b], $[Cu_2(dpp)(hfac)_4]$ (hfac = 1,1,1,5,5,5-hexafluoropentane-2,4-dionate) [Ishida T. *et al.*, 2002], $[Cu(dpp)(H_2O)(ox)]\cdot H_2O$ and $[Cu_2(dpp)_2(H_2O)_2(NO_3)_2(ox)]\cdot 4H_2O$ (ox = oxalate) [Carranza J. *et al.*, 2004].

Table 13. Bond lengths (Å) and angles (º) for the dpp ligand in **4**

C(10)-C(11)	1.373(9)	C(18)-C(17)	1.368(8)
C(11)-N(13)	1.342(8)	C(17)-C(16)	1.351(8)
N(13)-C(12)	1.334(7)	C(16)-C(15)	1.361(8)
C(12)-C(13)	1.395(7)	C(15)-C(14)	1.395(7)
C(13)-N(11)	1.349(6)	C(14)-N(12)	1.342(6)
N(11)-C(10)	1.331(7)	N(12)-C(18)	1.339(7)
C(12)-C(19)	1.519(8)	C(13)-C(14)	1.477(7)
C(19)-C(20)	1.395(9)	C(20)-C(21)	1.383(10)
C(21)-C(22)	1.350(11)	C(22)-C(23)	1.373(10)
C(23)-N(14)	1.326(8)	N(14)-C(19)	1.363(8)
C(10)-N(11)-C(13)	119.5(5)	C(18)-N(12)-C(14)	118.9(4)
C(11)-C(10)-N(11)	119.5(6)	C(17)-C(18)-N(12)	122.2(5)
N(13)-C(11)-C(10)	122.3(6)	C(16)-C(17)-C(18)	119.7(6)
C(12)-N(13)-C(11)	117.8(5)	C(15)-C(16)-C(17)	118.8(6)
C(13)-C(12)-N(13)	120.6(5)	C(14)-C(15)-C(16)	120.4(5)
N(11)-C(13)-C(12)	119.7(5)	N(12)-C(14)-C(15)	119.8(5)
N(11)-C(13)-C(14)	113.6(4)	N(12)-C(14)-C(13)	113.8(4)
C(12)-C(13)-C(14)	126.6(5)	C(15)-C(14)-C(13)	126.2(5)
N(13)-C(12)-C(19)	115.1(5)	C(13)-C(12)-C(19)	124.2(5)
C(12)-C(19)-N(14)	117.2(5)	C(12)-C(19)-C(20)	119.2(6)
C(19)-N(14)-C(23)	115.8(6)	C(20)-C(19)-N(14)	123.6(6)
C(21)-C(20)-C(19)	117.1(7)	C(22)-C(21)-C(20)	119.7(8)
C(23)-C(22)-C(21)	119.5(7)	N(14)-C(23)-C(22)	123.9(7)
C(10)-N(11)-Cu(1)	124.8(4)	C(18)-N(12)-Cu(1)	124.3(4)
C(13)-N(11)-Cu(1)	115.7(3)	C(14)-N(12)-Cu(1)	116.6(3)

The $[Cu(dpp)(mal)(H_2O)]$ units are stabilized by hydrogen bonds involving water molecules and pyridyl nitrogen atoms (see broken lines in Figure 13, middle). Symmetrically related (through a two-fold axis) copper(II) units are pairwise connected through hydrogen bonds involving the coordinated water molecules and malonate oxygen atoms [O(1w)···O(4a), see pale blue broken lines in Figures 13 and 15; the Cu(1)···Cu(1a) separation being 7.0576(11) Å]. These units are further connected through hydrogen bonds (Figure 15) involving O(1w) -the coordinated water molecule-, O(2w) -one of the solvent molecules- and O(3) -one of the outer malonate oxygen

atoms- affording double copper(II) chains that grow along the [½ ½ 0] and [½ -½ 0] directions (as shown in Figure 13 top and bottom). These chains are further held together by means of hydrogen bonds. Each [Cu(dpp)(mal)(H_2O)] mononuclear unit that belongs to one chain that grows along a given direction {[½ ½ 0] or [½ -½ 0]}, is connected through O-H···O and O-H···N hydrogen bonds [involving O(3w), see orange broken line in Figure 13] to other two units that belong to two adjacent copper(II) chains which grow along the perpendicular direction {[½, -½, 0] or [½, ½, 0], respectively} leading to a three-dimensional hydrogen bonded network.

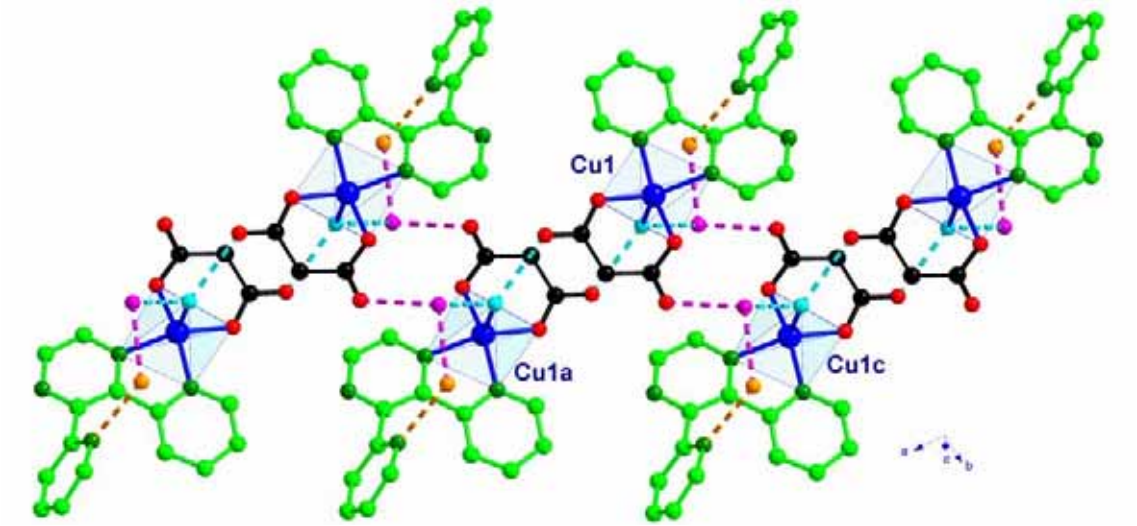

Figure 15. Perspective view of the [Cu(dpp)(mal)(H_2O)] units linked through hydrogen bonds (broken lines) involving O(1w) (pale blue), O(2w) (purple) and O(3w) (red).

Centrosymmetrically related [Cu(dpp)(mal)(H_2O)] units are additionally connected through hydrophobic interactions [see black dotted line in Figure 13] between the py1-dpp and the aliphatic chain of the malonate ligand [Cu(1)O(1)C(1)C(2)C(3)O(2)], stabilizing the whole structure and contributing to the crystal packing. The separation between the ring centroids and the dihedral angle between the normal vector to the mean pyridyl ring and the malonate aliphatic chain centroid are 3.540(4) Å and 14.05(13)º, respectively. These geometric values are within the range observed for the malonate-containing copper(II) complex of formula [Cu(mal)(phen)(H_2O)]·3/2H_2O where hydrophobic interactions were reported [Borghi E., 1987]. The copper···copper distance through this weak interaction is 4.0794(10) Å. Additional weak C-H···O hydrogen bonds contribute to stabilize the whole structure (see Table 11).

Description of the structure of [Cu(phen)(mal)(H_2O)]·H_2O (5)

The structure of **5** consists of [Cu(phen)(mal)(H_2O)] mononuclear units and water molecules of crystallization that are held together by means of hydrogen bonds and π-π interactions affording a three-dimensional network (see Figure 16).

Selected bond lengths and angles with the relevant hydrogen bonds in **5** are listed in Table 14.

Two crystallographically independent copper atoms are present in **5** (Figure 16). Both of them are five-coordinated and they exhibit a distorted [Cu(1)] and slightly distorted [Cu(2)] square pyramidal environment, the τ geometric value [Addison A. W. *et al.*, 1984] being 0.103 [Cu(1)] and 0.034 [Cu(2)].

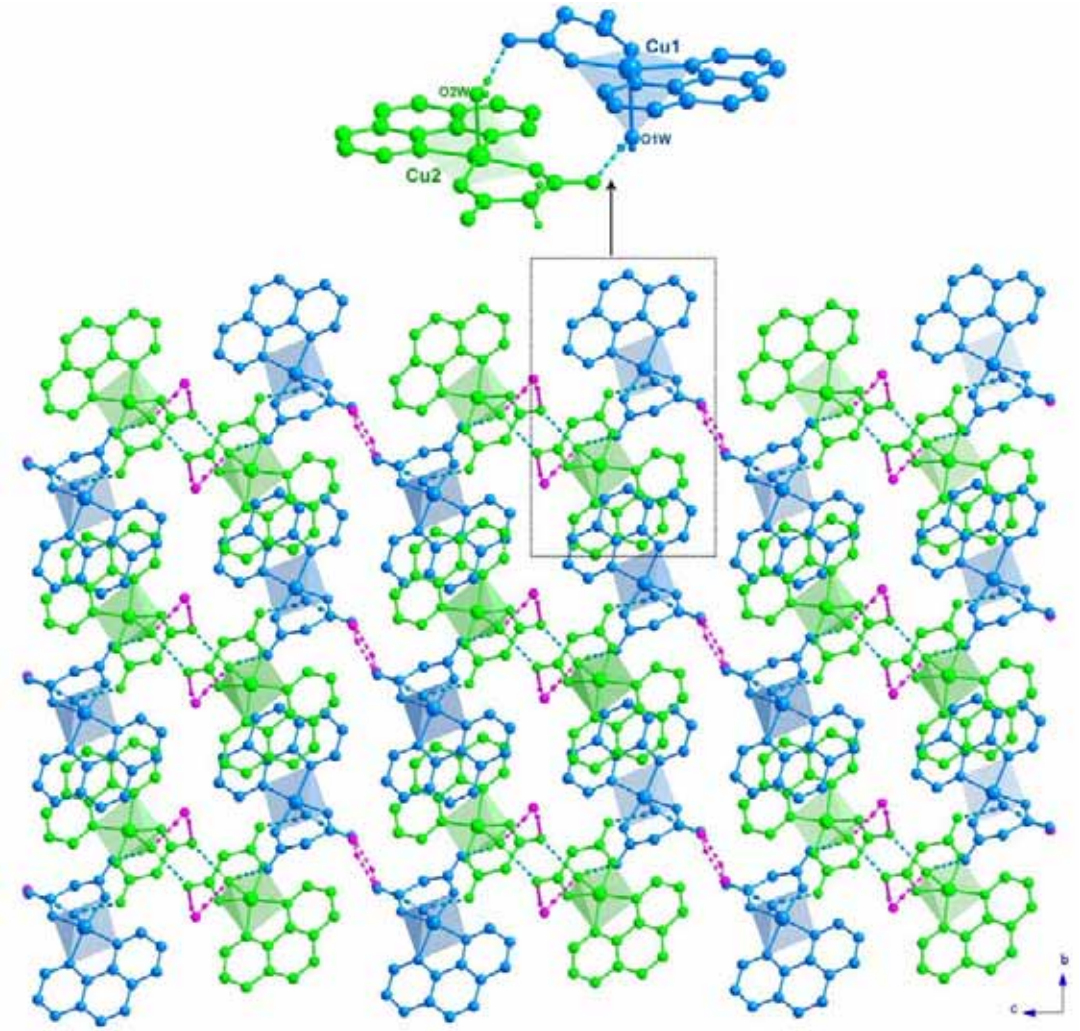

Figure 16. Perspective view, along the *a*-axis of the crystal packing in **5** with a view of a fragment showing the two crystallographically different [Cu(phen)(mal)(H_2O)] units which are present. Hydrogen bonds are drawn as dashed lines.

Table 14. Selected bonds lengths (Å) and angles (º) and hydrogen bonds for **5**[a,b]

Copper environment			
Cu(1)-O(1)	1.903(2)	Cu(1)-N(11)	2.000(2)
Cu(1)-O(2)	1.911(2)	Cu(1)-N(12)	2.015(2)
Cu(1)-O(1w)	2.254(2)		
O(1)-Cu(1)-O(2)	94.88(7)	N(11)-Cu(1)-N(12)	81.96(8)
O(1)-Cu(1)-N(11)	90.76(7)	O(2)-Cu(1)-N(11)	171.83(8)
O(1)-Cu(1)-N(12)	165.67(9)	O(2)-Cu(1)-N(12)	91.25(8)
O(1)-Cu(1)-O(1w)	100.34(9)	N(11)-Cu(1)-O(1w)	85.93(9)
O(2)-Cu(1)-O(1w)	98.84(10)	N(12)-Cu(1)-O(1w)	91.48(8)
Cu(2)-O(31)	1.917(2)	Cu(2)-N(41)	2.026(2)
Cu(2)-O(32)	1.897(2)	Cu(2)-N(42)	2.020(2)
Cu(2)-O(2w)	2.268(2)		
O(31)-Cu(2)-O(32)	95.02(7)	N(41)-Cu(2)-N(42)	80.82(8)
O(31)-Cu(2)-N(41)	92.87(7)	O(32)-Cu(2)-N(41)	166.15(8)
O(31)-Cu(2)-N(42)	168.21(8)	O(32)-Cu(2)-N(42)	89.35(7)
O(31)-Cu(2)-O(2w)	91.68(9)	N(41)-Cu(2)-O(2w)	91.27(8)
O(32)-Cu(2)-O(2w)	99.85(8)	N(42)-Cu(2)-O(2w)	98.37(9)

Hydroen bonds			
D-H···A	D···A/Å	H···A/Å	D-H···A/º
O(1w)-H(1w1)···O(3w)	2.759(4)	1.90(5)	171(4)
O(1w)-H(2w1)···O(34)	2.797(3)	2.18(4)	171(4)
O(2w)-H(1w2)···O(3)	2.705(3)	2.01(3)	170(4)
O(2w)-H(2w2)···O(33a)	2.765(3)	1.97(3)	172(4)
O(3w)-H(1w3)···O(4b)	2.813(4)	2.07(5)	178(5)
O(3w)-H(2w3)···O(4c)	2.799(3)	1.99(4)	163(4)
O(4w)-H(1w4)···O(2w)	2.836(4)	1.98(4)	171(4)
O(4w)-H(2w4)···O(33d)	2.885(4)	2.13(5)	167(4)
C(2)-H(2)···O(34d)	3.229(4)	2.45(4)	140(3)
C(10)-H(10)···O(33a)	3.319(3)	2.67(2)	128(2)
C(14)-H(14)···O(4we)	3.501(4)	2.71(3)	156(2)
C(15)-H(15)···O(3e)	3.169(3)	2.44(2)	141(2)
C(18)-H(18)···O(4f)	3.262(4)	2.65(3)	131(2)
C(41)-H(41)···O(4wg)	3.186(4)	2.36(3)	156(3)
C(42)-H(42)···O(34h)	3.330(3)	2.48(3)	160(3)

[a] Symmetry transformations: (a) -*x*+2, -*y*+2, -*z*; (b) *x*+1, *y*, *z*; (c) -*x*+1, -*y*+2, -*z*+1; (d) *x*-1, *y*, *z*; (e) *x*+1, *y*-1, *z*; (f) -*x*+1, -*y*+1, -*z*+1; (g) -*x*+1, -*y*+3, -*z*; (h) *x*-1, *y*+1, *z*. [b] A = acceptor; D = donor.

Two malonate-oxygen and two phenantroline-nitrogen atoms (see Figure 17) build the basal plane around the copper atoms [the mean Cu-O and Cu-N equatorial bond lengths are 1.907(2) and 2.008(2) Å for Cu(1) and 1.907(2) and 2.023(2) Å for Cu(2)] while the apical position is occupied by a water molecule [the Cu-O(w) bond

distance being 2.254(2) and 2.268(2) Å for Cu(1) and Cu(2), respectively]. Basal atoms around Cu(1) deviates from planarity [the maximum deviation from the mean basal plane being 0.070(2) Å for N(11)] meanwhile for Cu(2) basal atoms are coplanar within the experimental standard deviation. The copper atoms are shifted by 0.1527(4) Å [Cu(1)] and 0.1800(4) Å [Cu(2)] from the mean basal plane towards the apical water molecule. The bond length and angles are in good agreement with those reported for the complexes of formula: $[Cu(phen)(ox)(H_2O)]\cdot H_2O$ (ox = oxalate) [Fabretti A.C. *et al.*, 1985] and $[Cu(phen)(mal)(H_2O)]\cdot 3/2H_2O$ [Kwik W.-L. *et al.*, 1986; Borghi E., 1987].

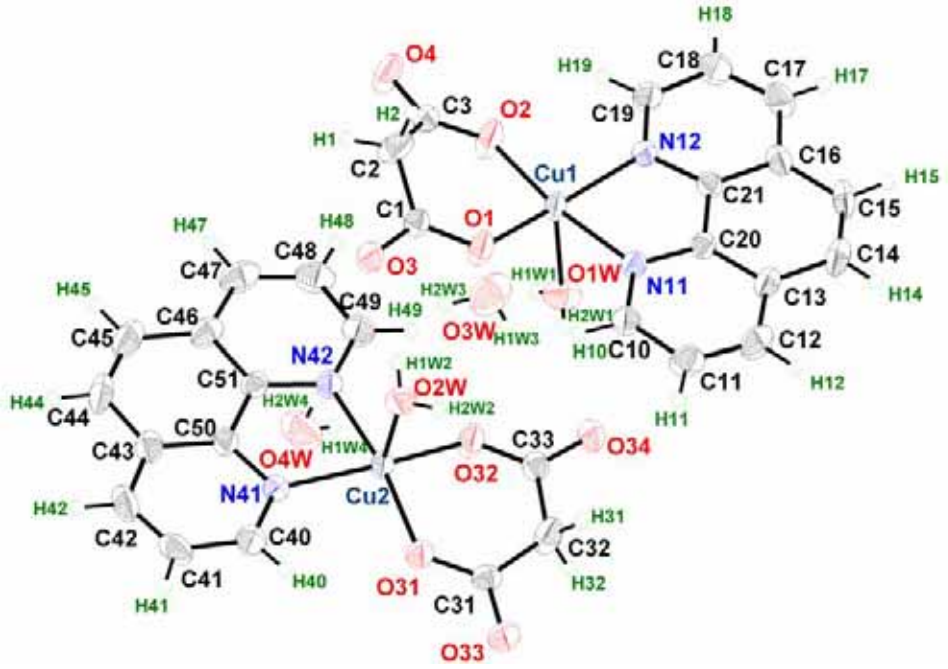

Figure 17. Perspective view of the asymmetric unit in **5** with the atom numbering. Thermal ellipsoids are drawn at the 50% probability level.

Two crystallographically independent malonate and phenantroline groups are present in **5**: [C(1)C(2)C(3)] L1 and [C(31)C(32)C(33)] L2 (Figure 17). Both malonate groups act as bidentate ligands [through O(1) and O(2) towards Cu(1) for L1 and through O(31) and O(32) towards Cu(2) for L2]. The values of the angle subtended at the metal atom by the malonate groups are 94.88(7) [at Cu(1)] and 95.02(7)º [at Cu(2)]. Both malonate ligands form a six-membered ring (including the copper atom), exhibiting a boat conformation [θ = 87.3(3)º and ϕ = 114.2(3)º] for L1 and a screw-boat conformation [θ = 63.6(9)º and ϕ = 149.8(9)] for L2 [Cremer D. *et al.*, 1975]. The bond lengths and angles of the malonate ligands (see Table 15) agree well with those reported for other malonate-containing copper(II) compounds [see the references concerning malonate-containing copper(II) complexes in the Introduction].

Table 15. Bond lengths (Å) and angles (º) for the malonate ligands in **5**

C(1)-C(2)	1.506(4)	C(2)-C(3)	1.504(3)
C(1)-O(1)	1.268(3)	C(3)-O(2)	1.265(3)
C(1)-O(3)	1.227(3)	C(3)-O(4)	1.233(3)
O(1)··· O(2)	2.809(3)	O(3)··· O(4)	4.544(3)
O(1)-C(1)-O(3)	122.5(2)	O(2)-C(3)-O(4)	122.1(2)
O(1)-C(1)-C(2)	119.7(2)	O(2)-C(3)-C(2)	120.4(2)
O(3)-C(1)-C(2)	117.8(2)	O(4)-C(3)-C(2)	117.5(2)
C(1)-C(2)-C(3)	121.1(2)		
C(1)-O(1)-Cu(1)	127.3(2)	C(3)-O(2)-Cu(1)	126.8(2)
O(1)C(1)O(3)-Cu(1)eq[a]	21.4(2)	O(2)C(3)O(4)-Cu(1)eq[a]	24.12(14)
C(31)-C(32)	1.508(4)	C(32)-C(33)	1.510(4)
C(31)-O(31)	1.275(3)	C(33)-O(32)	1.266(3)
C(31)-O(33)	1.237(3)	C(33)-O(34)	1.237(3)
O(31)···O(32)	2.812(2)	O(33)···O(34)	4.683(3)
O(31)-C(31)-O(33)	121.4(2)	O(32)-C(33)-O(34)	121.7(2)
O(31)-C(31)-C(32)	122.2(2)	O(32)-C(33)-C(32)	121.3(2)
O(33)-C(31)-C(32)	116.4(2)	O(34)-C(33)-C(32)	117.0(2)
C(31)-C(32)-C(33)	123.3(2)		
C(31)-O(31)-Cu(2)	127.60(15)	C(33)-O(32)-Cu(2)	128.45(16)
O(31)C(31)O(33)-Cu(2)eq[a]	5.30(15)	O(32)C(33)O(34)-Cu(2)eq[a]	6.28(11)

[a]dihedral angle (º) between the malonate carboxylate group and the mean equatorial plane of the metal.

The crystallographically independent phen ligands chelate the copper atoms, the values of the bite angles being 81.96(8) [N(11)-Cu(1)-N(12)] and 80.82(8)º [N(41)-Cu(2)-N(42)]. These values are somewhat far from the ideal value of 90º as expected because of the contrained geometry of the phenantroline ring system [MacCann M. *et al*., 1997; Castillo O. *et al*., 2001]. The phen ligands are almost planar, the maximum deviation from the mean plane being 0.022(2) and 0.034(3) Å for N(12) and C(41), respectively. The dihedral angle between pyridyl rings from phen ligands 1.75(8) [N(11)-phen] and 2.43(9)º [N(41)-phen]] are somewhat longer than the angle between the phenyl and pyridyl rings 0.62(9) [N(11)-ring], 1.34(7) [N(12)-ring], 1.68(8) [N(41)-ring] and 0.75(9)º [N(42)-ring]. The bond lengths and angles for the phenantroline ligands in **5** are listed in Table 16.

Table 16. Selected bond lengths (Å) and angles (°) for the phen ligands in **5**

C(10)-C(11)	1.393(4)	C(19)-C(18)	1.388(4)
C(11)-C(12)	1.361(4)	C(18)-C(17)	1.355(4)
C(12)-C(13)	1.400(4)	C(17)-C(16)	1.402(4)
C(13)-C(20)	1.392(3)	C(16)-C(21)	1.393(3)
C(20)-N(11)	1.352(3)	C(21)-N(12)	1.358(3)
N(11)-C(10)	1.323(3)	N(12)-C(19)	1.328(3)
C(13)-C(14)	1.437(3)	C(16)-C(15)	1.431(4)
C(14)-C(15)	1.341(4)	C(20)-C(21)	1.431(3)
C(10)-N(11)-C(20)	118.6(2)	C(19)-N(12)-C(21)	117.9(2)
C(11)-C(10)-N(11)	121.7(2)	C(18)-C(19)-N(12)	121.9(3)
C(12)-C(11)-C(10)	119.9(3)	C(17)-C(18)-C(19)	120.3(3)
C(13)-C(12)-C(11)	119.8(2)	C(16)-C(17)-C(18)	119.7(2)
C(20)-C(13)-C(12)	116.6(2)	C(21)-C(16)-C(17)	116.6(2)
N(11)-C(20)-C(13)	123.3(2)	N(12)-C(21)-C(16)	123.5(2)
N(11)-C(20)-C(21)	116.6(2)	N(12)-C(21)-C(20)	116.1(2)
C(12)-C(13)-C(14)	125.0(2)	C(17)-C(16)-C(15)	124.9(2)
C(13)-C(14)-C(15)	121.5(3)	C(16)-C(15)-C(14)	121.2(2)
C(13)-C(20)-C(21)	120.1(2)	C(16)-C(21)-C(20)	120.4(2)
C(14)-C(13)-C(20)	118.3(2)	C(15)-C(16)-C(21)	118.4(2)
C(10)-N(11)-Cu(1)	128.4(2)	C(19)-N(12)-Cu(1)	129.7(2)
C(20)-N(11)-Cu(1)	112.71(15)	C(21)-N(12)-Cu(1)	112.35(15)
C(40)-C(41)	1.394(4)	C(49)-C(48)	1.378(4)
C(41)-C(42)	1.347(4)	C(48)-C(47)	1.364(4)
C(42)-C(43)	1.408(4)	C(47)-C(46)	1.402(4)
C(43)-C(50)	1.398(3)	C(46)-C(51)	1.392(3)
C(50)-N(41)	1.348(3)	C(51)-N(42)	1.350(3)
N(41)-C(40)	1.327(3)	N(42)-C(49)	1.329(3)
C(43)-C(44)	1.429(4)	C(46)-C(45)	1.441(4)
C(44)-C(45)	1.346(4)	C(50)-C(51)	1.436(3)
C(40)-N(41)-C(50)	117.6(2)	C(49)-N(42)-C(51)	118.1(2)
C(41)-C(40)-N(41)	122.4(3)	C(48)-C(49)-N(42)	121.8(3)
C(42)-C(41)-C(40)	120.2(3)	C(47)-C(48)-C(49)	120.6(3)
C(43)-C(42)-C(41)	119.4(2)	C(46)-C(47)-C(48)	119.0(3)
C(50)-C(43)-C(42)	116.7(2)	C(51)-C(46)-C(47)	116.8(2)
N(41)-C(50)-C(43)	123.8(2)	N(42)-C(51)-C(46)	123.7(2)
N(41)-C(50)-C(51)	116.2(2)	N(42)-C(51)-C(50)	116.0(2)
C(42)-C(43)-C(44)	124.7(2)	C(47)-C(46)-C(45)	124.9(3)
C(43)-C(44)-C(45)	121.5(3)	C(46)-C(45)-C(44)	121.2(3)
C(43)-C(50)-C(51)	120.0(2)	C(46)-C(51)-C(50)	120.3(2)
C(44)-C(43)-C(50)	118.6(2)	C(45)-C(46)-C(51)	118.4(3)
C(40)-N(41)-Cu(2)	129.0(2)	C(49)-N(42)-Cu(2)	128.3(2)
C(50)-N(41)-Cu(2)	113.40(15)	C(51)-N(42)-Cu(2)	113.58(15)

The two crystallographically independent [Cu(phen)(mal)(H_2O)] units are pairwise connected through hydrogen bonds involving the coordinated water molecules and some outer malonate oxygen atoms [O(1w)···O(34) and O(2w)···O(3); see pale blue broken lines in Figure 16, top], the Cu(1)···Cu(2) separation being 5.6251(6) Å. These units are further hydrogen bonded through crystallization water molecules affording a two-dimensional network that grows in the *ac*-plane (Figure 18). It deserves to be noted that two different hydrogen patterns are present in the hydrogen bonded network. First, a $R_4^2(8)$ motif (blue coloured in Figure 18) connects four Cu(1) units through O(mal)···O(3w)···O(mal) [12.3908(8) Å for the copper···copper separation] and O(1w)···O(3w)···O(mal) interactions [8.0697(5) and 9.1378(7) Å being the copper···copper distances for O(1w)···O(3w)···O(4b) and O(1w)···O(3w)···O(4c), respectively]. Second, a $R_6^4(12)$ motif which exhibits a chair conformation (green colour in Figure 18) links four Cu(2) units (see Figure 18) through O(mal)···O(2w) [9.5627(7) Å for the copper···copper separation] and O(mal)···O(4w)···O(2w) interactions [8.0697(5) Å being the copper···copper distance]. And finally, a $R_6^6(20)$ motif formed by four water molecules and two malonate groups, all atoms being crystallographycally independent.

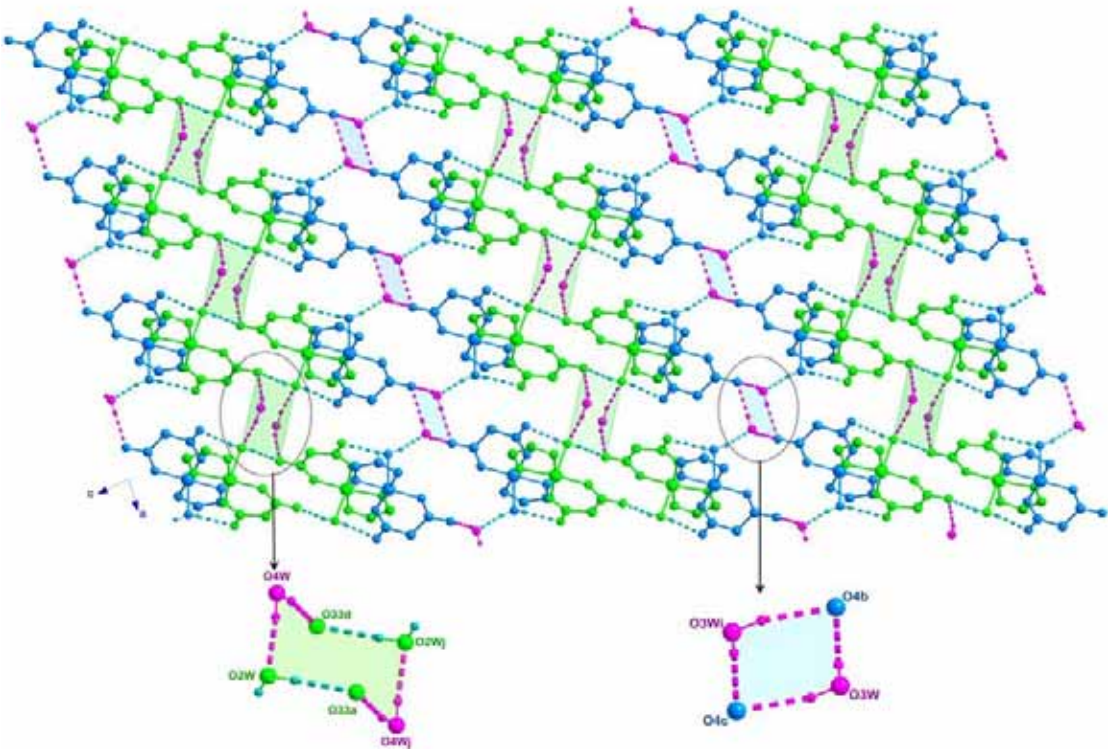

Figure 18. Perspective view, along the *b*-axis, of the two-dimensional hydrogen bonded network in **5** with a schematic view of the water arrangements. Hydrogen bonds are represented by broken lines.

Hydrogen bonded networks are further connected through offset face-to-face π-π interactions between the phenantroline rings bonded to Cu(1) and Cu(2) units belonging to adjacent layers (see Figure 19). The separation between phenantroline groups is around 3.5 Å. The dihedral angle between the mean planes defined by phenantroline groups is 2.56(3)º.

Finally, weak C-H···O interactions contribute to stabilize the whole three-dimensional structure (see Table 16).

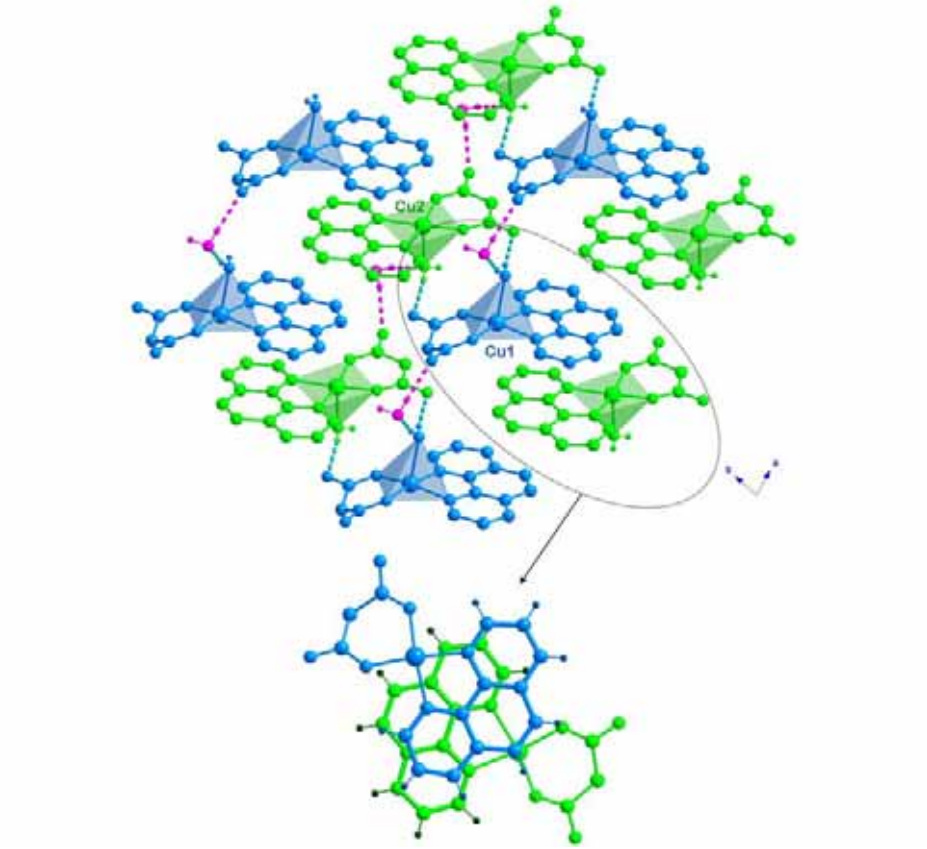

Figure 19. Perspective view of a fragment of the crystal structure of **5** showing the π-π stacking.

Let us finish with a comparison between the structure of **5** and that of the related compound [Cu(phen)(mal)(H_2O)]·3/2H_2O (**5i**) [Kwik W.-L. *et al.*, 1986; Borghi E., 1997]. Similarly to **5**, the structure of **5i** is made up of two crystallographically independent [Cu(phen)(mal)(H_2O)] mononuclear units and crystallization water molecules connected through hydrogen bonds to afford a hydrogen bonding two-dimensional networks that are further connected through offset face-to-face π-π interactions. The main difference between both compounds is the number of lattice water molecules in the crystal structure. This is at the origin of the different topology of

the two-dimensional hydrogen bonded network (as shown by comparing Figure 18 and 20).

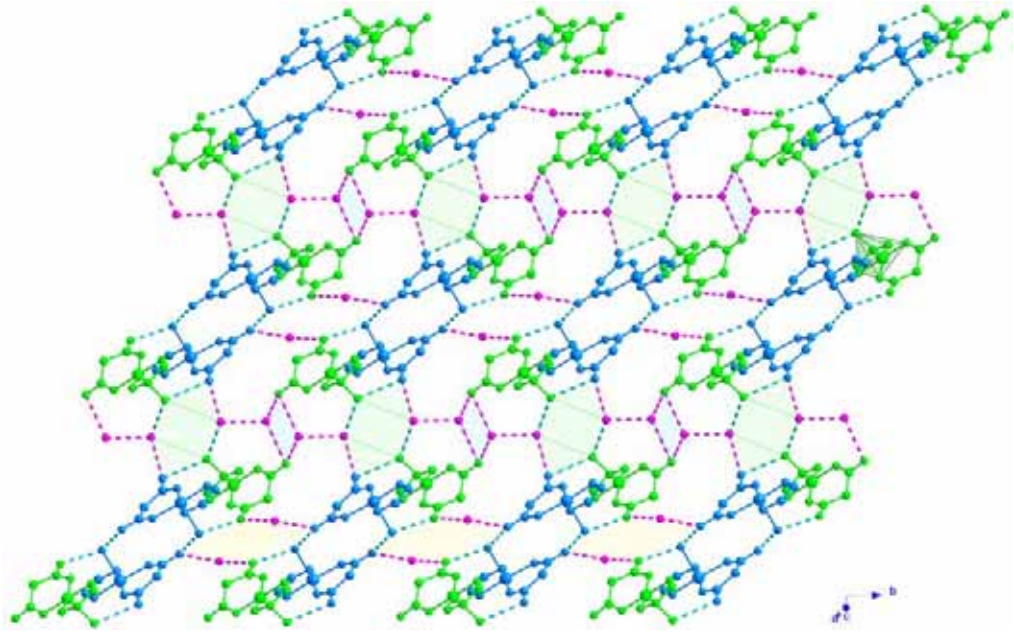

Figure 20. Perspective view of the two-dimensional hydrogen bonded network in the compound of formula [Cu(phen)(mal)(H_2O)]·3/2H_2O (**5i**). The colour areas illustrate the hydrogen-bond motifs. Hydrogen bonds are represented by broken lines.

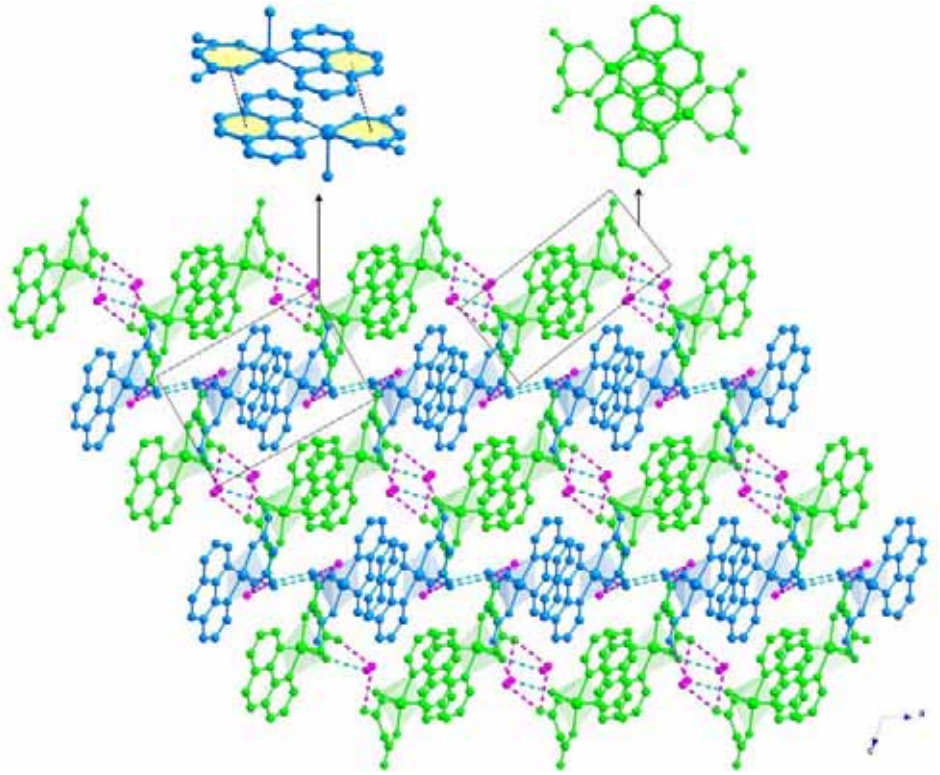

Figure 21. Perspective view of the crystal packing in the compound of formula [Cu(phen)(mal)(H_2O)]·3/2H_2O (**5i**) with fragments showing the π-π and aryl-π stackings. Hydrogen bonds are drawn as broken lines.

Unlike from **5**, three different oxygen arrays (four, six and eight-membered rings) involving water molecules and malonate oxygen atoms are present in **5i** (Figure

20). Also, the crystal packing through the phenantroline groups is quite different, two types of weak interactions being present in **5i.** First, offset face-to-face π-π interactions between phenantroline rings from Cu(2) units (Figure 21), the shortest atomic separations between phenantroline atoms range from 3.430 to 3.566 Å. Finally, hydrophobic interactions between the aromatic rings of phenantroline group and the aliphatic chains of the malonate ligand from the Cu(1) units [the separation between ring centroids being 3.53 Å] contribute to the crystal packing (Figure 21).

Description of the structure of $[Cu_2(phen)_2(mal)(H_2O)_3](NO_3)_2{\cdot}2H_2O$ (6)

The structure of **6** consists of dinuclear malonate-bridged phenantroline copper(II) units which are further linked through hydrogen bonds, π-π and hydrophobic interactions leading to a three-dimensional network (see Figure 22).

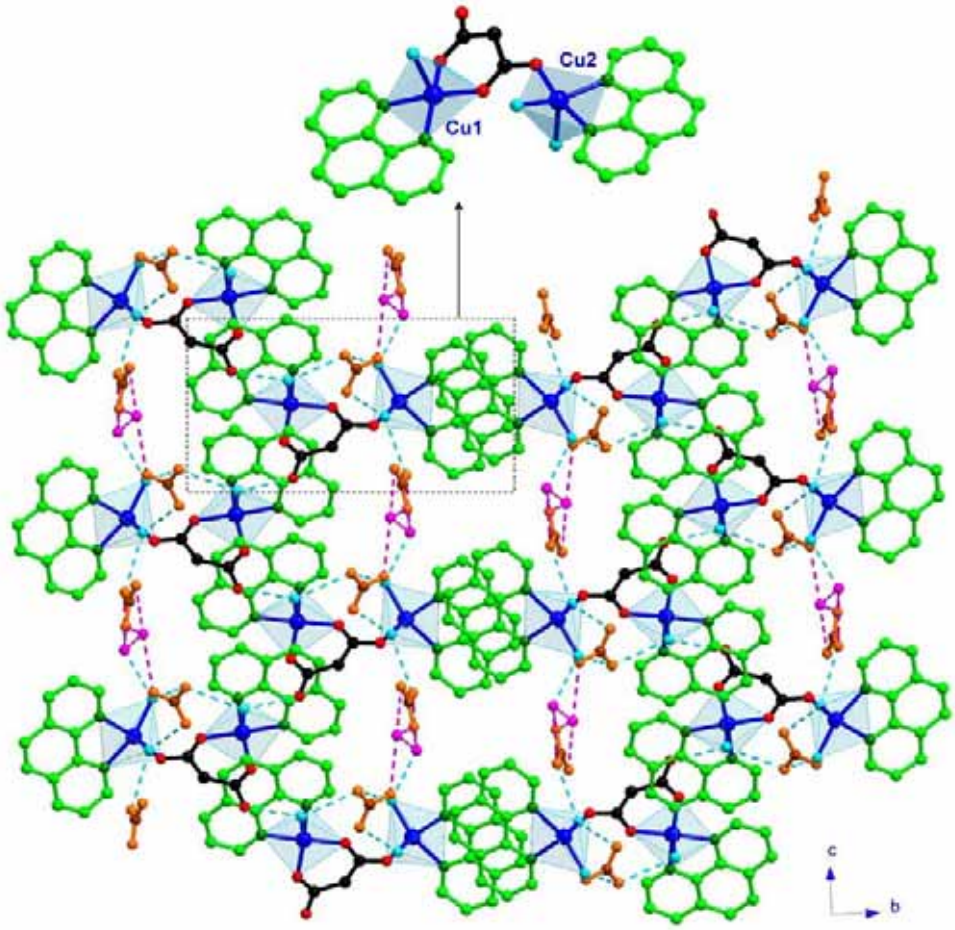

Figure 22. Perspective view along the *a*-axis of the crystal packing of the dinuclear malonate-bridged copper(II) units in **6**. Hydrogen bonds are drawn as broken lines. Nitrate groups and non-coordinated water molecules are orange and purple coloured, respectively.

Two crystallographically independent copper atoms are present in **6**. Both of them are five-coordinated and they exhibit distorted square pyramidal environments (see Figure 23), the τ values [Addison A.W. *et al.*, 1984] being 0.144 [Cu(1)] and 0.254 [Cu(2)]. Two malonate oxygens and two phenantroline-nitrogen atoms build the basal plane around Cu(1) [the mean Cu-O and Cu-N equatorial bond distances are 1.918(2) and 2.008(3) Å, respectively], the maximum deviation of the equatorial atoms from the mean basal plane being 0.093(3) for N(11). The apical position is occupied by a water molecule [Cu-O(w) = 2.257(3) Å].

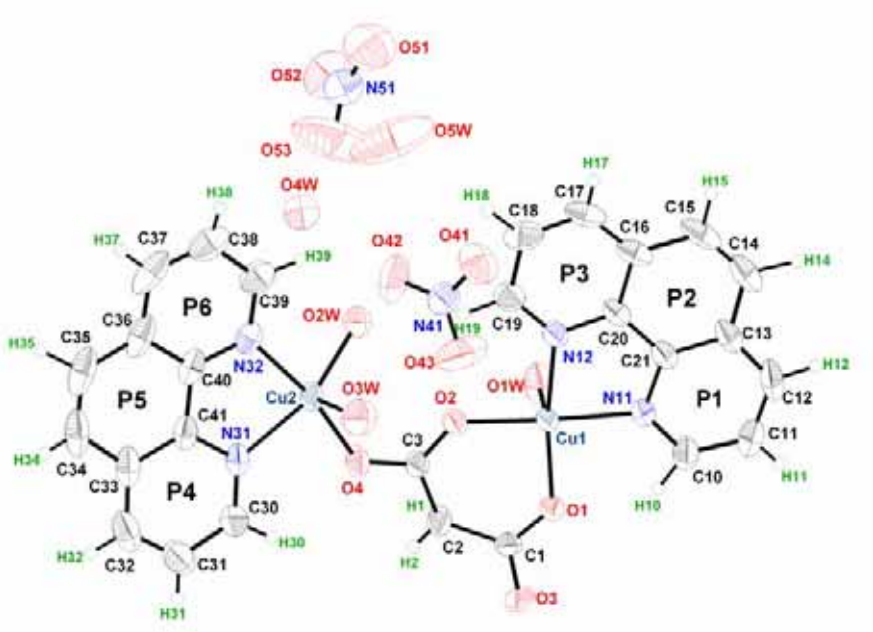

Figure 23. ORTEP view of the asymmetric unit in **6** with the atom numbering. Thermal ellipsoids are drawn at the 50% probability level.

One malonate-oxygen atom, a coordinated water molecule and the phenantroline-nitrogen atoms build the basal plane around Cu(2) [1.966(2) and 2.021(3) Å being the average Cu-N and Cu-O equatorial bond distances, respectively]. Whereas, one water molecule fills the apical position at Cu(2) [Cu-O(w) = 2.180(3) Å]. The deviation of the equatorial atoms around Cu(2) from the mean basal plane [the maximum deviation is 0.188(3) Å for N(31)] is longer than in Cu(1) because the greater distortion of the metal environment. Both copper atoms are shifted by 0.1546(4) [Cu(1)] and 0.2819(4) Å [Cu(2)] from the mean basal plane towards the apical position. Main bond lengths and angles for **6** are listed in Table 17.

Table 17. Selected bond lenghts (Å) and angles (º) and hydrogen bonds for **6**[a,b]

Copper environment			
Cu(1)-O(1)	1.900(2)	Cu(1)-N(11)	2.001(3)
Cu(1)-O(2)	1.936(2)	Cu(1)-N(12)	2.015(3)
Cu(1)-O(1w)	2.257(3)		
O(1)-Cu(1)-O(2)	93.80(10)	N(11)-Cu(1)-N(12)	82.34(12)
O(1)-Cu(1)-N(11)	90.50(11)	O(2)-Cu(1)-N(11)	173.26(11)
O(1)-Cu(1)-N(12)	164.64(12)	O(2)-Cu(1)-N(12)	92.24(11)
O(1)-Cu(1)-O(1w)	95.09(12)	N(11)-Cu(1)-O(1w)	91.56(11)
O(2)-Cu(1)-O(1w)	93.22(11)	N(12)-Cu(1)-O(1w)	98.65(12)
Cu(2)-O(4)	1.930(2)	Cu(2)-N(31)	2.026(3)
Cu(2)-O(2w)	2.001(3)	Cu(2)-N(32)	2.016(3)
Cu(2)-O(3w)	2.180(3)		
O(4)-Cu(2)-O(2w)	94.84(12)	N(31)-Cu(2)-N(32)	81.69(13)
O(4)-Cu(2)-N(31)	88.63(12)	O(2w)-Cu(2)-N(31)	153.59(12)
O(4)-Cu(2)-N(32)	168.85(12)	O(2w)-Cu(2)-N(32)	91.46(12)
O(4)-Cu(2)-O(3w)	96.28(12)	N(31)-Cu(2)-O(3w)	98.01(12)
O(2w)-Cu(2)-O(3w)	107.57(12)	N(32)-Cu(2)-O(3w)	90.55(12)

Hydrogen bonds			
D-H···A	D···A/Å	D-H···A	D···A/Å
O(1w)-H···O(3a)	2.786(4)	O(4w)-H···O(52)	3.053(5)
O(1w)-H···O(41b)	2.934(5)	O(4w)-H···O(53)	3.008(7)
O(2w)-H···O(41b)	2.867(4)	O(4w)-H···O(5wb)	2.669(6)
O(2w)-H···O(4w)	2.649(4)	O(5w)-H···O(42)	2.918(6)
O(3w)-H···O(43)	2.882(5)	O(5w)-H···O(51)	3.087(7)
O(3w)-H···O(52c)	2.888(5)	O(5w)-H···O(53)	2.904(8)

D-H···A	D···A/Å	H···A/Å	D-H···A/º
C(2)-H(1)···O(43c)	3.398(6)	2.46(5)	145(4)
C(12)-H(12)···O(52d)	3.516(6)	2.62(4)	160(3)
C(14)-H(14)···O(43a)	3.261(6)	2.53(4)	123(3)
C(14)-H(14)···O(3w)	3.655(6)	2.61(5)	158(4)
C(17)-H(17)···O(3e)	3.233(5)	2.47(4)	172(4)
C(32)-H(32)···O(4wf)	3.377(6)	2.56(5)	158(5)
C(39)-H(39)···O(53)	3.277(7)	2.58(4)	127(3)

[a] Symmetry transformations: (a) x, -y+1/2, z-1/2; (b) x+1, y, z; (c) x, y, z+1; (d) x, -y+1/2, z+1/2; (e) x-1, y, z-1; (f) -x+2, -y, -z+2. [b] A = acceptor; D = donor.

The malonate group (see Figure 24) in **6** acts simultaneously as monodentate [through O(4) towards Cu(2)] and bidentate ligand [through O(1) and O(2) towards Cu(1)]. It forms a six-membered ring including the copper atom that exhibits a boat conformation [θ = 80.8(6) and ϕ = 111.7(5)º] [Cremer D. *et al.*, 1975].

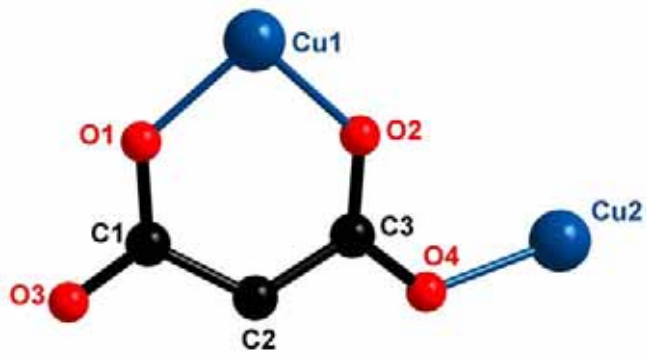

Figure 24. Coordination mode of the malonate ligand in **6**.

The *anti-syn* carboxylate-malonate group connects two equatorial positions from two adjacent copper atoms, the Cu···Cu separation being 5.097(6) Å. The dihedral angle between the basal planes of two adjacent copper atoms is 28.74(8)º. The values of the bond lengths and angles of the malonate ligand (see Table 18) are in good agreement with those reported for the previously malonate-bridged copper(II) complexes.

Table 18. Bond lengths (Å) and angles (º) for the malonate ligand present in **6**[a]

C(1)-C(2)	1.508(5)	C(2)-C(3)	1.516(5)
C(1)-O(1)	1.271(4)	C(3)-O(2)	1.250(4)
C(1)-O(3)	1.230(4)	C(3)-O(4)	1.257(4)
O(1)···O(2)	2.802(4)	O(3)···O(4)	4.632(4)
O(1)-C(1)-O(3)	121.9(4)	O(2)-C(3)-O(4)	122.7(3)
O(1)-C(1)-C(2)	120.7(3)	O(2)-C(3)-C(2)	122.2(3)
O(3)-C(1)-C(2)	117.5(3)	O(4)-C(3)-C(2)	115.1(3)
C(1)-C(2)-C(3)	121.5(3)		
C(1)-O(1)-Cu(1)	127.9(2)	C(3)-O(2)-Cu(1)	126.6(2)
C(3)-O(4)-Cu(2)	126.6(2)		
O(1)C(1)O(3)-Cu(1)eq[a]	14.1(3)	O(2)C(3)O(4)-Cu(1)eq[a]	9.8(2)
O(2)C(3)O(4)-Cu(2)eq[a]	32.4(2)		

[a]dihedral angle (º) between the carboxylate-malonate group and the mean plane defined by malonate oxygen atoms in the metal environment.

The two phenantroline groups act as terminal bidentate ligands [through N(11) and N(12) towards Cu(1) and through N(31) and N(32) towards Cu(2)]. The bite angles 83.34(12) [at Cu(1)] and 81.69(13)º [at Cu(2)] are somewhat far from the ideal value of 90º because of the constrained geometry of the five-membered chelate ring subtended at the copper atom by the phenantroline ligand. The phen ligands as a whole are quite planar, the maximum deviation from the planarity being 0.025(5) and 0.051(5) Å for C(14) and C(38), respectively. The bond lengths and angles of the phenantroline are within the range of those reported for other phenantroline-containing copper(II) complexes: $[Cu(ox)(phen)(H_2O)]\cdot H_2O$ [Fabretti A.C. *et al.*, 1985]

[Cu(phen)(mal)(H_2O)]·3/2H_2O [Kwik W.-L. *et al.*, 1986; Borghi E., 1987] and [Cu(phen)(mal)(H_2O)]·H_2O (**5**).

The [Cu(phen)(mal)(H_2O)] and [Cu(phen)(H_2O)$_2$]$^{2+}$ mononuclear units are connected through *anti-syn* carboxylate-malonate bridges to form anionic dinuclear units. These units are held together by means of hydrogen bonds, π···π and hydrophobic interactions (involving the phenantroline and the malonate ligands) affording thus a two-dimensional network.

First, dinuclear units are linked through O(1w)-H···O(3a) hydrogen bonds (see Table 17) affording helical zigzag chains which grow along the *c*-axis [5.7839(6) Å for the intrachain Cu(1)···Cu(1a) separation, see Figure 25]. Additionally, hydrogen bonds (involving coordinated water molecules and nitrate oxygen atoms), offset π···π interactions between P1- and P3-phenantroline rings (see Figure 23) [the distance between ring centroids is 3.7986(2) Å] and hydrophobic interactions between the P2 ring of the phenantroline group and the malonate aliphatic chain [Cu(1)-O(1)-C(1)-C(2)-C(3)-O(2)] contribute to stabilise the *zigzag* chains. The distance between ring centroids [3.795(4) Å] and the dihedral angle between the normal vector to the mean P2 ring plane and the vector defined by the two ring centroids [27.31(10)º] are within the range observed for other malonate-containing copper(II) complexes where hydrophobic interactions have been reported: [Cu(phen)(mal)(H_2O)]·3/2H_2O [Borghi E., 1987] and [Cu(dpp)(mal)(H_2O)]·H_2O (**4**). The *zigzag* chains are further held together by means of an extensive network of hydrogen bonds involving water molecules and the nitrate-oxygen atoms leading to a two-dimensional network.

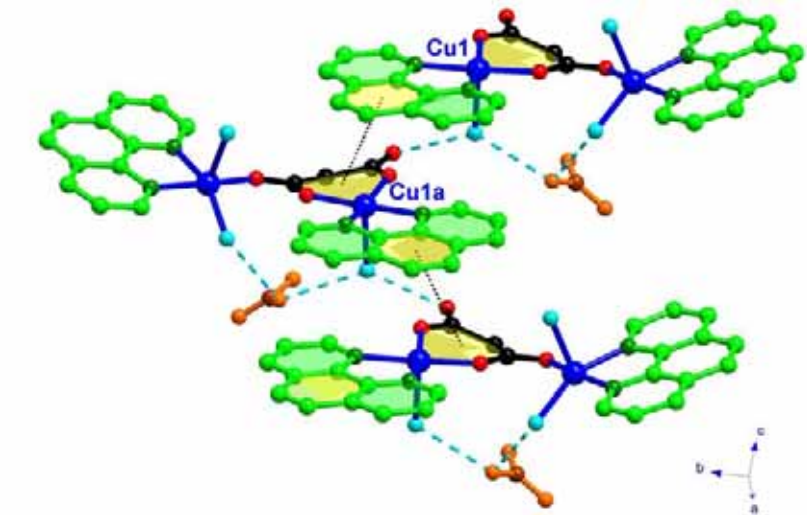

Figure 25. Perspective view of the helical copper(II) zigzag chains in **6**. Hydrogen atoms are skipped for the sake of clarity. Hydrogen bonds and hydrophobic interactions are represented by broken and dotted lines, respectively.

Finally, offset π-π interactions between the phenantroline groups that chelate Cu(2) atoms connect together the two-dimensional hydrogen bonded networks affording a three-dimensional structure (see Figure 22).

Magnetic properties

The magnetic properties of compounds **1**-**5** were not investigated because they are mononuclear. As we have seen in the previous chapter, hydrogen bonds are not able to mediate significant magnetic coupling between magnetic centres.

The magnetic behaviour of **6** in the form of $\chi_M T$ versus T plot [χ_M being the magnetic susceptibility per mol of two copper(II) ions] in the temperature range of 2-300 K is shown in Figure 26. The value of the $\chi_M T$ at 300 K is 0.84 $cm^3\ mol^{-1}$ K, a value which is as expected for two magnetically isolated spin doublets. Upon cooling, $\chi_M T$ remains practically constant up to 100 K, and then increases smoothly at lower temperatures, reaching a value of 1.086 $cm^3\ mol^{-1}$ K at 2 K. This behaviour indicates the occurrence of an overall ferromagnetic coupling between the magnetic centres. The structure of **6** consists of dinuclear units where two equatorial sites of copper(II) atoms are connected by an *anti-syn* carboxylate-malonate bridge. The dinuclear units are further connected through hydrogen bonds. We tried to fit the magnetic data through the Bleaney-Bowers equation [Bleaney B. *et al.*, 1952] for two interacting S = 1/2 including a θ term to take into account the weak intermolecular interactions between dinuclear units through hydrogen bonding.

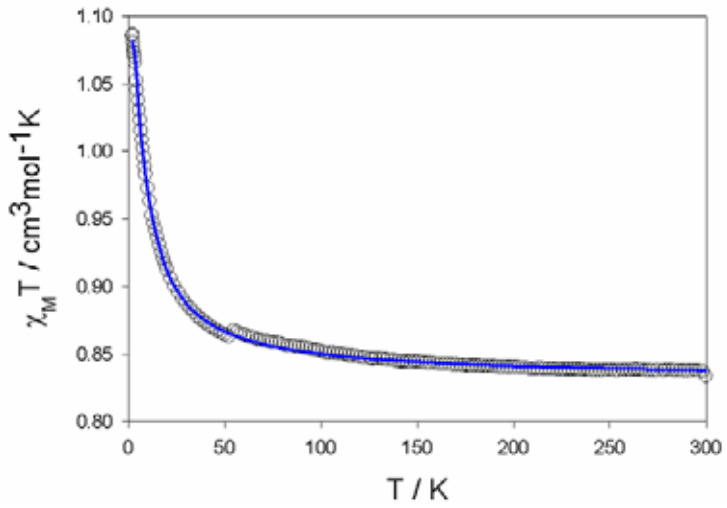

Figure 26. Thermal dependence of the $\chi_M T$ vs. T of **6**: (") experimental data and (C) best fit curve (see text).

The best least-squares fit parameters are J = +6.22(3) cm^{-1}, θ = -0.042(2) K , g = 2.106(1) and R = 4.15x10^{-6}. R is the agreement factor defined as $\Sigma[(\chi_M)_{obs} - (\chi_M)_{calc}]^2/\Sigma[(\chi_M)_{obs}]^2$. The value of the magnetic coupling agrees well with those reported for other malonate-containing copper(II) complexes which exhibits a similar exchange pathway: $\{[Cu(H_2O)_3][Cu(mal)_2(H_2O)]\}_n$ (J = +3 cm^{-1}) [Ruiz-Pérez C. *et al.*, 2000a], $\{[Cu(bpy)(H_2O)][Cu(bpy)(mal)(H_2O)]\}(ClO_4)_2$ (J = +4.6 cm^{-1}) [Ruiz-Pérez C. *et al.*, 2000b], $[Cu_2(mal)_2(H_2O)_2(4,4'\text{-bpy})]$ (J = +12.4 cm^{-1}) [Rodríguez-Martín Y. *et al.*, 2001], $[Cu_4(mal)_4(2,4'\text{-bpy})_4(H_2O)_4]\cdot 8H_2O$ (J = +12.3 cm^{-1}) [Rodríguez-Martín Y. *et al.*, 2002] and $\{[Cu_3(mal)_2(bpe)_3(H_2O)_2](NO_3)_2\}$n (J = +22 cm-1) [Sain S. *et al.*, 2003].

References

Addison A.W., Rao T.N., Reedijk J., Rijn J. and Verschoor G.C.J., *J. Chem. Soc., Dalton Trans.*, **1984**, 1349.

Allen F.H., *Acta Cryst., Sect. B*, **2002**, 58, 380.

Bleaney B. and Bowers K.D., *Proc. Roy. Soc. London Ser. A*, **1952**, 214, 151.

Borghi E., *Gazz. Chim. Ital.*, **1987**, 117, 557.

Breneman G.L., Aubol S.L. and Parker O.J., *Acta Cryst., Sect.E* , **2001**, 57, m288.

Carranza J., Brennan C., Sletten J., Vangdal B., Rillema P., Lloret F. and Miguel J., *New J. Chem.*, **2003**, 27, 1775.

Carranza J., Grove H. Sletten J., Lloret F., Julve M., Kruger P.E., Eller C. and Rillema D.P., *Eur. J. Inorg. Chem.*, **2004**, 24, 4836.

Castillo O., Luque A. and Román P., *J. Mol. Struct.*, **2001**, 570, 181.

Coronado E., Galán-Mascarós J.R., Gómez-García C.J., LaukhinV., *Nature*, **2000**, *408*, 447.

Cremer D. and Pople J.A., *J. Am. Chem. Soc.*, **1975**, 97, 1354.

Desiraju G.R., *Angew. Chem. Int. Ed. Engl.*, **1995**, 34, 2311.

Desiraju G.R., *Nature*, **2001**, *412*, 397.

DIAMOND 2.1d, Crystal Impact GbR, CRYSTAL IMPACT, K. Brandenburg & H. Putz GbR, Postfach 1251, D-53002 Bonn, Germany, **2000**.

Du M., Guo Y.-M., Chen S.-T., Bu X.-H. and Ribas J., *Inorg. Chim. Acta*, **2003**, 346 207.

Duisenberg A.J.M., Kroon-Batenburg, L.M.J. and Schreurs A.M.M., *J. Appl. Cryst.*, **2003**, 36, 220 (EVALCCD).

Earshaw A., *Introduction to Magnetochemistry*; Academic Press; London, **1968**.

Etter M.C., *Acc. Chem. Res.*, **1990**, 23 120.

Fabretti A.C., Franchini G., Zannini P. and Di Vaira M., *Inorg. Chim. Acta*, **1985**, 105, 187.

Farrugia L.J. (*WINGX*), *J. Appl. Cryst*, **1999**, *32*, 837.

Grove H., Sletten J., Julve M., Lloret F. and Lezama L., *Inorg. Chim. Acta*, **2000**, 310, 217.

Grove H., Julve M., Lloret F., Kruger P.E., Törnroos K.W. and Sletten J., *Inorg. Chim. Acta*, **2001a**, 325, 115.

Grove H., Sletten J., Julve M. and Lloret F., *J. Chem. Soc., Dalton Trans.*, **2001b**, 2487.

Hooft, R.W.W. *COLLECT*. Nonius BV, Delft, The Netherlands, **1999**.

Huang N.-T., Pennington W.T. and Petersen J.D., *Acta Cryst., Sect. C*, **1991**, 47, 2011.

Ishida T., Kawakami T., Mitsubori S., Nogami T., Yamaguchi K. and Iwamura H., *J. Chem. Soc., Dalton Trans.*, **2002**, 3177.

Karanovic L., Poleti D., Rogan J., Bogdanovic G.A. and Spasojevic-de-Biré A., *Acta Cryst., Sect. C*, **2002**, 58, m275.

Kwik W.-L., Ang K.-P., Chan H.S.-O., Chebolu V. and Koch S.A., *J. Chem. Soc., Dalton Trans.*, **1986**, 2519.

Lehn J.-M., *Supramolecular Chemistry*; VCH: Weinheim, Germany, **1995**.

Lu J.Y. and Schauss V., *Inorg. Chem. Comm.*, **2002**, 5, 1028.

MacCann M., Casey M.T., Devereux M., Curran M. and McKee V., *Polyhedron*, **1997**, 16, 2741.

Morgan L.W., Goodwin K.V., Pennington W.T. and Petersen J.D., *Inorg. Chem.*, **1992**, 31, 1103.

Morsali A., Ramazani A., Babaee M., Jamali F., Gouranlou F., Arjmandfar H. and Yanovsky A., *J. Coord. Chem.*, **2003**, 56, 455.

Nardelli M., *J. Appl. Crystallogr.*, **1995**, *28*, 659.

Parker O.J., Aubol S.L. and Breneman G.L., *Polyhedron*, **2000**, 19, 623.

Reeder K.A., Dose E.V. and Wilson L.J., *Inorg. Chem.*, **1978**, 17, 1071.

Reinoso S., Vitoria P., San Felices L., Lezama L. and Gutiérrez-Zorrilla J.M., *Acta Cryst., Sect. E* , **2003**, 58, m548.

Robertson K.N., Bakshi P.K., Lantos S.D., Cameron T.S. and Knop O., *Can. J. Chem.*, **1998**, 76, 583.

Robson R., *J. Chem. Soc., Dalton Trans.* **2000**, 3735.

Rodriguez-Martín Y., Ruiz-Pérez C., Sanchiz J., Lloret F. and Julve M., *Inorg. Chim. Acta*, **2001**, 318, 159.

Rodríguez-Martín Y., Hernández-Molina M., Delgado F.S., Pasán J., Ruiz-Pérez C., Sanchiz J., Lloret F. and Julve M., *CrystEngComm.*, **2002**, 4, 522.

Ruiz-Pérez C., Sanchiz J., Hernández-Molina M., Lloret F. and Julve M., *Inorg. Chem.*, **2000a**, 39, 1363.

Ruiz-Pérez C., Hernández-Molina M., Lorenzo-Luis P., Lloret F., Cano J. and Julve M., *Inorg. Chem.*, **2000b**, 39, 3845.

SADABS, version 2.03. Bruker AXS Inc.: Madison, WI, **2000**.

Sain S., Maji T.K., Mostafa G., Lu T.H. and Chanduri N.R., *New. J. Chem.*, **2003**, 27, 185.

Serna Z., Barandika M.G., Cortes R., Urtiaga M.K. and Arriortua M.I., *Polyhedron*, **1999**, 18, 249.

Sheldrick, G.M. *SHELX97*, *Programs for Crystal Structure Analysis (Release 97-2)*, Institüt für Anorganische Chemie der Universität, Tammanstrasse 4, D-3400 Göttingen, Germany, **1998**.

Sommerer S.O., Westcott B.L. and Timothy L.F., *Acta Cryst., Sect. C*, **1994**, 50, 2013.

Sletten J. and Bjorsvik O., *Acta Chem. Scand.*, **1998**, 52, 770.

Steel P.J. and Sumby C.J., *Dalton Trans.*, **2003**, 4505.

Stiefel E. I. and Brown G. F., *Inorg. Chem.*, **1972**, 11, 434.

Tong M.-L., Zhou A.-J. and Hu S., *Acta Cryst., Sect.E* , **2004**, 60, m657.

Tangoulis V., Raptopoulou C.P., Terzis A., Paschalidou S., Perlepes S.P. and Bakalbassis E.G., *Inorg.Chem.*, **1997**, 36, 3996.

Yaghi O.M., Li G., Li H., *Nature*, **1995**, 378, 703.

Yang C.-H., Chuo C.-M., Lee G.-H. and Wang C.-C., *Inorg. Chem. Comm.*, **2003**, 6, 135.

Yang G., Tong M.-L., Chen X.-M. and Ng S.W., *Acta Cryst., Sect. C*, **1998**, 54, 732.

Youngme S., van Aldaba G.A., Chaichit, N., Gunnasoot P., Kongsaeree P., Mutikainen I., Roubeau O., Reedijk J. and Turpeinen U., *Inorg. Chim. Acta*, **2003**, 353, 119.

Wang S.-L., Richardson J.W., Briggs S.J., Jacobson R.A. and Jensen W.P., *Inorg. Chim. Acta*, **1986**, 111, 67.

CHAPTER V.

From 1D to 3D networks: the use of a ligand to control the crystal structure.

Introduction

The interest in the design of supramolecular coordination networks has permanently increased during the last decade [Batten S.R. *et al.*, 1998; Robson R. *et al.*, 2000; Yaghi O.M. *et al.*, 1998; Hagrman P.J. *et al.*, 1999; O'Keeffe M. *et al.*, 2000; Braga D., 2000]. At this respect, the concept of molecular building block or tecton [O'Keeffe M. *et al.*, 2000], in the context of supramolecular synthesis [Lehn J.-M., 1995], afforded a large number of new coordination topologies with different metrics. The control of the network parameters through a careful selection of the metallic ion and the organic bridging ligands offers new possibilities for developing new functional materials with useful properties. Open framework structures promise catalysts with extra productivity that take advantage of the crystallinity [Fujita M. *et al*, 1994a], selective and/or reversible adsorbents, materials possessing new properties due to the incorporation in the tight pores with sides acting as scaffolds [Hagrman P.J. *et al.*, 1999], and acentric inclusion compounds that may exhibit useful electrical and optical features [Denti G. *et al.*, 1992]. Other interesting aspects of these networks are provided by factors such as their anisotropy or assembly [Garcia Y. *et al.*, 1999; Tangouolis V. *et al.*, 2000].

Polydentate N- or O-donor ligands are suitable examples of the tectons that are currently employed for the rational design of solid state functionality. The metal assembling into predictable multidimensional structures becomes easier having in mind the structural simplicity and well known coordination modes of these ligands. The control of the metrics of the resulting net arrays and their inherent properties by careful tuning the tecton structure, donor properties and mutual spatial alignment of binding sites, seems very attractive. In this context, novel perspectives for the design of coordination polymers may be offered by molecules that have the structural simplicity of the above ligands and special properties such as the ability to form coordination polymers both in neutral and anionic forms and to serve as efficient donors of hydrogen bonds for the effective control of the counter ion position and the enclathration of hydrophilic guest species.

In our recent works, an increasing attention has been paid to the construction of two- (2D) or three-dimensional (3D) magnetic systems in order to gain a better understanding of the correlation between structure and magnetism [Rodríguez-Martín

Y. *et al.*, 2002; Ruiz-Pérez C. *et al.*, 2003; Pasán J. *et al.*, 2003]. A suitable strategy to build a spatial well-spanned framework, is to use certain features of potential ligands, such as the conformational flexibility, diversity of binding modes, and ability to form hydrogen bonds. In this regard, malonate (mal) and 1,2-bis(4-pyridyl)ethylene (bpe) can be used as useful connectors to assemble paramagnetic centers into high-dimensional molecular arrangements.

The malonate ligand can form multidimensional compounds owing to its multi-binding ability with regard to metal ions [Rodríguez-Martín Y. *et al.*, 2002; Ruiz-Pérez C. *et al.*, 2003; Pasán J. *et al.*, 2003]. Concerning the bpe ligand, it has a broad relevance in the construction of the solid-state architectures and crystal engineering [Fujita M. *et al.*, 1994b; Real J.A. *et al.*, 1995; Hennigar T.L. *et al.*, 1997] due to its conformational flexibility and coordinating and hydrogen bonding abilities.

Hydrogen bonding, which is the important directional interaction responsible for the supramolecular arrangement and the significant factor in crystal engineering [Lehn J.-M., 1990; Palmans A.R.A. *et al.*, 1997], has a drawback in the field of molecular magnetism since hydrogen-bonded systems cannot provide enhanced magnetic interactions to the extent that covalent-bonded systems do. Therefore, the preparation of purely covalent-bonded high-dimensional systems is particularly crucial in the field of molecule-based magnets and the coupled use of types of bridging ligands seems to be a reasonable synthetic strategy, but examples still remain scarce [De Munno G. *et al.*, 1996]. In addition, the transformation of noncovalent/covalent systems to high-dimensional covalent systems has not been thoroughly investigated. Thus, we explored these two aspects employing the appropriate combinations of the mal and N-ligands and the hydrogen bonds to prepare new magnetically coupled systems with blended bridges.

Experimental

Materials and methods

Malonic acid, basic copper(II) carbonate [$CuCO_3 \cdot Cu(OH)_2$], 1,2-bis(4-pyridyl)ethylene, 2,3-bis(2-pyridyl)pyrazine, diethylenetriamine, 4,4'-bipyridine-N,N'-dioxide were purchased from Aldrich and used as received. Elemental analyses (C, H, N) were carried out using an EA 1108 CHNS-O elemental analyzer. Variable temperature (1.8-300 K) magnetic susceptibility measurements of crushed crystals of compound **1-6** out in a Quantum Design SQUID magnetometer operating at 100 G (**1** and **6**), 250 G (**2**) 500 G (**3** and **5**) and 1000 G (**4**) (T < 20) and at 1000 G (**1**, **4, 6**) or 10000 G (**2**, **3**, **5**) (T > 20) for **1** and **6**. Diamagnetic corrections of all the constituent atoms were estimated from Pascal's constants [Earshaw A., 1968] as -259×10^{-6}, -298×10^{-6}, -282×10^{-6}, -165×10^{-6}, 130×10^{-6} and -319×10^{-6} $cm^3\ mol^{-1}$ for **1-6**, respectively. Magnetic susceptibility data were also corrected for the temperature-independent paramagnetism [60×10^{-6} $cm^3\ mol^{-1}$ per copper(II) ion] and the magnetization of the sample holder.

Synthesis

$\{(H_2bpe)[Cu(mal)_2]\}_n \cdot 4nH_2O$ (1). Basic copper(II) carbonate (0.221 g, 1 mmol) is allowed to react with malonic acid (0.208 g, 2 mmol) in water (10 cm^3) to give an aqueous solution of copper(II) malonate. An ethanolic solution (20 cm^3) of bpe (0.364 g, 2 mmol) was mixed with an aqueous solution (10 cm^3) of malonic acid (0.208 g, 2 mmol) affording a colorless solution. The copper(II) malonate solution was transferred into a tube and then the colorless one was added dropwise. The white solid that was formed at the interface of both solutions redissolved after two days leading to a sky blue solution. Large rhombic pale blue single crystals of **1** were formed after a week. (Found: C, 41.4; H, 4.4; N, 6.4; calcd for $C_{18}H_{24}N_2O_{12}Cu$: C, 41.25; H, 4.58; N, 5.35%).

$[Cu_2(dpp)(mal)_2(H_2O)_2]_n \cdot 7nH_2O$ (2) [dpp = 2,3-bis(2-pyridyl)pyrazine]. Solid copper(II) basic carbonate (28 mg, 0.125 mmol) is allowed to react with malonic acid (26 mg, 0.25 mmol) in water (5 cm^3). This suspension is heated at 40-50 ºC, during one hour, under continuous stirring and then it is mixed with a solution of dpp (23 mg, 0.1 mmol) in a 1:1 H_2O:EtOH solution (5 cm^3). The dark green solution which results of the mixture is filtered and allowed to evaporate at room temperature. Single crystals of **2** as

green prisms were obtained within a week. (Found: C, 31.60; H, 4.15; N 7.20; calc. for $C_{20}H_{32}Cu_2N_4O_{17}$: C, 32.99; H, 4.40; N, 7.70%).

{[Cu(mal)$_2$(H$_2$O)$_2$][Cu(dien)]}$_n$·4nH$_2$O (3) [dien = diethylenetriamine]. Solid copper(II) basic carbonate (55 mg, 0.25 mmol) is added to an aqueous solution (15 cm^3) of malonic acid (52 mg, 0.5 mmol) under continuous stirring. The suspension is heated at 40-50 ºC, until a blue solution is obtained. This solution is filtered and mixed with dien (21 mg, 0.5 mmol) in EtOH (5 cm^3). Single crystals of **3** as pale blue prisms were grown from the solution by slow evaporation at room temperature within a week. (Found: C, 22.12; H, 4.71; N, 7.48;calc. for $C_{10}H_{29}Cu_2N_3O_{14}$: C, 22.12; H, 5.35; N, 7.74%).

[Cu(mal)(dpo)(H$_2$O)]$_n$ (4) [dpo = 4,4'-bipyridine-N,N'-dioxide]. Compound **4** is obtained by the same procedure as **3** using dpo (94 mg, 0.5 mmols) instead of dien. Single crystals suitable for X-ray diffraction as blue prisms were obtained by slow evaporation at room temperature within a week. (Found: C, 37.44; H, 3.26; N, 7.37;calc. for $C_{13}H_{12}CuN_2O_7$: C, 41.96; H, 3.23; N, 7.53%).

[Cu(mal)(bpe)$_{1/2}$(H$_2$O)]$_n$·nH$_2$O (5). Green rectangular crystals of **5** were grown by slow diffusion in an H-tube of an aqueous solution of copper(II) and malonic acid [1:1 molar ratio, 1 mmol of Cu(II)] in one arm and an ethanol/water (50:50 v/v) mixture containing bpe (1 mmol) in the other one. Blue rectangular crystals of **6** were also obtained. Crystals of **5** were collected and air dried and used for all measurements. (Found: C, 37.16; H, 3.80, N, 4.60; calc. for $C_9H_{11}NO_6Cu$: C, 36.89; H, 3.76; N, 4.78%).

[Cu$_4$(mal)$_4$(bpe)$_3$]$_n$·6nH$_2$O (6). Blue rectangular crystals of **6** were obtained together with the crystals of **5** following the same procedure described above. They were collected and air dried and used for all measurements. (Found: C, 43.9; H, 3.7, N, 6.4; calc. for $C_{24}H_{25}N_3O_{11}Cu_2$: C, 43.7; H, 3.8; N, 6.4%).

Crystal data collection and refinement

Suitable single crystals of compounds **1**-**5** were mounted on a Bruker Smart CCD diffractometer, whereas compound **6** was mounted on an Enraf-Nonius MACH3 diffractometer. For compounds **1**-**5**, orientation matrix and lattice parameters were obtained by least-squares refinement of the reflections obtained by a θ-χ scan (Dirax/lsq

method). For compound **6**, orientation matrix and lattice parameters were obtained by least-squares refinement of the diffraction data of 25 reflexions in the range $6 < \theta < 18^{\circ}$ [CAD4-EXPRESS, version 5.1/1.2, 1994; Harms K., 1996]. Diffraction data were collected at 293(2) K (**1**, **2a**, **3-6**) and at 100(2) (**2b**) using graphite-monochromated Mo-K_α radiation (λ = 0.71073 Å). Data collection and data reduction were done with the COLLECT [Hooft R.W.W., 1999] and EVALCCD [Duisenberg A.J.M., *et al.*, 2003] programs for compounds **1-5**, whereas for compound **6** data were collected using the ω-scan technique. Empirical absorption corrections were carried out using SADABS [SADABS, version 2.03, 2003] for compounds **1-5** whereas intensity data were corrected for Lorentz and polarization effects but not for absorption for compound **6**. The indexes of data collection were $-6 \le h \le 6$, $-13 \le k \le 12$, $-16 \le l \le 13$ for **1**; $-9 \le h \le 10$, $-14 \le k \le 16$, $-24 \le l \le 23$ for **2a**; $-9 \le h \le 9$, $-15 \le k \le 15$, $-22 \le l \le 22$ for **2b**; $-10 \le h \le 6$, $-22 \le k \le 24$, $-11 \le l \le 10$ for **3**; $-17 \le h \le 18$, $-14 \le k \le 14$, $-28 \le l \le 17$ for **4**; $-7 \le h \le 5$, $-28 \le k \le 31$, $-12 \le l \le 12$ for **5** and $-18 \le h \le 0$, $0 \le k \le -14$, $-26 \le l \le 27$ for **6**. Of the 4804 (**1**), 7950 (**2a**), 6414 (**2b**), 4804 (**3**), 3687 (**4**), 3037 (**5**), 7606 (**6**) measured independent reflections in the θ range 2.18 – 30.56º (**1**), 6.43 - 30º (**2a**), 4.51 – 27.50º (**2b**), 6.42 – 30.13º (**3**), 5.05 – 29.98º (**4**), 6.41 – 30.00º (**5**) and 2.53 - 29.99º (**6**), 3043 (**1**), 4815 (**2a**), 3858 (**2b**), 3662 (**3**), 2872 (**4**), 2021 (**5**) and 5860 (**6**) have $I \ge 2\sigma(I)$. All the measured independent reflections were used in the analysis. All calculations for data reduction, structure solution, and refinement were done by standard procedures (WINGX) [Farrugia L.J., 1999]. The structure was solved by direct methods and refined with full-matrix least-squares technique on F^2 using the SHELXS-97 and SHELXL-97 programs [Sheldrick, G.M. SHELX97, realease 97-2, 1998]. The malonate and water hydrogen atoms were located, for compounds **1, 3** and **6** from difference Fourier maps. For compounds **2** and **4-5,** the water hydrogen bonds were not found and pyridyl and malonate hydrogen atoms were set in calculated positions. For all compounds hydrogen atoms were refined with isotropic temperature factors. The final Fourier-difference map showed maximum and minimum height peaks of 0.375 and -0.328 e $Å^{-3}$ (**1**), 0.753 and -0.710 (**2a**), 2.487 and -1.060 e $Å^{-3}$ (**2b**), 0.565 and -0.479 e $Å^{-3}$ (**3**), 0.831 and -0.504 e $Å^{-3}$ (**4**) 0.521 and -0.657 e $Å^{-3}$ (**5**) and 1.492 and -2.412 e $Å^{-3}$ (**6**). A summary of the crystallographic data and structure refinement is given in Table 1. The final geometrical calculations and the graphical manipulations were carried out with PARST97 [Nardelli M., 1995] and DIAMOND [DIAMOND 2.1d, 2000] programs, respectively.

Table 1. Crystal data and details of structure determination for compounds **1**-**6**.

Compound	**1**	**2a**	**2b**	**3**	**4**	**5**	**6**
Formula	$C_{18}H_{24}CuN_2O_{12}$	$C_{20}H_{32}Cu_2N_4O_{17}$	$C_{20}H_{32}Cu_2N_4O_{17}$	$C_{10}H_{29}Cu_2N_3O_{14}$	$C_{13}H_{12}CuN_2O_7$	$C_9H_{11}CuNO_6$	$C_{24}H_{25}Cu_2N_3O_{11}$
M	523.9	727.58	727.58	542.44	371.79	292.73	658.5
Crystal system	triclinic	triclinic	triclinic	monoclinic	monoclinic	monoclinic	monoclinic
Space group	*P*-1	*P*-1	*P*-1	*P*21	*C*2/*c*	*P*21/n	*P*21/n
a, Å	4.8831(10)	7.2818(4)	7.1753(10)	7.2175(10)	12.918(3)	5.3547(3)	13.462(3)
b, Å	9.585(2)	11.8131(12)	11.863(3)	17.536(2)	10.348(2)	22.517(2)	10.275(5)
c, Å	11.813(2)	17.4336(13)	17.239(6)	7.9630(10)	20.404(4)	9.1684(11)	19.579(4)
α, deg	77.29(3)	74.128(8)	74.82(2)	-	-	-	-
β, deg	82.18(3)	82.298(6)	82.882(14)	96.224(10)	108.09(3)	101.346(7)	105.21
γ, deg	84.92(3)	86.668(6)	88.09(2)	-	-	-	-
V, Å^3	533.4(2)	1429.4(2)	1405.2(7)	1001.9(2)	2592.7(9)	1083.9(2)	2613.3(10)
Z	1	2	2	2	8	4	4
T, K	293(2)	293(2)	100(2)	293(2)	293(2)	293(2)	293(2)
ρ_{calc} (Mg m^{-3})	1.6312	1.691	1.720	1.798	1.729	1.794	1.6636
F(000)	271	748	748	560	1512	596	1344
λ (Mo-Kα Å)	0.71073	0.71070	0.71070	0.71073	0.71073	0.71073	0.71073
μ (MoK$_\alpha$) (mm^{-1})	1.093	1.573	1.600	2.197	1.905	2.032	1.694
Flack Parameter	0.057(5)	-	-	0.54(3)	-	-	-
Number parameters/restraints	179 / 0	388 / 0	388 / 0	263 / 1	256 / 0	192 / 0	437 / 0
Goodness of fit (*S*)	1.094	1.030	1.043	1.044	1.100	0.975	1.045
R1, $I > 2\sigma(I)$ (all)	0.0281 (0.0293)	0.0494 (0.1052)	0.0768 (0.1469)	0.0423 (0.0644)	0.398 (0.0624)	0.0427 (0.0788)	0.0548 (0.0794)
wR2, $I > 2s(I)$ (all)	0.0780 (0.0791)	0.1212 (0.1420)	0.1416 (0.1688)	0.0984 (0.1076)	0.792 (0.0858)	0.0933 (0.1014)	0.1438 (0.1576)
Max/min electron density (e/Å^3)	0.375 / -0.328	0.753 / -0.710	2.487* / -1.060	0.565 / -0.479	0.831 / -0.504	0.521 / -0.657	1.492 / -2.412
Measured reflections (R_{int})	4488 (0.0180)	16204 (0.0351)	25864 (0.0892)	6152 (0.0270)	11416 (0.0338)	7555 (0.0526)	7899 (0.0707)
Independent reflections [$I > 2\sigma(I)$]	3177 (1459)	7950 (4815)	6414 (3858)	4804 (3662)	3687 (2872)	3037 (2021)	7606 (5860)

*Maximum diffraction density at 1.95Å from O(8w). Although we tried to refine this density as a solvent molecule not good refinement was obtained.

Results and discussion

Description of the structure of $\{(H_2bpe)[Cu(mal)_2]\}_n \cdot 4nH_2O$ (1).

The structure of complex **1** is made up of $[Cu(mal)_2]^{2-}$ anions, H_2bpe^{2+} cations and crystallization water molecules (Figure 1). The anionic units are linked through axial copper to carboxylate-oxygen bonds leading to uniform copper(II) chains which run parallel to the *a*-axis (Figure 2). Each chain is weakly interconnected through hydrogen bonds involving non-coordinated water molecules [2.833(3) and 2.725(3) Å for O(1w)···O(2w) and O(2w)···O(1wb), respectively; (b) *x-1*, *y*, *z*], malonate oxygen atoms [2.847(3) and 2.787(2) Å for O(1w)···O(3) and O(2w)···O(3d), respectively; (d) *-x+1*, *-y+1*, *-z*] and protonated-bpe nitrogen atoms [2.669(2) Å for O(4e)···N(1); (e) *-x*, *-y*, *-z+1*]. Selected bond lengths and angles for **1** are listed in Table 2.

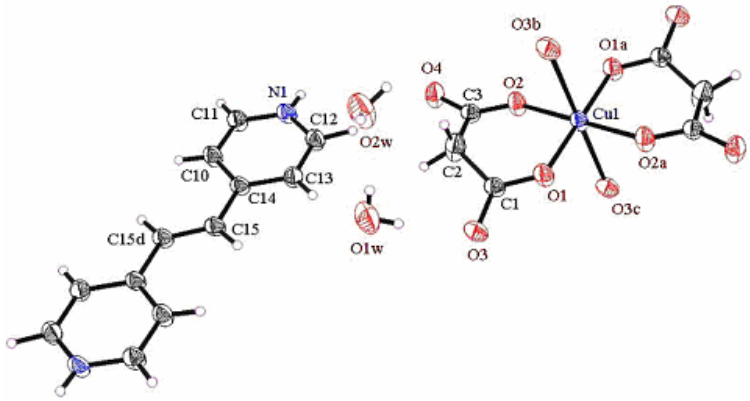

Figure 1. Perspective view of the $[Cu(mal)_2]^{2-}$ and H_2bpe^{2+} units of compound **1** with the atom numbering. Thermal ellipsoids are drawn at the 50% probability level.

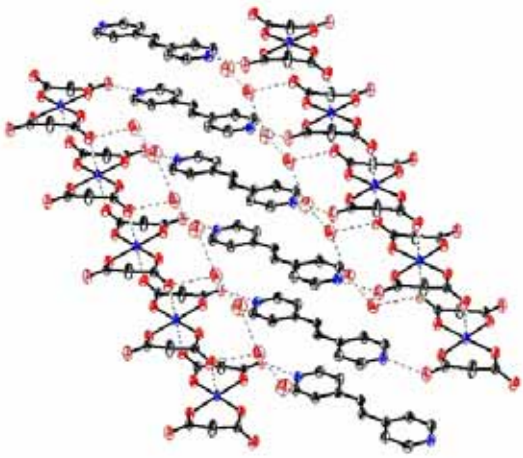

Figure 2. A view of the arrangement of the malonato-copper(II) chains and H_2bpe^{2+} units of **1** along the *a*-axis. Hydrogen bonds are illustrated by broken lines.

Table 2. Selected bond lenghts (Å) and angles (º) and hydrogen bonds for **1**[a,b]

Copper coordination sphere			
Cu(1)-O(1)	1.9314(11)	Cu(1)-O(2)	1.9367(10)
Cu(1)-O(3b)	2.6107(14)		
O(1)-Cu(1)-O(2)	93.88(5)	O(1)-Cu(1)-O(2a)	86.12(5)
O(1)-Cu(1)-O(3c)	91.25(5)	O(1)-Cu(1)-O(3b)	88.75(5)
O(2)-Cu(1)-O(3c)	93.60(5)	O(2)-Cu(1)-O(3b)	86.40(5)
O(1a)-Cu(1)-O(3c)	88.75(5)		

Hydrogen bonds			
D-H···A	D···A/Å	H···A/Å	D-H···A/º
O(1w)-H(1w1)···O(3)	2.847(3)	2.10(4)	164(3)
O(1w)-H(2w1)···O(2w)	2.833(3)	2.07(3)	169(4)
O(2w)-H(1w2)···O(1wb)	2.725(3)	1.91(3)	173(3)
O(2w)-H(2w2)···O(3d)	2.787(2)	2.14(3)	165(3)
N(1)-H(1N)···O(4e)	2.669(2)	1.884(1)	177.68(10)
C(10)-H(10)···O(2wf)	3.187(2)	2.285(2)	170.88(10)
C(11)-H(11)···O(1g)	3.394(2)	2.505(1)	167.77(9)
C(11)-H(11)···O(2e)	3.084(2)	2.472(1)	125.25(10)
C(12)-H(12)···O(4)	3.381(2)	2.377(1)	170.38(9)
C(13)-H(13)···O(1w)	2.438(2)	2.602(2)	157.85(9)

[a] Symmetry transformations: (a) *-x*, *-y*, *-z*; (b) *x*-1, *y*, *z*; (c) *-x*+1, *-y*, *-z*; (d) *-x*+1, *-y*+1, *-z*; (e) *-x*, *-y*, *-z*+1; (f) *-x*+1, *-y*+1, *-z*+1; (g) *x*, *y*, *z*+1. [b] A = acceptor; D = donor.

The copper(II) atoms are surrounded by six oxygen atoms from four different malonate groups forming an elongated octahedral environment with geometric values ϕ = 53.86º and *s/h* =1.52 (ϕ and *s/h* being the twist angle and compression ratio, respectively) [Stiefel E.I. *et al.*, 1972]. Four coplanar oxygen atoms from two bidentate malonate ligands build the equatorial plane around the copper atom, while the apical positions are filled by two carboxylate oxygen atoms from two neighbouring $[Cu(mal)_2]^{2-}$ units. The mean value of the equatorial Cu-O bond distances is 1.9341(11) Å and the angle subtended at the copper atom by the malonate ligand [O(1)-Cu(1)-O(2)] is 93.88(5)º. These structural parameters are within the range observed in previous malonate-containing copper(II) complexes [see malonate-containing Cu(II) complexes in the Introduction]. The value of the apical Cu-O bond length [2.6107(14) Å for Cu(1)-O(3c)] is significantly longer than the equatorial ones.

Each malonate group acts simultaneously (see Figure 3) as a monodentate [through O(3) towards Cu(1h); (h) *x+1*, *y*, *z*] and bidentate [through O(1) and O(2)

towards Cu(1)] ligand and it exhibits a twist-boat conformation with θ = 82.4(2) and ϕ = 94.5(2)º [Cremer D. *et al.*, 1987]. The values of the bond lengths and angles of the malonate ligand in **1** (see Table 3) well with those of previously observed in other malonate-containing copper(II) complexes [see Introduction].

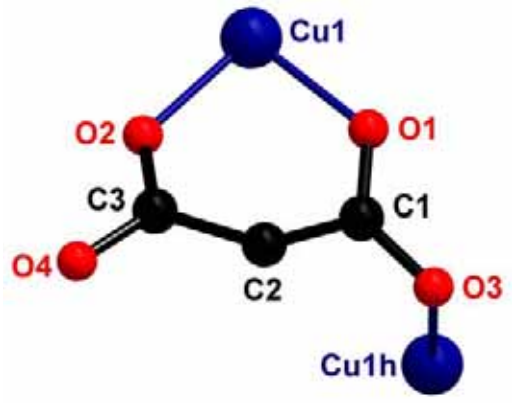

Figure 3. Coordination mode of the malonate ligand in **1**.

Table 3. Bond lengths (Å) and angles (º) for malonate ligands in **1**[a]

C(1)-C(2)	1.512(2)	C(2)-C(3)	1.507(2)
C(1)-O(1)	1.261(2)	C(3)-O(2)	1.260(2)
C(1)-O(3)	1.247(2)	C(3)-O(4)	1.254(2)
O(1)···O(2)	2.826(2)	O(3)···O(4)	4.560(2)
O(1)-C(1)-O(3)	123.37(12)	O(2)-C(3)-O(4)	122.18(11)
O(1)-C(1)-C(2)	120.10(12)	O(2)-C(3)-C(2)	121.21(11)
O(3)-C(1)-C(2)	116.47(13)	O(4)-C(3)-C(2)	116.59(12)
C(1)-C(2)-C(3)	119.95(12)		
C(1)-O(1)-Cu(1)	126.59(8)	C(3)-O(2)-Cu(1)	127.33(9)
C(1)-O(3)-Cu(1h)			
O(1)C(1)O(3)-Cu(1)eq[b]	22.17(11)	O(2)C(3)O(4)-Cu(1)eq[b]	15.48(9)
O(1)C(1)O(3)-Cu(1h)eq[b]	22.17(11)		

[a] Symmetry transformations: (h) *x+1, y, z*.
[b] dihedral angle (º) between the carboxylate-malonate group and the mean equatorial plane of the metal atom.

Within the uniform copper(II) chain, the carboxylate-bridge exhibits the *anti-syn* conformation and it connects an equatorial site of one copper atom with an apical site of the adjacent copper atom. The copper-copper separation through this carboxylate-bridge is 4.8831(10) Å [Cu(1)···Cu(1c); (c) *-x+1, -y, -z*], whereas the shortest interchain copper-copper distances are 9.585(2) [Cu(1)···Cu(1i); (i) *x, y+1, z*] and 11.813(2) Å [Cu(1)···Cu(1j); (j) *x, y, z+1*].

The protonated H_2bpe^{2+} unit is planar and it exhibits the *trans*-conformation. These structural features were previously observed in the free [Vansant, J. *et al.*, 1980]

and coordinated bpe molecules [Hagrman D. *et al.*, 1998a; Hagrman *et al.*, 1998b; Carlucci L. et *al.*, 2000; Lu J.Y. *et al.*, 2001; Zhang H.-X. *et al.*, 2001; Carlucci L. *et al.*, 2001; Visinescu D. *et al.*, 2002a]. Bond lengths and angles of the H_2bpe^{2+} agree well with those reported for the neutral bpe ligand. The H_2bpe^{2+} units are stacked along the *a*-axis in an eclipsed conformation (Figure 4). The value of the distance between planes of adjacent H_2bpe^{2+} units along this direction is 4.8831(10) Å revealing that π–π type interactions are negligible. The bpe ligand in **1** exhibits an eclipsed arrangement along the *a*-axis (Figure 4). This type of stacking is most likely imposed by the protonation of bpe ligand and the extensive hydrogen bonding associated with (see above).

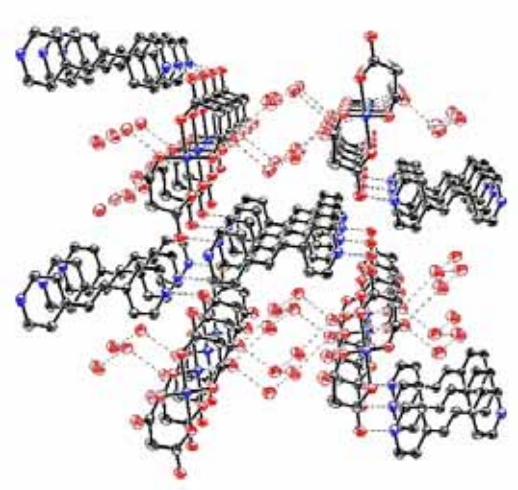

Figure 4. A view of the stacking of malonato-copper(II) chains and H_2bpe^{2+} units of **1** down the *a*-axis.

Description of the structure of $[Cu(dpp)(mal)_2(H_2O)_2]_n \cdot 7nH_2O$ (2)

The structure of **2** is made up of regular alternating zigzag copper(II) chains which run along the [-1 0 1] direction (see Figure 5). These chains are further linked through hydrogen bonds involving water molecules and malonate oxygen atoms that contribute to the crystal packing affording a three-dimensional structure.

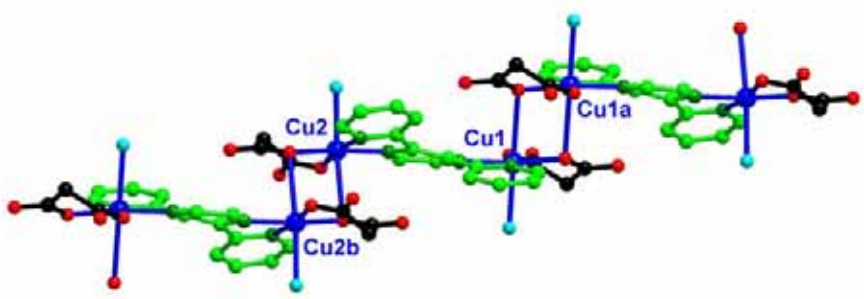

(a)

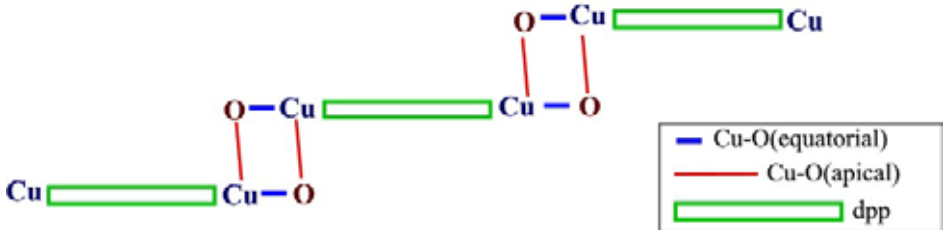

(b)

Figure 5. Perspective **(a)** and schematic **(b)** drawings of the regular alternating zigzag copper(II) chains in **2** which runs along the [-1 0 1] direction. Symmetry transformations: (a) -*x*+1, -*y*+2, -*z*; (b) -*x*, -*y*+2, -*z*+1.

Selected bond lengths and angles for **2** at room temperature (**2a**) and at 100 K (**2b**) are reported in Tables 4 and 5, respectively.

Table 4. Selected bond lenghts (Å) and angles (º) and hydrogen bonds for **2a**[a,b]

Copper coordination sphere			
Cu(1)-O(1)	1.931(2)	Cu(1)-N(11)	2.020(2)
Cu(1)-O(2)	1.904(2)	Cu(1)-N(12)	1.981(3)
Cu(1)-O(1w)	2.471(3)	Cu(1)-O(1a)	2.739(2)
O(1)-Cu(1)-O(2)	94.21(10)	N(11)-Cu(1)-N(12)	80.34(10)
O(1)-Cu(1)-N(11)	171.54(10)	O(2)-Cu(1)-N(11)	91.64(10)
O(1)-Cu(1)-N(12)	93.42(10)	O(2)-Cu(1)-N(12)	171.25(9)
O(1)-Cu(1)-O(1w)	97.83(9)	N(11)-Cu(1)-O(1w)	87.73(9)
O(2)-Cu(1)-O(1w)	95.11(9)	N(12)-Cu(1)-O(1w)	88.09(10)
O(1a)-Cu(1)-O(1)	80.67(8)	O(1a)-Cu(1)-O(2)	93.20(9)
O(1a)-Cu(1)-N(11)	92.91(9)	O(1a)-Cu(1)-N(12)	83.81(9)
O(1w)-Cu(1)-O(1w)	171.65(8)		
Cu(2)-O(31)	1.927(2)	Cu(2)-N(13)	2.015(2)
Cu(2)-O(32)	1.905(2)	Cu(2)-N(14)	1.992(3)
Cu(2)-O(2w)	2.451(3)	Cu(2)-O(31b)	2.810(3)
O(31)-Cu(2)-O(32)	93.62(10)	N(13)-Cu(2)-N(14)	80.44(10)
O(31)-Cu(2)-N(13)	171.61(11)	O(32)-Cu(2)-N(13)	91.81(10)
O(31)-Cu(2)-N(14)	93.49(10)	O(32)-Cu(2)-N(14)	170.45(10)
O(31)-Cu(2)-O(2w)	98.34(10)	N(13)-Cu(2)-O(2w)	87.59(10)
O(32)-Cu(2)-O(2w)	94.47(10)	N(14)-Cu(2)-O(2w)	90.80(10)
O(31b)-Cu(2)-O(31)	81.89(9)	O(31b)-Cu(2)-O(32)	92.86(9)
O(31b)-Cu(2)-N(13)	91.46(9)	O(31b)-Cu(2)-N(14)	81.83(9)
O(2w)-Cu(2)-O(31b)	172.63(8)		

Hydrogen bonds			
D-H···A	D···A/Å	D-H···A	D···A/Å
O(1w)···O(3c)	2.733(3)	O(5w)···O(5wh)	2.799(4)
O(1w)···O(3w)	2.779(5)	O(6w)···O(4)	2.917(4)
O(2w)···O(33d)	2.711(4)	O(6w)···O(5wi)	2.759(5)

O(2w)···O(1we)	2.876(4)	O(7w)···O(34)	2.927(8)
O(3w)···O(6wf)	2.886(7)	O(7w)···O(8w)	2.44(2)
O(3w)···O(8wg)	2.71(2)	O(8w)···O(34)	2.736(15)
O(4w)···O(2w)	3.13(2)	O(8w)···O(4wj)	2.57(2)
O(4w)···O(7wf)	3.015(15)	O(9w)···O(34)	2.798(6)
O(5w)···O(4)	2.784(4)	O(9w)···O(6wj)	2.814(7)

D-H···A	D···A/Å	H···A/Å	D-H···A/º
C(2)-H(1)···O(3w)	3.442(7)	2.643(6)	140.0(3)
C(2)-H(2)···O(5w)	3.405(5)	2.598(3)	140.8(2)
C(32)-H(32)···O(9w)	3.519(7)	2.718(6)	140.3(3)
C(32)-H(31)···O(2w)	3.392(5)	2.739(3)	125.2(3)
C(11)-H(11)···O(8wj)	3.525(15)	2.74(2)	143.2(4)
C(17)-H(17)···O(5wk)	3.431(4)	2.528(2)	163.9(2)
C(20)-H(20)···O(5wa)	3.348(4)	2.689(2)	128.5(2)

[a] Symmetry transformations: (a) -*x*+1, -*y*+2, -*z*; (b) -*x*, -*y*+2, -*z*+1; (c) -*x*+2, -*y*+2, -*z*; (d) -*x*-1, -*y*+2, -*z*+1; (e) *x*-1, *y*, *z*; (f) *x*+1, *y*, *z*; (g) -*x*+1, -*y*+1, -*z*+1; (h) -*x*+2, -*y*+1, -*z*; (i) -*x*+1, -*y*+1, -*z*; (j) -*x*, -*y*+1, -*z*+1; (k) *x*, *y*+1, *z*. [b] A = acceptor; D = donor.

Table 5. Selected bond lenghts (Å) and angles (º) and hydrogen bonds for **2b**[a,b]

Copper coordination sphere			
Cu(1)-O(1)	1.930(4)	Cu(1)-N(11)	2.009(5)
Cu(1)-O(2)	1.913(4)	Cu(1)-N(12)	1.984(5)
Cu(1)-O(1w)	2.425(4)	Cu(1)-O(1a)	2.751(4)
O(1)-Cu(1)-O(2)	94.3(2)	N(11)-Cu(1)-N(12)	80.9(2)
O(1)-Cu(1)-N(11)	171.6(2)	O(2)-Cu(1)-N(11)	91.1(2)
O(1)-Cu(1)-N(12)	93.2(2)	O(2)-Cu(1)-N(12)	170.7(2)
O(1)-Cu(1)-O(1w)	98.11(15)	N(11)-Cu(1)-O(1w)	88.0(2)
O(2)-Cu(1)-O(1w)	94.3(2)	N(12)-Cu(1)-O(1w)	90.2(2)
O(1a)-Cu(1)-O(1)	81.63(14)	O(1a)-Cu(1)-O(2)	93.14(15)
O(1a)-Cu(1)-N(11)	91.6(2)	O(1a)-Cu(1)-N(12)	82.4(2)
O(1a)-Cu(1)-O(1w)	175.52(13)		
Cu(2)-O(31)	1.932(5)	Cu(2)-N(13)	2.010(5)
Cu(2)-O(32)	1.916(6)	Cu(2)-N(14)	1.987(7)
Cu(2)-O(2w)	2.423(5)	Cu(2)-O(31b)	2.810(5)
O(31)-Cu(2)-O(32)	94.0(2)	N(13)-Cu(2)-N(14)	80.9(2)
O(31)-Cu(2)-N(13)	171.7(2)	O(32)-Cu(2)-N(13)	91.2(2)
O(31)-Cu(2)-N(14)	93.2(2)	O(32)-Cu(2)-N(14)	170.2(2)
O(31)-Cu(2)-O(2w)	98.2(2)	N(13)-Cu(2)-O(2w)	87.7(2)
O(32)-Cu(2)-O(2w)	94.7(2)	N(14)-Cu(2)-O(2w)	90.8(2)
O(31b)-Cu(2)-O(31)	83.0(2)	O(31b)-Cu(2)-O(32)	93.4(2)
O(31b)-Cu(2)-N(13)	90.3(2)	O(31b)-Cu(2)-N(14)	81.0(2)
O(31b)-Cu(2)-O(2w)	171.71(15)		

Hydrogen bonds

D-H···A	D···A/Å	D-H···A	D···A/Å
O(1w)···O(3c)	2.703(5)	O(5w)···O(5wg)	2.786(7)
O(1w)···O(3w)	2.798(7)	O(6w)···O(4)	2.872(6)
O(2w)···O(33d)	2.696(9)	O(6w)···O(5wh)	2.773(8)
O(2w)···O(1we)	2.861(7)	O(7w)···O(34)	2.855(12)
O(3w)···O(6wf)	2.808(8)	O(7w)···O(8wi)	2.790(15)
O(3w)···O(8wf)	2.781(11)	O(8w)···O(4w)	2.26(2)
O(4w)···O(2w)	2.75(2)	O(8w)···O(9wj)	2.642(14)
O(4w)···O(7we)	2.765(15)	O(9w)···O(34)	2.756(8)
O(5w)···O(4)	2.763(7)	O(9w)···O(6wi)	2.780(8)

D-H···A	D···A/Å	H···A/Å	D-H···A/º
C(2)-H(1)···O(3w)	3.406(9)	2.604(6)	140.2(4)
C(2)-H(2)···O(5w)	3.344(8)	2.529(5)	141.6(4)
C(32)-H(32)···O(9w)	3.415(11)	2.600(8)	141.7(5)
C(32)-H(31)···O(4w)	3.33(2)	2.51(2)	143.1(5)
C(22)-H(22)···O(8wk)	3.348(15)	2.487(12)	154.0(7)
C(17)-H(17)···O(5wk)	3.407(7)	2.507(4)	163.1(4)
C(20)-H(20)···O(5wa)	3.360(7)	2.695(4)	129.1(4)

[a] Symmetry codes: (a) -*x*+1, -*y*+2, -*z*; (b) -x, -y+2, -z+1; (c)-*x*+2, -*y*+2, -*z*; (d) -*x*-1, -*y*+2, -*z*+1; (e) *x*-1, *y*, *z*; (f) *x*+1, *y*, *z*; (g) -*x*+2, -*y*+1, -*z*; (h) -*x*+1, -*y*+1, -*z*; (i) -*x*, -*y*+1, -*z*+1; (j) -*x*-1, -*y*+1, -*z*+1; (k) *x*, *y*+1, *z*. [b] A = acceptor; D = donor.

Two crystallographically independent copper(II) atoms are present in **2**, both of them being six-coordinated (see Figure 6). They exhibit a distorted 4+1+1 octahedral environment. Each copper atom is bonded to four coplanar atoms [two malonate oxygens and two dpp-nitrogen atoms with average Cu(1)-O and Cu(1)-N bond distances of 1.918(2) and 2.001(3) Å (**2a**) and 1.922(4) and 1.997(3) Å (**2b**) for Cu(1) and 1.916(2) and 2.004(3) Å (**2a**) and 1.924(6) and 1.999(7) (**2b**) for Cu(2), respectively], which build the equatorial plane and two water molecules which fill the apical positions [one short and one long Cu-O(w) bond distances, see Tables 4 and 5]. The equatorial atoms around Cu(2) do not deviate from planarity meanwhile the maximum deviation from planarity around Cu(1) are 0.021(3) (**2a**), 0.012(5) Å (**2b**) for N(11). The metal atoms are shifted by 0.0841(4) (**2a**) and 0.0975(8) Å (**2b**) [Cu(1)] and 0.1031(4) (**2a**) and 0.1044(9) Å (**2b**) [Cu(2)] from the mean equatorial plane towards the short apical position.

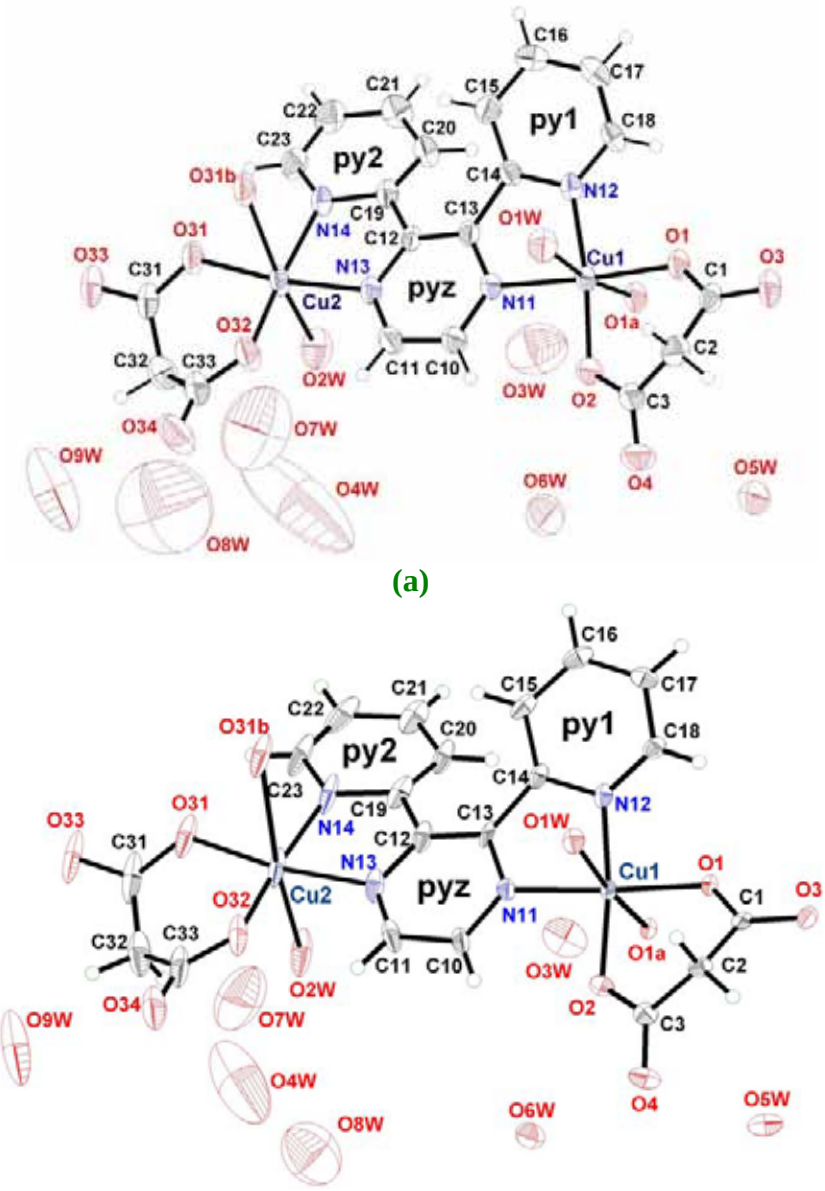

Figure 6. ORTEP view of the metal environments in **2** at room temperature **(a)** and at 100 K **(b)** with the atom numbering. Hydrogen atoms were not labelled for clarity. Thermal ellipsoids are drawn at the 50% probability level. Thermal ellipsoids evidence the occurrence of disordered crystallization water molecules. The measurement at 100K allowed to obtain better results **(b)**.

Two crystallographically independent malonate groups are present in **2** (see Figure 7). Both of them act as monodentate [through O(1) and O(31) towards Cu(1a) and Cu(2b), respectively] and bidentate ligands [through the inner oxygens towards the copper atoms], the angle subtended at the Cu(1) and Cu(2) atoms by the ligands being 94.22(9) and 93.62(10)º (**2a**) and 94.3(2) and 94.0(2)º (**2b**), respectively. Each malonate group forms a six-membered ring including the copper atoms that exhibits a boat conformation, the geometric values being θ = 90.0(3)/89.6(5) and ϕ = 125.3(3)/ 124.2(5)º [mal-Cu(1)] and θ = 91.7(3)/92.1(6) and ϕ = 121.2(3)/121.2(6)º [mal-Cu(2)]

for **2a**/**2b** [Cremer D. *et al.*, 1975]. The values of the bond lengths and angles of the malonate ligand agree well with those previously reported for other malonate-containing copper(II) complexes. Selected bond lengths and angles with other geometrical values are reported in Tables 6 and 7 for compound **2** at room temperature and 100 K, respectively.

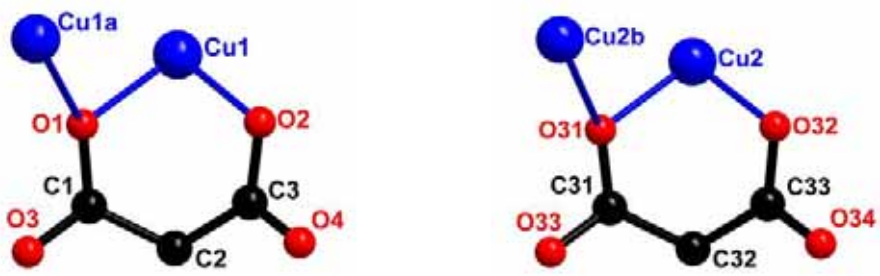

Figure 7. Coordination mode of the malonate ligands in **2**.

Table 6. Bond lengths (Å) and angles (º) for malonate ligands in **2a**[a]

C(1)-C(2)	1.506(5)	C(2)-C(3)	1.517(4)
C(1)-O(1)	1.287(4)	C(3)-O(2)	1.282(4)
C(1)-O(3)	1.231(4)	C(3)-O(4)	1.227(4)
O(1)···O(2)	2.809(3)	O(3)···O(4)	4.334(3)
O(1)-C(1)-O(3)	122.9(3)	O(2)-C(3)-O(4)	121.8(3)
O(1)-C(1)-C(2)	118.8(3)	O(2)-C(3)-C(2)	118.1(3)
O(3)-C(1)-C(2)	118.3(3)	O(4)-C(3)-C(2)	120.2(3)
C(1)-C(2)-C(3)	116.0(3)		
C(1)-O(1)-Cu(1)	122.8(2)	C(3)-O(2)-Cu(1)	123.8(2)
C(1)-O(1)-Cu(1a)	112.2(2)		
O(1)C(1)O(3)-Cu(1)eq[b]	29.0(2)	O(2)C(3)O(4)-Cu(1)eq[b]	29.9(3)
C(31)-C(32)	1.507(5)	C(32)-C(33)	1.511(5)
C(31)-O(31)	1.278(4)	C(33)-O(32)	1.284(4)
C(31)-O(33)	1.234(4)	C(33)-O(34)	1.232(5)
O(31)···O(32)	2.794(4)	O(33)···O(34)	4.351(4)
O(31)-C(31)-O(33)	122.8(4)	O(32)-C(33)-O(34)	121.7(3)
O(31)-C(31)-C(32)	119.2(3)	O(32)-C(33)-C(32)	118.7(3)
O(33)-C(31)-C(32)	117.9(3)	O(34)-C(33)-C(32)	119.6(3)
C(31)-C(32)-C(33)	115.8(3)		
C(31)-O(31)-Cu(2)	122.8(2)	C(33)-O(32)-Cu(2)	123.5(2)
C(31)-O(31)-Cu(2b)	112.8(2)		
O(31)C(31)O(33)-Cu(2)eq[b]	29.1(3)	O(32)C(33)O(34)-Cu(2)eq[b]	29.1(3)

[a] Symmetry transformations: (a) -*x*+1, -*y*+2, -*z*; (b) -*x*, -*y*+2, -*z*+1.
[b] dihedral angle (º) between the carboxylate-malonate group and the mean equatorial plane of the metal atom.

Table 7. Bond lengths (Å) and angles (º) for malonate ligands in **2b**[a]

C(1)-C(2)	1.507(8)	C(2)-C(3)	1.528(8)
C(1)-O(1)	1.287(7)	C(3)-O(2)	1.277(7)
C(1)-O(3)	1.244(7)	C(3)-O(4)	1.239(7)
O(1)···O(2)	2.817(5)	O(3)···O(4)	4.353(6)
O(1)-C(1)-O(3)	123.0(5)	O(2)-C(3)-O(4)	122.0(5)
O(1)-C(1)-C(2)	119.2(5)	O(2)-C(3)-C(2)	118.3(5)
O(3)-C(1)-C(2)	117.8(5)	O(4)-C(3)-C(2)	119.6(5)
C(1)-C(2)-C(3)	115.3(5)		
C(1)-O(1)-Cu(1)	122.7(4)	C(3)-O(2)-Cu(1)	123.6(4)
C(1)-O(1)-Cu(1a)	112.4(3)		
O(1)C(1)O(3)-Cu(1)eq[b]	27.8(4)	O(2)C(3)O(4)-Cu(1)eq[b]	29.1(5)
C(31)-C(32)	1.503(13)	C(32)-C(33)	1.501(11)
C(31)-O(31)	1.292(10)	C(33)-O(32)	1.278(8)
C(31)-O(33)	1.253(9)	C(33)-O(34)	1.236(10)
O(31)···O(32)	2.815(9)	O(33)···O(34)	4.367(10)
O(31)-C(31)-O(33)	121.5(9)	O(32)-C(33)-O(34)	122.0(7)
O(31)-C(31)-C(32)	120.3(7)	O(32)-C(33)-C(32)	119.2(8)
O(33)-C(31)-C(32)	118.2(8)	O(34)-C(33)-C(32)	118.7(7)
C(31)-C(32)-C(33)	116.2(7)		
C(31)-O(31)-Cu(2)	121.6(6)	C(33)-O(32)-Cu(2)	123.5(6)
C(31)-O(31)-Cu(2b)	113.7(4)		
O(1)C(1)O(3)-Cu(2)eq[b]	28.1(6)	O(2)C(3)O(4)-Cu(2)eq[b]	28.5(6)

[a] Symmetry transformations: (a) -*x*+1, -*y*+2, -*z*; (b) -*x*, -*y*+2, -*z*+1.
[b] dihedral angle (º) between the carboxylate- malonate group and the mean equatorial plane of the metal.

The dpp ligand acts as a bis-bidentate ligand [through the pyridyl- and pyrazine-nitrogen atoms at each side], the bite angles being 80.34(10)/80.9(2)º [at Cu(1)] and 80.44(10)/80.9(2)º [at Cu(2)] for **2a**/**2b**. The pyrazine (pyz) and the two pyridyl rings (py1 and py2) are essentially planar whereas the ligand as a whole deviates strongly from planarity. The dihedral angles between the mean pyrazine and pyridyl planes are 23.74(11)/22.1(2)º [py1-pyz], 22.81(10)/23.1(2)º [py2-pyz] and 42.81(11)/41.2(2)º [py1-py2] for **2a**/**2b**. Bond lengths and angles are in good agreement with those reported for the free dpp [Huang N.-T. *et al.*, 1991; Robertson K. N. *et al.*, 1998] and for the dpp-bridged dinuclear copper(II) complexes [Grove H. *et al.*, 2001a and 2001b, Ishida T. *et al.*, 2002; Carranza J. *et al.*, 2004].

Double μ-oxo bridges involving inner carboxylate-malonate oxygens link the {[Cu(mal)(H_2O)]$_2$(dpp)} dinuclear units leading to a regular alternating zigzag

copper(II) chains that grows along the [-1 0 1] direction (see Figure 5). The shortest copper···copper separations within the chain are: 6.7215(7)/6.710(2) Å [Cu(1)···Cu(2)], 3.5975(6)/3.5823(15) Å [Cu(1)···Cu(1a)] and 3.6242(6)/3.599(2) Å [Cu(2)···Cu(2b)] for **2a**/**2b**.

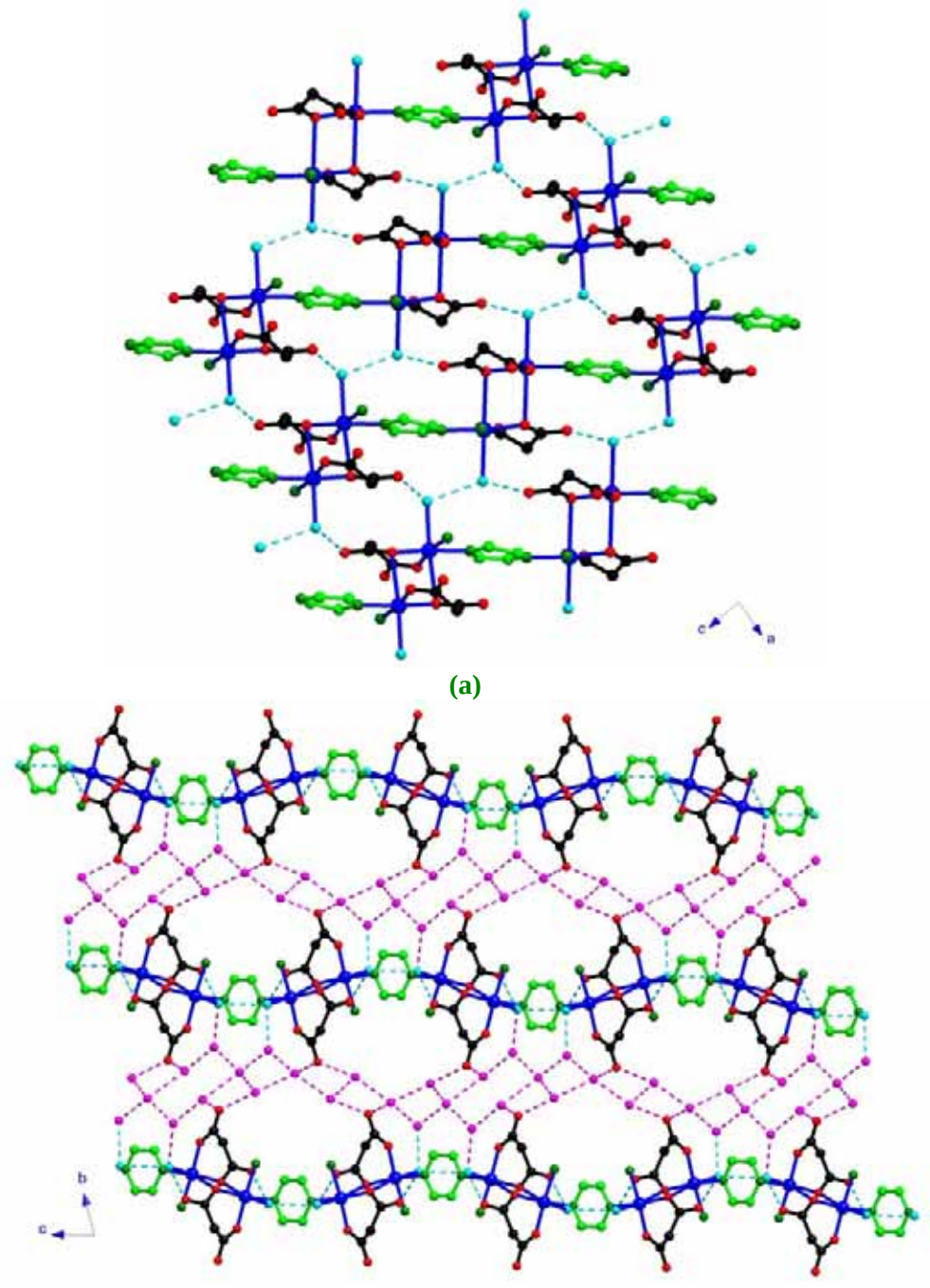

(a)

(b)

Figure 8. (a) Perspective view along the *b*-axis of the sheet-like structure of **2** showing the zigzag chains connected by hydrogen bonds. **(b)** View along the *a*-axis of the layers connected through hydrogen bonds involving crystallization water molecules (pink colour). The py1 and py2 rings of the dpp are skipped for clarity.

The chains are further connected through hydrogen bonds involving coordinated water molecules and malonate-oxygen atoms leading to a sheet-like structure that grows

in the *ac*-plane (see Figure 8a). Additionally, hydrogen bonds involving crystallization water molecules and malonate-oxygen atoms link the layers leading to a three-dimensional network (see Figure 8b).

Description of the structure of $\{[Cu(mal)_2(H_2O)_2][Cu(dien)]\}_n \cdot 4nH_2O$ (3)

The structure of **3** consists of zigzag chains of malonate-bridged copper(II) ions that exhibits a regular alternation of *trans*-diaquabis(malonate)copper(II) and (diethylenetriamine)copper(II) units (see Figure 9), the former units being linked to the latter as a bis-monodentate ligand through two *trans*-malonato oxygen atoms. These chains are further linked through hydrogen bonds involving water molecules and malonate oxygen atoms leading to a three-dimensional structure in which polymeric like layers of malonate-bridged copper(II) chains and water molecules stack alternatively.

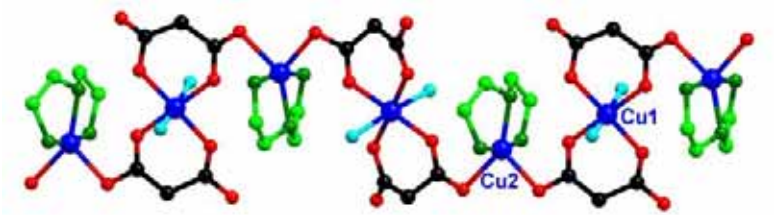

(a)

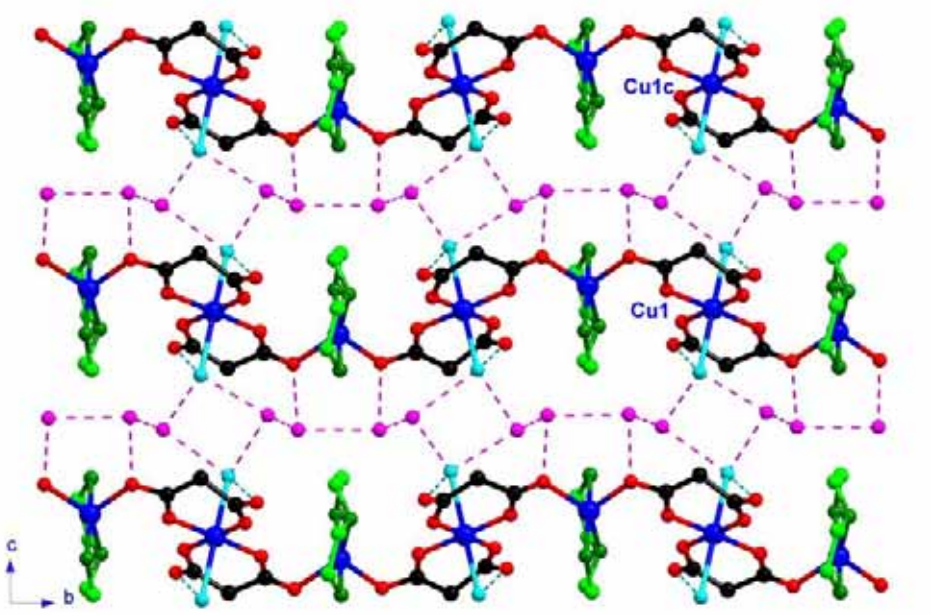

(b)

Figure 9. Perspective view of the malonate-bridged copper(II) chains in **3** **(a)** which are linked through hydrogen bonds involving water molecules, leading to a three-dimensional network **(b)**.

Main bond lengths and angles with the relevant hydrogen bonds are reported in Table 8.

Table 8. Selected bond lenghts (Å) and angles (º) and hydrogen bonds for **3**[a,b]

Copper coordination sphere			
Cu(1)-O(1)	1.941(6)	Cu(1)-O(11)	1.936(5)
Cu(1)-O(2)	1.948(5)	Cu(1)-O(12)	1.935(6)
Cu(1)-O(1w)	2.499(8)	Cu(1)-O(2w)	2.557(8)
O(1)-Cu(1)-O(2)	91.4(3)	O(11)-Cu(1)-O(12)	93.0(2)
O(1)-Cu(1)-O(11)	178.5(4)	O(2)-Cu(1)-O(11)	88.6(2)
O(1)-Cu(1)-O(12)	87.1(2)	O(2)-Cu(1)-O(12)	178.4(3)
O(1)-Cu(1)-O(1w)	94.9(3)	O(11)-Cu(1)-O(1w)	86.6(2)
O(2)-Cu(1)-O(1w)	95.4(3)	O(12)-Cu(1)-O(1w)	84.9(3)
O(1)-Cu(1)-O(2w)	87.2(3)	O(11)-Cu(1)-O(2w)	91.3(2)
O(2)-Cu(1)-O(2w)	87.4(3)	O(12)-Cu(1)-O(2w)	92.4(3)
O(1w)-Cu(1)-O(2w)	176.5(2)		
Cu(2)-O(3)	2.109(7)	Cu(2)-N(21)	1.981(3)
Cu(2)-N(22)	2.003(4)	Cu(2)-N(23)	2.014(4)
Cu(2)-O(13a)	2.202(6)		
O(3)-Cu(2)-N(22)	124.9(2)	N(21)-Cu(2)-N(23)	167.8(2)
O(3)-Cu(2)-N(21)	94.5(3)	N(22)-Cu(2)-N(21)	85.3(2)
O(3)-Cu(2)-N(23)	95.5(3)	N(22)-Cu(2)-N(23)	83.3(2)
O(3)-Cu(2)-O(13a)	91.20(11)	N(21)-Cu(2)-O(13a)	95.5(3)
N(22)-Cu(2)-O(13a)	143.8(2)	N(23)-Cu(2)-O(13a)	91.2(3)

Hydrogen bonds			
D-H···A	D···A/Å	D-H···A	D···A/Å
O(1w)-H···O(4b)	2.725(10)	O(4w)-H···O(4g)	3.067(12)
O(1w)-H···O(6wc)	2.838(10)	O(5w)-H···O(3h)	2.815(9)
O(2w)-H···O(14d)	2.856(9)	O(5w)-H···O(4wh)	2.865(10)
O(2w)-H···O(3w)	2.756(9)	O(5w)-H···O(14)	3.065(11)
O(3w)-H···O(1we)	2.897(9)	O(6w)-H···O(2w)	2.671(10)
O(3w)-H···O(4wf)	2.814(10)	O(6w)-H···O(5w)	2.733(10)
O(4w)-H···O(13a)	2.760(10)		

D-H···A	D···A/Å	H···A/Å	D-H···A/º
C(21)-H(23)···O(2a)	3.428(9)	2.733(7)	130.0(4)
C(21)-H(23)···O(3wa)	3.203(8)	2.631(6)	118.0(4)
C(22)-H(25)···O(2a)	3.311(14)	2.547(6)	135.7(7)
C(22)-H(26)···O(12)	3.366(13)	2.707(5)	125.7(7)
C(23)-H(28)···O(3wi)	3.421(15)	2.790(7)	123.5(5)
C(23)-H(29)···O(6w)	3.59(2)	2.793(7)	140.3(4)
N(21)-H(21)···O(3wa)	3.051(11)	2.304(6)	140.4(4)
N(21)-H(22)···O(6wc)	3.105(11)	2.238(7)	161.6(4)
N(22)-H(17)···O(1)	2.917(7)	2.302(6)	124.7(3)
N(22)-H(17)···O(22)	3.203(7)	2.388(6)	149.1(3)
N(23)-H(32)···O(4j)	3.095(12)	2.207(7)	168.9(5)
N(23)-H(33)···O(14d)	3.423(12)	2.647(6)	145.0(5)

[a] Symmetry codes: (a) -*x*, *y*-1/2, -*z*; (b) *x*-1, *y*, *z*; (c) *x*, *y*, *z*+1; (d) *x*+1, *y*, *z*; (e) *x*, *y*, *z*-1; (f) -*x*+1, *y*+1/2; -*z*; (g) -*x*+1, *y*-1/2, -*z*+1; (h) *x*-1, *y*, *z*-1; (i) -*x*, *y*-1/2, -*z*-1; (j) -*x*+1, *y*-1/2, -*z*. [b] A = acceptor; D = donor.

Two crystallographically independent copper(II) ions occur in **3** (see Figure 10). Cu(1) is six-coordinated and it exhibits a 4+2 distorted octahedral environment with ϕ = 54.16 and s/h = 1.47 (ϕ and s/h being the twist angle and the compression ratio, respectively) [Stiefel E.I. *et al.*, 1972]. Four coplanar oxygen atoms from two different malonate ligands build the equatorial plane around the metallic atom [1.940(6) Å being the average Cu-O bond distance]. Two water molecules occupy the apical positions, 2.499(8) and 2.552(8) Å being the Cu-O(w) bond distances. Cu(1) is shift by 0.016(2) Å from de mean equatorial plane towards O(1w).

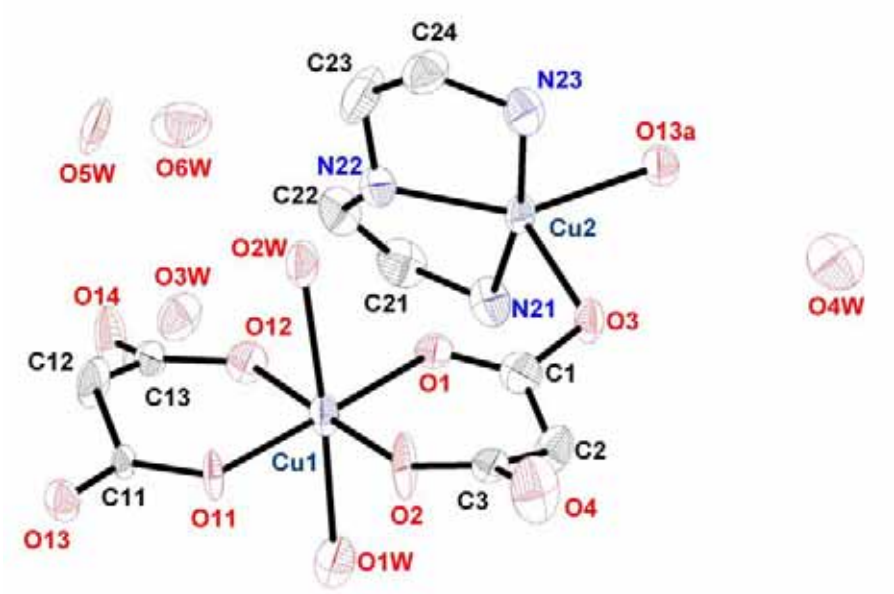

Figure 10. ORTEP view of the metal environments in **3** with the numbering scheme. Thermal ellipsoids are drawn at the 50 % probability level.

Cu(2) exhibits a highly distorted 4+1 square pyramidal environment. Three coplanar nitrogen atoms from the dien ligand [2.000(4) Å for the average Cu-N bond distance] and one malonate oxygen atom O(3) [2.109(7) for the Cu-O bond] build the basal plane around the Cu(2), whereas the apical position is filled by a carboxylate-oxygen atom O(13a) from a malonate ligand [2.202(6) Å for the Cu-O bond distance]. The basal atoms deviate significantly from planarity. There is an alternative description of the Cu(2) environment. Thus, as a distorted trigonal bipyramid where two carboxylate oxygen atoms [O(3) and O(13a)] and one nitrogen atom of the dien ligand, N(22), build the trigonal plane around the metal atom, whereas axial positions are occupied by two N atoms from the dien ligand. In this case, Cu(2) is outside the trigonal plane towards N(23) [the displacement out of plane being 0.0372(4) Å]. The geometry of the CuN_3O_2 environment can be characterized using the τ parameter (square pyramidal and trigonal bipyramidal surroundings correspond to τ = 0 and τ = 1,

respectively) [Addison A.W. *et al.*, 1984]. The calculated value of τ factor for Cu(2) is 0.40, a value that indicates a significant distortion of the square pyramidal environment towards trigonal bipyramidal conformation. Distorted environments (trigonal and square pyramidal) have been previously reported in other dien copper(II) complexes containing carboxylate groups [Stephens F.S., 1969; Davey G. *et al.*, 1971; Curtis N.F. *et al.*, 1973; Julve, M. *et al.*, 1984; Kruger P.E. *et al.*, 1994; Ye B.-H. *et al.*, 1998; Castillo, O. *et al.*, 1999; Patra, G.K. *et al.*, 2000].

Two crystallographically independent malonate groups are present in **3** (see Figure 11): L1 [C(1)C(2)C(3)] and L2 [C(11)C(12)C(13)]. Both of them act simultaneously as bidentate [through O(1), O(2) and through O(11), O(12) towards Cu(1)] and monodentate [through O(3) toward Cu(2) and through O(13) towards Cu(2k); (k) *-x*, *y*+1/2, *-z*] ligand. Both malonate groups describe together with the copper atom a six membered-ring that exhibits a twist-boat [θ= 84.6(9)º and ϕ =106(1)º] and a boat conformation [θ= 83.4(12) and ϕ= 124(1)º], for L1 and L2, respectively [Cremer D. *et al.*, 1975]. Two slightly different carboxylate bridges O(1)C(1)O(3) and O(11)C(11)O(13) which connects two equatorial-equatorial and equatorial-apical sites from adjacent copper atoms alternate regularly within each copper(II) chain, exhibiting the *anti-syn* conformation. The malonate bond lengths and angles with some geometrical features are reported in Table 9. These values agree well with those previously reported for other malonate-containing copper(II) complexes.

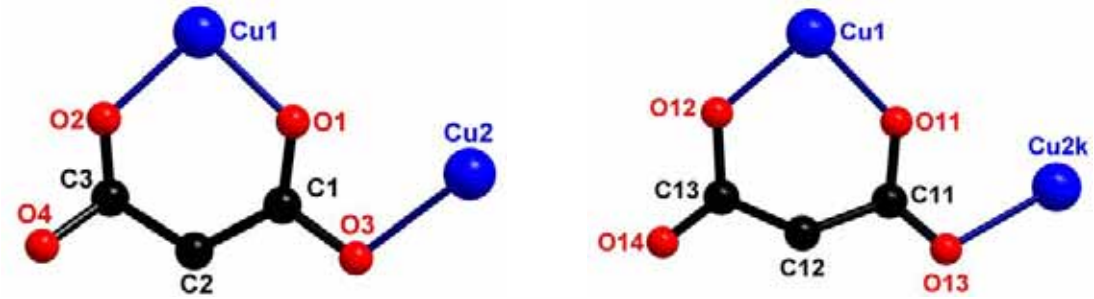

Figure 11. Coordination of the malonate ligands in **3**.

Table 9. Bond lengths (Å) and angles (º) for malonate ligands in **3**[a]

C(1)-C(2)	1.477(13)	C(2)-C(3)	1.543(11)
C(1)-O(1)	1.245(11)	C(3)-O(2)	1.191(10)
C(1)-O(3)	1.362(10)	C(3)-O(4)	1.316(11)
O(1)···O(2)	2.783(8)	O(3)···O(4)	4.647(9)
O(1)-C(1)-O(3)	117.9(8)	O(2)-C(3)-O(4)	121.9(8)
O(1)-C(1)-C(2)	123.8(8)	O(2)-C(3)-C(2)	120.1(8)
O(3)-C(1)-C(2)	118.3(8)	O(4)-C(3)-C(2)	117.4(8)

C(1)-C(2)-C(3)	115.2(7)		
C(1)-O(1)-Cu(1)	125.8(5)	C(3)-O(2)-Cu(1)	128.6(6)
C(1)-O(3)-Cu(2)	109.3(5)		
O(1)C(1)O(3)-Cu(1)eq[b]	21.3(5)	O(2)C(3)O(4)-Cu(1)eq[b]	17.7(8)
O(1)C(1)O(3)-Cu(2)eq[b]	85.9(8)		
C(11)-C(12)	1.549(10)	C(12)-C(13)	1.438(14)
C(11)-O(11)	1.263(8)	C(13)-O(12)	1.335(10)
C(11)-O(13)	1.168(9)	C(13)-O(14)	1.170(12)
O(11)···O(12)	2.807(7)	O(13)···O(14)	4.417(9)
O(11)-C(11)-O(13)	124.0(7)	O(12)-C(13)-O(14)	122.0(10)
O(11)-C(11)-C(12)	118.5(7)	O(12)-C(13)-C(12)	118.9(8)
O(13)-C(11)-C(12)	117.3(7)	O(14)-C(13)-C(12)	119.0(9)
C(11)-C(12)-C(13)	122.6(8)		
C(11)-O(11)-Cu(1)	129.4(5)	C(11)-O(13)-Cu(2k)	108.3(5)
C(13)-O(12)-Cu(1)	127.7(6)		
O(11)C(11)O(13)-Cu(1)eq[b]	13.7(4)	O(12)C(13)O(14)-Cu(1)eq[b]	22.9(8)
O(11)C(11)O(13)-Cu(2k)eq[b]	80.6(7)		

[a] Symmetry transformations: (k) -*x*, *y*-1/2, -*z*.
[b] dihedral angle (º) between the carboxylate- malonate group and the mean equatorial plane of the metal.

Trans-diaquabis(malonate)copper(II) and (diethylenetriamine)copper(II) units, are connected through carboxylate-malonate bridges leading to zigzag chains that run along the *b*-axis (see Figure 9a). The former units are linked to the latter as a bis-monodentate ligands through two *trans*-malonato oxygen atoms. Two different carboxylate bridges alternate within the chain: Cu(1)-O(1)-C(1)-O(3)-Cu(2) (equatorial-equatorial) and Cu(1)-O(11)-C(11)-O(13)-Cu(2k) (equatorial-apical). The dihedral angle between the equatorial planes of adyacent copper atoms are: 87.6(2)º [Cu(1)/Cu(2)] and 72.0(2)º [Cu(1)/Cu(2k)] (see Figure 12). The zigzag chains are further interconnected, along the *a*-axis, through hydrogen bonds involving the coordinated water molecules and carboxylate-malonate oxygen atoms of the adjacent chains affording a sheet like polymeric structure that grows within the *ab*-plane (Figure 12). Additional hydrogen bonds involving the crystallisation water molecules and carboxylate-malonate oxygen atoms contribute to stabilize the resulting three-dimensional network (see Figure 9b).

The two intrachain cooper···copper separations (see Figures 9 and 12)are 4.605(2) [Cu(1)···Cu(2)] and 4.586(2) Å [Cu(1)···Cu(2k); *x*, *y*+1/2, -*z*], whereas the

shortest interchain copper···copper separations are 7.2175(10) [Cu(1)···Cu(1d) and Cu(2)···Cu(2d); (d) *x*+1, *y*, *z*] and 7.963(3) Å [Cu(1)···Cu(1c) and Cu(2)···Cu(2c); (c) *x*, *y*, *z*+1].

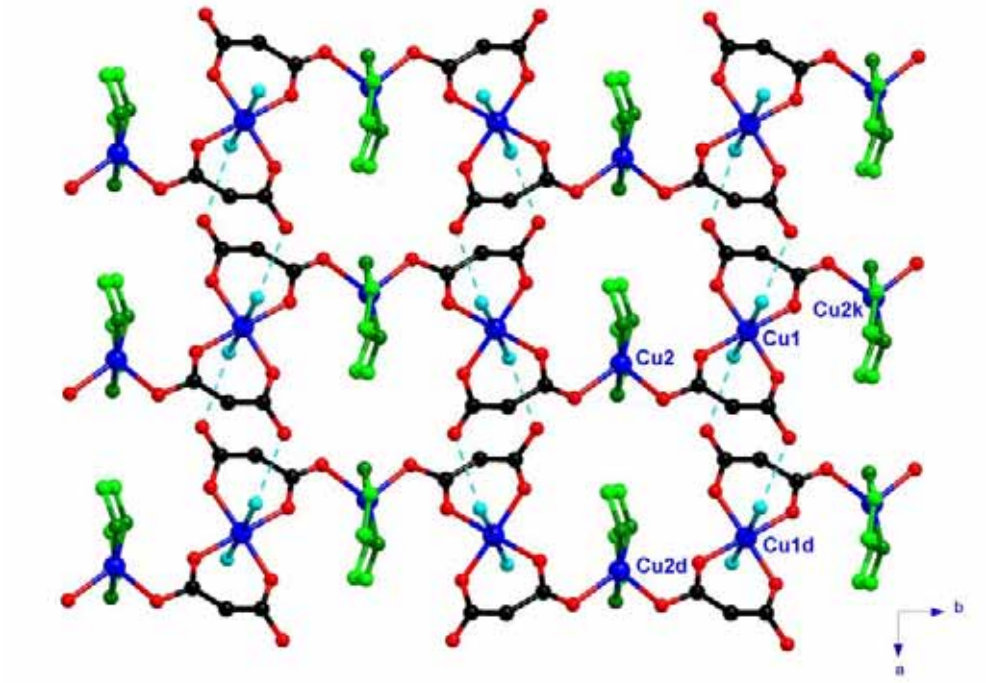

Figure 12. Perspective view, along the *c*-axis, of the zigzag copper(II) chains in **3** linked by hydrogen bonds involving the coordinated water molecules (cyan colour).

Description of the structure of $[Cu(mal)(dpo)(H_2O)]_n$ (4)

Compound **4** is made up of dpo-bridged aquamalonatecopper(II) units affording thus, helical chains which are pairwise through C(dpo)-H···O interactions (orange dashed lines in Figure 13) involving dpo- and malonate-oxygen atoms (see Table 10) to form nanochannels [6.6 x 3.5 Å] that grow along the *b*-axis. These channels are further connected through hydrogen bonds involving malonate-oxygen atoms and water molecules (cyan broken lines in Figure 14) and C(mal)-H···O(mal) (black dashed lines in Figure 14) hydrogen bonds to form a three-dimensional network.

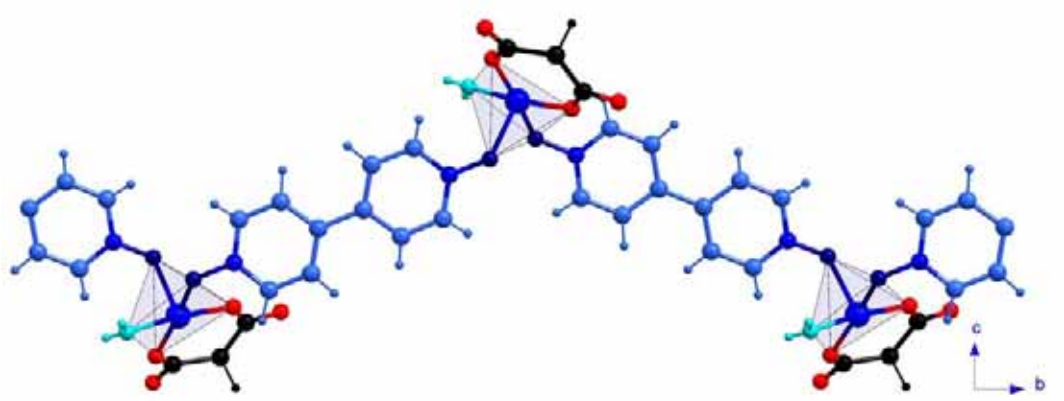

(a)

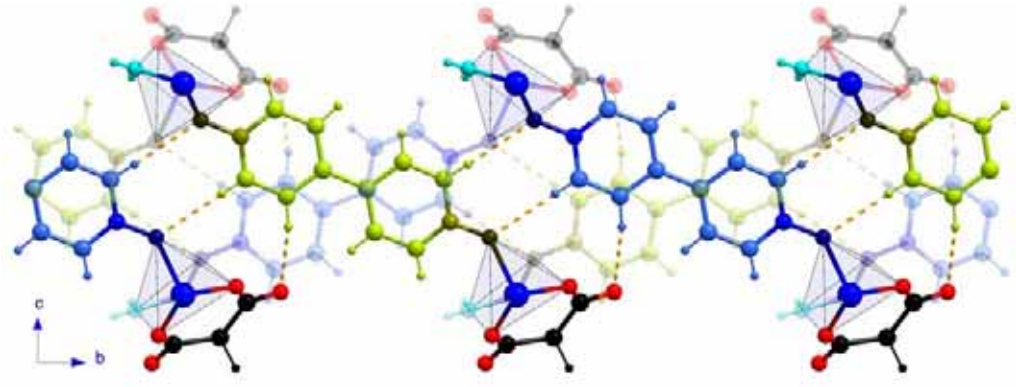

(b)

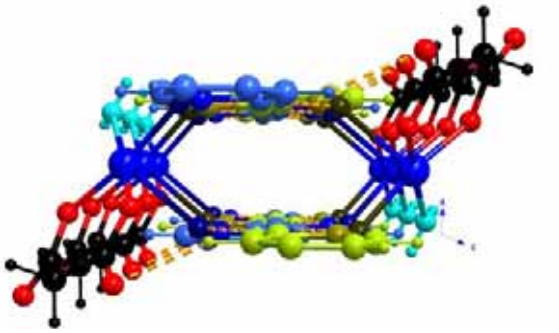

(c)

Figure 13. Perspective view along the *a*-axis **(a, b)** and *b*-axis **(c)** of the dpo-bridged aquamalonatecopper(II) chains **(a)** and nanochannels **(b, c)** in **4**. Orange dashed lines represent C(dpo)-H···O hydrogen bonds. For the sake of clarity only the stronger interactions have been drawn.

Table 10. Selected bond lengths (Å) and angles (º) and relevant hydrogen bonds for **4**[a,b]

Cu(1)-O(1)	1.915(2)	Cu(1)-O(12a)	1.962(2)
Cu(1)-O(2)	1.924(2)	Cu(1)-O(1w)	1.950(2)
Cu(1)-O(11)	2.376(2)		
O(1)-Cu(1)-O(2)	96.01(7)	O(12a)-Cu(1)-O(1w)	83.59(8)
O(1)-Cu(1)-O(12a)	93.60(7)	O(2)-Cu(1)-O(12a)	169.39(7)
O(1)-Cu(1)-O(1w)	169.68(10)	O(2)-Cu(1)-O(1w)	86.16(8)
O(1)-Cu(1)-O(11)	85.73(7)	O(12a)-Cu(1)-O(11)	95.64(8)
O(2)-Cu(1)-O(11)	89.57(8)	O(1w)-Cu(1)-O(11)	104.40(9)

Hydrogen bonds

D-H···A	D···A/Å	H···A/Å	D-H···A/º
O(1w)-H(1w1)···O(3b)	2.768(3)	2.00(4)	166(4)
O(1w)-H(2w1)···O(4c)	2.590(3)	1.86(4)	171(5)
C(2)-H(1)···O(4d)	3.343(4)	2.36(3)	179(3)
C(2)-H(2)···O(1e)	3.484(3)	2.53(3)	144(2)
C(2)-H(2)···O(3e)	3.420(4)	2.59(4)	131(2)
C(10)-H(10)···O(2c)	3.457(3)	2.70(3)	144(2)
C(11)-H(11)···O(12f)	3.362(3)	2.49(3)	174(3)
C(12)-H(12)···O(3g)	3.610(3)	2.70(3)	167(2)

C(16)-H(16)···O(1g)	3.269(3)	2.54(3)	132(2)
C(16)-H(16)···O(3g)	3.228(3)	2.33(2)	155(2)
C(17)-H(17)···O(4h)	3.553(3)	2.71(3)	152(3)
C(18)-H(18)···O(11g)	3.325(3)	2.45(3)	176(2)

[a] Symmetry transformations: (a) -*x*, *y*+1, -*z*+1/2; (b) *x*-1/2, *y*-1/2, *z*; (c) -*x*+1/2, -*y*+3/2, -*z*+1; (d) -*x*+1, -*y*+2, -*z*+1; (e) -*x*+1/2, -*y*+5/2, -*z*+1; (f) *x*, *y*+1, *z*; (g) *x*, *y*-1, *z*; (h) *x*-1/2, -*y*+3/2, *z*-1/2. [b] A = acceptor; D = donor.

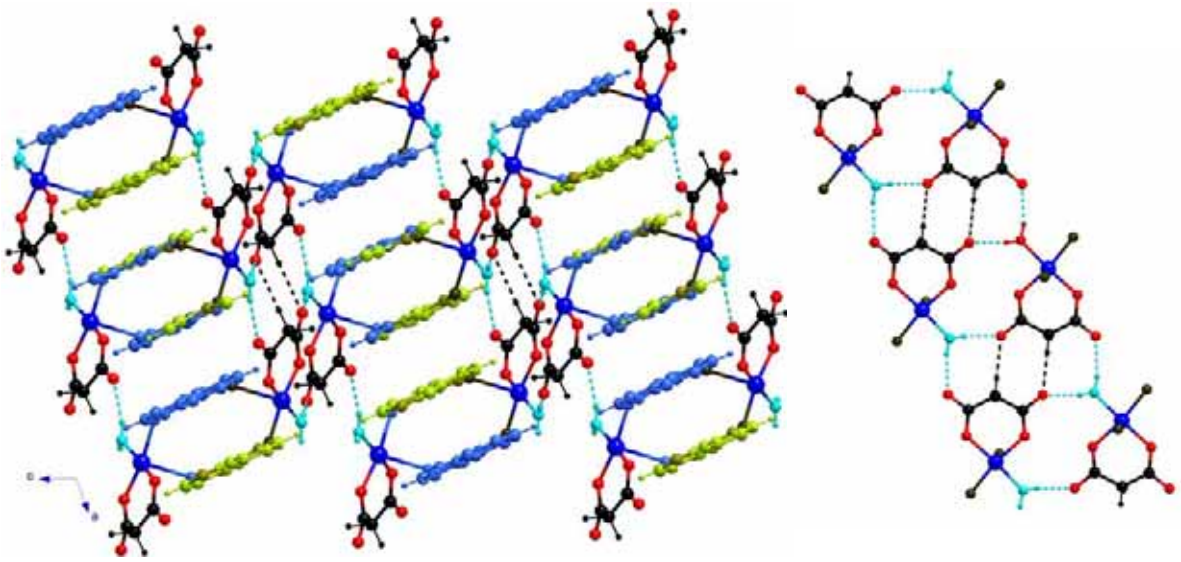

(a) **(b)**

Figure 14. Perspective view along the *b*-axis of the crystal packing in **4** **(a)** with a fragment of the structure **(b)** showing the Ow-H···O (cyan broken lines) and C(mal)-H···O (black dashed lines) hydrogen bonds that connects dpo-bridged copper(II) nanochannels.

Copper(II) is five-coordinated and it exhibits a slightly distorted square pyramidal environment (Figure 15), τ parameter [Addison A.W. *et al.*, 1984] being 0.04. The equatorial plane around the metal atom is formed by two malonate- and one dpo-oxygen atoms and a water molecule [the average Cu-O bond distance being 1.938(2) Å]. Only O(1w) deviates slightly from the mean equatorial plane [0.084(2) Å]. Apical position is occupied by one dpo oxygen atom [2.376(2) Å for the Cu-O(apical) bond length]. The metal atom is shifted by 0.1079 Å from the mean equatorial plane towards the apical position.

The malonate ligand quelates copper atom [through O(1) and O(2)], the angle subtended at the metal atom being 96.01(7)º. With the metal atom the malonate ligand forms a six-membered ring that exhibits a half-chair conformation [θ = 41.6(5) and ϕ = 146.0(1)] [Cremer D. *et al.*, 1975] which is quite unusual in malonate complexes. The malonate bond lengths and angles (see Table 11) agree well with those previously reported in other malonate-containing copper(II) complexes [see Introduction].

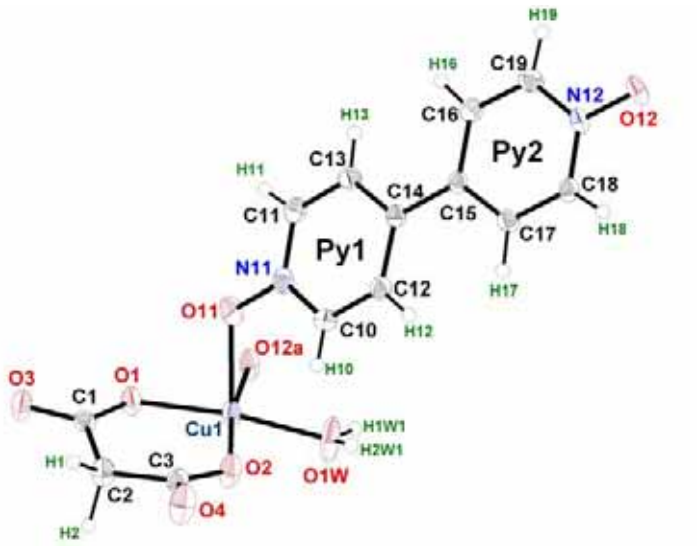

Figure 15. ORTEP view of the copper environment in **4** with the numbering scheme. Thermal ellipsoids are drawn at the 50% probability level.

Table 11. Bond lengths (Å) and angles (º) for the malonate present in **4**[a]

C(1)-C(2)	1.514(3)	C(2)-C(3)	1.511(3)
C(1)-O(1)	1.276(3)	C(3)-O(2)	1.258(3)
C(1)-O(3)	1.243(3)	C(3)-O(4)	1.240(3)
O(1)···O(2)	2.853(2)	O(3)···O(4)	4.603(3)
O(1)-C(1)-O(3)	122.2(2)	O(2)-C(3)-O(4)	123.6(2)
O(1)-C(1)-C(2)	121.0(2)	O(2)-C(3)-C(2)	121.4(2)
O(3)-C(1)-C(2)	116.6(2)	O(4)-C(3)-C(2)	114.7(2)
C(1)-C(2)-C(3)	121.9(2)		
C(1)-O(1)-Cu(1)	127.58(14)	C(3)-O(2)-Cu(1)	126.23(15)
O(1)C(1)O(3)-Cu(1)eq[a]	1.4(2)	O(2)C(3)O(4)-Cu(1)eq[a]	11.7(2)

[a]dihedral angle (º) between the malonate carboxylate group and the mean plane defined by malonate oxygen atoms in the metal environment.

The dpo acts as bis-monodentate [through O(11) and O(12) towards Cu(1) and Cu(1i); (i) -*x*, *y*-1, -*z*+1/2] adopting the *trans* coordination mode (see Figure 13b). The two dpo pyridyl rings are planar but the ligand as a whole deviates from planarity, the dihedral angle between the two pyridyl rings being 8.85(8)º. The dpo bond lengths and angles (listed in Table 12) are in good agreement with those previously reported in the literature for other dpo-containing copper(II) complexes [Plater M. *et al.*, 2000; Ma B.-Q. *et al.*, 2001; Visinescu D. *et al.*, 2002b; Nedelcu A. *et al.*, 2003] and for the free ligand [Thaimattam R. et *al.*, 1998]. It deserves to be note that in the literature the dpo ligand is well known not only for its capacity to coordinate metal atoms but also for acting as a good hydrogen acceptor because of the orientation of the lone pairs at the

oxygen atoms [Nedelcu A. *et al.*, 2003]. Even when the ligand is coordinated to metal atoms, it remains lone pair of electrons that may form hydrogen bonds with neighbouring hydrogen-bond donors. These hydrogen bonding interactions are considerably strong due to the participation of the strongly polarized NO group [Ma B.-Q. *et al.*, 2001]. We have to take into account this features of the dpo ligand in order to understand the crystal packing.

Table 12. Bond lengths (Å) and angles (º) for the dpo ligand in **4**[a]

O(11)-N(11)	1.318(2)	O(12)-N(12)	1.342(2)
N(11)-C(10)	1.356(3)	N(12)-C(18)	1.341(3)
N(11)-C(11)	1.351(3)	N(12)-C(19)	1.345(3)
C(10)-C(12)	1.381(3)	C(18)-C(16)	1.384(3)
C(11)-C(13)	1.371(3)	C(19)-C(17)	1.375(3)
C(12)-C(14)	1.399(3)	C(16)-C(15)	1.392(3)
C(13)-C(14)	1.401(3)	C(17)-C(15)	1.397(3)
C(14)-C(15)	1.481(3)		
O(11)-N(11)-C(10)	120.6(2)	O(12)-N(12)-C(18)	119.3(2)
O(11)-N(11)-C(11)	119.5(2)	O(12)-N(12)-C(19)	119.4(2)
N(11)-C(10)-C(12)	120.4(2)	N(12)-C(18)-C(16)	119.9(2)
N(11)-C(11)-C(13)	121.0(2)	N(12)-C(19)-C(17)	120.3(2)
C(10)-C(12)-C(14)	121.2(2)	C(18)-C(16)-C(15)	121.1(2)
C(10)-N(11)-C(11)	120.0(2)	C(18)-N(12)-C(19)	121.2(2)
C(11)-C(13)-C(14)	121.1(2)	C(19)-C(17)-C(15)	121.0(2)
C(12)-C(14)-C(13)	116.2(2)	C(16)-C(15)-C(17)	116.5(2)
C(12)-C(14)-C(15)	122.7(2)	C(16)-C(15)-C(14)	121.6(2)
C(13)-C(14)-C(15)	121.0(2)	C(17)-C(15)-C(14)	121.9(2)
N(11)-O(11)-Cu(1)	129.54(14)	N(12)-O(12)-Cu(1b)	122.57(12)

[a] Symmetry transformations: (b) *-x*, *y*-1, *-z*+1/2.

Aquamalonatecopper(II) units in **4** are bridged through dpo ligands, leading to helical chains that grow along the *b*-axis [12.267(2) Å for the metal···metal separation through the dpo]. The helical chains are further connected by C(dpo)-H···O hydrogen bonds involving dpo and malonate oxygens (see Figure 13) [2.33(2), 2.45(3) and 2.49(3) Å for H(16)···O(13g), H(18)···O(11g) and H(11)···O(12f); (f) *x*, *y*+1, *z*, (g) *x*, *y*-1, *z*], leading to dpo-bridged copper(II) nanochannels with 6.6 x 3.5 Å size. Within these channels dpo ligands stacked (see Figure 16) in a offset face-to-face paralell fashion [3.44 Å for the separation between the dpo groups] because of the repulsion of the pyridyl ring of adjacent dpo ligands.

Finally, the dpo-bridged channels are further held together by means of O(w)-H···O(mal) and C(mal)-H···O(mal), to form a three-dimensional supramolecular network (see Table 10 and Figures 14 and 15).

Figure 16. Perspective view of the stacking of the dpo groups in **4**. Hydrogen atoms have been skipped for clarity.

Description of the structure of $[Cu(mal)(bpe)_{1/2}(H_2O)]_n \cdot nH_2O$ (5)

The structure of **5** consists of corrugated copper(II) layers made up of aquacopper(II) units that are linked through bpe and malonate groups (see Figure 17a). These layers are further held together by means of hydrogen bonds involving water molecules and malonate oxygens which contribute to the crystal packing and afford a three-dimensional network (Figure 17b).

Looking at the crystal structure of **5**, one can realize that it exhibits a nanoporous structure. The stacking of the corrugated layers allows the formation of channels [9.2x 11.3 Å]. Within these channels, $C_1^1(3)$ water chains [Etter M.C., 1990] are hosted. The water chains are linked to the walls of the channel through H-bonds involving the outer O(3) malonate-oxygen atom (see Figure 17c).

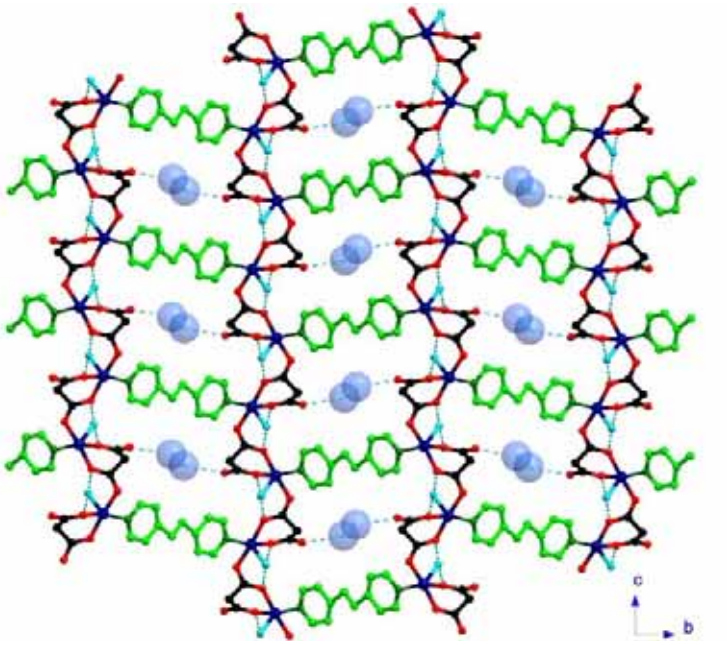

(a)

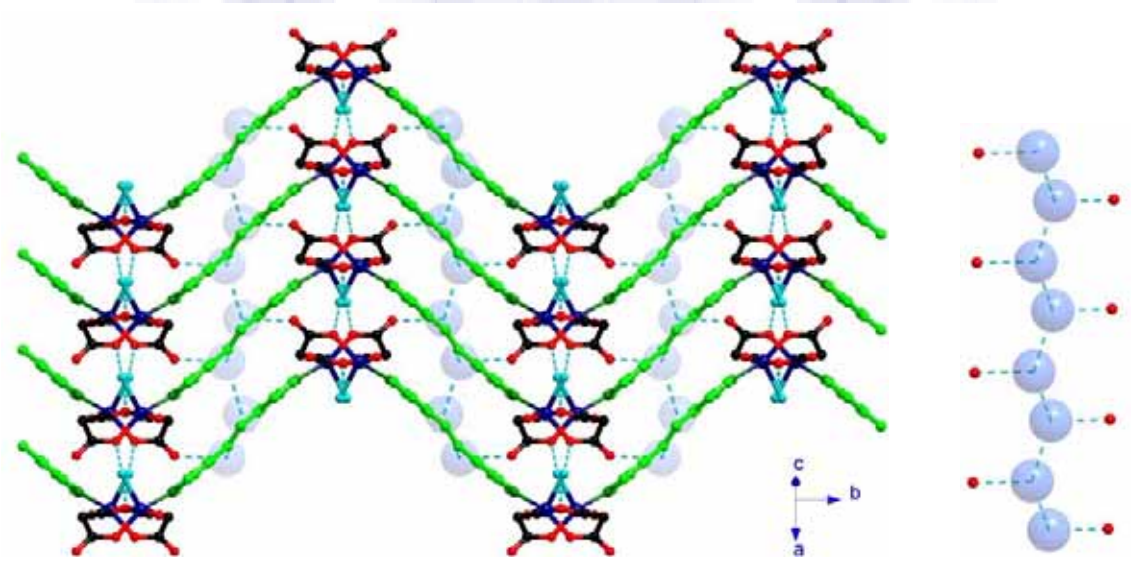

(b) **(c)**

Figure 17. Perspective view, along the *a*-axis, of the aquacopper(II) units linked through malonate and bpe ligands **(a)** and view of the stacking of these layers along the [3/2 0 3/2] direction **(b)** in **5**. **(c)** Perspective view of the water chains in **5** which are linked to the walls of the channels trough hydrogen bonds (broken lines).

Main bond lengths and angles for compound **5** are listed in Table 13.

Table 13. Selected bond lengths (Å) and angles (º) and hydrogen bonds for **5**[a,b]

Cu(1)-O(1)	1.959(2)	Cu(1)-O(4a)	1.946(2)
Cu(1)-O(2)	1.952(2)	Cu(1)-N(1)	2.027(2)
Cu(1)-O(1w)	2.221(2)		
O(1)-Cu(1)-O(2)	88.44(8)	O(4a)-Cu(1)-N(1)	89.43(9)
O(1)-Cu(1)-O(4a)	90.74(8)	O(2)-Cu(1)-O(4a)	173.16(9)
O(1)-Cu(1)-N(1)	161.30(10)	O(2)-Cu(1)-N(1)	89.18(9)
O(1)-Cu(1)-O(1w)	104.77(10)	O(4a)-Cu(1)-O(1w)	93.36(8)
O(2)-Cu(1)-O(1w)	93.41(8)	N(1)-Cu(1)-O(1w)	93.89(9)

Hydrogen bonds

D-H···A	D···A/Å	D-H···A	D···A/Å
O(1w)-H···O(1b)	2.761(3)	O(2w)-H···O(2wd)	2.890(5)
O(1w)-H···O(2c)	3.009(3)	O(2w)-H···O(2we)	2.889(5)
O(2w)-H···O(3)	2.736(4)		

D-H···A	D···A/Å	H···A/Å	D-H···A/º
C(2)-H(1)···O(3b)	3.251(4)	2.59(3)	127(2)
C(10)-H(10)···O(2)	2.842(5)	2.34(4)	124(4)
C(14)-H(14)···O(4c)	2.922(4)	2.46(4)	112(3)

[a] Symmetry transformations: (a) *x*-1/2, -*y*+1/2, *z*-1/2; (b) *x*+1, *y*, *z*; (c) *x*-1/2, -*y*+1/2, *z*-1/2; (d) -*x*, -*y*+1, -*z*+1; (e) -*x*+1, -*y*+1, -*z*+1. [b] A = acceptor; D = donor.

Copper atom in **5** is five-coordinated and it exhibits a distorted square pyramidal environment (see Figure 18), the geometrical τ [Addison A.W. *et al.*, 1984] value being

0.20. Three oxygen atoms from two malonate groups [1.952(2) Å for the average Cu-O bond distance] and one bpe-nitrogen atom [2.027(2) Å for the Cu-N] build the equatorial plane around the metal atom, whereas apical position is filled by a water molecule [the Cu-O(w) bond distance being 2.221(2) Å]. The equatorial atoms deviates from planarity, the maximum deviation from the mean equatorial plane being 0.134(2) Å for N(1). The copper atom is shifted by 0.2050 Å from the mean equatorial plane towards the apical position.

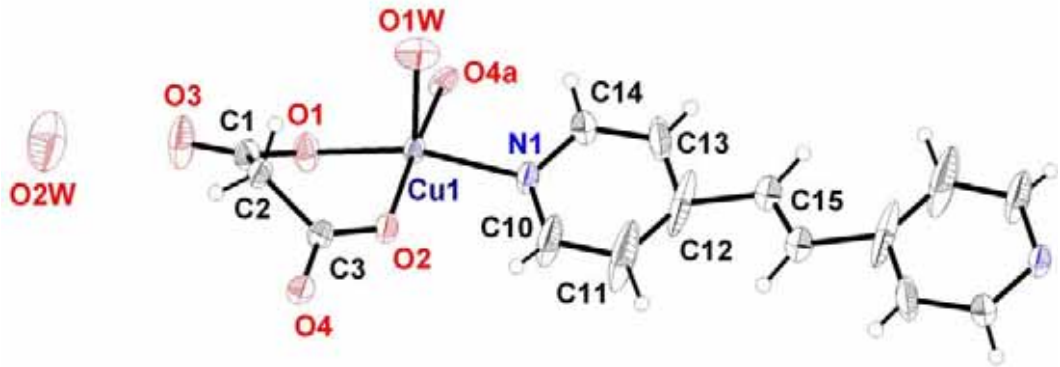

Figure 18. ORTEP drawing of the metal environment in **5**. Thermal ellipsoids are drawn at the 50% probability level.

The malonate group acts simultaneously as bidentate [through O(1) and O(2) towards Cu(1); the bite angle being 88.44(8)º] and monodentate [through O(4) towards Cu(1f); (f) *x*+1/2, -*y*+1/2, *z*+1/2] ligand (see Figure 19). It builds, including the metal atom, a six-membered ring that exhibits a slightly distorted twist-boat conformation [Cremer D. *et al.*, 1975]. The carboxylate group O(4)C(3)O(2) connects two equatorial sites of adjacent copper(II) ions and it exhibits the *anti-syn* conformation. The bond lengths and angles of the malonate ligand in **5** (listed in Table 14) are in good agreement with those of the previously reported malonate-containing copper(II) complexes [see references in the Introduction].

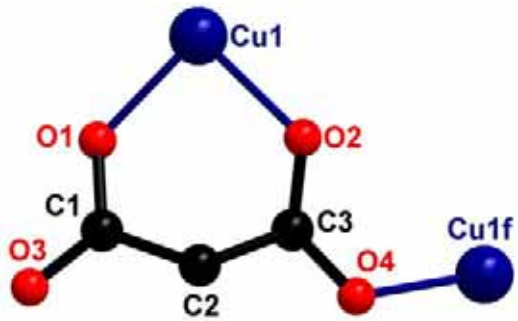

Figure 19. Coordination of the malonate ligand in **5**.

Table 14. Bond lengths (Å) and angles (º) for the malonate present in **5**[a]

C(1)-C(2)	1.511(4)	C(2)-C(3)	1.509(4)
C(1)-O(1)	1.282(4)	C(3)-O(2)	1.257(4)

C(1)-O(3)	1.217(3)	C(3)-O(4)	1.256(3)
O(1)···O(2)	2.727(3)	O(3)···O(4)	4.350(3)
O(1)-C(1)-O(3)	121.8(3)	O(2)-C(3)-O(4)	123.9(3)
O(1)-C(1)-C(2)	118.2(2)	O(2)-C(3)-C(2)	119.5(2)
O(3)-C(1)-C(2)	120.1(3)	O(4)-C(3)-C(2)	116.5(3)
C(1)-C(2)-C(3)	113.9(3)		
C(1)-O(1)-Cu(1)	124.2(2)	C(3)-O(2)-Cu(1)	124.4(2)
C(3)-O(4)-Cu(2f)	126.5(2)		
O(1)C(1)O(3)-Cu(1)eq[a]	31.2(2)	O(2)C(3)O(4)-Cu(1)eq[a]	27.4(2)
O(2)C(3)O(4)-Cu(1f)eq[a]	27.4(2)		

[a]dihedral angle (º) between the malonate carboxylate group and the mean plane defined by malonate oxygen atoms in the metal environment.

The bpe ligand exhibits the *trans*-conformation, acting as bis-monodentate ligand connecting two equatorial sites from the copper atoms it links. The geometrical values of the bpe are within the range of other bpe-containing copper(II) complexes.

Aquacopper(II) units are linked through carboxylate malonate bridges leading to a zigzag chain that runs along the *c*-axis (see Figure 20). These chains are further connected through bpe ligands to afford a corrugated layer that grows in the *bc*-plane (Figure 17a) [13.3768(9) Å being, the copper···copper distance across the bridging bpe].

Finally hydrogen bonds involving water molecules and malonate oxygens link adjacent copper layers (see Figure 20), stabilising the whole structure and leading to a three-dimensional network. The shortest interchain copper···copper distances through hydrogen bonds are: 5.3547(3) [Cu(1)···Cu(1b)] and 5.9590(7) Å [Cu(1)···Cu(1g)].

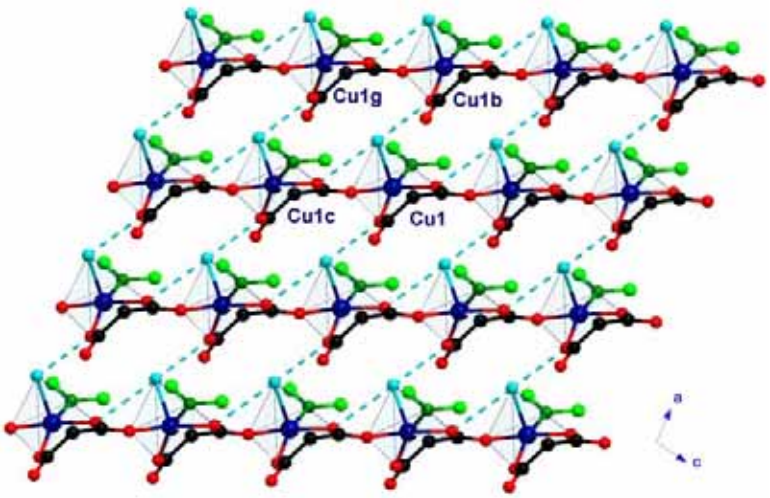

Figure 20. Perspective view, along the *b*-axis, of the malonate-bridged copper(II) chains held together by means of hydrogen bonds involving the coordinated water molecules and inner malonate-oxygen atoms.

Description of the structure of $[Cu_4(mal)_4(bpe)_3]_n \cdot 6nH_2O$ (6).

Complex **6** has a three-dimensional structure involving corrugated layers of malonato-bridged copper(II) ions (Figure 21a), which are linked by bis-monodentate bpe molecules (Figure 21b). The layers are stacked along the [-1 0 1] direction and the bis-monodentated bpe ligands run parallel to the [1 0 1] and [1 0 0] directions exhibiting a T-shape arrangement. The asymmetric unit with the atom numbering is shown in Figure 22.

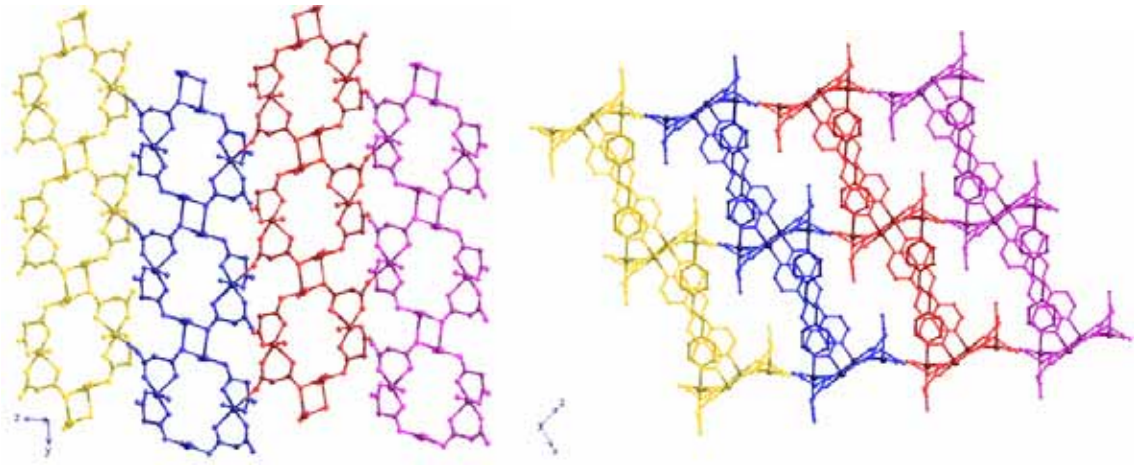

(a) **(b)**

Figure 21. Perspective views of **(a)** the malonato-bridged copper(II) corrugated plane and **(b)** its polymerization through bis-monodentate bpe in **6**.

Table 15. Selected bond lengths (Å) and angles (º) and hydrogen bonds for **6**[a,b]

Copper coordination sphere			
Cu(1)-O(4)	1.940(2)	Cu(1)-O(33a)	1.968(2)
Cu(1)-N(1)	2.080(2)	Cu(1)-N(2)	2.029(2)
Cu(1)-O(33)	2.370(2)		
O(4)-Cu(1)-N(1)	85.94(9)	O(33a)-Cu(1)-N(1)	91.06(9)
O(4)-Cu(1)-N(2)	91.78(9)	O(33a)-Cu(1)-N(2)	91.44(9)
O(4)-Cu(1)-O(33a)	175.25(8)	N(1)-Cu(1)-N(2)	175.79(10)
O(4)-Cu(1)-O(33)	99.73(8)	O(33a)-Cu(1)-O(33)	76.79(8)
N(1)-Cu(1)-O(33)	94.24(8)	N(2)-Cu(1)-O(33)	89.63(8)
Cu(2)-O(1)	1.980(2)	Cu(2)-O(2)	1.979(2)
Cu(2)-O(32b)	1.957(2)	Cu(2)-N(3)	2.022(3)
Cu(2)-O(31b)	2.278(2)	Cu(2)-O(34)	2.627(3)
O(1)-Cu(2)-O(2)	88.42(8)	O(32b)-Cu(2)-N(3)	88.71(10)
O(1)-Cu(2)-O(32b)	94.49(9)	O(1)-Cu(2)-N(3)	176.50(9)
O(2)-Cu(2)-N(3)	88.24(9)	O(2)-Cu(2)-O(32b)	172.89(9)
O(1)-Cu(2)-O(31b)	92.08(9)	O(1)-Cu(2)-O(34c)	95.01(9)
O(2)-Cu(2)-O(31b)	98.63(9)	O(2)-Cu(2)-O(34c)	88.21(8)
O(32b)-Cu(2)-O(31b)	87.77(8)	O(32b)-Cu(2)-O(34c)	85.07(8)
N(3)-Cu(2)-O(31b)	89.45(9)	N(3)-Cu(2)-O(34c)	83.85(9)
O(31b)-Cu(2)-O(34c)	170.29(8)		

Hydrogen bonds			
D-H···A	D···A/Å	D-H···A	D···A/Å
O(1w)-H···O(3)	2.836(5)	O(2w)-H···O(1wc)	2.817(6)
O(1w)-H···O(3wd)	3.085(6)	O(3w)-H···O(1)	3.085(6)
O(2w)-H···O(3)	2.975(6)	O(3w)-H···O(2wc)	2.785(8)
D-H···A	D···A/Å	H···A/Å	D-H···A/º
C(2)-H(2)···O(34)	3.080(4)	2.21(4)	134(3)
C(10)-H(10)···O(31a)	3.334(4)	2.70(4)	124(3)
C(10)-H(10)···O(33a)	3.056(4)	2.55(4)	113(3)
C(14)-H(14)···O(4)	2.802(4)	2.26(4)	120(3)
C(15)-H(15)···O(4)	2.950(4)	2.41(4)	115(3)
C(15)-H(15)···O(32e)	3.266(4)	2.61(3)	126(2)
C(16)-H(16)···O(1f)	3.315(4)	2.30(3)	168(3)
C(18)-H(18)···O(1wh)	3.414(5)	2.48(5)	175(3)
C(19)-H(19)···O(31a)	3.278(3)	2.64(4)	125(3)
C(19)-H(19)···O(33a)	2.986(3)	2.69(4)	104(3)
C(20)-H(20)···O(1wi)	3.671(4)	2.71(4)	177(4)
C(21)-H(21)···O(3f)	3.553(4)	2.53(5)	161(4)
C(31)-H(31)···O(1g)	3.240(4)	2.66(4)	121(3)
C(31)-H(31)···O(3wg)	3.332(7)	2.48(4)	153(3)
C(40)-H(40)···O(31b)	3.214(4)	2.75(5)	113(3)
C(43)-H(43)···O(2wj)	3.791(6)	2.89(6)	162(5)
C(44)-H(44)···O(32b)	2.982(5)	2.69(5)	104(3)

[a] Symmetry codes: (a) -*x*+1, -*y*+2, -*z*; (b) *x*, *y*-1, *z*; (c) -*x*+1/2, *y*-1/2, -*z*+1/2; (d) -*x*+1/2, *y*+1/2, -*z*+1/2; (e) -*x*+3/2, *y*-1/2, -*z*+1/2; (f) -*x*+3/2, *y*+1/2, -*z*+1/2; (g) *x*, *y*+1, *z*; (h) *x*+1/2, -*y*+3/2, *z*-1/2; (i) *x*-1/2, -*y*+3/2, *z*-1/2; (j) *x*+1, *y*, *z*.
[b] A = acceptor; D = donor.

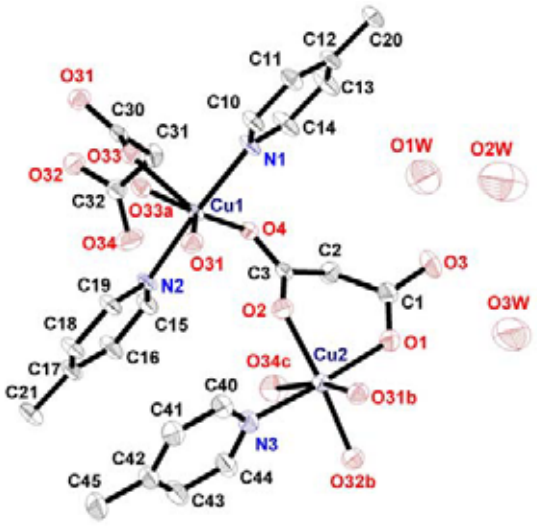

Figure 22. Perspective view of the asymmetric unit of **2**. Hydrogen atoms are ommited for simplicity. Thermal ellipsoids are drawn at the 50% probability level.

Two crystallographically independent copper(II) ions noted Cu(1) and Cu(2) occur in **6** (see Figure 22). Cu(1) exhibits a CuN_2O_3 slighty distorted square-pyramidal

environment, the τ value being 0.009 (square pyramidal and trigonal pyramidal surroundings correspond to $\tau = 0$ and $\tau = 1$, respectively) [Addison A.W. *et al.*, 1984]. Cu(2) is six coordinated $CuNO_5$ and has a 4+1+1 distorted octahedral conformation with $\phi = 54.69^{o}$ and *s/h* = 1.40 [Stiefel E.I. *et al.*, 1972]. The basal sites around Cu(1) are occupied by two bpe-nitrogen atoms and two carboxylate-oxygen atoms from two different malonate ligands. The Cu-N bond lengths [average value 2.055(2) Å] are somewhat longer than the Cu-O ones [mean value 1.954(2) Å]. The apical position is occupied by a malonate-oxygen atom [2.370(2) Å for Cu(1)-O(33)]. The equatorial plane around Cu(2) is built by a bpe-nitrogen atom and three carboxylate-oxygen atoms from two different malonate groups [the average value of Cu-N and mean Cu-O bonds being 2.022(3) and 1.972(2) Å, respectively]. These values are in good agreement with those observed in the previously reported structures of malonate- [see Introduction] and bpe-containing copper(II) complexes [Lu J.Y. *et al.*, 2001; Zhang H.-X. *et al.*, 2001; Carlucci L. *et al.*, 2001; Hagrman D. *et al.*, 1998a; Hagrman *et al.*, 1998b; Carlucci L. *et al.*, 2000; Visinescu D. *et al.*, 2002a]. Apical positions at Cu(2) are occupied by two structurally different malonate-oxygen atoms [2.278(2) and 2.627(3) Å for Cu(2)-O(31b) and for Cu(2)-O(34c), respectively; (b) *x*, *y-1*, *z*]. The longer axial Cu(2)-O bond corresponds to the monodentate malonate ligand whereas the shorter one comes from the bidentate malonate.

Two different malonate ligands occur in **6**: L1 [C(1)C(2)C(3)] and L2 [C(31)C(32)C(33)] (see Figure 23). L1 acts simultaneously as monodentate [through O(4) towards Cu(1)] and bidentate [through O(1), O(2) towards Cu(2)] ligand exhibiting the *anti-syn* conformation. It forms [including the Cu(2) atom] a the six-membered ring that exhibits a twist-boat conformation [$\theta = 97.2(2)^{o}$, $\phi = 107.9(2)^{o}$] [Addison A.W. *et al.*, 1984]. L2 bridges four copper atoms and it adopts simultaneously the tris-monodentate [O(34) toward Cu(2f) and O(33) towards Cu(1) and Cu(1a); (a) *-x+1*, *-y+2*, *-z*; (f) *-x+1.5*, *y+0.5*, *-z+0.5*] and bidentate [through O(32) and O(31) toward Cu(2g); (g) *x*, *y+1*, *z*] coordination modes and it exhibits a boat conformation [$\theta = 85.5(5)^{o}$ and $\phi = 121.3(2)^{o}$] [Addison A.W. *et al.*, 1984]. The carboxylate bridges of this latter malonate show the *anti-syn* [Cu(2g)-O(31)-C(30)-O(33)-Cu(1a)] and *anti-anti* [Cu(2g)-O(31)-C(30)-O(33)-Cu(1)] conformations. The bond lengths and angles of the two malonate ligands are in good agreement with those previously reported for malonate-containing copper(II) complexes [see Introduction].

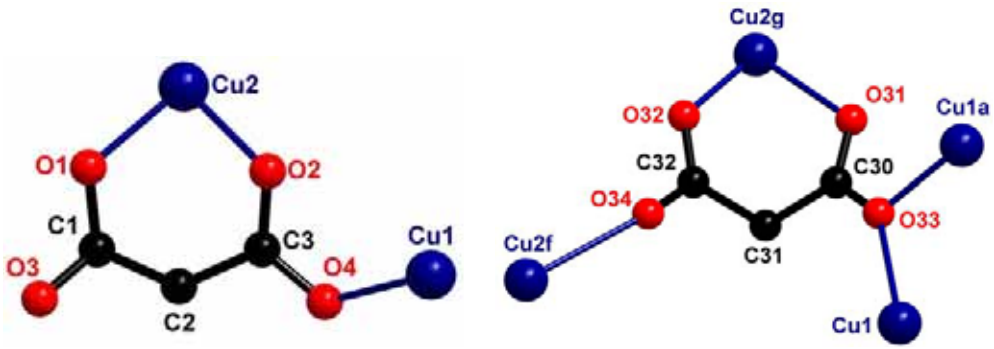

(a) **(b)**

Figure 23. Coordination mode of the malonate ligands in **6**.

Table 16. Bond lengths (Å) and angles (º) for malonate ligands in **6**[a]

C(1)-C(2)	1.513(4)	C(2)-C(3)	1.511(4)
C(1)-O(1)	1.271(4)	C(3)-O(2)	1.251(3)
C(1)-O(3)	1.239(4)	C(3)-O(4)	1.265(3)
O(1)···O(2)	2.761(3)	O(3)···O(4)	4.380(4)
O(1)-C(1)-O(3)	122.9(3)	O(2)-C(3)-O(4)	123.3(2)
O(1)-C(1)-C(2)	117.9(3)	O(2)-C(3)-C(2)	121.5(3)
O(3)-C(1)-C(2)	119.1(3)	O(4)-C(3)-C(2)	115.2(2)
C(1)-C(2)-C(3)	113.8(3)		
C(1)-O(1)-Cu(2)	123.6(2)	C(3)-O(2)-Cu(2)	120.0(2)
C(3)-O(4)-Cu(1)	122.7(2)		
C(30)-C(31)	1.507(4)	C(31)-C(32)	1.533(4)
C(30)-O(31)	1.243(3)	C(32)-O(32)	1.273(3)
C(30)-O(33)	1.283(3)	C(32)-O(34)	1.235(4)
O(31)···O(32)	2.945(3)	O(33)···O(34)	4.054(3)
O(31)-C(30)-O(33)	121.5(2)	O(32)-C(32)-O(34)	124.1(3)
O(31)-C(30)-C(31)	121.7(2)	O(32)-C(32)-C(31)	118.1(2)
O(33)-C(30)-C(31)	116.8(2)	O(34)-C(32)-C(32)	117.8(3)
C(30)-C(31)-C(32)	111.3(2)		
C(30)-O(31)-Cu(2g)	118.0(2)	C(30)-O(33)-Cu(1)	144.5(2)
C(32)-O(32)-Cu(2g)	128.6(2)	C(30)-O(33)-Cu(1a)	112.3(2)
C(32)-O(32)-Cu(2f)	162.0(2)		

[a] Symmetry transformations: (a) *-x*, *y*-1/2, *-z*; (g) *x*, *y*+1, z.

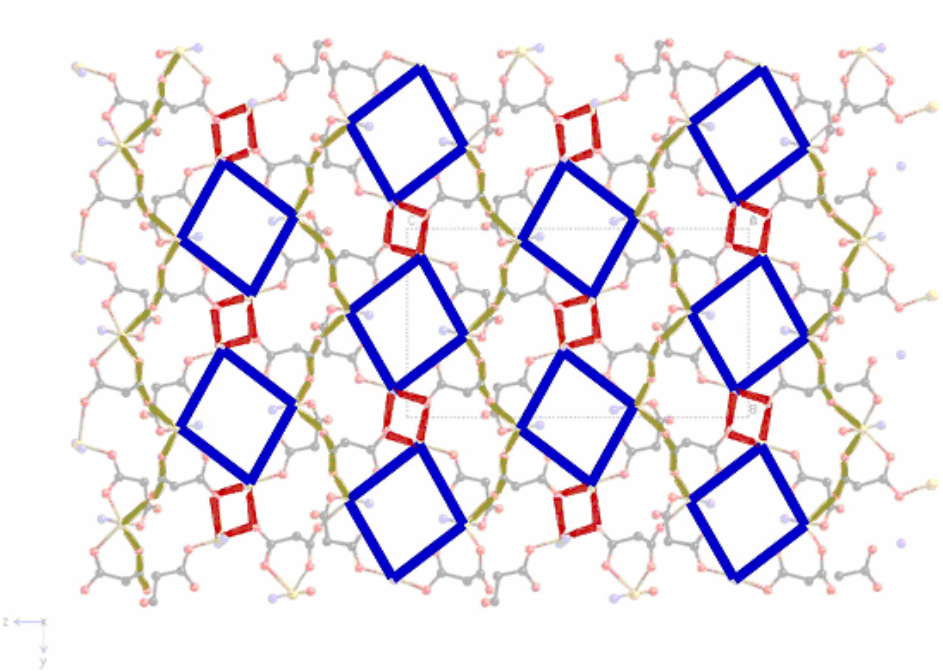

Figure 24. Tetranuclear copper(II) motifs (blue) connected through Cu(1) by double μ-oxo groups (red) and through Cu(2) by malonate-carboxylate bridges (yellow).

Within the malonate-bridged copper(II) layers, one can distinguish (Figure 24) tetranuclear units linked by double μ-oxo and single carboxylate bridges. Each tetranuclear unit forms a 16-membered ring [Cu(1)-O-C-O-Cu(2)]$_4$ with the four copper atoms located at the corners of a quasi planar parallelogram. Two different carboxylate-bridges are present in the tetranuclear unit: the equatorial-equatorial and the equatorial-axial linking pathways which lead to Cu(1)···Cu(2) separations of 5.0082(10) and 4.9488(11) Å, respectively. Each tetranuclear unit, within the layer is linked to six other ones through two μ-oxo [connecting Cu(1) atoms] and four carboxylate bridges [linking Cu(2) atoms]. Each Cu(1) atom is connected to another Cu(1) from a different tetranuclear unit through a double μ-oxo bridge [103.21(8)º for Cu(1)-O-Cu(1a)] with Cu(1)···Cu(1a) separation of 3.4095(7) Å. Each oxygen-oxo atom occupies an apical site at one copper atom and a basal site at the other one. Each Cu(2) is linked to two other Cu(2) atoms from two different tetranuclear units through single carboxylate bridges exhibiting the *anti-syn* conformation, the copper···copper separation being of 6.5268(13) Å [Cu(2)···Cu(2c)]. This carboxylate group exhibits the apical-equatorial bridging pathway.

The bpe molecule exhibits the *trans*-conformation and it acts as a bis-monodentate ligand connecting the corrugated layers of malonate-bridged copper(II) ions. The shortest interlayer separations across bridging bpe are 13.462(3)

[Cu(1)···Cu(1j); (j) *x+1, y, z*] and 13.406(2) Å [Cu(2)···Cu(2k); (k) *-x+2, -y+1, -z*]. These values are within the range reported in previous bpe-bridged copper(II) complexes.

Magnetic Properties

The magnetic behavior of **1** in the form of $\chi_M T$ *vs.* T plot [χ_M being the magnetic susceptibility *per* one copper(II) ion] is shown in Figure 25. $\chi_M T$ at 290 K is equal to 0.39 cm^3 mol^{-1} K, a value which is as expected for a magnetically isolated spin doublet. Upon cooling, $\chi_M T$ remains practically constant up to 50 K, and then it increases smoothly at lower temperatures, reaching a value of 0.43 cm^3 mol^{-1} K at 2.0 K. This curve reveals the occurrence of an overall weak ferromagnetic interaction. As the structure of **1** is made up of uniform chains of $[Cu(mal)_2]_n^{2n-}$ units which are well separated from each other by large $(H_2bpe)^{2+}$ cations, its magnetic data can be analyzed through the numerical expression for a ferromagnetically coupled regular chain of local spin doublets [Baker G.A. et *al.*, 1964]. Least-squares fit of the magnetic data leads to $J = +0.049(1)$ cm^{-1} and $g = 2.062(2)$.

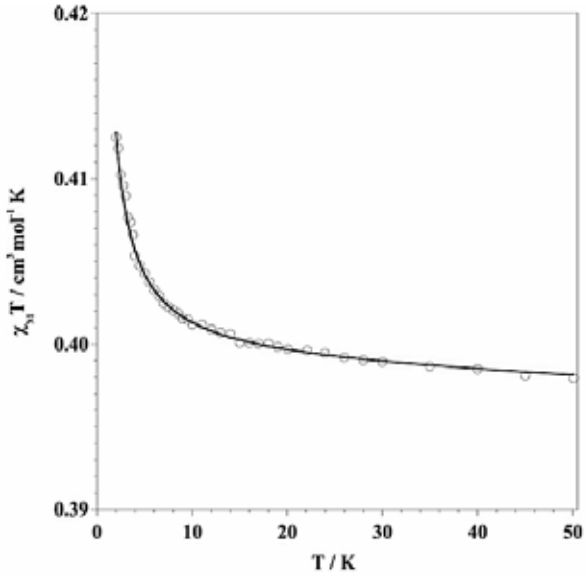

Figure 25. Temperature dependence of the $\chi_M T$ product of **1**: (o) experimental data; (-) best fit curve (see text).

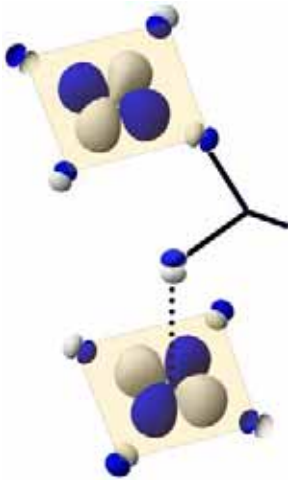

Scheme 1

An inspection of the structure of **1** allows to account for the observed weak ferromagnetic coupling. The unpaired electron of Cu(1) in the elongated six-coordinated environment is mainly located in the equatorial plane and it is of the $d_{x^2-y^2}$ type (magnetic orbital) [the *x* and *y* axes being roughly defined by the Cu(1)-O(1) and Cu(1)-O(2) bonds]. A weak spin density is thus expected in the apical positions (see Scheme 1). As the intrachain exchange pathway in **1** involves the equatorial-apical connection through carboxylate bridge [Cu(1)-O(1)-C(1)–O(3)···Cu(1h); (h) *x*+1, *y*, *z*] the overlap (*S*) between the magnetic orbitals of Cu(1) and Cu(1h) is predicted to be very small or zero (accidental orthogonality). Given that the magnitude of the antiferromagnetic interaction in a copper(II) dimmer is proportional to S^2 [Kahn O., 1993; Robson R., 2000], the ferromagnetic contribution is expected to be dominant and the resulting magnetic coupling in **1** is most likely ferromagnetic, as observed. In fact, previous experimental and theoretical studies of carboxylato-bridged copper(II) complexes have shown that the value of the exchange coupling between copper(II) ions through bridging carboxylate (*J*) is strongly dependent on the bridging mode of the carboxylate (*syn-syn*, *anti-anti* and *anti-syn*) and the type of Cu-O-C-O-Cu pathway involved (equatorial-equatorial or equatorial-apical) [Cano J. *et al.*, 1998; Cabrero J. *et al.*, 2000; Castillo O. *et al.*, 2001a; Castillo O. *et al.*, 2001b; Rodríguez-Martín *et al.*, 2001; Pasán J. *et al.*, 2003]. Finally, the value of the ferromagnetic coupling observed in compound **1** (J = +0.049(1) cm^{-1}) is very small compared with that of other compounds with similar orientations of the bridge and magnetic orbitals such us $[Cu_2(mal)_2(H_2O)_6]$ (J = +1.8 cm^{-1}) [Chattopadhyay D. *et al.*, 1993], $\{[Cu(H_2O)_3][Cu(mal)_2(H_2O)]\}_n$ (J = +1.9 cm^{-1}) [Ruiz-Pérez C. *et al.*, 2000], $[Cu(Im)_2(mal)]_n$ (J = +1.64 cm^{-1}) and [Cu(2-

MeIm)$_2$(mal)]$_n$ (J = +0.39 cm^{-1}) (Im = imidazole and 2-MeIm = 2-methylimidazole) [Sanchiz J. *et al.*, 2002]. This is mainly due to the somewhat greater value of the apical Cu(1)···O(malonate) distance in **1** (2.611 Å) compared with those observed in the related compounds (less than 2.39 Å).

The thermal dependence of the $\chi_M T$ product in the 2-100 K temperature range [$\chi_M T$ being the magnetic susceptibility per two copper(II) ions] for compound **2** is shown in Figure 26. The value of $\chi_M T$ at the highest temperature measured is 0.79 cm^3 mol^{-1} K, a value which is as expected for two magnetically isolated spin doublets. Upon cooling, $\chi_M T$ continuously increase to reach a value of 1.01 cm^3 mol^{-1} K at 2 K. This behaviour indicates the occurrence of an overall ferromagnetic coupling. Looking at the structure of **2**, it consists of regular alternating zigzag copper(II) chains where metal atoms are alternatively linked through pyrazine-dpp and μ-oxo bridges, these latter ones involving inner carboxylate-malonate oxygens (see Figure 5).

Previous magneto-structural studies on dpp-bridged copper(II) compounds have revealed that the exchange coupling through the bis-chelating dpp is very weak and antiferromagnetic, the values of J found in the literature ranging from -1.4 to -0.2 cm^{-1} [Sletten *et al.*, 1998; Grove H. *et al.*, 2000, 2001a and 2001b]. Bearing that in mind we tried to analyze the magnetic data of **2**, through the Bleaney-Bowers expression [Bleaney B. *et al.*, 1952], considering that we have μ-oxo bridged dinuclear units. Least-squares fit leads to the following paremeters: J = +2.866(4) cm^{-1}, g = 2.052(1) and R = 1.1x10^{-5}. R is the agreement factor defined as $\Sigma[(\chi_M T)_{obs} - (\chi_M T)_{calc}]^2/\Sigma[(\chi_M T)_{obs}]^2$. In order to take into account the interaction through the bis-bidentate/dpp bridge we introduced a θ term in the Bleaney-Bowers expression. Doing that, we obtain a negligible value of this term which confirms that the exchange through the dpp bridge must be very weak in according to the values previously reported in the literature.

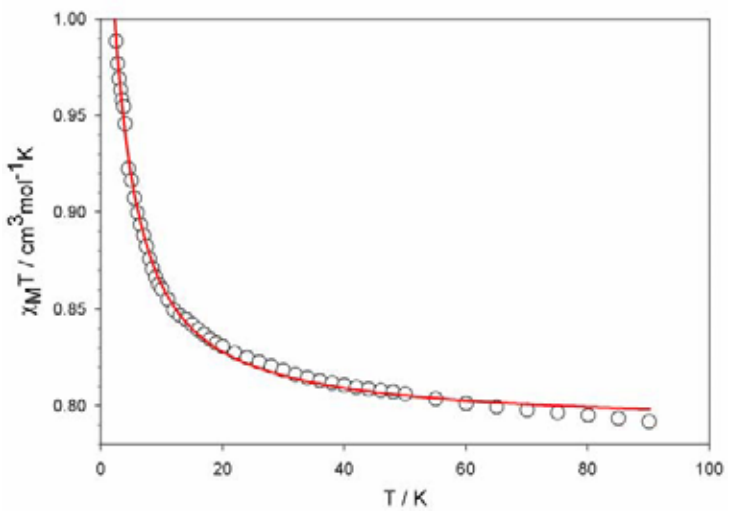

Figure 26. Thermal dependence of the $\chi_M T$ vs. T of **2**: (") experimental data and (C) best fit curve (see text).

The thermal dependence of the $\chi_M T$ product for **3** [$\chi_M T$ being the magnetic susceptibility per copper(II) ion] in the 2-100 K temperature range is shown in Figure 27. The value of the $\chi_M T$ at room temperature is 0.41 $cm^3\ mol^{-1}\ K$ a value which is as expected for a magnetically isolated copper(II) ion. Upon cooling, $\chi_M T$ smoothly increases to reach a value of 0.59 $cm^3\ mol^{-1}\ K$ at 4.5 K, and then it decreases reaching a value of 0.50 $cm^3 mol^{-1} K$ at 2 K. The shape of this curve is indicative of the occurrence simultaneously of a dominant ferromagnetic and a weak antiferromagnetic interaction.

Focusing on the structure of **3**, it consists of malonate-bridged copper(II) chains where *anti-syn* carboxylate groups connect adjacent copper(II) atoms (see Figure 9). After examining carefully the structure of this compound, one can see that two different carboxylate bridges alternate regularly within the chain: Cu(1)-O(1)-C(1)-O(3)-Cu(2) and Cu(1)-O(11)-C(11)-O(13)-Cu(2k) which exhibit the equatorial-equatorial and apical-equatorial conformation modes, respectively. Therefore, the alternating intrachain interactions are denoted as J_1 and J_2 (J_1 being the antiferromagnetic interaction). The appropriate Hamiltonian to model the magnetic behaviour of **3** is given by the following equation:

$$\hat{H} = -J_1 \sum_i \left[\hat{S}_{2i} \cdot \hat{S}_{2i+1} + \alpha \hat{S}_{2i} \cdot \hat{S}_{2i-1} \right] \qquad (1)$$

where α is the alternation parameter and J_2 is equal to $\alpha|J_1|$. A numerical extrapolated expression, based on rings of increasing size that contain only spin doublets (the calculations were limited up to 14 spins rings) [Borrás-Almenar J.J. *et al.*, 1994] allows us to successfully match the magnetic data. We also included in the fit a θ parameter to take into account the interchain interactions through hydrogen bonds. The best-fit

parameters are J_1 = -1.48(1) cm^{-1}, $J_2 = \alpha|J_1|$ = 10.4(1) cm^{-1}, g = 2.151(3), θ = 0.984(1) K and R = 8.3x10^{-6} [R being the agreement factor, R = $\Sigma[(\chi_M T)_{obs} - (\chi_M T)_{calc}]^2 / \Sigma[(\chi_M T)_{obs}]^2$].

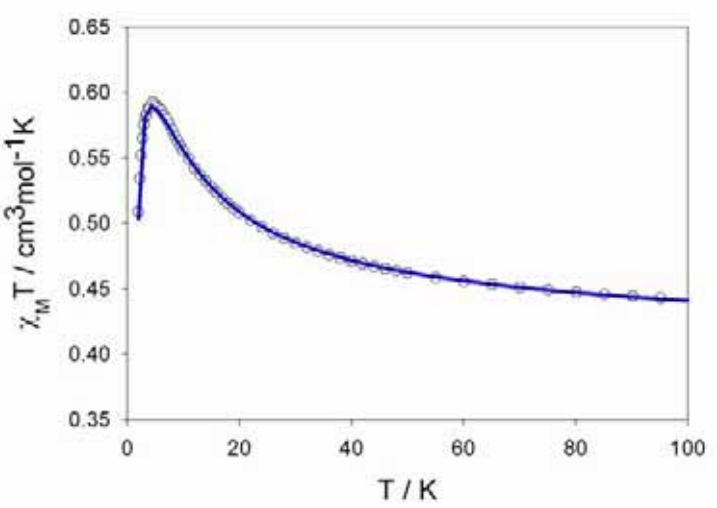

Figure 27. Thermal dependence of the $\chi_M T$ product for **3**: (") experimental data and (C) best fit curve (see text).

Without the introduction of the θ parameter the experimental data is roughly fitted through the magnetic susceptibility derived by the Hamiltonian of the eq. 1. [J_1 = -1.1 cm^{-1}, J_2 = +11.9 cm^{-1}, g = 2.18(2), R = 2.3 x 10^{-4}]. As the value of the antiferromagnetic coupling J_1 is small and we need a positive (ferromagnetic contribution) theta parameter to fit well the experimental curve it's also possible to think that the two intrachain magnetic coupling constants (J_1 and J_2) were ferromagnetic, and the antiferromagnetism observed in the experimental curve at low temperatures was due to the interchain interactions through hydrogen bonds.

The magnetic orbital at each copper atom in **3** is defined by the short equatorial bonds, and it is of the $d_{x^2-y^2}$ type with possibly some mixture of the d_{z^2} character in the axial position. It deserves to be noted that this mixture is quite important in the case of Cu(2) due to the highly distorted metal environment (τ = 0.40). The dihedral angle between the copper atoms linked through the equatorial-equatorial carboxylate bridge, [Cu(1)-O(1)-C(1)-O(3)-Cu(2)] which is nearly orthogonal [87.6(2)º], support the assignation of the stronger ferromagnetic coupling to this bridge. For the case of the equatorial-apical carboxylate bridge, a weaker interaction is expected due to the out-of-plane magnetic pathway. The strong distortion of the Cu(2) environment in **3**, accounts for the occurence of an important mixture of the magnetic orbital (located in the equatorial plane) towards the axial direction defined by Cu(2)-O(13a). Consecuently,

the overlap between the magnetic orbitals of adjacent copper atoms could be large enough to consider that the antiferromagnetic term is dominant. The value of the exchange interactions could be compared with those observed for other malonate-containing copper(II) complexes (see references of Table 17). As seen in Table 17, the values of the exchange interaction through the *anti-syn* equatorial-equatorial pathway is within the range observed for these type of bridge in malonate complexes. In the case of the equatorial-apical exchange pathway, **3** provides the first case of the occurrence of an antiferromagnetic interaction in a malonate-containing copper(II) complexes, this fact being due to the high distorted environment of the Cu(2) atom.

The magnetic properties of **4** under the form of $\chi_M T$ vs T plot [$\chi_M T$ being the magnetic susceptibility per copper(II) ion] in the 2-50 K temperature range are shown in Figure 28. The value of the $\chi_M T$ at the highest temperature measured is 0.42 cm^3 mol^{-1} K, a value which is near from that expected for a magnetically isolated spin doublet. Upon cooling $\chi_M T$ continuously decrease to reach a value of 0.21 cm^3 mol^{-1} K at 2 K.

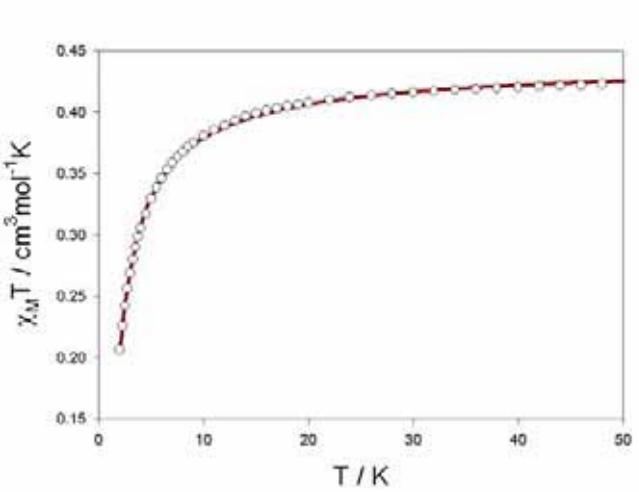

Figure 28. Thermal dependence of the $\chi_M T$ product of **4**: (") experimental data and (C) best fit curve (see text).

The structure of **4** consists of dpo-bridged aquamalonatecopper(II) chains which are further linked through hydrogen-bonds (see Figures 13 and 14). So, our first attempt was to interpretate the magnetic data using the Bonner and Fisher's expression for a regular copper(II) chain with an antiferromagnetic interaction between magnetic centres:

$$\chi_M = \frac{Ng^2\beta^2}{kT}\frac{0.25 + 0.074975x + 0.075235x^2}{1.0 + 0.9931x + 0.172135x^2 + 0.757825x^3}; \qquad (2)$$

$$\text{with } x = \frac{|J|}{kT}$$

The best least-squares fit through this expression leads to the following parameters: J = -1.72(1) cm^{-1}, g = 2.165(1) and R = 1.7x10^{-5}. Nevertheless the goodness of the fit, no magnetic exchange through the dpo ligand have been previously reported in the literature for other dpo-bridged copper(II) complexes [Ma B.-Q. *et al.*, 2000 and 2001; Plater M.J. *et al.*, 2000; Visinescu D. *et al.*, 2002b; Nedelcu A. *et al.*, 2003]. So we attempt to find another possible magnetic exchange pathways in **4** in order to explain the experimental magnetic data. An inspection of the structure of **4**, allow us to realize that other possible magnetic exchange pathways are present. First, the aquamalonatecopper(II) units are also connected through hydrogen bonds involving equatorial oxygen atoms [Cu-Ow-H···O-C-O-Cu] leading to a ladder-like chain (see Figure 14b). Second, another exchange pathway between copper(II) ions is possible through hydrogen bonds involving dpo atoms [Cu-O(apical)···H-C-N-O(equatorial)-Cu] (see Figure 13). In both cases, we expect weak ferro- or antiferromagnetic interaction. We are not able to introduce any assumption that allows us to neglect any of the three possible exchange pathways. In this respect, we can only conclude that the antiferromagnetic behaviour observed in **4** must be due to the contribution of the pathways described above. In order to get an estimation of the overall antiferromagnetic coupling, we consider the structure from a magnetic point of view as copper(II) monomers which interact each other through weak interactions. The lest-squares fit of the magnetic data through a Curie-Weiss law leads to: g = 2.09(3), θ = -1.65(2) K and R = 3.1x10^{-3} [$R = \Sigma[(\chi_M)_{obs} - (\chi_M)_{calc}]^2/\Sigma[(\chi_M)_{obs}]^2$].

The thermal dependence of the $\chi_M T$ product for compound **5** [$\chi_M T$ being the magnetic susceptibility per copper(II) ion] in the 2-300 K temperature range is shown in Figure 29. The value of the $\chi_M T$ at room temperature is 0.43 cm^3 mol^{-1} K, a value which is close to that expected for a magnetically isolated spin doublet. Upon cooling, $\chi_M T$ continuously increases to reach a value of 1.28 cm^3 mol^{-1} K at 2 K. This behaviour is characteristic of an overall ferromagnetic coupling between copper(II) ions. The structure of **5** consists of regular carboxylate-malonate copper(II) chains which are further linked through the bpe ligands affording corrugated layers (see Figure 17). Additionally, hydrogen bonds involving water molecules and carboxylate-malonate oxygen atoms held together these corrugated layers. The much larger copper···copper separation through the bpe ligands [13.3768(9) Å] compared with the shorter separation through the *anti-syn* carboxylate-malonate bridge [5.0845(7) Å] allow us to discard the

exchange pathways through the bpe. So, from a magnetic point of view, we can consider that compound **5** consists of regular copper(II) chains where the metal atoms are connected through *anti-syn* carboxylate bridges. Taking that into consideration, we tried to fit the magnetic data of **5** through the Baker and Rushbrooke expression for a ferromagnetic regular chain of local spins [Baker G.A. *et al.*, 1964] (eqs 1-4). The best-fit parameters are : J = +3.85(3) cm^{-1}, g = 2.155(3) and R = 1.9x10^{-4} [$R = \Sigma[(\chi_M T)_{obs} - (\chi_M T)_{calc}]^2/\Sigma[(\chi_M T)_{obs}]^2$].

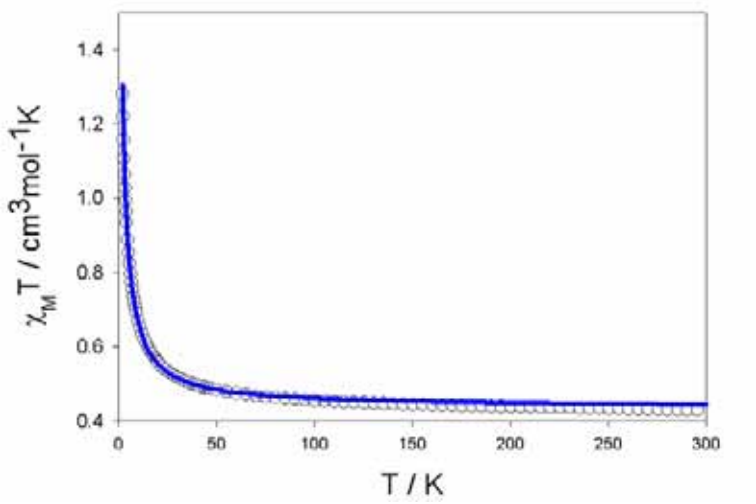

Figure 29. Thermal dependence of the $\chi_M T$ product for **5**: (") experimental data and (C) best-fit curve (see text).

Finally, the magnetic properties of **6** in the form of $\chi_M T$ *vs.* T plot [χ_M being the magnetic susceptibility *per* four Cu(II) ions] are shown in Figure 30. $\chi_M T$ at 290 K is 1.5 cm^3 mol^{-1} K, a value which corresponds to that expected for four magnetically isolated copper(II) ions. Upon cooling, this value continuously increases to reach a value of 2.66 cm^3 mol^{-1} K at 2 K. The shape of the curve is indicative of the occurrence of an overall ferromagnetic coupling in **6**.

The structure of **6** consist of $\{Cu(mal)\}_n$ corrugated layers interconnected through bpe ligands to give a 3D framework. From a magnetic point of view this is a very complicated system, since seven different exchange pathways can be operative: five within the $\{Cu(mal)\}_n$ layers (J_1-J_5 through carboxylate and double μ-oxo bridges, see Scheme 2), and other two through the two bpe bridges that connect the layers. It is clear that the much larger copper···copper separations across bridging bpe (more than 13 Å) when compared to the shorter values across double μ-oxo [3.4095(7) Å] and carboxylate bridges [values ranging from 4.9488(11) to 6.5285(13) Å] allow us to discard the exchange pathways through bpe. Thus, the magnetic behavior of **6** can be

explained by considering only the exchange pathways within the layer. Focusing on the layer, we have two different copper(II) ions The links of Cu(2) with its nearest neighbours are depicted in Scheme 2a. One can see there four different exchange pathways (J_1-J_4) through the carboxylate bridges: (i) equatorial positions at both Cu(1) and Cu(2) atoms are involved in J_1; (ii) J_2 concerns an axial position at Cu(2) and a basal position at Cu(1); (iii) J_3 involves an axial position at Cu(2) and an apical at Cu(1); (iv) finally, J_4 deals with two different symmetry related Cu(2) atoms connecting an axial position at Cu(2) and an equatorial one at Cu(2). An additional double μ-oxo bridge between Cu(1) and Cu(1a) atoms (exchange pathway corresponding to J_5) is illustrated by Scheme 2b.

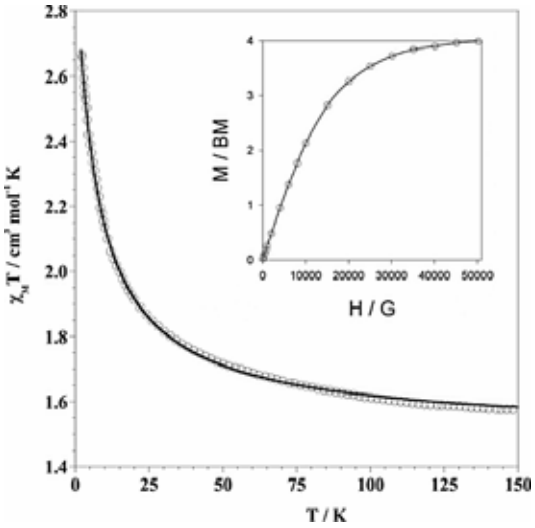

Figure 30. Temperature dependence of the $\chi_M T$ product of **6**: (o) experimental data; (-) best fit curve through eq (9) (see text).

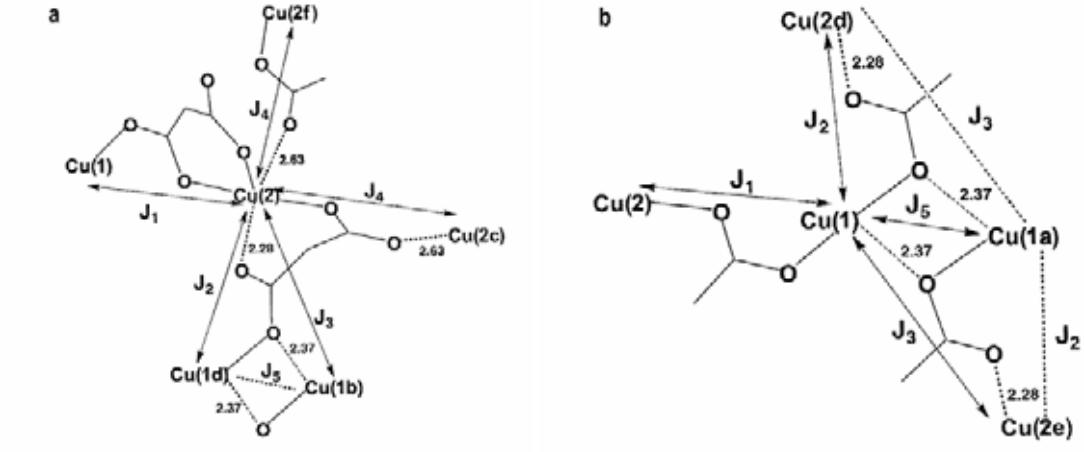

Scheme 2

Keeping in mind the above considerations, a rigorous description of the magnetic structure of **6** would require at least the evaluation of the five exchange coupling parameters. As there is no model to analyse such a complicated magnetic system, we have introduced several approximations that allowed us to determine the values for the main coupling constants and to check further their reliability by comparing them with those already known for this exchange pathways in lower nuclearity malonato-bridged copper(II) complexes. In this respect, and having in mind the overall path length via carboxylate bridges (Schemes 2a and 2b), the only relevant magnetic interactions are J_1 and J_2, the remaining ones being neglected in a first approach. So, we are dealing with a model of rectangles with alternating J_1 and J_2 parameters in the edges (blue motif in Figure 24). The corresponding spin Hamiltonian for this simplified model is given by the eq. (3):

$$\hat{H} = -\left[J_1(\hat{S}_1\hat{S}_2 + \hat{S}_{1A}\hat{S}_{2A}) + (J_2(\hat{S}_1\hat{S}_{2A} + \hat{S}_{1A}\hat{S}_2)\right] \quad (3)$$

The theoretical expression for the magnetic susceptibility of the tetranuclear complex derived through this Hamiltonian considering an average g value is then:

$$\chi_M = \frac{2Ng^2\beta^2}{kT}\frac{\left[5\exp(Q/kT + R\right]}{\left[5\exp(Q/kT) + 3R + \exp((S-Q)/kT) + \exp(-(S+Q)/kT)\right]} \quad (4)$$

$$Q = (J_1 + J_2)/2 \quad (5)$$

$$R = \exp((J_1 - J_2)/2kT) + \exp((J_2 - J_1)/2kT) + \exp(-(J_1 - J_2)/2kT) \quad (6)$$

$$S = (J_1^2 + J_2^2 - J_1J_2)^{1/2} \quad (7)$$

In order to take into account the interaction between tetranuclear units, a Weiss constant was introduced [eq (8)]

$$\chi' = \frac{\chi}{1-(2zJ'/Ng^2\beta^2)\chi} \quad (8)$$

Least-squares fit of the magnetic data leads to the following parameters: J_1 = +23(1) cm^{-1}, J_2 = +6.5(1) cm^{-1}, zJ' = -1.0(1) K and g = 2.002(2). The calculated curve matches well the magnetic data in the whole temperature range.

Let us to analyse and compare the values of the coupling constants. Relevant magneto-structural data for carboxylate(malonate)-bridged copper(II) complexes are listed in Table 4. One can see there that the magnetic coupling between copper(II) ions

through the carboxylate(malonate)-bridge is always ferromagnetic and also that the values through the equatorial-apical exchange pathway are smaller than those corresponding to the equatorial-equatorial ones, as expected. The values of J_1 and J_2 in **6** are in agreement with these observations and they are the upper-limits of both families. Concerning the value of J_5, a few studies involving Cu(II) ions bridged by a double μ-oxo bridges in an out-of-plane exchange pathway (Scheme 3) have been reported and weak ferro- and antiferromagnetic interactions were observed (values of J ranging from –4.30 cm^{-1} to + 1.26 cm^{-1}) [Greenway A.M. *et al.*, 1981; Chiari B. *et al.*, 1986; Escribá E., 1997; Pasini A. *et al.*, 2000]. These magneto-structural studies have shown that the nature and magnitude of the magnetic coupling between the parallel magnetic orbitals depends on the values of the angle at the bridge ϕ and the out-of-plane Cu···O bond distance (R_0). Values of ϕ = 103.21º and R_0 = 2.371 Å in **6** allow to predict a weak antiferromagnetic interaction through this bridge. Looking at the value of zJ' obtained by fit (*ca.* -1.0 K), the exchange pathway through the double μ-oxo bridge is most likely responsible for this coupling.

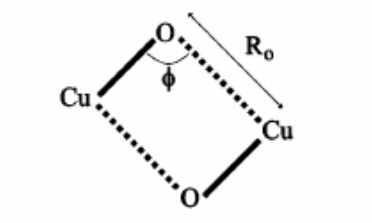

Scheme 3

Table 17. Selected Magneto-Structural Data for Some Carboxylate(malonate)-Bridged Copper(II) Complexes

Compound[a]	carboxylate pathway	J^b(cm^{-1})	Ref.
$\{[Cu(mal)_2(H_2O)_2][Cu(dien)]\}_n \cdot 4nH_2O$	equatorial-apical	-1.48	**3**
$\{(H_2bpe)[Cu(mal)_2]\}_n \cdot 4nH_2O$	equatorial-apical	+0.049	**1**
$[Cu(2\text{-}MeIm)_2(mal)]_n$	equatorial-apical	+0.4	Sanchiz J. *et al.*, 2002
$\{[Cu(H_2O)_4]_2[Cu(mal)_2(H_2O)]\}$	equatorial-apical	+1.2	Ruiz-Pérez C. *et al.*, 2000a
$[Cu(Im)_2(mal)]_n$	equatorial-apical	+1.6	Sanchiz J. *et al.*, 2002
$\{[Cu(H_2O)_4][Cu(mal)_2(H_2O)_2]\}$	equatorial-apical	+1.8	Chattopadhyay D. *et al.*, 1993
$\{[Cu(H_2O)_3][Cu(mal)_2(H_2O)]\}_n$	equatorial-apical	+1.9	Ruiz-Pérez C. *et al.*, 2000a
$[Cu_4(mal)_4(bpe)_3]_n \cdot 6nH_2O$	equatorial-apical	+6.5	**6**
$\{[Cu(H_2O)_3][Cu(mal)_2(H_2O)]\}_n$	equatorial-equatorial	+3.0	Ruiz-Pérez C. *et al.*, 2000a
$[Cu(mal)(bpe)_{1/2}(H_2O)]_n \cdot nH_2O$	equatorial-equatorial	+3.85	**5**
$\{[Cu(bpy)(H_2O)][Cu(bpy)(mal)(H_2O)]\}(ClO_4)_2$	equatorial-equatorial	+4.6	Ruiz-Pérez C. et al., 2000b
$\{[Cu(mal)_2(H_2O)_2][Cu(dien)]\}_n \cdot 4nH_2O$	equatorial-equatorial	+10.4	**3**
$[Cu_4(mal)_4(2,4'\text{-}bpy)_4(H_2O)_4] \cdot 8H_2O$	equatorial-equatorial	+12.3	Rodríguez-Martín. Y. *et al.*, 2002a
$[Cu_2(mal)_2(H_2O)_2(4,4'\text{-}bpy)]$	equatorial-equatorial	+12.4	Rodríguez-Martín. Y. *et al.*, 2002b
$[Cu_4(mal)(O_2CCH_2CO_2)_4] \cdot 7H_2O$	equatorial-equatorial	+13.5	Konar S. *et al.*, 2003
$[\{Cu_3(mal)_2(bpe)_3(H_2O)_2\}(NO_3)_2]_n$	equatorial-equatorial	+22	Sain S. *et al.*, 2003
$[Cu_4(mal)_4(bpe)_3]_n \cdot 6nH_2O$	equatorial-equatorial	+23	**6**

[a]Abbreviations used: dien = diethylenetriamine, bpe = 1,2-bis(4-pyridyl)ethylene, 2-MeIm = 2-methylimidazole, Im = imidazole, bpy = 2,2'-bipyridine, 2,4'-bpy = 2,4'-bipyridine and 4,4'-bpy = 4,4'bipyridine. [b]Values of the magnetic coupling.

References

Addison A.W., Rao T.N., Reedijk J., Rijn J. and Verschoor G.C.J., *J. Chem. Soc., Dalton Trans.*, **1984**, 1349.

Batten S.R. and Robson R., *Ang. Chem., Int. Ed. Engl.*, **1998**, *37*, 1460.

Baker G.A., Rushbrooke G.S. and Gilbert H.E., *Phys. Rev.*, **1964**, 135 A1272.

Bleaney B. and Bowers K.D., *Proc. Roy. Soc.* (*London*) *Ser. A* 214, **1952**, 451.

Borrás-Almenar J.J., Coronado E., Curely J., Georges R. and Gianduzzo J.C., *Inorg. Chem.*, **1994**, 33, 5171.

Braga D., *J. Chem. Soc., Dalton Trans.*, **2000**, *21*, 3705.

Cabrero J., Ben Amor N., de Graaf C., Illas F. and Caballol R., *J. Phys. Chem.* **2000**, 104, 9983.

CAD4-EXPRESS, version 5.1/1.2, Enraf-Nonius, Delft, The Netherlands, **1994**.

Cano J., Alemany P., Alvarez S., Verdaguer M. and Ruiz E., *Chem. Eur. J.* **1998**, 4, 476.

Carlucci L., Ciani G., Gramaccioli A., Proserpio D.M. and Rizzato S., *CrystEngComm*, **2000**, 29.

Carlucci L., Ciani G., Proserpio D.M. and Rizzato S., *Chem. Commun.* **2001**, 1198.

Carranza J., Grove H., Sletten J., Lloret F., Julve M., Kruger P.E., Eller C. and Rillema D.P., *Eur. J. Inorg. Chem.*, **2004**, 24, 4836.

Castillo O., Muga I., Luque A., Gutierrez-Zorrilla J.M., Serrucha J., Vitoria P. and Roman P., *Polyhedron*, **1999**, 18, 1235.

Castillo O., Luque A., Lloret F., Julve M. and Roman P., *Inorg. Chim. Acta* **2001a**, 315, 9.

Castillo O., Luque A., Lloret F. and Roman P., *Inorg. Chim. Acta* **2001b**, 324, 141.

Chattopadhyay D., Chattopadhyay S.K., Lowe P.R., Schwalbe C.H., Mazumder S.K., Rana A. and Ghosh S., *J. Chem. Soc., Dalton Trans.*, **1993**, 913.

Chiari B., Helms J.H., Piovesana O., Tarantelli T. and Zanazzi P.F., *Inorg. Chem.* **1986**, *25*, 2408.

Cremer D. and Pople J.A., *J. Am. Chem. Soc.*, **1975**, 97, 1354.

Curtis N.F., McCormick I.R.N. and Waters T.N., *J. Chem Soc., Dalton Trans.*, **1973**, 1537.

Davey G. and Stephens F.S., *J. Chem. Soc. A*, **1971**, 103.

De Munno G., Julve M., Viau G., Lloret F., Faus J. and Vitervo D., *Angew. Chem. Int. Ed. Engl.* **1996**, *35*, 1807.

Denti G., Seroni S., Campagna S., *Perspectives in Coordination Chemistry*, Williams A.F. and Floriani C., (Eds), VCH, Weinheim, Germany, **1992**, p.153.

DIAMOND 2.1d, Crystal Impact GbR, CRYSTAL IMPACT, K. Brandenburg & H. Putz GbR, Postfach 1251, D-53002 Bonn, Germany, **2000**.

Duisenberg A.J.M., Kroon-Batenburg, L.M.J. and Schreurs, A.M.M. *J. Appl. Cryst.*, **2003,** 36, 220 (EVALCCD).

Earshaw A., *Introduction to Magnetochemistry*; Academic Press; London, **1968**.

Escribá E., Server-Carrió J., Lezama L., Folgado J.V., Pizarro J.L., Ballesteros R. and Abarca B., *J. Chem. Soc., Dalton Trans*, **1997** , 2033.

Etter M.C., *Acc, Chem. Res.*, **1990**, 23, 120.

Farrugia L.J. (*WINGX*), *J. Appl. Cryst*, **1999**, *32*, 837.

Fujita M., Kwon Y.J., Washizu S. and Ogura K., *J. Am. Chem. Soc.*, **1994a**, *116*, 1151.

Fujita M., Kwon Y.J., Miyazawa M. and Ogura K., *J. Chem. Soc. Chem. Comm.*, **1994b**, 1977.

Garcia Y., Kahn O., Rabardel L., Chansou B., Salmon L. and Tuchagues J.P., *Inorg. Chem.*, **1999**, *38*, 4663.

Greenway A.M., O'Connor J.C., Overman J.W., and Sinn E., *Inorg. Chem.*, **1981**, 20, 1508.

Grove H., Sletten J., Julve M., Lloret F. and Lezama L., *Inorg. Chim. Acta*, **2000**, 310, 217.

Grove H., Julve M., Lloret F., Kruger P.E., Törnroos K.W. and Sletten J., *Inorg. Chim. Acta*, **2001a**, 325, 115.

Grove H., Sletten J., Julve M. and Lloret F. *J. Chem. Soc., Dalton Trans.*, **2001b**, 2487.

Hagrman D., Haushalter R.C. and Zubieta J., *Chemistry of Materials*, **1998a**, 10, 361.

Hagrman D., Hammond R.P., Haushalter R., Zubieta J., *Chemistry of Materials* **1998b**, 10, 2091.

Hagrman P.J., Hagrman D. and Zubieta J., *Angew. Chem., Int. Ed. Engl.*, **1999**, *38*, 2638.

Harms K., CAD4. Program for the Lp Correction of Nonius-CAD4-Diffractometer Data, University of Marburg, Germany, **1997**.

Hennigar T.L., MacQuarrie D.C., Losier P., Rogers R.D., Zaworotko M.J., *Ang. Chem. Int. Ed. Engl.*, **1997**, *36*, 972.

Hooft R.W.W., *COLLECT*. Nonius BV, Delft, The Netherlands, **1999**.

Huang N.-T., Pennington W.T. and Petersen J.D., *Acta Cryst., Sect. C*, **1991**, 47, 2011.

Ishida T., Kawakami T., Mitsubori S., Nogami T., Yamaguchi K. and Iwamura H. *J. Chem. Soc., Dalton Trans.*, **2002**, 3177.

Julve M., Verdaguer M., Gleizes A., Philoche-Levisalles M. and Kahn O. *Inorg. Chem.*, **1984**, *23*, 3808.

Kahn, O. in *Molecular Magnetism*, ed. VCH, New York, **1993** and references therein.

Kruger P.E., Murray K.S. and Tienkink E.R.T., *Z. Kristallogr.*, **1994**, 209, 624.

Ma B.-Q., Sun H.-L., Gao S. and Xu G.-X., *Inorg. Chem.*, **2001**, 40, 6247.

Nardelli M., *J. Appl. Crystallogr.*, **1995**, *28*, 659.

Nedelcu A., Žak Z., Madalan A.M., Pinkas J. and Andruh M., *Polyhedron*, **2003**, 22, 789.

O'Keeffe M., Edaoudi M., Li H., Reineke T. and Yaghi O.M., *J. Solid State Chem.*, **2000**, *152*, 3.

Palmans A.R.A., Vekemans J.A.J.M., Kooijman H., Speck A.L. and Meijer E.W., *J. Chem. Soc. Chem. Comm.* **1997**, 2247.

Pasán J., Delgado F.S., Rodriguez-Martín Y., Hernández-Molina M., Ruiz-Pérez C., Sanchiz J., Lloret F. and Julve M., *Polyhedron,* **2003**, 22, 2143.

Pasini A., Demartin F., Piovesana O., Chiari B., Cinti A., Crispu O., *J. Chem. Soc., Dalton Trans.,* **2000**, 3467.

Patra G.K., Mostafa G., Tocher D.A. and Datta D., *Inorg. Chem. Comm.*, **2000**, 3, 56.

Plater M.J., Foreman M.R.St.J. and Slawin A.M.Z., *Inorg. Chim. Acta*, **2000**, 303, 132.

Lehn, J.-M., *Ang. Chem. Int. Ed. Engl.*, **1990**, 29, 1304.

Lenh J.-M., *Supramolecular Chemistry: Concepts and Perspectives*, VCH, Weinheim, **1995**.

Lu J.Y., Babb A.M., *Inorg. Chem.*, **2001**, 40, 3261.

Real J.A., Andres E., Munoz M.C., Julve M., Granier T., Bousseksou A. and Varret F., *Science*, **1995**, *268*, 265.

Robertson K.N., Bakshi P.K., Lantos S.D., Cameron T.S. and Knop O., *Can. J. Chem.*, **1998**, 76, 583.

Robson R., *J. Chem. Soc., Dalton. Trans.*, **2000**, *21*, 3735.

Rodríguez-Martín Y., Ruiz-Pérez C., Sanchiz J., Lloret F. and Julve M., *Inorg. Chim. Acta* **2001**, 318, 159.

Rodríguez-Martín Y., Hernández-Molina M., Delgado F.S., Pasán J., Ruiz-Pérez C., Sanchiz J., Lloret F. and Julve M., *CrystEngComm*, **2002**, *4*, 522.

Ruiz-Pérez C., Sanchiz J., Hernández-Molina M., Lloret F. and Julve M., *Inorg. Chem.* **2000a**, 39, 1363.

Ruiz-Pérez C., Hernández-Molina M., Lorenzo-Luis P., Lloret F., Cano J. and Julve M., *Inorg. Chem.*, **2000b**, 39, 3845.

Ruiz-Pérez C., Rodríguez-Martín Y., Hernández-Molina M., Delgado F.S., Pasán J., Sanchiz J., Lloret F. and Julve M., *Polyhedron*, **2003**, 22, 2111.

SADABS, version 2.03. Bruker AXS Inc.: Madison, WI, **2000**.

Sain S., Maji T.K., Mostafa G., Lu T.H. and Chanduri N.R., *New J. Chem.*, **2003**, 27, 185.

Sanchiz J., Rodróguez-Martín Y., Ruiz-Pérez C., Mederos A., Lloret F. and Julve M., *New J.Chem.*, **2002**, 26, 1624**.**

Sheldrick G.M., *SHELX97*, *Programs for Crystal Structure Analysis (Release 97-2)*, Institüt für Anorganische Chemie der Universität, Tammanstrasse 4, D-3400 Göttingen, Germany, **1998**

Sletten J. and Bjorsvik O., *Acta Chem. Scand.*, **1998**, 52, 770.

Stephens F.S,. *J. Chem. Soc. A*, **1969**, 2493.

Stiefel E. I. and Brown G. F., *Inorg. Chem.*, **1972**, 11, 434.

Tangouolis V., Raptopolou C.P., Psycharis V., Terzis A., Korda K., Perlepes S.P., Cador O., Kahn O., Bakalbassis E.G., *Inorg. Chem.*, **2000**, *39*, 2522.

Thaimattam R., Reddy D.S., Xue F., Mak T.C.W., Nangia A. and Desiraju G.R., *J. Chem .Soc., Perkin Trans. 2*, **1998**, 1783.

Vansant J., Smets G., Declercq J.P., Germain G. and van Meerssche M., *J. Org. Chem.*, **1980**, 45, 1557.

Visinescu D., Andruh M., Muller A., Schmidtmann M. and Journaux Y., *Inorg. Chem. Comm.*, **2002a**, 5, 42.

Visinescu D., Pascu G.I., Andruh M., Magull J. and Roesky H.W., *Inorg. Chim. Acta*, **2002b**, 340, 201.

Yaghi, O.M., Li H., Davis C., Richardson D. and Groy T.L., *Acc. Chem. Soc.*, **1998**, *31*, 474.

Ye B.-H., Ji L.-N. and Mak T.C.W., *Polyhedron*, **1998**, 17, 2687.

Zhang H.-X., Kang H.-X., Zhou Z.-Y., Chan A.S.C., Chen Z.-N. and Ren C., *J. Chem. Soc., Dalton Trans*, **2001**, 1664.

CONCLUSIONS

Conclusions

Structural point of view. The addition of a ion in the malonate-containing copper(II) complexes, has afforded from mononuclear to three-dimensional structures, where the $[Cu(mal)_2]^{2-}$ behaves as a building block. The hydrogen-bonding play an important role in the crystal packing when the ions have donor groups as observed in chapter I and III. The size of the ion and its nature (type and number of donor groups, if it has got) control the stacking of the $[Cu(mal)_2]^{2-}$ units. It deserves to be note that usually, the stacking of the $[Cu(mal)_2]^{2-}$ units leads to anionic layers, where the copper atoms are located in the corners of a rhombus (that occurs for the compounds containing $Hmal^-$, Na^+, K^+, Rb^+, $MeNH_3^+$ and H_2pn^{2+}).

The combined used of Cu(II), malonate, and N- or O-exo ligands have afforded a great variety of crystal structures from mononuclear units to three dimensional structures. The pH, the copper(II):malonate:ligand molar ratio, the nature of the N- or O-exo ligand and the solvent used are the relevant parameters in the synthesis of the novel complexes. Bearing that in mind, it's clear that the malonate anion is a very versatile ligand to obtain novel and interesting new functional materials. Nevertheless, it remains difficult to predict its behaviour in the design of novel complexes.

The bisbidentate coordination mode dominant in the oxalato complexes is sterically forbidden for the malonate, this makes that the bidentate + monodentate and the bidentate + bis-monodentate coordination modes dominate in the chemistry of the malonate-containing compounds. This affects dramatically to the structure and the properties of the malonate complexes, being the ferromagnetic interactions much more frequent than in other dicarboxylic compounds. The malonate is a dissymmetric ligand. On one hand when the malonate anion acts as a bidentate ligand, it behaves as a strong complexing agent (due to the chelate effect) and it usually fills equatorial or basal positions displaying short M-O distances (M = metallic ion). On the other hand, when it acts as monodentate ligand it shows weaker interactions and longer M'-O distances. The metallic ion that is chelated usually remains in the same plane of the carboxylato groups with small deviations; meanwhile the monodentate coordinated metal can deviate considerably from the carboxylate plane, reducing notably the overlap between the magnetic orbitals of the paramagnetic centres that the malonate anion bridges. This

minimizes the antiferromagnetism and interactions expected to be antiferromagnetic can be turned to ferromagnetic. Another feature of the malonate anion is the fact that when these latter M'-O distances are long enough, this oxygen becomes axial or apical. Then, as a consequence of the coupling of orbitals of different symmetry the magnetic interaction is expected to be ferromagnetic in many copper(II) complexes.

Consequently we can conclude that the malonate is a very versatile ligand that is able to generate high dimensionality networks coupling paramagnetic centres ferromagnetically in much higher percentage than other dicarboxylic ligands. Within great versatility with the first transition metal ions the malonate anion it self can not lead to a three-dimensional array, [only one 3D structure have been obtained with copper(II)] [Yilmaz V.T. *et al.*, 2004], but combined with other ligands the three-dimensional networks can be obtained. We are now in the search of ligands, suitable to be combined with the malonate, capable to couple ferromagnetically the spin carriers in the remaining dimensions.

Magnetic point of view. The malonate is a very versatile ligand, allowing the out-of-plane conformation of the *anti-syn* and *anti-anti* modes. Hence, the magneto-structural assumptions applied to the oxalate bridge cannot be longer extended to more flexible ligands such as malonate, due to the oversimplification it implies.

As we commented in the introduction the magnetic coupling parameter between two paramagnetic centres can be expressed roughly by the addition of two terms [Kahn O., 1993]:

$$J = J_{AF} + J_{F}$$

J_{AF} being proportional to the overlap between the magnetic obitals of the paramagnetic centres that are coupled.

Bearing in mind this approximation, we can conclude that the parameter that governs, in first order, the magnetic interaction between metal centres is the relative position of the carboxylato bridge of the malonate anion in the coordination sphere of the copper(II) ions: equatorial-equatorial (strong interaction, scheme 1), equatorial-apical (weak interaction, scheme 2) and apical-apical (negligible interaction, scheme 3). Inside this division other parameters that become important are δ [the dihedral angle between copper(II) basal planes] and the distortion of the metal environment.

The synthesis and characterization of compounds of this family, and the wideness of this study to other flexible dicarboxylic ligands will allow these remarks to be definitely settled (see Table 17 in chapter III and Table 17 in chapter V).

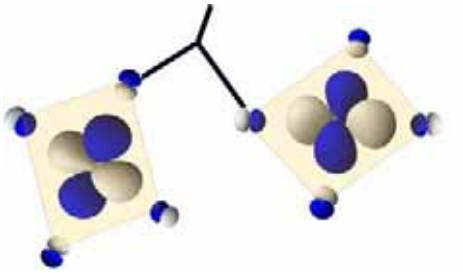

Scheme 1.

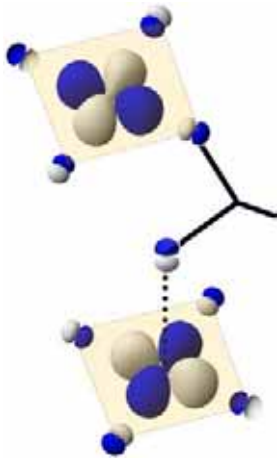

Scheme 2

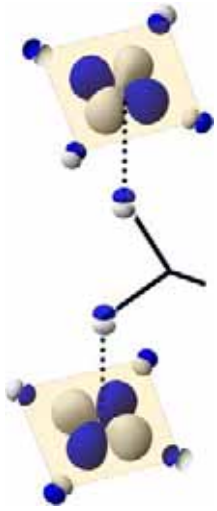

Scheme 3

References

Kahn, O. in *Molecular Magnetism*, ed. VCH, New York, **1993** and references therein.

Yilmaz V.T., Senel E. and Thone C., *Metal Transition Chemistry*, **2004**, 28, 336.

Universidad de La Laguna

DEPARTAMENTO DE FÍSICA FUNDAMENTAL II

"DESARROLLO DE NUEVOS MAGNETOS MOLECULARES CON ION MALONATO COMO LIGANDO"

"DEVELOPMENT OF NEW MOLECULAR MAGNETS BASED ON THE MALONATE ION"

TOMO II

FERNANDO SALVADOR DELGADO TRUJILLO

MEMORIA PARA OPTAR AL GRADO DE DOCTOR EN FÍSICA

PART II: WORKING WITH OTHER MALONATE COMPLEXES

CHAPTER VI. New homometallic malonate compounds: Co(II), Ni(II) and Mn(II).

CHAPTER VII. A structural revision of the heterometallic malonate complexes.

CHAPTER VIII. From low- to high-dimensional networks in Cobalt(II) malonate complexes.

CHAPTER IX. New lanthanide malonate complexes: Ho(III), Sm(III) and Ce(III).

CONCLUSIONS

CHAPTER VI.

New homometallic malonate compounds: Co(II), Ni(II) and Mn(II).

Section A: Co(II) and Ni(II)

Introduction

There has been an increasing interest in complexes containing paramagnetic metal ions exhibiting extended networks because of their potential applications in molecular magnetic materials [Miller J.S. *et al.*, 2001]. The ability of the bridging ligand to mediate magnetic coupling between the paramagnetic centers it links plays a fundamental role in these studies as shown by the oxalato [Kahn O., 1993; Pilkington M. *et al.*, 2004], cyano [Verdaguer M. *et al.*, 1999; Ohba M. *et al.*, 2000; Pilkington M. *et al.*, 2004], azide [Ribas J. *et al.*, 1999], oximato [Chaudhuri P., 2003] or dicyanamide [Batten S.R. *et al.*, 2003] ligands. The malonate group (the dianion of 1,3-propanedioic acid, H_2mal) is a suitable candidate in designing extended magnetic networks because it has been proved to be a very versatile ligand in crystal engineering and in materials science [Rodríguez-Martín Y. *et al.*, 2002a and 2002b; Ruiz-Pérez *et al.*, 2003]. The occurrence of two carboxylate groups in 1,3-positions allows this ligand to adopt several coordination modes. A great variety of crystal structures ranging from mononuclear species [Rodríguez-Martín Y. *et al.*, 2001 and 2002c] to three-dimensional networks [Rodríguez-Marín Y. *et al.*, 2003; Konar S. *et al.*, 2003; Liu T.F. *et al.*, 2003] can be built with the malonate ligand depending on the metal ions it bridges and on the presence of coligands.

Let us focus on the homometallic complexes with first-row transition metal ions that only contain malonate and water as ligands. Different topologies have been observed for the structures of the copper(II) complexes, their nuclearity ranging from discrete entities [Chattopadhyay D. *et al.*, 1993; Ruiz-Pérez C. *et al.*, 2000; Rodríguez-Martín *et al.*, 2002c] to chain compounds [Ruiz-Pérez C. *et al.*, 2000]. Most of these complexes have been magnetically characterized and they exhibit ferromagnetic coupling through the carboxylate-malonate bridge. On the other hand, two-dimensional structures with different topologies have been reported for the malonate complexes with zinc(II) [Ray N.J., 1982] and manganese(II) [Lis T. *et al.*, 1979] ions. An overall weak antiferromagnetic coupling and a spin-canting behaviour at very low temperature (T_c = 2.7 K) have been observed for the manganese(II) compound [Rodríguez-Martín Y. *et al.*, 2003]. No single crystals of the malonate-containing nickel(II) and cobalt(II)

complexes are available but the analysis of their X-ray powder diffraction data reveal that they are isostructural with the zinc(II) malonate [Walter-Levy L. *et al.*, 1973].

In the framework of our magneto-structural studies on malonate-containing metal complexes, we got single crystals of the two-dimensional compounds $\{[M(H_2O)_2][M(mal)_2(H_2O)_2]\}_n$ with M = Co(II) (**1**) and Ni(II) (**2**). We report here their preparation, crystal structure determination and magnetic characterization together with a brief discussion of the structural possibilities offered by this family of homometallic two-dimensional malonato complexes.

Experimental

Materials and methods

Malonic acid, cobalt(II) acetate tetrahydrate and nickel(II) acetate tetrahydrate were purchased from Aldrich and used as received. Elemental analyses (C, H) were performed on a EA 1108 CHNS-O microanalytical analyzer. IR spectra (450-4000 cm^{-1}) were recorded on a Brüker IF S55 spectrophotometer with the samples prepared as KBr pellets. Magnetic susceptibility measurements on polycrystalline samples of compounds **1** and **2** were carried out in the temperature range 1.9-295 K with a Quantum Design SQUID magnetometer. The applied magnetic field was 1 T for $T \geq 100$ K and 250 Oe for T < 100 K in order to avoid saturation phenomena. Diamagnetic corrections for the constituent atoms were estimated from Pascal's constants [Earshaw A., 1968] as -156×10^{-6}, and -160×10^{-6} cm^3 mol^{-1} for compounds **1** and **2**, respectively. Experimental susceptibilities were also corrected for the temperature-independent paramagnetism [100 x 10^{-6} cm^3 mol^{-1} per Ni(II) ion] and the magnetization of the sample holder.

Synthesis

$\{[Co(H_2O)_2][Co(mal)_2(H_2O)_2]\}_n$ (1). Malonic acid (11 mmol, 1.14 g) is added to an aqueous solution (100 cm^3) of cobalt(II) acetate (10 mmol, 2.49 g) under continuous stirring. The volume of the resulting solution is reduced to ca. *ca.* 50 cm^3 by heating in a steam bath at 60 ºC in order to evaporate the acetic acid. Single crystals of **1** as red prisms were grown on standing by keeping the temperature of steam bath at *ca.* 40 ºC. Yield: 75%. Anal. Calcd. for $C_6O_{12}H_{12}Co_2$: C, 18.28; H, 3.00. Found: C, 18.35; H, 3.10%. Selected IR peaks (KBr/cm^{-1}): ν(COO) 1663, 1581sh, 1565, 1451, 1373, 721.

{[Ni(H$_2$O)$_2$][Ni(mal)$_2$(H$_2$O)$_2$]}$_n$ (2). X-ray quality crystals of **2** as green needles were prepared by following the procedure detailed above for **1** but using nickel(II) acetate instead of the cobalt(II) one. Yield: 65%. Anal. Calcd. for $C_6O_{12}H_{12}Ni_2$: C, 18.30; H, 3.0. Found: C, 18.22; H, 3.12%. Selected IR peaks (KBr/cm^{1}): ν(COO) 1665, 1585sh, 1567, 1453, 1376, 726.

Crystal data collection and refinement of the structures

Single crystals of **1** and **2** were mounted on a Bruker-Nonius KappaCCD diffractometer. Orientation matrix and lattice parameters were obtained by least-squares refinement of the reflections obtained by a θ-χ scan (Dirax/lsq method). Diffraction data of **1** and **2** were collected at 293(2) K using graphite-monochromated Mo-K$_\alpha$ radiation (λ = 0.71073 Å). The indexes of data collection were $-15 \le h \le 16$, $-9 \le k \le 8$, $-9 \le l \le 7$ for **1** and $-17 \le h \le 10$, $-8 \le k \le 10$, $-10 \le l \le 10$ for **2**. Of the 723 (**1**) and 887 (**2**) measured independent reflections in the θ range 5.25 – 27.5º (**1**) and 6.43 – 30º (**2**) , 612 (**1**) and 637 (**2**) have $I \ge 2\sigma(I)$. All the measured independent reflections were used in the analysis. All calculations for data reduction, structure solution, and refinement were done by standard procedures (WINGX) [Farrugia L.J., 1999]. The structures were solved by direct methods and refined with full-matrix least-squares technique on F^2 using the SHELXS-97 and SHELXL-97 programs [Sheldrick G.M. SHELX97, release 97-2, 1998]. In both compounds the malonate hydrogen atoms were located from difference Fourier maps and refined with isotropic temperature factors. The hydrogen atoms of the water molecules were not found. The final Fourier-difference map showed maximum and minimum height peaks of 0.661 and -0.450 e Å^{-3} for **1** and of 0.682 and -0.539 e Å^{-3} for **2**. A summary of the crystallographic data and structure refinement is given in Table 1. The final geometrical calculations and the graphical manipulations were carried out with PARST97 [Nardelli M., 1995] and DIAMOND [DIAMOND 2.1d, 2000] programs, respectively.

Crystal structures were deposited at the Cambridge Crystallographic Data Centre, the CCDC reference numbers 231721 (**1**) and 231722 (**2**).

Table 1. Crystal data and details of the structure determination for **1** and **2**

Compound	**1**	**2**
Formula	$C_3H_6CoO_6$	$C_3H_6NiO_6$
M	197.01	196.79
Crystal system	monoclinic	monoclinic
Space group	*C*2/m	*C*2/m
a, Å	12.646(3)	12.5748(5)
b, Å	7.4040(10)	7.3781(6)
c, Å	7.2970(10)	7.2274(4)
α, deg	90.0	90.0
β, deg	120.18(3)	120.391(6)
γ, deg	90.0	90.0
V, Å^3	590.61(2)	578.41(6)
Z	4	4
T, K	293(2)	293(2)
ρ_{calc} (Mg m^{-3})	2.216	2.260
λ (Mo-K$_\alpha$ Å)	0.71073	0.71073
μ (Mo-K$_\alpha$ mm^{-1})	2.874	3.322
Number parameters/restrains	60 / 0	60 / 0
Goodness of fit (*S*)	1.165	1.095
R1, $I > 2\sigma(I)$ (all)	0.026 (0.034)	0.042 (0.071)
wR2, $I > 2\sigma(I)$ (all)	0.076 (0.079)	0.086 (0.092)
Max/min electron density (e/Å^3)	0.661 / -0.450	0.682 / -0.539
Measured reflections (R_{int})	1572 (0.016)	1943 (0.042)
Independent reflections [$I > 2\sigma(I)$]	723 (612)	887 (637)

Results and discussion

Description of the Structure of $\{[M(H_2O)_2][M(mal)_2(H_2O)_2]\}_n$ [M=Co(II) (1) and Ni(II)(2)]

Complexes **1** and **2** are isostructural compounds. Their structure consists of corrugated layers containing $[M(1)(mal)_2(H_2O)_2]^{2-}$ anions and $[M(2)(H_2O)_2]^{2+}$ cations with M(1) = M(2) = Co(II) (**1**) and Ni(II) (**2**) which are linked by carboxylate-malonate groups in the *anti-syn* bridging mode (Figure 1a). These layers grow in the *bc*-plane and they exhibit intralayer [between O(2w) and the O(1) and O(1f) malonate-oxygen atoms] and interlayer [between O(1w) and the O(2g) and O(2h) malonate oxygens] hydrogen bonds [see Table 2 and Figure 1b], the latter ones leading to a three-dimensional structure.

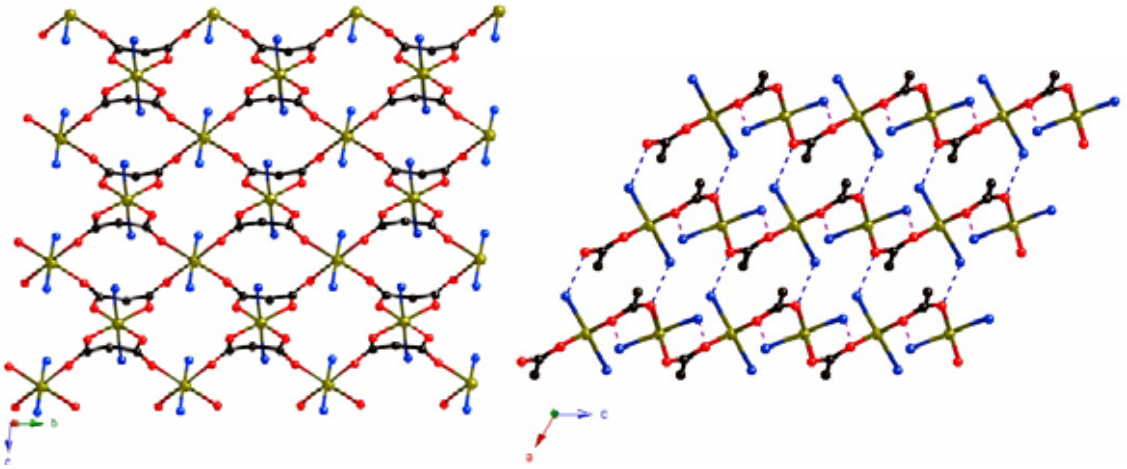

(a) **(b)**

Figure 1. (a) Perspective view of a fragment of the corrugated malonate-bridged layer of **1** [M = Co(II)] and **2** [M = Ni(II)] growing in the *bc*-plane. **(b)** Side view of three adjacent layers of **1** and **2** showing the intra- and interlayer hydrogen bonds (broken lines).

Table 2. Selected bond lenghts (Å) and angles (º) and relevant H-bonds for **1** and **2**[a,b]

Metal environment	**1**	**2**
M(1)-O(1)	2.050(2)	2.021(2)
M(1)-O(1w)	2.123(3)	2.090(4)
O(1)-M(1)-O(1a)	89.52(10)	90.55(13)
O(1)-M(1)-O(1c)	90.48(10)	89.45(13)
O(1)-M(1)-O(1w)	91.85(8)	92.20(10)
O(1)-M(1)-O(1wc)	88.15(8)	87.80(10)
O(2)-M(2)-O(2d)	86.45(11)	86.76(14)
M(2)-O(2)	2.119(2)	2.087(2)
M(2)-O(2w)	2.081(2)	2.058(3)
O(2)-M(2)-O(2f)	93.55(11)	93.24(14)
O(2)-M(2)-O(2w)	93.45(7)	93.92(9)
O(2)-M(2)-O(2wd)	86.55(7)	86.08(9)
Hydrogen bonds	**1**	**2**
D-H···A	D···A/Å	D···A/Å
Intralayer		
O(2w)···O(1)	2.680(2)	2.673(3)
O(2w)···O(1f)	2.680(2)	2.673(3)
Interlayer		
O(1w)···O(2g)	2.860(4)	2.853(5)
O(1w)···O(2h)	2.860(4)	2.853(5)

[a] Symmetry transformations: (a) *x*, -*y*, *z*; (b) 1-*x*, -*y*, 1-*z*; (c) 1-*x*, *y*, 1-*z*; (d) 1-*x*, *y*, 2-*z*; (e) 1-*x*, 1-*y*, 2-*z*; (f) *x*, 1-*y*, *z*; (g) 1/2-*x*, 1/2-*y*, 1-*z*; (h) 1/2-*x*, -1/2+*y*, 1-*z*. [b] A = acceptor; D = donor.

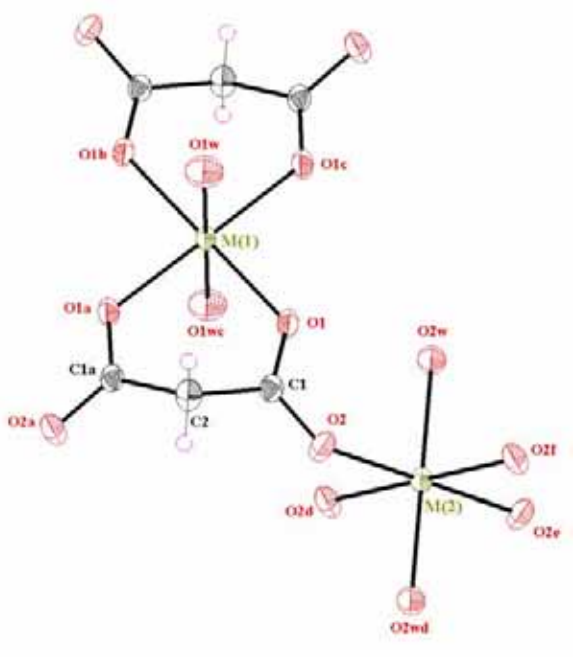

Figure 2. Perspective view showing the two crystallographically independent metal ions in **1** [M = Co(II)] and **2** [M = Ni(II)]. Thermal ellipsoids are drawn at the 50% probability level and they correspond to **1**.

There are two crystallographycally independent metal ions [M(1) and M(2)] which lie on a 2/*m* crystallographic site (Table 2, Figure 2). Both metal ions are six-coordinated in slightly distorted octahedral environments: they have in common the occurrence of two *trans* coordinated water molecules in the apical positions and four oxygen atoms from two [at M(1)] and four [at M(2)] malonate ligands in the equatorial plane. Some characteristic geometric values [Stiefel E.I. *et al.*, 1972] for **1** and **2** are listed in Table 3. The equatorial M(1)-O bond distances [2.050(2) and 2.021(2) Å for **1** and **2**, respectively] are somewhat shorter than the apical ones [2.123(3) (**1**) and 2.090(4) Å (**2**)], leading to an elongated distorted octahedral environment around M(1). The opposite trend is observed at M(2) whose octahedral environment is axially compressed, the values of the equatorial M(2)-O bond distances [2.119(2) (**1**) and 2.087(2) Å (**2**)] being longer than the apical ones [2.081(2) (**1**) and 2.058(3) Å (**2**)]. All geometric values are in good agreement with the those observed in the isostructural zinc(II) malonate [Ray N.J., 1982].

Table 3. Some geometric values for compounds **1** and **2**[a]

Compound	**1**	**2**
Geometric values for metal environment around M(1)		
s/h	1.247	1.246
Φ/º	58.8	56.9
Geometric values for metal environment around M(2)		
s/h	1.230	1.214
Φ/º	61.32	64.97
Ring puckering parameters (chelating malonate)		
Phase angle, ϕ/º	120.0(3)	120.0(4)
θ/º	73.2(2)	74.4(3)

Figure 3. Coordination mode of the malonate ligand in **1** [M = Co(II)] and **2** [M = Ni(II)].

The methylene-malonate group lies on a crystallographic mirror plane. Each malonate ligand adopts simultaneously the bidentate [through O(1) and O(1a) toward M(1)] and bis-monodentate [through O(2) and O(2a) toward M(2) and M(2i); (a) *x*, -*y*, *z*; (i) *x*, *y*-1, *z*] coordination modes and exhibits an envelope conformation (see geometric values in Table 3). The angle subtended by the malonate ligand at M(1) is 89.52(10) (**1**) and 90.55(13)º (**2**). The carboxylate-malonate groups exhibit the *anti-syn* conformation and they connect two equatorial positions of the M(1) and M(2) metal ions. The values of bond lengths and angles of the malonate ligands in **1** and **2**, listed in Table 4, agree well with those previously reported in other malonate-containing complexes [see references of malonate-containing cobalt(II) and nickel(II) complexes in the Introduction].

Table 4. Bond lengths (Å) and angles (º) for malonate ligands in **1**and **2**[a]

Malonate ligand	**1**	**2**
C(1)-C(2)	1.516(3)	1.518(4)
C(1)-O(1)	1.263(3)	1.262(4)
C(1)-O(2)	1.249(3)	1.253(4)
O(1)···O(1a)	2.886(2)	2.872(3)
O(2)···O(2a)	4.316(2)	4.344(3)
O(1)-C(1)-O(2)	123.0(2)	123.1(3)
O(1)-C(1)-C(2)	119.7(2)	119.8(3)
O(2)-C(1)-C(2)	117.3(2)	117.1(3)
C(1)-C(2)-C(1a)	115.8(3)	116.1(4)
C(1)-O(1)-M(1)	127.8(2)	127.7(2)
C(1)-O(2)-M(2)	126.8(2)	126.8(2)

[a] Symmetry transformations: (a) *x*, -*y*, *z*.

Each M(1) atom is connected to four M(2) atoms through *anti-syn* carboxylate groups from two malonate ligands to afford corrugated layers. The two crystallographically independent metal atoms [M(1) and M(2)] are set in the same plane within each layer, whereas the malonate ligands are shifted from these metal planes. The values of the dihedral angles between the equatorial plane of the M(1) and M(2) atoms and the O(1)-C(1)-O(2) mean plane are 22.6(2) and 77.64(13)º for **1** and 22.5(3) and 77.2(2)º for **2.** The equatorial planes of M(1) and M(2) form dihedral angles of 79.45(4) (**1**) and 80.17(6)º (**2**). The values of the shortest intra- and interlayer metal···metal distances are listed in Table 5.

Table 5. Values of the shortest metal···metal separations (Å) in compounds **1** and **2**[a]

Compound	**1**	**2**
Intralayer		
M(1)···M(2)	5.1977(5)	5.1641(3)
M(1)···M(1j)	7.4040(10)	7.3781(6)
M(2)···M(2k)	7.2970(10)	7.2274(4)
Interlayer		
M(1)···M(2l)	5.486(2)	5.4407(4)

[a] Symmetry code: (j) *x*, *y*+1, *z*; (k) *x*, *y*, *z*-1; (l) 1/2+*x*, -1/2+*y*, *z*.

Influence of the coligand on the structure of the homometallic malonate complexes

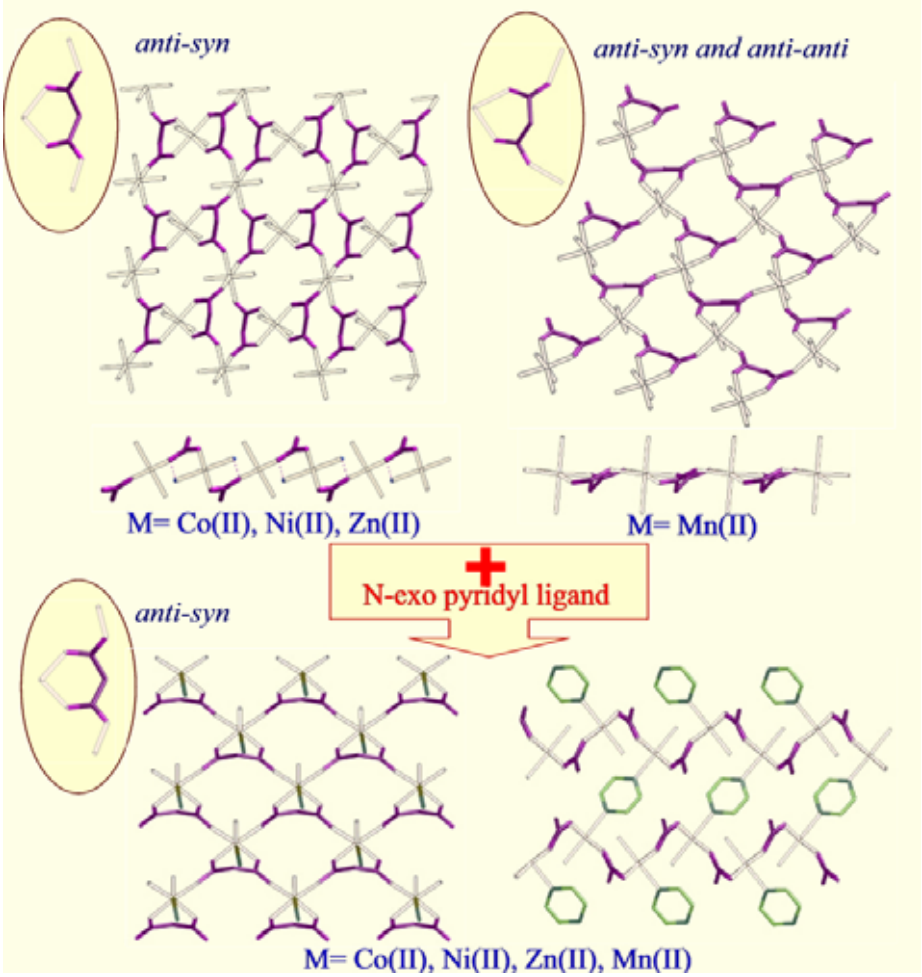

Scheme 1

Let us carry out a brief survey of the structural possibilities of the homometallic malonate complexes in the presence of a coligand. The structures of the hydrated phases of the manganese(II) and zinc(II) malonate complexes were previously described by Lys [Lys T. *et. al.*, 1979] and Ray [Ray N.J. ,1982], respectively. The structure of these compounds consists basically of layers of malonate-containing transition metal ions (see Scheme 1, top). In the case of manganese(II) the layers are built of *trans*-diaquamanganese(II) units bridged by carboxylate-malonate groups in the *anti-syn* and *anti-anti* bridging modes [intralayer Mn···Mn separations through the *anti-anti* and the *anti-syn* carboxylate bridges being 5.790(4) and 6.319(4) Å, respectively]. The malonate groups do not deviate significantly from the plane defined by the metal ions. On the other hand, two crystallographycally independent metal ions are present in the

isostructural zinc(II), cobalt(II) (**1**) and nickel(II) (**2**) malonate series. These three compounds have also a two-dimensional structures with *trans*-diaquabismalonatemetalate(II) and *trans*-diaquametal(II) units being bridged through *anti-syn* carboxylate-malonate groups [intralayer M···M separation ranging from 5.1566(5) to 5.2072(7) Å]. In contrast to the planar manganese(II) malonate structure, the layers in this series are corrugated, the malonate ligands within each layer being out the plane defined by the metal ions. In all homometallic malonate compounds with divalent first-row transition metal ions, hydrogen bonds involving coordinated water molecules and malonate oxygen atoms contribute to stabilize the crystal structure and lead to a three-dimensional network.

Although the homometallic malonate complexes have significant structural differences, when they react with N-exo pyridyl ligands such as pyrimidine (pym), pyrazine (pyz), 2,4'-bipyridine (2,4'-bpy) and 4,4'-bipyridine (4,4'-bpy), the layer containing the malonate and the metal ions is kept, the N-donor atom of the pyridyl ligand occupying an apical position of the metal environment for M = Mn(II) [Rodríguez-Martín Y. *et al.*, 2003; Maji T.K. *et al.*, 2003], Co(II) [Lightfoot P. *et al.*, 1999; Konar S. *et al.*, 2003; see also Chapter VIII], Zn(II) [Burrows A.D. *et al.*, 2000; Zhang X.T. *et al.*, 2003; see also compound8 in the cif files of Chapter VIII], and Ni(II) [see compound7 file in the cif files of Chapter VIII]. The topology of these layers (Scheme 1, bottom) is different from those of the diaquamalonatemetal(II) ones (Scheme 1, top). Aquametal(II) units linked by carboxylate-malonate groups in the *anti-syn* bridging mode build the corrugated layer in the complexes containing the N-donor. Additionally, weak π-π stacking interactions between pyridyl-rings in this family can contribute to the stabilization of the resulting network.

Several malonate complexes have been reported with other N-donor ligands. The reaction of manganese(II) malonate complexes with chelating ligands such as 2,2'-bipyridine (2,2'-bpy) [Shen L., 2003] and 1,10-phenantroline (phen) [Wang Z.X. *et al.*, 2000] afforded mononuclear neutral units which are linked by hydrogen bonds into three-dimensional networks. Finally, the reaction of Co(II) malonate with hexamethylenetetramine (urotropine) [Konar S. *et al.*, 2003] and benzimidazole [Xue Y.-H. *et al.*, 2004; Lin D.-D. *et al.*, 2004] yielded monomeric entities and two- and three-dimensional structures where corrugated malonate-bridging cobalt(II) layers are present.

Magnetic properties of 1 and 2

The thermal dependence of the $\chi_M T$ product [χ_M being the magnetic susceptibility *per* cobalt(II) ion] for compound **1** is shown in Figure 4. At room temperature, $\chi_M T$ is equal to 3.12 $cm^3\ mol^{-1}$ K, a value which is above of that expected for the spin-only one for a high spin cobalt(II) ion (1.87 $cm^3\ mol^{-1}$ K with g = 2.0). This is due to the occurrence of a unquenched orbital contribution typical of the $^4T_{1g}$ ground state in six-coordinated cobalt(II) complexes [Carlin R.L., 1986; Mabbs F.E. *et al.*, 1973]. Upon cooling, $\chi_M T$ continuously decreases reaching a minimum value of 1.35 $cm^3\ mol^{-1}$ K at 2.0 K. No maximum of susceptibility is observed in the χ_M versus T plot. The decrease of $\chi_M T$ with T can be due to depopulation of the higher energy Kramers doublets of cobalt(II) and/or to antiferromagnetic interactions. At this respect, the carboxylate group has shown to play the role of antiferromagnetic coupler in carboxylate-bridged cobalt(II) complexes [Rueff J.M. *et al.*, 2001; Kumagai H. *et al.*, 2002; Lee E.W. *et al.*, 2002; see Chapter V], the values of the exchange coupling (J) ranging from -3 to -1 cm^{-1}.

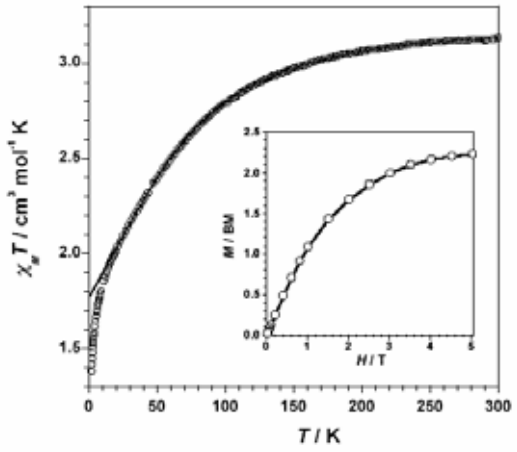

Figure 4. Thermal dependence of the $\chi_M T$ product for **1** per Co: (o) experimental; (—) best-fit curve (see text). The inset shows the magnetisation versus H plot at 2.0 K for **1**: (o) experimental; (—) eye-guide line.

Thus having in mind that the magnetic interactions in **1** are most likely very weak, its magnetic behaviour would be monitored by spin-orbit coupling effects. In order to test this assumption, and taking into account that the two crystallographically independent six-coordinated cobalt(II) ions are axially distorted (four carboxylate

malonate and two water molecules in *trans* positions), we have analyzed the magnetic data of **1** through the Hamiltonian of eq. (1) [Herrera J.M. *et al.*, 2003]:

$$\mathbf{H} = -A\kappa\lambda\mathbf{LS} + \Delta[\mathbf{L}_z^2 - (1/3)L(L+1)] + \beta(-A\kappa\mathbf{L} + g_e\mathbf{S})H \qquad (1)$$

where spin-orbit coupling (first term), axial distortion (second term) and Zeeman interaction (last term) are considered. No analytical expression for the magnetic susceptibility as a function of A, κ, λ and Δ can be derived and the values of these parameters were determined by matrix diagonalization. Taking into account that a value of A = 3/2 is used in most of the studies with Co(II) where the weak crystal field is involved (as in **1**) and in order to avoid the overparametrization, we introduced a fixed value of A of 1.5 in the fitting procedure. Best-fit parameters of the experimental data of **1** for T > 15 K are: A = 1.5 (fixed), κ = 0.98, λ = -137 cm^{-1} and Δ = 506 cm^{-1}. The calculated curve reproduces very well the experimental data in the temperature range 15-300 K and the computed values are within the range of those reported for high spin cobalt(II) in the literature. When T < 15 K, the magnetic data of Figure 3 are below the calculated curve indicating that a weak antiferromagnetic interaction between the cobalt(II) ions occurs. An inspection of the structure of **1** shows that the exchange pathways for these interactions are provided by intra- and interlayer hydrogen bonds and the carboxylate-malonate bridge but their evaluation is precluded by the lack of appropriate models.

The field dependence of the magnetization at 2.0 K, per cobalt(II) ion, of a polycrystalline sample of **1** (see inset of Figure 4) shows a quasi saturation value (M_S) of 2.25 $N_A\beta$ at 2 K and an applied magnetic field of 5 T. This value is smaller than the calculated M_S value of 3 (S_{Co} = 3/2) when g = 2. This difference is due to the fact that only the ground Kramers doublet is populated at 2.0 K [Carlin R.L., 1986; Coronado E. *et al.*, 1988], with an effective spin S_{eff} = 1/2 and g = (10 + 2$A\kappa$)/3. For A = 1.5 and κ = 0.98 (see above), M_S = 2.15 $N_A\beta$, a value which is close to the experimental one.

The thermal dependence of the $\chi_M T$ product [χ_M being the magnetic susceptibility *per* nickel(II) ion] for compound **2** is shown in Figure 5. At room temperature, $\chi_M T$ is equal to 1.22 cm^3 mol^{-1} K, a value which is as expected for a magnetically isolated spin triplet (1.21 cm^3 mol^{-1} K with g = 2.20). Upon cooling, $\chi_M T$

increases reaching a maximum value of 1.34 cm^3 mol^{-1} K at 7.5 K, and then decreases at lower temperatures. This behaviour is indicative of the occurrence of a very weak ferromagnetic coupling between the Ni(II) ions, the slight decrease in the low temperature range being due single-ion zero-field splitting of the Ni(II) ions (*D*) and/or very weak antiferromagnetic interactions. The absence of susceptibility maximum in the χ_M *vs. T* plot indicates that the decrease of $\chi_M T$ is mainly due to *D*. The magnetisation *vs. H* plot at 2.0 K, per nickel(II) ion, of a polycrystalline sample of **2** (see inset of Figure 5) shows a quasi paramagnetic behaviour, the value of the magnetization at 5 T (the maximum field available in our magnetometer) being 1.65 $N_A\beta$. This value is significantly below that expected for a spin triplet (ca. 2.20 $N_A\beta$ with g = 2.20) in agreement with the dominant role of the zero-field splitting term at low temperatures and the very weak ferromagnetic coupling observed.

Compound **2** has a two-dimensional and quasi quadratic structure in which the carboxylate-malonate groups act as bridges in the *anti-syn* conformation between the nickel(II) ions. In order to determine value of the weak ferromagnetic coupling observed in **2**, we have fitted the high temperature magnetic data (T > 16 K) of **2** through the high-temperature series expansion derived from the two-dimensional Heisenberg model for a S = 1 manifold ferromagnet square lattice [eq (2)] [Navarro R., 1990], assuming that the two nickel atoms are equivalent:

$$\chi = \left[Ng^2\beta^2/(3kT)\right]\cdot X\cdot\left(1+\sum_{n=1}^{8}A_n(X)K^n\right) \qquad (2)$$

with

$$A_n(X) = \sum_{i=1}^{n} a_n X^n$$
$$X = S(S+1)$$

and

$$K = J/\mathrm{kT}$$

In this expression, the parameters N, g, β and k are the Avogadro's number, Landé factor, Bohr magneton, Boltzman's constant respectively. A_n and a_n are the coefficients for the square lattice and J is the intralayer magnetic coupling between the local spins of the nearest-neighbours [Hamiltonian of eq (3)]

$$H = -\Sigma_i J S_i \cdot S_{i+1} \qquad (3)$$

In this approach, the single-ion zero-field splitting of the Ni(II) ions is not considered, assuming that its effect is not important in the temperature range considered [Castillo O. *et al.*, 2001]. This expression is valid for systems in which all the nickel(II) ions are equivalent, which is not the case of compound **2**, so we will have an approximate value for J and a mean value for the Landé factor for both nickel(II) ions. The best-fit parameters using a nonlinear regression analysis are: $J = +0.18(2)$ cm^{-1}, $g = 2.20(1)$ and $R = 3.8 \times 10^{-4}$ where R is the agreement factor defined as $\Sigma_i[(\chi_M T)_{obs}(i) - (\chi_M T)_{calc}(i)]^2/\Sigma[(\chi_M T)_{obs}(i)]^2$. The calculated curve matches very well the experimental data in the temperature range 16 –295 K.

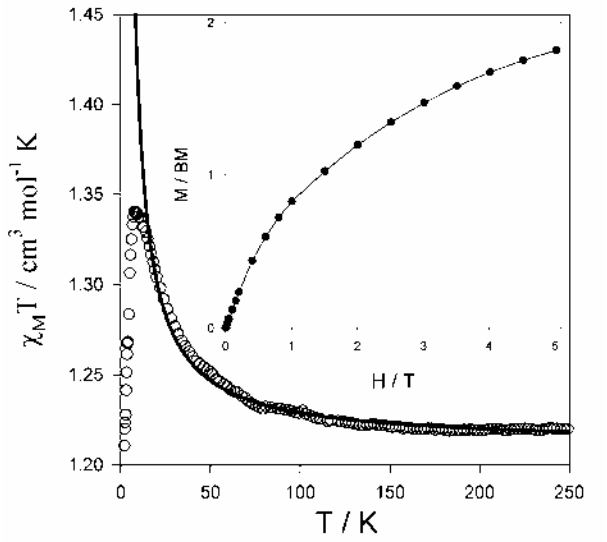

Figure 5. Thermal dependence of the $\chi_M T$ product for **2** per Ni: (o) experimental; (—) best-fit curve (see text). The inset shows the magnetisation versus H plot at 2.0 K for **2**: (o) experimental; (—) eye-guide line.

A literature survey of the magneto-structural data on carboxylate-malonate copper(II) complexes where the carboxylate exhibits the *anti-syn* coordination mode reveals the occurrence of moderate (when linking equatorial positions of adjacent copper atoms) to weak (when linking equatorial and axial positions of adjacent copper atoms) ferromagnetic interactions [Pasán J. *et al.*, 2003a and 2003b; see Chapter V]. This ability of the carboxylate group to mediate ferromagnetic interactions between copper(II) ions when acting as a bridge through the *anti-syn* coordination mode has been substantiated by DFT type calculations [Rodríguez-Fortea A. *et al.*, 2001]. The orthogonality between the two copper centred magnetic orbitals (which lie mainly in the

equatorial plane of the copper atom) through this carboxylate bridge accounts for the ferromagnetic coupling observed. Although magneto-structural studies on carboxylate-bridged nickel(II) with the carboxylate adopting the *anti-syn* bridging mode are rare, ferromagnetic interactions through this exchange pathway are known [Whitfield T. *et al.*, 2001]. This exchange pathway is most likely responsible for the ferromagnetic coupling observed in **2**, the disagreement between the experimental data and calculated curve in the low temperature range being due to influence of the zero-field splitting and or very weak antiferromagnetic interactions through hydrogen bonds.

Finally, a point which deserves a brief comment is the fact that the magnetic coupling between the cobalt(II) (**1**) and nickel(II) ions (**2**) through the carboxylate-malonate bridge is antiferro- (**1**) and ferromagnetic (**2**). The different electronic configuration of the metal ions involved with three (**1**) and two (**2**) unpaired electrons [$t_{2g}^5 e_g^2$ for Co(II) and $t_{2g}^6 e_g^2$ for Ni(II), O_h symmetry] would account for that. As the ferromagnetic coupling in **2** is very weak, the presence of one unpaired electron in the t_{2g} type orbital for **1** would increase the possibility of net overlap between the magnetic orbitals [Pilkington M. *et al.*, 2004] enhancing thus the antiferromagnetic contributions in **1** and the ferromagnetic terms would be overcome. The weak antiferromagnetic coupling observed between the manganese(II) ions [$t_{2g}^3 e_g^2$ electronic configuration] bridged by carboxylate-malonate units [Rodríguez-Martín Y. *et al.*, 2003] where the three t_{2g} type orbitals are half filled supports additional support to this suggestion.

Section B: Mn(II) [Neutron diffraction study]

Introduction

The crystal structure of $[Mn(mal)(H_2O)_2]_n$ is well known [Lys T. *et al.*, 1979; Rodríguez-Martín et *al.*, 2003]. Its structure consits of layers containing $[Mn(mal)(H_2O)_2]$ mononuclear units linked by *anti-anti* and *anti-syn* carboxylate bridges (see Figure 6) [the intralayer Mn···Mn separations being 6.319(4) and 5.790(4) Å, through the *anti-anti* and *anti-syn* bridge, respectively].

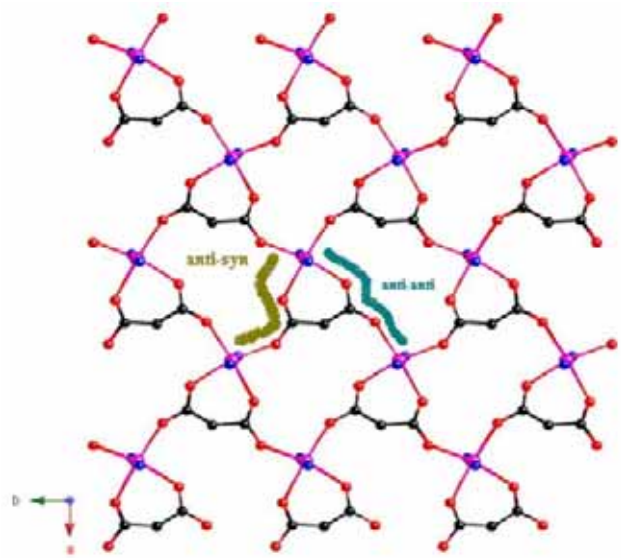

Figure 6. Perspective view, along the *c*-axis of a fragment of the malonate-bridged manganese(II) layer.

Magnetic measurements (d.c. and a.c. magnetic susceptibilities, zero-field cooled and field-cooled magnetizations) have shown that this compound exhibits a long range magnetic ordering below T_c = 2.7(1) K (this behaviour being characteristic of a spontaneuos moment due to the spin canting) [Rodríguez-Martín et *al.*, 2003]. From these data and $T > 3$ K, the magnitude of the exchange couplings through the *anti-anti* and *anti-syn* carboxylate bridges was obtained. Although both bridges are able to mediate significant magnetic coupling among paramagnetic centres, the *anti-syn* gives much weaker interactions than the *anti-anti* [Colacio E. *et al.*, 1999; Ruiz-Pérez C. *et al.*, 2000; Rodríguez-Fortea P. *et al.*, 2001]. Under this approach and from a magnetic point of view, the structure of $[Mn(mal)(H_2O)_2]_n$ was described as *anti-anti* carboxylate-malonate bridged manganese(II) chains linked through *anti-syn* carboxylate groups (see Figure 7) [Rodríguez-Martín *et al.*, 2003]; *J* and *j* are the exchange couplings across the *anti-anti* and *anti-syn* carboxylate bridges, respectively. Having this in mind, the magnetic data were analysed through the Fisher [Fisher M.E., 1964] expression. In both cases, the nature of the

magnetic exchange is antiferromagnetic, the values being J = -0.64(1) and j = -0.0075 cm^{-1}.

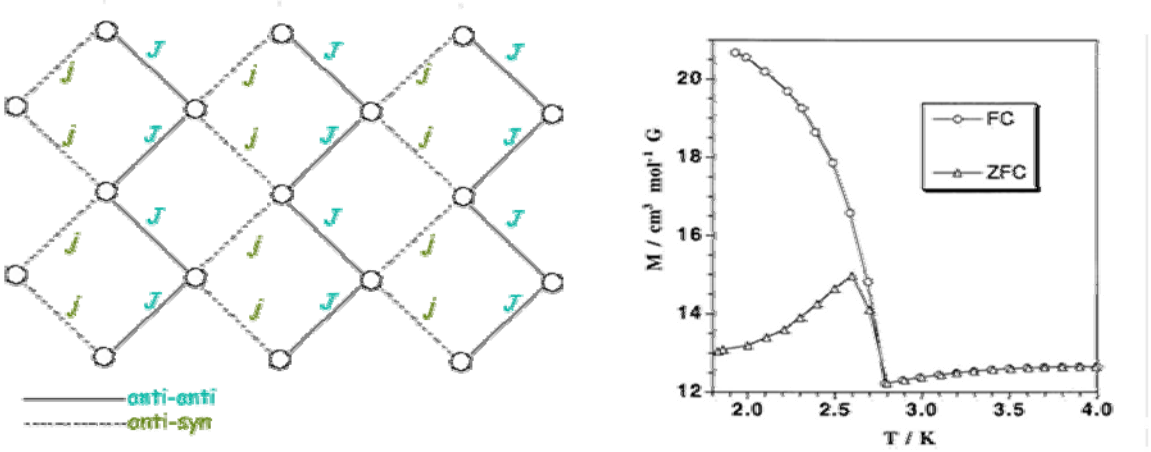

(a) **(b)**

Figure 7. (a) Schematic view of the magnetic interactions within the carboxylate-bridged manganese(II) layers. **(b)** Zero-field cooled (Δ) and field-cooled magnetisation (") as a function of the temperature for $[Mn(mal)(H_2O)_2]_n$. The solid line is an eye-guide line and the inset shows the temperature dependence of the out-of-phase ac susceptibility (χ'') measured in an oscillatory field of 1 G and at 333 Hz.

In this work, our aim is to establish the magnetic structure below T_c = 2.7(1) K, using powder neutron diffraction.

The presence of hydrogen atoms and the low density of magnetic centres in the sample [only four Mn(II) by unit cell] were the first problems we have to face up in order to solve the magnetic structure of **3** because of the noise (due to the presence of hydrogen atoms) and the low intensity in the signal (due to the small amount of magnetic centres in the unit cell). In order to obtain appropriated neutron powder diffraction patterns we made a good statistics of the data.

Unpolarizated neutron powder diffraction data from G4.2 diffractometer at 280 and 5 K were used to determine the complete crystal structure including hydrogen atoms which have not been located by X-ray diffraction.

Once, we knew the complete crystal structure we used the neutron powder diffraction data from the G4.1 diffractometer to obtain the magnetic structure of $[Mn(mal)(H_2O)_2]_n$ below the ordering temperature and to refine it. We present here the obtained results.

Experimental
Searching for the hydrogen atoms

X-Ray Diffraction Data. Structure Solution and Refinement

Crystals of $[Mn(mal)(H_2O)_2]_n$ (**3**) were prepared following the procedure described in the literature [Rodríguez-Martín et *al.*, 2003]. Suitable crystals of **3** were mounted on a Bruker-Nonius KappaCCD diffractometer. Orientation matrix and lattice parameters were obtained by least-squares refinement of the reflections obtained by a θ-χ scan (Dirax/lsq method). Diffraction data were collected at 293(2) (**3a**) and at 100(2) K (**3b**) using graphite-monochromated Mo-K_α radiation (λ = 0.71073 Å). Data collection and data reduction were done with the COLLECT [Hooft R.W.W., 1999] and EVALCCD [Duisenberg A.J.M. *et al.*, 2003] programs. Empirical absorption corrections were carried out using SADABS [SADABS, version 2.03, 2003] for all compounds. All calculations for data reduction, structure solution, and refinement were done by standard procedures (WINGX) [Farrugia L.J., 1999]. The structure was solved by direct methods and refined with full-matrix least-squares technique on F^2 using the SHELXS-97 and SHELXL-97 programs [Sheldrick G.M., SHELX97, realease 97-2, 1998]. For both compounds, the water hydrogen atoms were not found and the malonate hydrogen atoms were set in calculated positions. The hydrogen atoms were refined with isotropic temperature factors. A summary of the crystallographic data and the structure refinement is given in Table 6. Selected bond lengths and angles for **3** are listed in Table 7.

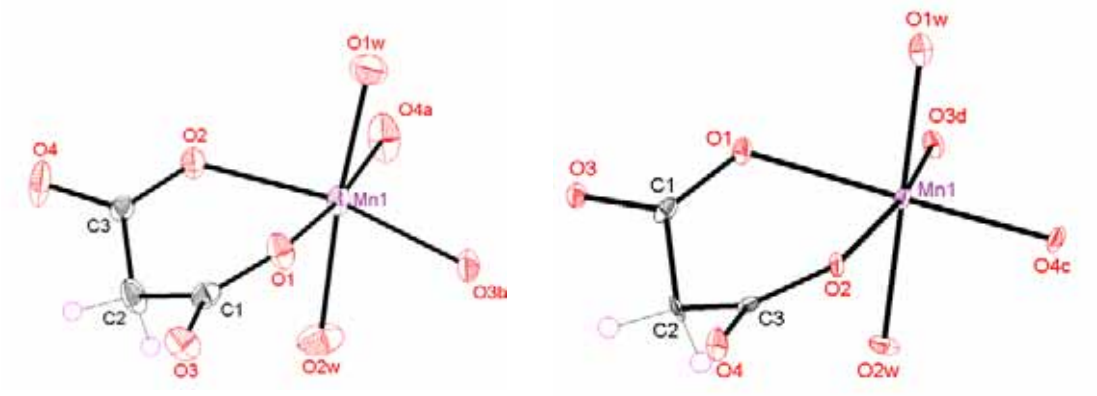

(a) (b)

Figure 8. ORTEP view of the manganese(II) environment at room temperature **(a)** and at 100 K **(b)** with the atom numbering. Thermal ellipsoids are drawn at the 50% probability level.

Table 6. Crystal data and details of structure determination for **3**

Compound	**3a**	**3b**
Formula	$C_3H_6MnO_6$	$C_3H_6MnO_6$
M	193.02	193.02
Crystal system	orthorhombic	orthorhombic
Space group	$Pca2_1$	$Pca2_1$
a, Å	9.6050(4)	9.615(2)
b, Å	7.3602(3)	7.3350(10)
c, Å	8.3263(4)	8.232(2)
V, Å^3	588.63(4)	580.6(2)
Z	4	4
T(K)	293(2)	100(2)
ρ_{calc} (Mg m^{-3})	2.178	2.208
F(000)	388	388
λ (Mo-Kα Å)	0.71073	0.71073
μ(MoK$_\alpha$) (mm^{-1})	2.211	2.241
Flack Parameter	0.06(3)	0.04(4)
Number parameters/restraints	92 / 1	91 / 1
Goodness of fit (S)	1.086	1.078
R1, $I > 2\sigma(I)$ (all)	0.0400 (0.0624)	0.0414 (0.0576)
wR2, $I > 2\sigma(I)$ (all)	0.0816 (0.0864)	0.0908 (0.0954)
Max/min electron density (e/Å^3)	0.513 / -0.503	0.788 / -0.520
Measured reflections (R_{int})	3691 (0.0366)	2268 (0.0417)
Independent reflections [$I > 2\sigma(I)$]	1673 (1305)	1157 (966)

Selected bond lengths and angles for 3 are listed in Table 7.

Table 7. Selected bond lengths (Å) and angles (º) for **3a** and **3b**[a]

3a			
Mn(1)-O(1)	2.200(2)	Mn(1)-O(2)	2.160(2)
Mn(1)-O(4a)	2.122(2)	Mn(1)-O(3b)	2.150(3)
Mn(1)-O(1w)	2.164(3)	Mn(1)-O(2w)	2.241(3)
O(1)-Mn(1)-O(2)	81.87(9)	O(4a)-Mn(1)-O(3b)	99.36(11)
O(1)-Mn(1)-O(4a)	173.50(12)	O(2)-Mn(1)-O(3b)	165.67(11)
O(1)-Mn(1)-O(3b)	86.11(10)	O(2)-Mn(1)-O(4a)	93.15(10)
O(1w)-Mn(1)-O(1)	86.75(11)	O(2w)-Mn(1)-O(1)	93.49(11)
O(1w)-Mn(1)-O(2)	92.96(12)	O(2w)-Mn(1)-O(2)	92.19(11)
O(1w)-Mn(1)-O(4a)	89.34(13)	O(2w)-Mn(1)-O(4a)	90.87(13)
O(1w)-Mn(1)-O(3b)	94.13(12)	O(2w)-Mn(1)-O(3b)	80.74(11)
O(1w)-Mn(1)-O(2w)	174.83(14)		

		3b	
Mn(1)-O(1)	2.194(3)	Mn(1)-O(2)	2.159(3)
Mn(1)-O(4c)	2.123(3)	Mn(1)-O(3d)	2.142(3)
Mn(1)-O(1w)	2.152(5)	Mn(1)-O(2w)	2.230(5)
O(1)-Mn(1)-O(2)	82.40(12)	O(4c)-Mn(1)-O(3d)	98.35(13)
O(1)-Mn(1)-O(4c)	174.15(15)	O(2)-Mn(1)-O(3d)	166.01(14)
O(1)-Mn(1)-O(3d)	86.49(13)	O(2)-Mn(1)-O(4c)	93.27(12)
O(1w)-Mn(1)-O(1)	85.52(13)	O(2w)-Mn(1)-O(1)	93.42(13)
O(1w)-Mn(1)-O(2)	92.70(15)	O(2w)-Mn(1)-O(2)	91.43(13)
O(1w)-Mn(1)-O(4c)	90.77(16)	O(2w)-Mn(1)-O(4c)	90.61(16)
O(1w)-Mn(1)-O(3d)	94.90(14)	O(2w)-Mn(1)-O(3d)	80.72(14)
O(1w)-Mn(1)-O(2w)	175.56(16)		

[a]Symmetry codes: (a) *x*-1/2, -*y*-2, *z*; (b) *x*-1/2, -*y*-1, *z*; (c) x-1/2, -y+1, z; (d) x+1/2, -y+2, z.

Once the crystal structure was solved using the normal procedures (WinGX and SHELX programs), the obtained results were used to make a final refinement of the structure using the program Fullprof [Rodríguez-Carvajal J., Fullprof 2.60, March 2004] (see Figure 9).

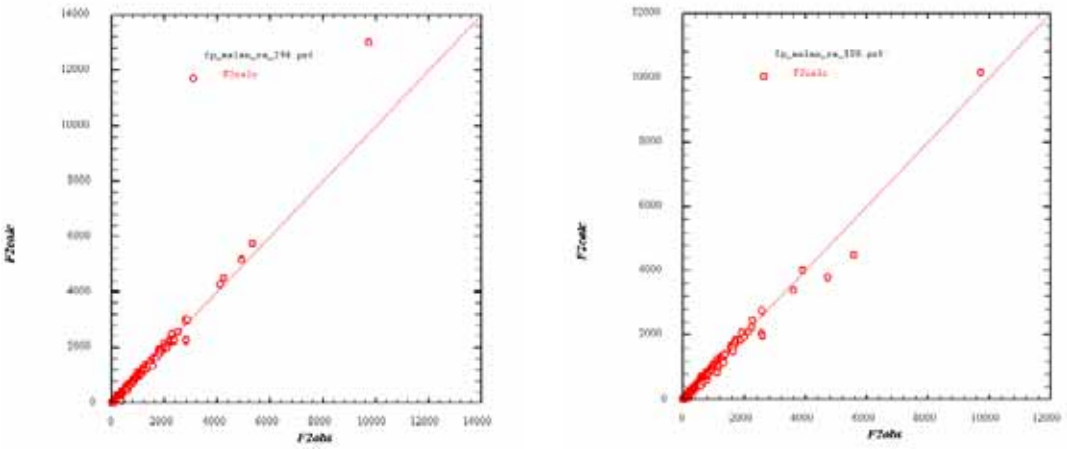

(a) **(b)**

Figure 9. Calculated vs. experimental structure factors for compound **1** using the Fullprof procedure to refine single crystal data at 298 K **(a)** and 100 K **(b)**.

Tabla 8. Values of the goodness of the crystal structure refinement using Fullprof

Compound	**1a**	**1b**
RF2 -factor	6.75	7.32
RF2w-factor	7.07	9.37
RF -factor	5.19	5.25
χ^2(Intensity)	0.542	0.934

G4.2 Powder Neutron Diffraction Data. Structure Refinement.

Neutron diffraction patterns at 280 and 5 K were obtained from a powder sample of **3**, using the equipment G4.2 at the LLB. These data are used to determine the structural parameters (the atomic positions and thermal displacements) of the hydrogen atoms in **3**.

.

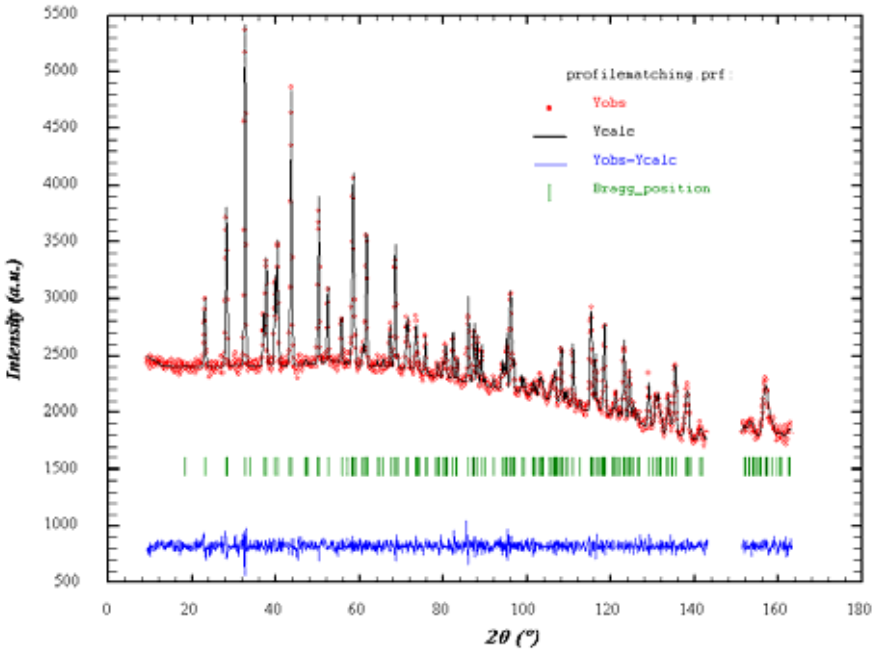

(a)

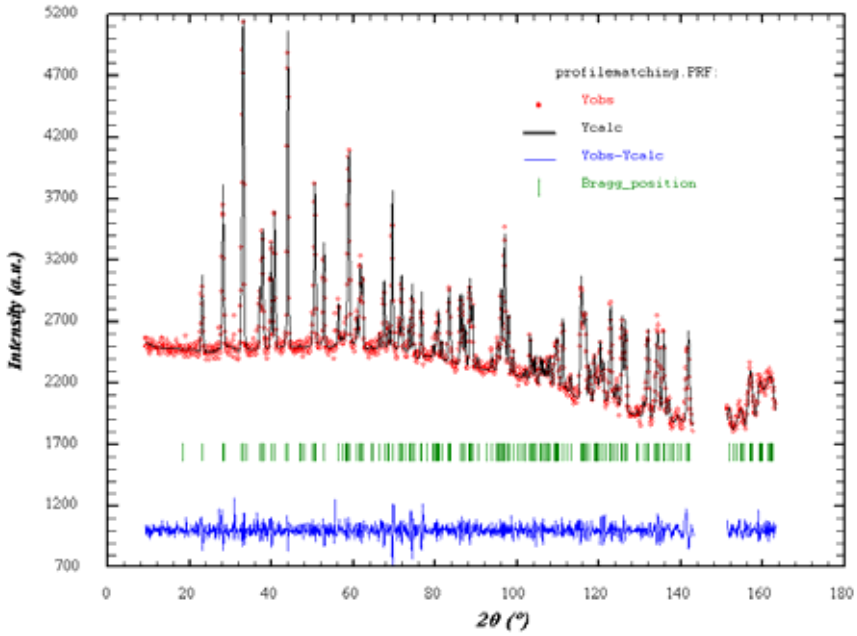

(b)

Figure 10. Profile Matching of the G4.2 unpolarised powder neutron diffraction data at 298 **(a)** and 5 K **(b)**.

The crystallographic information obtained from the X-ray diffraction data was used to refine the unit cell parameters (which determine the position of the peaks in the diffraction pattern) and the characteristic experimental values of the powder diffraction pattern (background and the zero displacement), using the Profile Matching procedure included in the Fullprof program [Rodríguez-Carvajal J., Fullprof 2.60, March 2004]. The fit of the experimental diffraction pattern which is showed in Figure 10, allow us to have good starting values to look for the hydrogen atoms in **3**

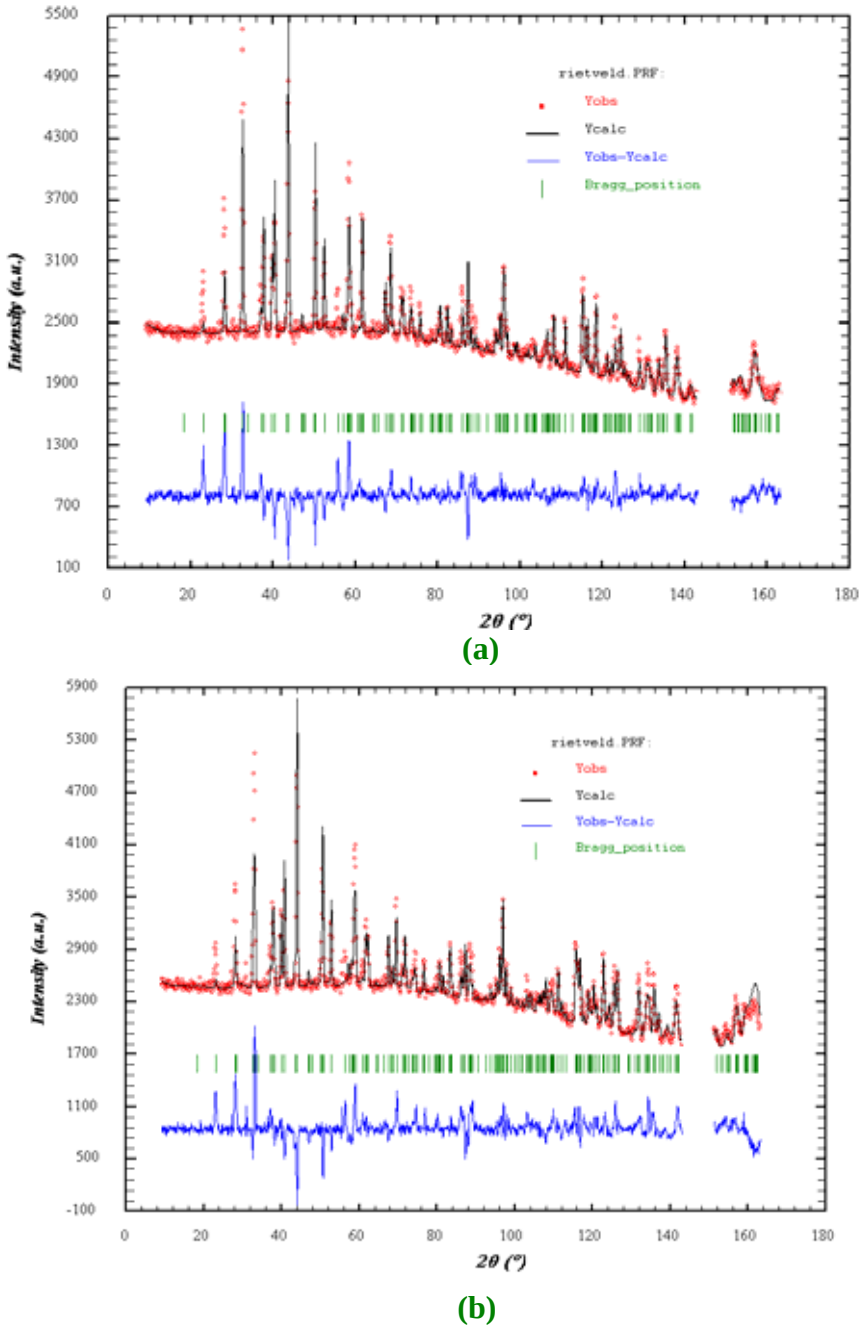

Figure 11. Best-fit of the powder diffraction patterns with the initial structural data (mainly obtained by single crystal X-ray diffraction), before searching the hydrogen atoms in **3**.

Before searching the hydrogen atoms in **3**, we checked the structural data we have. In order to do that, we calculated the theoretical diffraction pattern from the crystallographic data we disposed (atomic and thermal displacements obtained from single crystal X-ray diffraction and the cell unit, the zero displacement and the background parameters we have previously obtained by the Profile Matching procedure using neutron diffraction data) and we refined a scale factor by the Rietveld method (fixing all the structural data) to fit the theoretical pattern with the experimental one. The result obtained is showed in Figure 11.

The Simulated Annealing routine, in the Fullprof package, allowed us to locate the water hydrogen atoms that we could not find by single crystal X-ray diffraction. In order to simplify the problem, we introduced some restrains, using the model shown in Scheme 1 for the water molecule with the following restraints:

(1) The values of the O-H bond distance ranging from 0.85 to 1.15 Å.

(2) The values of the H-O-H bond angle variying between 100 and 120º.

So, we introduced the water molecule as a rigid body for which some geometrical parameters could be varied. This feature is also implemented in the Fullprof package.

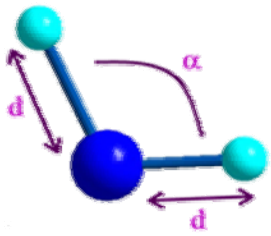

Scheme 1

We refined the two parameters (d and α) together with the three angles that define the orientation of the water hydrogen atoms, in the Simulated Annealing subroutine. Of course, we used all the information we have, placing the rigid body in the atomic positions of the oxygen atoms, which were well determined by X-ray diffraction.

The results after the convergence of the simulated annealing procedure were good, a good agreement between the calculated structural factors and the experimental data (see Figure 12) being achieved.

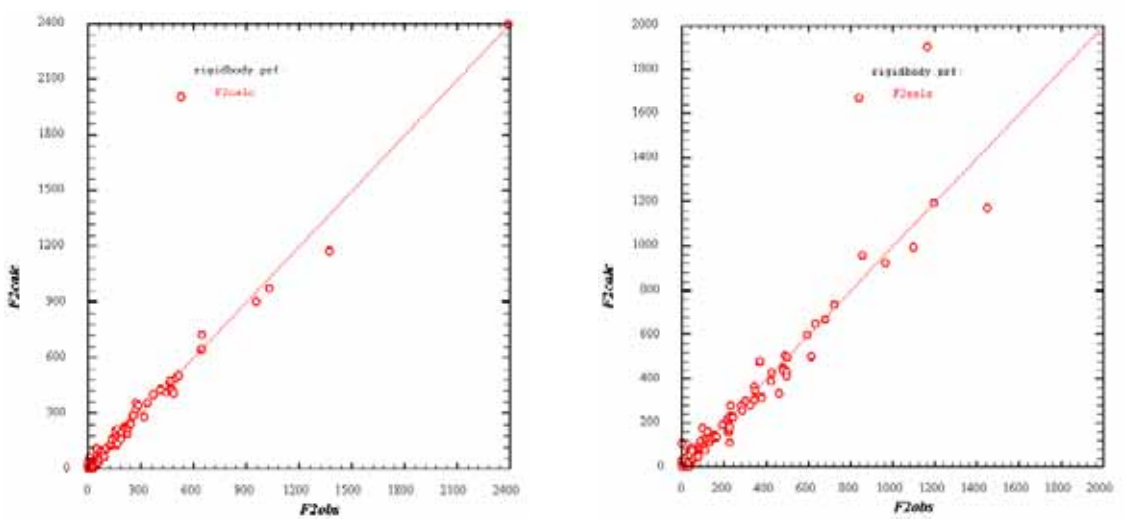

Figure 12. Calculated vs. observed neutron structure factors after searching the water hydrogen atoms using the Simulated Annealing routine.

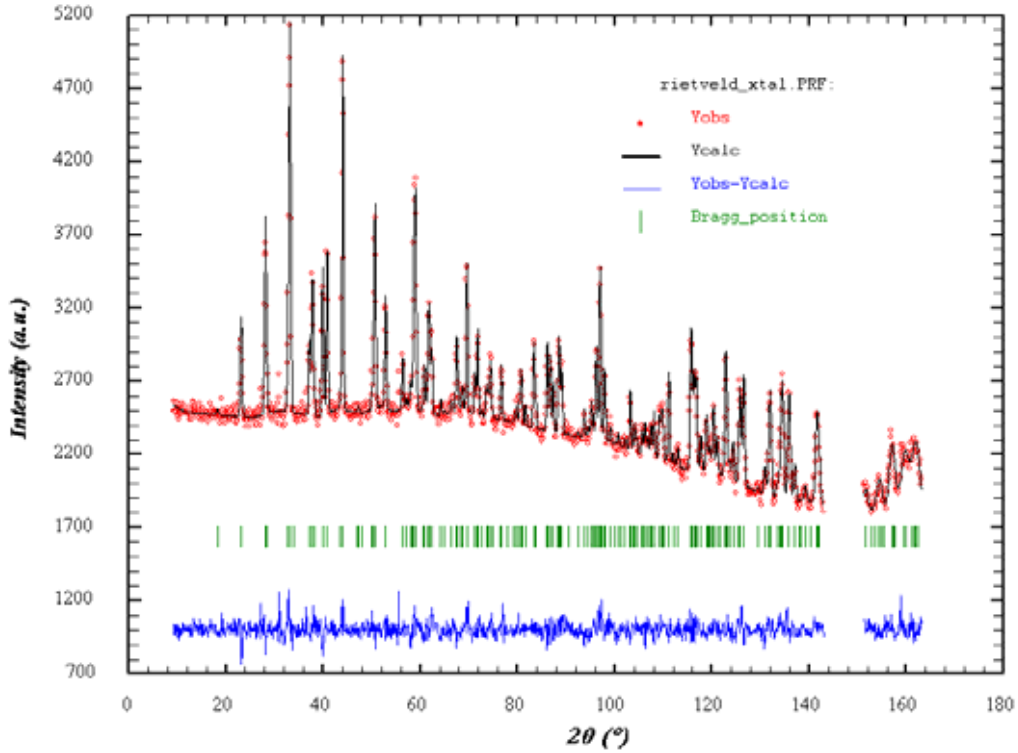

Figure 13. Best-fit of the G4.2 neutron diffraction pattern registered at 5 K after finding hydrogen atoms and refining some parameters (see text) by using the Rietveld Method.

Finally, by means of the Rietveld Method we refined, using the neutron diffraction pattern at 5 K, the following parameters:

(1) the scale factor together with the zero displacement of the neutron diffraction pattern

(2) the unit cell parameters and a global thermal scale that takes into account a general reduction of the thermal ellipsoids for the neutron data registered at 5 K (we remind here that we have used the atomic positions and thermal displacements determined by X-ray diffraction at 100 K as starting point)

(3) and the geometry and thermal parameters of the water molecules together with the methyl groups of the malonate ligands.

The results of the final refinements of the structure of **3**, using the Rietveld Method, can be monitored in Figure 13, the fit of the experimental neutron diffraction pattern being shown.

X-ray and G4.2 neutron diffraction data. Final refinement of the structure.

A final refinement of the structure (including the atomic position and thermal displacements of all the components of **3**) was done using both the single X-ray (at 100 K) and the G4.2 unpolarised neutron diffraction data (at 5 K), combining the Rietveld Method with the refinement of the single crystal data in the Fullprof program. The Figure 14 shows the goodness of the refinement for both X-ray and neutron diffraction data.

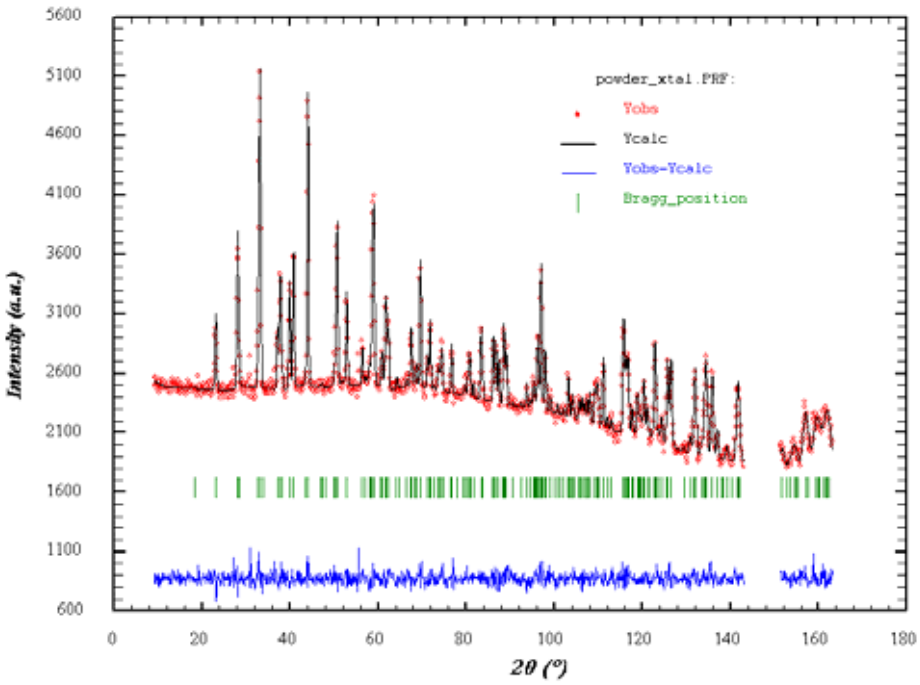

(a)

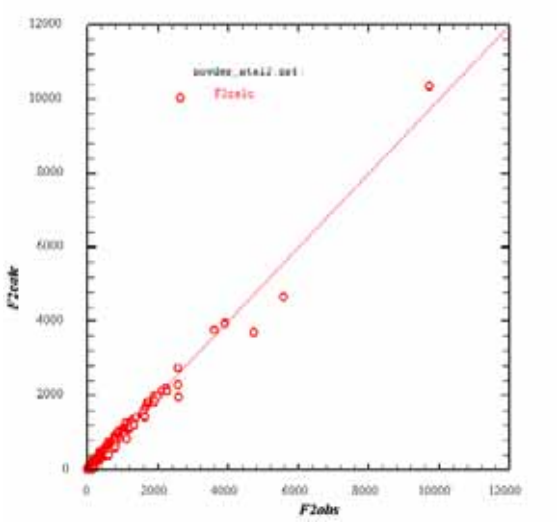

(b)

Figure 14. Results of the refinement of the structure of **3**, using both the neutron and the X-ray diffraction data: **(a)** final fit of the neutron diffraction data and **(b)** calculated *versus* experimental structure factors of the X-ray diffraction.

The hydrogen atoms found with the neutron diffraction data agree well with the hydrogen bonding network that occurs in **3** (see Figure 15).

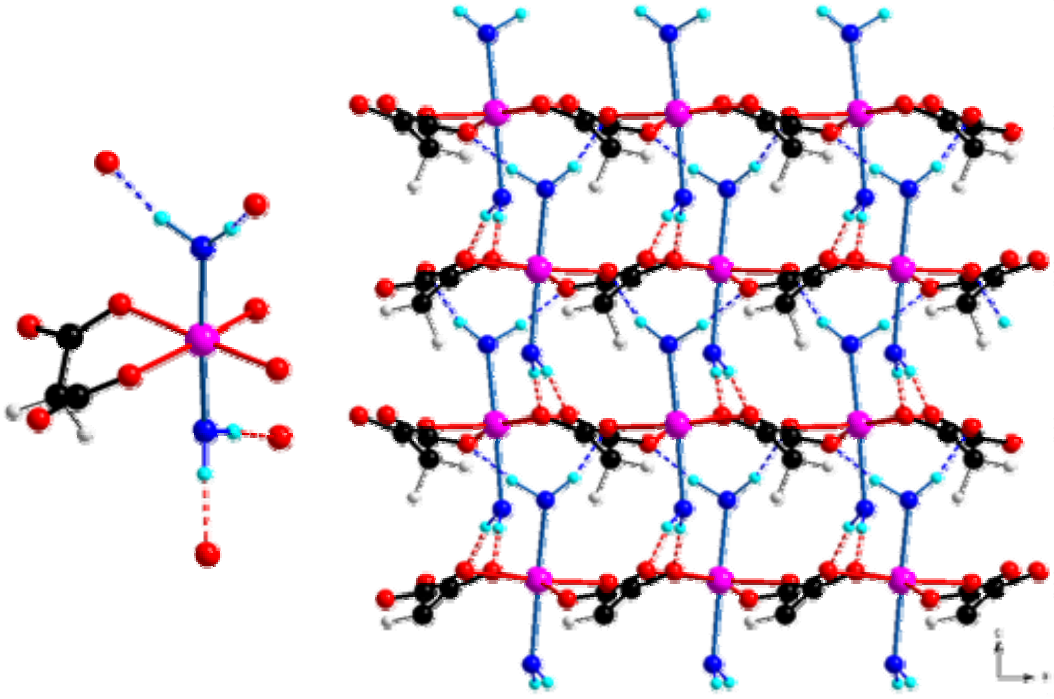

(a) **(b)**

Figure 15. Perspective views of the metal environment of metal atom in **3** **(a)** and the hydrogen bonding network **(b)**. Cyan circles are water hydrogen atoms and hydrogen atoms are represented as dashed lines.

Determination of the Magnetic Structure

G4.1 Powder Neutron Diffraction Data. Determination of the Magnetic Structure.

In order to study the magnetic structure, a powder sample of **3** was put in the holder sample of the G4.1 equipment at the LLB and the powder diffraction of this product was registered below and above the order temperature T_c = 2.7(1) K, as determined by the ac measurements.

For each measured pattern, we first refine some characteristic parameters of the measured pattern [zero displacement, background, global thermal parameter (Boverall)]. In Figure 16, the experimental pattern at 5 K together with the calculated one from the final structural parameters, including hydrogen atoms obtained and refined previously, allowed us to check the goodness of the structural data we got.

New diffraction peaks appear (magnetic peaks) in the pattern (see Figure 17) for the experimental data measured below the order temperature, as expected, due to the magnetic phase transition.

We analyse the magnetic phase through the magnetic propagation vector $\vec{k} = (0,0,0)$.

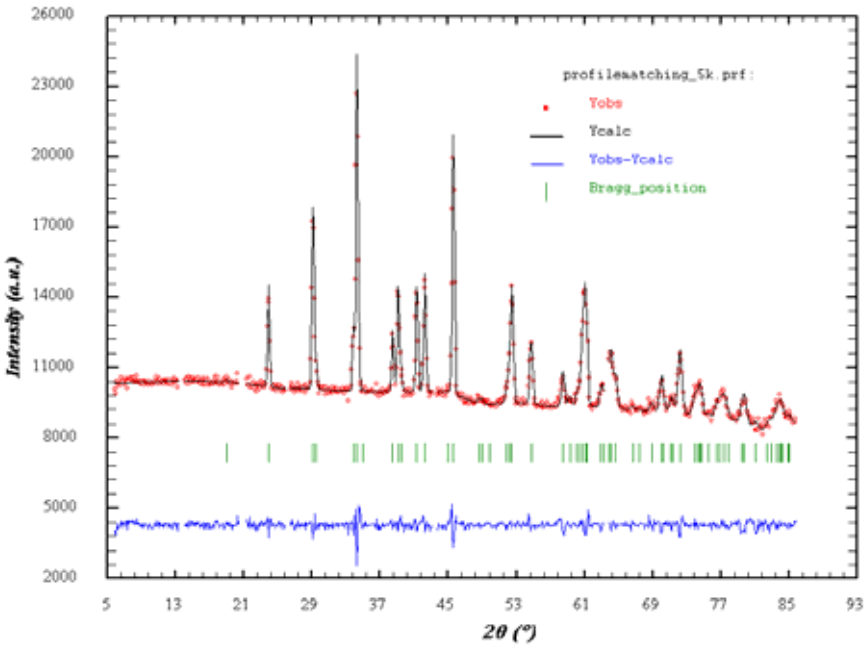

Figure 16. G4.1 neutron diffraction pattern at 5 K (") together with the calculated one (C) using the structural data obtained and refined by single crystal X-ray and G4.2 powder neutron diffraction.

Taking into account the space group of **3** ($Pca2_1$) we calculated the possible irreducible representations for the magnetic moment corresponding for each Mn(II) atom that occurs in the unit cell of **3**, using the program GBASIREPS (included in Fullprof).

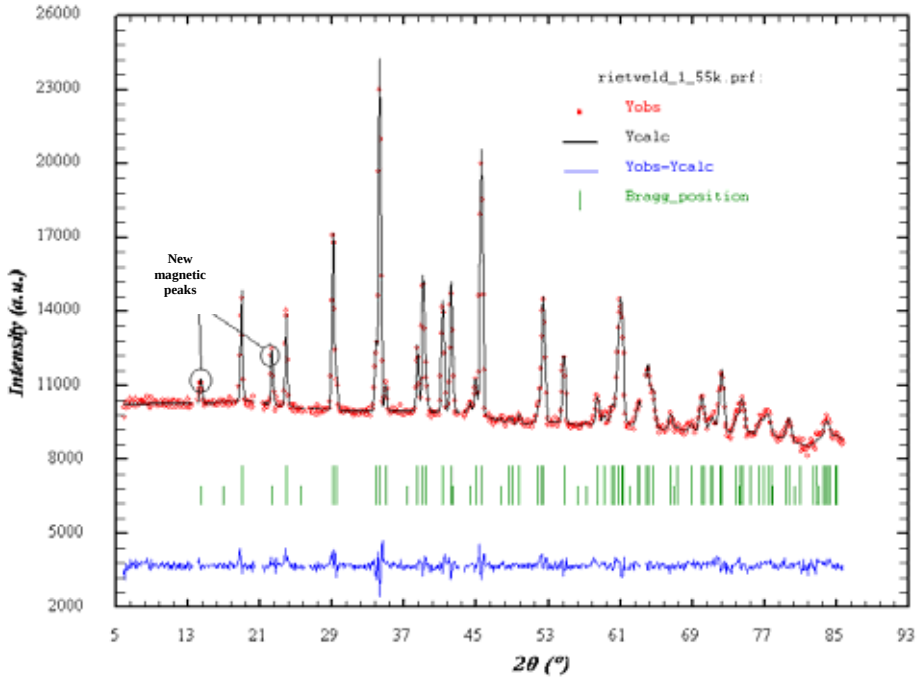

Figure 17. G4.1 neutron diffraction data at 1.55 K showing the additional peaks that appear below the order temperature: (") experimental data; (C) calculated pattern using the IRrep(4) and the (0, 0, 0) magnetic propagation vector.

Here we reported the four irreducible representations for the magnetic moment compatible with the space group of **3** (u, v, w being the components of the magnetic moment):

++

Basis functions of Representation **IRrep(1)** of dimension 1

++

Symmetry code: *x*, *y*, *z* Atom: Mn1 0.0581 0.7803 0.1373
Magnetic vector: (u, v, w)

Symmetry code: -*x*+1, -*y*+1, *z*+1/2 Atom: Mn1a 0.9419 0.2197 0.6373
Magnetic vector: (-u, -v, w)

Symmetry code: *x*+1/2, -*y*+1,*z* Atom: Mn1b 0.5581 0.2197 0.1373
Magnetic vector: (u, -v, w)

Symmetry code: -*x*+1/2, *y*, *z*+1/2 Atom: Mn1c 0.4419 0.7803 0.6373
Sk(4): (-u, v, w)

++

Basis functions of Representation **IRrep(2)** of dimension 1

++

Symmetry code: *x*, *y*, *z* Atom: Mn1 0.0581 0.7803 0.1373
Magnetic vector: (u, v, w)

Symmetry code: -*x*+1, -*y*+1, *z*+1/2 Atom: Mn1a 0.9419 0.2197 0.6373
Magnetic vector: (-u, -v, w)

Symmetry code: *x*+1/2, -*y*+1,*z* Atom: Mn1b 0.5581 0.2197 0.1373
Magnetic vector: (-u, v, -w)

Symmetry code: -*x*+1/2, *y*, *z*+1/2 Atom: Mn1c 0.4419 0.7803 0.6373
Sk(4): (u, -v, -w)

++

Basis functions of Representation **IRrep(3)** of dimension 1

++

Symmetry code: *x*, *y*, *z* Atom: Mn1 0.0581 0.7803 0.1373
Magnetic vector: (u, v, w)

Symmetry code: -*x*+1, -*y*+1, *z*+1/2 Atom: Mn1a 0.9419 0.2197 0.6373
Magnetic vector: (u, v, -w)

Symmetry code: *x*+1/2, -*y*+1,*z* Atom: Mn1b 0.5581 0.2197 0.1373
Magnetic vector: (u, -v, w)

Symmetry code: -*x*+1/2, *y*, *z*+1/2 Atom: Mn1c 0.4419 0.7803 0.6373
Sk(4): (u, -v, -w)

++

Basis functions of Representation **IRrep(4)** of dimension 1

++

Symmetry code: *x*, *y*, *z* Atom: Mn1 0.0581 0.7803 0.1373
Magnetic vector: (u, v, w)

Symmetry code: -*x*+1, -*y*+1, *z*+1/2 Atom: Mn1a 0.9419 0.2197 0.6373
Magnetic vector: (u, -v, -w)

Symmetry code: *x*+1/2, -*y*+1,*z* Atom: Mn1b 0.5581 0.2197 0.1373
Magnetic vector: (-u, v, -w)

Symmetry code: -*x*+1/2, *y*, *z*+1/2 Atom: Mn1c 0.4419 0.7803 0.6373
Sk(4): (-u, v, w)

The magnetic data below the order temperature can be only interpretate, by using the parameters for the magnetic moment of the IRrep(4) irreducible representation. The results of the analysis of the experimental data below the order temperature are reported in Table 9 and a schematic view of the magnetic structure is shown in Figure 18.

These results confirm the existence of the spin-canting in **3** below the order temperature. One can see the appearance of a spontaneous magnetic moment below T = 2.7 K (the order temperature), in Table 9.

Table 9. Crystal data and details of structure determination for **1**

T(K)	M(MB)	My(BM)	Mz(BM)	Global χ^2 [a]	Bragg R-factor [b]	Mag. R-factor [c]
1.55	4.26(9)	1.85(15)	3.84(3)	5.43	5.36	8.24
1.75	4.00(10)	1.6(2)	3.66(6)	3.18	5.29	8.99
2.17	3.62(10)	1.7(2)	3.17(6)	3.21	6.32	12.8
2.25	3.42(11)	1.7(2)	2.97(7)	3.32	6.26	12.0
2.32	3.35(11)	1.6(2)	2.93(7)	3.16	5.25	12.3
2.39	3.21(12)	1.8(2)	2.66(7)	3.03	5.72	11.0
2.44	2.96(12)	1.6(2)	2.48(8)	3.03	6.12	14.7
2.53	2.54(14)	1.8(2)	1.83(10)	3.08	6.14	18.7
2.58	2.0(2)	1.5(2)	1.25(15)	3.29	5.66	26.3
2.67	1.8(2)	1.8(2)	0.0	3.06	6.03	10.6
2.79	1.8(2)	1.8(2)	0.0	3.08	5.70	15.7

[a]Global user-weigthed χ^2 (Bragg contribution). [b]Bragg R-factor for the crystalline structure. [c]R-factor for the magnetic structure.

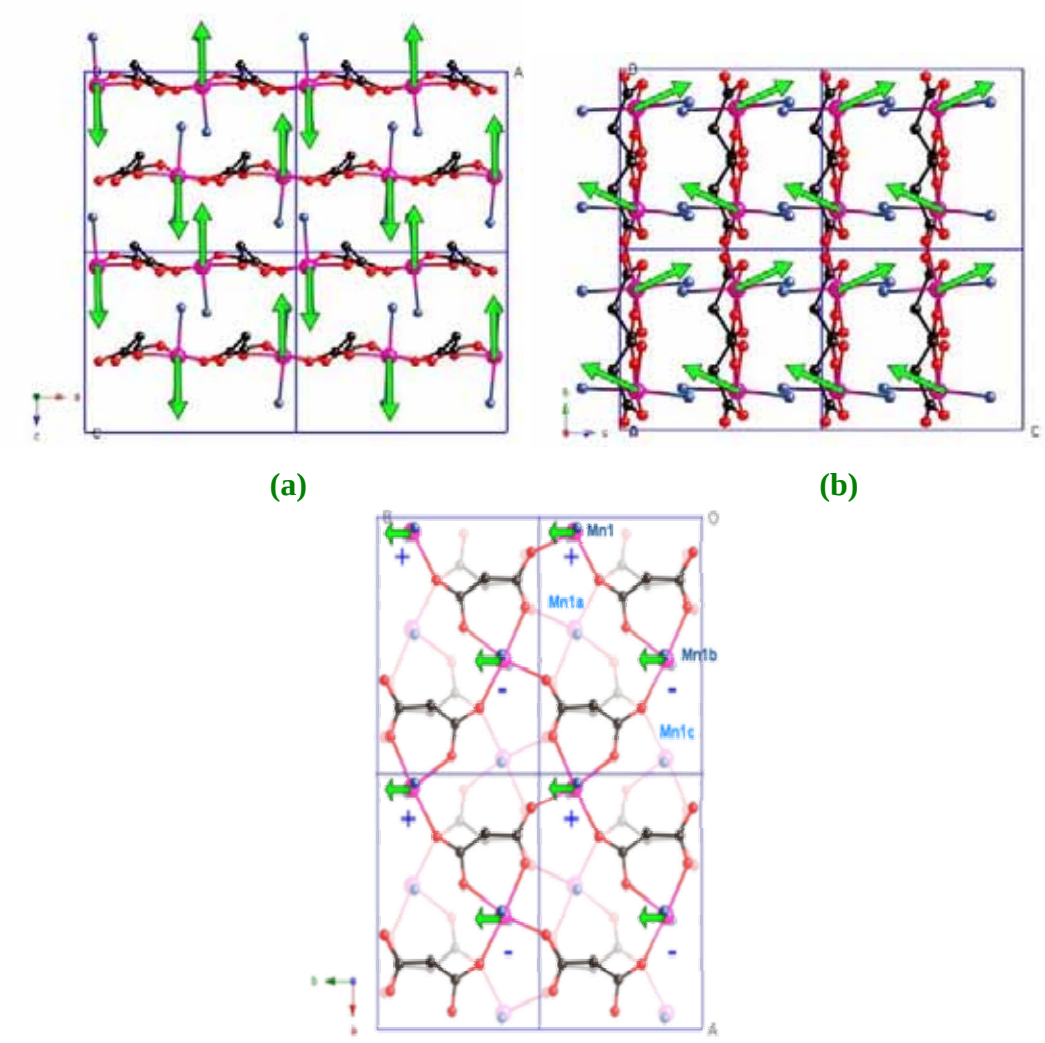

(a) **(b)**

(c)

Figure 18. Perspective view along the *b*- **(a)**, *a*- **(b)** and *c*-axis **(c)** of the structure of **1** with a vector showing the magnetic moment in the manganese(II) atoms.

References

Section A: Co(II) and Ni(II)

Carlin R.L., *Magnetochemistry*, Springer-Verlag, Berlin, Heidelberg, **1986**.

Castillo O., Luque A., Román P., Lloret F. and Julve M., *Inorg. Chem.*, **2001**, 40, 5526.

Coronado E., Drillon M., Nutgeren P.R., De Jongh L.J. and Beltrán D., *J. Am. Chem. Soc.*, **1988**, 110, 3907.

Batten S.R. and Murray K.S., *Coord. Chem. Rev.*, **2003**, 246, 103.

Burrows A.D., Harrington R.W., Mahon M.F. and Price C.E., *Danton Trans.*, **2000**, 3845.

Chattopadhyay D., Chattopadhyay S.K., Lowe P.R., Schwalbe C.H., Mazumder S.K., Rana A. and Ghosh S., *Dalton Trans.*, **1993**, 913.

Chaudhuri P., *Coord, Chem. Rev.*, **2003**, 243, 143.

DIAMOND 2.1d, Crystal Impact GbR, CRYSTAL IMPACT, K. Brandenburg & H. Putz GbR, Postfach 1251, D-53002 Bonn, Germany, 2000

Earshaw A., *Introduction to Magnetochemistry*; Academic Press; London, **1968**.

Farrugia L.J. (*WINGX*), *J. Appl. Cryst*, **1999**, *32*, 837.

Herrera J.M., Bleuzen A., Dromzée Y., Julve M., Lloret F. and Verdaguer M., *Inorg. Chem.*, **2003**, 42, 7052.

Kahn O., *Molecular Magnetism*, VCH, Weinheim, **1993**.

Konar S., Mukherjee P.S., Drew M.G.B., Ribas J. and Chaudhuri N.R., *Inorg. Chem.*, **2003**, 42, 2545.

Kumagai H., Oka Y., Inoue K. and Kurmoo M., *Dalton Trans.*, **2002**, 3442.

Lee E.W., Kim Y.J.and Jung D.K., *Inorg. Chem.*, **2002**, 41, 501.

Lightfoot P. and Snedden A., *Dalton Trans.*, **1999**, 3549.

Lin D.-D., Liu Y. And Xu D.-J., *Acta Cryst., Sect E*, **2004**, 59, m771.

Lis T. and Matuszewski J., *Acta Crystallogr., Sect. B*, **1979**, 35, 2212.

Liu T.F., Sun H.L., Gao S., Zhang S.W. and Lau T.C., *Inorg. Chem.*, **2003**, 42, 4792.

Mabbs F.E. and Machin D.J., *Magnetism and Transition Metal Complexes*, Chapman and Hall Ltd., London, **1973**.

Maji T.K., Sain S., Mostafa G., Lu T.-H., Ribas J., Monfort M. and Chaudhuri N.R., *Inorg. Chem.*, **2003**, 42 709.

Miller J.S. and Drillon M. (Eds.), *Molecule Based Materials*, Wiley - VCH, Weinheim, **2001**.

Nardelli M. *J. Appl. Crystallogr.*, **1995**, *28*, 659.

Navarro R., *Application of High- and Low-Temperature Series Expansions to Two-Dimensional Magnetic Systems*, ed. L. J. de Jongh, Kluwer Academic Publishers, The Netherlands, **1990**.

Ohba M. and Okawa H., *Coord. Chem. Rev.*, **2000**, 198, 313.

Pilkington M. and Decurtins S., *In Comprehensive Coordination Chemistry II. From Biology to Nanotechnology*; Mc Cleverty J.A. and Meyer T.J. (Eds.), Elsevier, **2004**, Vol. 7, p 177.

Pasán J., Delgado F.S., Rodríguez-Martín Y., Hernández-Molina M., Ruiz-Pérez, C. Sanchiz J., Lloret F. and Julve M., *Polyhedron*, **2003**, 22, 2143.

Pasán J., Sanchiz J., Ruiz-Pérez C., Lloret F. and Julve M., *New J. Chem.*, **2003**, 27, 1557.

Ray N.J., *Acta Crystallogr., Sect. B*, **1982**, 38, 770.

Ribas J., Escuer A., Monfort M., Vicente R., Cortés R., Lezama L. and Rojo T., *Coord. Chem. Rev.*, **1999**, 193, 1027.

Rodríguez-Fortea A., Alemany P., Álvarez S. and Ruiz E., *Chem. Eur. J.*, **2001**, 7, 627.

Rodríguez-Martín Y., Sanchiz J., Ruiz-Pérez C., Lloret F. and Julve M., *Inorg. Chim. Acta*, **2001**, 326, 20.

Rodríguez-Martín Y., Hernández-Molina M., Delgado F.S., Pasán J., Ruiz-Pérez C., Sanchiz J., Lloret F. and Julve M., *CrystEngComm.*, **2002a**, 4, 522.

Rodríguez-Martín Y., Hernández-Molina M., Delgado F.S., Pasán J., Ruiz-Pérez C., Sanchiz J., Lloret F. and Julve M., *CrystEngComm.*, **2002b**, 4, 440.

Rodríguez-Martín Y., Sanchiz J., Ruiz-Pérez C., Lloret F. and Julve M., *CrystEngComm.*, **2002c**, 4, 631.

Rodríguez-Martín Y., Hernández-Molina M., Sanchiz J., Ruiz-Pérez C., Lloret F. and Julve M., *Dalton Trans.*, **2003**, 2359.

Rueff J.M., Masciocchi N., Rabu P., Sironi A. and Skoulios A., *Eur. J. Inorg. Chem.*, **2001**, 2843.

Ruiz-Pérez C., Sanchiz J., Hernández-Molina M., Lloret F. and Julve M., *Inorg. Chem.*, **2000**, 39, 1363.

Ruiz-Pérez C., Rodríguez-Martín Y., Hernández-Molina M., Delgado F.S., Pasán J., Sanchiz J., Lloret F. and Julve M., *Polyhedron*, **2003**, 22, 2111.

Sheldrick, G.M. *SHELX97*, *Programs for Crystal Structure Analysis (Release 97-2)*, Institüt für Anorganische Chemie der Universität, Tammanstrasse 4, D-3400 Göttingen, Germany, **1998**.

Shen L., *Acta Cryst., Sect. C*, **2003**, 59, m128.

Stiefel E. I., Brown G. F. *Inorg. Chem.*, **1972**, 11, 434.

Verdaguer M., Bleuzen A., Marvaud V., Vaissermann J., Seuleiman M., Desplanches C., Scuiller A., Train C., Garde R., Gelly G., Lamenech C., Rosenman I., Veillet P., Cartier C. and Villain F., *Coord. Chem. Rev.*, **1999**, 1023, 190.

Walter-Levy L., Perrotey J. and Visser J.W., *Bull. Soc. Chim. Fr.*, **1973**, 2596.

Wang Z.-X., Zhou X.-H., Yu W.-T. and Fu Y.-J., *Z. Kristallogr.-New Cryst. Struct.*, **2000**, 215, 423.

Whitfield T., Zheng L.M., Wang X. and Jacobson A.J., *Sol. St. Sci.*, **2001**, 3, 829.

Xue Y.-H., Lin D.-D. and Xu D.-J., *Acta Cryst., Sect. E*, **2004**, 59, m750.

Zhang X.T., Lu C.Z., Zhang Q.Z., Lu S.F., Yang W.B., Liu J.C. and Zhuang H.H., *Eur. J. Inorg. Chem.*, **2003**, 1181.

Section B: Mn(II)

Colacio E., Domínguez-Vera J.M., Ghazi M., Kivekkäs R., Moreno J.M., Romerosa A. And Ruiz J. Inorg. Chem., **1993**, 212, 115.

Hooft, R.W.W. *COLLECT*. Nonius BV, Delft, The Netherlands, **1999**

Duisenberg A.J.M., Kroon-Batenburg, L.M.J. and Schreurs, A.M.M. *J. Appl. Cryst.*, **2003,** 36, 220 (EVALCCD)

Farrugia L.J. (*WINGX*), *J. Appl. Cryst*, **1999**, *32*, 837.

Rodríguez-Carvajal J., FULLPROF version 2.60, March **2004**, ILL (unpublished).

Fisher M.E. *Am. J. Phys.*, **1964**, 32, 343

Rodríguez-Fortea A., Alemany P., Alvarez S. and Ruiz E. *Chem. Eur. J.*, **2001**, 7, 627.

Rodriguez-Martín Y., Hernández-Molina M., Sanchíz J., Ruíz-Pérez C., Lloret F. and Julve M., *Dalton Trans.*, **2003**, 2359.

Ruiz-Pérez C., Sanchiz J., Hernández-Molina M., Lloret F. and Julve M. *Inorg. Chem.*, **2000**, 39, 1363.

SADABS, version 2.03. Bruker AXS Inc.: Madison, WI, **2000**.

Sheldrick, G.M. *SHELX97*, *Programs for Crystal Structure Analysis (Release 97-2)*, Institüt für Anorganische Chemie der Universität, Tammanstrasse 4, D-3400 Göttingen, Germany, **1998**

CHAPTER VII.

A structural revision of the heterometallic malonate complexes.

Introduction

We have shown in the previous chapters that malonate-containing homometallic complexes provided a wide variety of structures and properties.

Previous studies on malonate-containing bimetallic MM' complexes [M and M' = Mn(II), Co(II), Ni(II), Cu(II) and Zn(II)] [Rodríguez-Martín Y. *et al.*, 2002a] have afforded very interesting magneto-structural results. The structural analysis by single crystal X-ray diffraction could not be carried out only on two compounds [namely, (CoMn) and (NiMn)], the problem being the lack of suitable crystals for them.

Among the strategies to control the molecular self-assembling during crystallization, hydrogen bonding appears as one of the most relevant. The key role of this type of interactions is due to their strong directing capability to organise molecules into supramolecular aggregates that have well-defined structures. These supramolecular aggregates often have unique chemical and physical properties due to the collective behaviour of these weakly bound molecules. Hydrogen bonds have been used to generate supramolecular assemblies with structures that can be controlled selectively in one and two dimensions. In addition, a well known and effective strategy in the design of supramolecular hosts and complexes, is the matching of complementary hydrogen bond donors and acceptors, in order to form hydrogen bonded aggregates. In particular, metal aqua-ions act as excellent, readily available hydrogen bond donors with very limited acceptor properties, and hence little intermolecular self complementarity. The O–H···O hydrogen bonds formed by –COOH and –OH groups are among the strongest neutral bonds. It is well known, however, that the O–H···O bond can be further strengthened if the polarity of the acceptor systems is increased *via* deprotonation of the carboxylic group. These interactions are sufficiently strong to control recognition and self-assembly of carboxylic acid/carboxylate anions in robust three-dimensional superstructures.

In this context and following our systematic studies on the malonato-containing metal complexes concerning the design of high-dimensional heterometallic species, we have obtained the malonte-containing bimetallic compounds MM' (MM' being CoMn and NiMn). Unfortunately, the task of obtaining a pure sample of these compound to make magnetic measurements is difficult and we have to improve the synthesis.

It's also a difficult task to characterise by X-ray diffraction bimetallic complexes when the two metal ions we can use to prepare the new materials are close in the periodic table because the low difference between their electron densities.

Experimental

Materials and methods

Malonic acid, cobalt(II) acetate tetrahydrate, cobalt(II) carbonate hydrate, nickel(II) acetate tetrahydrate and manganese(II) carbonate were purchased from Aldrich and used as received. Elemental analyses (C, H, N) were not carried out due to the small amount of product obtained in the synthesis.

Synthesis

$[Mn(H_2O)_6][Ni(mal)_2(H_2O)_2]$ (1). A suspension of manganese(II) malonate (0.242 mg, 1.25 mmol) (prepared as described in the previous chapter), nickel(II) malonate (0.246 mg, 1.25 mmol) and malonic acid (0.010 mg, 0.10 mmol) in water (10 cm^3) was put into a hydrothermal cell and it was allowed to stand at 110 ºC during 72 h. Then, the hydrothermal cell was allowed to reach the room temperature. Green single-crystals of **1** were taken out from the hydrothermal cell, washed with a small amount of water and dried on filter paper.

$\{[Mn(H_2O)_2][Co(mal)_2(H_2O)_2]\}$ (2). A mixture of manganese(II) carbonate (345 mg, 3 mmol) and malonic acid (312 mg, 3 mmol) is added to an aqueous solution (40 cm^3) and the resulting suspension was heated under continuous stirring during 1 h and a half. At the same time, a mixture of cobalt(II) carbonate hydrate (357 mg, 3 mmol) and malonic acid (624 mg, 6 mmol) is suspended in water (20 cm^3) and heated under continuous stirring during 1 h. The two resulting solutions are allowed to react being heated under continuous stirring during 1 h. Finally, this solution is filtered and allowed to evaporate at room temperature. Within 2 days, crystals of **2** as red rectangular prisms were collected from the solution. It deserved to be noted here that crystals of cobalt(II) and manganese(II) malonates appeared when leaving the solution more time, this fact making difficult the manual separation of the bimetallic crystals from the mesh.

Quantitative Analysis (SEM Microscopy)

In order to determine the amount of Mn and Co ions in **2** we made a quantitative analysis of a crystal of the sample through the X-ray microanalysis technique by using a copper pattern. The results are reported herein.

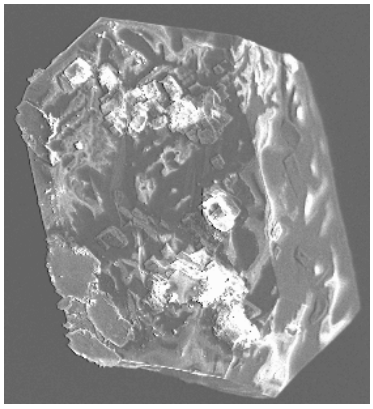

SEM image of the sample

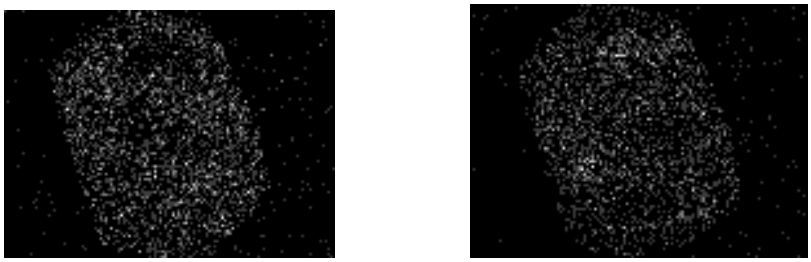

(a) **(b)**

Images of the sample showing the distribution of Mn(II) **(a)** and Co(II) **(b)** ions

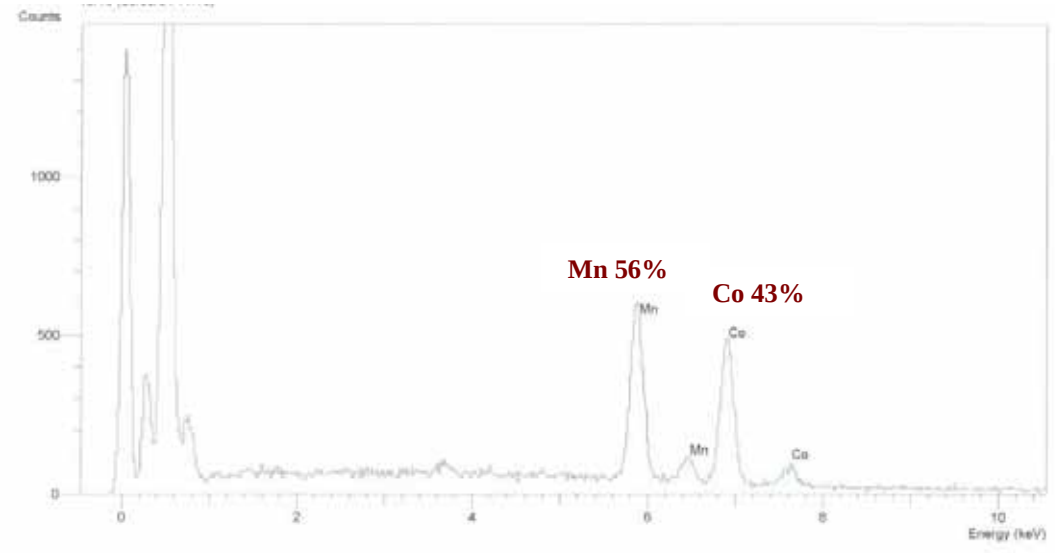

From the qualitative analysis we conclude that Mn(II) and Co(II) ions are present in **2** in a 1:1 molar ratio.

Crystal data collection and refinement

Suitable single crystals of compounds **1** and **2** were mounted on a Bruker-Nonius KappaCCD diffractometer. Orientation matrix and lattice parameters were obtained by least-squares refinement of the reflections obtained by a θ-χ scan (Dirax/lsq method). Diffraction data for the two compounds were collected at 293(2) K using graphite-monochromated Mo-K_α radiation (λ = 0.71073 Å). Data collection and data reduction were done with the COLLECT [Hooft R.W.W., 1999] and EVALCCD [Duisenberg A.J.M. *et al.*, 2003] programs. Empirical absorption corrections for **1** and **2** were carried out through SADABS [SADABS, version 2.03, 2003]. The indexes of data collection were $-6 \leq h \leq 6$, $-9 \leq k \leq 8$ and $-13 \leq l \leq 13$ for **1**, $-18 \leq h \leq 19$, $-10 \leq k \leq 10$ and $-17 \leq l \leq 18$ for **2**. Of the 1687 (**1**) and 1718 (**2**) measured independent reflections in the θ ranges 6.47 – 27.48º (**1**) and 6.44 - 30º (**2**), 1181 (**1**) and 1440 (**2**) have $I \geq 2\sigma(I)$. All the measured independent reflections were used in the analysis. All calculations for data reduction, structure solution, and refinement were done by standard procedures (WINGX) [Farrugia L.J., 1999]. The structures were solved by direct methods and refined with full-matrix least-squares technique on F^2 using the SHELXS-97 and SHELXL-97 programs [Sheldrick G.M. SHELX97, realease 97-2, 1998]. The hydrogen atoms of the malonate and water molecules in **1** were located from a difference Fourier map. For compound **2**, the hydrogen atoms of the water molecules were not found and those of the malonate were set in calculated positions. The hydrogen atoms of **1** and **2** were refined with isotropic temperature factors. The final Fourier-difference map showed maximum and minimum height peaks of 0.392 and -0.441 e $Å^{-3}$ (**1**), 0.665 and -0.517 e $Å^{-3}$ (**2**). A summary of the crystallographic data and structure refinement is given in Table 1. The final geometrical calculations and the graphical manipulations were carried out with PARST97 [Nardelli M., 1995] and DIAMOND [DIAMOND 2.1d, 2000] programs, respectively.

Table 1. Crystal data and details of structure determination of **1** and **2**

Compound	**1**	**2**
Formula	$C_6H_{20}MnNiO_{16}$	$C_6H_{12}CoMnO_{12}$
M	461.87	390.03
Crystal system	triclinic	monoclinic
Space group	*P*-1	*C*2/*c*
a, Å	5.2160(10)	14.1677(10)
b, Å	7.3800(10)	7.299(2)
c, Å	10.309(2)	12.853(2)
α, deg	105.22(3)	-
β, deg	98.64(3)	116.549(2)
γ, deg	97.20(3)	-
V, Å^3	372.88(11)	1189.0(4)
Z	1	4
T(K)	293(2)	293(2)
ρ_{calc} (Mg m^{-3})	2.057	2.179
F(000)	237	784
λ (Mo-K$_\alpha$ Å)	0.71073	0.71073
μ (MoK$_\alpha$) (mm^{-1})	2.197	2.522
Number parameters/restraints	158 / 0	102 / 0
Goodness of fit (*S*)	1.002	1.206
R1, $I > 2\sigma(I)$ (all)	0.0409 / 0.0755	0.0387 / 0.0508
wR2, $I > 2\sigma(I)$ (all)	0.0714 / 0.0793	0.1015 / 0.1046
Max/min electron density (e/Å^3)	0.392 / -0.441	0.665 / -0.517
Measured reflections (R_{int})	3394 (0.0334)	6817 (0.0256)
Independent reflections [$I > 2\sigma(I)$]	1687 (1181)	1718 (1440)

Results and discussion

Description of the structure of $[Mn(H_2O)_6][Ni(mal)_2(H_2O)_2]$ (1)

Compound **1** is isostructural with the complexes of formula $[M^{II}(H_2O)_6][Cu(mal)_2(H_2O)_2]$ [M = Mn, Co, Ni, Cu and Zn] [Rodríguez-Martín Y. *et al.*, 2002b]. Its structure consists of alternating layers of $[Ni(mal)_2(H_2O)_2]^{2-}$ anions and $[Mn(H_2O)_6]^{2+}$ cations (see Figure 1).

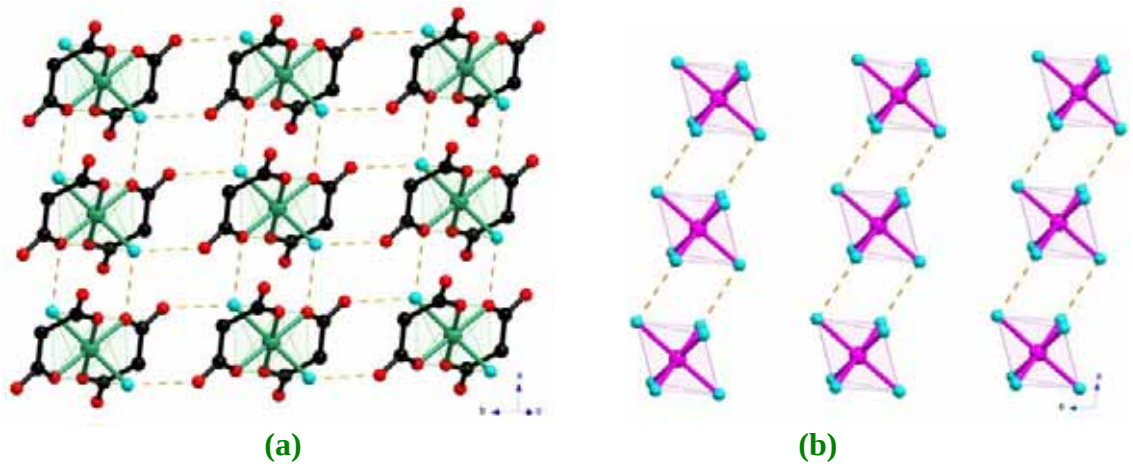

(a) **(b)**

Figure 1. Perspective view of the $[Ni(mal)_2(H_2O)_2]^{2-}$ anionic **(a)** and $[Mn(H_2O)_6]^{2+}$ cationic **(b)** layers showing the hydrogen bonds as broken lines. Hydrogen atoms were removed for clarity.

These layers are connected through an extensive network of hydrogen bonds (see Table 2) involving all the water molecules and some of the carboxylate-malonate oxygen atoms leading to a three-dimensional network with regular alternating of anionic and cationic layers (see Figure 2).

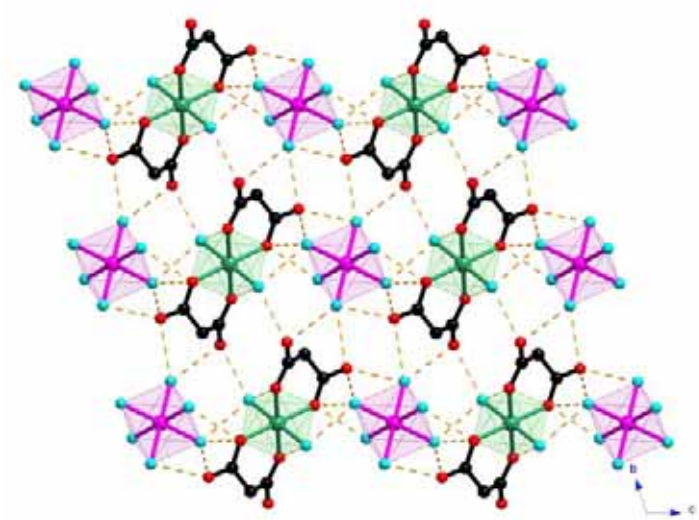

Figure 2. Perspective view down the *a*-axis of the $[Ni(mal)_2(H_2O)_2]^{2-}$ anionic and $[Mn(H_2O)_6]^{2+}$ cationic layers linked through an extensive network of hydrogen bonds.

Selected bond lengths and angles for **1** are reported in Table 2 together with hydrogen bonds and C-H···O type interactions.

Table 2. Bond lengths (Å) and angles (º) with the relevant hydrogen bonds for **1**[a,b]

Mn(1)-O(1w)	2.109(2)	Mn(1)-O(2w)	2.170(3)
Mn(1)-O(3w)	2.103(3)		
O(1w)-Mn(1)-O(2w)	90.69(11)	O(1w)-Mn(1)-O(3w)	92.80(11)
O(2w)-Mn(1)-O(3w)	88.63(11)	O(1w)-Mn(1)-O(2wa)	89.31(11)
O(1w)-Mn(1)-O(3wa)	87.20(11)	O(2w)-Mn(1)-O(3wa)	91.37(11)
Ni(1)-O(1)	2.004(2)	Ni(1)-O(2)	2.025(2)
Ni(1)-O(4w)	2.151(2)		
O(1)-Ni(1)-O(2)	91.36(9)	O(1)-Ni(1)-O(4w)	89.53(10)
O(2)-Ni(1)-O(4w)	93.18(10)	O(1)-Ni(1)-O(2b)	88.64(9)
O(1)-Ni(1)-O(4wb)	90.47(10)	O(2)-Ni(1)-O(4wb)	86.82(10)

D-H···A	D···A/Å	H···A/Å	D-H···A/º
O(1w)-H(1w1)···O(2w)	2.901(4)	2.02(5)	171(4)
O(1w)-H(2w1)···O(1)	2.691(4)	1.94(6)	156(5)
O(2w)-H(1w2)···O(4c)	2.801(4)	1.90(5)	166(5)
O(2w)-H(1w2)···O(3d)	2.985(4)	2.71(6)	98(4)
O(2w)-H(2w2)···O(3)	2.826(4)	2.03(5)	147(4)
O(2w)-H(2w2)···O(3d)	2.985(4)	2.43(4)	120(4)
O(3w)-H(1w3)···O(3e)	2.675(4)	1.88(5)	167(5)
O(3w)-H(2w3)···O(4wf)	2.823(4)	1.94(4)	167(4)
O(3w)-H(2w3)···O(1a)	3.045(4)	2.71(4)	103(3)
O(4w)-H(1w4)···O(4g)	2.771(4)	1.89(7)	170(6)
O(4w)-H(2w4)···O(2h)	2.778(4)	2.00(4)	170(4)
C(2)-H(1)···O(4h)	3.197(5)	2.38(5)	136(4)
C(2)-H(2)···O(1wi)	3.356(5)	2.46(5)	142(4)

[a] Symmetry transformations: (a) *-x*, *-y*, *-z*+1; (b) *-x*, *-y*, *-z*; (c) *-x*, *-y*+1, *-z*+1; (d) *-x*+1, *-y*+1, *-z*+1; (e) *-x*+1, *-y*, *-z*+1; (f) *x*, *y*, *z*+1; (g) *-x*, *-y*+1, *-z*; (h) *x*+1, *y*, *z*; (i) *x*, *y*+1, *z*. [b] A = acceptor; D = donor.

Both metal ions [Mn(1) and Ni(1)] lie on an inversion centre. They are six-coordinated and exhibit distorted octahedral environments (see Figure 3). Four carboxylate-oxygen atoms from two malonate ligands build the equatorial plane around the nickel atom [2.015(2) Å for the average Ni-O(mal) bond distance], the apical positions being occupied by two symmetrically related water molecules [2.151 Å for Ni-O(4w)]. Six water molecules are coordinated to each manganese atom building a 4+2 octahedral environment around the metal atom [see the Mn-O(w) bond distances in Table 2].

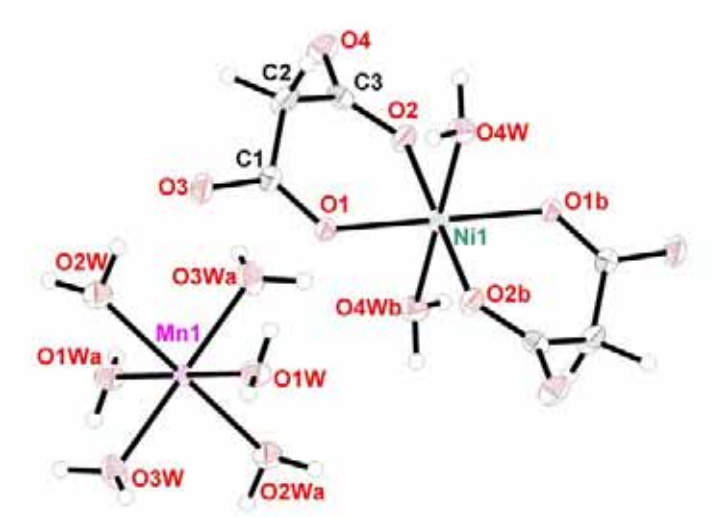

Figure 3. ORTEP view of the metal environments in **1** with the numbering scheme. Thermal ellipsoids are drawn at the 50% probability level.

Each malonate group in **1** acts as a bidentate ligand through O(1) and O(2) towards Ni(1) (see Figure 3), the O(1)-Ni(1)-O(2) bite angle being 91.36º. The malonate ligand forms a six-membered ring, including the nickel atom, that exhibits a boat conformation [θ = 90.8(4)º and ϕ = 122.4º] [Cremer D. et *al.*, 1975]. The values of the bond distances and angles for the malonate ligand in **1** (see Table 3) compare well with those reported for other malonate-containing nickel(II) complexes [see references in the Introduction].

Table 3. Bond lengths (Å) and angles (º) for the malonate ligand in **1**

C(1)-C(2)	1.524(5)	C(2)-C(3)	1.500(5)
C(1)-O(1)	1.265(4)	C(3)-O(2)	1.272(4)
C(1)-O(3)	1.252(4)	C(3)-O(4)	1.251(4)
O(1)···O(2)	2.883(4)	O(3)···O(4)	4.523(4)
O(1)-C(1)-O(3)	122.5(3)	O(2)-C(3)-O(4)	122.2(3)
O(1)-C(1)-C(2)	120.8(3)	O(2)-C(3)-C(2)	121.0(3)
O(3)-C(1)-C(2)	116.7(3)	O(4)-C(3)-C(2)	116.8(3)
C(1)-C(2)-C(3)	120.4(3)		
C(1)-O(1)-Ni(1)	126.7(2)	C(3)-O(2)-Ni(1)	126.0(2)

The $[Ni(mal)_2(H_2O)_2]^{2-}$ units are held together by means of hydrogen bonds involving the O(4w) coordinated water molecule and some malonate oxygen atoms [O(2) and O(4)] affording thus anionic layers that grow in the *ab*-plane (see Figure 2). The $[Mn(H_2O)_6]^{2+}$ units are linked through hydrogen bonds involving coordinated water molecules [O(1w) and O(2w)] leading to cationic chains that run along the *a*-axis. These chains are stacked along the *b*-axis, giving rise to cationic layers within the *ab*-plane.

Finally, additional hydrogen bonds involving all water molecules and all the malonate oxygen atoms (see Table 2) hold together the cationic and anionic layers affording a three-dimensional network (Figure 2).

Description of the structure of {[Mn(H$_2$O)$_2$][Co(mal)$_2$(H$_2$O)$_2$]} (2)

The structure of **2** consists of corrugated layers of malonate-bridged $[Co(mal)_2(H_2O)_2]^{2-}$ and $[Mn(H_2O)_2]^{2+}$ units (Figure 4a) which grow in the plane perpendicular to the [1 0 -1] direction. Additionally, hydrogen bonds involving water molecules and carboxylate oxygen atoms contribute to the crystal packing stabilizing the bimetallic layers and also linking them into a three-dimensional network (Figure 4b). Selected bond lengths and angles for compound **2** are listed in Table 4.

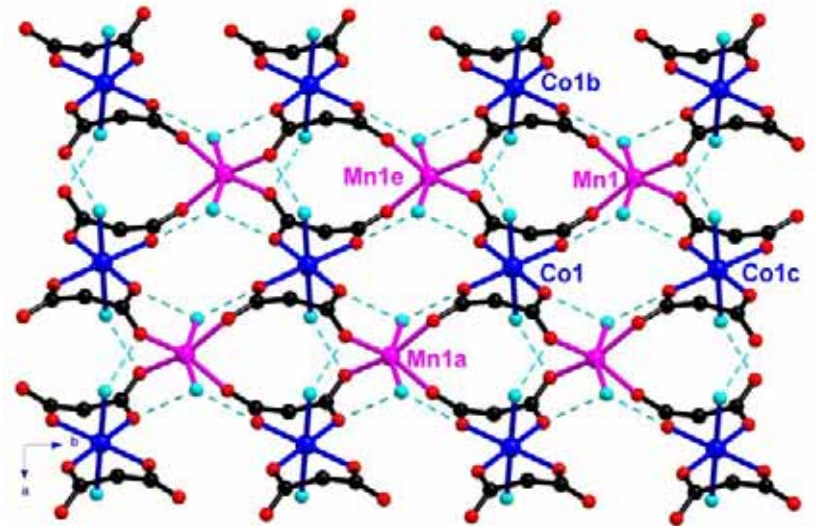

(a)

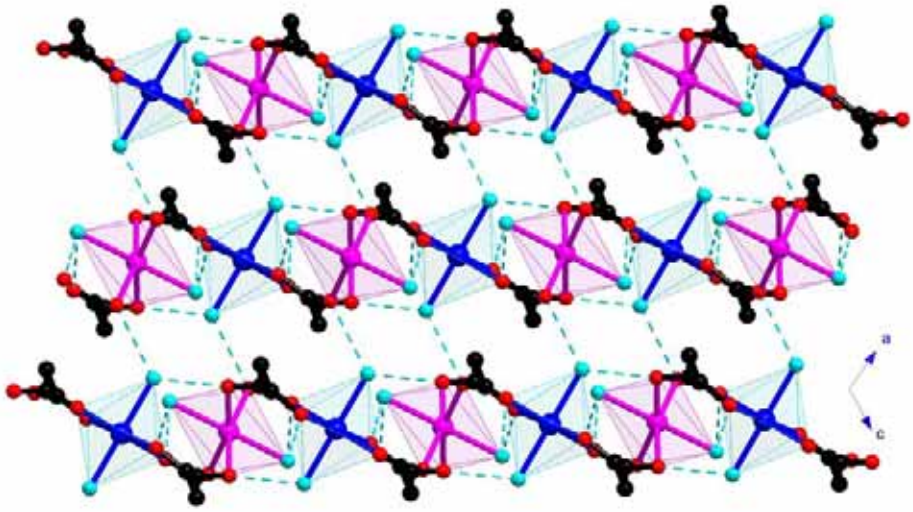

(b)

Figure 4. **(a)** Perspective view down the *c*-axis of a fragment of the malonate-bridged bimetallic layer of **2** (cobalt and manganese in blue and pink colours, respectively). **(b)** Stacking of these layers along the [10-1] direction. The hydrogen bonds are drawn as dashed lines. Symmetry codes are listed in Tables 4-6.

Table 4. Main bond lengths (Å) and angles (º) for **2**[a]

Co(1)-O(1)	2.056(2)	Co(1)-O(2)	2.132(2)
Co(1)-O(1w)	2.127(2)		
O(1)-Co(1)-O(2)	88.05(8)	O(1)-Co(1)-O(2a)	91.95(8)
O(1w)-Co(1)-O(1)	91.53(9)	O(1w)-Co(1)-O(1a)	88.47(9)
O(1w)-Co(1)-O(2)	91.15(10)	O(1w)-Co(1)-O(2a)	88.85(10)
Mn(1)-O(3c)	2.194(2)	Mn(1)-O(4)	2.192(2)
Mn(1)-O(2w)	2.238(2)		
O(3c)-Mn(1)-O(3d)	85.62(13)	O(4)-Mn(1)-O(4b)	92.51(13)
O(3c)-Mn(1)-O(4)	93.72(9)	O(4)-Mn(1)-O(2w)	81.52(9)
O(3c)-Mn(1)-O(4b)	161.73(8)	O(4)-Mn(1)-O(2wb)	84.06(9)
O(3c)-Mn(1)-O(2w)	79.90(8)	O(2w)-Mn(1)-O(2wb)	159.09(12)
O(3c)-Mn(1)-O(2wb)	116.20(8)		

[a] Symmetry transformations: (a) -*x*+1/2, -*y*+1/2, -*z*+1; (b) -*x*, *y*, -*z*+1/2; (c) *x*, *y*+1, *z*; (d) -*x*, *y*+1, -*z*+1/2.

Each cobalt atom lies on an inversion centre (see Figure 5). Four carboxylate-oxygen atoms from two malonate groups [2.056(2) and 2.131(2) Å for the Co-O(mal) bonds] and two water molecules in *cis* positions [2.127(2) Å = Co-O(1w)] build a slightly distorted octahedron around the metal atom.

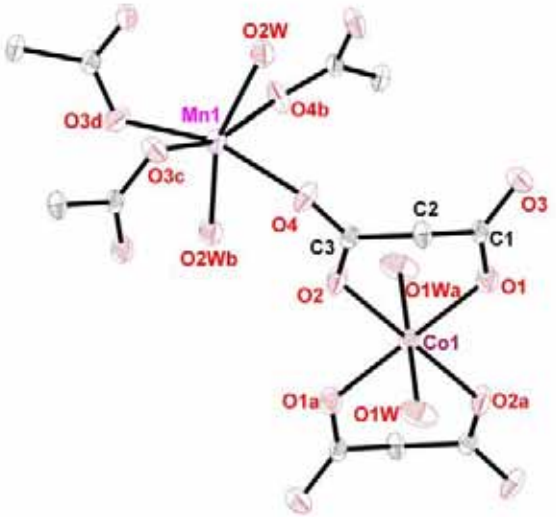

Figure 5. ORTEP view of the metal environments in **2** with the atom numbering. Thermal ellipsoids are drawn at the 50% probability level.

Each manganese atom lies on a two-fold axis (see Figure 5). Four carboxylate-oxygen atoms from four malonate groups [bond lengths of 2.194(2) and 2.192(2) Å] and two water molecules in *cis* positions [the bond distance being 2.238(2) Å] are coordinated to the manganese atom building a highly distorted octahedron environment around the metal atom (see the values of the O-Mn-O bond angles in Table 4).

The malonate group acts simultaneously as bidentate [through O(1) and O(2) towards Co(1)] and bis-monodentate [through O(3) and O(4) towards Mn(1) and Mn(1e); (e) *x*, *y*-1, *z*] ligand (see Figure 6). The malonate ligand forms a six-membered ring, including the cobalt atom, that exhibits a slightly distorted screw-boat conformation [θ = 73.5(3)º and ϕ = 131.4(3)º] [Cremer D. *et al.*, 1975]. Each carboxylate-malonate connects two adjacent metal ions [values of 5.5981(10) and 4.6459(7) Å for the Co(1)···Mn(1) and Co(1)···Mn(1e) separations, respectively] adopting the *anti-syn* conformation. The bond lengths and angles for the malonate group in **2** are listed in Table 5.

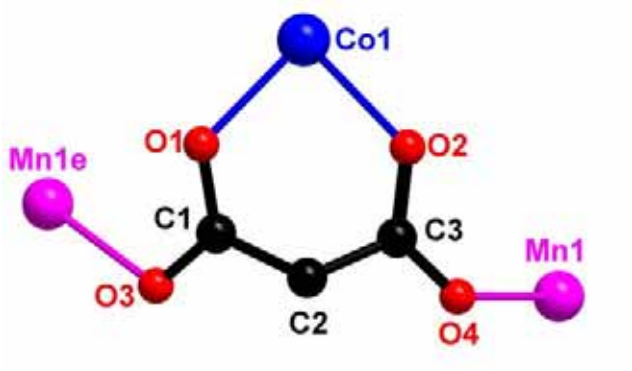

Figure 6. Coordination modes of the malonate ligand in **2**.

Table 5. Bond lengths (Å) and angles (º) for the malonate ligand in **2**[a]

C(1)-C(2)	1.509(4)	C(2)-C(3)	1.514(4)
C(1)-O(1)	1.261(4)	C(3)-O(2)	1.264(3)
C(1)-O(3)	1.255(3)	C(3)-O(4)	1.254(3)
O(1)···O(2)	2.911(3)	O(3)···O(4)	4.231(3)
O(1)-C(1)-O(3)	121.1(3)	O(2)-C(3)-O(4)	123.8(3)
O(1)-C(1)-C(2)	120.4(3)	O(2)-C(3)-C(2)	119.4(2)
O(3)-C(1)-C(2)	118.5(3)	O(4)-C(3)-C(2)	116.8(2)
C(1)-C(2)-C(3)	114.2(2)		
C(1)-O(1)-Co(1)	126.0(2)	C(3)-O(2)-Co(1)	127.9(2)
C(1)-O(3)-Mn(1e)	112.7(2)	C(3)-O(4)-Mn(1)	133.4(2)

[a] Symmetry transformations: (e) *x*, *y*-1, *z*.

The $[Co(mal)_2(H_2O)_2]^{2-}$ and $[Mn(H_2O)_2]^{2+}$ units are connected through carboxylate bridges leading corrugated bimetallic layers that grow in the plane perpendicular to the [1 0 -1] direction.. The shortest intralayer metal···metal distances are (see Figure 4a): 7.299(2) [Mn(1)···Mn(1e) and Co(1)···Co(1c)], 7.2506(6) [Mn(1a)···Mn(1e)] and 7.1264(6) Å [Co(1)···Co(1b)].

The bimetallic layers are further connected through hydrogen bonds (see Table 6) involving the O(1w) water molecule and some malonate oxygen atoms. The corrugated layers are stacked along the [1 0 -1] direction affording a three-dimensional network.

Table 6. Relevant strong and weak hydrogen bonds for **1**[a,b]

D-H···A	D···A/Å	D-H···A	D···A/Å
O(1w)-H···O(3f)	2.846(3)	O(2w)-H···O(1h)	2.961(4)
O(1w)-H···O(4g)	2.966(4)	O(2w)-H···O(2i)	2.724(4)
O(2w)-H···O(4)	2.893(3)		
D-H···A	D···A/Å	H···A/Å	D-H···A/º
C(2)-H(1)···O(4g)	3.482(4)	2.65(4)	157(4)
C(2)-H(2)···O(2wj)	3.373(4)	2.62(4)	135(3)

[a] Symmetry transformations: (f) *x*+1/2, -*y*+1/2, *z*+1/2; (g) -*x*+1/2, *y*-1/2, -*z*+1/2; (h) -*x*, *y*+1, -*z*+1/2; (i) -*x*, *y*, -*z*+1/2; (j) -*x*, -*y*+1, -*z*. [b] A = acceptor; D = donor.

References

Cremer D. and Pople J.A., *J. Am. Chem. Soc.*, **1975**, 97, 1354.

DIAMOND 2.1d, *Crystal Impact GbR, CRYSTAL IMPACT, K. Brandenburg & H. Putz GbR, Postfach 1251, D-53002 Bonn, Germany,* **2000.**

Duisenberg A.J.M., Kroon-Batenburg, L.M.J. and Schreurs, A.M.M., *J. Appl. Cryst.,* **2003,** 36, 220 (EVALCCD).

Farrugia L.J. (*WINGX*), *J. Appl. Cryst*, **1999**, 32, 837.

Hooft, R.W.W. *COLLECT*. Nonius BV, Delft, The Netherlands, **1999**.

Nardelli M. *J. Appl. Crystallogr.*, **1995**, 28, 659.

Rodríguez-Martín Y., Tesis Doctoral: *Malonato y azinas: una nueva alternativa en el diseño de materiales moleculares magnéticos*, **2002a**.

Rodríguez-Martín Y., Sanchiz J., Ruiz-Pérez C., Lloret F. and Julve M. *CrystEngComm*, **2002b**, 4, 631.

SADABS, version 2.03. Bruker AXS Inc.: Madison, WI, **2000**.

Sheldrick, G.M. *SHELX97*, *Programs for Crystal Structure Analysis (Release 97-2)*, Institüt für Anorganische Chemie der Universität, Tammanstrasse 4, D-3400 Göttingen, Germany, **1998**.

CHAPTER VIII.

From low- to high-dimensional networks in Cobalt(II) malonate complexes.

Introduction

Low dimensional coordination polymers, generally including one-dimensional (1D) chainlike and two-dimensional (2D) layer-like structures, have received much attention owing to their interesting structural features and unique electro-conductive, non-linear optical and magnetic properties, which are different from those of three-dimensional (3D) coordination polymers. One of the attractive challenges in this field is to predict the crystal packing from molecular structures. A reasonable approach to build three-dimensional structures based on layered structural motifs is to control the packing of layers by organic pillars of changeable lengths and/or type. This approach has been demonstrated to be effective towards assembly of both non-covalent and covalent pillared networks [Kondo M. *et al.*, 1999]. Pillared structures are potentially important for applications in absorption, separation and catalysis [Mitchel I.V., 1990]. A variety of pillar-layered structures including positively and negatively charged or neutral layers have been synthesized.

We are interested in the building-block approach for the network construction of coordination polymers focusing both on the role of the metal-ion geometry and that of the bridging ligands. A survey of the synthetic attempts reveals that most of them deal with rod-like and rigid bridging ligands, and consequently, the use of more flexible spacers deserves to be explored [Fujita *et al.*, 1996; Lu J. *et al.*, 1999]. From this respect, the malonate ligand (dianion of the propanedioic acid, H_2mal) seems a suitable candidate. The occurrence of two carboxylate groups in 1,3-positions allows this ligand to adopt simultaneously chelating bidentate and different carboxylato bridging modes (*syn-syn, syn-anti* and *anti-anti* trought one or both carboxylate groups). The well known ability of the carboxylato bridge to mediate significant ferro- and antiferromagnetic interactions between the paramagnetic metal ions that it bridges makes the malonate ligand very interesting in the design of extended magnetic systems.

In the context of our magneto-structural research with malonate-bridged homometallic complexes, we extended our work with the preparation, structural characterization and magnetic properties of several Co-metallic complexes. Cobalt is an essential metal ion involved in key biomolecules, regulating processes in human physiology. As a metal ion, Co(II) assumes forms, which are dictated by the nature of

organic binders in biological fluids, and the conditions under which metal ion ligand interactions arise.

The magnetism of dinuclear high-spin cobalt(II) complexes is a challenging area because the orbital angular momentum causes difficulties in the magnetic analysis [Kahn O., 1993]. In general, the orbital angular momentum is partially quenched in a ligand field of a certain symmetry [Figgis B.N. *et al.*, 2000]. For instance, in a ligand field of O_h symmetry, only the orbital angular momenta of T terms (T_{1g}, T_{1u}, T_{2g}, and T_{2u}) remain as a result of the quenching. When the symmetry is decreased to D_{3h}, only E terms (E' and E'') have orbital angular momenta. Thus, the effect of the orbital angular momentum is highly dependent on the symmetry around the metal ion. To our knowledge, the magnetism of the high-spin cobalt(II) complexes is classified into three groups: (1) an ideal octahedral or slightly distorted octahedral case, in which a ground term possesses an orbital angular momentum; (2) a tetrahedral, square-planer, trigonal, bipyramidal, or highly distorted octahedral case, in which a ground term does not have an orbital angular momentum; and (3) a highly distorted lower symmetric case, in which a ground term has an orbital angular momentum. In group 1, under an ideal O_h symmetry, the ground $^4T_{1g}$ term possesses the orbital angular momentum. Thus, to analyze the magnetic data, the effect of the orbital angular momentum should be taken into account [Kahn O., 1993]. In group 2, the ground term does not have an orbital angular momentum; thus, a spin-only treatment is valid for the complexes in this group. The effect of the higher term possessing an orbital momentum can be treated as a second-order Zeeman effect [Figgis B.N. *et al.*, 2000]. In group 3, the ground term possesses an orbital angular momentum due to the admixture with higher states [Figgis B.N. *et al.*, 2000]. At this stage, an appropriate method should be selected to consider the symmetry around the cobalt(II) ion for magnetic analysis. In the magnetic analysis of homo dinuclear high-spin cobalt(II) complexes, the classification above is also valuable. It is not difficult to understand the magnetism of the dinuclear complexes containing two cobalt(II) ions classified into group 2 because the spin-only treatment is possible. However, it is much more difficult to elucidate the magnetism of the dinuclear complexes containing two cobalt(II) ions classified into group 1 because of the T ground term with an orbital angular momentum, and there have been only a few successful examples [Lines M.E., 1971; Coronado E. *et al.*, 1988; De Munno G. *et al.*, 1994; Sakiyama H. *et al.*, 2001]. In 1971, Lines reported a theory for the analysis of the

magnetic coupling between two highspin cobalt(II) ions of pure O_h symmetry using a temperature dependent Hamiltonian [Lines M.E., 1971]. This remarkable theory enabled the analysis of the magnetic data of some dinuclear cobalt(II) complexes [De Munno G. *et al.*, 1994], but it was limited to only highly symmetrical cases. This limitation sometimes causes problems in the magnetic analysis since the symmetry around the real cobalt(II) ions is at best axial [Kahn O., 1993]. Taking the anisotropy into account, Drillon and co-workers made a successful low temperature study [Coronado E. *et al.*, 1988].

Experimental

Materials and methods

Malonic acid, cobalt(II) acetate tetrahydrate, cobalt(II) nitrate hexahydrate, cadmium(II) acetate, 4,4'-bipyridine-N,N'-dioxide, o-phenantroline, 3-cyanopyridine, pyrazine and pyrimidine were purchased from Aldrich and used as received. Elemental analyses (C, H, N) were carried out using an EA 1108 CHNS-O elemental analyzer. Variable temperature (1.8-300 K) magnetic susceptibility measurements of crushed crystals of **1-6** were carried out in a Quantum Design SQUID magnetometer operating at 250 G (T < 10 K) and 10000 G (T > 10 K). Diamagnetic corrections of all the constituent atoms were estimated from Pascal's constants as [Earshaw, 1968] -125 x 10^{-6} (**1**), -366 x 10^{-6} (**2**), -195 x 10^{-6} (**3**), -120 x 10^{-6} (**4**) -194 × 10^{-6} (**5** and **6**) cm^3mol^{-1}. Magnetic susceptibility data were also corrected for the magnetization of the sample holder.

Synthesis

{[Co(mal)$_2$(H$_2$O)$_2$]Cd(H$_2$O)$_2$} (1). A mixture of solid cobalt(II) malonate (0.197 mg, 1 mmol) (prepared as described in the previous chapter) and malonic acid (0.104 mg, 1 mmol) is added to an aqueous solution (10 cm^3). To this solution, we add under continuous stirring cadmium acetate (1 mmol) in aqueous solution (10 cm^3). This suspension is filtered. Red single-crystals of **1** appeared from the solution by slow evaporation at room temperature within ten days. (Found: C, 16.42; H, 2.72; calc. for $C_6H_{12}CdCoO_{12}$: C, 16.09; H, 2.68).

[Co$_2$(mal)$_2$(dpo)(H$_2$O)$_6$]·2H$_2$O (2) [dpo = 4,4'-bipyridine-N,N'-dioxide]. To an aqueous solution (10 cm^3) of copper malonate (104 mg, 1 mmol) is added 4,4'-

bipyridine-N,N'-dioxide (140 mg, 0.55 mmol) in aqueous solution (5 cm^3) under continuous stirring. The suspension is filtered and red single crystals of **2** were obtained by slow evaporation at room temperature within five days. (Found: C, 30.02; H, 4.30; N, 4.17; calc. for $C_{16}H_{28}Co_2N_2O_{18}$: C, 29.35; H, 4.28; N, 4.28 %).

[Co(mal)(phen)(H_2O)]·2H_2O (3) [phen = 1,10-phenantroline]. Solid cobalt(II) acetate tetrahydrate (498 mg, 2 mmol) is added to an aqueous solution (15 cm^3) of malonic acid (208 mg, 2 mmol) under continuous stirring. The suspension is heated at 40-50 ºC, until a rose solution is obtained. This solution is filtered and mixed with a 1:1 H_2O:EtOH solution (5 cm^3) of o-phenanthroline (235 mg, 1 mmol). Single crystals of **3** as light plates prisms were grown from the resulting solution by slow evaporation at room temperature within three weeks. (Found: C, 37.45; H, 3.67; N, 11.30; calc. for $C_{11}H_{13}CuN_3O_6$: C, 38.06; H, 3.75; N, 12.11%)**.**

[Co(mal)(3-cnpy)(H_2O)] (4) [3-cnpy = 3-cyanopyridine]. The formation of crystals of **4** is accomplished by the reaction of malonic acid, 3-cnpy and cobalt(II) nitrate hexahydrate in sodium metasilicate gels. The silica gel was prepared by hydrolysis and polycondensation of sodium metasilicate nonahydrate in water solution under acidic conditions [Henish H.K., 1970]. First, solid 3-cyanopyridine (2.605 g, 33.4 mmol) is added to an aqueous solution (25 ml, 1 M) under continuous stirring. To the resulting solution a proper amount of $Na_2SiO_3·9H_2O$ (1 M) is added to adjust the pH value at the mixed solution to about 4.5. The mixture was run into test tubes, covered, and allowed to set for 48 hours at room temperature in a dark place. 0.1 M solution of cobalt(II) nitrate hexahydrate was then added dropwise on top of the gel, so that the surface of the gel would not break, and the tubes were stored at 25ºC. Three months later, red crystals appeared suitable for X-ray analysis. They were mounted from the gel, washed and dried at room temperature (Found: C, 44.94; H, 3.76; N 11.40; calc. for $C_{17}H_{17}CuN_4O_{6.5}$: C, 45.85; H, 3.82; N, 12.59%).

[Co_2(mal)$_2$(pym)(H_2O)]$_n$ (5) [pym = pyrimidine]. To an aqueous solution (100 cm^3) of cobalt(II) acetate (0.500 g, 2.00 mmol) malonic acid (0.210 g, 2.02 mmol) was added and the solution was evaporated in a steam bath to a volume of *ca.* 50 cm^3. Then the solution was cooled to room temperature and an aqueous solution (10 cm^3) of pyrimidine (0.093 g, 1.12 mmol) was added. Red single-crystals of **2** (yield > 50%) appeared from the pink solution within two weeks. (Found: C, 27.4; H, 2.9; N, 6.4; calc. for $C_5H_6NO_5Co$: C, 27.4; H, 2.8; N, 6.4%).

$[Co_2(mal)_2(pyz)(H_2O)]_n$ (6) [pyz = pyrazine]. Compound **6** is obtained as red single-crystals following a similar procedure to that of **5**, using pyrazine instead of pyrimidine. (Found: C, 27.3; H, 2.8; N, 6.3.; calc. for $C_5H_6NO_5Co$: C, 27.4; H, 2.8; N, 6.4%).

Crystal data collection and refinement

Suitable single crystals of compounds **1-4** were mounted on a Bruker-Nonius KappaCCD diffractometer. Orientation matrix and lattice parameters were obtained by least-squares refinement of the reflections obtained by a θ-χ scan (Dirax/lsq method). For compounds **5-6** single crystals were mounted on an Enraf-Nonius MACH3 diffractometer. Orientation matrix and lattice parameters were obtained by least-squares refinement of the diffraction data of 25 reflexions in the range $6 < \theta < 18^\circ$ [CAD4-EXPRESS, version 5.1/1.2, 1994; Harms K., 1996]. Diffraction data for all compounds were collected at 293(2) K using graphite-monochromated Mo-K_α radiation (λ = 0.71073 Å). Data collection and data reduction were done with the COLLECT [Hooft R.W.W., 1999] and EVALCCD [Duisenberg A.J.M. *et al.*, 2003] programs for compounds **1-4**, whereas for compounds **5** and **6** data were collected using the ω-scan technique. Empirical absorption corrections were carried out using SADABS [SADABS, version 2.03, 2003] for compounds **1-4** whereas intensity data were corrected for Lorentz and polarization effects but not for absorption for compounds **5-6**. The indexes of data collection were $-18 \le h \le 18$, $-9 \le k \le 8$, $-16 \le l \le 16$ for **1**; $-6 \le h \le 10$, $-44 \le k \le 42$, $-13 \le l \le 14$ for **2**; $-18 \le h \le 17$, $-7 \le k \le 7$, $-18 \le l \le 18$ for **3**; $-10 \le h \le 6$, $-9 \le k \le 9$, $-15 \le l \le 14$ for **4**; $-21 \le h \le 23$, $-9 \le k \le 0$, $-10 \le l \le 0$ for **5** and $-9 \le h \le 0$, $-20 \le k \le 0$, $-10 \le l \le 10$ for **6**. Of the 1362 (**1**), 6859 (**2**), 2759 (**3**), 2963 (**4**), 1225 (**5**), 2174 (**6**) measured independent reflections in the θ range 6.40 – 27.50º (**1**), 6.41 - 30º (**2**), 6.40 – 25.02º (**3**), 6.45 – 30.00º (**4**), 2.68 – 27.50º (**5**) and 2.82 - 29.95º (**6**), 1216 (**1**), 3213 (**2**), 1820 (**3**), 2376 (**4**), 1153 (**5**) and 1543 (**6**) have $I \ge 2\sigma(I)$. All the measured independent reflections were used in the analysis. All calculations for data reduction, structure solution, and refinement were done by standard procedures (WINGX) [Farrugia, L. J., 1999]. The structures were solved by direct methods and refined with full-matrix least-squares technique on F^2 using the SHELXS-97 and SHELXL-97 programs [Sheldrick G.M. SHELX97, realease 97-2, 1998]. The malonate and water hydrogen atoms were located, for compounds **1, 3** and **6** from difference Fourier maps. For compounds **2** and **4-5,** the water hydrogen bonds were not found and pyridyl and

malonate hydrogen atoms were set in calculated positions. For all compounds hydrogen atoms were refined with isotropic temperature factors. The final Fourier-difference map showed maximum and minimum height peaks of 0.975 and -2.025 e $Å^{-3}$ (**1**), 0.641 and -0.451 e $Å^{-3}$ (**2**), 0.331 and -0.339 e $Å^{-3}$ (**3**), 0.544 and -0.367 e $Å^{-3}$ (**4**) 4.032 [at 0.82 Å from Co(1)] and -1.469 e $Å^{-3}$ (**5**) [an empirical absorption correction was tried for **2** but no improvement was obtained] and 0.587 and -0.714 e $Å^{-3}$ (**6**). A summary of the crystallographic data and structure refinement is given in Table 1. The final geometrical calculations and the graphical manipulations were carried out with PARST97 [Nardelli, M., 1995] and DIAMOND [DIAMOND 2.1d, 2000] programs, respectively.

Table 1. Crystal data and details of structure determination for compounds **1**-**5**.

Compound	**1**	**2**	**3**	**4**	**5**	**6**
Formula	$C_6H_{12}CdCoO_{12}$	$C_{16}H_{28}Co_2N_2O_{18}$	$C_{15}H_{16}CoN_2O_7$	$C_9H_8CoN_2O_5$	$C_5H_6CoNO_5$	$C_5H_6CoNO_5$
M	447.49	654.26	395.23	283.10	219.04	219.04
Crystal system	monoclinic	monoclinic	monoclinic	monoclinic	monoclinic	monoclinic
Space group	*C*2/*c*	*P*21/*n*	*P*21/*n*	*P*21	*C*2	*P*21/*n*
a, Å	14.174(3)	7.308(3)	15.149(3)	7.5502(6)	16.802(2)	6.9610(10)
b, Å	7.3950(10)	32.068(7)	6.6200(10)	6.7565(3)	6.8884(4)	14.442(3)
c, Å	12.984(3)	10.378(2)	15.936(3)	10.8651(7)	7.4787(11)	7.4340(10)
α, deg	-	-	-	-	-	-
β, deg	117.69(3)	93.66(2)	90.62(3)	106.156(5)	115.119(10)	92.02(3)
γ, deg	-	-	-	-	-	-
V, Å^3	1205.1(4)	2427.2(12)	1598.1(5)	532.37(6)	783.7(2)	746.9(2)
Z	4	4	4	2	4	4
T(K)	293(2)	293(2)	293(2)	293(2)	293(2)	293(2)
ρ_{calc} (Mg m^{-3})	2.467	1.790	1.643	1.766	1.856	1.948
F(000)	876	1344	812	286	440	440
λ (Mo-Kα Å)	0.71073	0.71073	0.71073	0.71073	0.71073	0.71073
μ(MoK$_\alpha$) (mm^{-1})	3.205	1.458	1.116	1.623	2.171	2.278
Flack Parameter	-	-	-	0.00	0.14(6)	-
Number parameters/restraints	117 / 0	343 / 0	290 / 0	178 / 1	112 / 1	133 / 0
Goodness of fit (S)	1.059	1.009	1.015	0.999	1.144	1.002
R1, $I > 2\sigma(I)$ (all)	0.0376 / 0.0442	0.0744 / 0.1934	0.0448 / 0.0942	0.0436 / 0.0642	0.0793 / 0.0747	0.0360 / 0.0774
wR2, $I > 2s(I)$ (all)	0.0950 / 0.0980	0.1220 / 0.1506	0.0659 / 0.0753	0.0898 / 0.0962	0.1915 / 0.1962	0.0826 / 0.0934
Max/min electron density (e/Å^3)	0.975 / -2.025	0.641 / -0.451	0.331 / -0.339	0.544 / -0.367	4.0321[a] / -1.469	0.587 / -0.714
Measured reflections (R_{int})	3293 (0.0515)	16976 (0.0918)	12757 (0.0861)	4628 (0.0315)	1309 (0.0170)	2331 (0.0313)
Independent reflections [$I > 2\sigma(I)$]	1362 (1216)	6859 (3213)	2759 (1820)	2963 (2376)	1225 (1153)	2174 (1543)

[a]Maximum diffraction density at 0.82 Å from Co(1) (an empirical absorption was tried for **5** but not improvement was observed).

Results and discussion

Description of the structure of {[Co(mal)$_2$(H$_2$O)$_2$]·Cd(H$_2$O)$_2$} (1)

The structure of **1** consists of corrugated layers of malonate-bridged $[Co(mal)_2(H_2O)_2]^{2-}$ and $[Cd(H_2O)_2]^{2+}$ units (Figure 1a) which grow in the *ab*-plane. Additionally, hydrogen bonds involving water molecules and carboxylate-oxygen atoms contribute to the crystal packing stabilizing the bimetallic layers and also connecting them into a three-dimensional network (Figure 1b).

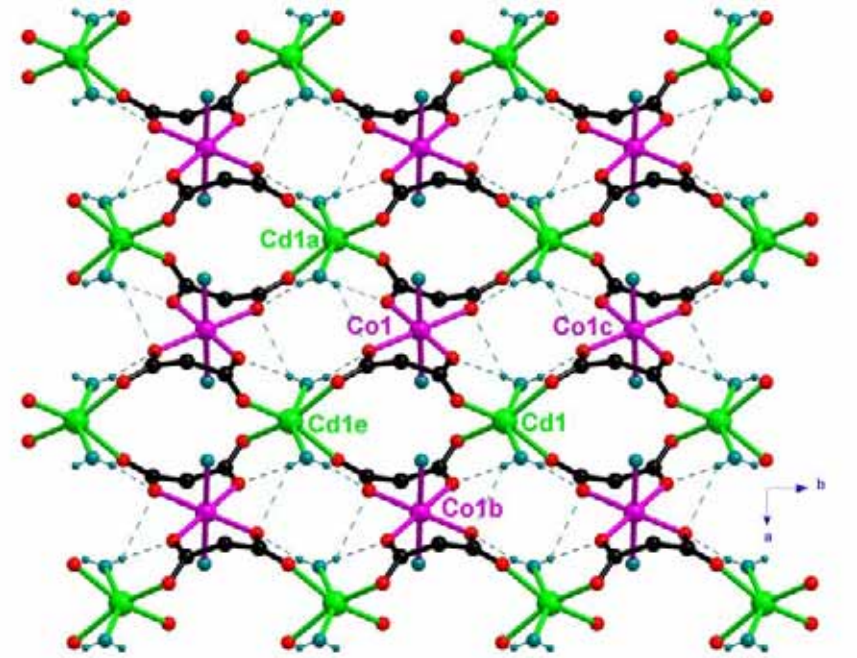

(a)

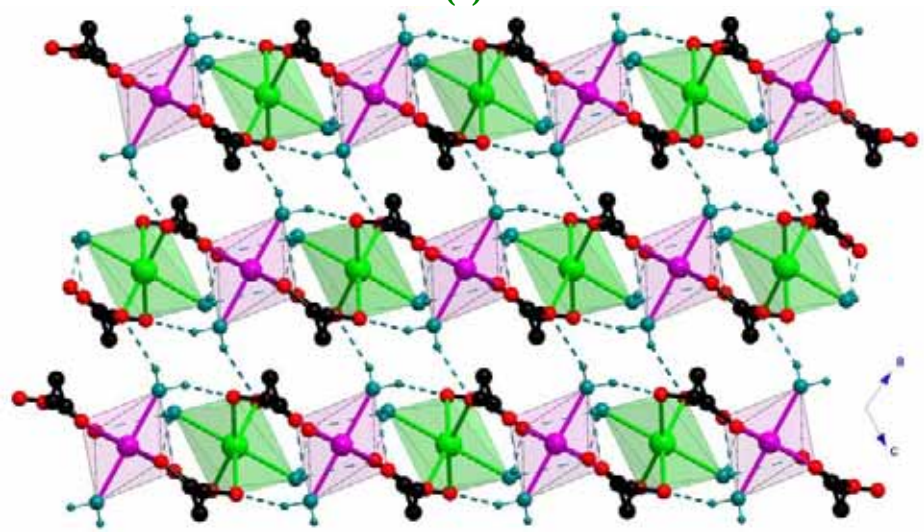

(b)

Figure 1. (a) Perspective view of a fragment of the malonate-bridged bimetallic layer of **1** (cobalt, pink; cadmium, green), along the *c*-axis. **(b)** Stacking of these layers along the [1 0 -1] direction. The hydrogen bonds are drawn as dotted lines. Symmetry codes are reported in Tables 2 and 3.

Selected bond lengths and angles for **1** are listed in Table 2.

Table 2. Main bond lengths (Å) and angles (º) for **1**[a]

Co(1)-O(1)	2.130(3)	Co(1)-O(2)	2.062(3)
Co(1)-O(1w)	2.121(4)		
O(1)-Co(1)-O(2)	88.57(13)	O(1)-Co(1)-O(2a)	91.43(13)
O(1w)-Co(1)-O(1)	91.1(2)	O(1w)-Co(1)-O(1a)	88.9(2)
O(1w)-Co(1)-O(2)	91.3(2)	O(1w)-Co(1)-O(2a)	88.7(2)
Cd(1)-O(3c)	2.318(3)	Cd(1)-O(4)	2.294(3)
Cd(1)-O(2w)	2.346(2)		
O(3c)-Cd(1)-O(3d)	91.2(2)	O(4)-Cd(1)-O(4b)	88.9(2)
O(3c)-Cd(1)-O(4)	93.48(12)	O(4)-Cd(1)-O(2w)	120.83(14)
O(3c)-Cd(1)-O(4b)	159.85(12)	O(4)-Cd(1)-O(2wb)	79.76(14)
O(3c)-Cd(1)-O(2w)	81.88(14)	O(2w)-Cd(1)-O(2wb)	152.9(3)
O(3c)-Cd(1)-O(2wb)	79.23(15)		

[a] Symmetry transformations: (a) *-x*-1/2, *-y*-1/2, *-z*; (b) *-x*, *y*, *-z*+1/2; (c) *x*, *y*+1, *z*; (d) *-x*, *y*+1, *-z*+1/2.

Each cobalt atom lies on an inversion centre and it is six coordinated (see Figure 2). Four malonate oxygen atoms [2.130(3) and 2.062(3) Å for Co-O(mal)] and two water molecules [2.121(4) Å for Co-O(w)] in *trans* positions are bound to the cobalt atom building a slightly distorted octahedral environment around the metal ion (*s*/*h* = 1.22, ϕ = 59.16º) [Stiefel E.I. *et al.*, 1972]. It deserves to be noted that the geometry of the cobalt environment is close to that of the ideal octahedron (*s*/*h* = 1.22 and ϕ = 60º for the regular octahedron).

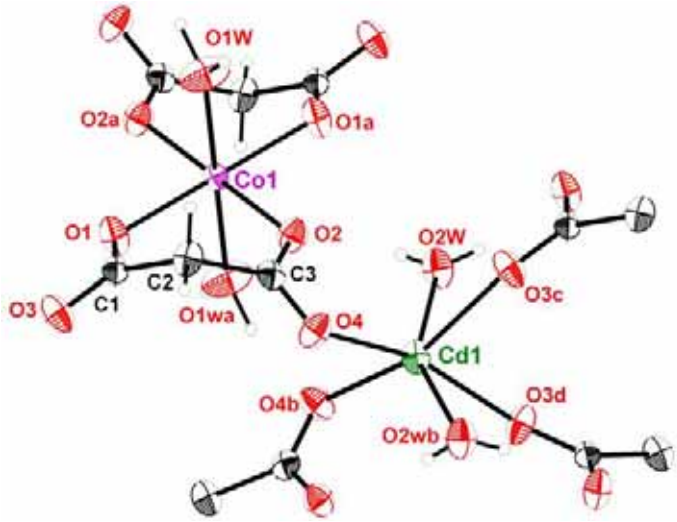

Figure 2. Perspective view of the metal environments in **1** with the atom numbering. Thermal ellipsoids are drawn at the 50% probability level.

Each cadmium atom lies on a two-fold axis (Figure 2). Four malonate oxygen atoms [2.318(3) and 2.294(3) for Cd-O(mal)] and two water molecules [2.346(2) for Cd-O(2w)] build a highly distorted octahedral environment around the metal atom (see bond angles in Table 2).

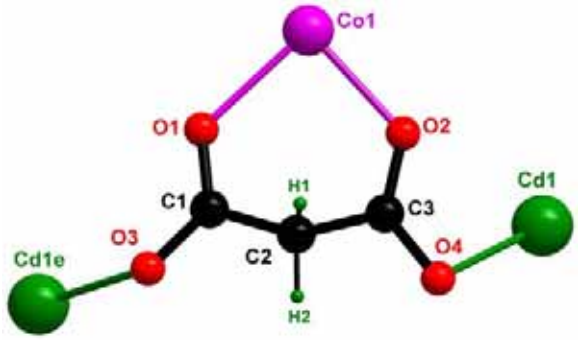

Figure 3. Coordination mode of the malonate ligand in **1**.

The malonate group acts simultaneously as bidentate [through O(1) and O(2) towards Co(1), the O(1)-Cu(1)-O(2) angle being 88.57(13)º] and bis-monodentate [through O(4) towards Cd(1) and through O(3) towards Cd(1e); (e) *x*, *y*-1, *z*] ligand. It forms a six-membered ring including the cobalt atom that exhibits a slightly screw boat conformation [θ = 78.3(5) and ϕ = 113.5(5)º] [Cremer D. *et al.*, 1975]. Each carboxylate-malonate group bridges two adjacent metal ions [4.5774(13) and 5.6915(12) Å for the Co(1)···Cd(1) and Co(1)···Cd(1e) distances, respectively] in an *anti-syn* conformation. The values of the bond lengths and angles of the malonate ligand in 1 are listed in Table 3.

Table 3. Selected bond lengths (Å) and angles (º) for the malonate present in **1**[a]

C(1)-C(2)	1.514(6)	C(2)-C(3)	1.521(6)
C(1)-O(1)	1.267(5)	C(3)-O(2)	1.252(6)
C(1)-O(3)	1.249(5)	C(3)-O(4)	1.249(5)
O(1)···O(2)	2.928(5)	O(3)···O(4)	4.213(5)
O(1)-C(1)-O(3)	123.7(4)	O(2)-C(3)-O(4)	121.9(4)
O(1)-C(1)-C(2)	119.5(4)	O(2)-C(3)-C(2)	120.3(4)
O(3)-C(1)-C(2)	116.8(4)	O(4)-C(3)-C(2)	117.7(4)
C(1)-C(2)-C(3)	113.9(4)		
C(1)-O(1)-Co(1)	126.2(3)	C(3)-O(2)-Co(1)	125.9(3)
C(1)-O(3)-Cd(1e)	133.1(3)	C(3)-O(4)-Cd(1)	106.4(3)

[a] Symmetry code: (e) *x*, *y*-1, *z*.

$[Co(mal)(H_2O)_2]^{2-}$ and $[Cd(H_2O)_2]^{2+}$ units are linked through carboxylate bridges leading to corrugate malonate bimetallic layers that grow in the *ab*-plane. The shortest intralayer metal···metal distances are: 7.3950(12) [Cd(1)···Cd(1e)], 7.212(3) [Cd(1)···Cd(1a)], 7.044(3) [Co(1)···Co(1b)] and 7.3950(10) Å [Co(1)···Co(1c)] (see Figure 1).

Finally, corrugated layers are held together by means of hydrogen bonds (see Table 4) involving the O(1w) and malonate oxygen atoms [the distance between the mean planes defined by atoms belonging to consecutive corrugated layers being 5.7839(3) Å]. The bimetallic layers stack along the [1 0 -1] direction affording a three-dimensional network through hydrogen bonding.

Table 4. Relevant strong and weak hydrogen bonds for **1**[a,b]

D-H···A	D···A/Å	H···A/Å	D-H···A/º
O(1w)-H(1w1)···O(3f)	2.896(7)	2.17(10)	156(8)
O(1w)-H(2w1)···O(4g)	2.749(5)	1.89(5)	154(6)
O(2w)-H(1w2)···O(1c)	2.739(7)	2.05(8)	156(8)
O(2w)-H(2w2)···O(2)	3.056(7)	2.61(10)	130(9)
O(2w)-H(2w2)···O(1a)	3.184(5)	2.66(7)	141(10)
C(2)-H(1)···O(3f)	3.355(7)	2.54(6)	153(5)
C(2)-H(2)···O(2wh)	3.354(7)	2.54(7)	143(4)

[a] Symmetry transformations: (a) *-x*-1/2, *-y*-1/2, *-z*; (c) *x*, *y*+1, *z*; (f) *-x*-1/2, *y*-1/2, *-z*+1/2; (g) *x*-1/2, *-y*-1/2, *z*-1/2; (h) *-x*-1/2, *y*+1/2, *-z*+1/2. [b] A = acceptor; D = donor.

Description of the structure of $[Co_2(mal)_2(dpo)(H_2O)_6]\cdot 2H_2O$ (2)

The structure of **2** consists of malonato-bridged heterobimetallic $[Co_2(mal)_2(dpo)(H_2O)_6]$ dinuclear units and crystallisation water molecules which are held together by means of hydrogen bonds and weak π-π interactions (3.36 Å being the distance between dpo ligands) affording a three-dimensional network with regular alternating hydrophilic (A) and hydrophobic (B) layers (see Figure 4).

Selected bond lengths and angles for the metal environments in **2** are reported in Table 5.

Two crystallographically independent cobalt atoms occur in **2**: Co(1) and Co(2). Both of them are six-coordinated (see Figure 5) in a slightly distorted octahedral environment [*s*/*h* = 1.24 and ϕ = 58.99º for Co(1) and *s*/*h* = 1.25 and ϕ = 59.29º for Co(2)] [Stiefel E.I. *et al.*, 1972].

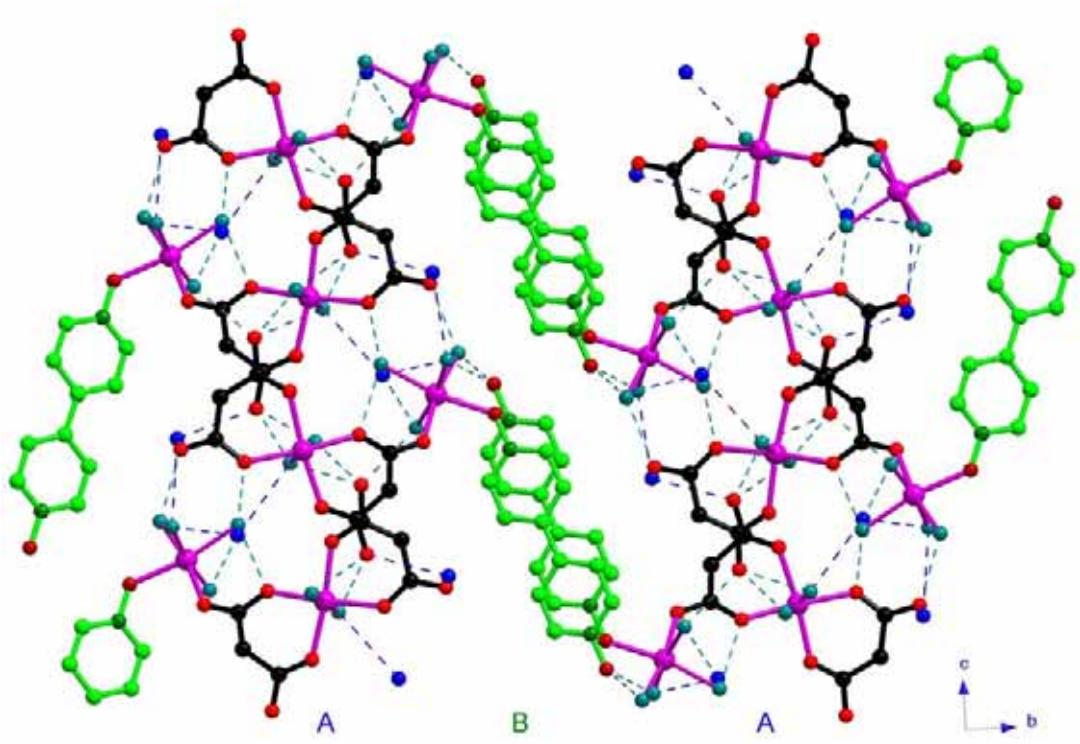

(a)

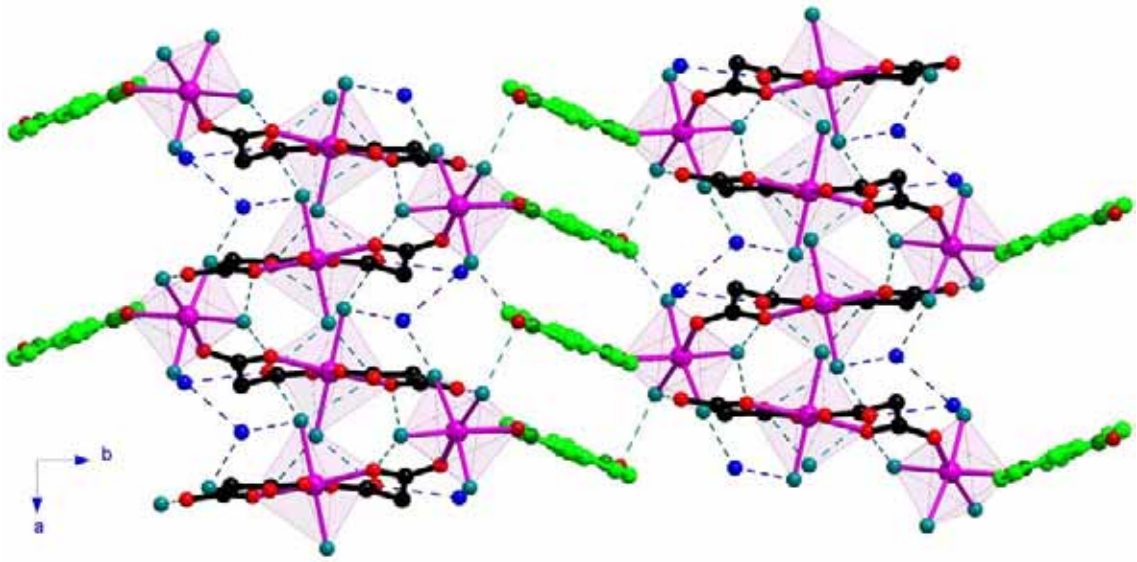

(b)

Figure 4. Perspective views along the *a*- **(a)** and *c*-axis **(b)** of the crystal packing in **2**. The hydrogen bonds are represented by broken lines.

Table 5. Selected bond lengths (Å) and angles (º) for **2**

Co(1)-O(1)	2.057(3)	Co(1)-O(2)	2.044(3)
Co(1)-O(11)	2.061(3)	Co(1)-O(12)	2.044(3)
Co(1)-O(1w)	2.112(4)	Co(1)-O(2w)	2.118(4)
O(1)-Co(1)-O(2)	88.38(12)	O(11)-Co(1)-O(12)	89.49(12)
O(1)-Co(1)-O(11)	96.24(12)	O(2)-Co(1)-O(11)	174.53(12)
O(1)-Co(1)-O(12)	174.12(12)	O(2)-Co(1)-O(12)	85.96(12)
O(1w)-Co(1)-O(1)	90.27(14)	O(1w)-Co(1)-O(2)	91.13(15)
O(1w)-Co(1)-O(11)	91.76(15)	O(1w)-Co(1)-O(12)	88.25(15)

O(2w)-Co(1)-O(1)	86.75(13)	O(2w)-Co(1)-O(2)	89.79(14)
O(2w)-Co(1)-O(11)	87.56(14)	O(2w)-Co(1)-O(12)	94.82(14)
O(1w)-Co(1)-O(2w)	176.85(13)		
Co(2)-O(4)	2.047(3)	Co(2)-O(21)	2.106(3)
Co(2)-O(3w)	2.123(3)	Co(2)-O(4w)	2.056(3)
Co(2)-O(5w)	2.141(3)	Co(2)-O(6w)	2.132(4)
O(4)-Co(2)-O(21)	88.53(12)	O(3w)-Co(2)-O(4w)	91.49(12)
O(4)-Co(2)-O(3w)	99.13(12)	O(21)-Co(2)-O(3w)	169.49(12)
O(4)-Co(2)-O(4w)	169.07(12)	O(21)-Co(2)-O(4w)	81.28(12)
O(5w)-Co(2)-O(4)	89.48(13)	O(5w)-Co(2)-O(21)	97.22(13)
O(5w)-Co(2)-O(3w)	90.07(13)	O(5w)-Co(2)-O(4w)	87.92(13)
O(6w)-Co(2)-O(4)	88.91(14)	O(6w)-Co(2)-O(21)	90.79(14)
O(6w)-Co(2)-O(3w)	82.23(13)	O(6w)-Co(2)-O(4w)	95.11(13)
O(5w)-Co(2)-O(6w)	171.78(13)		

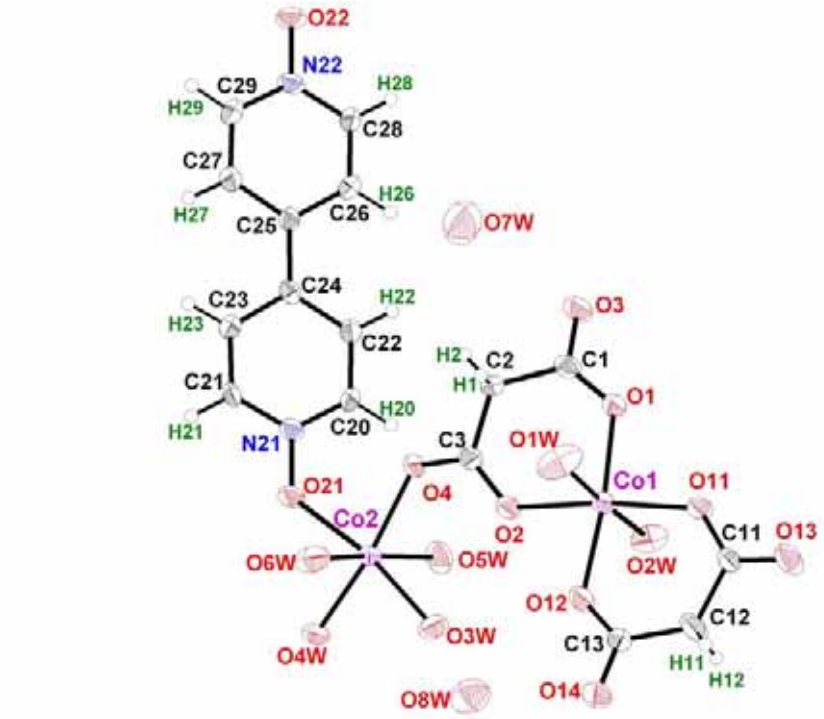

Figure 5. Perspective view of the asymmetric unit in **2** with the atom numbering. Thermal ellipsoids are drawn at the 50% probability level.

Four coplanar malonate-oxygen atoms build the equatorial plane around Co(1) [the average Co(1)-O(mal) bond distance is 2.052(3) Å], whereas two water molecules in *trans* configuration fill the apical positions [2.115(4) Å for the mean Co(1)-O(w) bond distance]. The metal atom is shifted by 0.0157(7) Å from the mean equatorial plane towards O(1w).

Two water molecules [O(3w) and O(4w)] and two oxygen atoms [O(21) and O(4)] from the dpo and malonate group build the equatorial plane around Co(2) [2.083(3) Å being the mean Co(2)-O bond distance], whereas the apical positions are

occupied by two water molecules [2.141(3) and 2.132(4) Å for Co(2)-O(1w) and Co(2)-O(2w), respectively]. The Co(2) atom is shifted by 0.0352(7) Å from the mean equatorial plane towards O(5w).

Two crystallographically independent malonate ligands noted L1 [C(1)-C(2)-C(3)] and L2 [C(11)-C(12)-C(13)] are present in **2** (see Figure 5). L1 acts simultaneously as a bidentate [through O(1) and O(2) towards Co(1)] and monodentate [through O(4) towards Co(1)] ligand (see Figure 6), whereas L2 adopts a bidentate coordination mode [through O(11) and O(12) towards Co(1)]. The values of the angle subtended by L1 and L2 at Co(1) are 88.38(12) and 89.49(12)º, respectively. Both malonate groups form six-membered rings including the metal atom corresponding to a boat [θ = 87.7(4) and ϕ = 122.6(5)º] and twist-boat [θ = 89.74(14) and ϕ = 101.96(13)º] conformations [Cremer D. *et al.*, 1975] for L1 and L2, respectively. The O(4)-C(3)-O(2) carboxylate group connects two equatorial sites from two adjacent cobalt atoms [Co(1)···Co(2) = 5.2566(13) Å] showing the *anti-syn* confomation. Selected bond lengths and angles for the malonate ligand are reported in Table 6.

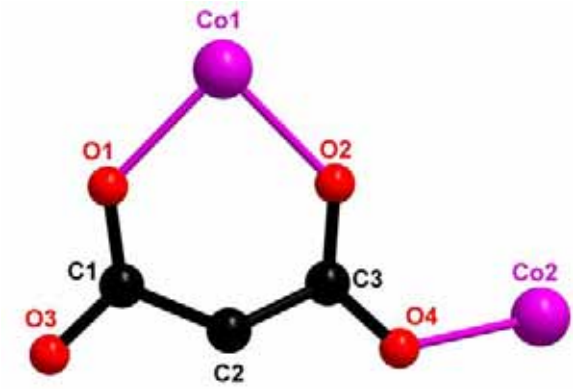

Figure 6. Coordination mode for malonate ligand L1 in **2**.

Table 6. Bond lengths (Å) and angles (º) for the malonate ligands present in **2**.[a]

C(1)-C(2)	1.520(6)	C(2)-C(3)	1.511(6)
C(1)-O(1)	1.246(5)	C(3)-O(2)	1.249(5)
C(1)-O(3)	1.265(5)	C(3)-O(4)	1.253(5)
O(1)···O(2)	2.859(4)	O(3)···O(4)	4.396(4)
O(1)-C(1)-O(3)	124.3(4)	O(2)-C(3)-O(4)	123.8(4)
O(1)-C(1)-C(2)	120.5(4)	O(2)-C(3)-C(2)	120.2(4)
O(3)-C(1)-C(2)	115.2(4)	O(4)-C(3)-C(2)	116.1(4)
C(1)-C(2)-C(3)	117.3(4)		
C(1)-O(1)-Co(1)	127.0(3)	C(3)-O(2)-Co(1)	127.9(3)
C(3)-O(4)-Co(2)	127.8(3)		

C(11)-C(12)	1.484(6)	C(12)-C(13)	1.467(6)
C(11)-O(11)	1.258(5)	C(13)-O(12)	1.237(5)
C(11)-O(13)	1.242(5)	C(13)-O(14)	1.257(5)
O(11)···O(12)	2.890(4)	O(13)···O(14)	4.561(5)
O(11)-C(11)-O(13)	123.5(4)	O(12)-C(13)-O(14)	122.3(4)
O(11)-C(11)-C(12)	122.2(4)	O(12)-C(13)-C(12)	121.8(4)
O(13)-C(11)-C(12)	114.3(4)	O(14)-C(13)-C(12)	116.0(4)
C(11)-C(12)-C(13)	126.0(4)		
C(11)-O(11)-Co(1)	127.9(3)	C(13)-O(12)-Co(1)	129.7(3)

The 4,4'-bipyridine-N,N'-dioxide (dpo) group acts as a monodentate ligand through O(1) towards Co(2). This coordination mode has been observed in other structurally characterised dpo-containing cobalt(II) complexes [Blake A.J. *et al.*, 2001; Nedelcu A. *et al.*, 2003]. The values of the bond lengths and angles of the dpo ligand are listed in Table 7 and they agree well with those reported for the free ligand [Thaimattam R. *et al.*, 1998]. The dpo as a whole does not deviates significantly from planarity [the dihedral angle between pyridyl rings being 2.2(2)º]. The maximum deviation from the mean equatorial plane is 0.047(4) Å for O(21).

Table 7. Bond lengths (Å) and angles (º) for the dpo ligand in **2**

O(21)-N(21)	1.341(4)	O(22)-N(22)	1.330(4)
N(21)-C(20)	1.336(5)	N(22)-C(28)	1.344(5)
N(21)-C(21)	1.344(5)	N(22)-C(29)	1.350(5)
C(20)-C(22)	1.364(6)	C(28)-C(26)	1.373(6)
C(21)-C(23)	1.366(6)	C(29)-C(27)	1.363(6)
C(22)-C(24)	1.404(6)	C(26)-C(25)	1.395(6)
C(23)-C(24)	1.398(6)	C(27)-C(25)	1.387(6)
C(24)-C(25)	1.473(6)		
O(21)-N(21)-C(20)	120.0(4)	O(22)-N(22)-C(28)	119.6(4)
O(21)-N(21)-C(21)	119.1(3)	O(22)-N(22)-C(29)	119.7(4)
N(21)-C(20)-C(22)	120.6(4)	N(22)-C(28)-C(26)	119.3(4)
N(21)-C(21)-C(23)	120.3(4)	N(22)-C(29)-C(27)	120.6(4)
C(20)-C(22)-C(24)	121.2(4)	C(28)-C(26)-C(25)	122.1(4)
C(20)-N(21)-C(21)	120.9(4)	C(28)-N(22)-C(29)	120.7(4)
C(21)-C(23)-C(24)	121.3(4)	C(29)-C(27)-C(25)	121.3(4)
C(22)-C(24)-C(23)	115.7(4)	C(26)-C(25)-C(27)	115.9(4)
C(22)-C(24)-C(25)	121.9(4)	C(26)-C(25)-C(24)	120.9(4)
C(23)-C(24)-C(25)	122.4(4)	C(27)-C(25)-C(24)	123.2(4)
N(21)-O(21)-Co(2)	129.2(2)		

Within the malonate-bridged cobalt(II) dinuclear unit, the dihedral angle between the mean equatorial planes of Co(1) and Co(2) is 27.09(8)º. An extensive network of hydrogen bonds involving malonate-oxygen atoms and water molecules (see Table 8) hold together the cobalt dinuclear units affording hydrophilic layers that grow in the *ac*-plane (see Figure 4). Additionally, weak offset π···π interactions between the hydrophobic dpo groups [3.35 Å being the mean distance between adjacent dpo groups] connect the dinuclear units belonging to adjacent hydrophilic layers leading to a three-dimensional network (see Figure 4).

Table 8. Relevant strong and weak hydrogen bonds for **2**[a,b]

D-H···A	D···A/Å	D-H···A	D···A/Å
O(1w)-H···O(3a)	2.757(5)	O(5w)-H···O(14d)	2.717(4)
O(1w)-H···O(14b)	2.863(5)	O(5w)-H···O(8w)	2.848(5)
O(2w)-H···O(3c)	2.781(5)	O(6w)-H···O(22f)	2.671(5)
O(2w)-H···O(14d)	2.863(5)	O(7w)-H···O(3)	2.905(5)
O(3w)-H···O(2)	2.793(4)	O(7w)-H···O(6wg)	3.030(5)
O(3w)-H···O(11c)	2.803(5)	O(8w)-H···O(2wc)	3.104(5)
O(4w)-H···O(13c)	2.580(4)	O(8w)-H···O(6wh)	2.963(5)
O(4w)-H···O(22e)	2.782(5)		

D-H···A	D···A/Å	H···A/Å	D-H···A/º
C(2)-H(1)···O(14b)	3.518(6)	2.612(4)	155.6(3)
C(2)-H(2)···O(7w)	3.573(6)	2.763(4)	141.4(3)
C(20)-H(20)···O(5w)	3.519(5)	2.739(3)	142.0(3)
C(21)-H(21)···O(22i)	3.264(5)	2.343(3)	170.2(3)
C(22)-H(22)···O(13d)	3.337(6)	2.433(4)	163.9(3)
C(23)-H(23)···O(7wf)	3.564(6)	2.663(5)	163.4(3)
C(26)-H(26)···O(13d)	3.613(6)	2.688(4)	173.0(3)
C(26)-H(26)···O(4wg)	3.374(5)	2.782(3)	122.5(3)
C(28)-H(28)···O(21g)	3.293(5)	2.377(3)	168.1(3)
C(28)-H(28)···O(4wg)	3.310(5)	2.669(3)	126.7(3)
C(29)-H(29)···O(4f)	3.291(6)	2.452(3)	150.2(3)

[a] Symmetry transformations: (a) *x*+1/2, -*y*+1/2, *z*+1/2; (b) *x*+1/2, -*y*+1/2, *z*-1/2; (c) *x*-1/2, -*y*+1/2, *z*+1/2 (d) *x*-1/2, -*y*+1/2, *z*-1/2; (e)-*x*+1, -*y*+1, -*z*+1; (f) -*x*+2, -*y*+1, -*z*+1; (g) *x*, *y*, *z*-1; (h) *x*-1, *y*, *z*; (i) *x*, *y*, *z*+1. [b] A = acceptor; D = donor.

Description of the structure of [Co(mal)(phen)(H_2O)]·2H_2O (3)

The structure of **3** consists of malonate-bridged cobalt(II) zigzag chains and crystallisation water molecules (see Figure 7a). The chains are interlinked through hydrogen bonds (involving malonate-oxygen atoms and solvent water molecules) and weak C-H···π and π···π interactions leading to a three-dimensional network (see Figure 7b).

Each cobalt atom is six-coordinated (see Figure 8). Three oxygen atoms from two different malonate ligands [2.084(2) Å for the mean Co-O(mal) bond distance], a water molecule and two phenantroline nitrogens [2.123(3) for the mean Co-N(phen)] build a distorted octahedral environment around the metal ions with geometric values s/h = 1.23 and θ = 54.8º [Stiefel E.I. *et al.*, 1972].

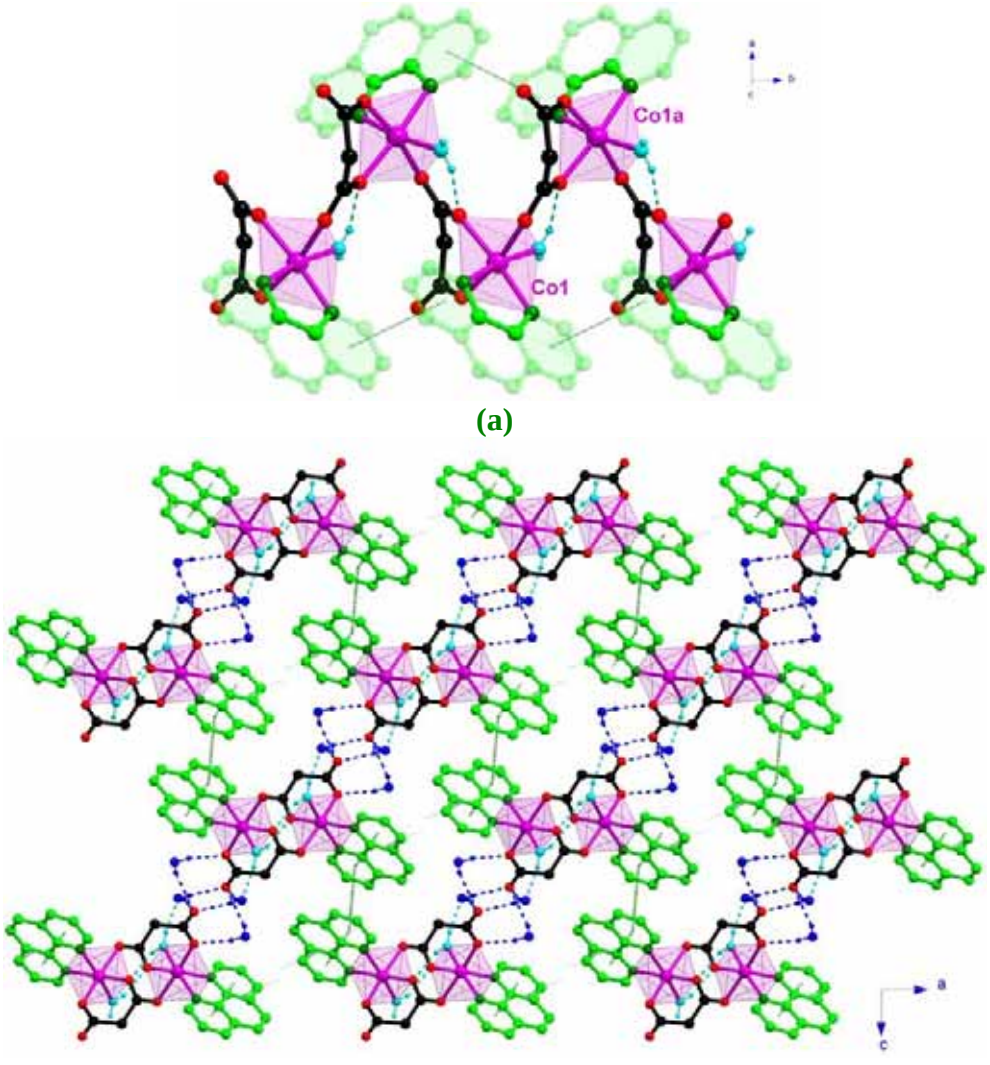

(a)

(b)

Figure 7. Perspective view of the malonate-bridged cobalt(II) chains growing parallel to the *b*-axis **(a)** and the crystal packing of these chains in the *bc*-plane **(b)**. Hydrogen bonds are drawn as broken lines whereas the weak π···π and C-H···π interactions are represented by dotted lines.

Selected bond lengths and angles for compound **3** are listed in Table 9.

Table 9. Selected bond lengths (Å) and angles (º) for **3**[a]

Co(1)-O(1)	2.066(2)	Co(1)-O(2)	2.070(2)
Co(1)-N(11)	2.121(3)	Co(1)-N(12)	2.124(2)
Co(1)-O(1w)	2.077(3)	Co(1)-O(3a)	2.117(2)

O(1)-Co(1)-O(2)	85.61(9)	N(11)-Co(1)-N(12)	78.13(10)
O(1)-Co(1)-N(11)	95.84(10)	O(2)-Co(1)-N(11)	89.29(9)
O(1)-Co(1)-N(12)	173.50(10)	O(2)-Co(1)-N(12)	91.83(9)
O(1w)-Co(1)-O(1)	93.85(11)	O(1w)-Co(1)-O(2)	93.20(12)
O(1w)-Co(1)-N(11)	170.15(11)	O(1w)-Co(1)-N(12)	92.26(11)
O(3a)-Co(1)-O(1)	85.38(9)	O(3a)-Co(1)-O(2)	169.94(9)
O(3a)-Co(1)-N(11)	87.16(9)	O(3a)-Co(1)-N(12)	96.64(9)
O(1w)-Co(1)-O(3a)	91.88(12)		

[a] Symmetry code: (a) -*x*+3/2, *y*+1/2, -*z*+1/2

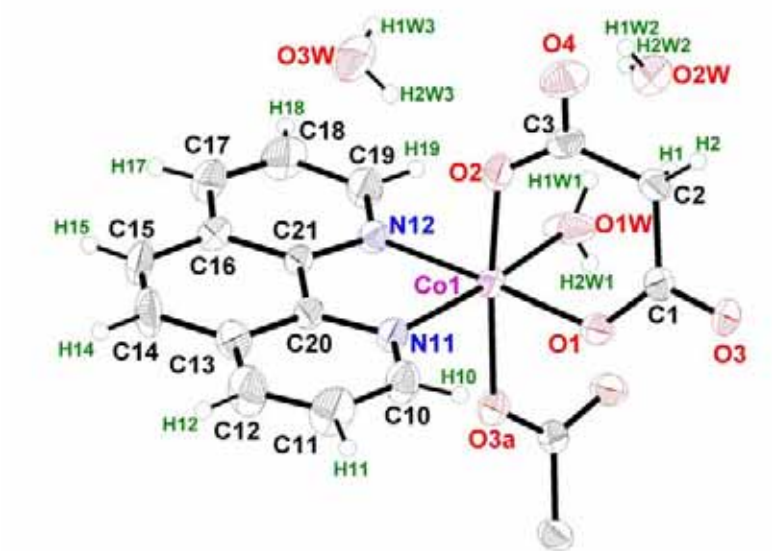

Figure 8. Perspective view of the metal environment in **3** with the numbering scheme. Thermal ellipsoids are drawn at the 50% probability level.

The malonate ligand adopts simultaneously bidentate [through O(1) and O(2) towards Co(1); 85.61(9)º is the bite angle] and monodentate [through O(3) towards Co(1b)] coordination modes (see Figure 9). It forms a six-membered ring, including the metal atom, that exhibits a boat conformation [$\theta = 93.6(3)$ and $\phi = 125.7(3)$] [Cremer D. *et al.*, 1975]. The O(1)-C(1)-O(3) carboxylate group links two sites from two adjacent cobalt environments exhibiting an *anti-syn* configuration. The bond lengths and angles of the malonate ligand (see Table 10) are in good agreement with those reported for other malonate-containing cobalt(II) complexes.

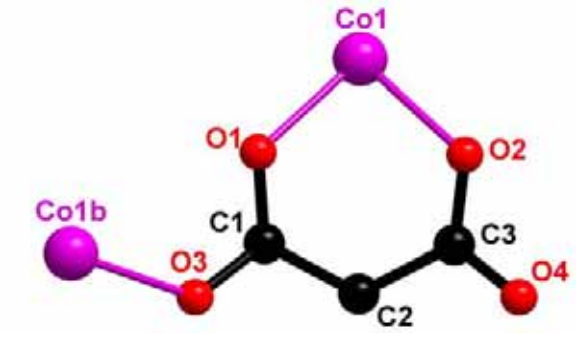

Figure 9. Coordination mode for the malonate ligand in **3**.

Table 10. Bond lengths (Å) and angles (º) for the malonate ligand present in **3**[a]

C(1)-C(2)	1.510(5)	C(2)-C(3)	1.520(5)
C(1)-O(1)	1.256(4)	C(3)-O(2)	1.262(4)
C(1)-O(3)	1.259(4)	C(3)-O(4)	1.249(4)
O(1)···O(2)	2.811(3)	O(3)···O(4)	4.401(3)
O(1)-C(1)-O(3)	123.8(3)	O(2)-C(3)-O(4)	123.8(3)
O(1)-C(1)-C(2)	119.6(3)	O(2)-C(3)-C(2)	118.8(3)
O(3)-C(1)-C(2)	116.6(3)	O(4)-C(3)-C(2)	117.4(3)
C(1)-C(2)-C(3)	116.7(3)		
C(1)-O(1)-Co(1)	127.1(2)	C(3)-O(2)-Co(1)	127.3(2)
C(1)-O(3)-Co(1b)	126.6(2)		

[a] Symmetry code: (b) -*x*+3/2, *y*-1/2, -*z*+1/2.

The phenantroline is coordinated to the cobalt atom as a bidentate ligand with a bite angle of 78.13(10)º. As commented in the Chapter IV this value is far from the ideal value of 90º due to the constrained geometry of the phenantroline ligand [Castillo O. *et al.*, 2001; MacCann M. *et al.*, 1997]. The phenantroline ligand as a whole is planar [the maximum deviation from the ligand mean plane being 0.038(4) Å for C(17)]. Selected bond lengths and angles for the phenantroline ligand in **3** are reported in Table 11.

Table 11. Selected bond lengths (Å) and angles (º) for the phen ligand in **3**

C(10)-C(11)	1.381(5)	C(19)-C(18)	1.388(5)
C(11)-C(12)	1.366(5)	C(18)-C(17)	1.353(5)
C(12)-C(13)	1.394(5)	C(17)-C(16)	1.400(5)
C(13)-C(20)	1.398(4)	C(16)-C(21)	1.397(4)
C(20)-N(11)	1.359(4)	C(21)-N(12)	1.359(4)
N(11)-C(10)	1.319(4)	N(12)-C(19)	1.325(4)
C(13)-C(14)	1.429(5)	C(16)-C(15)	1.428(5)
C(14)-C(15)	1.330(5)	C(20)-C(21)	1.436(4)
C(10)-N(11)-C(20)	117.7(3)	C(19)-N(12)-C(21)	117.5(3)
C(11)-C(10)-N(11)	122.7(4)	C(18)-C(19)-N(12)	123.0(4)
C(12)-C(11)-C(10)	120.0(4)	C(17)-C(18)-C(19)	119.7(4)
C(13)-C(12)-C(11)	119.4(4)	C(16)-C(17)-C(18)	119.4(4)
C(20)-C(13)-C(12)	116.9(3)	C(21)-C(16)-C(17)	117.5(3)
N(11)-C(20)-C(13)	123.3(3)	N(12)-C(21)-C(16)	122.9(3)
N(11)-C(20)-C(21)	117.1(3)	N(12)-C(21)-C(20)	117.2(3)
C(12)-C(13)-C(14)	124.3(4)	C(17)-C(16)-C(15)	124.0(4)
C(13)-C(14)-C(15)	121.4(4)	C(16)-C(15)-C(14)	121.7(4)
C(13)-C(20)-C(21)	119.6(3)	C(16)-C(21)-C(20)	120.0(3)
C(14)-C(13)-C(20)	118.8(3)	C(15)-C(16)-C(21)	118.5(3)
C(10)-N(11)-Co(1)	128.3(2)	C(19)-N(12)-Co(1)	128.7(2)
C(20)-N(11)-Co(1)	113.9(2)	C(21)-N(12)-Co(1)	113.7(2)

The [Co(mal)(phen)(H_2O)] units are held together by means of carboxylate-malonate bridges affording cobalt(II) chains which run along the *b*-axis (Figure 7a) [5.3482(10) Å being the Co···Co distance through the carboxylate bridge]. Hydrogen bonds (see Table 12) involving the coordinated water molecules and malonate oxygen atoms and weak face-to-face π···π interactions contribute to stabilise the structure (see broken lines and coloured pyridyl rings in Figure 7a). Additional hydrogen bonds involving malonate oxygen atoms and crystallisation water molecules, link adjacent chains leading to a two-dimensional network. Focusing on the hydrogen bonding, one can see (see Figure 10) the alternation of $R_4^2(8)$ and $R_4^4(12)$ hydrogen motifs [Etter M.C., 1990] which share one edge (two malonate-oxygens). The shortest interchain cobalt···cobalt separations (see Figure 10) are 8.735(2) [Co(1)···Co(1c); (c) -*x*+1, -*y*, -*z*+1] and 9.576(2) Å [Co(1)···Co(1d); (d) -x+1, -y+1, -z+1].

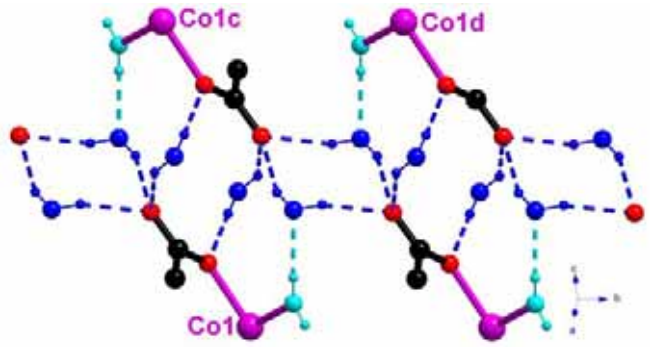

Figure 10. Partial view of the hydrogen bonding in **3**. The phenantroline and some malonate atoms have been omitted for the sake of clarity.

Finally, weak offset π···π and C-H···π interactions (see dotted lines in Figure 7b) between layers contribute to stabilise the crystal structure and they lead to a three-dimensional network.

Table 12. Relevant strong and weak hydrogen bonds for **3**[a]

D-H···A	D···A/Å	H···A/Å	D-H···A/º
O(1w)-H(1w1)···O(2wc)	2.694(5)	1.91(4)	169(4)
O(1w)-H(2w1)···O(1a)	2.648(4)	1.98(4)	151(4)
O(2w)-H(1w2)···O(4d)	2.860(4)	2.09(5)	158(5)
O(2w)-H(2w2)···O(4)	2.779(4)	2.00(5)	163(5)
O(3w)-H(1w3)···O(4e)	3.021(4)	2.33(6)	140(5)
O(3w)-H(2w3)···O(2)	2.814(4)	2.03(6)	170(5)
C(15)-H(15)···O(3wf)	3.490(6)	2.74(3)	149(3)
C(17)-H(17)···O(3wf)	3.350(6)	2.54(4)	154(3)

[a] Symmetry transformations: (a) -*x*+3/2, *y*+1/2, -*z*+1/2; (c) *x*, *y*+1, *z*; (d) -*x*+1, -*y*-1, -*z*+1; (e) -*x*+1, -*y*, -*z*+1; (f) -*x*+1/2, *y*+1/2, -*z*+1/2. [b] A = acceptor; D = donor.

Description of the structure of [Co(mal)(3-cnpy)(H$_2$O)](4)

The structure of **4** consists of malonate-bridged cobalt(II) corrugated layers which are held together by means of C-H···π and weak C-H···N interactions affording a three-dimensional network (see Figure 11). The cobalt(II) layers are further stabilized by hydrogen bonds involving coordinated water molecules and malonate-oxygen atoms. Selected bond lengths and angles for compound **4** are reported in Table 13.

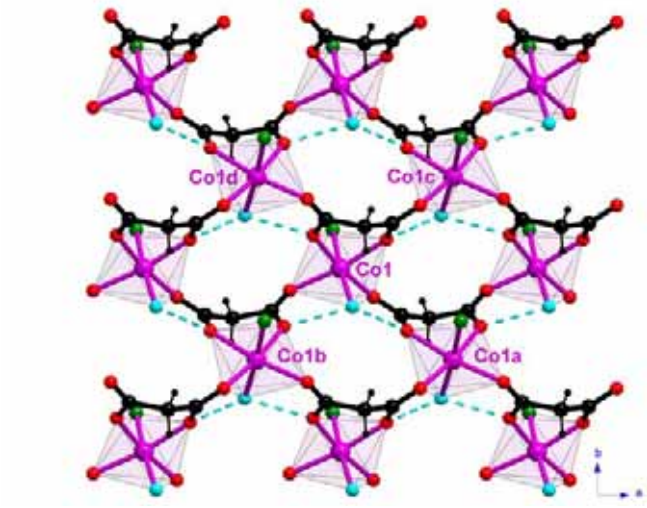

(a)

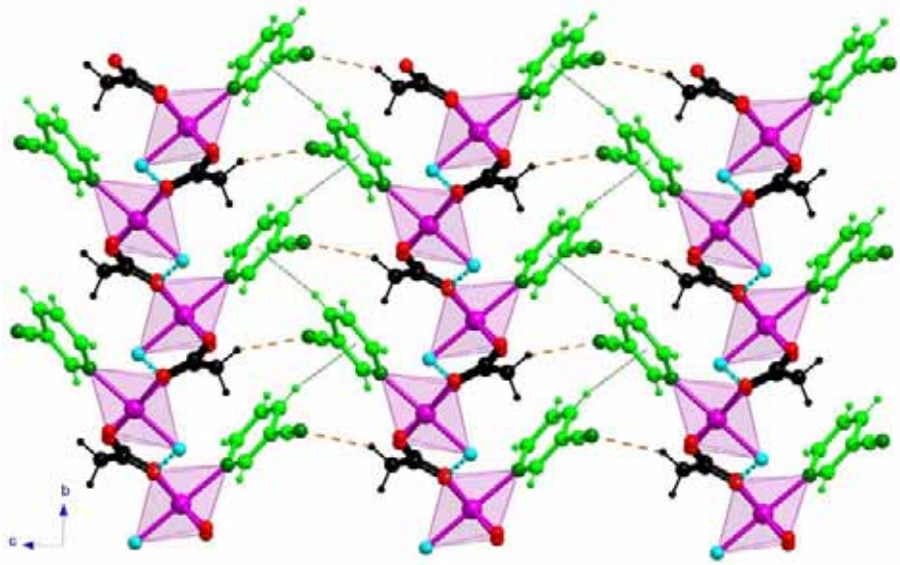

(b)

Figure 11. Perspective view of a fragment of the malonate-bridged cobalt(II) corrugated layer in **4** **(a)** and view of the stacking of these layers by means of π···π (green dotted lines) and weak C-H···π (orange broken lines) interactions **(b)**. Hydrogen bonds are represented by blue broken lines.

Each cobalt atom is six-coordinated and it exhibits a slightly distorted 4+2 octahedral environment (s/h = 1.25, ϕ = 58.25º) [Stiefel E.I. *et al.*, 1972] (Figure 12). Four carboxylate-oxygen atoms from three different malonate groups [2.078(3) Å being the average Co-M bond distance] build the equatorial plane around the metal atom. The

apical positions are filled by a water molecule and a nitrogen atom from the 3-cnpy ligand [2.157(3) Å and 2.184(3) Å for the Co-Ow and Co-N bond distance, respectively). The cobalt atom is shifted by 0.0386(4) Å from the mean equatorial plane towards O(1w).

Table 13. Selected bond lengths (Å) and angles (º) for **4**[a]

Co(1)-O(1)	2.082(3)	Co(1)-O(2)	2.070(3)
Co(1)-O(3a)	2.073(2)	Co(1)-O(4b)	2.085(3)
Co(1)-N(11)	2.184(3)	Co(1)-O(1w)	2.157(3)
O(1)-Co(1)-O(2)	85.76(10)	O(3a)-Co(1)-O(4b)	101.58(10)
O(1)-Co(1)-O(3a)	87.05(10)	O(2)-Co(1)-O(4b)	85.54(10)
O(1)-Co(1)-O(4b)	170.98(10)	O(2)-Co(1)-O(3a)	172.62(11)
N(11)-Co(1)-O(1)	88.17(11)	N(11)-Co(1)-O(2)	91.58(11)
N(11)-Co(1)-O(3a)	86.55(11)	N(11)-Co(1)-O(4b)	89.73(11)
O(1w)-Co(1)-O(1)	88.85(10)	O(1w)-Co(1)-O(2)	91.56(10)
O(1w)-Co(1)-O(3a)	89.92(10)	O(1w)-Co(1)-O(4b)	93.73(10)
N(11)-Co(1)-O(1w)	175.49(11)		

[a] Symmetry code: (a) -*x*+1, *y*-1/2, -*z*+1; (b) -*x*, *y*-1/2, -*z*+1

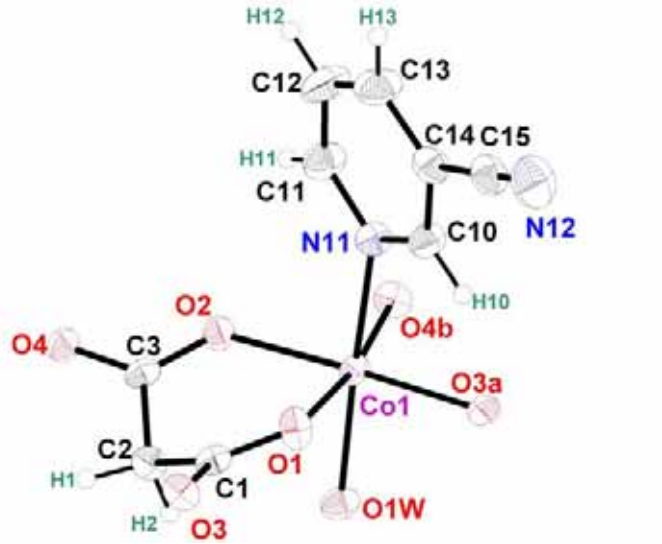

Figure 12. Perspective view of the asymmetric unit in **4** with the numbering scheme. Thermal ellipsoids are drawn at the 50% probability level.

The malonate group in **4** acts simultaneously as bidentate [through O(1) and O(2) towards Co(1), 85.76(10)º being the value of the angle subtended at the metal atom] and bis-monodentate [through O(3a) and O(4b) towards Co(1c) and Co(1d), respectively] ligand (Figure 13). The malonate group forms (including the cobalt atom) a six-membered ring that exhibits a boat conformation [$\theta = 90.8(3)$ and $\phi = 119.5(3)$º] [Cremer D. *et al.*, 1975]. Each carboxylate-malonate group connects two equatorial sites from adjacent cobalt atoms exhibiting the *anti-syn* conformation. The bond lengths and

angles for the malonate ligand (see Table 14) agree well with those of the previously reported malonate-containing cobalt(II) complexes [see references in the Introduction].

The 3-cnpy molecule acts as a monodentate ligand through N(11) towards Co(1). Its pyridyl ring is planar and the ligand as a whole does not deviate significantly from planarity. The 3-cnpy bond lengths and angles (see Table 15) agree well with those of the previously reported cobalt(II) 3-cnpy complexes [Sekine A. *et al.*, 1991; Arimoto Y. *et al.*, 2003] and the free ligand [Kubiak R. *et al.*, 2002].

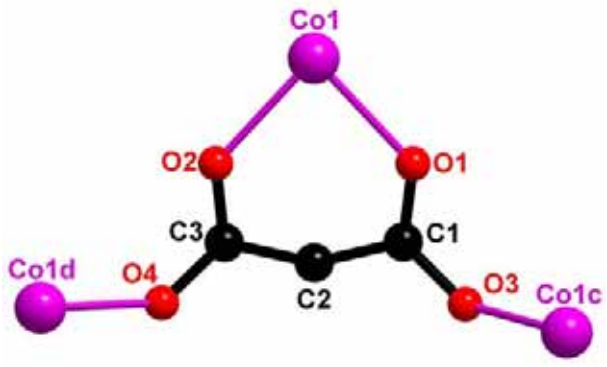

Figure 13. Coordination mode of the malonate ligand in **4**.

Table 14. Bond lengths (Å) and angles (º) for the malonate ligand in **4**[a]

C(1)-C(2)	1.511(5)	C(2)-C(3)	1.514(5)
C(1)-O(1)	1.265(4)	C(3)-O(2)	1.270(4)
C(1)-O(3)	1.257(4)	C(3)-O(4)	1.245(4)
O(1)···O(2)	2.825(4)	O(3)···O(4)	4.344(4)
O(1)-C(1)-O(3)	123.5(3)	O(2)-C(3)-O(4)	128.8(3)
O(1)-C(1)-C(2)	119.8(3)	O(2)-C(3)-C(2)	118.3(3)
O(3)-C(1)-C(2)	116.7(3)	O(4)-C(3)-C(2)	117.8(3)
C(1)-C(2)-C(3)	115.7(3)		
C(1)-O(1)-Co(1)	126.7(2)	C(3)-O(2)-Co(1)	128.1(2)
C(1)-O(3)-Co(1c)	128.9(2)	C(3)-O(4)-Co(1d)	127.6(2)

[a] Symmetry code: (c) -*x*+1, *y*+1/2, -*z*+1; (d) -*x*, *y*+1/2, -*z*+1.

Each cobalt atom is connected to other four ones through carboxylate-malonate bridges, affording thus, rectangular layers (Figure 11a). The metal ions are placed in two different planes, within each layer, whereas malonate ligands are located out of these metal planes (Figure 11a). The value of the dihedral angle between the equatorial plane of the metal ion and the O(1)-O(2)-C(1)-C(3) plane is 20.02(12)º. The shortest Co···Co intralayer distances are: 5.3876(6) [Co(1)···Co(1a) and Co(1)···Co(1c); (a) -*x*+1, *y*-1/2, -*z*+1; (b) -*x*, *y*-1/2, -*z*+1], 5.3135(7) [for, Co(1)···Co(1b) and Co(1)···Co(1d); (c) -*x*+1, *y*+1/2, -*z*+1; (d) -*x*, *y*+1/2, -*z*+1] (see Figure 11a). Within each layer, the dihedral

angle between equatorial planes of adjacent metal ions are 84.50(5)º. These corrugated layers are stabilised by means of hydrogen bonds involving water molecules and malonate-oxygen atoms.

Table 15. Selected bond lengths (Å) and angles (º) for the 3-CNpy ligand in **4**

N(11)-C(10)	1.333(5)	N(11)-C(11)	1.336(5)
C(10)-C(14)	1.396(5)	C(11)-C(12)	1.375(7)
C(14)-C(13)	1.376(6)	C(12)-C(13)	1.376(6)
C(14)-C(15)	1.443(6)	C(15)-N(12)	1.131(5)
N(11)-C(10)-C(14)	122.2(4)	N(11)-C(11)-C(12)	123.8(4)
C(10)-C(14)-C(13)	119.5(4)	C(11)-C(12)-C(13)	118.9(5)
C(10)-N(11)-C(11)	117.4(3)	C(12)-C(13)-C(14)	118.2(5)
C(10)-C(14)-C(15)	117.7(4)	C(13)-C(14)-C(15)	122.8(4)
C(14)-C(15)-N(12)	178.7(4)		
C(10)-N(11)-Co(1)	118.8(2)	C(11)-N(11)-Co(1)	123.2(3)

Finally, the malonate-bridged cobalt layers are connected through C-H···π interactions (Table 16) involving the pyridyl ring of the 3-cnpy ligand, giving thus a three-dimensional network where hydrophilic and hydrophobic layers stacked sequentially. Additionally, very weak C-H···N interactions (due to the long H···N distance, see Table 16) interactions contribute to stabilize the resulting three-dimensional structure.

Table 16. Relevant weak interactions in **4**.[a]

D-H···A	D···A/Å	H···A/Å	D-H···A/º
O(1w)-H···O(1f)	2.668(4)		
O(1w)-H···O(2b)	2.645(4)		
C(2)-H(1)···N(12e)	3.611(5)	2.748(4)	148.6(2)
C(10)-H(10)···O(3f)	2.938(4)	2.355(3)	120.5(3)
C(11)-H(11)···O(1wd)	3.604(6)	2.686(3)	169.3(3)
C(17)-H(17)···π	0.930(5)	3.272(3)	133.2(3)

[a] Symmetry transformations: (b) -*x*, *y*-1/2, -*z*+1; (d) -*x*, *y*+1/2, -*z*+1; (e) *x*, *y*, *z*+1; (f) -*x*+1, *y*-1/2, -*z*+1;. [b] A = acceptor; D = donor.

Description of the structure of {[Co(mal)(L)(H_2O)] [L = pym(5),pyz (6)]

Complexes **5** and **6** exhibit a three-dimensional network involving malonate-bridged cobalt(II) corrugated layers (see Figure 14) which are pillared by pyrimidine (pym) (**5**) or pyrazine (pyz) (**6**) ligands (Figure 15).

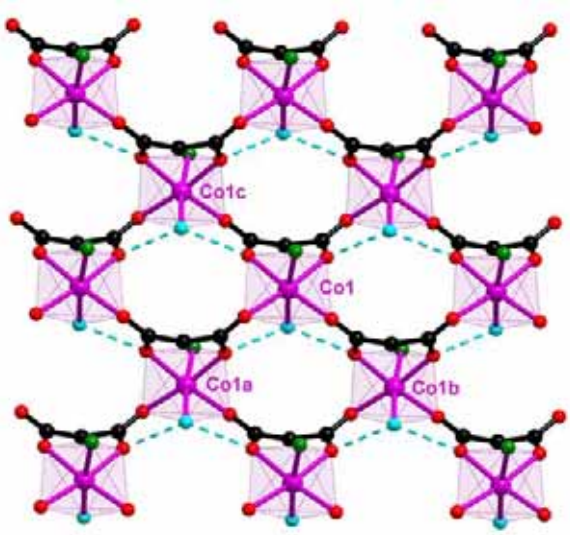

Figure 14. Perspective view of a fragment of the malonate-bridged layer of metal ions in compounds **5** and **6**. The green circle corresponds to the coordinated nitrogen atoms of the pym/pyz groups. Symmetry codes are reported in Table 17.

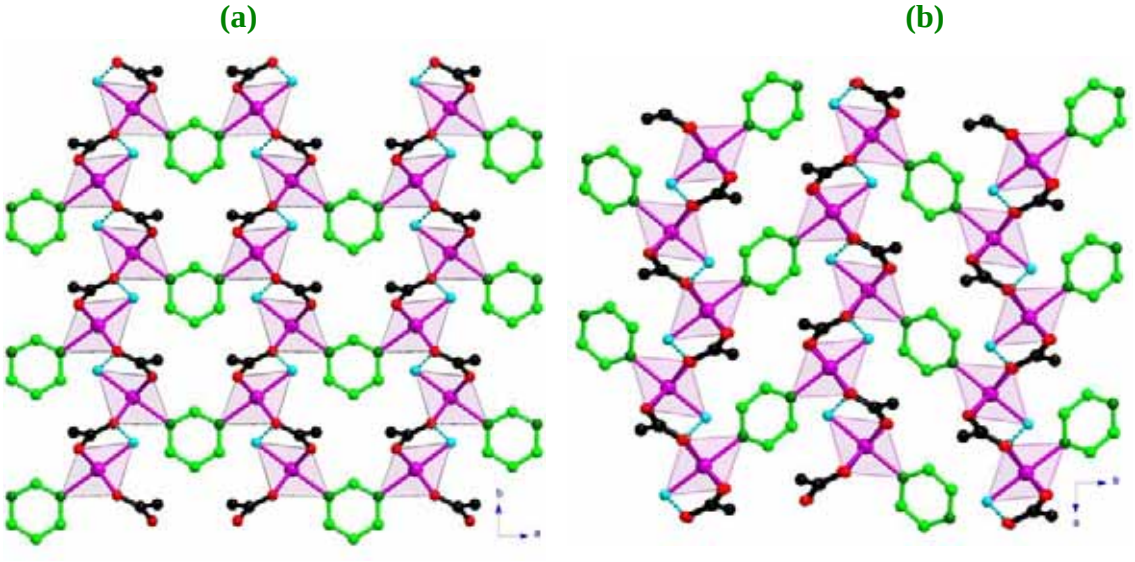

Figure 15. Projection of $[Co(mal)_2(L)(H_2O)]_n$ [L = pym **(5)** , pyz **(6)**] down the *c*-axis showing the malonate-bridged cobalt(II) parallel layers pillared by pym **(a)** and pyz **(b)** ligands.

Selected bond lengths and angles for compounds **5** and **6** are listed in Table 17.

Table 17. Selected bond lengths (Å) and angles (º) for compounds **5** and **6**[a]

Cobalt(II) pyrimidine complex (**5**)			
Co(1)-O(1)	2.080(6)	Co(1)-O(2)	2.091(6)
Co(1)-O(3b)	2.047(6)	Co(1)-O(4a)	2.052(6)
Co(1)-N(1)	2.200(6)	Co(1)-O(1w)	2.134(6)
O(1)-Co(1)-O(2)	84.7(2)	O(3b)-Co(1)-O(4a)	97.4(3)
O(1)-Co(1)-O(3b)	88.8(3)	O(2)-Co(1)-O(4a)	88.7(3)
O(1)-Co(1)-O(4a)	172.2(3)	O(2)-Co(1)-O(3b)	172.5(3)
N(1)-Co(1)-O(1)	90.3(3)	O(1w)-Co(1)-O(1)	90.4(3)
N(1)-Co(1)-O(1)	91.2(3)	O(1w)-Co(1)-O(2)	90.5(3)
N(1)-Co(1)-O(3b)	85.0(2)	O(1w)-Co(1)-O(3b)	93.4(3)
N(1)-Co(1)-O(4a)	85.6(2)	O(1w)-Co(1)-O(4a)	93.9(2)
N(1)-Co(1)-O(1w)	173.89(9)		

[a] Symmetry code: (a) -*x*+1/2, *y*+1/2, -*z*; (b) -*x*+1/2, *y*+1/2, -*z*+1.

Cobalt(II) pyrazine complex (**6**)			
Co(1)-O(1)	2.061(2)	Co(1)-O(2)	2.068(2)
Co(1)-O(3b)	2.083(2)	Co(1)-O(4a)	2.062(2)
Co(1)-N(1)	2.212(2)	Co(1)-O(1w)	2.170(2)
O(1)-Co(1)-O(2)	85.84(8)	O3b-Co1-O4a	97.51(9)
O(1)-Co(1)-O(3b)	172.84(8)	O2-Co1-O4a	174.42(9)
O(1)-Co(1)-O(4a)	89.15(8)	O2-Co1-O3b	87.39(8)
N(1)-Co(1)-O(1)	87.90(9)	O(1w)-Co(1)-O(1)	87.69(9)
N(1)-Co(1)-O(2)	92.34(9)	O(1w)-Co(1)-O(2)	91.56(9)
N(1)-Co(1)-O(3b)	90.06(9)	O(1w)-Co(1)-O(3b)	94.82(9)
N(1)-Co(1)-O(4a)	85.00(9)	O(1w)-Co(1)-O(4a)	90.70(9)
N(1)-Co(1)-O(1w)	173.89(9)		

[a] Symmetry code: (a) *x*-1/2, -*y*+1/2, *z*+1/2; (b) *x*-1/2, -*y*+1/2, *z*-1/2.

The divalent metal ions are six-coordinated (Figure 16) and they exhibit a slightly distorted octahedral environment [s/h = 1.255 and ϕ = 58.2º (**5**) and s/h =1.262 and ϕ = 57.8º (**6**)] [Stiefel E.I. *et al.*, 1972]. Four coplanar oxygen atoms from three different malonate ligands build the equatorial plane of the metal ion, whereas apical positions are filled by a water molecule and a nitrogen atom from a pym (**5**) or a pyz (**5**) ligand. The metal ion is shifted by 0.0769(10) (**5**) 0.0455(3) Å (**6**) from the mean equatorial plane towards O(1w). The values of the average Co-O bond distance in the equatorial plane is 2.068(6) and 2.069(2) Å for compounds **5** and **6** respectively, in good agreement within the range observed in the previous reported malonate-containing cobalt(II) complexes.

The Co-N(pym) and Co-N(pyz) distances also agree well with those reported for other pym- [Lloret F. *et al.*, 1998; Nakayama K. *et al.*, 1998; Hashizume D. *et al.*, 1999;

Kusaka T. *et al.*, 2000; Doi Y. *et al.*, 2002; Takagami N. *et al.*, 2004a and 2004b] and pyz- [Carreck P.W. *et al.*, 1971; Kubel F. *et al.*, 1981; Jung O.-S. *et al.*, 1994; Fetzer Th. *et al.*, 1994; Gairing C. *et al.*, 1996; Lu J. *et al.*, 1997; Groeneman R.H. *et al.*, 1998; Jensen P. *et al.*, 2001; Ma B.Q. *et al.*, 2001; Zheng L.-M. *et al.*, 2001; James M., 2002; Kumagai H. *et al.*, 2002; Dreos R. *et al.*, 2003; Nather C. *et al.*, 2003; Yang S.-Y. *et al.*, 2003; Chang W.-K. *et al.*, 2004; Xie L. *et al.*, 2004; Zhang K.-L. *et al.*, 2004; Holman K.T. *et al.*, 2005; Zhang J. *et al.*, 2005] bridged cobalt(II) complexes.

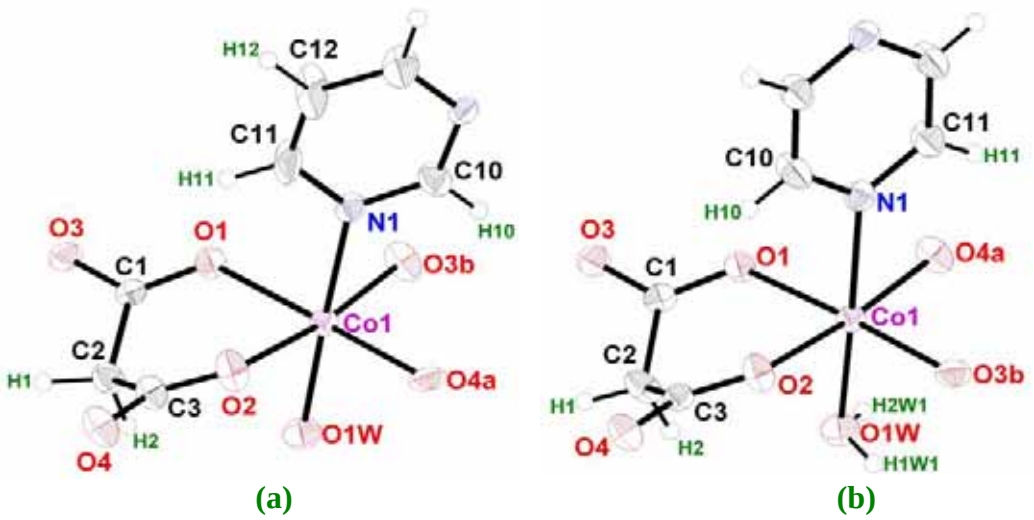

Figure 16. Perspective view of the metal environment in compounds **5** **(a)** and **6** **(b)** with the numbering scheme. Thermal ellipsoids are drawn at the 50% probability level.

Each malonate group acts simultaneously as bis-monodentate [through O(3) and O(4) towards Co(1c) and Co(1d), respectively; see symmetry codes in Table 17] and bidentate [through O(1) and O(2) towards Co(1)] ligand (see Figure 17). Malonate ion exhibits a boat conformation [the geometric values being θ= 82.7(7)º and ϕ= -0.4(8)º for compound **5** and θ = 87.2(2) and ϕ = -2.4(2)º for **6**] [Cremer *et al.*, 1975]. The bridging carboxylate groups of the malonate ion exhibit the *anti-syn* conformation. The bond lengths and angles of the malonate ligand (Table 17) agree with those of previously reported malonate-containing cobalt(II) complexes.

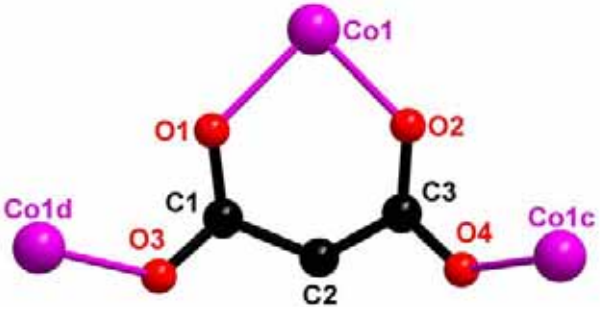

Figure 17. Coordination mode for the malonate ligand in **5** and **6**. Symmetry codes are reported in Table 17.

Table 17. Bond lengths (Å) and angles (º) for the malonate ligands present in **5** and **6**[a]

Compound **5**			
C(1)-C(2)	1.528(10)	C(2)-C(3)	1.526(10)
C(1)-O(1)	1.257(9)	C(3)-O(2)	1.250(9)
C(1)-O(3)	1.255(9)	C(3)-O(4)	1.252(9)
O(1)···O(2)	2.810(10)	O(3)···O(4)	4.399(10)
O(1)-C(1)-O(3)	123.9(7)	O(2)-C(3)-O(4)	124.6(7)
O(1)-C(1)-C(2)	121.1(6)	O(2)-C(3)-C(2)	120.3(6)
O(3)-C(1)-C(2)	115.0(6)	O(4)-C(3)-C(2)	115.1(6)
C(1)-C(2)-C(3)	115.7(6)		
C(1)-O(1)-Co(1)	126.1(5)	C(3)-O(2)-Co(1)	126.8(5)
C(1)-O(3)-Co(1d)	126.8(5)	C(3)-O(4)-Co(1c)	127.4(5)

[a] Symmetry code: (c) -*x*+1/2, *y*-1/2, -*z*; (d) -*x*+1/2, *y*-1/2, -*z*+1.

Compound **6**			
C(1)-C(2)	1.517(4)	C(2)-C(3)	1.517(4)
C(1)-O(1)	1.265(3)	C(3)-O(2)	1.261(3)
C(1)-O(3)	1.253(3)	C(3)-O(4)	1.247(3)
O(1)···O(2)	2.813(3)	O(3)···O(4)	4.325(3)
O(1)-C(1)-O(3)	124.0(3)	O(2)-C(3)-O(4)	124.2(2)
O(1)-C(1)-C(2)	118.5(2)	O(2)-C(3)-C(2)	120.1(2)
O(3)-C(1)-C(2)	117.5(3)	O(4)-C(3)-C(2)	115.7(2)
C(1)-C(2)-C(3)	115.1(2)		
C(1)-O(1)-Co(1)	127.2(2)	C(3)-O(2)-Co(1)	125.8(2)
C(1)-O(3)-Co(1d)	125.4(2)	C(3)-O(4)-Co(1c)	131.6(2)

[a] Symmetry code: (c) *x*+1/2, -*y*+1/2, *z*-1/2; (d) *x*+1/2, -*y*+1/2, *z*+1/2.

The pyrimidine ring for compound **5** lies on a crystallographic two-fold axis whereas the pyrazine ring for compound **6** lies about an inversion centre. In both cases the heterocyclic nitrogen donors act as a bis-monodentate ligands [through N(11) and N(12) towards two symmetrically related cobalt atoms]. The bond lengths and angles pym and pyz agree (reported in Table 18) with those of the previously reported pym- and pyz- bridged cobalt(II) complexes.

Table 18. Bond lengths (Å) and angles (º) for the pym and pyz ligands from **5** and **6**[a]

Pym ligand			
N(1)-C(10)	1.324(9)	N(1)-C(11)	1.335(11)
C(11)-C(12)	1.358(12)		
C(10)-N(1)-C(11)	116.9(9)	N(1)-C(11)-C(12)	120.5(9)

N(1)-C(10)-N(1e)	125.7(13)	C(11)-C(12)-C(11e)	119.4(12)
C(10)-N(1)-Co(1)	117.2(7)	C(11)-N(1)-Co(1)	125.8(6)

[a] Symmetry code: (e) -*x*+1, *y*, -*z*+1.

Pyz ligand

N(1)-C(10)	1.334(4)	N(1)-C(11)	1.332(4)
C(10)-C(11e)	1.380(4)		
C(10)-N(1)-C(11)	115.4(3)	N(1)-C(10)-C(11e)	122.3(3)
N(1)-C(11)-C(10e)	122.3(3)		
C(10)-N(1)-Co(1)	122.3(2)	C(11)-N(1)-Co(1)	122.1(1)

[a] Symmetry code: (e) -*x*+1, -*y*+1, -*z*+1.

Each cobalt atom is connected to four other ones by four carboxylate groups from three malonate ligands to form rectangular grids (Figure 14). The cobalt atoms are placed in two different planes, within each layer, whereas the malonate ligands are located out of these metal planes (Figure 15). The values of the dihedral angle between the equatorial plane of the metal ion and the O(1)-O(2)-C(1)-C(3) plane are 24.4(3) and 22.70(9)º for compounds **5** and **6**, respectively. The values of the shortest intralayer Co···Co distances are: 5.3491(14), 5.3568(15), 6.8884(16) and 7.4787(14) Å in **5** and 5.2721(15), 5.4424(14), 6.9610(11) and 7.4340(11) Å in **6**, for Co(1)···Co(1a), Co(1)···Co(1b), Co(1a)···Co(1c) and Co(1a)···Co(1b), respectively (see Figure 14). The value of the angle between equatorial planes of adjacent metal atoms, within each layer, are 79.01(15)º and 80.80(5)º for **5** and **6**, respectively.

The malonate-bridged cobalt(II) layers are further pillared by pym (**5**) and pyz (**6**) ligands affording a three-dimensional network. The shortest interlayer metal···metal distances are 5.9333(14) and 7.2229(11) Å for compounds **5** and **6**, respectively. These values are somewhat longer than those reported for structurally characterized pym- and pyz-bridged cobalt(II) complexes.

Magnetic Properties

The thermal dependence of the $\chi_M T$ products for compounds **1-4** [$\chi_M T$ being the susceptibility per cobalt(II) ion for **1**, **3** and **4** and per two cobalt(II) ions for **2**] are shown in Figures 18-21. The value of the $\chi_M T$ at the highest temperature measured is 2.63 (for **1**) and 2.92 $cm^3\ mol^{-1}\ K$ (for **3** and **4**), values which are greater than that expected for the spin-only one for a magnetically isolated ions with S = 3/2 (1.87 $cm^3\ mol^{-1}\ K$ with $g = 2$). Also for **2**, the value $\chi_M T$ at 250 K (6.02 $cm^3\ mol^{-1}\ K$) is greater than that expected for the spin-only (3.74 $cm^3\ mol^{-1}\ K$ with $g = 2$). This difference is due to the occurrence of an unquenched orbital contribution typical of the $^4T_{1g}$ ground state in six-coordinated cobalt(II) complexes [Carlin R.L., 1986; Mabbs F.E., 1973], as commented in the Chapter VI. Upon cooling $\chi_M T$ continuously decrease to reach a value of 1.49, 1.87, 2.18 and 1.44 $cm^3\ mol^{-1}\ K$ for compounds **1-4**, respectively. This behaviour can be due to the depopulation of the higher energy Kramers doublets and/or to antiferromagnetic interactions. The carboxylate group usually behaves as an antiferromagnetic coupler in carboxylate-bridged cobalt(II) complexes [Rueff J.M. *et al.*, 2001; Kumagai H. *et al.*, 2002; Lee E.W. *et al.*, 2002] the values of the exchange coupling (J) ranging from -3 to -1 cm^{-1}.

Let us focusing on the structures of compounds **1-4** in order to interpretate their magnetic behaviour. First, compound **1** consists of rectangular grids build up from *trans*-diaquabismalonatecobalt(II) and *trans*-diaquacadmium(II) units which are carboxylate-bridged (see Figure 1). These layers are further connected through an extensive network of hydrogen bonds. From a magnetic point of view, compound **1** could be consider as quasi-isolated cobalt(II) ions, bearing in mind that cadmium(II) is a diamagnetic ion. So, we have analysed its magnetic data through the halmiltonian of eq. (1) [Herrera J.M. *et al.*, 2003].

$$\mathbf{H} = -A\kappa\lambda\mathbf{LS} + \Delta[\mathbf{L}_z^2 - (1/3)L(L+1)] + \beta(-A\kappa\mathbf{L} + g_e\mathbf{S})H \qquad (1)$$

where spin-orbit coupling (first term), axial distortion (second term) and Zeeman interaction (last term) are considered. No analytical expression for the magnetic susceptibility as a function of A, κ, λ and Δ can be derived and the values of these parameters were determined by matrix diagonalization. Taking into account that a value of A = 3/2 is used in most of the studies with Co(II) where the weak crystal field is

involved (as in **1**) and in order to avoid the overparametrization, we introduced a fixed value of A of 1.5 in the fitting procedure. Best-fit parameters of the experimental data of **1** are: A = -1.5, κ = 0.81, λ = -159 cm^{-1}, Δ = 506 cm^{-1}, R = 1.93x10^{-4}. R is the agreement factor defined as $\Sigma[(\chi_M T)_{obs} - (\chi_M T)_{calc}]^2/\Sigma[(\chi_M T)_{obs}]^2$. Below 10 K, the experimental data lie down the theoretical ones (see Figure 18), indicating the occurence of weak antiferromagnetic intermolecular interactions.

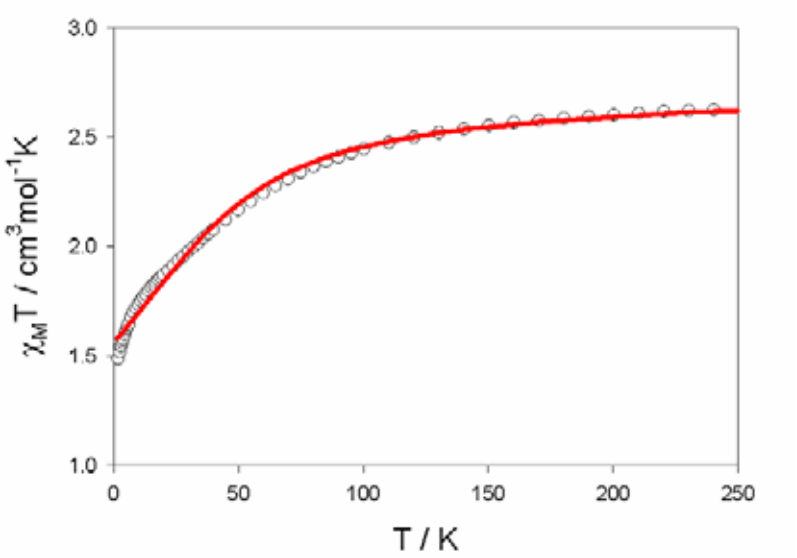

Figure 18. Thermal dependence of $\chi_M T$ product for compound **1**: (") experimental data, (C) best-fit curve (see text).

Structurally, compound **2** consists of dinuclear malonate-bridged cobalt(II) units which are further linked through hydrogen bonds and weak π···π (see Figure 4). As the extensive hydrogen bonding interactions present in both compounds are expected to not able to mediate any significant coupling, we try to analyse the magnetic behaviour of **2** considering it, as isolated cobalt(II) dimers.

We analize the magnetic data through the Hamiltonian of eq. (2):

$$\mathbf{H} = -(25/9)J\mathbf{S}_1\mathbf{S}_2 - A\kappa\lambda\mathbf{LS} + \Delta[\mathbf{L}_z^2 - (1/3)L(L+1)] + \beta(-A\kappa\mathbf{L} + g_e\mathbf{S})H \qquad (2)$$

where the first term takes into account the magnetic interaction between the dimmer considering that each ion has an effective spin S = ½. The value 25/9 is due to the use of the ½ effective spin approach ($S_{eff} = 5/3 \cdot S_{real}$). The other terms has the same meaning that in eq (1).

The best-fit parameters are: A = -1.5, κ = 0.94, λ = -143 cm^{-1}, Δ = -433 cm^{-1}, J = 0.0 (this result indicating the interaction between cobalt ions being negligible) and R =

$5.6x10^{-5}$ (see Figure 19). The magnetic coupling in **2** between the cobalt(II) atoms through the *anti-syn* carboxylate group is small enough to be detected magnetically.

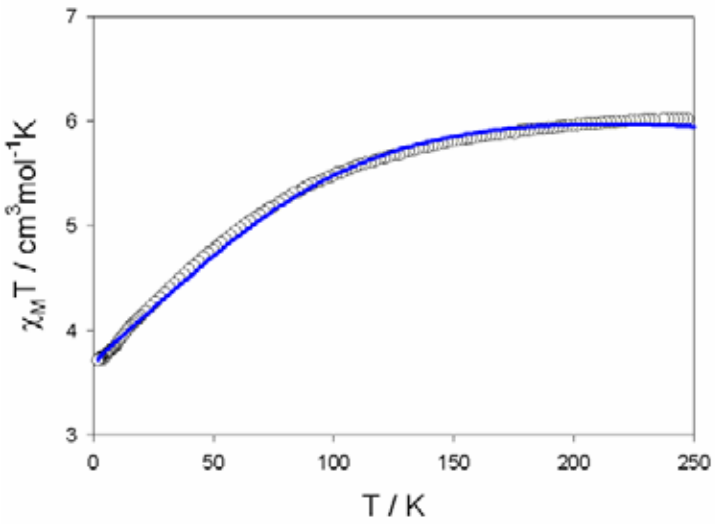

Figure 19. Thermal dependence of $\chi_M T$ product for compound **2**: (") experimental data, (C) best-fit curve (see text).

Compound **3** is made up of regular malonate-bridged cobalt(II) chains which are further held together by means of hydrogen bonds involving solvent molecules. Therefore, we analyse the magnetic data of **3** considering that we have chains of cobalt(II) ions. In order to do that we have used a numerical method developed by Prof. F. Lloret based on the Lines approach. An effective spin of $S_{eff} = 1/2$ is considered (a Kramers doublet is the fundamental state) and the excited states are taken into account by means of the introduction of a *g* factor which is temperature dependent. The *g* factor (see eq. 3) is calculated through the magnetic susceptibility derived from the eq. (1).

$$[g(T)]^2 = \frac{4k}{N\beta^2}\chi_M T \qquad (3)$$

The value of the g(T), calculated through eq. (3) is introduced in the equation of the magnetic susceptibility for a chain of magnetically coupling S=1/2. In this case, as the magnetic interaction was weak ferromagnetic, the expression derived by Baker, Rushbrooke and Gilbert was used [Kahn O., 1993].

The best-fit paramets being: $A = -1.5$, $\kappa = 0.97$, $\lambda = -167$ cm^{-1}, $\Delta = 930$ cm^{-1}, $J = +0.06$ cm^{-1} and $R = 5.3x10^{-5}$ (see Figure 20).

The value of the magnetic coupling reveals the occurrence of a weak ferromagnetic interaction within the chain. This fact causes the minimum in the $\chi_M T$ vs T curve observed at low temperatures (see Figure 20).

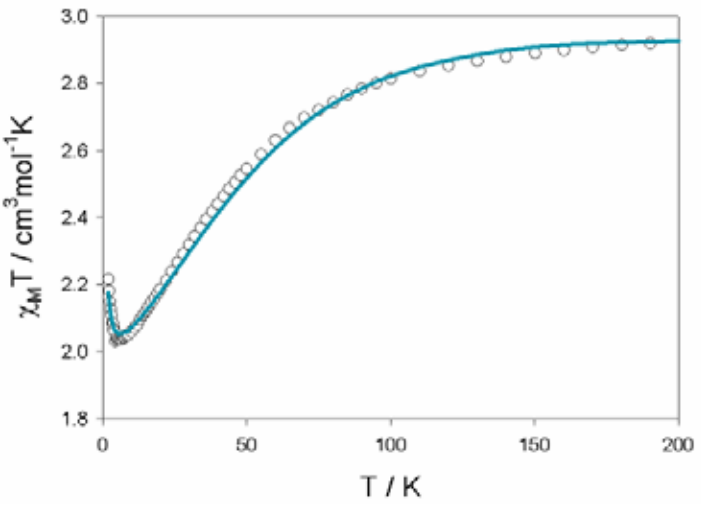

Figure 20. Thermal dependence of $\chi_M T$ product for compound **3**: (") experimental data, (C) best-fit curve (see text).

Finally, compound **4** consists of rectangular grids of malonate-bridged cobalt(II) ions which are linked through weak interactions (hydrogen bonds and C-H···π) which are not able to mediate significant magnetic interactions.

In order to analyse the magnetic data of **4**, we used the method described above in compound **3,** but using the expression derived by Lines for a square plane of S = ½ instead of the expression for a chain. The best-fit parameters are: A = -1.5, κ = 0.89, λ = -175 cm^{-1}, Δ = -717 cm^{-1}, J = -0.13 cm^{-1} and R = 6.4x10^{-5} (see Figure 21). The J value reveals the occurrence of a weak antiferromagnetic interaction.

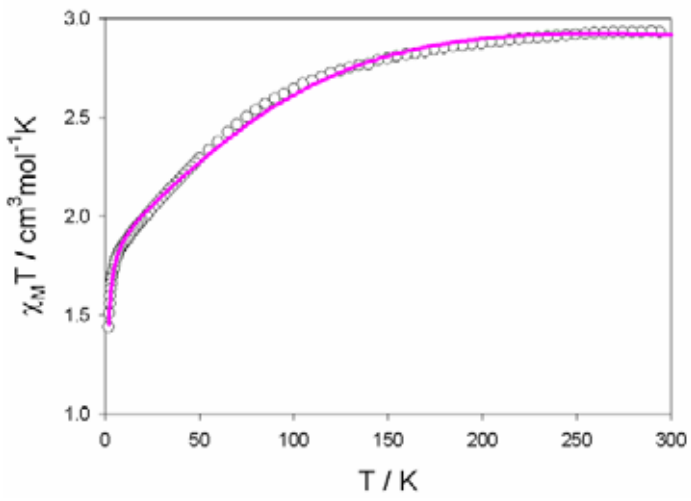

Figure 21. Thermal dependence of $\chi_M T$ product for compound **4**: (") experimental data, (C) best-fit curve (see text).

The calculated curve reproduces very well the experimental data in the measured temperature range for all compounds and the computed values are within the range of those reported for high spin cobalt(II) in the literature.

The temperature dependence of the $\chi_M T$ products per cobalt(II) ion for compounds **5** and **6** is shown in Figure 22. The inset shows the temperature dependence of the magnetic susceptibility in the low temperature range. The value of $\chi_M T$ regularly decrease from 3.35 at 300 K to 0.75 cm^3 mol^{-1} K at 1.8 K for **5** and from 3.55 at 300 K to 1.45 cm^3 mol^{-1} K at 1.8 K for **6**. Upon cooling, the magnetic susceptibility per mol of Co(II) ion for **5** continuously increases reaches a maximum value of 0.41 cm^3 mol^{-1} at 2 K and then decreases at lower temperatures.

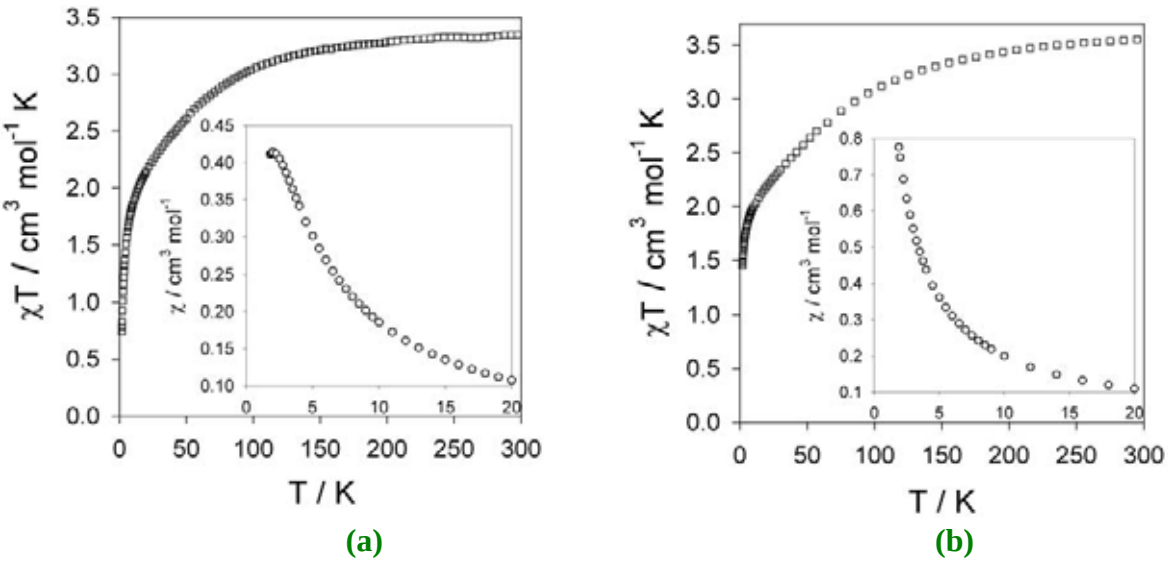

Figure 22. Thermal dependence of $\chi_M T$ product for compounds **5** **(a)** and **6** **(b)**. The inset shows the variation of the magnetic susceptibility (χ) at very low temperatures.

In the case of **6**, the magnetic susceptibility increases monotonically to reach a value of 0.80 cm^3 mol^{-1} at 1.80 K. The $1/\chi$ *versus* T plot shows a linear dependence with the temperature in the high temperature regime (T > 150 K) for both compounds, and the data follow well a the Curie-Weiss law giving C = 3.50 cm^3 mol^{-1} K and θ = -13.3 K for **5** and C = 3.86 cm^3 mol^{-1} K and θ = -24.3 K for **6**. The values of the Curie constants are slightly higher than those expected for six-coordinated high-spin Co(II) ions [Carling R.L., 1986] and the negative sign of the Weiss temperatures suggest the occurrence of overall antiferromagnetic exchange interactions, also supported by the values of χT at 2 K, smaller than those expected (1.8 cm^3 mol^{-1} K) for isolated Co(II) magnetic centres and by the maximum observed in χ for **5**. The effect of the spin-orbit

coupling contributes to the decay of the χT product, but it is not the only phenomenon occurring in **5** and **6**. Weak antiferromagnetic interactions through the carboxylate and/or through the pyrazine or pyrimidine ligands may also take place in **6** and are evident in **5**. The carboxylate and the pyrazine bridges have shown to play the role of antiferromagnetic couplers in cobalt(II) complexes, values of the exchange coupling constant ranging from -9 to -0.7 cm^{-1} (for pyrazine) [Ishida T. et *al.*, 2002; Liang Y.C. et *al.*, 2002] and from -3 to -1 cm^{-1} (through carboxylato) [Rueff J.M. et *al.*, 2001; Lee E.W. et *al.*, 2002; Kumagai H. et *al.*, 2002]. The pyrimidine has been observed to couple the cobalt(II) ions either ferro- [Lloret F. et *al.*, 1998] or antiferromagnetically [Nakayama K. et *al.*, 1998; Lloret F. et *al.*, 1998; Kusaka T. et *al.*, 2000; Doi Y. et *al.*, 2002; Ishida T. et *al.*, 2002], depending on the symmetry of the metal orbitals involved and on the σ or π character of the overlaps between the metal and the nitrogen orbitals [Rueff J.M. et *al.*, 2001]. In principle, the values of the exchange coupling constants through any of the bridges (carboxylate, pyrazine or pyrimidine) are of the same order of magnitude and none of them can be neglected. Thus, under a magnetic point of view compounds **5** and **6** should be considered as 3D arrays of antiferromagnetically coupled Co(II) ions exhibiting spin-orbit coupling. As there is no analytical expression for the magnetic susceptibility of this type of systems, a detailed analysis of the magnetic properties is precluded. Significant spin-orbit coupling and overall weak antiferromagnetic interaction in **5** and **6** are the two main conclusions in the light of their magnetic data

References

Addison A.W., Rao T.N., Reedijk J., Rijn J. and Verschoor G.C.J., *J. Chem. Soc., Dalton Trans.*, **1984**, 1349

Arimoto Y., Ohkoshi S., Zhong Z.J., Seino H., Mizobe Y. and Hashimo K. *J. Am.Chem. Soc.*, **2003**, 125, 9240.

Blake A.J., Brett M.T., Champness N.R., Khlobystov A.N., Long D.-L., Wilson C. And Schröder M. *Chem. Comm.*, **2001**, 2258

CAD4-EXPRESS, version 5.1/1.2, Enraf-Nonius, Delft, The Netherlands, **1994**.

Carling R.L., *Magnetochemistry*, Springer-Verlag, Berlin, Heidelberg, **1986**.

Carreck P.W., Goldstein M., McPartlin E.M. and Unsworth W.D. *J. Chem. Soc. D*, **1971**, 1634.

Castillo O., Luque A. and Román P. *J. Mol. Struct.*, **2001**, 570, 181.

Chang W.-K., Chiang R.-K., Jiang Y.-C., Wang S.-L., Lee S.-F. and Lii K.-H. *Inorg. Chem.*, **2004**, 43, 2564.

Coronado, E.; Drillon, M.; Nugteren, P. R.; de Jongh, L. J.; Beltran, D. *J. Am. Chem. Soc*. **1988**, *110*, 3907-3913.

Cremer D. and Pople J.A., *J. Am. Chem. Soc.*, **1975**, 97, 1354

DIAMOND 2.1d, Crystal Impact GbR, CRYSTAL IMPACT, K. Brandenburg & H. Putz GbR, Postfach 1251, D-53002 Bonn, Germany, 2000

De Munno, G.; Julve, M.; Lloret, F.; Faus, J.; Caneschi, A. *J. Chem.Soc., Dalton Trans.* **1994**, 1175-1183.

Doi Y., Ishida T. and Nogami T. Bull. *Chem. Soc. Jpn.*, **2002**, 75, 2455.

Dreos R., Nardin G., Randaccio L., Siega P. and Tauzher G. *Inorg. Chem.*, **2003**, 42, 612.

Duisenberg A.J.M., Kroon-Batenburg, L.M.J. and Schreurs, A.M.M. *J. Appl. Cryst.*, **2003,** 36, 220 (EVALCCD)

Earshaw A., *Introduction to Magnetochemistry*; Academic Press; London, **1968**.

Etter M.C., *Acc. Chem. Res.*, **1990**, 23 120.

Farrugia L.J. (*WINGX*), *J. Appl. Cryst*, **1999**, *32*, 837.

Fetzer Th., Jooss R., Lentz A. and Debaerdemaeker T. *Z. Anorg. Allg. Chem.*, **1994**, 620, 1750.

Figgis, B. N.; Hitchman, M. A. *Ligand Field Theory and its Application*; Wiley-VCH: New York, 2000.

Fujita M., Sasaki O., Mitsuhashi T. and Fujita T., *J. Chem. Soc., Chem.Comm.*, **1996**, 1535.

Gairing C., Lentz A., Grosse E., Haseidl M., and Walz L. *Z. Kristallogr.*, **1996**, 211, 804.

Groeneman R.H., MacGillivray and Atwood J.L. *Chem.Comm.*, **1998**, 2735.

Harms K., CAD4. Program for the Lp Correction of Nonius-CAD4-Diffractometer Data, University of Marburg, Germany, **1997**.

Hashizume D., Takayama R., Nakayama K., Ishida T., Nogami T., Yasui M. and Iwasaki *Acta Cryst., Sect. C*, **1999**, 55, 1793.

Henisch H.K., Crystal Growth in Gels, The Pennsylvania State, Univ.Press., Pittsburgh, **1970**.

Herrera J.M., Bleuzen A., Dromzée Y., Julve M., Lloret F. and Verdaguer M. *Inorg. Chem.*, **2003**, 42, 7052.

Hooft, R.W.W. *COLLECT*. Nonius BV, Delft, The Netherlands, **1999**

Holman K.T., Hammud H.H., Isber S. and Tabbal M. *Polyhedron*, **2005**, 24, 221.

Ishida T., Kawakami T., Mitsubori S., Nogami T., Yamaguchi K. and Iwamura H. *J. Chem. Soc., Dalton Trans.*, **2002**, 3177.

James M. *Aus. J. Chem.*, **2002**, 55, 219.

Jensen P., Batten S.R., Moubaraki B. and Murray K.S. *J Solid Sate Chem.*, **2001**, 159, 352.

Jung O.-K.and Pierpont C.G. *J. Am. Chem. Soc.*, **1994**, 116, 2229.

Kahn, O. *Molecular Magnetism*; VCH Publishers: New York, 1993.

Kondo M., Okubo T., Asami A., Noro S., Yoshitomi T., Kitagawa S., Ishii T., Matsuzaka H.and Seki K., *Ang. Chem., Int. Ed.*, 1999, **38**, 140.

Kubel F. and Strahle J. *Z. Naturforsch., B*, **1981**, 36, 441.

Kubiak R., Janczak J. and Sledz M. *J.Mol. Struct.*, **2002**, 610, 59.

Kumagai H., Oka Y., Inoue K. And Kurmoo M. *J. Chem. Soc., Dalton Trans.*, **2002**, 3442.

Kusaka T., Ishida T., Hashizune D., Iwasaki F. and Nogami T. *Chem. Lett.*, **2000**, 1146.

Lee E.W., Kim Y.J. and Jung D.K. *Inorg. Chem.*, **2002**, 41, 501.

Liang Y.C., Hong M.C., Liu J.C. and Cao R. *Inorg. Chim. Acta*, **2002**, 328, 152.

Lines, M. E. *J. Chem. Phys*. **1971**, *55*, 2977.

Lloret F., De Munno G., Julve M., Cano J., Ruiz R. and Caneschi A. *Angew. Chem., Int. Ed. Engl.*, **1998**, 37, 135.

Lu J., Paliwala T., Lim S.C., Yu C., Niu T. and Jacobson A.J. Inorg. Chem., **1997**, 36, 923.

Ma B.-Q., Gao S., Yi T. and Xu G.-X. Polyhedron, **2001**, 20, 1255.

Mabbs F.E. and Machin D.J. *Magnetism and Transition Metal Complexes*, Chapman and Hall Ltd., London, **1973**.

MacCann M., Casey M.T., Devereux M., Curran M. and McKee V. *Polyhedron*, **1997**, 16, 2741.

Mitchell I.V., *Pillared Layered Structures: Current Trends and Applications,* ed., Elsevier, London, **1990.**

Nardelli M. *J. Appl. Crystallogr.*, **1995**, 28, 659.

Nakayama K., Ishida T., Takayama R., Hashizume D., Yasui M., Iwasaki F. and Nogami T. *Chem. Lett.*, **1998**, 497.

Nakayama K., Ishida T., Takayama R., Hashizume D., Yasui M. And Iwasaki F. *Acta Cryst., Sect. C*, **1999**, 55, 1793.

Nather C., Greve J. and Jess I. *Z. Naturforsh., B*, **2003**, 58, 52

Nedelcu A., Žak Z., Madalan A.M., Pinkas J. and Andruh M *Polyhedron*, **2003**, 22, 789.

Thaimattam R., Reddy D.S., Xue F., Mak T.C.W., Nangia A. and Desiraju G.R. *J. Chem .Soc., Perkin Trans. 2*, **1998**, 1783.

Rueff J.M., Masciocchi N., Rabu P., Sironi A. and Skoulios A. *Eur. J. Inorg. Chem.*, **2001**, 2843.

SADABS, version 2.03. Bruker AXS Inc.: Madison, WI, **2000**.

Sakiyama, H.; Ito, R.; Kumagai, H.; Inoue, K.; Sakamoto, M.; Nishida, Y.; Yamasaki, M. *Eur. J. Inorg. Chem*. **2001**, 2027-2032.

Sekine A., Ohashi Y. and Hori K., *Acta Cryst., Sect. C*, **1991**, 47, 525.

Sheldrick, G.M. *SHELX97*, *Programs for Crystal Structure Anlysis (Release 97-2)*, Institüt für Anorganische Chemie der Universität, Tammanstrasse 4, D-3400 Göttingen, Germany, **1998**

Stiefel E. I., Brown G. F. *Inorg. Chem.*, **1972**, 11, 434

Takami N., Ishida T. and Nogami T. *Bull. Chem. Soc. Jpn.*, **2004**, 77, 1125.

Xie L., Wei Y., Wang Y., Hou H., Fan Y. and Zhu Y. *J. Mol. Struct.*, **2004**, 692, 201.

Yang S.-H., Long L.S., Huang R.-B., Zheng L.S. and Ng S.W., *Acta Cryst., Sect. E*, **2003**, 59, m841.

Zhang K.-L., Wang Z., Huang H., Zhu Y. and You X.-Z. *J. Mol. Struct.*, **2004**, 693, 193.

Zhang J., Li Z.-J., Cheng J.K., Kang Y., Qin Y.-Y. and Yao Y.-Y. *New J. Chem.*, **2005**, 29, 421.

Zheng L.-M., Wang X., Wang Y. and Jacobson A.J. *J. Mater. Chem.*, **2001**, 11, 1100.

CHAPTER IX.

New lanthanide malonate complexes: Ho(III), Sm(III) and Ce(III).

Introduction

Metal coordination polymers with one-, two- and three dimensional frameworks have been the subject of intensive research for several decades. Major advances have been made in their synthesis, theoretical description and in their applications as new materials [Desiraju G.R., 1995]. The chemistry of metal coordination polymers is among one of the most promising interfaces between synthetic chemistry and materials science. In this context, the field is important as it provides a foundation for the understanding of molecular organisation in the solid state. The structural design or modification of frameworks has become a very active field of crystal engineering. An example of the advance in this field is the generation of polymeric structures in metal complexes using di-carboxylate-ligands, which develop theoretical models of the exchange interaction in extended lattices [Robson R. *et al*., 1992]. Recent studies show that the flexibility of the molecular backbones, their conformational preferences, the metal ions employed and their counter ions, all have a profound influence on the polymeric structures obtained [Robson R. *et al*., 1992]. In our work we have used the malonate dianion (*i.e* the dianion of malonic acid, hereafter denoted mal) as a bridging ligand in metal complexes because of its ability to form extended networks. The structures formed — which depend on factors such as type of metal, the nature of the organic functionality of the ligand and reaction conditions — are mostly polymeric; either chains or two- and three-dimensional networks [Hernández-Molina M. *et al*., 2000; Ruiz-Pérez C. *et al*., 2000a, 2000b, 2000c and 2000d].

The expansion of research activity in the chemistry of malonic acid derivatives as ligands for lanthanide and transition metals, reflects the growing interest in their practical applications as fluorescence probes [Wang Z.-M. *et al*,. 2000] and molecular magnetic materials [Hernández-Molina M. *et al*., 2000] as well as precursors for oxides [Insausti M. *et al.* 1993; Gil De Muro I. *et al*., 1998 and 1999]. Therefore, studies of the new complexes of lanthanides with malonic acid are important both inherently and in their applications.

There are six isostructural series in the malonate-containing lanthanide complexes of general formula $[Ln_2(mal)_3(H_2O)_n]\cdot mH_2O$ and $[Ln(mal)_2]\cdot {}_pH_2O$ with Ln = lanthanide element, $n = 2$ ($m = 3$ and 4) and 5 ($m = 3$) and $p = 3$, 4 and 5, where the total number of water molecules and the oxidation state of the rare earth element are structure

determining factors [Hansson E, 1973a, 1973b and 1973c; WenMei X. *et al.* 1992; Hernández-Molina M. *et al.*, 2000; Wang Z.-M. *et al.*, 2000].

Experimental

Materials and methods

Malonic acid, sodium metalsilicate nonahydrate $Na_2SiO_3 \cdot 9H_2O$, holmium nitrate hexahydrate, samarium nitrate hexahydrate and cerium nitrate hexahydrate were purchased from commercial sources and used as received. Variable temperature (1.8-300 K) magnetic susceptibility measurements of crushed crystals of **1-3** were carried out in a Quantum Design SQUID magnetometer operating at 250 (**1**), 500 (**2**), 10000 (**3**) G (T < 20 K) and 10000 G (**1-3**) (T > 20 K). Diamagnetic corrections of all the constituent atoms were estimated from Pascal's constants as [Earshaw, 1968] -241 x 10^{-6} (**1**), -228 x 10^{-6} (**2** and **3**) cm^3mol^{-1}. Magnetic susceptibility data were also corrected for the magnetization of the sample holder. Elemental analyses (C, H, N) were performed on an EA 1108 CHNS-O microanalytical analyser.

Synthesis

$[Ho_2(mal)_3(H_2O)_5]\cdot 2H_2O$ (1). The formation of holmium malonate is accomplished by the reaction between malonic acid and europium nitrate in sodium metasilicate gels. The silica gel were prepared by hydrolysis and polycondensation of sodium metasilicate nonahydrate in water solution under acidic conditions [Henisch H.K., 1970]. Preparation involved primary mixing of proper amounts $Na_2SiO_3 \cdot 9H_2O$ 1M, and $C_3H_4O_4$ 2M, to adjust the pH value at the mixed solutions to about 4.5. The mixture run into test tubes, covered, and allowed to set for 24 hours at room temperature. 0.5 M solution of holmium nitrate hexahydrate was then added on top of the gel dropwise, so that the surface of the gel would not break, and the tubes were stored at 30ºC. Three weeks later, colourless crystals appeared suitable for X-ray analysis. They were removed from the gel, washed and dried at room temperature. (Found: C, 13.84; H, 2.62. Calc. for $C_9H_{20}Ho_2O_{19}$: C, 14.17, H, 2.32%).

$[Sm_2(mal)_3(H_2O)_6]$ (2). The formation of samarium malonate is accomplished by the same procedure used for **1** but replacing holmium nitrate by samarium nitrate. Colourless needle crystals, suitable for X-ray analysis, appeared within three weeks.

They were removed from the gel, washed and dried at room temperature. (Found: C, 15.11; H, 2.52. Calc. for $C_9H_{18}Sm_2O_{18}$: C, 15.05, H, 2.41%).

$[Ce_2(mal)_3(H_2O)_6]$ (3). The formation of cerium malonate is accomplished by the same procedure used for **1** but replacing the holmium nitrate by cerium nitrate. Colourless prism crystals suitable for X-ray analysis appeared within one month. They were removed from the gel, washed and dried at room temperature. (Found: C, 14.43; H, 2.89. Calc. for $C_9H_{22}Ce_2O_{20}$: C, 14.78, H, 3.01%).

Crystal data collection and refinement

Single crystals of three compounds were mounted on a Bruker-Nonius KappaCCD diffractometer. Orientation matrix and lattice parameters were obtained by least-squares refinement of the reflections obtained by a θ-χ scan (Dirax/lsq method). Diffraction data for all compounds were collected at 293(2) K using graphite-monochromated Mo-K_α radiation (λ = 0.71073 Å). Data collection and data reduction were done with the COLLECT [Hooft R.W.W., 1999] and EVALCCD [Duisenberg, A.J..M. *et al.*, 2003] programs. Empirical absorption corrections were carried out using SADABS [SADABS, version 2.03, 2003] for all compounds. The indexes of data collection were $-15 \le h \le 15$, $-10 \le k \le 10$, $-26 \le l \le 26$ for **1**; $-24 \le h \le 20$, $-15 \le k \le 17$, $-15 \le l \le 15$ for **2**; $-15 \le h \le 14$, $-17 \le k \le 17$, $-19 \le l \le 20$ for **3**. Of the 2418 (**1**), 2708 (**2**), 3051 (**3**) measured independent reflections in the θ range 3.20 – 27.51º (**1**), 2.23 – 39.99º (2), 2.78 – 30.07º (**3**), 2247 (**1**), 2366 (**2**), 2324 (**3**) have $I \ge 2\sigma(I)$. All the measured independent reflections were used in the analysis. All calculations for data reduction, structure solution, and refinement were done by standard procedures (WINGX) [Farrugia L.J., 1999]. The structure was solved by direct methods and refined with full-matrix least-squares technique on F^2 using the SHELXS-97 and SHELXL-97 programs [Sheldrick G.M., SHELX97, realease 97-2, 1998]. The malonate hydrogen atoms were set in calculated positions for compounds **1** and **3,** whereas for compound **2** they were found from difference Fourier maps. For all compounds hydrogen atoms were refined with isotropic temperature factors. The final Fourier-difference map showed maximum and minimum height peaks of 1.363 and -1.606 e $Å^{-3}$ (**1**), 1.147 and -2.334 e $Å^{-3}$ (**2**), 1.400 and -2.095 e $Å^{-3}$ (**3**). A summary of the crystallographic data and structure refinement is given in Table 1. The final geometrical calculations and the graphical

manipulations were carried out with PARST97 [Nardelli M., 1995] and DIAMOND [DIAMOND 2.1d, 2000] programs, respectively.

Table 1. Crystal data and details of structure determination for compounds **1-3**.

Compound	**1**	**2**	**3**
Formula	$C_9H_{20}Ho_2O_{19}$	$C_9H_{18}Sm_2O_{18}$	$C_9H_{22}Ce_2O_{20}$
M	762.11	714.93	730.51
Crystal system	orthorhombic	monoclinic	orthorhombic
Space group	*Pnma*	*C*2/*c*	*Pbcn*
a, Å	12.0794(12)	17.120(2)	11.3106(7)
b, Å	8.0555(9)	12.284(2)	12.6698(12)
c, Å	20.207(3)	11.144(2)	14.7397(15)
β, deg	-	127.549(13)	-
V, Å^3	1966.3 (4)	1861.3(5)	2112.2(3)
Z	4	4	4
T, K	293(2)	293(2)	293(2)
ρ_{calc} (Mg m^{-3})	2.574	2.551	2.297
F(000)	1440	1360	1408
λ (Mo-K$_\alpha$ Å)	0.71073	0.71073	0.71073
μ (MoK$_\alpha$) (mm^{-1})	8.083	6.339	4.349
Number parameters/restraints	151 / 0	144 / 0	142 / 0
Goodness of fit (*S*)	1.227	1.160	1.109
R1, $I > 2\sigma(I)$ (all)	0.0333 (0.0376)	0.0321 (0.0430)	0.0415 (0.0624)
wR2, $I > 2s(I)$ (all)	0.0814 (0.0831)	0.0797 (0.0897)	0.0926 (0.1024)
Max/min electron density (e/Å^3)	1.363 / -1.606	1.147 / -2.334	1.400 / -2.095
Measured reflections (R_{int})	50047 (0.0711)	8232(0.0525)	13060(0.0962)
Independent reflections [$I > 2\sigma(I)$]	2418 (2247)	2708 (2366)	3051 (2324)

Results and discussion

Description of the structure of $[Ho_2(mal)_3(H_2O)_5]\cdot 2H_2O$ (1)

The structure of **1** consists of malonate-bridged diaqua- and triaquaholmium(III) units that lead to a two-dimensional network (see Figure 1).

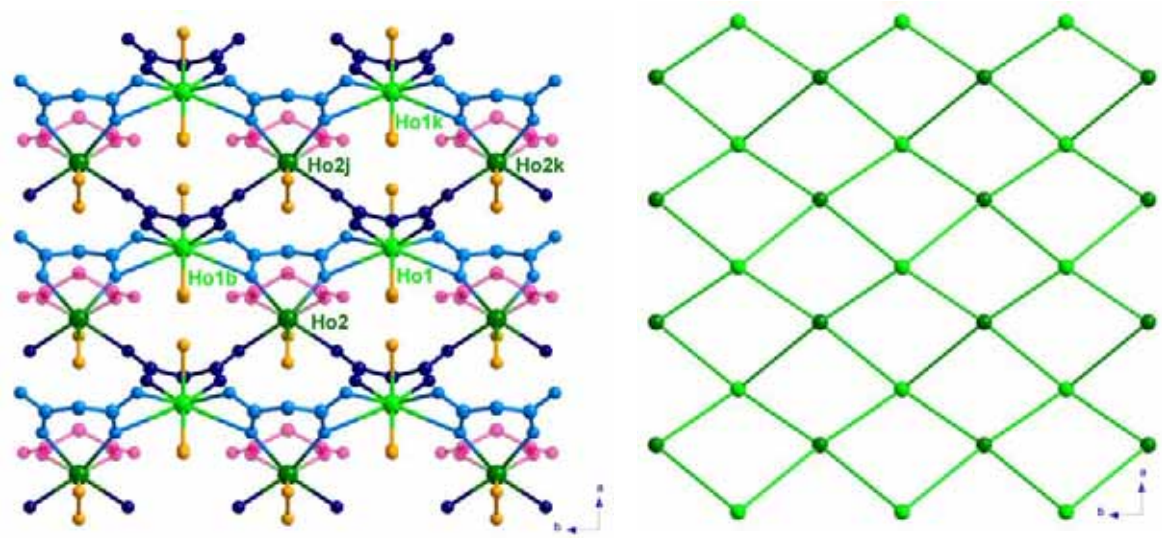

(a) **(b)**

Figure 1. Perspective **(a)** and schematic view **(b)**, along the *c*-axis of the malonate-bridged holmium(III) layers in **1**.

These malonate-bridged holmium(III) networks are further linked together by means of hydrogen bonds (Table 2) affording a three-dimensional structure (Figure 2).

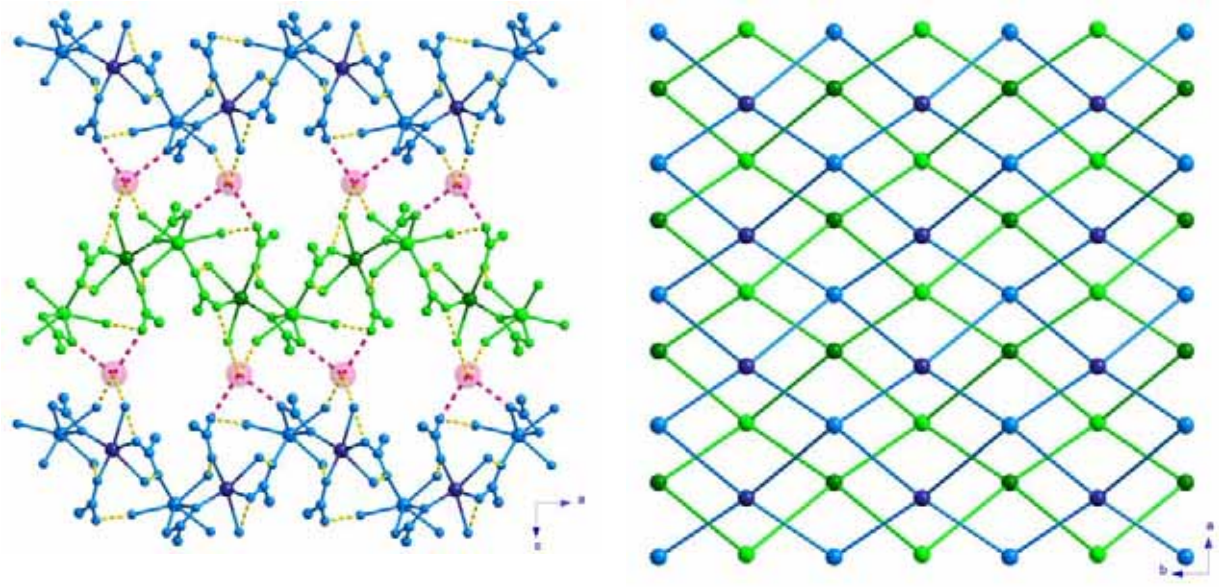

(a) **(b)**

Figure 2. Perspective view, along the *b*-axis (a) and schematic view slong the *c*-axis (b) of the stacking of the holmium(III) malonate layers in **1**.

Table 2. Selected bond lengths (Å) and angles (°) for **1**[a, b]

Holmium coordination sphere			
Ho(1)-O(1)	2.843(4)	Ho(1)-O(11)	2.307(4)
Ho(1)-O(2)	2.363(4)	Ho(1)-O(1w)	2.366(6)
Ho(1)-O(2w)	2.346(6)	Ho(1)-O(3w)	2.343(6)
O(1)-Ho(1)-O(2)	48.56(13)	O(2)-Ho(1)-O(1a)	136.48(13)
O(1)-Ho(1)-O(1a)	134.3(2)	O(2)-Ho(1)-O(2a)	97.6(2)
O(1)-Ho(1)-O(2a)	136.48(13)	O(2)-Ho(1)-O(11)	84.06(15)
O(1)-Ho(1)-O(11)	68.01(13)	O(2)-Ho(1)-O(11a)	145.36(15)
O(1)-Ho(1)-O(11a)	139.46(13)	O(2)-Ho(1)-O(1w)	76.41(15)
O(1)-Ho(1)-O(1w)	69.96(9)	O(2)-Ho(1)-O(2w)	71.2(2)
O(1)-Ho(1)-O(2w)	111.06(9)	O(2)-Ho(1)-O(3w)	124.00(12)
O(1)-Ho(1)-O(3w)	75.86(9)	O(2a)-Ho(1)-O(11)	145.36(15)
O(1a)-Ho(1)-O(2a)	48.56(13)	O(2a)-Ho(1)-O(11a)	84.06(15)
O(1a)-Ho(1)-O(11)	139.46(13)	O(2a)-Ho(1)-O(1w)	76.41(15)
O(1a)-Ho(1)-O(11a)	68.01(13)	O(2a)-Ho(1)-O(2w)	71.2(2)
O(1a)-Ho(1)-O(1w)	136.53(13)	O(2a)-Ho(1)-O(3w)	124.00(12)
O(1a)-Ho(1)-O(2w)	111.06(9)	O(11a)-Ho(1)-O(1w)	136.53(13)
O(1a)-Ho(1)-O(3w)	75.86(9)	O(11a)-Ho(1)-O(2w)	76.9(2)
O(11)-Ho(1)-O(11a)	76.0(2)	O(11a)-Ho(1)-O(3w)	80.6(2)
O(11)-Ho(1)-O(1w)	136.53(13)	O(1w)-Ho(1)-O(2w)	129.7(3)
O(11)-Ho(1)-O(2w)	76.9(2)	O(1w)-Ho(1)-O(3w)	79.0(2)
O(11)-Ho(1)-O(3w)	80.6(2)	O(2w)-Ho(1)-O(3w)	151.3(3)
Ho(2)-O(1)	2.377(4)	Ho(2)-O(12c)	2.318(4)
Ho(2)-O(21)	2.313(4)	Ho(2)-O(4w)	2.404(6)
Ho(2)-O(5w)	2.366(6)		
O(1)-Ho(2)-O(1b)	72.7(2)	O(1b)-Ho(2)-O(12c)	79.04(15)
O(1)-Ho(2)-O(12c)	141.12(14)	O(1b)-Ho(2)-O(12d)	141.12(14)
O(1)-Ho(2)-O(12d)	79.04(15)	O(1b)-Ho(2)-O(21)	115.43(15)
O(1)-Ho(2)-O(21)	72.74(14)	O(1b)-Ho(2)-O(21b)	72.74(14)
O(1)-Ho(2)-O(21b)	115.43(15)	O(1b)-Ho(2)-O(4w)	141.71(11)
O(1)-Ho(2)-O(4w)	141.71(11)	O(1b)-Ho(2)-O(5w)	77.9(2)
O(1)-Ho(2)-O(5w)	77.9(2)	O(12d)-Ho(2)-O(21)	79.5(2)
O(12c)-Ho(2)-O(12d)	109.7(2)	O(12d)-Ho(2)-O(21b)	145.17(15)
O(12c)-Ho(2)-O(21)	145.17(15)	O(12d)-Ho(2)-O(4w)	75.22(15)
O(12c)-Ho(2)-O(21b)	79.5(2)	O(12d)-Ho(2)-O(5w)	70.44(14)
O(12c)-Ho(2)-O(4w)	75.22(15)	O(21b)-Ho(2)-O(4w)	75.1(2)
O(12c)-Ho(2)-O(5w)	70.44(14)	O(21b)-Ho(2)-O(5w)	141.28(11)
O(21)-Ho(2)-O(21b)	75.6(2)	O(4w)-Ho(2)-O(5w)	118.1(3)
O(21)-Ho(2)-O(4w)	75.1(2)	O(21)-Ho(2)-O(5w)	141.28(11)

Hydrogen bonds[c]			
D-H···A	D···A/Å	D-H···A	D···A/Å
O(1w)-H···O(6wf)	2.755(9)	O(4w)-H···O(11c)	2.740(5)
O(1w)-H···O(6wg)	2.755(9)	O(4w)-H···O(11d)	2.740(5)
O(2w)-H···O(22h)	2.691(7)	O(5w)-H···O(6wi)	2.790(8)
O(2w)-H···O(22e)	2.691(7)	O(5w)-H···O(6wj)	2.790(8)
O(3w)-H···O(21)	2.771(5)	O(6w)-H···O(2)	2.842(9)
O(3w)-H···O(21a)	2.771(5)	O(6w)-H···O(22h)	2.796(9)

[a] Symmetry codes: (a) *x*, -*y*-1/2, *z*; (b) *x*, -*y*+1/2, *z*; (c) *x*-1/2, -*y*+1/2, -*z*-1/2; (d) *x*-1/2, *y*, -*z*-1/2; (k) *x*+1/2, -*y*-1/2, -*z*-1/2; (f) –*x*+1, -*y*, -*z*+1; (g) –*x*+1, *y*-1/2, -*z*-1; (h) *x*+1/2, *y*, -*z*-1/2; (i) –*x* +1, -*y*, -*z*-1; (j) –*x*+1, *y*+1/2, -*z*-1. [b] A = acceptor; D = donor. [c] Symmetry operators apply to acceptor atoms

Two crystallographically independent holmium(III) which are nine- [Ho(1)] and eight- [Ho(2)] coordinated, occur in **1** (see Figure 3).

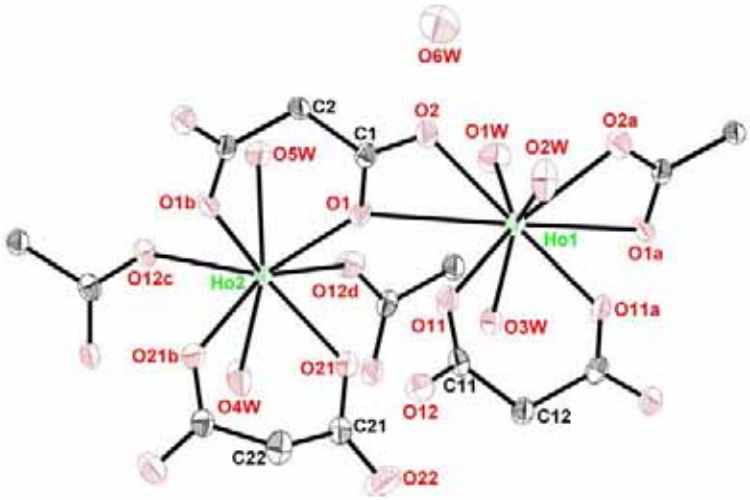

Figure 3. ORTEP view of the holmium environments in **1**. Thermal ellipsoids are drawn at 50% probability level.

They lie on a mirror plane. Six oxygen atoms from three different malonate groups [the Ho(1)-O(mal) bond distances being 2.307(4), 2.363(4) and 2.843(4)] and three water molecules [the Ho(1)-O(w) = 2.366(6), 2.343(6) and 2.346(6) Å] build a distorted tricapped trigonal prism around the Ho(1) atom (see Figure 4a). Ho(2) is bonded to six oxygen atoms from four different malonate groups [Ho(2)-O(mal) bond distances being 2.313(4), 2.318(4) and 2.377(4) Å] and two water molecules [Ho(2)-O(w) = 2.366(6) and 2.404(6) Å], forming thus, a distorted square antiprism (Figure 4b). Similar geometries have been observed in the isostructural related compound $[Eu_2(mal)_3(H_2O)_5]\cdot 3H_2O$ [Hansson, E., 1973b]. Two aspects concerning the holmium environment deserves to be noted: (i) a long bond between Ho(1) and the carboxylate-

malonate oxygen O(1) [2.843(4) Å] occurs, the O(1) atom being involved in the oxo bridge Ho(1)-O(1)-Ho(2); (ii) the mean values of the Ho-O(w) bond distance [2.358(6) Å] is longer than that of the Ho-O(mal) ones [2.336(4) Å, keeping out the longer Ho(1)-O(1) bond distance]. All coordinated water molecules lie on a mirror plane.

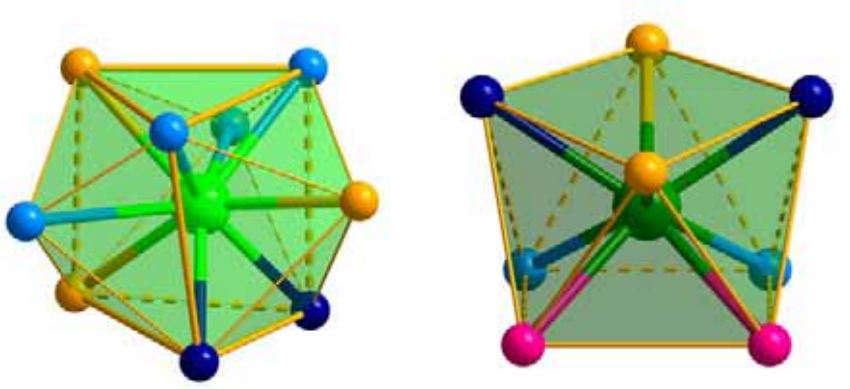

(a) **(b)**

Figure 4. Coordination geometry of the two holmium cations: Ho(1) **(a)** and Ho(2) **(b)** that occur in **1**.

Three crystallographically independent malonate groups are present in **1**: L1 [C(1)C(2)C(1b)], L2 [C(11)-C(12)-C(11a)] and L3 [C(21)-C(22)-C(21b)]. The three methylene carbon atoms belonging to the independent malonate groups lie on a mirror plane. L1 (see Figure 5a) acts as bis-bidentate ligand through its carboxylate groups towards Ho(1) and Ho(1b) atoms [the angle subtended by the carboxylate groups at the lanthanide atoms is 48.56(13)º] and also chelates Ho(2) through the inner O(1) and O(1b) malonate oxygen atoms [72.7(2)º being the angle subtended by the malonate ligand at the rare earth atom]. L1 forms a six-membered ring including the rare earth atom that exhibits a boat conformation with θ = 97.0(5) and ϕ = 120.0(5)º. L2 adopts (Figure 5b) simultaneously bis-monodentate [through O(12) and O(12a) towards Ho(2) and Ho(2a), respectively] and bidentate [through O(11) and O(11a) towards Ho(2)] coordination modes. The chelate ring of L2 has a boat conformation [θ = 78.5(5) and ϕ = 120.0(5)º] and the angle subtended by the malonate ligand at Ho(2) is 76.0(2)º. Finally, L3 (see Figure 5c) acts as bidentate ligand towards Ho(2) [O(21)-Ho(2)-O(21b) = 75.6º]. The chelate ring has a boat conformation [θ = 36.3 and ϕ = 120.0(13)º]. The carboxylate groups of L1 and L2 connect two holmium atoms exhibiting the *anti-syn* conformation.

(a)

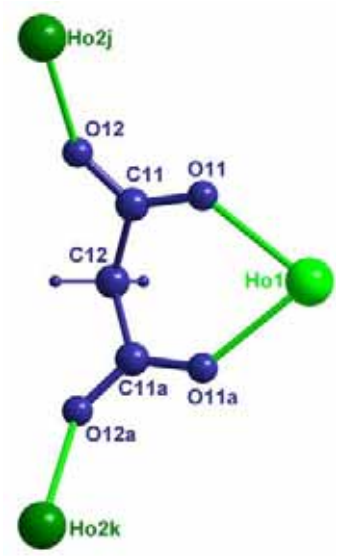

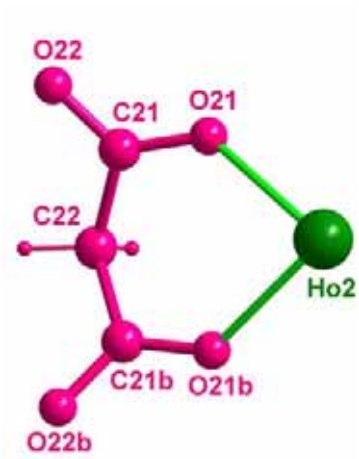

(b) **(c)**

Figure 5. Coordination modes of the three malonate ligands crystallographically independent that occur in **1**.

Each triaquaholmium(III) unit is connected to four diaquaholmium(III) entities by four carboxylate groups from three different malonate ligands to form corrugated layers (see Figure 2). The shortest separation between the holmium atoms, within the lanthanide malonate-bridged layer (see Figure 1), are: 4.9314(5) [Ho(1)···Ho(2) separation through L1], 5.9648(6) [Ho(1)···Ho(2j) separation through L2], 8.0555(9) [Ho(1)···Ho(1b) and Ho(2j)···Ho(2k) separations through L1 and L2, respectively], 7.0905(8) [Ho(1)···Ho(1k)] and 6.384(8) Å [Ho(2)···Ho(2j)].

The corrugated layers of holmium atoms are linked by hydrogen bonds involving water molecules and malonate oxygen atoms (see Figure 2) and they are stacked in a ABAB sequence, leading to a three-dimensional network. The distance between the mean planes defined by the holmium atoms belonging to adjacent planes is 10.104(3) Å.

Description of the structures of $[Sm_2(mal)_3(H_2O)_6]$ (2) and $[Ce_2(mal)_3(H_2O)_6]\cdot 2(H_2O)$ (3)

The structure of complexes **2** and **3** consists of three-dimensional malonate-bridged triaqualanthanide(III) networks (see Figures 6a and 6b) which result from the cross-linking of double lanthanide (Ln) [Ln = Sm(III) and Ce(III)] chains which grow along the [101] direction (see Figures 7a and 8a) and single chains which run parallel to the *b*-axis (see Figures 7b and 8b). Extensive hydrogen bonds (see Tables 3 and 4, for compounds **2** and **3**, respectively) involving coordinated (in **2**) and non-coordinated water molecules (in **3**) contribute to stabilize the crystal structure.

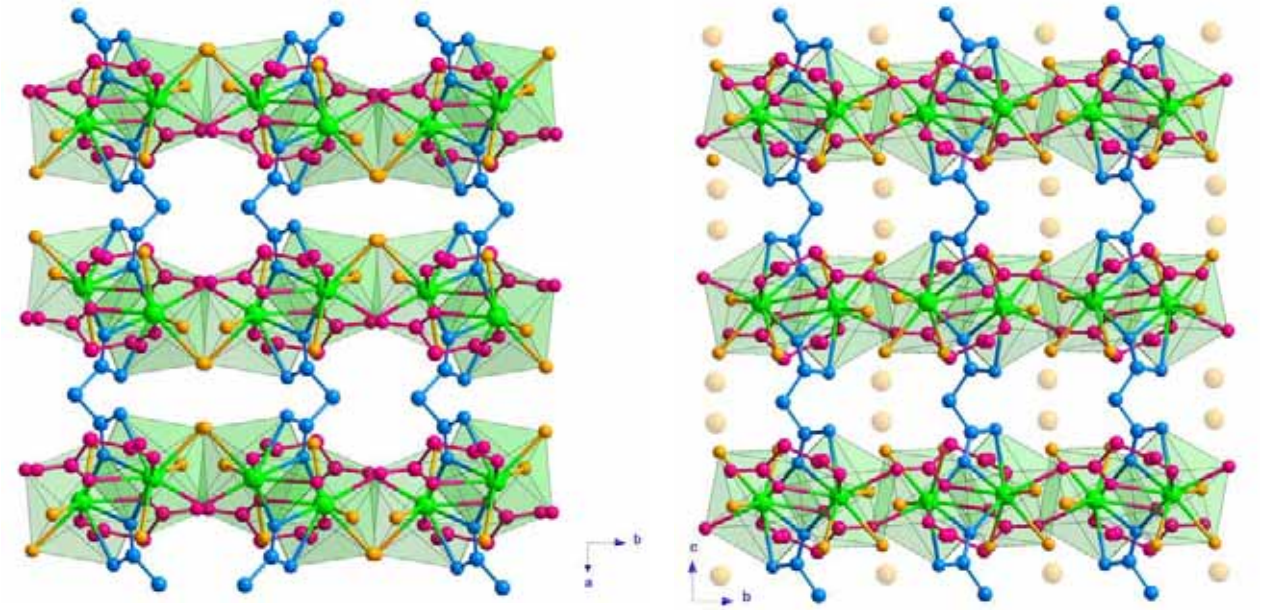

(a) **(b)**

Figure 6. Perspective view of the crystal packing in compounds **2** **(a)** and **3** **(b)**. The two crystallographically different malonate ligands that occur in both compounds are pink and blue coloured. Hydrogen bonds were not drawn for clarity.

The samarium and cerium atoms are nine-coordinated (see Figure 9). Six carboxylate oxygen atoms from three different malonate groups [the Ln-O(mal) bond distances range from 2.321(5) to 2.602(4) Å in **2** and from 2.436(4) to 2.729(3) Å in **3**] and three water molecules [Ln-O(w) bond distances ranging from 2.484(4)-2.532(4) Å (**2**) and 2.507(4)-2.557(4) (**3**) Å] build a distorted monocapped square antiprism around the rare earth atoms (see Figure 10).

Table 3. Selected bond lengths (Å) and angles (°) for **2**[a]

Samarium coordination sphere			
Sm(1)-O(1)	2.371(4)	Sm(1)-O(11)	2.549(4)
Sm(1)-O(2)	2.427(4)	Sm(1)-O(12)	2.602(4)
Sm(1)-O(4b)	2.321(4)	Sm(1)-O(12a)	2.448(3)
Sm(1)-O(1w)	2.532(4)	Sm(1)-O(2w)	2.504(5)
Sm(1)-O(3w)	2.484(4)		
O(1)-Sm(1)-O(2)	71.54(12)	O(2)-Sm(1)-O(4b)	138.93(15)
O(1)-Sm(1)-O(4b)	92.87(14)	O(2)-Sm(1)-O(11)	70.13(13)
O(1)-Sm(1)-O(11)	80.97(13)	O(2)-Sm(1)-O(12)	68.82(12)
O(1)-Sm(1)-O(12)	124.71(12)	O(2)-Sm(1)-O(12a)	85.32(13)
O(1)-Sm(1)-O(12a)	146.97(13)	O(2)-Sm(1)-O(1w)	68.17(13)
O(1)-Sm(1)-O(1w)	77.00(14)	O(2)-Sm(1)-O(2w)	131.97(14)
O(1)-Sm(1)-O(2w)	74.04(15)	O(2)-Sm(1)-O(3w)	136.41(14)
O(1)-Sm(1)-O(3w)	141.45(14)	O(11)-Sm(1)-O(12)	50.16(11)
O(4b)-Sm(1)-O(11)	146.50(15)	O(11)-Sm(1)-O(12a)	113.52(12)
O(4b)-Sm(1)-O(12)	141.82(13)	O(11)-Sm(1)-O(1w)	137.14(13)
O(4b)-Sm(1)-O(12a)	89.41(14)	O(11)-Sm(1)-O(2w)	72.3(2)
O(4b)-Sm(1)-O(1w)	71.39(15)	O(11)-Sm(1)-O(3w)	86.01(15)
O(4b)-Sm(1)-O(2w)	74.4(2)	O(12a)-Sm(1)-O(1w)	72.56(12)
O(4b)-Sm(1)-O(3w)	78.5(2)	O(12a)-Sm(1)-O(2w)	137.68(14)
O(12)-Sm(1)-O(12a)	63.43(13)	O(12a)-Sm(1)-O(3w)	71.16(13)
O(12)-Sm(1)-O(1w)	119.48	O(1w)-Sm(1)-O(2w)	133.4(2)
O(12)-Sm(1)-O(2w)	107.1(2)	O(1w)-Sm(1)-O(3w)	132.44(15)
O(12)-Sm(1)-O(3w)	67.89(13)	O(2w)-Sm(1)-O(3w)	67.43(15)

Hydrogen bonds[b,c]

D-H···A	D···A/Å	D-H···A	D···A/Å
O(1w)-H···O(3g)	2.715(8)	O(1w)-H···O(11h)	2.839(7)
O(2w)-H···O(3i)	2.756(8)	O(2w)-H···O(2wj)	2.827(11)
O(3w)-H···O(1i)	2.791(6)	O(3w)-H···O(2a)	2.733(9)

[a] Symmetry transformations: (a) –*x*-1/2, -*y*-1/2, -*z*+1; (b) –*x*-1/2, *y*-1/2, -*z*+1/2. [b] A = acceptor; D = donor. [c] Symmetry operators apply to acceptor atoms

Table 4. Selected bond lengths (Å) and angles (°) for **3**[a]

Cerium coordination sphere			
Ce(1)-O(1)	2.461(3)	Ce(1)-O(11)	2.557(3)
Ce(1)-O(2)	2.481(4)	Ce(1)-O(12)	2.729(3)
Ce(1)-O(4b)	2.436(4)	Ce(1)-O(12a)	2.502(3)
Ce(1)-O(1w)	2.557(3)	Ce(1)-O(2w)	2.507(4)
Ce(1)-O(3w)	2.557(4)		
O(1)-Ce(1)-O(2)	69.59(11)	O(2)-Ce(1)-O(4b)	136.95(12)
O(1)-Ce(1)-O(4b)	73.18(12)	O(2)-Ce(1)-O(11)	78.08(12)
O(1)-Ce(1)-O(11)	82.53(13)	O(2)-Ce(1)-O(12)	67.86(10)

O(1)-Ce(1)-O(12)	119.66(11)	O(2)-Ce(1)-O(12a)	77.51(11)
O(1)-Ce(1)-O(12a)	140.80(12)	O(2)-Ce(1)-O(1w)	72.23(12)
O(1)-Ce(1)-O(1w)	72.75(12)	O(2)-Ce(1)-O(2w)	137.61(12)
O(1)-Ce(1)-O(2w)	107.43(13)	O(2)-Ce(1)-O(3w)	134.48(11)
O(1)-Ce(1)-O(3w)	144.69(12)	O(11)-Ce(1)-O(12)	48.47(11)
O(4b)-Ce(1)-O(11)	76.36(12)	O(11)-Ce(1)-O(12a)	111.32(11)
O(4b)-Ce(1)-O(12)	115.64(11)	O(11)-Ce(1)-O(1w)	146.40(12)
O(4b)-Ce(1)-O(12a)	144.52(12)	O(11)-Ce(1)-O(2w)	144.32(13)
O(4b)-Ce(1)-O(1w)	116.07(13)	O(11)-Ce(1)-O(3w)	79.69(12)
O(4b)-Ce(1)-O(2w)	74.22(13)	O(12a)-Ce(1)-O(1w)	77.44(12)
O(4b)-Ce(1)-O(3w)	73.10(12)	O(12a)-Ce(1)-O(2w)	82.90(12)
O(12)-Ce(1)-O(12a)	62.85(13)	O(12a)-Ce(1)-O(3w)	74.43(11)
O(12)-Ce(1)-O(1w)	128.13(11)	O(1w)-Ce(1)-O(2w)	66.95(12)
O(12)-Ce(1)-O(2w)	132.84(12)	O(1w)-Ce(1)-O(3w)	132.99(11)
O(12)-Ce(1)-O(3w)	67.61(11)	O(2w)-Ce(1)-O(3w)	72.79(12)

Hydrogen bonds[b,c]

D-H···A	D···A/Å	D-H···A	D···A/Å
O(1w)-H···O(4w)	2.747(6)	O(1w)-H···O(3f)	2.693(5)
O(2w)-H···O(3w)	2.656(6)	O(2w)-H···O(4b)	2.983(5)
O(3w)-H···O(1g)	2.756(5)	O(3w)-H···O(2h)	2.684(5)

[a] Symmetry transformations: (a) –*x*, -*y*, -*z*-1; (b) –*x*+1/2, *y*-1/2, *z*. [b] A = acceptor; D = donor.
[c] Symmetry operators apply to acceptor atoms.

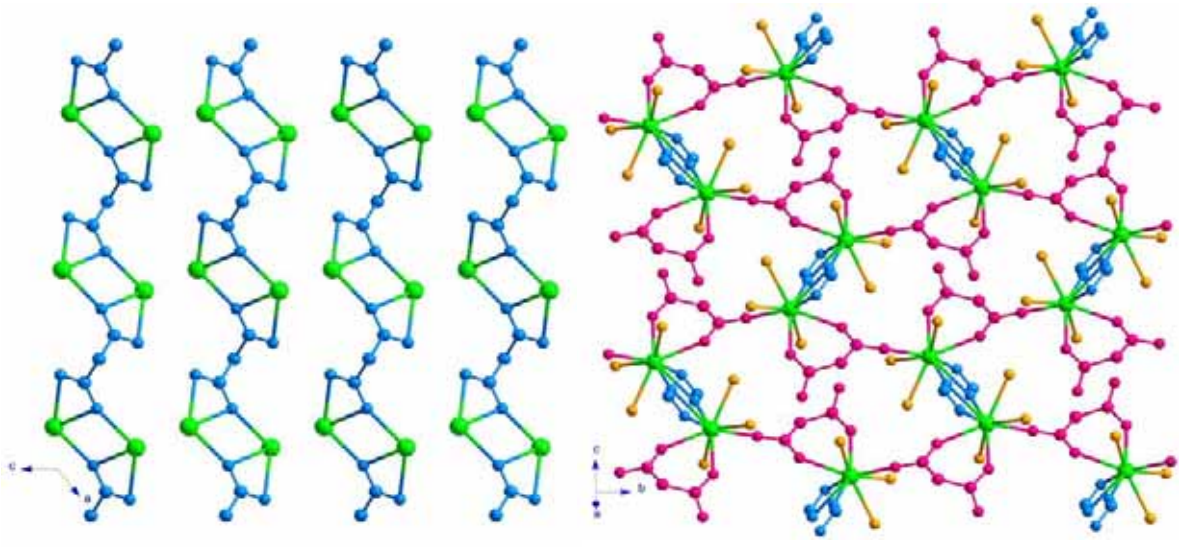

(a) **(b)**

Figure 7. Perspective view of the double Sm(III) chains that grow along the [101] direction **(a)** and the single chains that run parallel to the *c*-axis **(b)** in compound **2**.

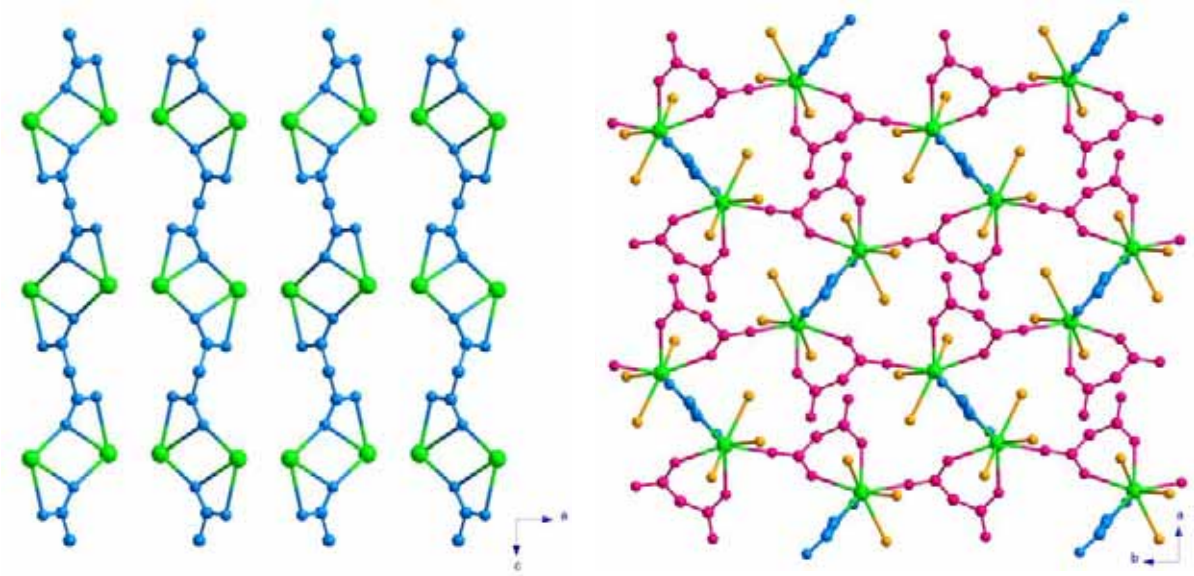

Figure 8. Perspective view of the double Ce(III) chains that grow along the [101] direction (a) and the single chains that run parallel to the c-axis (b) in compound **3**.

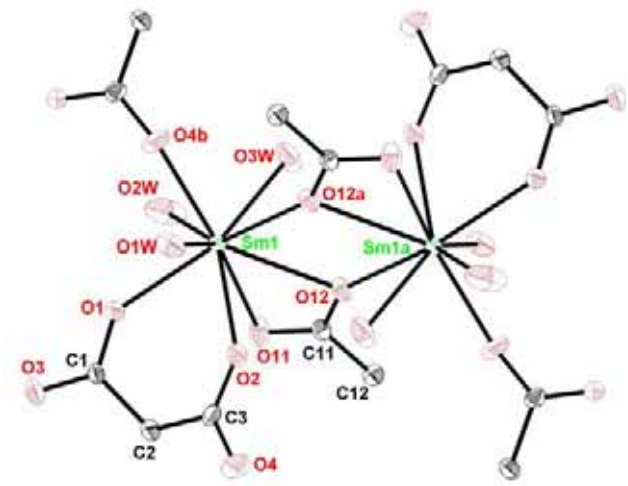

(a)

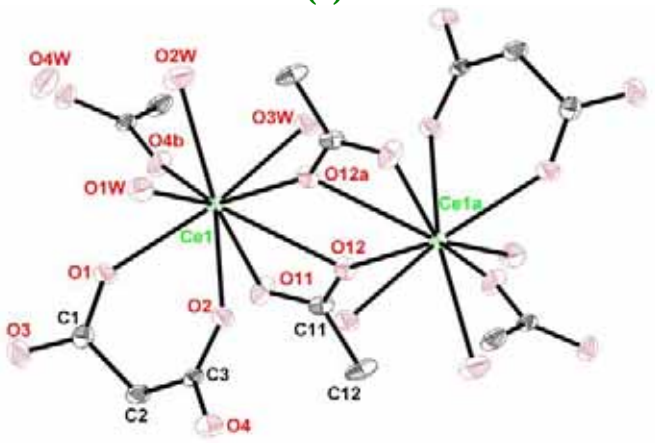

(b)

Figure 9. ORTEP view of the samarium (a) and cerium (b) environments in compounds 2 and 3, respectively. Thermal ellipsoids are drawn at 50% probability level.

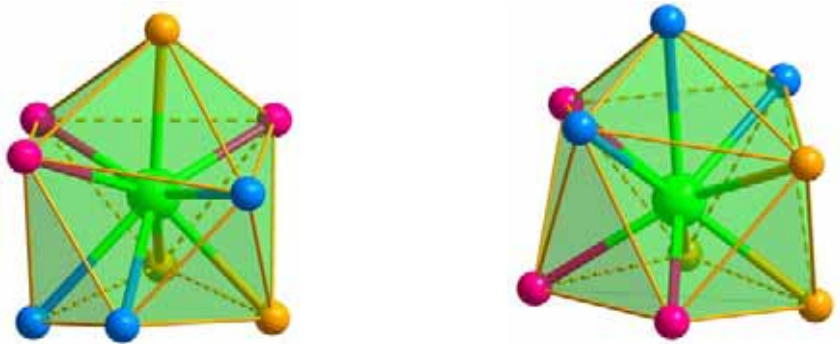

(a) **(b)**

Figure 10. Coordination geometry of the samarium **(a)** and cerium **(b)** ions for compound **2** and **3**, respectively.

Two crystallographically independent malonate groups are present in **2** and **3**: L1 [C(1)-C(2)-C(3)] and L2 [C(11)-C(12)-C(11)] (see Figures 11 and 12). L1 acts simultaneously as monodentate [through O(4) towards Sm(1g) and Ce(1f)] and bidentate ligand [through O(1) and O(2) towards Sm(1) and Ce(1)], the value of the angle subtended by the malonate ligand at the lanthanide atom being 71.54(12) and 69.59(11)º for compounds **2** and **3**, respectively. It forms a six-membered ring including the rare-earth atom that exhibits a boat conformation in **2** and **3** [Cremer D. *et al.*, 1975] with θ = 83.6(4) and ϕ = 112.4(4)º (**2**) and θ = 89.1(6) and ϕ = 128.3(6)º (**3**). The C(3)O(4)O(2) carboxylate bridge adopts the *anti-syn* conformation. The central atom of L2 group lies on a two-fold axis. L2 links four lanthanide atoms acting simultaneously as bis-monodentate [through O(12) towards Sm(1j) and Ce(1h)] and bis-bidentate ligand [through the carboxylate-malonate oxygen atoms towards lanthanide ions], the value of the angle subtended by carboxylate-malonate group at the rare earth atoms being 50.16(11)º (**2**) and 48.47(11)º (**3**). The geometric values of the malonate group agree well with those reported for other malonate-containing complexes.

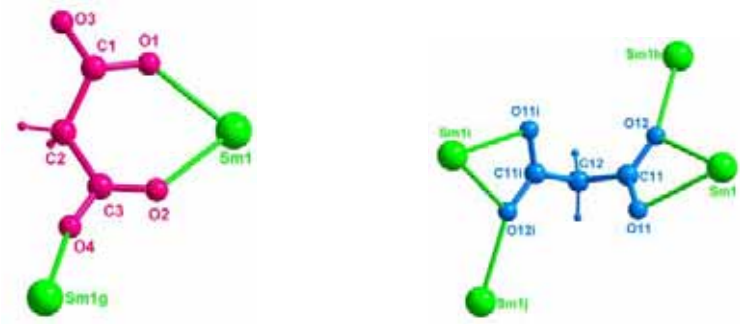

(a) **(b)**

Figure 11. Coordination modes of the two malonate ligands crystallographically independent that occur in **2**.

Each triaqualanthanide(III) units are linked by the malonate skeleton of the L1 group leading to a single lanthanide chain growing along the *b*-axis. The shortest intrachain Ln···Ln distance being 6.5858(10) and 6.7313(7) Å, for **2** and **3**, respectively. These malonate-bridged lanthanide chains are further linked through the carboxylate-malonate unit of the L2 group, the distance through the double μ-oxo bridge being 4.2971(7) (**2**) and 4.4656(4) Å (**3**). The malonate-bridged lanthanide layers are pillared by the L2 group affording a three-dimensional structure, (see Figure 6) the shortest interlayer Ln···Ln distance being 6.971(2) Å (**2**) and 7.9207 Å (**3**). The stacking of these layers following the trends ABABA and AAAA for **2** and **3**, respectively. Finally, hydrogen bonds involving water molecules and malonate oxygen atoms contribute to the stabilization of the whole structure. It deserve to be note that crystallization water molecules are present in the crystal structure of compound **3**.

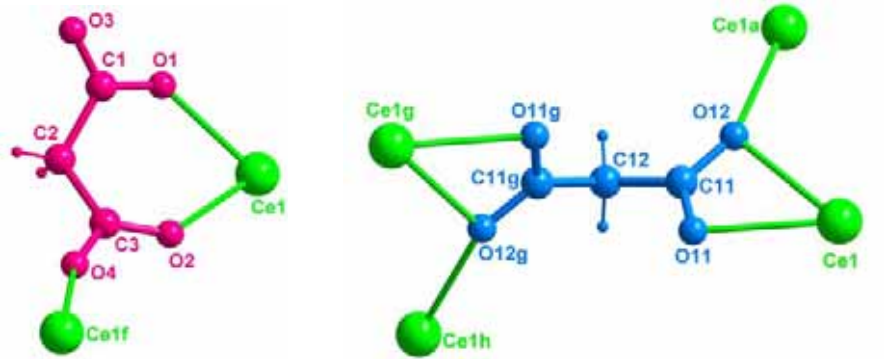

(a) **(b)**

Figure 12. Coordination modes of the two malonate ligands crystallographically independent that occur in **3**.

Magnetic properties

A summary of the magnetic behaviour of the rare-earth containing compounds is reported in the Appendix C. It's well known that the ground configuration of the rare-earth ions is $4f^{n}5s^{2}5p^{6}$. So, the 4*f* orbitals, where the magnetically active electrons are located, are partially shielded by the external 5*s* and 5*p* orbitals. Moreover, these 4*f* orbitals are almost uninvolved in the bonds between the rare-earth ions and its nearest neighbours. Therefore, the influence of the rare-earth environment in the magnetic properties of these compounds is much less pronounced than in the transition metal compounds and consequently, in a first approximation we can consider that a rare-earth

ion in a molecular compound behaves magnetically as a free-ion (free-ion approximation) [Kahn O., 1993].

Nevertheless, the $^{2S+1}\Gamma_J$ ground state is always partially split by the ligand field giving rise to a multiplet which witdh in energy depends on the symmetry and the intensity of the ligand field. For this reason, the free-ion approximation is only valid at high temperatures, when the width in energy of the multiple is small enough to consider that all the components of the multiple are statistically populated at room temperature. On cooling, this approximation becomes less and less valid due to the depopulation of the components of higher energy arising from the splitting of the $^{2S+1}\Gamma_J$ ground state.

The magnetic behaviour of **1** in the form of $\chi_M T$ versus T plot [χ_M being the magnetic susceptibility per holmium(III) ion] in the temperature range of 2-300 K is shown in **Figure 13**. The value of the $\chi_M T$ product at room temperature is 13.46 cm^3 mol^{-1} K, a value which is close to that expected for a magnetically isolated holmium ion (14.07 cm^3 mol^{-1} K). Upon cooling, $\chi_M T$ remains practically constant up to 100 K, and then quickly decrease to reach a value of 7.42 cm^3 mol^{-1} K at 2 K.

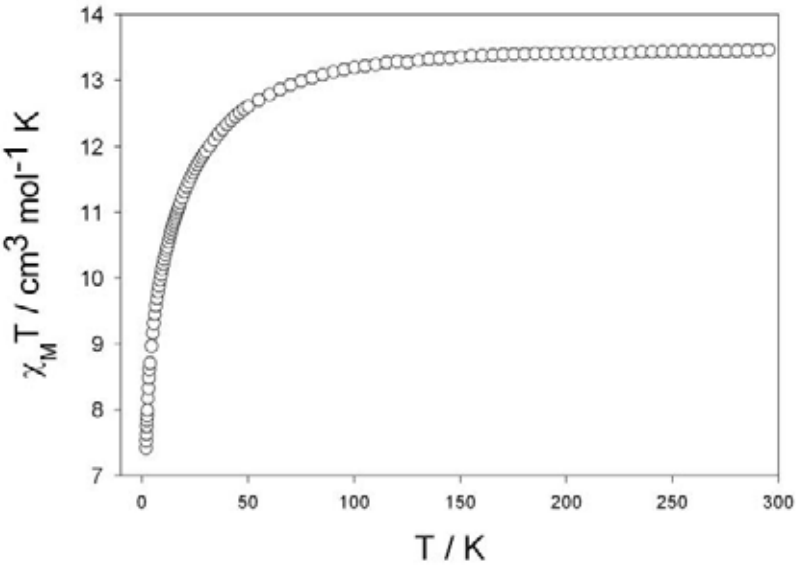

Figure 13. Thermal dependence of the $\chi_M T$ product for **1**.

The thermal dependence at high temperatures follows a Curie Law, as expected for a free-holmium(III) ion. The energy separation between the ground ($^5I_8$) and the first excited state ($^5I_7$) is ~5000 cm^{-1}, large enough to consider that only the ground state is termally populated at room temperature. The decrease of the thermal dependence of the $\chi_M T$ product may be due to:

- the statistical depopulation of the components of the higher energy arising from the splitting of the ground state due to the influence of the ligand field.

- the occurence of an overall antiferromagnetic coupling between the rare-earth ions through the carboxylate-malonate bridges that link the metal ions in **1** (see **Figure 1**).

The magnetic behaviour of **2** in the form of χ_M *versus* T plot [χ_M being the magnetic susceptibility per samarium(III) ion] in the temperature range of 2-300 K is shown in **Figure 14**. The value of the χ_M at room temperature is 1.17×10^{-3} cm^3 mol^{-1} a value which is somewhat lower that the value expected for a free-samarium(III) ion (1.96x10-3 cm3 mol-1). Upon cooling χ_M remains practically constant up to 150 K. Then, it smoothly increases to reach a value of 1.75×10^{-2} cm^3 mol^{-1}.

For the free-samarium(III), the ^6H ground term splits by spin-orbit coupling into six levels, the energies of these levels being:

$$E(J) = \lambda[J(J+1) - 35/4]/2 \qquad (1)$$

where λ is the spin orbit coupling which is of the order of 200 cm^{-1}. Consequently, the first excited state $^6H_{7/2}$ may be populated at room temperature and we have to take into account in the expression of the magnetic susceptibility (see Appendix C) the six states arising from the ^6H ground state due to the spin-orbit coupling. Taking that into consideration, the expression for the magnetic susceptibility is as follows [Kahn O., 1993]:

$$\chi_M = (N\beta^2/3kTx)[a_1x + b_1 + (a_2x + b_2)e^{-7x/2} + (a_3x + b_3)e^{-8x} + (a_4x+b_4)e^{-27x/2} + (a_5x + b_5)e^{-20x} + (a_6x + b_6)e^{-55x/2}] / [3 + 4e^{-7x/2} + 5e^{-8x} + 6e^{-27x/2} + 7e^{-20x} + 8e^{-55x/2}] \qquad (2)$$

with

$x = \lambda/kT$

$a_1 = 2.143$ $\quad b_1 = 7.437$

$a_2 = 42.92$ $\quad b_2 = 1.641$

$a_3 = 283.7$ $\quad b_3 = -0.6571$

$a_4 = 620.6$ $\quad b_4 = -1.9400$

$a_5 = 1122$ $\quad b_5 = -2.835$

$a_6 = 1813$ $\quad b_6 = -3.556$

This equation is only valid in the high temperature range. So, we analyse through this expression the magnetic data over 200 K. The least-squares fit leads to: λ =

241(2) cm^{-1}, R = 1.3x10^{-3}. R is the agreement factor defined as $\Sigma[(\chi_M)_{obs} - (\chi_M)_{calc}]^2/\Sigma[(\chi_M)_{obs}]^2$.

It deserves to be note here that deviations of this law one can observe at low temperatures (below 200 K) are due to the influence of the ligand field that split the $^{2S+1}\Gamma_J$ ground state.

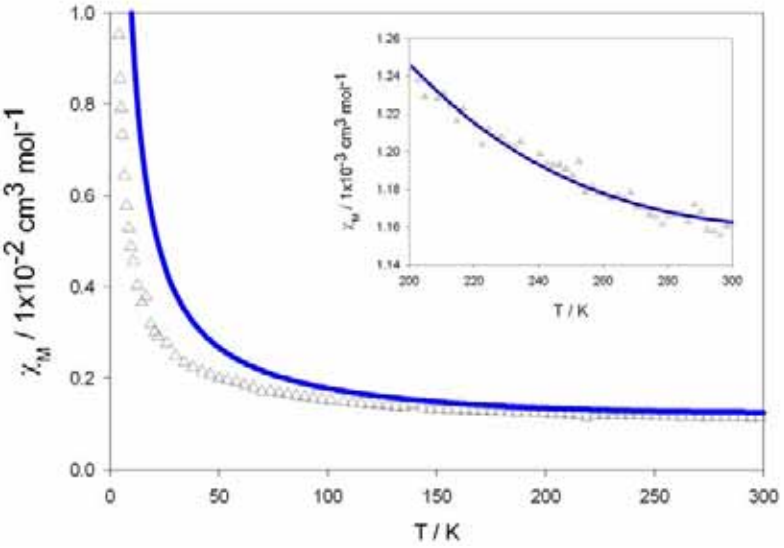

Figure 14. Thermal dependence of the $\chi_M T$ product for **2**. The inset shows the fit in the 200-300 K temperature range.

The thermal dependence of the $\chi_M T$ product for **3** [χ_M being the magnetic susceptibility per cerium(III) ion] in the temperature range of 2-300 K is shown in **Figure 15**. The value of the $\chi_M T$ product at room temperature is 0.80 cm^3 mol^{-1} K, a value which is as expected for a free cerium(III) ion. Upon cooling, $\chi_M T$ remains practically constant up to 200 K and then smoothly decrease to reach a value of 0.47 cm^3 mol^{-1} K at 2 K. The free-cerium(III) ion has a $^2F_{5/2}$ ground state, the first excited state $^2F_{7/2}$ being at ~2200 cm^{-1}, so at room temperature only the ground state is thermally populated. At high temperatures the thermal dependence of the $\chi_M T$ product follows a Curie Law as expected for a free-cerium(III). As in **1**, the deviation of the $\chi_M T$ product from the Curie Law at lower temperatures may be due to:

- the thermally depopulation of the components arising from the splitting of the ground state due to the influence of the ligand field.
- the ocurrence of an overall antiferromagnetic coupling between the cerium ions in **3**.

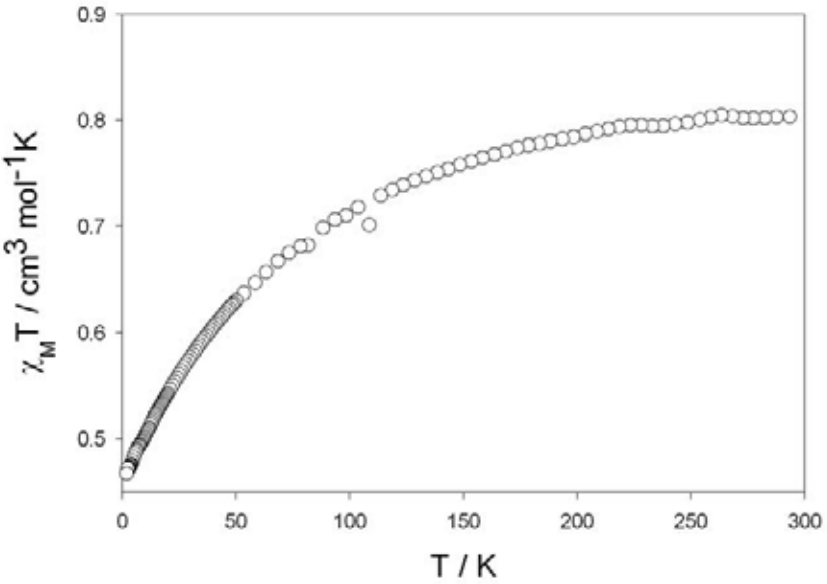

Figure 15. Temperature dependence of the $\chi_M T$ product of **3**.

A more detailed study, including the effect of the crystal field is necesary to interpretate the magnetic data. Only the diagonalization of the hamiltonian including the spin-orbit coupling, the influence of the crystal field and the Zeeman perturbations using all the eigenfunctions associated with the states thermally populated will allow us to interpretate the magnetic data in the whole temperature range.

References

Desiraju G.R. (De.) *The Crystal as a Supramolecular Entity*, Wiley, New York, **1995**.

DIAMOND 2.1d, Crystal Impact GbR, CRYSTAL IMPACT, K. Brandenburg & H. Putz GbR, Postfach 1251, D-53002 Bonn, Germany, **2000**.

Duisenberg A.J.M., Kroon-Batenburg, L.M.J. and Schreurs, A.M.M., *J. Appl. Cryst.*, **2003**, 36, 220 (EVALCCD).

Earshaw A., *Introduction to Magnetochemistry*; Academic Press; London, **1968**.

Farrugia L.J. (*WINGX*), *J. Appl. Cryst*, **1999**, 32, 837.

Gil de Muro I., Mautner F.A., Insausti M., Lezama I., Arriortua M.I. and Rojo T., *Inorg. Chem.*, **1998**, 37, 3243.

Gil de Muro I., Insausti M., Lezama L., Pizarro J.L., Arriortua M.I. and Rojo T., *Eur. J. Inorg. Chem.*, **1999**, 935.

Hansson E., *Acta Chem. Scand.*, **1973a**, 27, 2441.

Hansson E., *Acta Chem. Scand.*, **1973b**, 27, 2827.

Hansson E., *Acta Chem. Scand.*, **1973c**, 27, 2841.

Henisch H.K., *Crystal Growth in Gels*, The Pennsylvania State, Univ. Press, Pittsburgh, **1970**.

Hernández-Molina M., Lorenzo-Luis P. A., López T., Ruiz-Pérez C., Lloret F. and Julve M., *CrystEngComm*, **2000**, 31, 1.

Hooft, R.W.W. *COLLECT*. Nonius BV, Delft, The Netherlands, **1999**.

Insausti M., Cortés R., Arriortua M.I., Rojo T. and Bocanegra E.H., *Solid State Ionics*, **1993**, 63, 351.

Nardelli M. *J. Appl. Crystallogr.*, **1995**, 28, 659.

Robson R., Abrahams B.F., Batten S.R., Gable R.W., Hoskins B.F. and Liu J., *Supramolecular Architecture*, ACS, Washington, DC, **1992**.

Ruiz-Pérez C., Hernández-Molina M., Lorenzo-Luis P. A., Lloret F., Cano J. and Julve M., *Inorg. Chem.*, **2000a**, 39, 3845.

Ruiz-Pérez C., Hernández-Molina M., Sanchiz J., López T., Lloret F. and Julve M. *Inorg. Chim. Acta* **2000b**, 298, 245.

Ruiz-Pérez C., Sanchiz J., Hernández-Molina M., Lloret F. and Julve M. *Inorg. Chim. Acta* **2000c**, 298, 202.

Ruiz-Pérez C., Sanchiz J., Hernández-Molina M., Lloret F. andx Julve F., *Inorg. Chem.*, **2000d**, 39, 1363.

SADABS, version 2.03. Bruker AXS Inc.: Madison, WI, **2000**.

Sheldrick, G.M. *SHELX97*, *Programs for Crystal Structure Analysis (Release 97-2)*, Institüt für Anorganische Chemie der Universität, Tammanstrasse 4, D-3400 Göttingen, Germany, **1998**.

Wang Z.-M., van de Burgt L.J. and Choppin G.R. *Inorg. Chim. Acta* **2000**, 310, 248.

WenMei X., Qiguang W., Lan Y.and Rudong Y., *Polyhedron*, **1992**, 11, 2051.

CONCLUSIONS

Conclusions

Structural point of view. Homometallic malonate-containing complexes with the first-row transition metal ions Co(II), Ni(II), Zn(II) and Mn(II) have two-dimensional structures exhibiting two different topologies (see Scheme 1). Co(II), Ni(II) and Zn(II) malonate complexes are isostructural and their structure exhibit corrugated layers of metal(II) ions bridged through carboxylate-malonate in the *anti-syn* conformation. Coexistence of *anti-syn* and *anti-anti* bridging modes occurs in the case of Mn(II). The reaction of these homometallic malonate complexes with N-exo-pyridyl ligands affords two- and three-dimensional structures where malonate-bridged metal(II) layers (*anti-syn* conformation of the carboxylate-malonate groups) with the same topology are observed, this topology being different from that of the original homometallic malonate complexes.

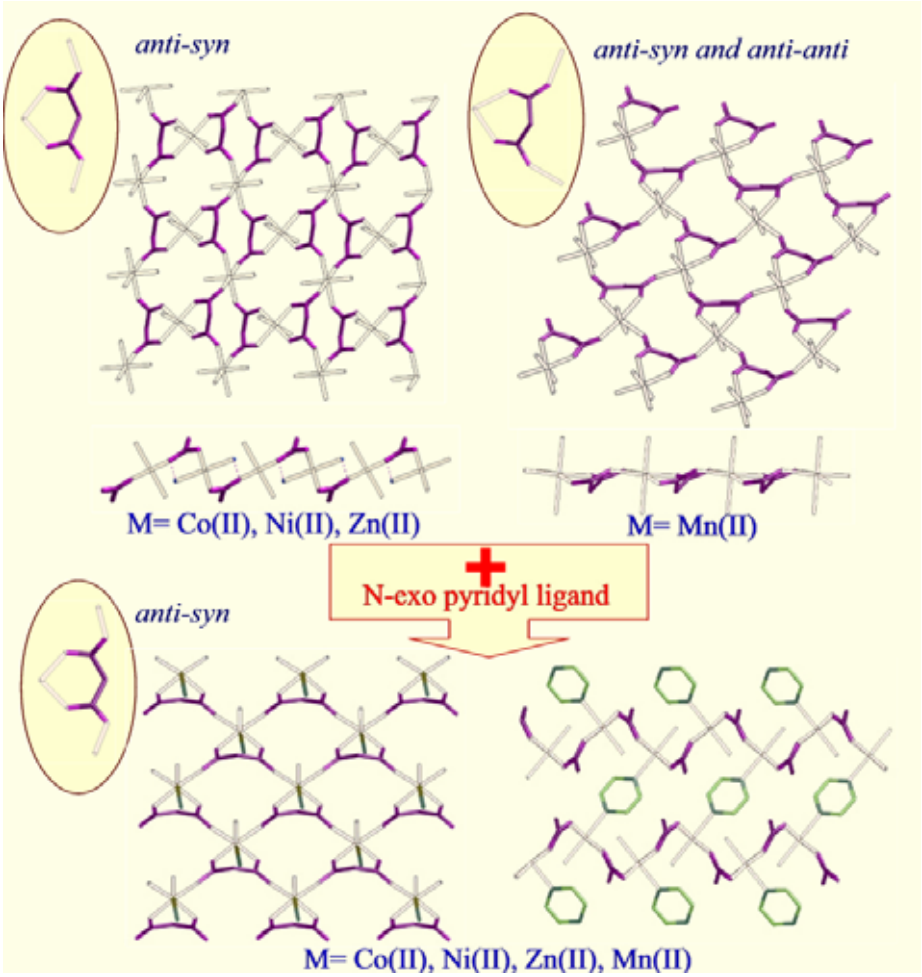

Scheme 1

It deserves to be note here that seven new malonate-containing cobalt(II) compounds have been synthesised, leading to a great variety of crystal structures (from dimmers to three-dimensional networks). The dimensionality of this complexes seems to be controled by the nature of the additional bridging ligand we use.

The design of new solid-state architectures has recently driven much attention and increasing interest. Advanced crystal engineering by selecting structural ligands and the coordination geometry of lanthanide(III) metal centers as a building block may given a series of novel inorganic frameworks with an interesting variety of crystal-packing motifs. This is in accordance with the experience that the crystal structures of the lanthanide compounds frequently change along the series as a result of the lanthanide contraction.

Among a number of ligands used as building blocks, the two end functional groups of dicarboxylic acids could yield a variety of crystal structures of coordination compounds even with close chemical formulas depending on the conformation of the carbon chains and the end functional groups. Those compounds are characterized as organic/inorganic hybrids with pillared sheete-like structures assembled from the molecular precursor in solution.

In order to check the ability of the rare earth ions to lead to high dimensional materials, we have thus undertake a study of the lanthanide malonate complexes (where malonate stands for the dianion of the propanedioic acid, H_2mal). This ligand has, indeed, a great ability to form infinite connections with metal ions and a remarkable versatility in adopting several different modes of bonding (monodentate, chelating and bridging modes) sometimes in more than one way in the same compound. Seven bonding modes have been observed according to the coordination environment of COO^- groups.

Magnetic point of view. Weak antiferro- and ferromagnetic interactions between the cobalt(II) and nickel(II) ions through carboxylate-malonate bridges with the *anti-syn* conformation are observed supporting the ability of the malonate bridge to mediate magnetic interactions between metal ions other than copper(II).

The difficulty in studying the magnetic properties of species containing paramagnetic Ln(III) ions arises from the fact that most of the Ln(III) ions possess a

first-order angular momentum. For the $4f^n$ configuration of a Ln(III) ion, it splits into $^{2S+1}L_J$ states by interelectronic repulsion and spin-orbit coupling. Further splitting of this ground state is caused by crystal-field perturbation. At room temperature, all these levels are populated, but as the temperature decreases, the effective magnetic moment of the lanthanide ion will change by thermal depopulation of the energy levels, even for a mononuclear Ln(III) complex; the temperature dependence causes the magnetic susceptibility to deviate from the Curie behaviour. This phenomenon is intrinsic to the lanthanide ion and it is modulated by the ligand field and the symmetry of the compound.

PART III: NEW PERSPECTIVES OF MALONATE COMPLEXES

CHAPTER X. Malonate-containing Manganese(III) compounds an attempt to obtain precursors.

CHAPTER XI. The complex as precursor: Chromium(III) complexes.

CONCLUSIONS

CHAPTER X.

Malonate-containing Manganese(III) compounds an attempt to obtain precursors.

Introduction

The use of deprotonated dicarboxylic acids as bridging ligands between paramagnetic transition metal ions to afford polynuclear compounds is an area of continuous interest both in molecular magnetism [Oldham C., 1987; Kahn O., 1993] and in biology [Christou G., 1989; Weighardt K., 1989]. Among the first-row transition metal ions, the case of carboxylato-bridged manganese(II) complexes is specially relevant because such systems are known to exist at the active centers of some manganese-containing enzimes [Pecoraro V.L., 1992; Waldo G.S. *et al.*, 1992; Tan X.S. *et al.*, 1997; Policar C. *et al.*, 1999; Tangoulis V. *et al.*, 1996; Albela B. *et al.*, 1998, Xen X.M. *et al.*, 1995]. Focusing on the magnetic studies and without being exhaustive, examples are known of structurally characterized oxalate- [Verdaguer M., 1984; Deguenon D. *et al.*, 1990; Ménage S. *et al.*, 1991; Gleup J. *et al.*, 1995; Marinescu G. *et al.*, 2000], terephthalate- [Cano J. *et al.*, 1994], adipate- [Kim Y.J. *et al.*, 2000] and malonate-bridged [Lis T. *et al.*, 1979; Sain S. *et al.*, 2003a; Rodríguez-Martín Y. *et al.*, 2003; Maji M. *et al.*, 2003; see also Introduction of the Thesis] manganese(II) compounds with antiferromagnetic interactions ranging from maximum values of –2.5 (through oxalato) to –0.70 cm^{-1} (through carboxylato-malonate). The case of the malonate dianion (hereafter noted as mal) is very appealing mainly due to two features which are well illustrated by its copper(II) complexes: (i) the great versatility as a ligand given that it can adopt not only the chelating bidentate coordination mode but also the *syn-syn*, *syn-anti* and *anti-anti* carboxylate bridiging modes (ii) the ability to mediate ferromagnetic interactions between the metal ions it bridges [Sain S. *et al.*, 2003b; Pasán J. *et al.*, 2003a; Ruiz-Pérez C. *et al.*, 2003, see also malonate-containing compounds in the Introduction of the Thesis]. Interestingly, this ferromagnetic interaction between the copper(II) ions through the carboxylate-malonate bridge is kept when one of the hydrogen atoms of the methylene group is replaced by a phenyl group [Pasán J. *et al.*, 2003b and 2004] (that is the phenylmalonate as ligand instead of malonate)

The extensive magneto-structural work which has been carried out with the malonato complexes with divalent first-row transition metal ions [see references concerning malonate-containing compounds in the Introduction of the Thesis] contrasts with the paucity of investigations concerning the manganese(III) ion [Lis T. *et al.*, 1977; Lis T. *et al.*, 1980a and 1980b; Kirk M.L. *et al.*, 1991; Wei Y.G. *et al.*, 1996]. The

coordination chemistry of the cation is not an easy task because its fairly oxidising power and easy disproportion. However, it has caught the eyes of magnetochemists interested in the design of molecular magnets, that is discrete polynuclear transition metal complexes which exhibit slow relaxation of the magnetization [Barra A.L. *et al.*, 1977; Yoo J. *et al.*, 2001; Gatteschi D. *et al.*, 2003]. This property is strongly related the occurrence of a large spin in the ground state and a strong axial anisotropy in the cluster. This last requierment can be fulfilled by the presence of Mn(III), known to posess a promounced magnetic anisotropy. In the search for stable manganese(III) building blocks to be used as precursors of these so-called single molecule magnets, we have prepared the new manganese(III) complexes $PPh_4[Mn(mal)_2(H_2O)_2]$ (**1**) and $AsPh_4[Mn(mal)_2(H_2O)_2]$ (**2**) (PPh_4^+ = tetraphenylphosphonium cation, $AsPh_4$ = tetraphenylarsonium cation and H_2mal = malonic acid). Their preparation, structural characterization, magnetic study and theoretical analysis of the exchange pathway are presented here. The magnetic properties of the previously reported chain compound $K_2[Mn(mal)_2(MeOH)_2][Mn(mal)_2]$ (**3**) [Kirk M.L. *et al.*, 1991] were investigated for comparison.

Experimental

Materials and methods

Malonic acid, potassium permanganate. tetraphenylphosphonium chloride and tetraphenylarsonium chloride monohydrate were purchased from commercial sources and used as recieved. Polycrystalline samples of $K_2[Mn(mal)_2(MeOH)_2][Mn(mal)_2]$ (**3**) were prepared by the method of Cartledge and Nichols [Cartledge G.H. *et al.*, 1940] and well formed green crystals of this compound were grown by the receipt of Lis and Matuszewski [Lis T. *et al.*, 1980a]. These crystals once crushed were used for the magnetic measurements. Elemental analyses (C, H) were carried out by the Microanalytical Service of the Universidad Autónoma de Madrid. The X:Mn [X = P (**1**), As (**2**) and K (**3**)] molar ratio was determined by elecron probe X-ray microanalysis at the Servicio Interdepartamental de Investigación de la Universidad de Valencia. Variable-temperature (1.9-295 K) magnetic susceptibility measurements on polycrystalline samples of **1-3** were carried out with a Quantum Design SQUID operating at 5000 Oe in the high temperature range (30-295 K) and at 250 Oe at $T < 30$ K in order to avoid saturation phenomena. Diamagnetic corrections for the molar units

were estimated from Pascal constants [Earnshaw, A., 1968] as -365 x 10^{-6} (**1**), -370 x 10^{-6} (**2**) and -141 x 10^{-6} cm^3 mol^{-1} (**3**) [per mol of manganese(III)].

Synthesis

$PPh_4[Mn(mal)_2(H_2O)_2]$ (1) and $AsPh_4[Mn(mal)_2(H_2O)_2]$ (2). Compounds **1** and **2** are obtained as polycrystalline olive green powders by adding solid PPh_4Cl (1 mmol, **1**) and $AsPh_4Cl \cdot H_2O$ (1 mmol, **2**) to an aqueous solution (30 mL) 0.05 M H_2mal of $K_2[Mn(mal)_2(MeOH)_2][Mn(mal)_2]$ (1 mmol, **1** and **2**). The yield is about 70 %. The recrystallization of these powder samples in a H_2O-MeOH 1:2 (v/v) mixture in a hood afforded plate-like crystals of **1** and rods of **2**. The rods were suitable for X-ray diffraction whereas the plates poorly diffract. Anal. Calcd for $C_{30}H_{28}MnO_{10}P$ (**1**): C, 56.81; H, 4.42. Found: C, 56.45; H, 4.36 %. Anal. Calc for $C_{30}H_{28}AsMnO_{10}$ (**2**): C, 53.13; H, 4.12. Found: C, 52.93; H, 4.06 %.

Computational Strategy.

All theoretical calculations were carried out with the hybrid B3LYP method [Lee C. *et al.*, 1988; Becke A.D., 1988 and 1993], as is implemented in Gaussian03 program [Gaussian 03, Revision C.02]. Double- and triple-ζ quality basis sets proposed by Ahlrichs and co-workers have been used for all atoms [Schaefer A. *et al.*, 1992 and. 1994]. The broken-symmetry approach has been employed to describe the unrestricted solutions of the antiferromagnetic spin states [Cano J. *et al.*, 1998; Ruiz E. *et al.*, 1998 and 1999; Cano J. *et al.*, 1999]. To analyse the magnetic interactions between the manganese(III) ions in **2** and **3**, two models have been built from the experimental crystal structure. A quadratic convergence method was used to determine the more stable wave functions in the SCF process [Bacskay G.B., 1981]. The atomic spin densities were obtained from Natural Bond Orbital (NBO) analysis [Carpenter J.E. *et al.*, 1988; Reed A.E. *et al.*, 1988; Weinhold F. *et al.*, 1988].

Crystal data collection and refinement

A single crystal of **2** was mounted on a Bruker-Nonius KappaCCD diffractometer. Orientation matrix and lattice parameters were obtained by least-squares refinement of the reflections obtained by a θ-χ scan (Dirax/lsq method). Diffraction data of **2** were collected at 293(2) K using graphite-monochromated Mo-K_α radiation (λ =

0.71073 Å). A summary of the crystallographic data and structure refinement is given in Table 1. The indexes of data collection were $-11 \le h \le 11$, $-12 \le k \le 12$, $-11 \le l \le 17$. Of the 5426 measured independent reflections in the θ range 1.98 - 26º (1), 3526 have $I \ge 2\sigma(I)$. Over 26º the sample diffracts weakly. All the measured independent reflections were used in the analysis. All calculations for data reduction, structure solution, and refinement were done by standard procedures (WINGX) [Farrugia L.J., 1999]. The structure was solved by direct methods and refined with full-matrix least-squares technique on F^2 using the SHELXS-97 and SHELXL-97 programs [Sheldrick G.M., SHELX97, realease 97-2, 1998]. The malonate hydrogen atoms were located from difference Fourier maps and refined with isotropic temperature factors. The hydrogen atoms of the water molecules were not found. The final Fourier-difference map showed maximum and minimum height peaks of 0.843 and -0.806 e $Å^{-3}$. The final geometrical calculations and the graphical manipulations were carried out with PARST97 [Nardelli M., 1995] and DIAMOND [DIAMOND 2.1d, 2000] programs, respectively.

Table 1 Crystal data and details of structure determination

Compound	**2**
Formula	$C_{30}H_{24}AsMnO_{10}$
M	674.35
Crystal system	triclinic
Space group	*P*-1
a, Å	9.8890(8)
b, Å	10.3410(13)
c, Å	14.136(2)
α, deg	85.499(4)
β, deg	84.737(6)
γ, deg	89.975(7)
V, $Å^3$	1435.0(3)
Z	2
T, K	293(2)
ρ_{calc} (Mg m^{-3})	1.561
F(000)	684
λ (Mo-Kα Å)	0.71073
μ (Mo-Kα, mm^{-1})	1.662
Number parameters/restrains	382 / 0
Goodness of fit (*S*)	1.117
R1, $I > 2\sigma(I)$ (all)	0.090 (0.150)
wR2, $I > 2s(I)$ (all)	0.205 (0.255)
Max/min electron density (e/$Å^3$)	0.843 / -0.806
Measured reflections (R_{int})	11083 (0.074)
Independent reflections [$I > 2\sigma(I)$]	5426 (3526)

Results and discussion

Description of the structure of $AsPh_4[Mn(mal)_2(H_2O)_2]$ (2)

The solid state structure of **2** comprises *trans*-diaquabis(malonato)manganese(III) anions and tetraphenylarsonium cations which are linked through electrostatic forces, hydrogen bonds and van der Waals interactions. Two crystallographycally independent manganese(III) units [Mn(1) and Mn(2)] occur in **2** (see Figure 1), the manganese atoms being located on crystallographic inversion centers. The manganese atoms are six-coordinated with four coplanar oxygen atoms from two bidentate malonate ligands in the equatorial plane [Mn-O(mal) bond distances being 1.927 and 1.909 Å for Mn(1) and Mn(2), respectively], whereas the axial positions are filled by two water molecules [2.245(6) and 2.268(6) Å for Mn(1)-O(1w) and Mn(2)-O(2w), respectively]. The resulting MnO_6 elongated octahedron has geometric values $\phi = 55.88$ and $s/h = 1.341$ at Mn(1) and $\phi = 55.57$ and $s/h = 1.361$ at Mn(2), ϕ and s/h being the twist angle and the compression ratio, respectively [Stiefel E.I. *et al.*, 1972].

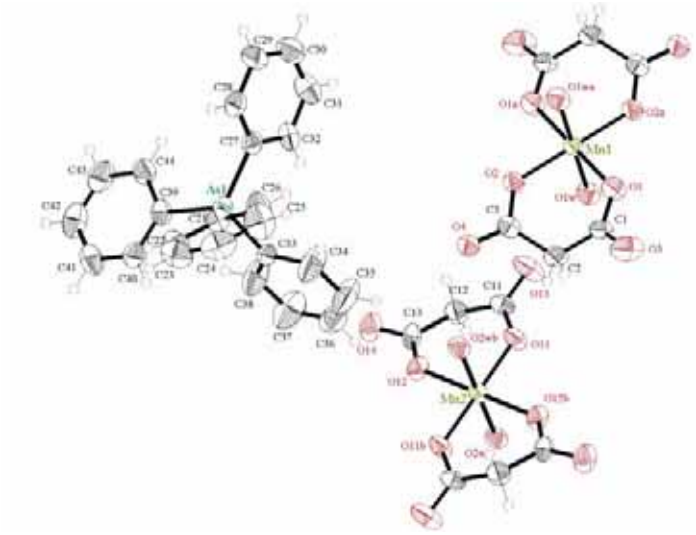

Figure 1. Perspective view showing the two crystallographycally independent metal ions [Mn(1), Mn(2)] and the $AsPh_4^+$ cation in **2**. Thermal ellipsoids are drawn at the 50% probability level.

The values of the average Mn-O(malonate) bonds of **2** agree with that observed in the related mononuclear compound $K[Mn(mal)_2(H_2O)_2] \cdot 2H_2O$ (1.90 Å) [Lis T. *et al.*, 1979]. As far as for the values of 2.245(6) and 2.268(6) Å for the Mn-Ow bond distance in **2**, they are rather long for coordinated water indicating that this bond is quite weak. However, they compare well with the vaue of 2.30 A reported for this bond in the

compound $K[Mn(mal)_2(H_2O)_2] \cdot 2H_2O$ [Lis T. *et al.*, 1979]. It deserves to be noted that such marked axial elongations are typical of high-spin d^4 systems.

Table 2 Selected bond lengths (Å) and angles (º) for compound **2**[a]

Mn(1)-O(1)	1.923(6)	Mn(2)-O(11)	1.894(6)
Mn(1)-O(2)	1.932(6)	Mn(2)-O(12)	1.925(6)
Mn(1)-O(1w)	2.245(6)	Mn(2)-O(2w)	2.268(6)
O(1)-Mn(1)-O(2)	91.7(3)	O(11)-Mn(2)-O(12)	91.5(3)
O(1)-Mn(1)-O(2a)	88.3(3)	O(11)-Mn(2)-O(12b)	88.5(3)
O(1)-Mn(1)-O(1w)	90.9(2)	O(11)-Mn(2)-O(2w)	89.5(2)
O(1)-Mn(1)-O(1wa)	89.1(2)	O(11)-Mn(2)-O(2wb)	90.5(2)
O(2)-Mn(1)-O(1w)	93.1(2)	O(12)-Mn(2)-O(2w)	88.7(2)
O(2)-Mn(1)-O(1wa)	86.9(2)	O(12)-Mn(2)-O(2wb)	91.3(2)

[a] Symmetry codes: (a) *-x, -y, -z*; (b) *-x+1, -y+1, -z*.

Two crystallographycally independent malonate ions are present in **2**. They act as bidentate ligands towards the manganese(III) ions, the values of the angles subtended at the metal atom being 91.7(3) [O(1)-Mn(1)-O(2)] and 91.5(3)º [O(11)-Mn(1)-O(12)]. Each malonate ligand exhibits a twist-boat conformation [Cremer D. *et al.*, 1975]. The values of the C-C [1.488(13)-1.518(13) Å] and C-O [1.219(10)-1.289(10) Å] malonate bond distances and O-C-O [118.3(8)-121.2(9)º] bond angles agree well with those previously reported for the malonic acid [Goedkoop J.A. *et al.*, 1957] and other malonate-containing metal complexes [see malonate-containing complexes in the Thesis Introduction; Lis T. *et al.*, 1979]. The $[Mn^{III}(mal)_2(H_2O)_2]^-$ units are linked through hydrogen-bonds involving the free malonate-oxygen atoms and the coordinated water molecules (see Table 3), leading to a quasi square two-dimensional anionic network in the *ab* plane (see Figure 2). The shortest manganese···manganese intralayer distances are 7.1557(7) [Mn(1)···Mn(2)], 7.1526(7) [Mn(1)···Mn(2e); (e) *x*-1, *y*, *z*], 9.8890(8) [Mn(1)···Mn(1f); (f) *x*, *y*+1, *z*] and 10.3410(13) Å [Mn(2)···Mn(2e)].

Table 3 Relevant hydrogen-bond distances for compound **2**

D-H···A	D···A (Å)
O(1w)-H···O(13)	2.634(10)
O(1w)-H···O(14c)	2.753(9)
O(2w)-H···O(3d)	2.672(9)
O(2w)-H···O(4)	2.760(9)

[a] Symmetry code: (c) *–x+1, -y, -z*; (d) *–x+1, -y+1, -z*

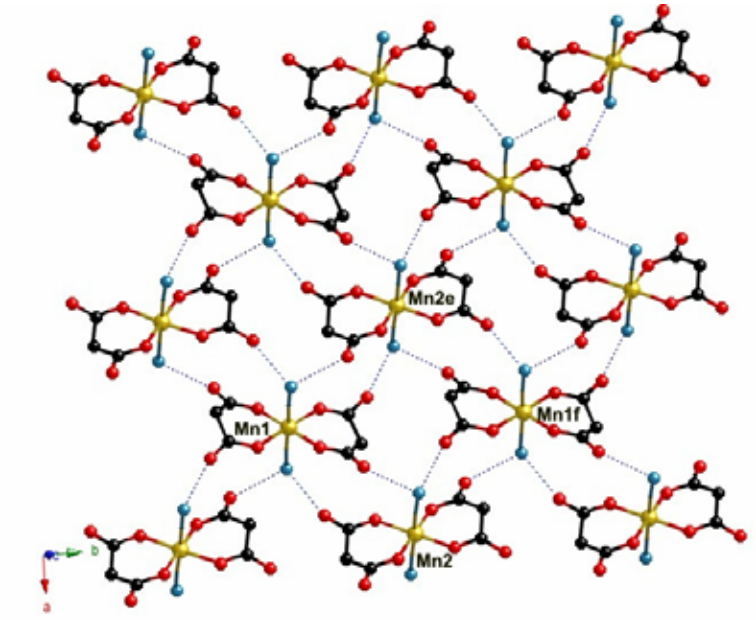

Figure 2. Perspective view of the manganese(III) malonato-bridged layer of **2** growing in the *ab* plane. Hydrogens bonds are drawn as blue broken lines.

The $AsPh_4^+$ cations exhibit the expected tetrahedral shape with average As-C bond distance of 1.917(9) Å and average C-As-C bond angle of 109.4(4)º. Its bond distances and angles are in agreement with those observed in previous $AsPh_4^+$-containing compounds [Baldas J. et al. 1988; Vicente R. et al. 1987; Grenz R. et al. 1986; Muñoz M.C. *et al.*, 1998; De Munno G. *et al.* 1999; Marinescu G. *et al.*, 2000; Lescouëzec R. *et al.*, 2001]. Mutilple phenyl embraces involving $AsPh_4^+$ lead to a two-dimensional cationic network (see Figure 3). Interestingly, alternating sextuple (SPE) and double phenyl embraces (DPE) [Dance I. *et al.*, 1996 and 1998] between $AsPh_4^+$ cations occur along the *a* and *b* axis, the arsonium-arsonium distances involved being 6.4369(15) [(SPE):As(1)···As(1g); (g) -*x*+1, -*y*, -*z*+1], 8.6321(15) [(DPE) along the *a*-axis: As(1)···As(1h); (h) –*x*, -*y*, -*z*+1], 7.5371(15) Å [(DPE) along the *b*-axis: As(1)···As(1i); (i) –*x*+1, -*y*+1, -*z*+1]. In the case of double phenyl embrace where the offset face-to-face interaction occurs between two phenyl rings of two adjacent cations, the interplanar distances are 3.961(13) (along the *a*-axis) and 4.95(2) Å (along the *b* axis). Regular alternating of anionic and cationic layers occur along the *c* axis, as shown in Figure 4. Weak hydrogen bonds involving aromatic C-H groups and oxygen atoms from malonate or water molecules lead to a three-dimensional network, the relevant C-H···O interactions being listed in Table 4.

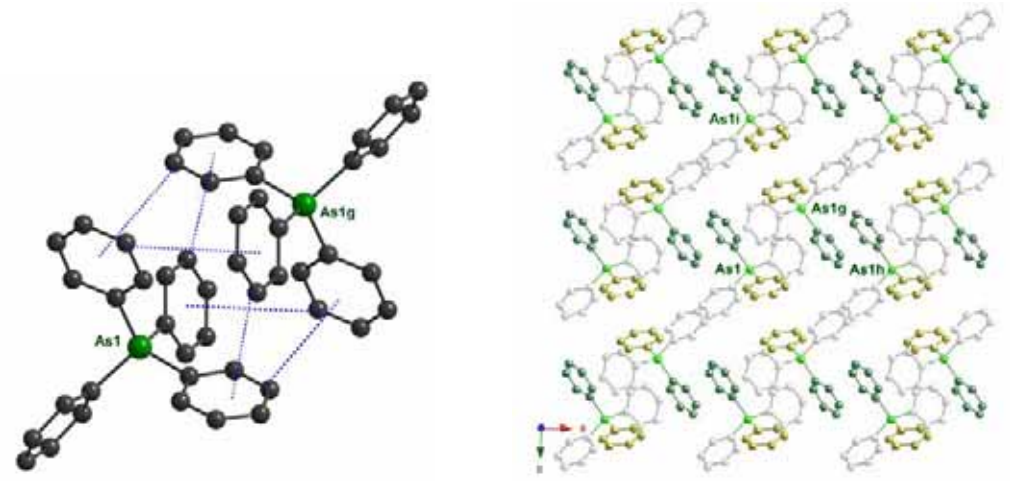

(a) **(b)**

Figure 3. (a) Perpective view of the sextuple phenyl embrace between $AsPh_4^+$ groups. **(b)** Perspective view of a $AsPh_4^+$ layer of **2** growing in the a*b* plane, showing the multiple phenyl embrace. Double phenyl embraces (DPE) along *a* (green rings) and *b-axis* (yellow rings) between $AsPh_4^+$ cations are shown.

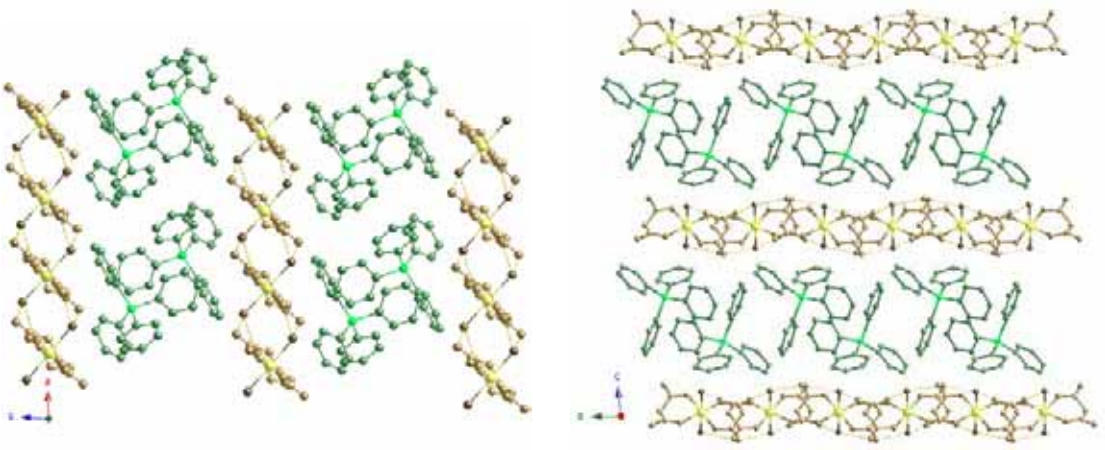

(a) **(b)**

Figure 4. (a) Perspective view of the stacking of the manganese(III) malonato-bridged anionic (yellow) and $AsPh_4^+$ cationic layers (green) of **2** along *a-axis*. **(b)** Perspective view of the stacking of the anionic (yellow) and cationic layers (green) of **2** along *b-axis*. Hydrogen bonds are drawn as yellow broken lines.

Table 4 Weak hydrogen bonds involving C-aromatic and oxygen atoms for **2**[a]

D–H···A	D···A	∠D–H···A	Symmetry Operator[b]
C(22)–H(22)···O(11)	3.506(12)	141.3(6)	*x*, *y*, *z*+1
C(23)–H(23)···O(12)	3.418(14)	141.3(7)	-*x*+1, -*y*+1, -*z*+1
C(23)–H(23)···O(14)	3.537(14)	138.2(7)	-*x*+1,-*y*+1,-*z*+1
C(24)–H(24)···O(4)	3.564(14)	169.0(8)	-*x*, -*y*+1, -*z*+1
C(28)–H(28)···O(1w)	3.227(13)	137.6(6)	*x*, *y*, *z*+1
C(29)–H(29)···O(4)	3.623(14)	177.4(8)	-*x*, -*y*, -*z*+1
C(29)–H(29)···O(2)	3.635(14)	135.7(8)	-*x*, -*y*, -*z*+1
C(35)–H(35)···O(2w)	3.394(15)	132.9(8)	*x*, *y*, *z*
C(36)–H(36)···O(12)	3.317(13)	154.5(8)	*x*, *y*, *z*
C(42)–H(42)···O(1)	3.560(14)	135.7(7)	*x*+1, *y*, *z*+1

C(42)–H(42)···O(2)	3.357(13)	154.7(7)	-*x*+1, -*y*, -*z*+1
C(43)–H(43)···O(4)	3.469(14)	140.2(8)	-*x*+1, -*y*, -*z*+1
C(44)–H(44)···O(14)	3.543(12)	122.1(6)	-*x*+1, -*y*, -*z*+1

[a] D = donor and A = acceptor; values of D···A and ∠D-H···A in Å and degrees, respectively. [b] Symmetry operators appy to acceptor atoms.

We would like to finish this structural discussion by recalling the structure of $K_2[Mn(mal)_2(MeOH)_2][Mn(mal)_2]$ (**3**) [Kirk M. *et al.*, 1991] and comparing it with that of **2** The structure of **3** is made up of chains of regular alternating $[Mn(mal)_2(MeOH)_2]$ and $[Mn(mal)_2]$ units, bridged by *anti-syn* carboxylate-malonate groups, that are connected together by means of potassium atoms (see Figure 5). Two crystallographically independent manganese(III) atoms are present in **3**, the manganese atoms being located on a crystallographic inversion center. Both metal atoms are six-coordinated and they exhibit a slightly distorted 4+2 elongated octahedron. Four oxygen atoms from two bidentate malonate ions [the bite angle at the metal atom is 91.5(2)º] conform the equatorial plane around Mn(1) [the Mn(1)-O(equatorial) bond distances are 1.901(5) and 1.913(5) Å], the apical positions being occupied by two malonate oxygen atoms [the Mn(1)-O(apical) bond distance being 2.262(5) Å]. Mn(2) is bound to four oxygen atoms from two bidentate malonate groups [bite angle = 92.1(2)º] in the equatorial plane [the Mn(2)-O(equatorial) bond distances are 1.901(4) and 1.918(5) Å], and to two oxygen atoms from two methanol molecules [the Mn(2)-O(MeOH) bond length being 2.203(7) Å]. The potassium atom is bound to six carboxylate-oxygen atoms from six different malonate groups [the K-O bond lengths ranging from 2.714(5) to 2.904(5) Å]. It exhibits a highly distorted octahedral environment the maximum deviations from the ideal value of 90º being 55.3 and 116.5º.

The $[Mn(mal)_2(MeOH)_2]^-$ and $[Mn(mal)_2]^-$ units are bridged by *anti-syn* carboxylate groups (Figure 5a) which involve an apical oxygen atom at Mn(1) and an equatorial one at Mn(2) affording an alternating manganese(III) chain which grows along the [110] direction. These units are further connected through O-K-O bridges (see bronze broken lines in Figure 5) and hydrogen bonds involving the hydroxyl group of the methanol molecule and the malonate oxygen atoms. The intrachain Mn(1)···Mn(2) separation through the carboxylate-malonate group is 5.501 Å and the dihedral angle between the adjacent mean equatorial planes is 49.4º. The manganese(III) chains are held together by means of potassium cations. Each chain is connected to nine adjacent ones through O-K-O bridges (see purple broken lines in Figure 5b) leading to a three-dimensional network. The shortest interchain Mn···Mn separation being 6.552 and 8.562

Å for Mn(1)···Mn(2a) and Mn(1)···Mn(2b), respectively [(a) *x*+1, *y*, *z*; (b) *x*, *y*, *z*+1]. Additional weak C-H···O interactions involving the methyl groups of the methanol molecule and the carboxylate oxygen atoms contribute to stabilize the whole structure.

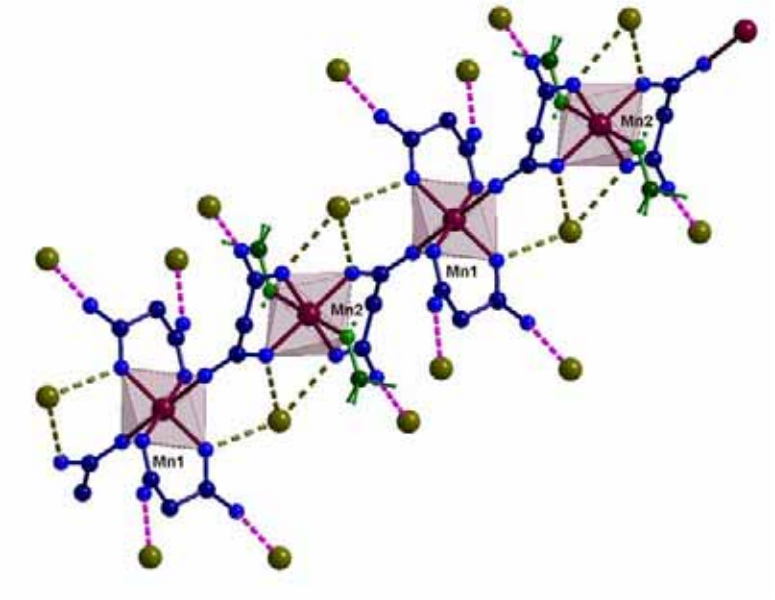

(a)

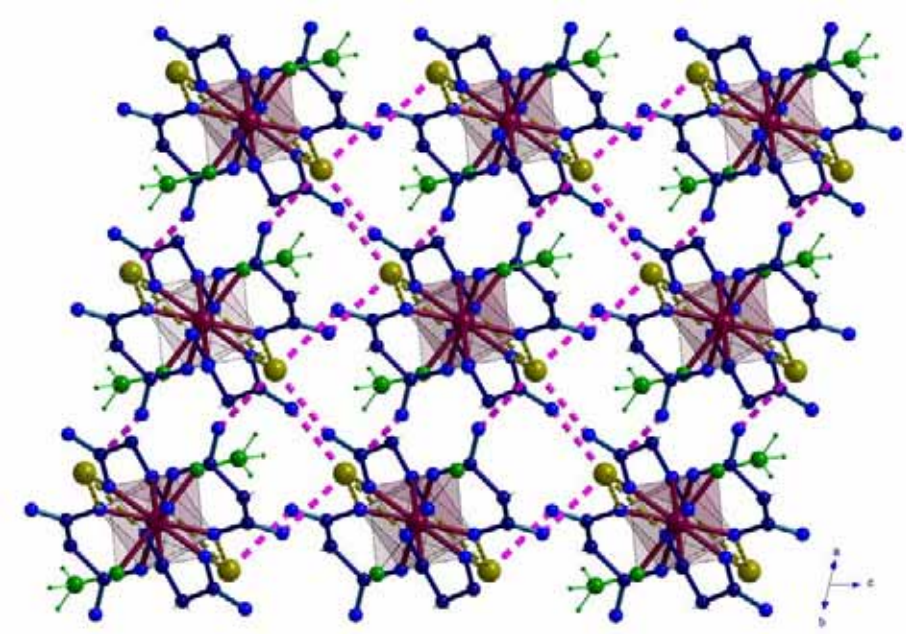

(b)

Figure 5. (a) Perspective view of a fragment of the alternating carboxylate-malonate bridged manganese(III) chain growing along the [110] direction. **(b)** Perspective view of the arrangement of the manganese(III) chains and the potassium cations.. Bronze and purple broken lines represent the intra- and interchain O-K-O bridging units.

In contrast to **2**, where the $[Mn(III)(mal)_2](H_2O)_2]^-$ units are connected by hydrogen bonds involving the water molecules and the uncoordinated malonate-

oxygens to create quasi square layer of manganese(III) ions, the $[Mn(III)(mal)_2](CH_3OH)_2]^-$ entities in **3** are linked to the $[Mn(III)(mal)_2]^-$ units through *anti-syn* carboxylate bridges affording chains. The main difference between **2** and **3** is the character and the size of the counterion present in both compounds. In **2,** the hydrophobic and aromatic character of the $AsPh_4^+$ cation are at the origin of the two-dimensional structure with alternating hydrophobic and hydrophilic units. As described above for **2**, the cationic and anionic layers are connected through weak C-H···O(malonate) interactions. The bulky $AsPh_4^+$ group keeps away the manganese(III) units of adjacent layers. The smaller size of the potassium cation and its ability to coordinate the oxygen atoms, make closer the $[Mn(III)(mal)_2]^+$ units.

Magnetic properties

The magnetic properties of the complexes **1-3** are shown in Figures 6-8 under the form of $\chi_M T$ versus T plot [χ_M is the magnetic susceptibility per Mn(III) ion]. The values $\chi_M T$ at 300 K are 2.93 (**1**), 2.95 (**2**) and 3.0 $cm^3\ mol^{-1}\ K$ (**3**). They are in agreement for the spin-only value of a magnetically isolated high-spin d^4 ion [$\chi_M T$ = 3.0 $cm^3\ mol^{-1}\ K$ with g = 2.0]. Upon cooling, $\chi_M T$ for **1** smoothly increases to reach a maximum value of *ca.* 2.97 $cm^3\ mol^{-1}\ K$ at 17 K, then it decreases to a minimum of 2.85 $cm^3\ mol^{-1}\ K$ at 4.5 K and it increases further to 3.12 $cm^3\ mol^{-1}\ K$ at 1.9 K. In the case of **2**, the value of $\chi_M T$ remains practically constant from room temperature to 30 K, then it decreases to reach a minimum of *ca.* 2.76 $cm^3\ mol^{-1}\ K$ at 4.0 K and it increases further to 2.95 $cm^3\ mol^{-1}\ K$ at 1.9 K. finally, in the case of **3**, a Curie law behaviour is observed from room temperature to 90 K followed by a sharp decrease of $\chi_M T$ alt lower temperatures to reach 1.4 $cm^3\ mol^{-1}\ K$ at 1.9 K. The magnetic plots of **1** and **2** are as expected for the coexistence of large single-ion zero-field splitting effects (D) and ferromagnetic coupling whereas in the case of **3**, the significant reduction of $\chi_M T$ at $T < 90$ K is attributed to the simultaneous occurrence of D and antiferromagnetic interactions. An inspection of the M versus H plot at 2.0 K for **2** and **3** (see inset of Figure 8) supports the occurrence of a weak ferromagnetic interaction in **2** given that its magnetization data are well above those of **3**. No susceptibility maximum is observed in the magnetic plots of **1-3** in the temperature range explored. Finally, the lack of ac signals for **1-3** down to 1.9 K reveals the absence of magnetic ordering in this series.

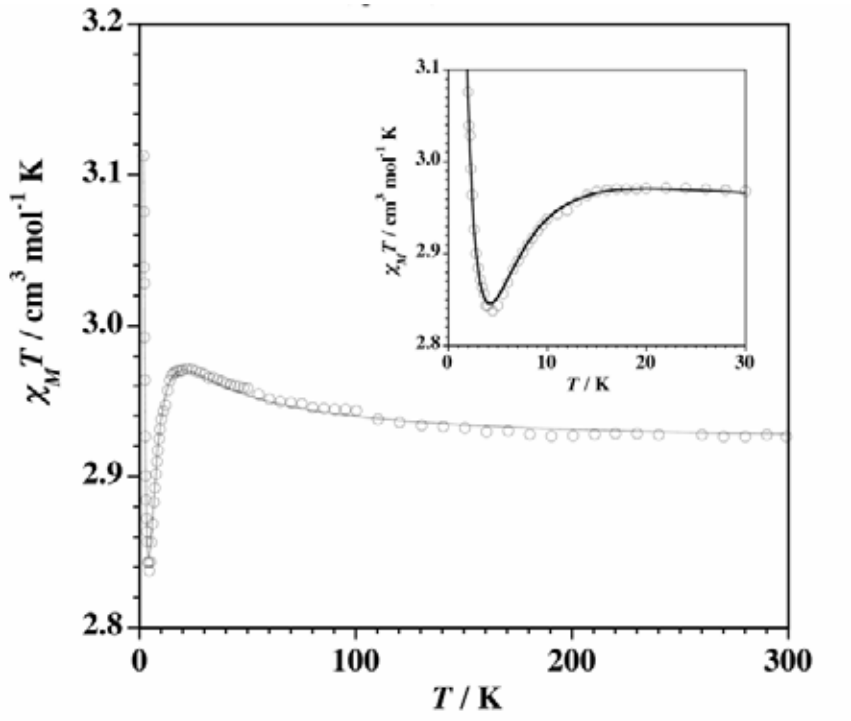

Figure 6. Thermal dependence of the $\chi_M T$ product for complex **1**: (O) experimental data; (–) best-fit curve (see text). The inset shows the low temperature region in detail.

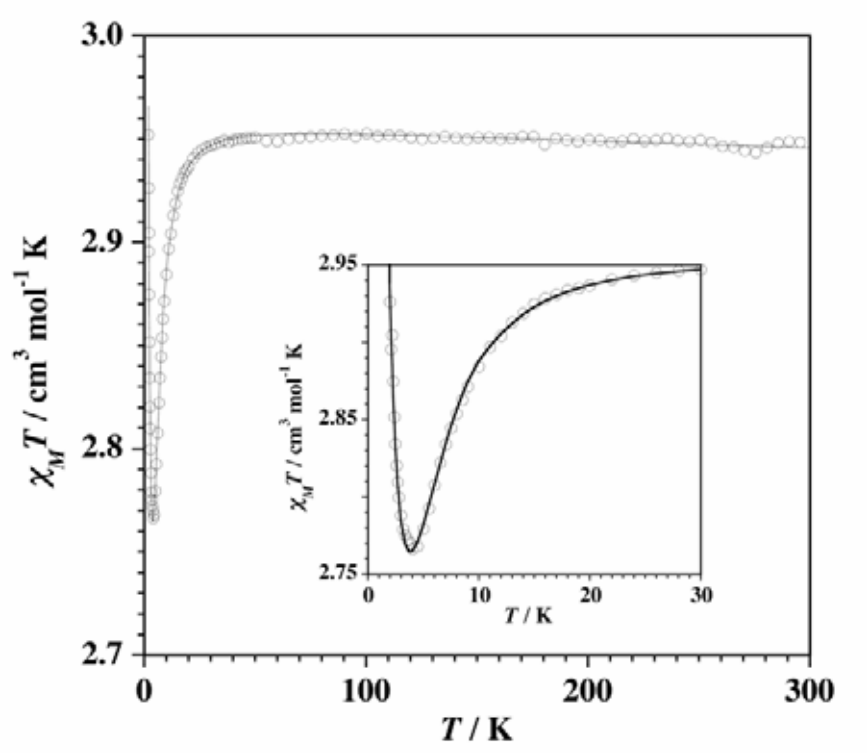

Figure 7. Thermal dependence of the $\chi_M T$ product for complex **2**: (O) experimental data; (–) best-fit curve (see text). The inset shows the low temperature region in detail.

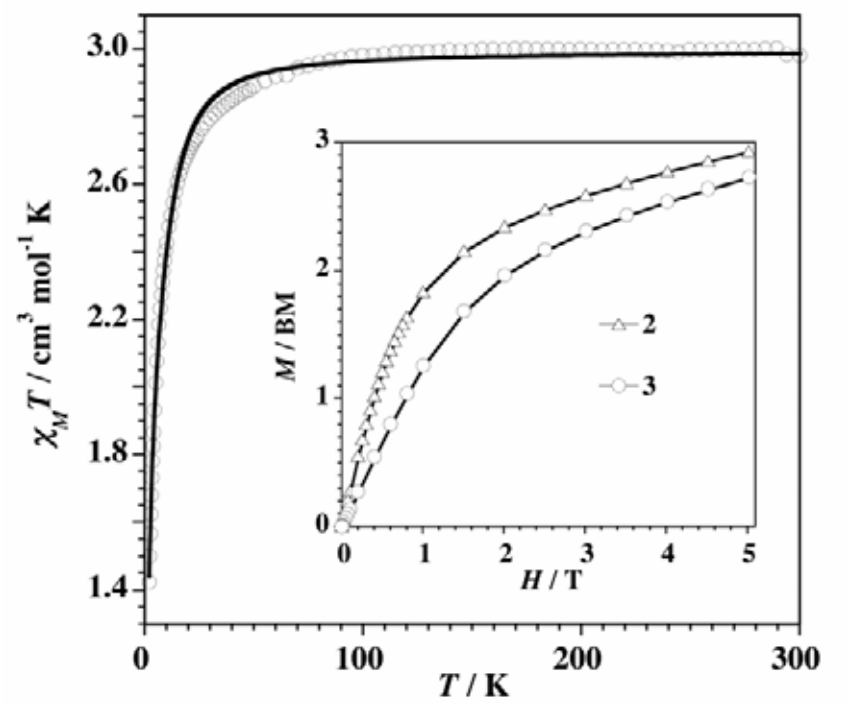

Figure 8. Thermal dependence of the $\chi_M T$ product for complex **3**: (O) experimental data; (—) best-fit curve (see text). The inset shows the magnetization versus *H* plot at 2.0 K for **3** (O) and **2** (Δ). The solid line is an eye-guide line.

The analysis of the magnetic behaviour of complexes containing high-spin Mn(III) centers (d^4 ions) in a magnetic field is quite complex due to the different numbers of parameters involved namely, the exchange interaction, low-symmetry ligand fields, *g*-tensor anisotropy and the Jahn-Teller effect. The appropriate Hamiltonian to account for all these factors is given by eq (1)

$$\mathrm{H} = D\sum_{i=1}^{N}\left[S_{iz}^2 - 1/3S(S+1)\right] + E\sum_{i=1}^{N}\left[S_{ix}^2 - S_{iy}^2\right] - J\sum_{i=1}^{N}\left[S_i S_{i+1}\right] + g_{\|}\beta\sum_{i=1}^{N} S_z H_z + g_{\perp}\beta\sum_{i=1}^{N}\left(S_x H_x + S_y H_y\right)$$

eq (1)

where *D*, *E*, $g_{\|}$ and $g_{\perp}$ apply for each ion. The application of this Hamiltonian becomes very complicated because of the large number of parameters involved. As the dependence of the magnetic susceptibility on the rhombic splitting parameter (*E*) is negligible, this term was discarded. In addition, we considered that *D*, $g_{//}$ and $g_{\perp}$ are the same for the two manganese sites in **2** and **3** (and also in **1** whose structure most likely is like that of **2**). Under these assumptions, the number of parameters is reduced to a reasonable size.

Taking into account that the size of local interacting spins in **1**-**3** (S = 2) is large enough to be considered as classical and that we are dealing with a uniform chain

(compound **3**) and quasi quadratic layers (compounds **1** and **2**), eqns (2) and (3), which were derived by Fisher [Fisher M.E., 1964] and Curély [Curély J., 1995 and 1998] for isotropic Heisenberg systems, can be used to analyze their magnetic properties:

$$\chi_{chain} = \frac{N\beta^2 g^2}{3kT} S(S+1) \frac{1+u}{1-u} \qquad \text{eq (2)}$$

$$\chi_{2Dsquare} = \frac{N\beta^2}{3kT} S(S+1) \frac{(g_1^2 + g_2^2)W_1 + 2g_1 g_2 W_2}{2(1-u_1^2)(1-u_2^2)} \qquad \text{eq (3)}$$

where

$$W_1 = (1+u_1^2)(1+u_2^2) + 4u_1u_2$$

$$W_2 = 2u_1(1+u_2^2) + 2u_2(1+u_1^2)$$

and

$$u_i = \coth\left[\frac{J_i S(S+1)}{kT}\right] - \frac{kT}{J_i S(S+1)}$$

As the for the inclusion of the zero-field splitting is concerned, its influence on the on the powder susceptibility measurements is expressed by eqns (4)-(6)

$$\chi_{\parallel} = \frac{2N\beta^2 g_{\parallel}^2}{kT} \frac{\exp(-D/kT) + 4\exp(-4D/kT)}{1 + 2\exp(-D/kT) + 2\exp(-4D/kT)} \qquad \text{eq (4)}$$

$$\chi_{\perp} = \frac{2N\beta^2 g_{\perp}^2}{3D} \frac{9 - 7\exp(-D/kT) - 2\exp(-4D/kT)}{1 + 2\exp(-D/kT) + 2\exp(-4D/kT)} \qquad \text{eqn (5)}$$

$$\chi_{ZFS} = \frac{\chi_{\parallel} + 2\chi_{\perp}}{3} \qquad \text{eqn (5)}$$

Keeping in mind that the magnetic plots in **1**-**3** are dominated by *D* [the ferro- (**1** and **2**) and antiferromagnetic (**3**) interactions are predicted to be very weak in the light of their structures and shape of their magnetic plots], a perturbational approach [Lloret F. *et al.*, 1992; Rodríguez-Martín Y. *et al.*, 2001] would be a suitable model to analyze their magnetic data [eqns (6) and (7)].

$$\chi_{comp(1)} = \chi_{ZFS} \frac{1+u}{1-u} \qquad \text{eq (6)}$$

$$\chi_{comp(2,3)} = \chi_{ZFS} \frac{(g_1^2 + g_2^2)W_1 + 2g_1 g_2 W_2}{2(1-u_1^2)(1-u_2^2)} \quad \text{with } g_1 = g_2 \text{ and } u_1 = u_2 \qquad \text{eq (7)}$$

So, the magnetic behavior of **1**-**3** which is dictated by the dominant *D* factor is slightly perturbed by the weak magnetic interactions observed in the very low temperature region. Best-fit parameters through eqns (7) (**1** and **2**) and (6) (**3**) are: D = -3.91 cm^{-1}, J = +0.081 cm^{-1} and g = 1.98 for **1**, D = -3.96 cm^{-1}, J = +0.072 cm^{-1} and g = 1.99 for **2** and D = -5.90 cm^{-1}, J = -0.14 cm^{-1} and g = 1.98 for **3**. As seen in Figures 6-8, a satisfactory match is obtained between the magnetic data and the theoretical curve in the whole temperature range explored.

Analyse of the Echange Pathways in 2 and 3.

In order to substantiate the magnetic interactions between manganese(III) ions in **2** and **3** and to get an orbital picture of the exchange pathways involved in them, we have performed DFT type calculations on two model fragments whose structural parameters were taken from the respective crystal structures: a dinuclear unit of the chain structure of **3** [Figure 9(a)] and a trinuclear manganese(III) entity corresponding to the two edges of the quasi squares units of the anionic layers of **2** [Figure 9(b)].

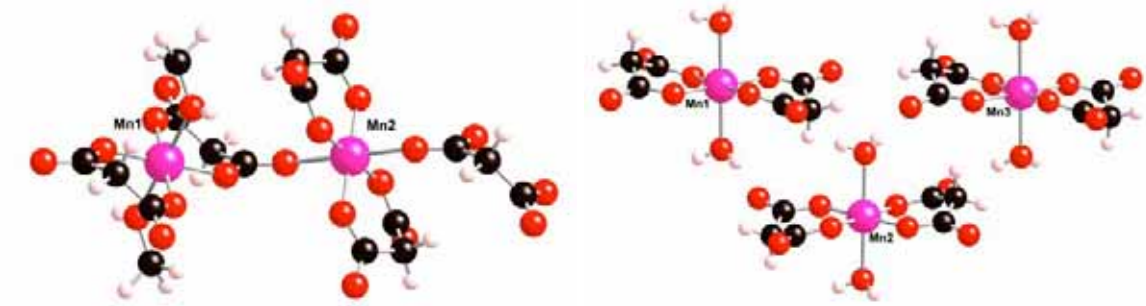

(a) **(b)**

Figure 9. Structural models used in the DFT calculations concerning compounds **3** **(a)** and **2** **(b)**. Bond lengths and angles of the models are those of the corresponding crystal structures.

Let us start the analysis with compound **3** for the sake of simplicity. This compound can be considered as a one-dimensional system where two crystallographically independent manganese(III) ions are connected in a regular way by a carboxylate group of a malonate ligand which exhibis the *anti-syn* briging mode. A nonet A (2,2) and broken-symmetry singlet B (2,-2) spin configurations were calculated [A and B being defined as ($M_{S\ Mn1}$, $M_{S\ Mn2}$)]. From the energies of these configurations and eq (8), we have evaluated the exchange coupling constant between the

manganese(III) ions in **3** which is J = -4.7 cm^{-1}. This value has the same sign and it is not far from that obtained for **3** by fit (J = -0.14 cm^{-1}) and also for the family of the

$$E_B - E_A = -10J \qquad (8)$$

chain compounds of formula $(cat)_2[Mn^{III}(sal)_2(CH_3OH)_2]Mn^{III}(sal)_2]$ with sal = salicylate and cat = Na^+ (J = -0.46 cm^{-1}), K^+ (J = -0.46 cm^{-1}) and NH_4^+ (J = -1.40 cm^{-1}) [Kirk M.L. *et al.*, 1991], where the same type of carboxylate-malonate bridge occurs. An inspection of the magnetic orbitals involved accounts for the antiferromagnetic nature of the magnetic coupling. In fact, the manganese(III) ions in **3** (also in **2**) exhibits elongated octahedral environments with an idealized D_{4h} symmetry. Consequently, if one takes the elongation axis as the z direction, one unpaired electron is placed in the d_{z^2} orbital and the $d_{x^2-y^2}$ orbital is nonmagnetic, given that this last orbital has the highest energy. The relative orientation of the two d_{z^2} magnetic orbitals is represented in Figure 10. Although an *anti-syn* coordination topology occurs in **3** with the two metal ions and the carboxylate group being practically coplanar, the strict orthogonality is avoided because of the values of the Mn-O-C angles [127.3(5) and 137.8(5)º] [Lis T. *et al.*, 1980a]. One can see that the equatorial d_{z^2} electron density in a manganese atom and the axial d_{z^2} in the other manganese center are involved in the exchange pathway; so, a small overlap between the two magnetic orbitals through the carboxylate-malonate bridge is predicted and a weak antiferromagnetic interaction is expected, as observed. Indeed, the small magnitude of the magnetic interaction is also related to the weak spin delocalization observed in the atomic spin densities [3.98 electron units for the manganese(III) ion].

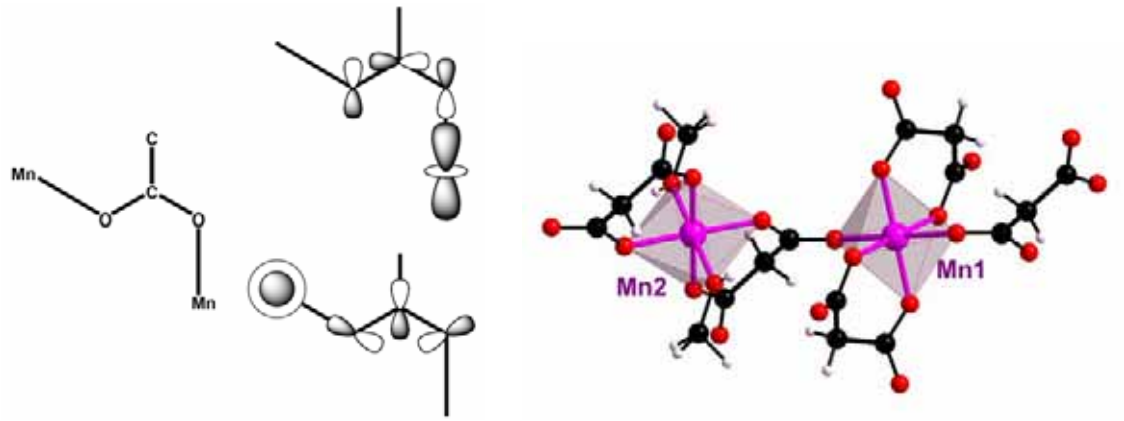

Figure 10. Schematic drawing showing the orientation of the d_{z^2} type magnetic orbitals in the dinuclear fragment of compound 3 [model Figure 9a].

The hydrogen bonds between the mononuclear $[Mn^{III}(mal)_2(H_2O)_2]^-$ units in **2** have to be responsible for the ferromagnetic coupling it exhibits. Recently, Desplanches *et al.* have shown that the hydrogen-bonds can mediate weak magnetic interactions in metal complexes [Desplanches E. *et al.*, 2002]. As described in the structural part, the $[Mn^{III}(mal)_2(H_2O)_2]^-$ units in **2** are linked by hydrogen bonds to form an anionic quasi quadratic layer of manganese(III) ions (Figure 2) with two intralayer magnetic interactions noted J_1 [between Mn(1) and Mn(2)] and J_2 [between Mn(1) and Mn(2e)]. These layers are well separated from each other by the bulky tetraphenylarsonium cations (Figure 4). The only intralayer exchange pathway occurring in **2** involves the axially coordinated water molecule of one manganese unit and a carboxylate-malonate fron the neighboring unit. Two of these pathways connect each pair of manganese(III) ions. Small structural differences in them lead to an alternating character of the network. So, in the model used for **2** three metal ions and two exchange coupling constants have been considered [Figure 9(b)]. Using the equations (9) and (10) applied to the energy obtained for the configurations C (2,2,2), D (-2,2,2) and F (2,2,-2) [C, D and E being defined as ($M_{S\ Mn1}$, $M_{S\ Mn2}$, $M_{S\ Mn3}$)], we have obtained the values +0.04 and +0.02 cm^{-1} for J_1 and J_2 respectively. So,

$$E_D - E_C = -10J_1 \qquad (2)$$

$$E_F - E_C = -10J_2 \qquad (3)$$

a weak ferromagnetic interactions between the metal ions are obtained by DFT calculations whose values are close to mean value obtained by fit.

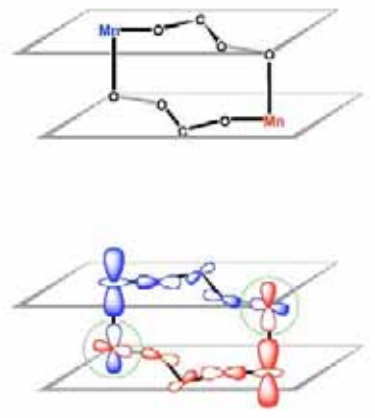

Figure 11. (Top) Schematic drawing of a $Mn(OCO^{\cdots}Ow)_2Mn$ couple in **2**. (Bottom) Orbital picture of the exchange pathway in **2**.

A close inspection of of the dinuclear fragment Mn-$(OCO\cdots O_w)_2$Mn of **2** depicted on the top of Fig. 11 shows that the two Mn-$OCO\cdots O_w$ units are in parallel planes, the axial Mn-O_w bonds being quasi perpendicular to these planes. The corresponding orbital picture is shown in the bottom of Figure 11. One can see there that the spin density in the ring of d_z^2 orbital leads to a delocalization via σ exchange pathway of carboxylate (blue), while the axial spin density in the same orbital involves a delocalization via π exchange pathway (red). This situation corresponds to a orthogonality case and consequently, a ferromagnetic coupling is predicted, as observed.

References

Albela B., Corbella M., Ribas J., Castro I., Sletten J. and Stoeckli-Evans H., *Inorg. Chem.*, **1998**, 37, 788.

Bacskay G. B., *Chem. Phys.* **1981**, 61, 385.

Baldas J., Colmanet S.F. and Mackay M.F., *J. Chem. Soc., Dalton Trans.* **1988**, 1725.

Barra A.L., Gatteschi D. and Sessoli R., *Phys. Rev.*, **1997**, B56, 8192.

Becke A.D., *Phys. Rev. A*, **1988**, 38, 3098.

Becke A.D., *J. Chem. Phys.*, **1993**, 98, 5648.

Cano J., De Munno G., Sanz J., Ruiz R., Lloret F., Faus J. and Julve M., *J. Chem. Soc., Dalton Trans.*, **1994**, 3465.

Cano J., Alemany P., Alvarez S., Verdaguer M. and Ruiz E., *Chem. Eur. J.*, **1998**, 4, 476.

Cano J., Ruiz E., Alemany P., Lloret F. and Alvarez S., *J. Chem. Soc., Dalton Trans.*, **1999**, 1669.

Carpenter J.E. and Weinhold F., *J. Mol. Struct. (TEOCHEM)*, **1988**, 169, 41.

Cartledge G.H. and Nichols P.M., *J. Am. Chem. Soc.*, **1940**, 62, 3057.

Christou G., *Acc. Chem. Res.*, **1989**, 22, 328.

Cremer D. and Pople J.A., *J. Am. Chem. Soc.*, **1975**, 97, 1354.

CRYSTAL MAKER 4.2.1., Crystalmaker Sofware., P.O. Box 183, Bicester, Oxfordside, OX26 3TA, UK, **2001**.

Curély J., *Europhys. Lett.*, **1995**, 32, 529.

Curély J., *Physica B*, **1998**, 245, 263.

Dance I. and Scudder M., *J. Chem. Soc., Dalton Trans.*, **1998**, 1341.

Dance I. and Scudder M., *Chem. Eur. J.*, **1996**, 2, 481.

De Munno G., Armentano D., Julve M., Lloret F., Lescouëzec R. and Faus J., *Inorg. Chem.*, **1999**, 38, 2234.

Deguenon D., Bernardelli G., Tuchagues J.P. and Castan P., *Inorg. Chem.*, **1990**, 29, 3031.

Desplanches E., Ruiz E., Rodriguez-Fortea A. and Alvarez S., *J. Am. Chem. Soc.*, **2002**, 124, 5197.

DIAMOND 2.1d, Crystal Impact GbR, CRYSTAL IMPACT, K. Brandenburg & H. Putz GbR, Postfach 1251, D-53002 Bonn, Germany, **2000**.

Earnshaw, A. *Introduction to Magnetochemistry*, Academic Press, London and New York, **1968**.

Farrugia L.J., WINGX, *J. Appl. Cryst*, **1999**, 32, 837.

Fisher M.E., *Am. J. Phys.*, **1964**, 32, 343.

Gatteschi D. and Sessoli R., *Angew. Chem. Int. Ed.*, **2003**, 42, 269.

GAUSSIAN 03, Revision C.02.: Frisch M.J., Trucks G.W., Schlegel H.B., Scuseria G.E., Robb M.A., Cheeseman J.R., Montgomery J.A., Vreven Jr.T., Kudin K.N., Burant J.C., Millam J.M., Iyengar S.S., Tomasi J., Barone V., Mennucci B., Cossi M., Scalmani G., Rega N., Petersson G.A., Nakatsuji H., Hada M., Ehara M., Toyota K., Fukuda R., Hasegawa J., Ishida M., Nakajima T., Honda Y., Kitao O., Nakai H., Klene M., Li X., Knox J.E., Hratchian H.P., Cross J.B., Bakken V., Adamo C., Jaramillo J., Gomperts R., Stratmann R.E., Yazyev O., Austin A.J., Cammi R., Pomelli C., Ochterski J.W., Ayala P.Y., Morokuma K., Voth G.A., Salvador P., Dannenberg J.J., Zakrzewski V.G., Dapprich S., Daniels A.D., Strain M.C., Farkas O., Malick D.K., Rabuck A.D., Raghavachari K., Foresman J.B., Ortiz J.V., Cui Q., Baboul A.G., Clifford S., Cioslowski J., Stefanov B.B., Liu G., Liashenko A., Piskorz P., Komaromi I., Martin R.L., Fox D.J., Keith T., Al-Laham M.A., Peng C.Y., Nanayakkara A., Challacombe M., Gill P.M.W., Johnson B., Chen W., Wong M.W., González C. and Pople J.A., Gaussian, Inc., Wallingford CT, **2004**.

Glerup J., Goodson P.A., Hodgson D.J. and Michelsen K., *Inorg. Chem.*, **1995**, 34, 6255.

Goedkoop J.A. and MacGillavry C.H., *Acta Crystallogr.*, **1957**, 10, 125.

Grenz R., Götzfried F., Nagel U. and Beck W., *Chem. Ber.*, **1986**, 119, 1217.

Kahn O., *Molecular Magnetism*; VCH: New York, **1993**.

Kim Y.J. and Jung D.Y., *Inorg. Chem.*, **2000**, 39, 1470.

Kirk M.L., Lah M.S., Raptopoulou C., Kessissoglou D.P., Hatfield W.E. and Pecoraro V.L., *Inorg. Chem.*, **1991**, 30, 3900.

Lee C., Yang W. and Parr R.G., *Phys. Rev. B*, **1988**, 37, 785.

Lescouëzec R., Marinescu G., Muñoz M.C., Luneau D., Andruh M., Lloret F., Faus J., Julve M., Mata J.A., Llusar R. and Cano J., *New. J. Chem.*, **2001**, *25*, 1224.

Lis T., Matuszewski J. and Jezowska-Trzebiatowska B., *Acta Crystallogr.*, **1977**, B33, 1943.

Lis T. and Matuszewski J., *Acta Crystallogr.*, **1979**, B35, 2212.

Lis T. and Matuszewski J., *J. Chem. Soc., Dalton Trans.*, **1980a**, 996.

Lis T. and Matuszewski J., *Polish J. Chem.*, **1980b**, 54, 163.

Liu T.F., Sun H.L., Gao S., Zhang S.W. and Lau T.C., *Inorg. Chem.*, **2003**, 42, 4792.

Lloret F., Ruiz R., Julve M., Faus J., Journaux Y., Castro I. and Verdaguer M., *Chem. Mater.*, **1992**, 4, 1150.

Marinescu G., Andruh M., Lescouëzec R., Muñoz M.C., Cano J. and Lloret F., *New J. Chem.*, **2000**, 24, 527.

Ménage S., Vítols S.E., Bergerat P., Codjovi E., Kahn O., Girerd J.J., Guillot M., Solans X. and Calvet T., *Inorg. Chem.*, **1991**, 30, 2666.

Muñoz M.C., Julve M., Lloret F., Faus J. and Andruh M., *J. Chem. Soc., Dalton Trans.*, **1998**, 3125.

Nardelli M., *J. Appl. Crystallogr.*, **1995**, 28, 659.

Oldham C., In *Comprehensive Coordination Chemistry*; Wilkinson G., Gillard R.D., McCleverty J.A., Eds.; Pergamon Press: Oxford, U.K., **1987**; Vol. 2, p 435.

Pasán J., Delgado F.S., Rodríguez-Martín Y., Hernández-Molina M., Ruiz-Pérez C., Sanchiz J., Lloret F. and Julve M., *Polyhedron*, **2003a**, 22, 2143.

Pasán J., Sanchiz J., Ruiz-Pérez C., Lloret F. and Julve M., *New J. Chem.*, **2003b**, 27, 1557.

Pasán J., Sanchiz J., Ruiz-Pérez C., Lloret F. and Julve M., *Eur. J. Inorg. Chem.*, **2004**, 4081.

Pecoraro V.L., *Manganese Redox Enzymes*; Ed.VCH: New York, **1992**.

Policar C., Lambert F., Cesario M. and Morgenstern-Badarau I., *Eur. J. Inorg. Chem.*, **1999**, 2201.

Reed A.E., Curtis L.A. and Weinhold F., *Chem. Rev.* **1988**, 88, 899.

Rodríguez-Martín Y., Ruiz-Pérez C., Sanchiz J., Lloret F. and Julve M., *Inorg. Chim. Acta*, **2001**, 318, 159.

Rodríguez-Martín Y., Hernández-Molina M., Sanchiz J., Ruiz-Pérez C., Lloret F. and Julve M., *Dalton Trans.*, **2003**, 2359.

Ruiz E., Cano J., Alvarez S. and Alemany P., *J. Am. Chem. Soc.*, **1998**, 120, 11122.

Ruiz E., Cano J., Alvarez S. and Alemany P., *J. Comput. Chem.*, **1999**, 20, 1391.

Ruiz-Pérez C., Rodríguez-Martín Y., Hernández-Molina M., Delgado F.S., Pasán J., Sanchiz J., Lloret, F. and Julve M., *Polyhedron*, **2003**, 22, 2111.

Sain S., Maji T.K., Mostafa G., Lu T.H. and Chaudhuri N.R., *Inorg. Chim. Acta*, **2003a**, 351, 12.

Sain S., Maji T.K., Mostafa G., Lu T.H. and Chaudhuri N.R., *New J. Chem.*, **2003b**, 27, 185.

Schaefer A., Horn A. and Ahlrichs R., *J. Chem. Phys.*, **1992**, 97, 2571.

Schaefer A., Huber C. and Ahlrichs R., *J. Chem. Phys.*, **1994**, 100, 5829.

Sheldrick G.M., SHELX97, *Programs for Crystal Structure Analysis (Release 97-2)*, Institüt für Anorganische Chemie der Universität, Tammanstrasse 4, D-3400 Göttingen, Germany, **1998**.

Stiefel E.I. and Brown G.F., *Inorg. Chem.*, **1972**, 2, 434.

Tan X.S., Xiang D.F., Tang W.X. and Sun J., *Polyhedron*, **1997**, 16, 689.

Tangoulis V., Psomas G., Dendrinou-Samara C., Raptopoulou C.P., Terzis A. and Kessissoglou D.P., *Inorg. Chem.*, **1996**, 35, 7655.

Verdaguer M., Ph. D. Thesis, University of Orsay, France, **1984**.

Vicente R., Ribas J., Alvarez S., Seguí A., Solans X. and Verdaguer M, *Inorg. Chem.*, **1987**, 26, 4004.

Waldo G.S., Yu S. and Penner-Hahn J.E., *J. Am. Chem. Soc.* **1992**, 114, 5869.

Wei Y.G., Zhang S.W., Shao M.C., Shao M.C., Liu Q., Tang Y.Q., *Polyhedron*, **1996**, 15, 4303.

Weinhold F. and Carpenter J.E., *The Structure of Small Molecules and Ions*, Plenum,

1988, p 227.

Wieghardt K., *Angew. Chem. Int. Ed. Engl.*, **1989**, 28, 1153.

Xen X.M., Tong Y.X., Xu Z.T. and Mak T.C.W., *J. Chem. Soc., Dalton Trans.*, **1995**, 4001.

Yoo J., Yamaguchi A., Nakano M., Krzystek J., Streib W.E., Brunel L.C., Ishimoto H., Christou G. and Hendrickson D.N., *Inorg. Chem.*, **2001**, 40, 4604.

Zhang X., Lu C., Zhang Q., Lu S., Yang W., Liu J. and Zhuang H., *Eur. J. Inorg. Chem.,* **2003**, 1181.

CHAPTER XI.

The complex as precursor: Chromium(III) complexes.

Introduction

In the previous work presented in this thesis, we have shown how the malonate ion can be used to prepare and design new magnetic materials. As commented, the malonate anion is a useful tool in Materials Science (especially in Crystal Engineering and Molecular Magnetism) for the preparation of novel functional materials due to its versatility as a ligand towards metal ions to afford high-dimensional networks. It deserves to be noted that sometimes, this versatility is a problem in the design because of the difficulty to predict the coordination modes of the malonate ion in its metal complexes [especially with copper(II)] and consequently to foresee the crystal structure and, so on, the properties of these new materials.

A rational procedure which is used with other ligands such as the cyanide and oxalate anions consists of preparing a stable complex which can be used as a ligand to build extended networks where this complex remains unchanged and behaves as the fundamental unit. This procedure is known as the building-block approach or complex as ligand strategy.

Keeping this in mind and aiming at testing this strategy in the malonate-containing complexes, we have prepared and characterized by X-ray diffraction three-new chromium(III) complexes with the malonate ligand, where the dinuclear $[Cr_2(mal)_4(OH)_2]^{4-}$ unit acts as a building-block.

Experimental

Materials and methods

Malonic acid, copper(II) perchlorate hexahydrate, nickel(II) perchlorate hexahydrate, tris(2-aminoethyl)amine (tren) and potassium dichromate were purchased from commercial sources and used as received. Elemental analyses (C, H, N) were performed on an EA 1108 CHNS-O microanalytical analyser.

Synthesis

$K_4[Cr(OH)(mal)_2]_2 \cdot 6H_2O$ (1)

The complex *cis*-$K[Cr(mal)_2(H_2O)_2]$ which is the precursor of **1** was prepared as follows: a hot aqueous solution (10 ml) of malonic acid (20.8 g, 83.3 mmol) was slowly added to a suspension of $K_2Cr_2O_7$ (11.8 g, 40 mmol) in hot water (25 ml). The resulting suspension is diluted to 200 ml and then its volume is reduced to *ca.* 50 ml in a steam bath at 80 ºC. The resulting solution is allowed to cool at the room temperature and then, ethanol (95%) is added dropwise under continuous stirring to precipitate the solid (*cis*-$K[Cr(mal)_2(H_2O)_2]$ which is is filtered, washed with ethanol and dried in the open air (yield 75%).

An aqueous solution (24 ml) of *cis*-$K[Cr(mal)_2(H_2O)_2]$ (15.4 g, 47 mmol) was reacted with mixed with KOH (2.64 g, 47 mmol) dissolved in water (9 ml). The resulting solution is allowed to stand at room temperature. After a week, dark brown prism crystals of **1** separated from the mother liquor. The yield is *ca.* 35%.

$\{[Cu(tren)]_4[Cr_2(mal)_4(OH)_2]\}(ClO_4)_4 \cdot 8H_2O$ (2)

A methanolic solution (5 ml) of tren (7.31 mg, 0.5 mmol) was added to an aqueous solution (5 ml) of $Cu(ClO_4)_2 \cdot 6 H_2O$ (186 mg, 0.5 mmol). An aqueous solution (10 ml) of **1** (202.6 mg, 0.25 mmol) was poured into the resulting dark blue under continuous stirring. Dark blue prisms of **2** were obtained by slow evaporation of the mother liquor at room temperature after three days (yield *ca.* 30%).

$[Ni(Htren)_2][Cr_2(mal)_4(OH)_2] \cdot 8H_2O$ (3)

A methanolic solution (5 ml) of tren (14.96 mg, 1 mmol) was added to an aqueous solution (5 ml) of $Ni(ClO_4)_2 \cdot 6H_2O$ (365.7 mg, 1 mmol). An aqueous solution (10 ml) of **1** (202.6 mg, 0.25 mmol) was poured into the resulting solution with continuous stirring.

Dark violet prisms of **3** were obtained by slow evaporation at room temperature after four days, (yield *ca.* 30%).

Crystal data collection and refinement

Single crystals of **1-3** were mounted on a Bruker-Nonius KappaCCD diffractometer. Orientation matrix and lattice parameters were obtained by least-squares refinement of the reflections obtained by a θ-χ scan (Dirax/lsq method). Diffraction data were collected at 293(2) K using graphite-monochromated Mo-K_α radiation (λ = 0.71073 Å). Data collection and data reduction were done with the COLLECT [Hooft R.W.W., 1999] and EVALCCD [Duisenberg A.J.M. *et al.*, 2003] programs. Empirical absorption corrections were carried out using SADABS [SADABS, version 2.03, 2003] for all compounds. The indexes of data collection were $-11 \leq h \leq 11$, $-13 \leq k \leq 13$ and $-12 \leq l \leq 13$ for **1**; $-23 \leq h \leq 22$, $-15 \leq k \leq 14$ and $-28 \leq l \leq 17$ for **2** and $-12 \leq h \leq 12$, $-13 \leq k \leq 12$ and $-18 \leq l \leq 18$ for **3**. Of the 3945 (**1**), 9739 (**2**) and 5987 (**3**) measured independent reflections in the θ ranges 6.41 – 30º (**1**), 6.40 - 30º (**2**) and 6.41 – 30.00º (**3**), 3086 (**1**), 5835 (**2**) and 3564 (**3**) have $I \geq 2\sigma(I)$. All the measured independent reflections were used in the analysis. All calculations for data reduction, structure solution, and refinement were done by standard procedures (WINGX) [Farrugia L.J., 1999]. The structure was solved by direct methods and refined with full-matrix least-squares technique on F^2 using the SHELXS-97 and SHELXL-97 programs [Sheldrick, G. M. SHELX97, realease 97-2, 1998]. The hydrogen atoms of the water molecules for **1-3** were not found. The amine and malonate hydrogen atoms of **1** and **2** were set in calculated positions whereas they were located from difference Fourier maps for **3**. All hydrogen atoms were refined with isotropic temperature factors. The perchlorate groups in **2** are thermally disordered and some restrains were introduced in the refinement (concerning their bond distances and angles) in order to improve the final refinement. In spite of all our attempts to improve the refinement of the perchlorate groups, some of the perchlorate oxygens have high thermal displacements. The final Fourier-difference map showed maximum/minimum height peaks of 0.918/-0.749 (**1**), 1.225/-1.401 (**2**) and 0.880/-0.788 e $Å^{-3}$ (**3**). A summary of the crystallographic data and structure refinement is given in Table 1. The final geometrical calculations and the graphical manipulations were carried out with PARST97 [Nardelli M., 1995] and DIAMOND [DIAMOND 2.1d, 2000] programs, respectively.

Table 1. Crystal data and details of structure determination for compounds **1-3**

Compound	**1**	**2**	**3**
Formula	$C_{12}H_{22}O_{24}K_4Cr_2$	$C_{36}H_{98}Cl_4Cr_2Cu_4N_{16}O_{42}$	$C_{24}H_{64}Cr_2N_8NiO_{26}$
M	810.70	1927.26	1043.54
Crystal system	triclinic	monoclinic	triclinic
Space group	*P*-1	$P2_1/n$	*P*-1
a, Å	8.2948(7)	16.7161(4)	9.1804(5)
b, Å	9.4737(10)	11.3208(10)	9.6532(5)
c, Å	9.7296(8)	20.1947(14)	13.0261(6)
α, deg	102.028(6)	-	106.313(4)
β, deg	100.085(6)	102.637(5)	103.821(4)
γ, deg	106.708(6)	-	95.435(5)
V, Å^3	693.21(11)	3729.1(4)	1059.48(9)
Z	1	2	1
T(K)	293(2)	293(2)	293(2)
ρ_{calc} (Mg m^{-3})	1.942	1.716	1.636
F(000)	410	1988	548
λ (Mo-Kα Å)	0.71073	0.71073	0.071073
μ (Mo-Kα, mm^{-1})	1.484	1.649	1.043
Extinction coefficient	0.036(3)	-	-
Number parameters/restraints	191 / 0	470 / 21	372 / 0
Goodness of fit (*S*)	1.040	1.045	1.027
R1, $I > 2\sigma(I)$ (all)	0.0379 (0.0568)	0.0629 (0.1193)	0.0542 (0.1165)
wR2, $I > 2s(I)$ (all)	0.0907 (0.0964)	0.1682 (0.1997)	0.1158 (0.1366)
Max/min electron density (e/Å^3)	0.918 / -0.749	1.225 / -1.401	0.880 / -0.788
Measured reflections (R_{int})	7745 (0.0226)	23087 (0.0285)	12468 (0.0384)
Independent reflections [$I > 2\sigma(I)$]	3945 (3086)	9739 (5835)	5987 (3564)

Results and discussion

Description of the structure of $K_4[Cr_2(mal)_4(OH)_2] \cdot 6H_2O$ (1)

The structure of **1** is made up of $[Cr_2(mal)_4(OH)_2]^{4-}$ dinuclear units which are linked through $[K_2(H_2O)_3]^{2+}$ entities to afford a three-dimensional network (see Figure 1). Additional hydrogen bonds involving water molecules, and malonate- and hydroxo-oxygen atoms contribute to stabilise the whole structure.

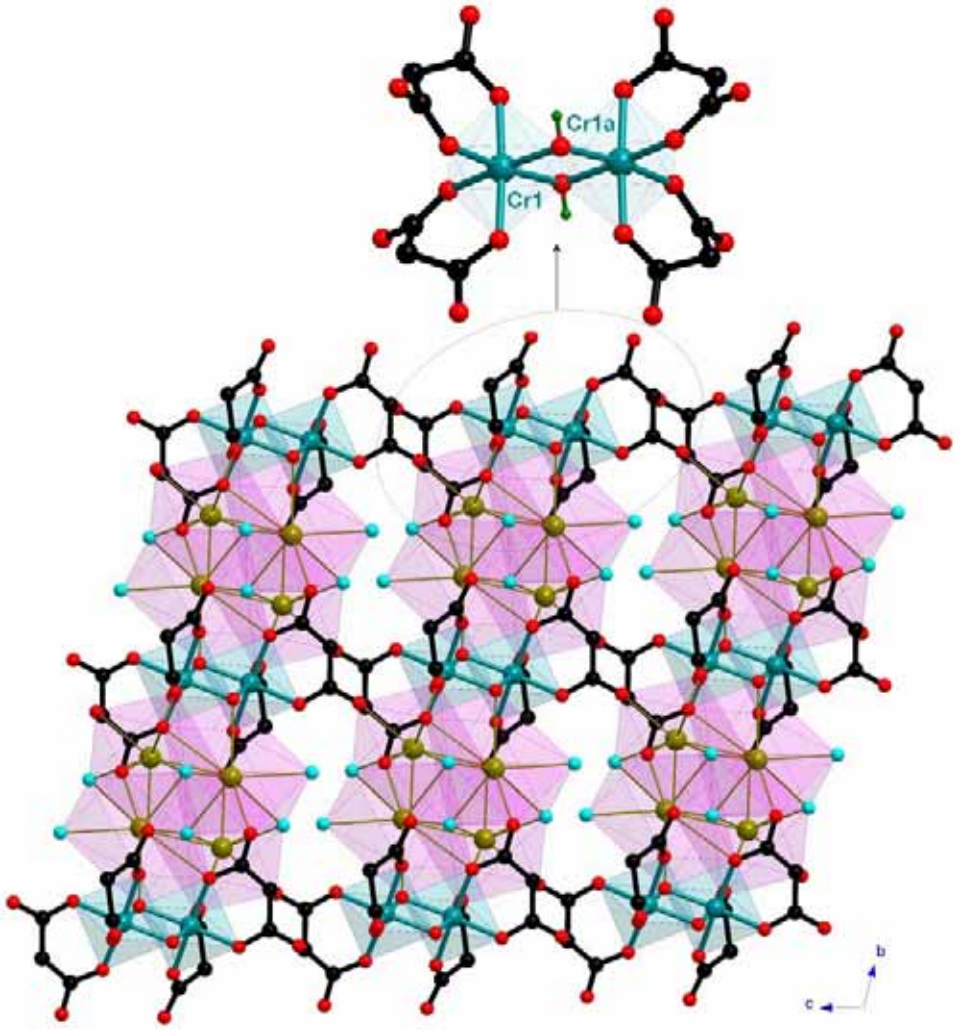

Figure 1. Perspective view of the crystal packing in **1** showing the $[Cr_2(mal)_4(OH)_2]^{4-}$ dinuclear unit. Hydrogen atoms have been skipped for clarity. The coordination polyhedra of the chromium and potassium atoms are denoted by blue and pink colours.

Main bond lengths and angles for compound **1** are reported in Table 2.

Table 2. Selected bond lengths (Å) and angles (º) for compound **1**[a]

Cr(1)-O(1)	1.973(2)	Cr(1)-O(2)	1.9728(15)
Cr(1)-O(11)	1.973(2)	Cr(1)-O(12)	1.958(2)
Cr(1)-O(20)	1.9790(15)	Cr(1)-O(20a)	1.9702(14)
O(1)-Cr(1)-O(2)	89.74(7)	O(1)-Cr(1)-O(11)	176.42(7)

O(1)-Cr(1)-O(12)	88.41(7)	O(1)-Cr(1)-O(20)	91.20(7)
O(1)-Cr(1)-O(20a)	87.41(6)	O(2)-Cr(1)-O(11)	88.14(7)
O(2)-Cr(1)-O(12)	94.03(7)	O(2)-Cr(1)-O(20)	91.29(6)
O(2)-Cr(1)-O(20a)	171.27(6)	O(11)-Cr(1)-O(12)	88.86(7)
O(11)-Cr(1)-O(20)	91.74(6)	O(11)-Cr(1)-O(20a)	95.10(6)
O(12)-Cr(1)-O(20)	174.66(7)	O(12)-Cr(1)-O(20a)	94.14(7)
O(20)-Cr(1)-O(20a)	80.52(6)		
K(1)-O(1)	2.760(2)	K(1)-O(11a)	3.116(2)
K(1)-O(13b)	2.910(2)	K(1)-O(20a)	2.853(2)
K(1)-O(1w)	2.713(2)	K(1)-O(1wc)	2.808(2)
K(1)-O(2w)	2.937(3)	K(1)-O(3wd)	3.119(4)
O(1)-K(1)-O(11a)	64.19(5)	O(1)-K(1)-O(13b)	162.42(6)
O(1)-K(1)-O(20a)	58.05(4)	O(1)-K(1)-O(1w)	104.11(6)
O(1)-K(1)-O(1wc)	127.42(6)	O(1)-K(1)-O(2w)	86.24(8)
O(1)-K(1)-O(3wd)	82.52(9)	O(11a)-K(1)-O(13b)	133.37(5)
O(11a)-K(1)-O(20a)	56.54(4)	O(11a)-K(1)-O(1w)	85.40(5)
O(11a)-K(1)-O(1wc)	65.46(5)	O(11a)-K(1)-O(2w)	139.97(7)
O(11a)-K(1)-O(3wd)	137.25(8)	O(13b)-K(1)-O(20a)	128.59(5)
O(13b)-K(1)-O(1w)	79.37(6)	O(13b)-K(1)-O(1wc)	69.65(6)
O(13b)-K(1)-O(2w)	78.67(8)	O(13b)-K(1)-O(3wd)	81.49(9)
O(20a)-K(1)-O(1w)	141.70(6)	O(20a)-K(1)-O(1wc)	82.14(5)
O(20a)-K(1)-O(2w)	85.47(7)	O(20a)-K(1)-O(3wd)	126.73(9)
O(1w)-K(1)-O(1wc)	85.88(6)	O(1w)-K(1)-O(2w)	129.81(9)
O(1w)-K(1)-O(3wd)	77.19(10)	O(1wc)-K(1)-O(2w)	126.28(10)
O(1wc)-K(1)-O(3wd)	148.82(10)	O(2w)-K(1)-O(3wd)	55.27(12)
K(2)-O(3a)	2.825(2)	K(2)-O(3e)	2.651(2)
K(2)-O(4f)	2.703(2)	K(2)-O(11)	2.975(2)
K(2)-O(13)	2.874(2)	K(2)-O(14g)	2.589(3)
K(2)-O(1we)	3.231(2)	K(2)-O(3w)	3.044(4)
O(3a)-K(2)-O(3e)	79.22(6)	O(3a)-K(2)-O(4f)	78.90(6)
O(3a)-K(2)-O(11)	96.34(5)	O(3a)-K(2)-O(13)	118.82(6)
O(3a)-K(2)-O(14g)	152.61(8)	O(3a)-K(2)-O(1we)	54.02(5)
O(3a)-K(2)-O(3w)	121.24(9)	O(3e)-K(2)-O(4f)	152.60(6)
O(3e)-K(2)-O(11)	112.84(5)	O(3e)-K(2)-O(13)	79.71(6)
O(3e)-K(2)-O(14g)	127.91(9)	O(3e)-K(2)-O(1we)	80.80(5)
O(3e)-K(2)-O(3w)	72.48(9)	O(4f)-K(2)-O(11)	85.85(5)
O(4f)-K(2)-O(13)	125.69(6)	O(4f)-K(2)-O(14g)	74.07(8)
O(4f)-K(2)-O(1we)	73.04(5)	O(4f)-K(2)-O(3w)	105.65(10)
O(11)-K(2)-O(13)	44.17(5)	O(11)-K(2)-O(14g)	77.53(11)
O(11)-K(2)-O(1we)	145.85(5)	O(11)-K(2)-O(3w)	141.95(9)
O(13)-K(2)-O(14g)	75.21(10)	O(13)-K(2)-O(1we)	160.31(5)
O(13)-K(2)-O(3w)	105.41(10)	O(14g)-K(2)-O(1we)	119.90(11)
O(14g)-K(2)-O(3w)	71.41(13)	O(1we)-K(2)-O(3w)	71.10(9)

[a] Symmetry codes: (a) -*x*, -*y*, -*z*; (b) *x*, *y*+1, *z*; (c) -*x*, -*y*+1, -*z*; (d) *x*+1, *y*+1, *z*; (e) *x*-1, *y*-1, *z*; (f) *x*-1, *y*, *z*; (g) -*x*, -*y*, -*z*+1.

Two *cis*-hydroxo oxygens and four carboxylate-oxygen atoms from two malonate ions adopting the *cis* conformation are coordinated to each chromium atom building a somewhat distorted octahedral environment (see Figure 2). The Cr-O(mal) bond distances which range from 1.958(2) to 1.9773(2) Å are in agreement with those reported for $Na_4[Cr_2(mal)_4(OH)_2]\cdot 5H_2O$ [Scaringe R.P. *et al.*, 1977a] and $Na_4[Cr_2(ox)_4(OH)_2]\cdot 6H_2O$ [Scaringe R.P. *et al.*, 1977b]. Even though the Cr-O(OH) bond distances [1.9790(15) and 1.9702(14) in **1**] are somewhat shorter than the values reported for the sodium/malonate salt [1.987 and 1.988 Å] they are within the range of the values observed for the oxalate compound [1.950 and 1.976 Å].

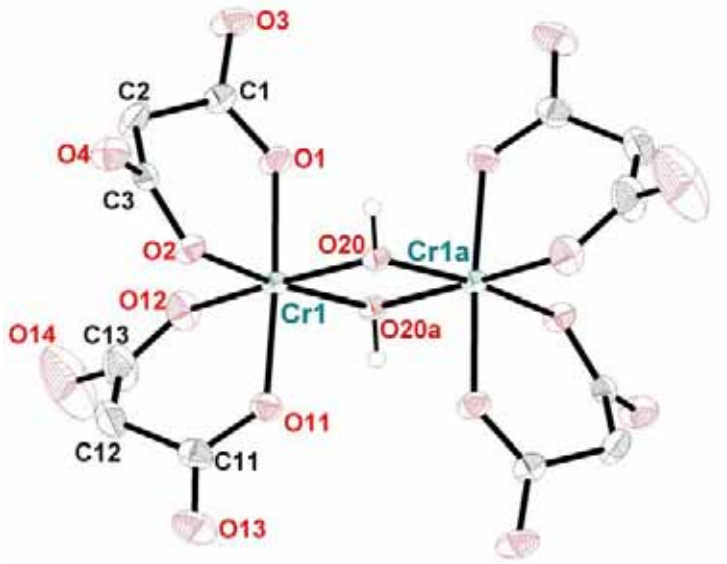

Figure 2. ORTEP view of the $[Cr_2(mal)_4(OH)_2]^{4-}$ dinuclear unit with the atom numbering. Thermal ellipsoids are drawn at the 50% probability level.

The dinuclear chromium anion is centrosymmetric, the inversion centre being located in the middle point of the $Cr_2(\mu\text{-}OH)_2$ unit. For this reason, this unit is planar. The value of the Cr-O-Cr bond angle [99.48(7)º] agree well with the values reported for the above mentioned sodium salts [99.34(7)º (malonate) and 99.63º (oxalate)].

Two crystallographically independent potassium ions occur in **1**. They are eight-coordinated adopting highly distorted square antiprism environments (see Figure 3). Four malonate-oxygen atoms and four water molecules are coordinated to K(1) [K(1)-O bond distances ranging from 2.760(2) to 3.119(4) Å] whereas six malonate oxygens and two water molecules are coordinated to K(2) [K(2)-O bond distances ranging from 2.651(2) to 3.231(2) Å]. The upper limit of the bond distances is somewhat longer than that observed for the potassium salt of formula $[K(H_2O)_{1.5}]_2[Cu(mal)_2]$ reported in Chapter II.

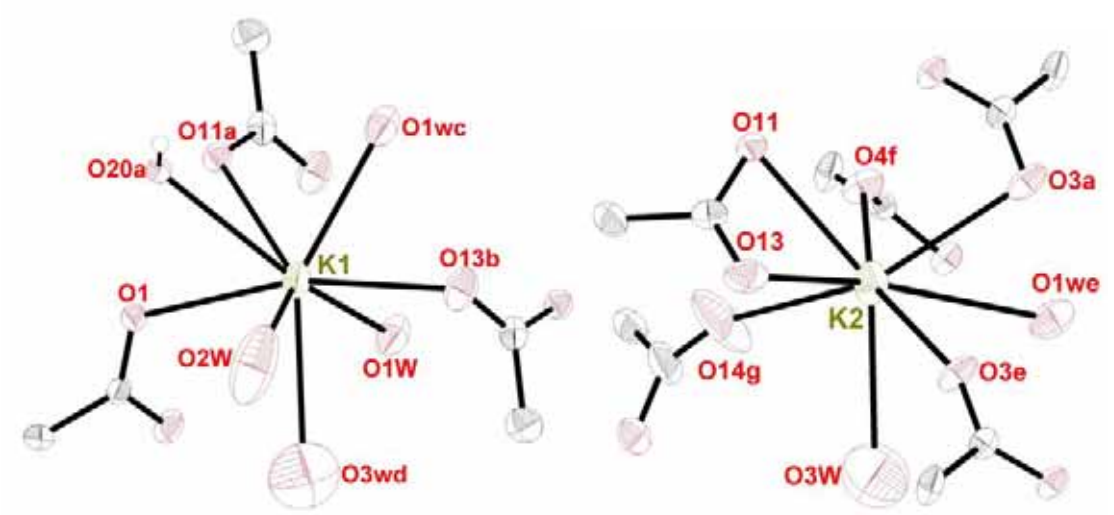

(a) **(b)**

Figure 3. ORTEP view of the potassium environments [K(1) **(a)** and K(2) **(b)**] in **1** with the numbering scheme. Thermal ellipsoids are drawn at the 50% probability level.

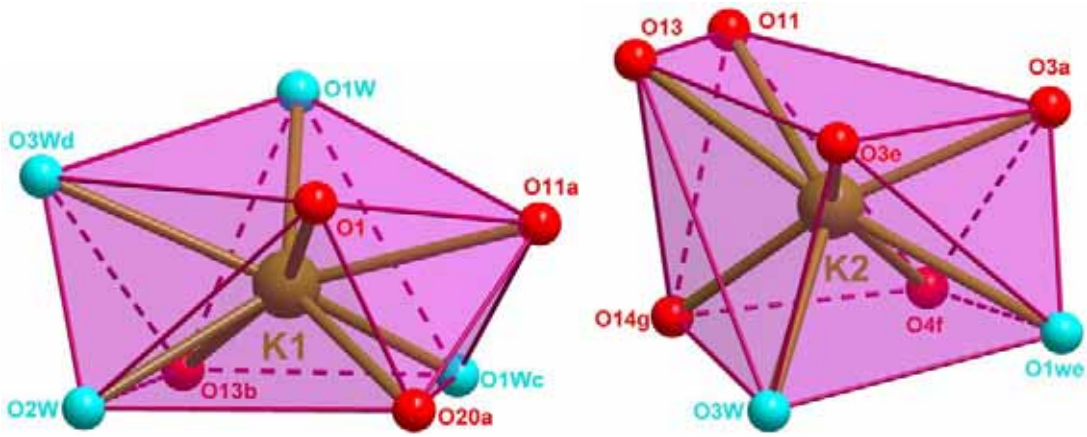

(a) **(b)**

Figure 4. Perspective drawing of the potassium environments [K(1) **(a)** and K(2) **(b)**] in **1** showing the polyhedron around the metal ions.

Two crystallographically independent malonate ions occur in **1**: C(1)C(2)C(3) [L1] and C(11)C(12)C(13) [L2]. L1 acts (see Figure 5a) simultaneously as bidentate [through O(1) and O(2) towards Cr(1), the bite angle being 89.74(1)º], bis-monodentate [across O(1) and O(4) towards K(1) and K(2h), respectively; (h) *x*+1, *y*, *z*] and bridging bis-monodentate [through O(3) towards K(2a) and K(2d); (a) -*x*, -*y*, -*z* and (d) *x*+1, *y*+1, *z*] ligand. L1 forms a six-membered ring, including the Cr(1) atom, which exhibits a slightly distorted boat conformation [$\theta = 79.8(2)^{\circ}$ and $\phi = 127.1(2)^{\circ}$] [Cremer D. *et al.*, 1975]. L2 adopts (see Figure 5b) simultaneously two bidentate [through O(11) and O(12) towards Cr(2), and O(1) and O(13) towards K(2), the values of the bite angles being 88.86(7) and 44.17(5)º, respectively] and three monodentate [through O(11), O(13) and O(14) towards K(1a), K(1i) and K(2g), respectively; (a) -*x*, -*y*, -*z*; (g) -*x*, -*y*, -

z+1; (i) *x*, *y*-1, *z*] coordination modes. L2 build a six-membered ring, including the Cr(1) atom that has a boat conformation [θ = 95.0(3)º and ϕ = 124.8(3)º] [Cremer D. *et al.*, 1975]. The bond lengths and angles for the malonate ligands (see Table 3) in **1** compares well with those reported for the compound of formula $Na_4[Cr_2(mal)_4(OH)_2]\cdot 5H_2O$ [Scaringe R.P. *et al.*, 1977a].

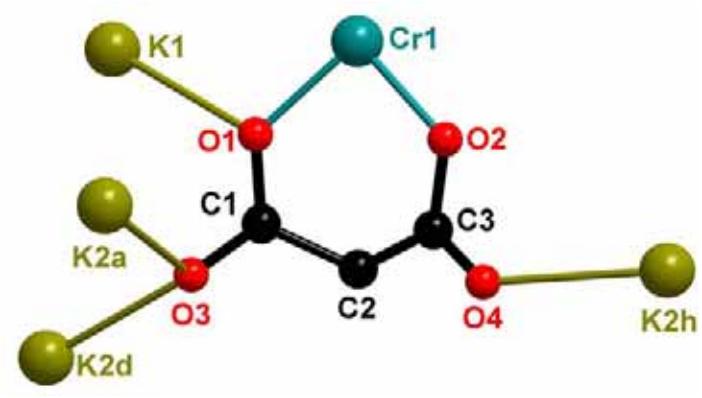

(a)

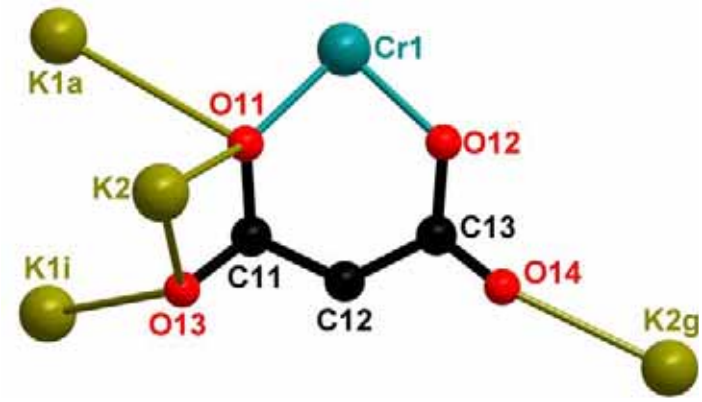

(b)

Figure 5. Coordination modes of the malonate ligands L1 **(a)** and L2 **(b)** in **1**.

Table 3. Bond lengths (Å) and angles (º) for the malonate ligands in **1**

C(1)-C(2)	1.525(3)	C(2)-C(3)	1.507(3)
C(1)-O(1)	1.273(3)	C(3)-O(2)	1.288(3)
C(1)-O(3)	1.232(3)	C(3)-O(4)	1.227(3)
O(1)···O(2)	2.784(3)	O(3)···O(4)	4.373(3)
O(1)-C(1)-O(3)	122.2(2)	O(2)-C(3)-O(4)	121.9(2)
O(1)-C(1)-C(2)	119.1(2)	O(2)-C(3)-C(2)	117.6(2)
O(3)-C(1)-C(2)	118.8(2)	O(4)-C(3)-C(2)	120.4(2)
C(1)-C(2)-C(3)	115.1(2)		
C(1)-O(1)-Cr(1)	129.05(14)	C(3)-O(2)-Cr(1)	128.84(14)
C(11)-C(12)	1.513(4)	C(12)-C(13)	1.513(4)
C(11)-O(11)	1.280(3)	C(13)-O(12)	1.278(3)

C(11)-O(13)	1.238(3)	C(13)-O(14)	1.229(4)
O(11)···O(12)	2.751(2)	O(13)···O(14)	4.452(3)
O(11)-C(11)-O(13)	121.8(2)	O(12)-C(13)-O(14)	121.4(3)
O(11)-C(11)-C(12)	119.6(2)	O(12)-C(13)-C(12)	119.7(2)
O(13)-C(11)-C(12)	118.6(2)	O(14)-C(13)-C(12)	119.0(3)
C(11)-C(12)-C(13)	116.4(2)		
C(11)-O(11)-Cr(1)	126.25(15)	C(13)-O(12)-Cr(1)	126.8(2)

The $[Cr_2(mal)_4(OH)_2]^{4-}$ dinuclear units are linked through potassium atoms and water molecules leading to a three-dimensional network where the chromium units are well separated by means of potassium clusters (see Figure 1). The shortest metal···metal separations are: 3.0137(6) [Cr(1)···Cr(1a)], 3.7999(9) [Cr(1)···K(1)] and 3.9790 Å [Cr(1a)···K(2)]. Additional hydrogen bonds involving the water molecules and the hydroxo and malonate oxygens (see Table 3) contribute to the crystal packing and the stabilisation of the three-dimensional network in **1**.

Table 4. Hydrogen bonds for **1**[a-c]

D-H···A	D···A/Å	D-H···A	D···A/Å
O(1w)-H···O(2b)	2.783(3)	O(2w)···O(12)	2.828(4)
O(1w)-H···O(3j)	2.774(3)	O(2w)···O(13g)	2.939(5)
D-H···A	D···A/Å	H···A/Å	D-H···A/º
O(20)-H20)···O(4k)	2.831(2)	2.032(2)	164.75(12)
C(2)-H(2)···O(3wg)	3.699(5)	2.778(4)	158.8(2)

[a] Symmetry transformations: (b) -*x*+1/4, *y*+1/4, *z*+1/4; (g) *x*, *y*, *z*+1; (j) -*x*+1, -*y*+1, -*z*; (k) -*x*+1, -*y*, -*z*. [b] A = acceptor; D = donor. [c] Symmetry operators apply to acceptor atoms.

Description of the structure of $\{[Cu(tren)]_4[Cr_2(mal)_4(OH)_2]\}(ClO_4)_4 \cdot 8H_2O$ (2)

The structure of **2** consists of hexanuclear units where the *cis*-$[Cr_2(mal)_4(OH)_2]^{4-}$ anions are liked to four $[Cu(tren)]^{2+}$ cations through carboxylate-malonate bridges. These heterometallic units are further connected through hydrogen bonds involving hydroxo groups and water molecules together with perchlorate- and malonate-oxygen atoms affording a three-dimensional network (see Figure 6).

Main bond lengths and angles for compound **2** are listed in Table 5.

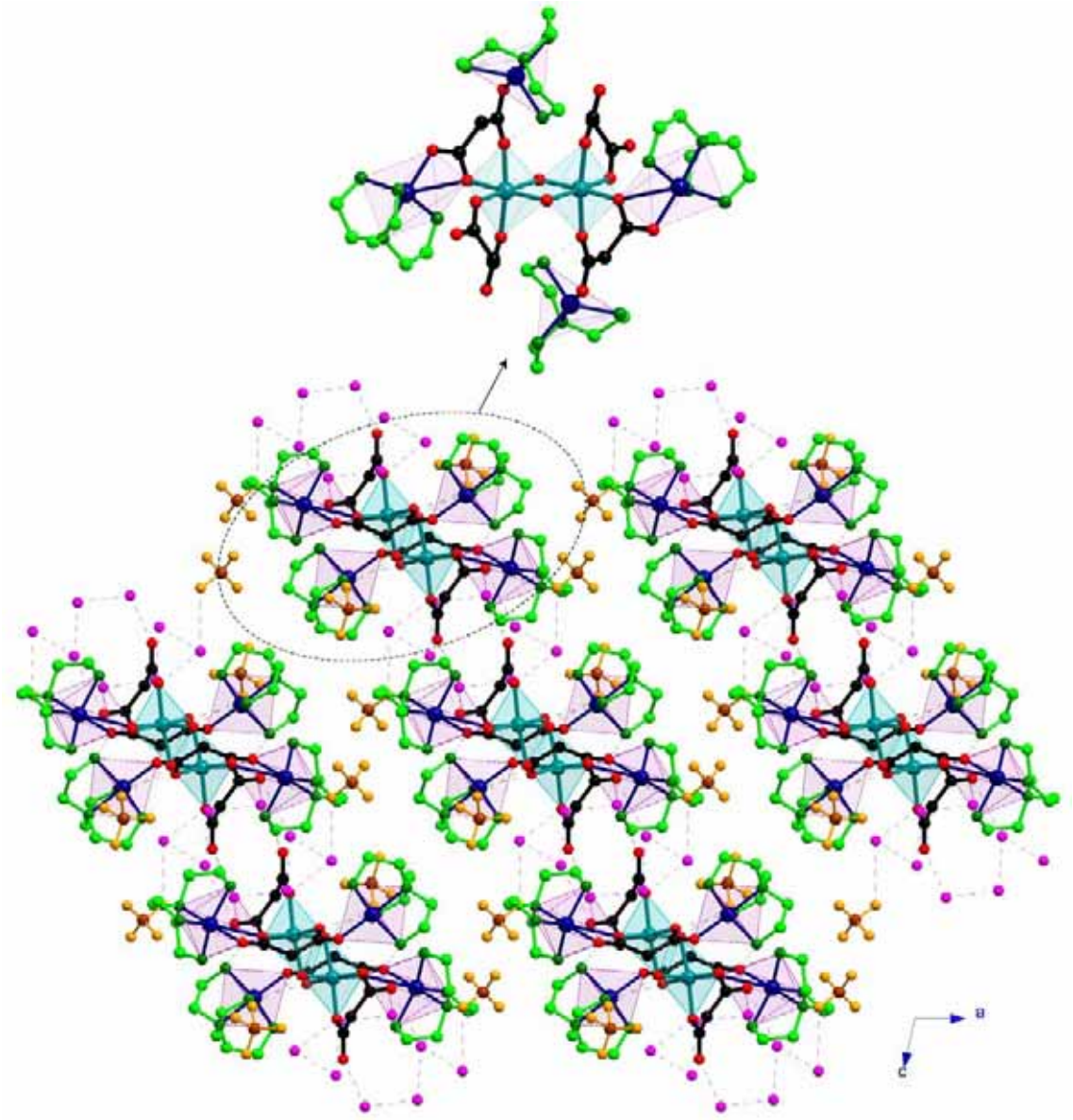

Figure 6. Perspective view, along the *b*-axis, of the crystal packing in **2** showing the $\{[Cu(tren)]_4[Cr_2(mal)_4(OH)_2]\}^{4+}$ units linked through hydrogen bonds (only relevant hydrogen bonds have been drawn). Hydrogen atoms were skipped for clarity. The coordination polyhedra of the chromium and copper atoms are denoted in blue and violet colours, respectively.

Table 5. Main bond lengths (Å) and angles (º) for compound **2**[a]

Cr(1)-O(1)	1.977(3)	Cr(1)-O(2)	1.956(3)
Cr(1)-O(11)	1.967(3)	Cr(1)-O(12)	1.967(3)
Cr(1)-O(20)	1.953(3)	Cr(1)-O(20a)	1.950(3)
O(1)-Cr(1)-O(2)	86.63(12)	O(1)-Cr(1)-O(11)	172.04(13)
O(1)-Cr(1)-O(12)	88.16(13)	O(1)-Cr(1)-O(20)	90.14(13)
O(1)-Cr(1)-O(20a)	93.78(13)	O(2)-Cr(1)-O(11)	85.88(13)
O(2)-Cr(1)-O(12)	91.48(13)	O(2)-Cr(1)-O(20)	94.66(12)
O(2)-Cr(1)-O(20a)	174.20(13)	O(11)-Cr(1)-O(12)	89.34(13)
O(11)-Cr(1)-O(20)	93.14(13)	O(11)-Cr(1)-O(20a)	93.94(13)
O(12)-Cr(1)-O(20)	173.52(13)	O(12)-Cr(1)-O(20a)	94.31(13)

O(20)-Cr(1)-O(20a)	79.56(13)		
Cu(1)-N(31)	2.094(5)	Cu(1)-N(32)	2.058(4)
Cu(1)-N(33)	2.049(6)	Cu(1)-N(34)	2.053(4)
Cu(1)-O(3)	1.975(3)		
N(31)-Cu(1)-N(32)	110.6(2)	N(31)-Cu(1)-N(33)	120.9(3)
N(32)-Cu(1)-N(33)	125.8(3)	N(34)-Cu(1)-N(31)	84.4(2)
N(34)-Cu(1)-N(32)	84.1(2)	N(34)-Cu(1)-N(33)	85.0(2)
O(3)-Cu(1)-N(31)	95.2(2)	O(3)-Cu(1)-N(32)	101.9(2)
O(3)-Cu(1)-N(33)	89.7(2)	N(34)-Cu(1)-O(3)	173.7(2)
Cu(2)-N(51)	2.041(5)	Cu(2)-N(52)	2.055(4)
Cu(2)-N(53)	2.126(5)	Cu(2)-N(54)	2.046(4)
Cu(2)-O(2)	2.717(3)	Cu(2)-O(4)	2.008(3)
N(51)-Cu(2)-N(52)	137.7(3)	N(51)-Cu(2)-N(53)	111.7(3)
N(52)-Cu(2)-N(53)	107.2(2)	N(54)-Cu(2)-N(51)	83.4(2)
N(54)-Cu(2)-N(52)	84.1(2)	N(54)-Cu(2)-N(53)	84.7(2)
O(2)-Cu(2)-N(51)	78.3(2)	O(2)-Cu(2)-N(52)	74.72(15)
O(2)-Cu(2)-N(53)	152.8(2)	O(4)-Cu(2)-N(51)	94.3(2)
O(4)-Cu(2)-N(52)	94.2(2)	O(4)-Cu(2)-N(53)	100.9(2)
O(2)-Cu(2)-O(4)	52.20(11)	O(2)-Cu(2)-N(54)	152.8(2)
O(4)-Cu(2)-N(54)	174.38(15)		

[a] Symmetry codes: (a) -*x*, -*y*, -*z*.

Similarly to **1**, each chromium atom in **2** is bonded to four carboxylate-oxygen atoms from two malonate groups in *cis*-conformation and two *cis*-hydroxo oxygens, building thus, a distorted octahedral environment around the metal atom (see Figure 7). The Cr-O(mal) bond distances [from 1.956(3) to 1.977(3) Å] compares well with those reported for compound **1** and for the related complexes of formula $Na_4[Cr_2(mal)_4(OH)_2]\cdot 5H_2O$ [Scaringe R.P. *et al.*, 1977a] and $Na_4[Cr_2(ox)_4(OH)_2]\cdot 6H_2O$ [Scaringe R.P. *et al.*, 1977b]. As far as the Cr-O(OH) bond distances are concerned [1.950(3) and 1.953(3) Å], they are in the range observed for the oxalate compound [Scaringe R.P. *et al.*, 1977b], but they are somewhat shorter that those reported for **1** and $Na_4[Cr_2(mal)_4(OH)_2]\cdot 5H_2O$ [Scaringe R.P. *et al.*, 1977a]. Each chromium atom is connected to another one through a double μ-hydroxo bridge [2.9993(8) Å for the Cr(1)···Cr(1a) separation; (a) -*x*, -*y*, -*z*], the dinuclear chromium entity being centrosymmetric. The value of the Cr-O-Cr bond angle [100.44(13)º] in **2** is a little larger than the values reported for the malonate and oxalate sodium salts and also for **1** [values ranging from 99.34-99.63º] but it agrees well with them.

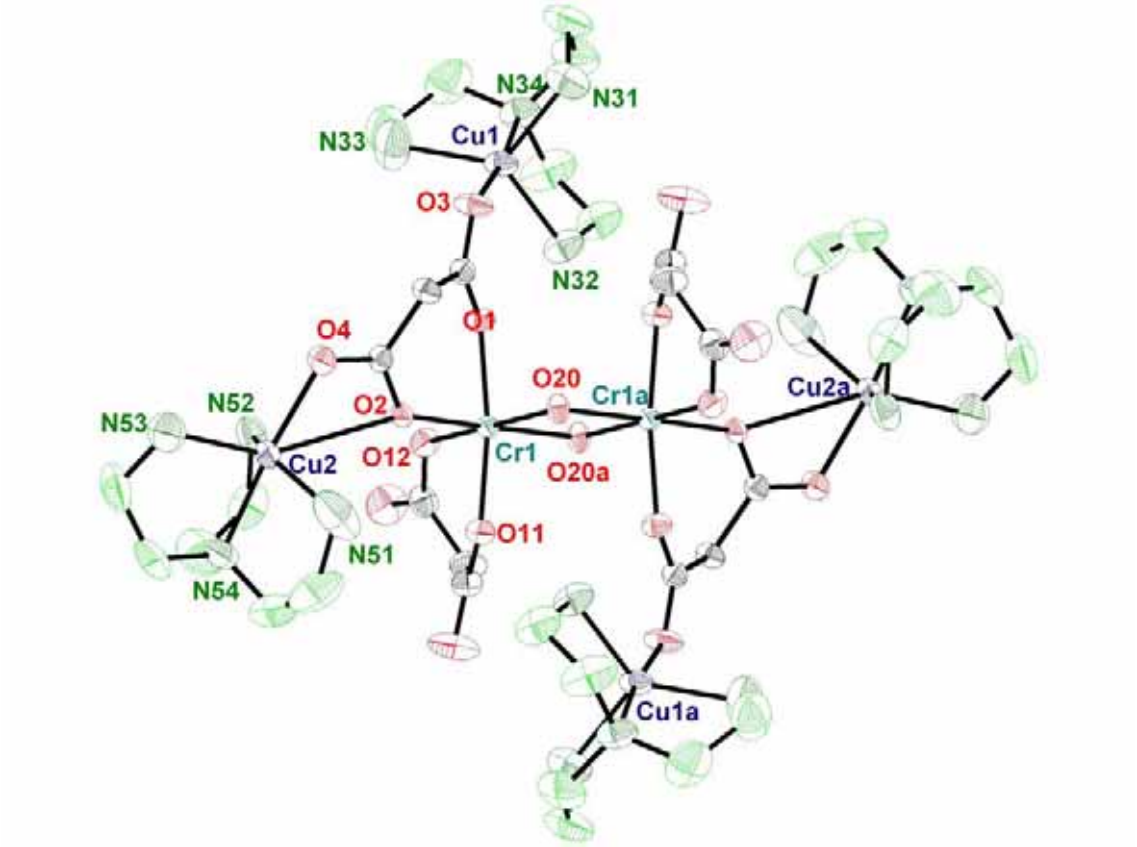

Figure 7. ORTEP view of the $\{[Cu(tren)]_4[Cr_2(mal)_4(OH)_2]\}^{4+}$ hexanuclear unit with the atom numbering. The hydrogen atoms and the perchlorate groups were omitted for the sake of clarity. Thermal ellipsoids are drawn at the 50% probability level.

Two crystallographically independent copper atoms occur in **2** [Cu(1) and Cu(2)] which are five- [Cu(1)] and six-coordinated [Cu(2)] (see Figure 7). Four tren-nitrogen atoms and one malonate-oxygen atom are coordinated to Cu(1) building a trigonal prism around the metal atom. The equatorial plane is formed by three coplanar nitrogen atoms [N(31), N(32) and N(34)], the metal atom being shifted by 0.1964(6) Å from the mean equatorial plane towards the O(3) malonate oxygen. The equatorial bond lengths [ranging from 2.049(6) to 2.094(5) Å] are somewhat longer than the apical ones [1.975(3) and 2.053(4) Å], the Cu-O(mal) bond distance being shorter than that of the Cu-N(tren). Cu(2) is surrounded by to four tren-nitrogen [the Cu-N bond distances ranging from 2.041(5) to 2.126(5) Å] atoms and two carboxylate-malonate oxygens [2.008(3) Å. and 2.717(3) Å for the Cu-O(mal) bond distances]. It exhibits a highly distorted octahedron environment. If one neglects the long Cu(2)-O(2) interaction, the environment of the Cu(2) atom can be viewed as trigonal bipyramidal with the equatorial plane being built by three coplanar tren nitrogens atoms [N(51), N(52) and N(53)] and the metal atom being shifted by 0.2166(6) Å from the mean equatorial plane

towards the O(4) malonate oxygen atom. The remaining apical position is filled by the N(54) atom. The apical bond distances are in average shorter than the equatorial ones. The value of the dihedral angle between the equatorial planes of Cu(1) and Cu(2) is 72.9(2)º.

Two independent malonate groups L1 [C(1)C(2)C(3)] and L2 [C(11)C(12)C(13)] occur in **2**. L1 adopts simultaneously (see Figure 8) a monodentate [through O(3) towards Cu(1)] and two bidentate [through O(2) and O(4) towards Cu(2) and through O(1) and O(2) towards Cr(1), the bite angles being 52.20(11) and 86.63(12)º, respectively] coordination modes. L1 forms a six-membered ring, including the Cr(1) atom, that exhibits a slightly distorted boat conformation [θ = 96.5(4)º and ϕ = 110.9(4)º] [Cremer D. *et al.*, 1975]. The two carboxylate groups in L1 show the *anti-syn* conformation and they connect the Cr(1) atom with two adjacent copper atoms [the separations through the carboxylate bridges being 5.0363(9) [Cr(1)···Cu(1)] and 4.5552(9) Å [Cr(1)···Cu(2)]]. L2 adopts a bidentate conformation [through O(11) and O(12) towards Cr(1), the bite angle being 89.34(13)º]. L2 forms a six-membered ring, including the chromium atom, which exhibits a boat conformation [θ = 90.9(4)º and ϕ = 127.2(4)º] [Cremer D. *et al.*, 1975]. Bond lengths and angles for the malonate ligands in **2** are listed in Table 6.

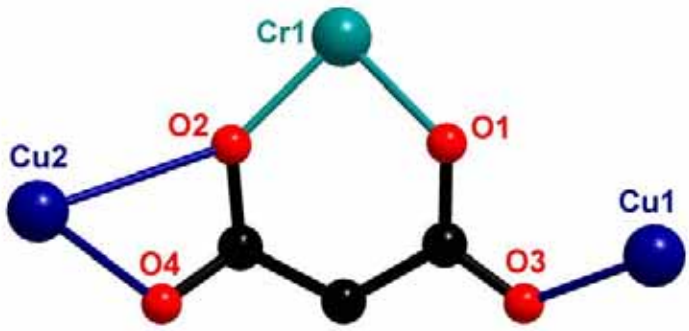

Figure 7. Coordination mode of the L1 malonate ligand in **2**.

Table 6. Bond lengths (Å) and angles (º) for the malonate ligands in **2**

C(1)-C(2)	1.519(6)	C(2)-C(3)	1.501(6)
C(1)-O(1)	1.259(5)	C(3)-O(2)	1.268(5)
C(1)-O(3)	1.243(5)	C(3)-O(4)	1.246(5)
O(1)···O(2)	2.698(4)	O(3)···O(4)	4.508(5)
O(1)-C(1)-O(3)	122.9(4)	O(2)-C(3)-O(4)	119.7(4)
O(1)-C(1)-C(2)	120.8(4)	O(2)-C(3)-C(2)	120.7(4)
O(3)-C(1)-C(2)	116.3(4)	O(4)-C(3)-C(2)	119.6(4)
C(1)-C(2)-C(3)	114.9(4)		

C(1)-O(1)-Cr(1)	127.3(3)	C(3)-O(2)-Cr(1)	128.6(3)
C(1)-O(3)-Cu(1)	124.2(3)	C(3)-O(2)-Cu(2)	111.2(3)
C(3)-O(4)-Cu(2)			
C(11)-C(12)	1.514(7)	C(12)-C(13)	1.489(7)
C(11)-O(11)	1.269(5)	C(13)-O(12)	1.296(5)
C(11)-O(13)	1.230(6)	C(13)-O(14)	1.229(6)
O(11)···O(12)	2.766(5)	O(13)···O(14)	4.361(7)
O(11)-C(11)-O(13)	122.9(5)	O(12)-C(13)-O(14)	121.7(5)
O(11)-C(11)-C(12)	118.0(4)	O(12)-C(13)-C(12)	118.2(4)
O(13)-C(11)-C(12)	119.2(4)	O(14)-C(13)-C(12)	120.1(4)
C(11)-C(12)-C(13)	116.2(4)		
C(11)-O(11)-Cr(1)	126.5(3)	C(13)-O(12)-Cr(1)	126.0(3)

Two crystallographically tren groups are present in **2**, each one acting as a tetradentate ligand through its four nitrogen atoms towards the copper atom. The geometry of the tren as well as the Cu-N(tren) bond distances [2.041(5)-2.126(5) Å] and the chelating N(tren)-Cu-N(tren) bond angles [83.4(2)-85.0(2)º] compares well with the values reported in the literature for other tren-containing copper(II) complexes where the metal environment of the metal ion is filled by four tren-nitrogens and one oxygen atom [Castro I. *et al.*, 1995; Duan C.-Y. *et al.*, 1998; Mao Z.-W. *et al.*, 2001].

Each $[Cr_2(mal)_4(OH)_2]^{4-}$ dinuclear unit in **2** is connected to four $[Cu(tren)]^{2+}$ entities through four carboxylate-malonate bridges leading to an hexanuclear complex (see Figure 7). These cationic units are held together by means of hydrogen bonds involving the hydroxo groups, the perchlorate and malonate oxygen atoms and the amine-tren nitrogens (see Figure 6) affording a two-dimensional network. In addition, hydrogen bonds involving the water molecules, amine-tren nitrogens and carboxylate-malonate and perchlorate oxygens (see Table 7) connect the two-dimensional layers contributing to the crystal packing in **2** and leading a three-dimensional network.

Table 7. Hydrogen bonds and relevant short contacts for **2**[a-c]

D-H···A	D···A/Å	D-H···A	D···A/Å
O(1w)···O(13)	3.073(12)	O(3w)···O(1w)	2.810(14)
O(1w)···O(2w)	2.831(14)	O(3w)···O(4w)	2.950(10)
O(2w)···O(12b)	2.837(9)	O(4w)···O(13c)	2.892(7)
O(2w)···O(27)	3.003(16)	O(4w)···O(14)	2.813(6)
D-H···A	D···A/Å	H···A/Å	D-H···A/º
O(20)-H(20)···O(23d)	2.835(10)	2.096(10)	149.8(3)

C(2)-H(1)···O(24d)	3.552(10)	2.618(9)	161.9(3)
C(2)-H(2)···O(3e)	3.578(5)	2.662(3)	157.7(3)
C(12)-H(11)···O(24b)	3.517(11)	2.698(9)	142.4(4)
N(31)-H(30)···O(4e)	3.042(6)	2.195(3)	156.6(3)
N(31)-H(31)···O(13a)	3.253(7)	2.492(5)	142.7(4)
N(32)-H(36)···O(11a)	3.120(6)	2.246(3)	164.0(3)
N(32)-H(37)···O(1)	2.817(6)	2.444(3)	105.1(3)
N(32)-H(37)···O(2wc)	3.239(8)	2.475(7)	143.0(4)
N(33)-H(42)···O(3wc)	3.133(9)	2.291(7)	155.6(4)
N(33)-H(43)···O(24c)	3.315(12)	2.474(10)	155.8(5)
N(51)-H(50)···O(2)	3.050(7)	2.555(3)	115.3(4)
N(51)-H(50)···O(23d)	3.262(10)	2.557(8)	135.7(5)
N(52)-H(56)···O(14c)	3.010(6)	2.114(4)	173.2(3)
N(52)-H(57)···O(2)	2.943(5)	2.470(3)	113.2(3)
N(53)-H(62)···O(25f)	3.222(13)	2.404(11)	151.2(5)
N(53)-H(63)···O(27g)	3.077(13)	2.468(13)	125.3(5)
N(53)-H(63)···O(4wc)	3.398(9)	2.598(7)	148.4(4)
C(31)-H(32)···O(21c)	3.59(2)	2.64(2)	166.1(6)
C(31)-H(33)···O(25h)	3.473(12)	2.721(11)	134.7(5)
C(31)-H(33)···N(53e)	3.558(10)	2.836(6)	131.9(5)
C(32)-H(34)···O(22i)	3.406(12)	2.697(10)	130.4(5)
C(33)-H(39)···O(23b)	3.272(11)	2.562(10)	130.1(4)
C(34)-H(40)···O(22i)	3.464(14)	2.638(12)	143.3(6)
C(35)-H(44)···O(28c)	3.52(2)	2.724(14)	139.3(6)
C(35)-H(44)···O(2wc)	3.516(12)	2.738(9)	137.7(6)
C(37)-H(47)···O(21c)	3.57(2)	2.71(2)	147.7(6)
C(54)-H(60)···O(24)	3.469(11)	2.617(8)	146.7(5)
C(55)-H(65)···O(14c)	3.685(9)	2.887(5)	140.2(4)
C(56)-H(67)···O(22)	3.505(12)	2.805(12)	129.7(5)

[a] Symmetry transformations: (a) -*x*, -*y*, -*z*; (b) -*x*+1/2, *y*-1/2, -*z*+1/2; (c) -*x*+1/2, *y*+1/2, -*z*+1/2; (d) *x*-1/2, -*y*+1/2, *z*-1/2; (e) -*x*, -*y*+1, -*z*; (f) -*x*+1, -*y*, -*z*; (g) *x*, *y*+1, *z*; (h) *x*-1, *y*+1, *z*; (i) *x*-1, *y*, *z*. [b] A = acceptor; D = donor. [c] Symmetry operators apply to acceptor atoms.

Description of the structure of $[Ni(Htren)_2][Cr_2(mal)_4(OH)_2]\cdot 8H_2O$ (3)

The structure of **3** is made up of $[Cr_2(mal)_4(OH)_2]^{4-}$ dinuclear anions and $[Ni(Htren)_2]^{4+}$ cations which are held together by means of hydrogen bonds involving the water molecules, the amine-tren groups and the malonate-oxygen atoms to afford a three-dimensional network (see Figure 9). Additional O-H···O, N-H···O and C-H···O hydrogen bonds contribute to stabilize the whole structure.

Selected bond lengths and angles for compound **3** are listed in Table 8.

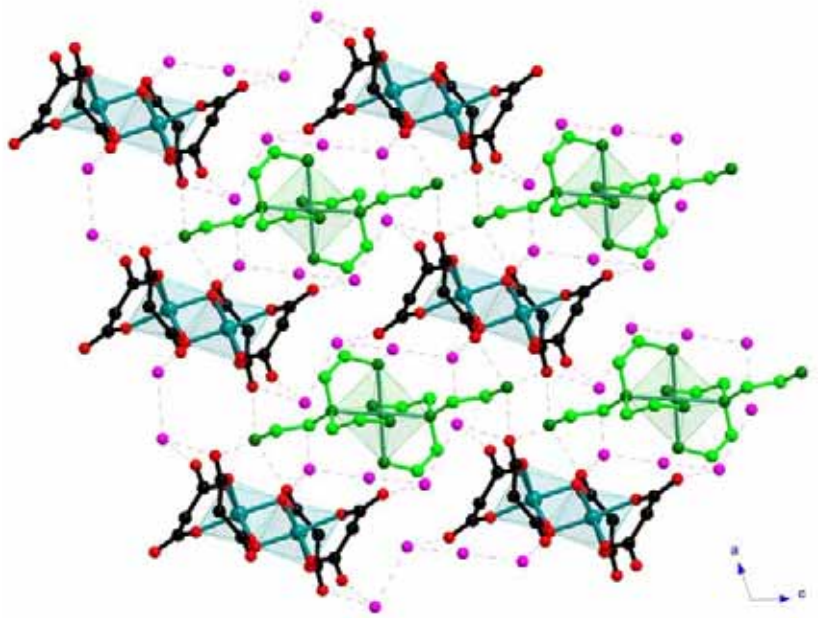

(a)

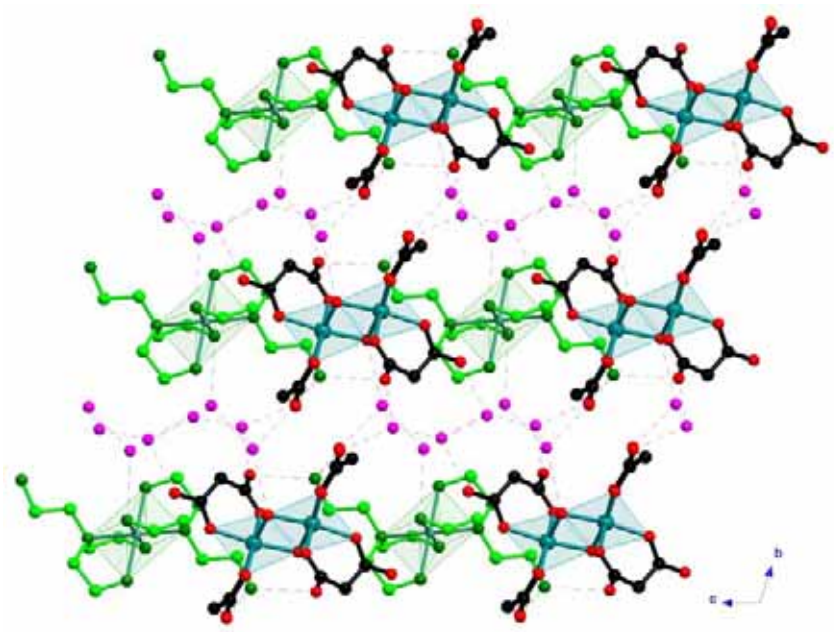

(b)

Figure 9. Perspective view of the crystal packing in **3** along the *b*- (a) and *c*-axes (b). Hydrogen atoms were omitted for clarity. Blue and green colours were adopted to denote the coordination polyhedra of the Cr(1) and Ni(1) atoms, respectively.

Table 8. Main bond lengths (Å) and angles (º) for **3**[a]

Cr(1)-O(1)	1.972(2)	Cr(1)-O(2)	1.971(2)
Cr(1)-O(11)	1.959(2)	Cr(1)-O(12)	1.983(2)
Cr(1)-O(20)	1.945(3)	Cr(1)-O(20a)	1.963(3)
O(1)-Cr(1)-O(2)	88.40(9)	O(1)-Cr(1)-O(11)	174.17(9)
O(1)-Cr(1)-O(12)	90.23(10)	O(1)-Cr(1)-O(20)	92.20(11)
O(1)-Cr(1)-O(20a)	90.38(11)	O(2)-Cr(1)-O(11)	85.86(10)

O(2)-Cr(1)-O(12)	93.57(10)	O(2)-Cr(1)-O(20)	94.01(11)
O(2)-Cr(1)-O(20a)	173.30(11)	O(11)-Cr(1)-O(12)	89.12(9)
O(11)-Cr(1)-O(20)	89.21(11)	O(11)-Cr(1)-O(20a)	95.43(11)
O(12)-Cr(1)-O(20)	172.10(11)	O(12)-Cr(1)-O(20a)	93.03(11)
O(20)-Cr(1)-O(20a)	79.45(13)		
Ni(1)-N(31)	2.100(3)	Ni(1)-N(32)	2.140(3)
Ni(1)-N(34)	2.213(2)		
N(31)-Ni(1)-N(32)	92.7(2)	N(31)-Ni(1)-N(34)	81.61(10)
N(31)-Ni(1)-N(34b)	98.39(10)	N(31)-Ni(1)-N(32b)	87.3(2)
N(32)-Ni(1)-N(34b)	99.06(11)	N(32)-Ni(1)-N(34)	80.94(11)

[a] Symmetry codes: (a) -*x*, -*y*, -*z*; (b) -*x*-1, -*y*-2, -*z*+1.

Each chromium atom in **3** is coordinated to four carboxylate-oxygen atoms from two malonate groups in a *cis* conformation and two *cis*-hydroxo oxygens building a distorted octahedral environment (see Figure 10). The Cr-O(mal) [1.959(2)-1.983(2) Å] and the Cr-O(OH) [1.945(3) and 1.963(3)Å] bond distances agree with the values observed in **1** and **2** as well as with those reported in the literature for the compounds of formula $Na_4[Cr_2(mal)_4(OH)_2]\cdot 5H_2O$ [Scaringe R.P. *et al.*, 1977a] and $Na_4[Cr_2(ox)_4(OH)_2]\cdot 6H_2O$ [Scaringe R.P. *et al.*, 1977b].

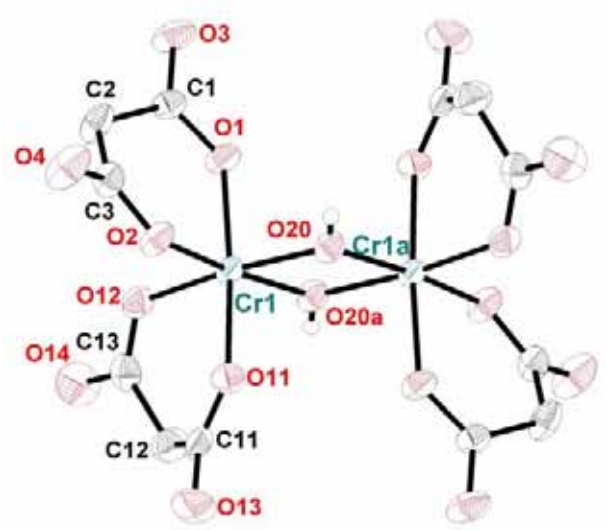

Figure 10. ORTEP view of the $[Cr_2(mal)_4(OH)_2]^{4-}$ dinuclear anion with the numbering scheme. Thermal ellipsoids are drawn at the 50% probability level.

As in **1** and **2**, the di-μ-hydroxo bridge in **3** is centrosymmetric. The value of the Cr-(OH)-Cr bond angle [100.55(13)º] compares well with those previously reported for similar compounds in this chapter (**1**, **2**) and in the literature [Scaringe R.P. *et al.*, 1977a, 1977b].

Each nickel atom in **3** lies on an inversion centre. Six nitrogen atoms from two monoprotonted $Htren^+$ groups, build a 4+2 octahedron environment around each metal atom (see Figure 11). Four coplanar nitrogens [N(31), N(32), N(31b) and N(32b); (b) -*x*-1, -*y*-2, -*z*+1] form the equatorial plane [2.120(3) Å being the average Ni-N(eq) bond distance], whereas the apical positions are filled by two symmetrically related nitrogen atoms [2.213(2) Å for Ni-N(ap)].

Similarly to **1** and **2**, two crystallographically independent malonate ligands L1 [C(1)C(2)C(3)] and L2 [C(11)C(12)C(13)] occur in **3**. They act as bidentate ligands towards the Cr(1) atom through their inner carboxylate-oxygen atoms (see Figure 10). Each malonate ligand forms a six-membered ring, including the chromium atom, that adopts a boat conformation [θ = 90.6(4)º and ϕ = 121.7(4)º for L1 and θ = 96.1(4)º and ϕ = 133.4(4)º for L2] [Cremer D. *et al.*, 1975]. Bond lengths and angles for the malonate ligands that occur in **3** are listed in Table 9.

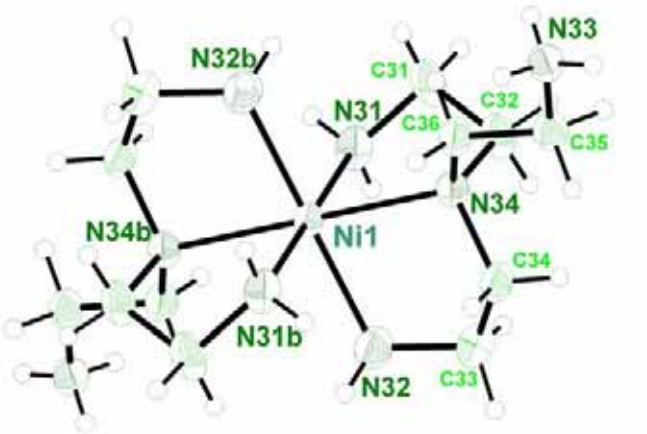

Figure 11. ORTEP view of the nickel environment in **3** with the numbering scheme. Thermal ellipsoids are drawn at the 50% probability level.

Table 9. Bond lengths (Å) and angles (º) for the malonate ligands in **3**

C(1)-C(2)	1.499(5)	C(2)-C(3)	1.499(5)
C(1)-O(1)	1.268(4)	C(3)-O(2)	1.259(4)
C(1)-O(3)	1.250(4)	C(3)-O(4)	1.246(4)
O(1)···O(2)	2.749(3)	O(3)···O(4)	4.543(4)
O(1)-C(1)-O(3)	120.6(3)	O(2)-C(3)-O(4)	122.1(3)
O(1)-C(1)-C(2)	120.4(3)	O(2)-C(3)-C(2)	120.0(3)
O(3)-C(1)-C(2)	119.0(3)	O(4)-C(3)-C(2)	117.9(3)
C(1)-C(2)-C(3)	118.5(3)		
C(1)-O(1)-Cr(1)	129.4(2)	C(3)-O(2)-Cr(1)	130.2(2)
C(11)-C(12)	1.494(5)	C(12)-C(13)	1.502(5)
C(11)-O(11)	1.247(4)	C(13)-O(12)	1.266(4)
C(11)-O(13)	1.253(4)	C(13)-O(14)	1.230(4)

O(11)···O(12)	2.766(3)	O(13)···O(14)	4.531(4)
O(11)-C(11)-O(13)	121.4(3)	O(12)-C(13)-O(14)	121.6(3)
O(11)-C(11)-C(12)	120.0(3)	O(12)-C(13)-C(12)	120.6(3)
O(13)-C(11)-C(12)	118.6(3)	O(14)-C(13)-C(12)	117.8(3)
C(11)-C(12)-C(13)	119.0(3)		
C(11)-O(11)-Cr(1)	128.6(2)	C(13)-O(12)-Cr(1)	125.9(2)

The $Htren^+$ ligand in **3** acts as a tridentate ligand [through N(31), N(32) and N(34) towards Ni(1); the values of N-Ni-N bite angles are 80.94(11) and 81.61(10)º], the protonated amino group of the $Htren^+$ ligand being free. The Ni-N bond distances range from 2.100(3) to 2.213(2) Å. This coordination mode of the $Htren^+$ ligand was previously observed in other $Htren^+$-containing metal complexes [Colpas G.J. et *al.*, 1990; Ellermeier J. et *al.*, 2002] but not in nickel(II) compounds. A literature survey on the behaviour of the $Htren^+$ as ligand shows monodentate towards Mn(II) [Schaefer M. *et al.*, 2003] and tridentate towards Ru(III) [Sakai K. *et al.*, 1996], Pt(II) [Davies M.S. *et al.*, 2000] and Cu(II) [Chen C.-H. *et al.*, 2002] coordination modes.

The $[Cr_2(mal)_4(OH)_2]^{4-}$ and $[Ni(Htren)_2]^{4+}$ units are connected through hydrogen bonds (see Table 10) involving the hydroxo group, some of the malonate oxygens and two amine-tren groups affording a two-dimensional network (see Figure 9a). Additional hydrogen bonds involving water molecules and malonate oxygen atoms connect adjacent layers contributing to the stabilisation of the resulting three-dimensional network (see Figure 9b).

Table 10. Hydrogen bonds and relevant short contacts for **3**[a-c]

D-H···A	D···A/Å	D-H···A	D···A/Å
O(1w)···O(4)	2.796(6)	O(3w)···O(2w)	2.891(6)
O(1w)···O(13c)	2.701(5)	O(3w)···O(4wc)	3.195(14)
O(2w)···O(3)	2.711(5)	O(4w)···O(14)	2.605(11)
O(2w)···O(1wd)	2.879(5)	O(4w)···O(1we)	2.924(11)
D-H···A	D···A/Å	H···A/Å	D-H···A/º
O(20)-H(20)···O(2wf)	2.966(4)	2.42(4)	162(6)
C(12)-H(11)···O(4wg)	3.371(12)	2.49(5)	156(4)
C(12)-H(12)···O(2wh)	3.360(6)	2.58(5)	167(5)
N(31)-H(30)···O(3wi)	3.006(5)	2.17(4)	164(4)
N(31)-H(31)···O(12i)	3.344(4)	2.48(4)	170(3)
N(31)-H(31)···O(14i)	3.078(5)	2.43(4)	131(3)

N(32)-H(36)···O(14j)	3.106(5)	2.36(5)	139(4)
N(32)-H(37)···O(3wi)	3.244(6)	2.65(5)	136(4)
N(33)-H(42)···O(4c)	2.824(5)	2.08(4)	172(4)
N(33)-H(43)···O(3j)	2.844(5)	2.00(4)	170(4)
N(33)-H(44)···O(13k)	2.834(5)	2.01(4)	172(4)
C(31)-H(32)···O(14c)	3.471(5)	2.55(5)	152(3)
C(31)-H(33)···O(14i)	3.158(6)	2.67(5)	112(3)
C(33)-H(39)···O(3wi)	3.308(6)	2.52(3)	139(3)
C(34)-H(40)···O(12b)	3.663(5)	2.77(4)	171(4)
C(35)-H(45)···O(2c)	3.398(5)	2.74(4)	123(3)
C(35)-H(46)···O(11k)	3.346(4)	2.66(3)	128(3)
C(36)-H(48)···O(3j)	3.459(4)	2.79(3)	132(3)

[a] Symmetry transformations: (b) -*x*-1, -*y*-2, -*z*+1; (c) *x*, *y*-1, *z*; (d) *x*+1, *y*, *z*; (e) -*x*, -*y*, -*z*+1; (f) -*x*, -*y*-1, -*z*; (g) -*x*, -*y*+1, -*z*+1; (h) *x*, *y*+1, *z*; (i) -*x*, -*y*-1, -*z*+1; (j) *x*-1, *y*-1, *z*; (k) -*x*-1, -*y*-1, -*z*. [b] A = acceptor; D = donor. [c] Symmetry operators apply to acceptor atoms.

References

Castro I., Sletten J., Calatayud M.L., Julve M., Cano J., Lloret F. and Caneschi A. *Inorg. Chem.*, **1995**, 34, 4903

Chen C.-H., Cai J. and Chen X.-M. *Acta Cryst., Sect. C*, **2002**, 58, m59.

Colpas G.J., Kumar M., Day R.O. and Maroney M.J. *Inorg. Chem.*, **1990**, 29, 4779

Cremer D. and Pople J.A., *J. Am. Chem. Soc.*, **1975**, 97, 1354.

Davies M.S., Fenton R.R., Huq F., Ling E.C.H., Hambley T.W. *Aust.J.Chem.*, **2000**, 53, 451.

DIAMOND 2.1d, Crystal Impact GbR, CRYSTAL IMPACT, K. Brandenburg & H. Putz GbR, Postfach 1251, D-53002 Bonn, Germany, 2000

Duan C.-Y., Lu Z.-L., You X.-Z. and Mak T.C.W. *Transition Met. Chem.*, **1998**, 23, 77.

Duisenberg A.J.M., Kroon-Batenburg, L.M.J. and Schreurs, A.M.M. *J. Appl. Cryst.*, **2003,** 36, 220 (EVALCCD)

Ellermeier J., Stahler R. and Bensch W. *Acta Cryst., Sect. C*, **2002**, 58, m70

Farrugia L.J. (*WINGX*), *J. Appl. Cryst*, **1999**, *32*, 837

Hooft, R.W.W. *COLLECT*. Nonius BV, Delft, The Netherlands, **1999**

Nardelli M. *J. Appl. Crystallogr.*, **1995**, *28*, 659

SADABS, version 2.03. Bruker AXS Inc.: Madison, WI, **2000**.

Sakai K., Yamada Y. and Tsubomura T. *Inorg. Chem.*, **1996**, 35, 3163.

Scaringe R.P., Hatfield W.E. and Hodgson D.J. *Inog. Chem.*, **1977a**, 16, 1600.

Scaringe R.P., Hatfield W.E. and Hodgson D.J. *Inorg. Chim. Acta*, **1977b**, 22, 175.

Schaefer M., Engelke L. and Bensch W. *Z. Anorg. Allg. Chem.*, **2003**, 629, 1912.

Sheldrick, G.M. *SHELX97*, *Programs for Crystal Structure Analysis (Release 97-2)*, Institüt für Anorganische Chemie der Universität, Tammanstrasse 4, D-3400 Göttingen, Germany, **1998**.

Mao Z.-W., Liehr G. and Eldik R.van *J. Chem. Soc., Dalton Trans.*, **2001**, 1593.

CONCLUSIONS

Conclusions

Following the demand for the rational design of clearly identified target molecules, an impressive synthetic work has been performed since the 1990's tending towards the nuclearity control of the transition metal compounds. The commonest used synthetic strategy consists of reacting the metal ions [A^{a+}] with coordinately ligands [L], where the number of available coordination sites and their relative position (for instance, *cis*- or *trans*- in the case of two labile sites and *mer*- or *fac*- in the case of three) around the metal ion A^{a+} is determined by the denticity and stereochemistry of the ligand L. Another more elaborated strategy consists in a better control of the polymerization possibilities using precursors. This *bottom up* strategy is throroughly analyzed and discussed in Chapters X and XI.

Synthetic strategy: choice of the precursors and analysis of the relevant parameters

One of the best methods for the rational design of nuclearity tailored polynuclear complexes is the use of a stable building block which can act as a ligand (complex as ligand strategy). All the tools associated to the flexibility of the coordination chemistry are used in this strategy. Three of the best rewarding examples are represented by the oxamidatocopper(II) complexes, the tris(oxalato)chromate(III) entity and the hexacyanometallate family which have provided a plethora of new extended systems with interesting magnetic properties. These precursors have in common a high solubility in water, a great stability (their nature being kept in solution), an anionic character (important parameter when thinking at their reaction with cationic species fully solvated cations or preformed cationic complexes) and a good complexing ability (chelating and bis-chelating character of the oxamide and oxalate and remarkable capability of the cyanide to act as a bridge). The carboxylate group has several singularities: first, its asymmetric character makes it a very appropriated ligand for selective binding of two different metal ions; second, it is able to mediate strong magnetic interactions between the paramagnetic centres that it bridges; and third, the nature of the magnetic coupling is easily predicted and its value is tuned by choosing the metal centres M and M' involved. *A priori*, this allows to foresee the nature of the ground spin state of the carboxylate-bridged entities.

As mentioned above, in an attempt to extend the vast carboxylate chemistry to molecular regime, we have developed an alternative synthetic route which consists of using stable malonate-bearing complexes of general formula $[M_2(mal)_4(OH)_2]^{4-}$ as ligand towards either fully solvated metal ions or partially blocked metal complexes. The possibilities that offer these types of precursors and the main parameters to play will be investigated.

Let us to outline briefly some of the points associated with the choice of these building blocks and their advantages. Concerning the malonate-bearing species, we will focus here on the preparative routes and characterization of a precursor of formula $[M_2(mal)_4(OH)_2]^{4-}$ with M = Cr^{III}. This unit is a quite stable paramagnetic and anionic building block with local spins of 3/2 (Cr^{III}). In general, we use two types of cations as precipitating agents: univalent alkaline cations (sodium and potassium essentially) and bulky organic cations (tetraphenylphosphonium or tetraphenylarsonium). This allows us to isolate high purity precursors which can be solubilized in common solvents (both polar and non polar). They were characterized by chemical analysis, X-ray diffraction on single crystals.

APPENDIX

APPENDIX A. X-RAY DIFFRACTION

X-Ray Diffraction

Equipment

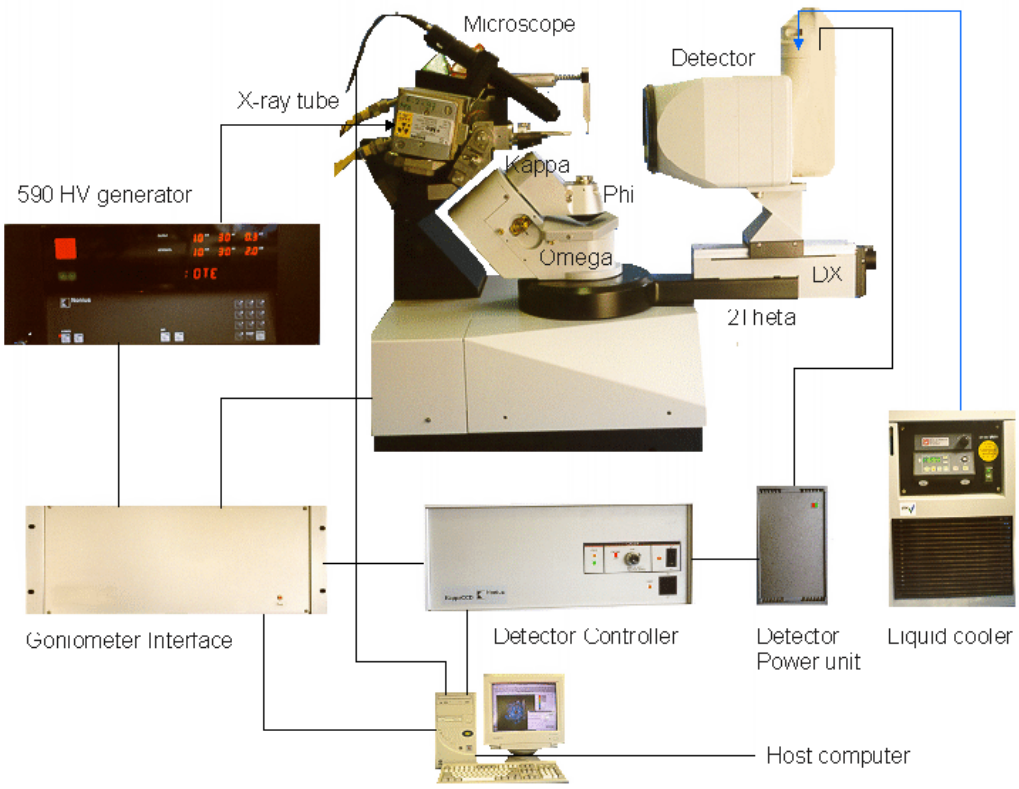

Scheme of a KappaCCD Diffractometer

The equipment used in all the X-ray measurements was a KappaCCD Difractometer.

The KappaCCD (see Scheme above) consists of a CCD detector, X-ray source, three axes goniometer (Omega, Kappa and Phi) to position the crystal and a Theta axis and displacement axis (DX) to position the detector. The CCD (Charge-Coupled Devide) is a two-dimensional detector that measures the X-ray, which is reflected in the crystal.

The X-ray is generated by a Mo tube which is a part of a high voltage generator (HV). The X-ray optics consists of a main shutter, a fast shutter, a monochromator to suppress the β- and brehms radiation and a collimator to get a small bundle. A

microscope displays the crystal on the PC monitor allowing us to centre the crystal. In the two-dimensional detector a phosphor converts the X-ray to light, a fibre optic taper reduces the image and a cooled scientific grade CCD measures the light signal.

Theoretical basis

Roentgen discovered in 1895 the X-rays while experimenting with vacuum tubes but it was Max von Laue who has shown in 1912 that X-rays behave as a wave when he observed the X-ray diffraction by crystals.

X-rays lie in the electromagnetic spectrum between the ultraviolet light and gamma radiation and have an approximate range of wavelenghts of 0.1-100 Å.

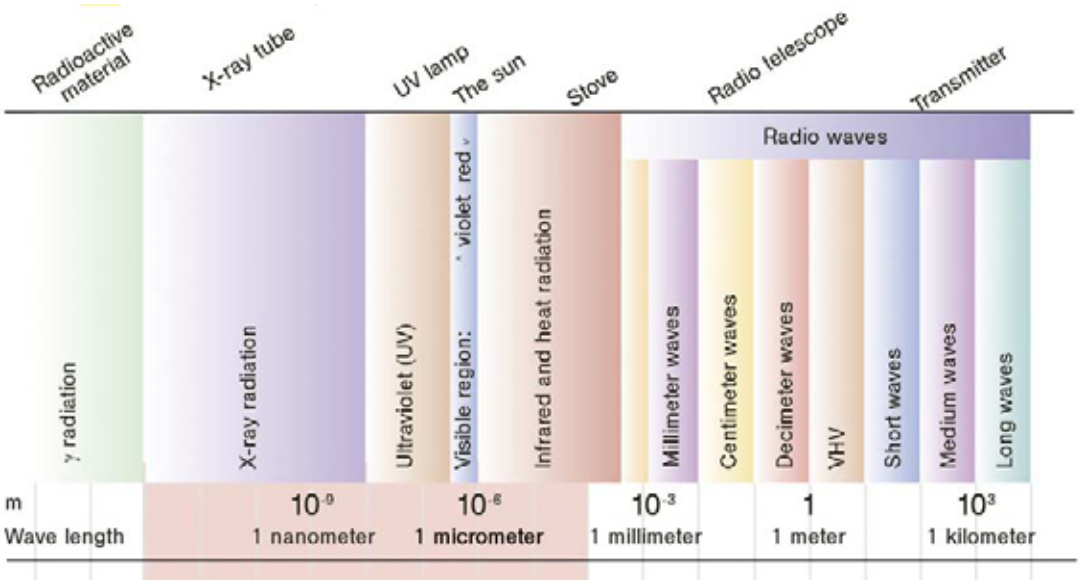

Scheme of the Electromagnetic Spectrum

To generate X-rays, electrons are accelerated by an electric field and directed against a metal target which produce a X-ray spectra. This spectra shows a continuum of radiation (bremsstrahlung component) which shows characteristic peaks and some spectral lines which are characteristic for the element of which the target is made (Figure 1).

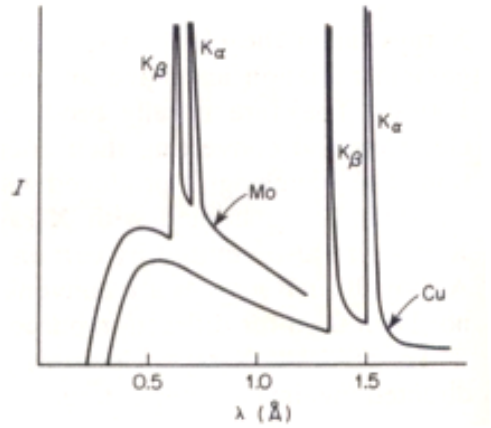

Figure 1. X-ray spectra with characteristic peaks; Mo-K_α, 50 kV; Cu-K_α, 35 kV.

A crystal is a solid which is composed by a set of atoms, molecules or ions arranged in a particular way (unit cell), which is periodically repeated in the three dimensions affording a regular lattice. X-ray diffraction can be used to determine the crystal structure (the arrangement of the atoms in a crystal) because its wavelength ($\lambda \sim$ 1 Å) has the same order of magnitude that the separation between the atoms, molecules or ions in a crystal.

The diffraction can be easily understood in the basis of the Bragg's law. He considered that a crystal is formed by families of lattice planes (hkl) which reflect the X-ray incident beams.

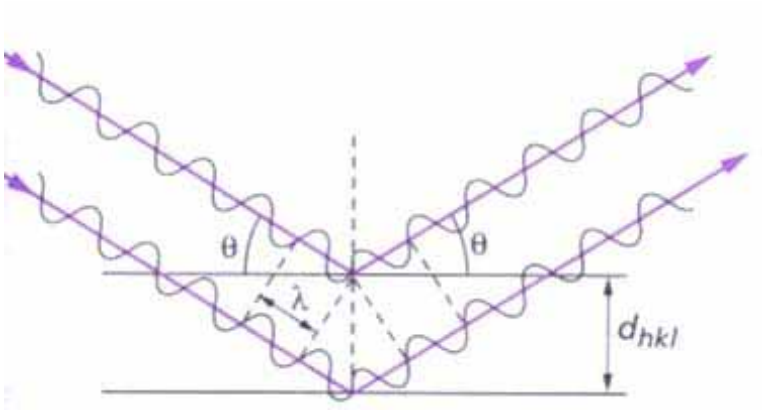

Scheme of the reflection on the lattice planes (Bragg's law)

Treating the diffraction as "reflection" from planes in the lattice he obtained the following equation, known as Bragg's law:

$$2d \sin\theta = n\lambda \qquad (1)$$

where d is the distance between lattice planes (hkl) and θ is the incident angle, λ is the wavelength of the incident beam and n is an integer. So, the directions where a maximum in the diffraction pattern is observed depends only on the lattice parameters. Nevertheless, the intensity of a diffracted beam in one direction depends on the nature and the position of the atoms in the crystal structure:

$$I_{hkl} \propto |F_{hkl}|^2 \tag{2}$$

where F_{hkl} is the structure factor defined as:

$$F_{hkl} = \sum_{m=1}^{1} f_m e^{i2\pi(hx_m+ky_m+lz_m)} = |F_{hkl}| e^{i\alpha} \tag{3}$$

f_m being the scattering factor of the mth atom in the unit cell and x_m, y_m and z_m the position of this atom.

The structure factor is related with the electron density:

$$\rho(x,y,z) = \frac{1}{V} \sum_{h,k,l} F_{hkl}\, e^{-2\pi i(hx+ky+lz)} \tag{4}$$

Combining equations (2)-(3) one can calculate the diffracted intensities by a crystal knowing its crystal structure. Unfortunately, measuring the intensity we loose some the information about the phase α:

$$I_{hkl} \propto F_{hkl} \cdot F_{hkl}^{*} = |F_{hkl}|^2 \tag{5}$$

Several methods have been developed to solve the phase problem: direct methods (where the phases are randomly assigned in an initial stage) and Patterson methods (which analyse the intensity by the way of the Patterson function). Both methods are iterative and how the intensities calculated from the theoretical crystal structure match the experimental ones.

More information about Crystallography and X-ray diffraction is available on the website of the IUCR (International Union of Crystalloraphy):

http://www.iucr.org/

where it's possible to find interesting educational resources.

It also quite interesting to have a look at the Interactive Course of Crystallography by Gervais Chapuis and Wes Hardaker available on the website:

http://lcr.epfl.ch/page37304.html

Some interesting text books:

Stout G.H. and Jensen L.H., "X-Ray Structure Determination: A Practical Guide", Ed. John Wiley & Sons, 1998.

Rousseau J.-J., "Cristallographie Géometrique et Radiocrystallographie", Ed. Dunod, 2000.

.

APPENDIX B. NEUTRON DIFFRACTION FACILITIES

Neutron Diffraction Facilities

G 4-1. Cold Neutron Two-Axis Diffractometer PYRRHIAS,

G 4-1 is a two-axis powder diffractometer equipped with a vertical focusing pyrolytic graphite monochromator and a 800-cells multidetector covering a 80° - 2θ range (step 0.1° between 2 cells). The most frequently used wavelength is 2.43 Å but can occasionaly be varied between 2.43 and 5.5 Å. The accessible 2θ diffusion angle covers the range 3° - 105°; in that range it is possible to perform diagrams with 0.02° step (2θ). The instrumental resolution of the spectrometer being minimal at low 2θ diffusion angle (2θ < 60°), G 4-1 is particularly well adapted for magnetic structure determination. The high acquisition rate of the multidetector allows to perform diffraction studies (structural or magnetic) as a function of external parameters (temperature, pressure…) and to follow in situ kinetic reactions or phase transitions; the minimal acquisition time is of the order of one minute. With longer acquisition time (a few hours) it becomes possible to detect and quantify minority phases present in a multiphase compound, generally down to 0.1% (weight percentage).

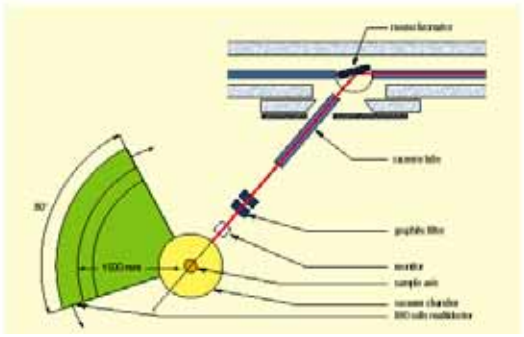

Fig.1 General layout of the cold neutron two axis difractometer G 4-1.

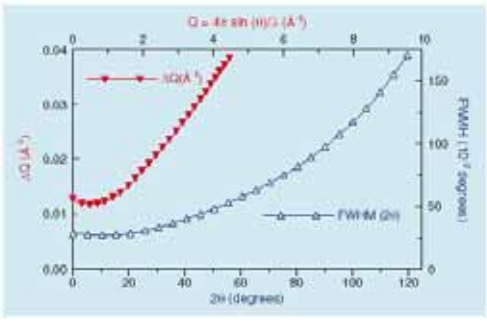

Fig.2 Resolution curves full width at half maximum (FWHM versus 2θ) (blue), Q variation of the resolution ΔQ (λ=0.245nm) (red)

G 4-2. High Resolution Powder Diffractometer

This diffractometer was designed and constructed in the Materials Science Research Laboratory of PNPI, Russia. It is installed at the G 4-2 site and has been in operation since january 1997. The diffractometer is designed for determination and refinement of the crystal and/or magnetic structure of powder materials especially with an elementary cell volume up to 1500 $Å^3$. The original feature of the diffractometer

consists of the way in which its 70 detectors are arranged, i.e., inside 7 dependent sections (each with a step motor and an absolute position encoder). Each section contains ten neutron detectors with a Soller collimator in front of each detector. The encoder of each section measures the angular position of the first detector in the section with a precision of 18" in the range of 0 - 360°. The other detectors in the section are positioned at 2° from each other. In the stage of preliminary data processing their positions are refined by the angular position of the transmission neutron beam measured by each detector. The sections are set in motion by step motors with the help of three air cushions lifting them over the base surface. The diffractometer mainly operates in the superposition mode: each part of the neutron diffraction pattern is measured successively by all detectors and the results are added up. The procedure is as follows: the detectors assembly as a whole (all seven sections) starts motion from the initial position at a given step and has the specified monitor counts (or specified exposition time) for each position. At the same time, the smallest technological gap between the sections is preserved. As soon as the first section reaches the specified final position, all sections stop and the transport velocity is switched on, at which the first section moves to the end of the detector assembly. The measuring procedure continues till the second section reaches the final position, then the third, etc… As a result, each detector measures the entire diffraction pattern. In further measurements of the same sample, the movement of the detector assembly can be accomplished in the backward direction. This determines a high luminosity of the diffractometer and considerably simplifies the correction for the efficiency of counting channels and the relative positions of the detectors. Simpler algorithms of operation in the non-superposition mode are also possible. In this case, for calibrating the counting channels and relative positions of the detectors, the efficiency file obtained during measurements in superposition mode is used. The collimator window is 11 x 110 mm^2, the working length is 200 mm, and the distance between the films is 1 mm ; the collimators are made of a thin polymer film with a gadolinium oxide-based absorber. The mean transmission coefficient measured for all 70 collimators is 85% and the beam divergence is 12 - 13'. The focusing Ge monochromator provides the possibility of using three wavelengths. This allows the diffractometer to be easily adjusted for many physical problems. The neutron monochromator is a set of 11 plates made from a plastically deformed Ge single crystal. The vertical axis is the rotation axis of the monochromator and coincides with the

crystallographic direction [110] within an accuracy of several minutes of arc. The plates are arranged one over another in a computercontrolled vertical focusing device which enables precision turning of the plates around the horizontal axis for the monochromator to have the form of a degenerated parabola. Turning of the monochromator as a whole around the vertical axis allows us to use the Ge (115), (004) and (113) reflections in the experiment. At the same time the resolution of the diffractometer changes and the neutron wavelength range changes from 1.8 Å to 2.8 Å. This allows us to optimise the conditions of a particular neutron diffraction experiment.

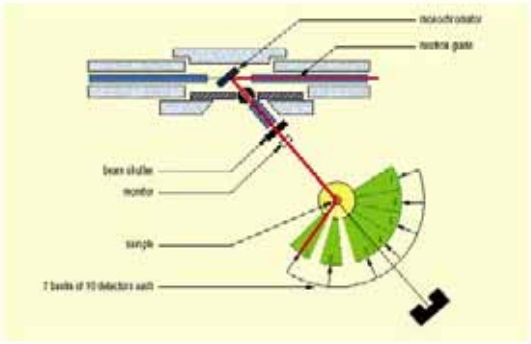

Fig.3 General layout of the cold neutron difractometer G 4-2.

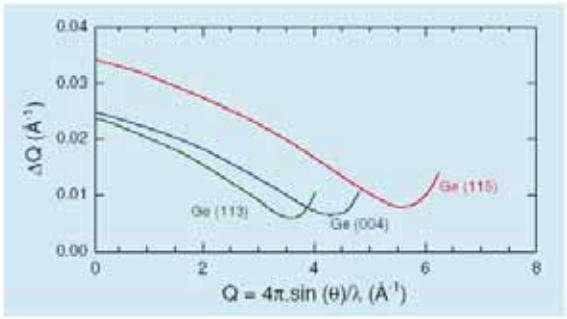

Fig.4 Resolution curves for the Ge(113), Ge(004) and Ge(115) (green, blue and red respectively) for the difractometer G 4-2.

APPENDIX C. MOLECULAR MAGNETISM

Molecular Magnetism

Magnetization and Magnetic Susceptibility

Diamagnetic and Paramagnetic Susceptibilities

In this first section we establish some key equations in molecular magnetism. To begin with, we consider a sample containing 1 mol of a molecular compound within an homogeneous magnetic field *H*. The sample acquires a molar magnetization *M* related to *H* through

$$\partial M / \partial H = \chi \tag{1}$$

where χ is the molar magnetic susceptibility. *M*, which is also called the molar magnetic moment, is a vector, *H* is an axial vector, and χ is a second rank tensor. It is always possible to choose the reference axes in order for χ to be diagonal with the χ_u *(u = x, y, z)* principal values. If the sample is magnetically isotropic, then χ becomes a scalar. When the magnetic field is weak enough, χ is independent of *H*, such that one can write

$$M = \chi H \tag{2}$$

Let us examine these equations. In principle χ is the algebraic sum of two contributions associated with different phenomena:

$$\chi = \chi^D + \chi^P \tag{3}$$

where χ^D and χ^P represent the diamagnetic and paramagnetic susceptibilities, respectively. The former is negative and the latter positive. When χ^D dominates, the sample is said to be diamagnetic; it is repelled by the magnetic field. When χ^P is the leading contribution, the sample is said to be paramagnetic; it is attracted by the applied field.

Diamagnetism is an underlying property of matter. It is always present, even when it is masked by the paramagnetism. The diamagnetism is due to the interaction of the magnetic field with the motion of the electrons in their orbits. The theory of this phenomenon has been well understood for several decades, and, for some small molecules, *ab initio* ca1culations of the molar diamagnetic susceptibility afford reasonably good results. It is sufficient to specify that χ^D is independent of the temperature and the strength of the applied field. Empirical formulas have been proposed to estimate its value. They are based on the idea that the diamagnetic susceptibility is essentially additive. χ^D can then be roughly ca1culated either from atomic susceptibilities and

constitutive corrections, or from group susceptibilities (group meaning here ligand or counterion). The constitutive corrections are generally positive. They account for the fact that a molecule with multiple or conjugated bonds is less diamagnetic than a rather similar molecule with only single bonds. In the 1940s Pascal tabulated data allowing the application of these additive methods.

Fundamental Equations in Molecular Magnetism

The molar paramagnetic susceptibility (hereafter χ) characterizes the way in which an applied magnetic field H interacts with the angular momenta associated with the thermally populated states of a molecule. In classical mechanics, when a sample is perturbed by an external magnetic field, its magnetization is related to its energy variation through

$$M = -\partial E / \partial H \tag{4}$$

This equation may be easily translated into the language of quantum mechanics. We consider a molecule with an energy spectrum E_n (n = 1, 2, ...) in the presence of a magnetic field H. For each energy level we can define a microscopic magnetization μ_n as

$$\mu_n = -\partial E_n / \partial H \tag{5}$$

The macroscopic molar magnetization M is then obtained by summing the microscopic magnetizations weighted according to the Boltzmann distribution law, which leads to

$$M = \frac{N\sum_n (-\partial E_n / \partial H)\exp(-E_n / kT)}{\sum_n \exp(-E_n / kT)} \tag{6}$$

where T is the temperature and k is the Boltzmann constant.

This expression (6) may be considered as the fundamental expression in molecular magnetism. It does not lean on any approximation. The molar magnetic susceptibility is deduced from (6) through (1), or, if H/kT is not too large, through (2).

Equation (6) may be transformed in a different way which will be used later on. For this we define the partition function Z as

$$Z = \sum_n \exp(-E_n / kT) \tag{7}$$

We can now write:

$$\partial \ln Z / \partial H = (1/kT) \frac{\sum_n (-\partial E_n / \partial H) \exp(-E_n / kT)}{\sum_n \exp(-En / kT)} \quad (8)$$

which leads to

$$M = NkT\left(\partial \ln Z / \partial H\right) \quad (9)$$

and

$$\chi = NkT(\partial^2 \ln Z / \partial H^2) \quad (10)$$

Van Vleck Formula

Although Eq. (6) is general, it is often difficult to apply. Indeed it requires knowledge on the $E_n = f(H)$ variations for all thermally populated states to calculate the $\partial E_n / \partial H$ derivatives. In 1932 Van Vleck proposed a simplification based on a few approximations [Van Vleck J.H., 1932]. The first of them is that it is legitimate to expand the energies E_n according to the increasing powers of H:

$$E_n = E_n^{(0)} + E_n^{(1)} H + E_n^{(2)} H^2 + \cdots \quad (11)$$

where $E_n^{(0)}$ is the energy of level n in zero field. $E_n^{(1)}$ and $E_n^{(2)}$ are called first- and second-order Zeemann coefficients, respectively. From (11), μ_n in (5) becomes

$$\mu_n = -E_n^{(1)} - 2E_n^{(2)} H + \cdots \quad (12)$$

The second approximation is that H/kT is small with respect to unity. In other words, it is assumed that H is not too large and T not too small. The exponential in (6) may then be written as

$$\exp\left(-E_n/kT\right) = \exp\left(-E_n^{(0)}/kT\right)\left(1 - E_n^{(1)} H/kT\right) \quad (13)$$

From these two approximations, we obtain

$$M = \frac{N\sum_n (-E_n^{(1)} - 2E_n^{(2)} H)(1 - E_n^{(1)} H / kT) \exp(-E_n^{(0)} / kT)}{\sum_n (1 - E_n^{(1)} H / kT) \exp(-E_n^{(0)} / kT)} \quad (14)$$

In zero field, the magnetization vanishes, such that

$$\sum_n E_n^{(1)} \exp\left(-E_n^{(0)}/kT\right) = 0 \quad (15)$$

This condition (15) exc1udes molecular-based compounds exhibiting a spontaneous magnetization.

Substituting (15) into (14) and retaining only terms linear in H results in

$$M = \frac{NH\sum_n \left(E_n^{(1)2}/kT - 2E_n^{(2)}\right)\exp\left(-E_n^{(0)}/kT\right)}{\sum_n \exp\left(-E_n^{(0)}/kT\right)} \tag{16}$$

and finally

$$\chi = \frac{N\sum_n (E_n^{(1)^2}/kT - 2E_n^{(2)})\exp(-E_n^{(0)}/kT)}{\sum_n \exp(-E_n^{(0)}/kT)} \tag{17}$$

which is the Van Vleck formula. To apply this formula we only need to know the $E_n^{(0)}$, $E_n^{(1)}$, and $E_n^{(2)}$ quantities. It is no longer necessary to calculate the derivatives $\partial E_n / \partial H$. From a theoretical point of view, the Van Vleck formula can be utilized when the eigenvalues $E_n^{(0)}$ and eigenfunctions $|n\rangle$ of the Hamiltonian in zero-field associated with the molecule under consideration are known. $E_n^{(1)}$ and $E_n^{(2)}$ are then calculated through perturbation theory as

$$E_n^{(1)} = \langle n|\overline{H_{ZE}}|n\rangle \tag{18}$$

$$E_n^{(2)} = \sum_m{}' \frac{\langle n|\overline{H_{ZE}}|m\rangle^2}{(E_n^{(0)} - E_m^{(0)})} \tag{19}$$

where Σ' means that the summation runs over the levels m with $E_m^{(0)} \neq E_n^{(0)}$. $\mathbf{H}_{ZE}$ is the Zeeman operator, which accounts for the interaction between the magnetic field and the electronic angular momenta:

$$\overline{H_{ZE}} = \beta\sum_i \left(\overline{l_i} + g_e\overline{s_i}\right)\cdot H \tag{20}$$

where $\mathbf{l}_i$ is the orbital momentum of electron i and $\mathbf{s}_i$ is the spin momentum of the same electron. g_e is the gyromagnetic factor, or the g-factor, of the free electron (equal to 2.0023), and β is the Bohr magneton (1 $N\beta$ = 5585 cm^3 G mol^{-1}). In principle the summation in (20) runs over all electrons of the system. In a molecular orbital approach (without configuration interaction) only electrons occupying singly occupied orbitals contribute to the Zeeman perturbation. The expressions for $E_n^{(1)}$, in (18), and $E_n^{(2)}$, in (19), suppose implicit1y that the Zeeman perturbation is diagonal using the functions $|n\rangle$ as a basis set. We would like to stress here that before using Van Vleck's equation, it is always necessary to check that the approximations on which it leans are valid. In particular, the Van Vleck equation gives the magnetic susceptibility only in the magnetic field range where the M versus H plot is linear.

When all energies E_n are linear in H, the second-order Zeeman coefficients $E_n^{(2)}$ vanish and (17) becomes

$$\chi = \frac{N\sum_n E_n^{(1)^2} \exp(-E_n^{(0)}/kT)}{kT\sum_n \exp(-E_n^{(0)}/kT)} \tag{21}$$

Temperature-Independent Paramagnetism

If the only thermally populated state of a molecule is a spin singlet without first-order angular momentum, then the paramagnetic susceptibility is intuitively expected to be zero, and the measured susceptibility will be negative. In a few cases a somewhat different situation is encountered, which the Van Vleck formula easily accounts for.

Let the energy $E_0^{(0)}$ of the ground state be the energy origin. Since this state has no angular momentum-it is said to be diamagnetic-$E_0^{(1)}$ is zero and (17) becomes

$$\chi = 2NE_0^{(2)} \tag{22}$$

or, from (19)

$$\chi = -2N\sum_{m\neq 0} \frac{\langle 0|\overline{H}_{ZE}|m\rangle^2}{\left(E_0^{(0)} - E_m^{(0)}\right)} \tag{23}$$

The diamagnetic ground state may couple with excited states through the Zeeman perturbation provided that the energy gaps are not too large. χ in (23) is positive since all denominators are negative, and temperature independent. This contribution is often called temperature-independent paramagnetism (TIP). The TIP is actually rather small, often of the same order of magnitude as the diamagnetism, but of opposite sing. For example it is estimated to be about 60 x 10^{-6} cm^3 mol^{-1} for copper(II) mononuclear species.

TIP is not restricted to compounds with a diamagnetic ground state. The coupling between a magnetic ground state and nonthermally populated excited states may also give a weak temperature-independent contribution, which then superimposes to the dominant temperature-dependent contribution arising from the ground state. In the following we will assume that the measured susceptibilities have been corrected not only for diamagnetism, but also for TIP

Magnetic Properties in Co(II) Complexes

Cobalt(II) Mononuclear Complexes

The mononuclear cobalt(II) complexes (high spin S = 3/2) where the metal ion is six-coordinated have magnetic properties which deviate substantially from the magnetic behaviour of the free ion and this fact makes difficult the interpretation of the magnetic properties of these compounds.

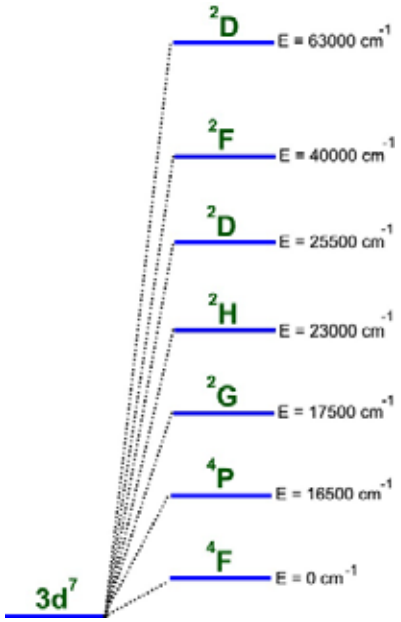

Scheme 1

The existence of an important orbital contribution in the hexacoordinated cobalt(II) complexes that cannot be neglected is the main problem in the interpretation of the magnetic properties of these compounds.

The free Co(II) ion presents a d^7 electronic configuration (see scheme 1) and consequently a ^4F ground state. The first excited term, ^4P is located at 16500 cm^{-1} from the ground state so its contribution to the magnetic properties is basically negligible (only a short mixture with the fundamental state due to a second order spin-orbit coupling could appears).

Obviously in the coordination chemistry compounds, the cobalt(II) ion is not free. It's coordinated to other atoms which form a given environment around the metal ion, and we have to take into account the influence of the chemical bonds in the electronic configuration of the metal ion. This influence is known as the crystal field.

Usually Co(II) ion is six-coordinated. In the pure O_h symmetry (see scheme 2), the term ^4F splits into three levels: $^4T_{1g}$, $^4T_{2g}$ and $^4A_{2g}$ ($^4T_{1g}$ being the ground state). The excited levels are enough far in energy from the ground state (> 8000 cm^{-1}) to consider that only the $^4T_{1g}$ is thermally populated.

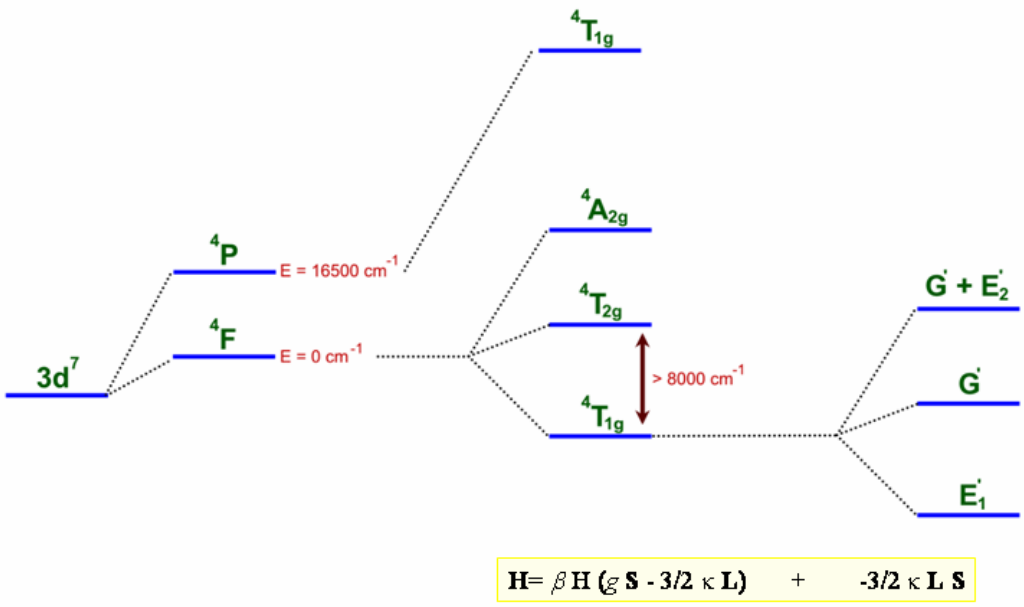

Scheme 2

The $^4T_{1g}$ ground state is an orbital triplet. It has a first-order orbital momentum that couples with the spin momentum and this spin-orbit coupling partially removes the degeneracy of the $^4T_{1g}$ ground state that splits into three levels: a sextet (G'+E_2'), a quartet (G') and a Kramers doublet (E_1').

At this point, we use the isomorphism that exits between the T_{1g} triplet orbital and the L = 1 triplet (M_L = 0, ±1). The eigenvalues of the matrix corresponding to the T_{1g} are the same of the L = 1 when we multiply them by -3/2. Moreover, the calculation requires the introduction of an additional parameter, the orbital reduction factor κ that takes into account both the covalence of the Co-ligand bonds and the admixture of the $^4T_{1g}$ (from the ^4P of the free ion) excited state and the $^4T_{1g}$ (from the ^4F) ground state. For cobalt(II), the spin-orbit coupling parameter λ is negative and of the order of 170 cm^{-1}. So, to calculate the eigenvalues of the eigenfunctions we have to diagonalise the spin-orbit coupling operator:

$$\hat{H}_{SO} = -3/2\kappa\lambda\ \hat{L}\cdot\hat{S} \qquad (1)$$

which acts on the basis set $|m_l, m_s\rangle$ where $m_l = 0, \pm1$ y $m_s = \pm1/2, \pm3/2$ (κ and λ being the orbital reduction factor and the spin-orbit coupling, respectively).

Taking into account the spin-orbit-coupling together with the Zeeman interaction (eq. 2), when the cobalt(II) ion is six-coordinated in the pure O_h symmetry we can obtain an expression for the magnetic susceptibility (eq. 3)

$$\hat{H} = (-3/2)\kappa\lambda\hat{L}\cdot\hat{S} + \beta[(-3/2)\kappa\hat{L} + g_e\hat{S}]H; \quad (2)$$

$$\chi_M = \frac{N\beta^2}{\kappa T}\frac{F_1}{F_2};$$

$$F_1 = \frac{63}{20}(-2+k)^2 x + \frac{2(4+3k)^2}{25k} + \left[\frac{2}{45}\left(11-3k)^2 x + \frac{88(4+3k)^2}{2025k}\right)\right]\exp\left(-\frac{15kx}{4}\right) + \left[\frac{1}{36}(10+3k)^2 x - \frac{10(4+3k)^2}{81k}\right]\exp(-6kx); \quad (3)$$

$$F_2 = \left[3 + 2\exp\left(\frac{15kx}{4}\right) + \exp(-6kx)\right]x;$$

The fundamental Kramers doublet is separated 9/4λ (J = 1/2) in energy from the first excited state and 6λ from the second one. Taking a value of -170 for λ (decreasing this value when the covalent character of the compound increases) the energy gap between the ground state (E_1')and the first excited states (G' and G' + E_2') will be: 300 cm^{-1} (G') and 900 cm^{-1} (G + E_2').

At room temperature, the sextet (G'+E') will be poorly populated because it's well separate in energy from the ground state and it could be discarded from the interpretation of the magnetic properties. So, the magnetic behaviour of Co(II) in a pure O_h symmetry is due mainly to the fundamental Kramers doublet (E') and the first excited quartet (G'). Upon cooling, the population of the quartet state decrease in favour of the Kramers doublet ground state. In this respect, the susceptibility below 30 K could be interpreted by means of the Ising model, where an effective spin of ½ is supposed for the fundamental doublet.

Up to now, we have considered the cobalt(II) ion in a O_h pure symmetry, but in the coordination chemistry of the cobalt(II) complexes, the environment of the metal ion is often distorted, being the cobalt in a lower symmetry environment (D_{4h}, C_{4v}). This distortion of the metal environment breaks the degeneration of the $^4T_{1g}$ orbital triplet state and if this distortion is important, the magnetic behaviour of the cobalt(II) ion

approach to that of the isolated high-spin ion. Under an axial distortion (D_{4h} or C_{4v} point group), the orbital triplet removes its degeneracy and it splits into two levels (see scheme 3): an orbital singlet $^4A_{2g}$ and an orbital doublet ^4E_g [more important the axial distortion, more higher the gap (Δ) between the $^4A_{2g}$ and ^4E_g levels]. When $^4A_{2g}$ is the fundamental state and the environment of the cobalt(II) is highly distorted, the Δ value could be bigger enough to consider that the singlet orbital is the only state thermally populated at room temperature and consequently we can treat these cobalt(II) complexes through an isolated spin Hamiltonian. In such a case we have to take into account the zero-field splitting due the second-order spin-orbit coupling. Thus, the energy levels of (scheme 3 left) due to this second-order coupling give rise to that of the (scheme 3 right), where we used the double group D'_4 irreducible representation to label the levels arising from the axial symmetry, so that $\Gamma_6(E_2')$ makes references to the M = ± 1/2 values and $\Gamma_7(E_3')$ to the M = ± 3/2. The interaction between the levels with the same symmetry from the ^4E and $^4A_2$ terms leads to the splitting of the $\Gamma_6(E_2')$ and $\Gamma_7(E_3')$ levels.

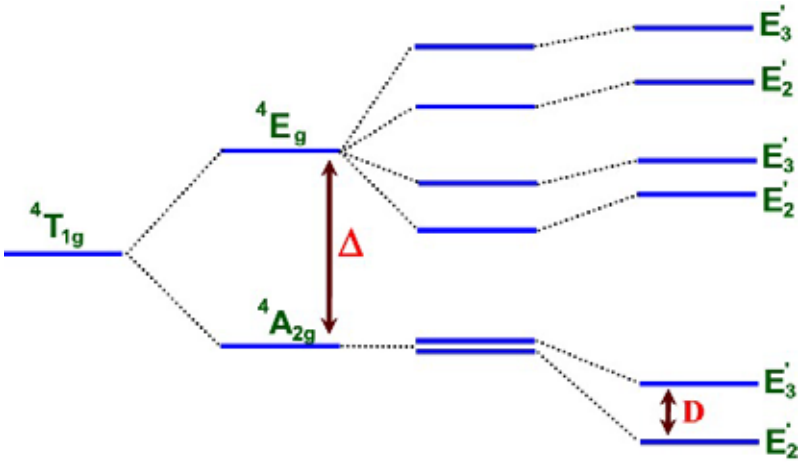

Scheme 3

The resulting expression for the magnetic susceptibility bearing in mind this approximation and taking into account the zero-field splitting is:

$$\chi = \frac{\chi_{\parallel} + 2\chi_{\perp}}{3} \tag{4}$$

where

$$\chi_{\parallel} = \frac{Ng_z^2\beta^2}{4kT}\frac{1+9\exp(-2D/kT)}{1+\exp(-2D/kT)} \tag{5}$$

$$\chi_{\perp} = \frac{Ng_x^2\beta^2}{kT}\frac{1+(3/4x)[1-\exp(-2x)]}{1+\exp(-2x)} \quad (6)$$

being $x = \frac{D}{kT}$;

Nevertheless, although most of the cobalt(II) compounds show this type of distortion, it is not large enough to neglect the population of the first excited state (^4E_g) at room temperature. So, we usually cannot use the isolated spin Halmiltonian. When the energy difference (Δ) between the ground and the first excited state is not large enough to consider that only the ground state is thermally populated at room temperature, we must take into account the ^4E_g term and we have to introduce in the Hamiltonian a crystal field operator with axial symmetry. Then, the magnetic susceptibility depends on λ (spin-orbit coupling), κ (orbital reduction factor) and Δ (the energy difference between the ground and the first excited state). The matrix obtained using the new Hamiltonian is not diagonal and therefore, no analytic expression can be deduced and the matrix must be solved numerically.

Co(II) Dinuclear complexes

In order to deal with the cobalt(II) dinuclear complexes we are going to analyze first the complexes where the distortion of the metal environment from the octahedral symmetry (O_h) is large enough to consider that the energy levels arising from the splitting of the $^4T_{1g}$ term are well separated in energy (Δ>>kT). In this case, we can use the isolated spin Hamiltonian because there is no orbital momentum:

$$\hat{H} = -J\,\hat{S}_A\cdot\hat{S}_B \quad (7)$$

When $S_A = S_B = 3/2$, the magnetic susceptibility is given by the following expression:

$$\chi_M = \frac{2N\beta^2g^2}{kT}\left\{\frac{e^x+5e^{3x}+14e^{6x}}{1+e^x+5e^{3x}+7e^{6x}}\right\} \quad (8)$$

with $x = \frac{J}{kT}$;

Moreover, at very low temperatures the $^4A_{2g}$ ground state of each cobalt ion splits into two Kramers doublets due to the second order spin-orbit coupling (zero-field

splitting, see scheme 3). For such a case, no analytical expression for the magnetic susceptibility can be obtained.

Only few six-coordinated high-spin cobalt dinuclear complexes show magnetic properties that can be analyzed through this model. Between them we have to emphasize those where the magnetic exchange coupling J is the dominant parameter and/or those which show highly distorted environments ($\Delta >> kT$). Unfortunately, the distortion of the metal environment is not large enough to neglect the orbital momentum of the $^4T_{1g}$ ground state.

In spite of everything, bearing in mind that the spin-orbit coupling of the ground state leads to a Kramers doublet which is separated 300 cm^{-1} from the first excited states, we can consider that below 30K, only the Kramers doublet is thermally populated. Within this approximation, we can use the 1/2 effective spin approach. It's possible to demonstrate that the real spin operator (S = 3/2) $\hat{S}$, is the effective spin (S = 1/2) $\hat{s}$ multiplied by 3/5:

$$\hat{S} = 3/5\,\hat{s} \tag{9}$$

Under this approach, the Hamiltonian is given by the eq. 7. If we consider an isotropic spin, $g_x = g_y = g_z = g_0$ we obtain:

$$\hat{H} = \frac{25}{9} J\,\hat{S}_1\hat{S}_2 + g_o\beta H_z(\hat{S}_{1,z} + \hat{S}_{2,z}) \tag{10}$$

$$\chi_M = \frac{2N\beta^2 g_0^2}{kT}\left[3 + \exp\left(\frac{-25J}{9kT}\right)\right]^{-1} \tag{11}$$

where N is the Avogradro constant, β is the Bohr magneton and k is the Boltzmann constant. Unfortunately, the Kramers doublet is highly anisotropic ($g_{\parallel} \neq g_{\perp}$). Hence, bearing in mind this anisotropy, it's possible to deduce the eq. 12, which correspond to an Ising dinuclear complex [Coronado E. *et al.*, 1998]:

$$\chi_M = \frac{(\chi_{\parallel} + 2\chi_{\perp})}{3} \tag{12}$$

$$\chi_{\parallel} = \frac{N\beta^2 g_{\parallel}^2}{2kT}\frac{\exp\left(\frac{25J}{18kT}\right)}{\cosh\left(\frac{25J}{18kT}\right)} \tag{13}$$

$$\chi_{\perp} = \frac{18N\beta^2 g_{\perp}^2}{25J}\tanh\left(\frac{25J}{36k}\right) \tag{14}$$

This approach can only be used when the Kramers doublet is the only thermally populated state (T < 30 K). If we want to analyse the experimental data at higher temperatures we must take into account the orbital momentum of the high-spin cobalt ions. Then, the Hamiltonian is given by:

$$\hat{H} = -J\ \hat{S}_1\hat{S}_2 - \beta H_z\,[2(\hat{S}_{1,z} + \hat{S}_{2,z}) - \frac{3}{2}\kappa\lambda(\hat{L}_{1,z} + \hat{L}_{2,z})] \tag{15}$$

This Hamiltonian leads to a 144x144 matrix which is difficult to diagonalise. In order to obtain an analytical expression for the magnetic susceptibility, Lines used the following approach: the matrix is diagonalised considering only the Kramers doublet and the first excited terms are introduced as a molecular field. In this way, the magnetic susceptibility for a cobalt(II) dinuclear complex where the metal ions show an octahedral symmetry and are magnetically coupled is given by the following equation:

$$\chi_M = \frac{2N\beta^2}{kT}[g(T)]^2\left[3 + \exp\left(\frac{-25J}{9kT}\right)\right]^{-1} \tag{16}$$

where *g(T)* is a temperature dependent function. The cM value needs to be calculated in an iterative routine which converge when $|Xi\text{-}1 - Xi| < 10^{-9}$, being $Xi = (\langle \mathbf{S_z} \rangle / \beta H_o)_i$.

Recently, an expression for an axially distorted cobalt(II) dinuclear compound have been deduced using the Lines approach.

For higher nuclearity compounds (n high-spin cobalt ions) we need to diagonalise a $12^n x 12^n$ matrix in order to obtain a expression for the magnetic susceptibility. So, in a first approach we can only obtain an analytical expression for the magnetic susceptibility considering that only the Kramers doublet is thermally populated (T < 30 K). So that, for a cobalt(II) chain, the magnetic susceptibility derived from the Ising model is given by the expression [Fisher M. E., 1963]:

$$\chi_M = \frac{(\chi_{\parallel} + 2\chi_{\perp})}{3} \tag{17}$$

$$\chi_{\parallel} = \frac{Ng_{\parallel}^2\beta^2}{4kT}\exp\left(\frac{J}{2kT}\right) \tag{18}$$

$$\chi_{\perp} = \frac{Ng_{\perp}^2}{2J}\left[\tanh\left(\frac{J}{2kT}\right) + \left(\frac{J}{4kT}\right)\mathrm{senh}^2\left(\frac{J}{4kT}\right)\right] \qquad (19)$$

Magnetic Properties in Rare-Earth Complexes

The rare earth ions have a $4f^n5s^25p^6$ ground configuration. This electronic feature confers on the lanthanides a characteristic magnetic behaviour, quite different from that of the transition metal ions ($3d^n$ ground configuration). Comparing to the behaviour of the transition metal ions, the magnetic properties of the rare earths are much less influenced by the environment because in the latter the 4*f* orbitals, partially occupied by magnetically active electrons, are very efficiently shielded by the fully occupied 5*s* and 5*p* orbitals. Therefore, in a first approximation a rare earth ion in a molecular compound magnetically behaves as a free ion. It also deserves to be note that the magnitude of the spin-orbit coupling is much larger for rare earth than for a $3d^n$ ion, and it increases from the left to the right of the Periodic Table. So, the Russel-Sunders model is a good approximation to describe the energy levels of the lanthanides. Consequently, the spin-orbit coupling partially remove the degeneracy of the $^{2S+1}\Gamma$ ground term, giving rise to $^{2S+1}\Gamma_J$ states, with *J* varying and integer value from $|L - S|$ to $L + S$. *J* is the quantum number associated with the total angular momentum $\hat{\mathrm{J}}$ defined as:

$$\hat{\mathrm{J}} = \hat{\mathrm{L}} + \hat{\mathrm{S}} \qquad (1)$$

The lowest state in energy has the smallest *J* for the configurations $4f^1$-$4f^6$, and the highest *J* for the configurations $4f^8$-$4f^{13}$. For the configuration $4f^7$, there is no first-order angular momentum.

The energy separations between the ground state and the first excited state for rare earth ions are reported in Table 1 and a schematic view of the energy levels of the earth rare ions are depicted in Scheme 1.

Table 1. Ground and first excited states with the energy separation between these levels for the Rare Earth Ions

Lantanide Ion	$4f^n$	S	L	J	Ground State	First Excited State	ΔE (cm^{-1})
Ce(III)	$4f^1$	1/2	3	5/2	$^2F_{5/2}$	$^2F_{7/2}$	2200
Pr(III)	$4f^2$	1	5	4	$^3H_4$	$^3H_5$	2100
Nd(III)	$4f^3$	3/2	6	9/2	$^4I_{9/2}$	$^4I_{11/2}$	1900
Pm(III)	$4f^4$	2	6	4	$^5I_4$	$^5I_5$	1600
Sm(III)	$4f^5$	5/2	5	5/2	$^6H_{5/2}$	$^6H_{7/2}$	1000
Eu(III), Sm(II)	$4f^6$	3	3	0	$^7F_0$	$^7F_1$	300
Gd(III), Eu(II)	$4f^7$	7/2	0	7/2	$^8S_{7/2}$	$^6P_{7/2}$	30000
Tb(III)	$4f^8$	3	3	6	$^7F_6$	$^7F_5$	2000
Dy(III)	$4f^9$	5/2	5	15/2	$^6H_{15/2}$	$^6H_{13/2}$	-

Ho(III)	$4f^{10}$	2	6	8	$^5I_8$	$^5I_7$	-
Er(III)	$4f^{11}$	3/2	6	15/2	$^4I_{5/2}$	$^4I_{13/2}$	6500
Tm(III)	$4f^{12}$	1	5	6	$^3H_6$	$^3H_5$	-
Yb(III)	$4f^{13}$	1/2	3	7/2	$^2F_{7/2}$	$^2F_{5/2}$	10000

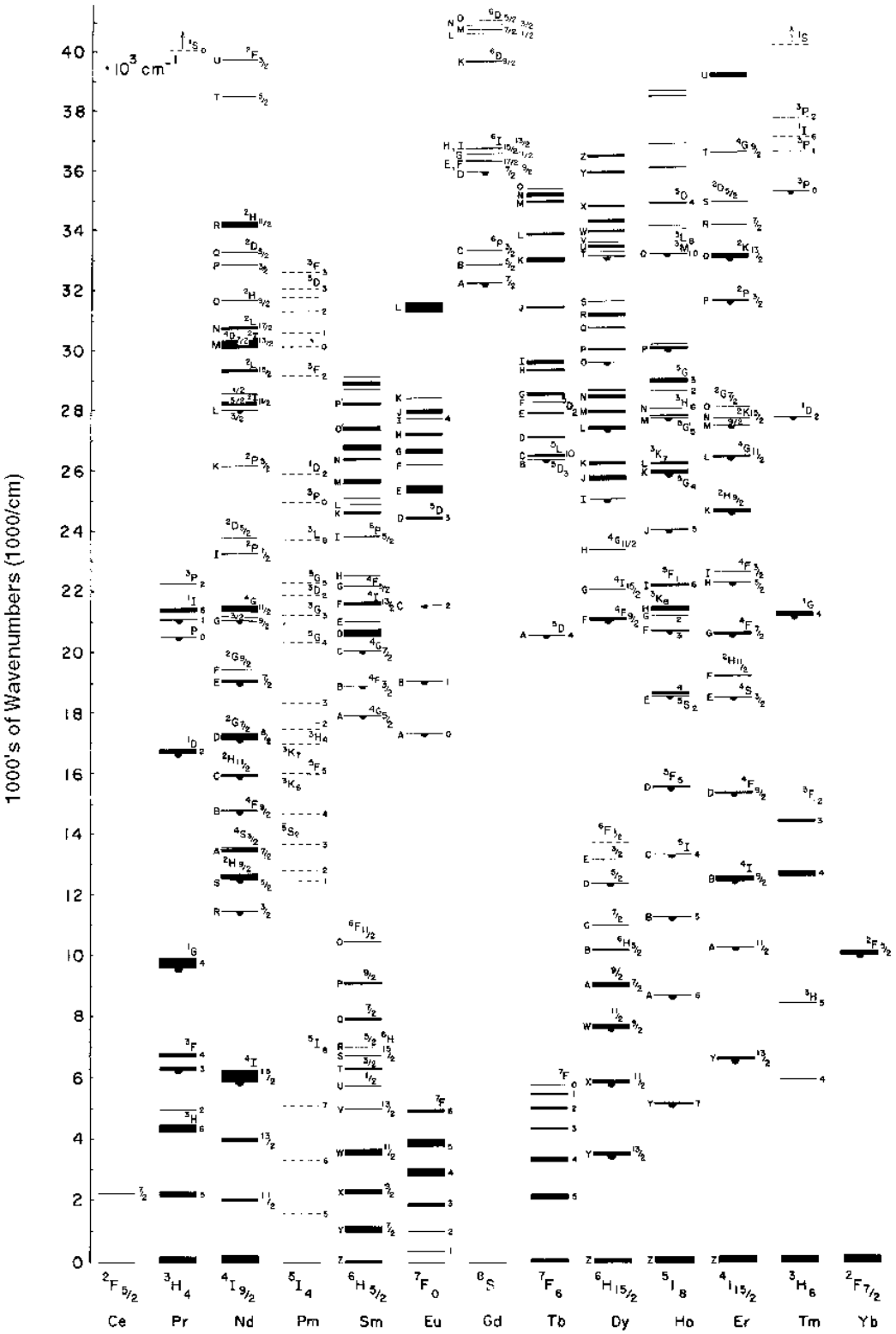

Scheme 1. Spectra and energy levels of Rare Earth Ions [Dieke G.H., 1968].

When the energy separation between the ground and the first excited states is weak, the first state may be thermally populated; when it is large, only the ground state is thermally populated. At room temperature, only the ground state is thermally populated for most of the rare earth, because the strong spin-orbit coupling. Therefore, the magnetic behaviour for the rare earth ions at high temperatures is similar to that of the free ion. Only for Eu(III) and Sm(III) lanthanide ions, the energy separation between the ground and the first excited states is not enough consider that only this former is thermally populated at room temperature and we have to take into account the first excited state to explain the magnetic behaviour at high temperatures.

When the magnetic behaviour of the rare earth ions can be interpretated in the light of the free ion approximation (considering that only the ground state is thermally populated), we face with the magnetism of a system with a well isolated $^{2S+1}\Gamma_J$ ground state, and J, L and S are good quantum numbers. When we applied a magnetic field H, the $^{2S+1}\Gamma_J$ state is split into $2J+1$ levels, the wavefunctions of which being noted $|J, M_J>$, with M_J varying by an integer value from $-J$ to J. M_J is the quantum number associated with the magnetic momentum $\hat{M}$ defined as:

$$\hat{M} = \hat{L} + 2\hat{S} \tag{2}$$

and then we have to applied the Zeeman Hamiltonian

$$\hat{H}_{ZE} = \beta \hat{M} H \tag{3}$$

in order to obtain the energy $E(J, M_J)$ of the $|J, M_J>$ energy levels [Kahn O., 1993]

$$E(J, M_J) = < J, M_J \mid \hat{H}_{ZE} \mid J, M_J > = \beta g_J M_J H \tag{4}$$

with

$$g_J = \frac{3}{2} + \frac{S(S+1) - L(L+1)}{2J(J+1)} \tag{5}$$

Therefore, the magnetic susceptibility is given by the following equation:

$$\chi_M = \frac{N g_J^2 \beta^2}{3kT} J(J+1) \tag{6}$$

So, in the approximation of the free ion, the magnetic susceptibility obeys the Curie Law. The g_J parameter and the value of the $\chi_M T$ at high temperature for the lanthanide ions are listed in Table 2.

Table 2. Values of g_J and $\chi_M T$ at high temperature for lanthanides in the Free-Ion Approximation

Lantanide Ion	Configuration $4f^n$, n =	g_J	$\chi_M T$ (cm^3 K mol^{-1})
Ce(III)	1	6/7	0.80
Pr(III)	2	4/5	1.60
Nd(III)	3	8/11	1.64
Pm(III)	4	3/5	0.90
Sm(III)	5	2/7	0.09
Eu(III), Sm(II)	6	5	0.00
Gd(III), Eu(II)	7	2	7.88
Tb(III)	8	3/2	11.82
Dy(III)	9	4/3	14.17
Ho(III)	10	5/4	14.07
Er(III)	11	6/5	11.48
Tm(III)	12	7/6	7.15
Yb(III)	13	8/7	2.57

The presence of excited states not too far from the ground state [as it occurs for Eu(III) and Sm(III)] may add a significant temperature-independent contribution χ'_M to the magnetic susceptibility calculated in eq. 6.

$$\chi'_M = \frac{2N\beta^2(g_J - 1)(g_J - 2)}{3\lambda} \tag{7}$$

where λ is the spin-orbit coupling parameter ocurring in the spin-orbit coupling operator $\lambda\hat{L}\hat{S}$ acting on the $^{2S+1}\Gamma$ term.

Consequently for Eu(III) and Sm(III), we have to take into account all the thermally populated levels when we calculate the molar magnetic susceptibility which follows the following equation:

$$\chi_M = \frac{\sum_J (2J+1)\chi(J)\exp[-E(J)/kT]}{\sum_J (2J+1)\exp[-E(J)/kT]} \tag{8}$$

the $\chi(J)$ term takes into account the temperature-dependent contribution:

$$\chi(J) = \frac{Ng_J^2\beta^2 J(J+1)}{3kT} + \frac{2N\beta^2(g_J - 1)(g_J - 2)}{3\lambda} \tag{9}$$

and the E(J) term is the energy corresponding to the J term which results from the spin-orbit coupling

$$E(J) = \lambda\frac{J(J+1) - L(L+1) - S(S+1)}{2} \tag{10}$$

All the results we have obtained until now are within the free-ion approximation. They are only valid in the high temperature ($kT >> 100$ cm^{-1}) limit. At lower temperatures, the ligand field effect cannot be neglected and we have to take into account the rare earth environment to understand the magnetic behaviour in the whole temperature range. Thus makes quite difficult the interpretation of the magnetic susceptibility for lanthanides.

In most cases, the $^{2S+1}\Gamma_J$ ground state is partially split by the ligand field, depending on the symmetry of the rare earth environment. If it has a rhombic symmetry, which is most likely in molecular compounds, the ground state splits into $2J + 1$ (for J integer) or $J + 1/2$ (for half-integer J) components. In the latter case the components are Kramers doublets. The total width of the resulting multiplet may vary from a few tens to a few hundreds of wavenumbers. If this width is small enough, all the components of this multiple arising from the splitting of the ground state are thermally populated at room temperature, and the free-ion approximation is valid. Nevertheless, upon cooling, the components of higher energies are successively depopulated and the free-ion approximation becomes less and less valid. This may have two consequences:

- the magnetic susceptibility deviates from the Curie law
- the system becomes more and more anisotropic at lower temperatures.

When the total width of the multiplet is larger, the components of higher energies could be statistically depopulated, even at room temperature, and the compound may present a significant magnetic anisotropy.

The magnetic anisotropy always increases on cooling. Consequently, in order to understand and interpretate the magnetic behaviour of a molecular rare-earth compound, we have to describe the effect of the crystal field in a satisfying fashion. The diagonalization of the spin-orbit coupling, the ligand field and the Zeeman perturbations using all the eigenfunctions associated with the $^{2S+1}\Gamma_J$ free-ion states arising from the $4f^n$ electronic configuration allows us to interpretate the magnetic behaviour of this compounds.

References:

Coronado, E.; Drillon, M.; Nugteren, P. R.; de Jongh, L. J.; Beltran, D. *J. Am. Chem. Soc*. **1988**, *110*, 3907-3913.

Dieke G.H., Spectra and energy levels of rare earth ions in crystals, Interscience Publishers. New York, 1968.

Kahn O., *Molecular Magnetism*, VCH, Weinheim, **1993** and references therein.